Development of 2D materials incorporated multi-functional nickel composite coatings by electrodeposition

By

Revathy Sreekumar

10CC19A39021

A thesis submitted to the
Academy of Scientific and Innovative Research
for the award of degree of
DOCTOR OF PHILOSOPHY

In

SCIENCE

Under the supervision of

Dr. Sreejakumari S.S.

CSIR-National Institute for Interdisciplinary Science and Technology (NIIST)
Thiruvananthapuram – 695019

Academy of Scientific and Innovative Research
AcSIR Headquarters, CSIR-HRDC Campus
Sector 19, Kamla Nehru Nagar,
Ghaziabad, U.P. – 201002, India

March 2025

राष्ट्रीय अंतर्विषयी विज्ञान तथा प्रौद्योगिकी संस्थान
वैज्ञानिक तथा औद्योगिक अनुसंधान परिषद् | विज्ञान तथा प्रौद्योगिकी मंत्रालय, भारत सरकार
इंडस्ट्रियल इस्टेट पी.ओ., पाप्पनंकोड, तिरुवनंतपुरम, भारत-695 019

CSIR-NATIONAL INSTITUTE FOR INTERDISCIPLINARY SCIENCE AND TECHNOLOGY (CSIR-NIIST)
Council of Scientific & Industrial Research | Ministry of Science and Technology, Govt. of India
Industrial Estate P.O., Pappanamcode, Thiruvananthapuram, India-695 019

Dr. Sreejakumari S.S.
Principal Scientist
Material Sciences &Technology Division

Email: sreejakumari@niist.res.in
Mobile: 9442217259

CERTIFICATE

This is to certify that the work incorporated in this Ph.D. thesis entitled, **"Development of 2D materials incorporated multi-functional nickel composite coatings by electrodeposition"**, submitted by ***Ms. Revathy Sreekumar,*** to the Academy of Scientific and Innovative Research (AcSIR) in fulfilment of the requirements for the award of the Degree of ***Doctor of Philosophy in Science***, embodies original research work carried out by the student. We further certify that this work has not been submitted to any other University or Institution in part or full for the award of any degree or diploma. Research materials obtained from other sources and used in this research work has been duly acknowledged in the thesis. Images, illustrations, figures, tables etc., used in the thesis from other sources, have also been duly cited and acknowledged.

Revathy 14/03/2025
Revathy Sreekumar

14/03/2025
Dr. Sreejakumari S.S.
(Thesis Supervisor)

March 14th, 2025
Thiruvananthapuram

Tel : 91 471 2515226 | 2515234 | E-mail : director@niist.res.in | Website : http://niist.res.in

STATEMENTS OF ACADEMIC INTEGRITY

I, **Revathy Sreekumar,** a Ph.D. student of the Academy of Scientific and Innovative Research (AcSIR) with Registration No. 10CC19A39021 hereby undertake that, the thesis entitled **"Development of 2D materials incorporated multi-functional nickel composite coatings by electrodeposition"** has been prepared by me and that the document reports original work carried out by me and is free of any plagiarism in compliance with the UGC Regulations on *"Promotion of Academic Integrity and Prevention of Plagiarism in Higher Educational Institutions (2018)"* and the CSIR Guidelines for *"Ethics in Research and in Governance (2020)".*

14/03/2025
Revathy Sreekumar

March 14th, 2025
Thiruvananthapuram

It is hereby certified that the work done by the student, under my supervision, is plagiarism-free in accordance with the UGC Regulations on *"Promotion of Academic Integrity and Prevention of Plagiarism in Higher Educational Institutions (2018)"* and the CSIR Guidelines for *"Ethics in Research and in Governance (2020)".*

14/03/2025
Dr. Sreejakumari S.S.

March 14th, 2025
Thiruvananthapuram

Dedicated to all women and girls in science &

my beloved family

Acknowledgements

I would like to take this opportunity to express my profound gratitude and appreciation to each and everyone who have helped me from the very first day to till date in completing this research work.

With deep regards and respect, I would like to express my sincere gratitude to my research supervisor Dr. Sreejakumari S.S., Principal Scientist, Materials Science and Technology Division, CSIR-National Institute for Interdisciplinary Science and Technology (CSIR-NIIST), Thiruvananthapuram, for suggesting this exciting area, creative suggestions, dedicated help, encouragement, advice, and useful corrections of this research work. I'm very grateful for her unwavering support not only as my guide but also being my best friend who always had my back and provided me with ample space and intellectual freedom to grow as a researcher.

I am thankful to Dr. C. Anandharamakrishnan, and Dr. A. Ajayaghosh, present and former Directors of CSIR-NIIST, Thiruvananthapuram for providing me all the necessary facilities for carrying out the work.

I extend my sincere gratitude towards Dr. S. Ananthakumar, Dr. M. Ravi, and Dr. S. Savithri present and former heads of the Materials Science and Technology division for all the help and support. I thank Dr. P. Jayamurthy, Dr. Karunakaran Venugopal and Dr. C. H. Suresh, the present and former AcSIR program coordinators CSIR-NIIST, for the timely conduction of course work, help and advice regarding the academic procedures of AcSIR.

I wish to acknowledge Dr. T.P.D. Rajan, Dr. A. Srinivasan and Dr. Achu Chandran (my doctoral advisory committee members) for their encouragement, insightful suggestions and discussions which helped me to widen my research. I would like to express my sincere gratitude to Dr. Rakhi R.B. for the fruitful collaboration, academic support and inspiring presence during my Ph.D. I gratefully acknowledge all the scientists and staffs of CSIR-NIIST, Thiruvananthapuram, for their help, support and encouragement.

My wholehearted thanks to Mr. Harish Raj, Mr. Amalraj, Mr. Peer Mohammad, Mr. Chandrakanth C.K. for their technical support by extending different instrumental facilities. Mr. Arun, Mr. Giri and Mr. Nandhakumar of NIIST workshop are specially acknowledged for their support regarding the initial sample cutting and preparation.

Words are insufficient to express my gratitude to my seniors, colleagues and friends who made my life at CSIR-NIIST enjoyable and memorable. Former group members, Ms. Aswathy, Ms. Ancin, Mr. Aashamz and Ms. Sreevalsa are specially thanked for their love, care and support throughout my research period. Dr. Raji, Dr. Jerin, Mr. Akhil M.G., Mr. Arunkumar, Dr. Jithu, Dr. Arsha, Dr. Hari, my seniors are greatly acknowledged for all their help, support and friendship.

My sincere thanks to my colleague and best friend Mr. Visakh Manoj for believing in me and my potential and for his immense support at both professional and personal level throughout my Ph.D. journey. Mr. Muhammad, Ms. Anjana, Ms. Bashida, Ms. Shilpa R, Mr. Arun V.S., Ms. Suja, Dr. Sujith are greatly acknowledged for their companionship and love.

I extend my gratitude to all the scientists and students of MMM group: Dr. Parijath Pallab Jana, Dr. Jayasankar K, Mr. Venkatesan J, Ms. Sreedevi, Ms. Gayathri, Mr. Atly, Dr. Simi, Ms. Anju, Mr. Riyas, Mr. Vineeth, Mr. Justin, Mr. Isahaq and Mr. Harikrishnan. I thank Ms. Sangeetha, Ms. Parvathy, Mr. Christan, Ms. Ragi, Ms. Angitha, Mr. Ben, Ms. Bavya and Mr. Nandhu, my friends at NIIST.

I express my heartfelt thanks to all my MSc project students Ms. Priyalekshmi, Ms. Swapna, Ms. Kavya, Ms. Sreenanda, Ms. Parvathy, Ms. Ansi, Ms. Gopika and Ms. Navya without whom I wouldn't have completed my work and for their friendship, help and useful discussions. I would like to acknowledge my longtime friends Ms. Nishitha, Mr. Navin, Ms. Uthara and Mr. Muhammad Nasik who were part of my Ph.D. journey. A huge shout out to all my throw ball team mates who made my NIIST life more colourful. Mr. Merin, Ms. Aswathy, Mr. Rejith are specially thanked for all their help and support during my Ph.D. All my co-Inspire fellows are thanked. The sitcom program Uppum Mulakum helped me to retain my sanity during this period.

I feel a deep sense of gratefulness to my parents (Mr. Sreekumar and Mrs. Rekha Sreekumar); without their support I couldn't have made this far. They dreamed the best for me and inculcated good values in me. Their unfailing love, care, patience and academic support will remain my inspiration throughout my life. I greatly acknowledge my teacher, Dr. Digna Varghese for her prayers and support. Mrs. Rani T.J. and Ms. Aswathy, my cousin sister are thanked for their wholehearted care, love and support.

I would like to acknowledge the financial support received from the Department of Science & Technology, in the form of Inspire fellowship grant. Above all, I thank God the Almighty for bestowing blessings upon me and giving all these people to help and encourage me, for the successful completion of the work.

Last but not the least, I would like to thank myself- for never quitting, for always believing that there is light at the end of the tunnel. Self, it has been a rollercoaster ride, thank you for holding up all these years of studying, writing, crying, trying and most importantly trusting the process. You deserve all the happiness and success.

Revathy Sreekumar

TABLE OF CONTENTS

List of Tables

List of Figures

LIST OF ABBREVIATIONS

°C	:	Degree Celsius
µm	:	Micro meter
1-D	:	One dimensional
2-D	:	Two dimensional
3-D	:	Three dimensional
A	:	Ampere
AC	:	Alternating current
AFM	:	Atomic force microscopy
CA	:	Chronoamperometry
CD	:	Current density
Cdl	:	Double layer capacitance
cm	:	Centimeter
COF	:	Coefficient of Friction
CPE	:	Constant phase element
CTAB	:	Cetyl trimethyl ammonium bromide
CV	:	Cyclic voltammetry
CVD	:	Chemical vapor deposition
DC	:	Direct Current
DCM	:	Dichloromethane
dec	:	Decade
DI	:	De-ionized
DLC	:	Diamond like coating
dm^2	:	Decimeter square
E	:	Potential
E_{corr}	:	Corrosion potential
EDS	:	Energy dispersive spectroscopy

EEE	:	Equivalent electrochemical circuit
EIS	:	Electrochemical impedance spectroscopy
FCC	;	Face centered cubic
FE-SEM	:	Field emission scanning electron microscopy
g	:	gram
GDP	:	Gross domestic product
gf	:	gram force
g/l	:	gram per litre
GO	:	Graphene oxide
Gr	:	Graphene
h	:	hour
HER	:	Hydrogen evolution reaction
HV	:	Vickers hardness
Hz	:	Hertz
i	:	Current
$\mathbf{I_{corr}}$	:	Corrosion current
IE	:	Inhibition efficiency
IF	:	Inorganic fullerene
JCPDS	:	Joint committee on powder diffraction standards
kHz	:	Kilohertz
LDH	:	Layered double hydroxide
MA	:	Myristic acid
MB	:	Methylene blue
MEMS	:	Micro-electromechanical systems
mg	:	milligram
MHz	:	Megahertz

min	:	minutes
mm	:	millimetre
mmpy:	:	Millimeter per year
MOF	:	Metal organic framework
MS	:	Mild steel
mV	:	Milli volt
NPs	:	Nano particles
NCs	:	Nano cubes
OCP	:	Open circuit potential
PC	:	Pulse current
PP	:	Potentiodynamic polarisation
PRC	:	Pulse reverse current
PTFE	:	Poly tetra fluoro ethylene
PVAc	:	Poly vinyl acetate
PVA	:	Poly vinyl alcohol
PVD	:	Physical vapor deposition
R_c	:	Coating resistance
R_{ct}	:	Charge transfer resistance
r-GO	:	Reduced graphene oxide
R_p	:	Polarisation resistance
rpm	:	revolutions per minute
R_s	:	Solution resistance
RT	:	Room temperature
s	:	second
SA	:	Stearic acid
SCE	:	Standard calomel electrode
SDS	:	Sodium dodecyl sulphate

SHSM	:	Superhydrophobic stainless steel mesh
SLS	:	Sodium lauryl sulphate
SS	:	Stainless steel
SSM	:	Stainless steel mesh
TMDs	:	Transition metal dichalcogenides
TPa	:	Terapascal
V	:	Voltage
WCA	:	Water contact angle
wt	:	weight
XRD	:	X-ray diffraction
Z'	:	Impedance (real)
Z''	:	Impedance (imaginary)
η	:	Eta (here, inhibition efficiency)
η_{10}	:	Overpotential
μAcm^{-2}	:	Micro ampere per centimeter square
μF	:	Microfarad

PREFACE

Material deterioration and excessive energy consumption are closely linked, especially in industries where the performance and longevity of materials are critical. According to the World Energy Council, it is expected that rapid industrialisation will increase the worldwide energy demand from 45% to 60% by 2030. The deterioration of materials due to corrosion, wear, friction, oxidation, fatigue, etc., can lead to increased energy use in several ways, primarily due to the loss of efficiency, increased maintenance requirements, and the need for more frequent replacement or repairs. It is estimated that annually, about $2.5 trillion loss occurs due to corrosion and wear. Excessive energy consumption can have economic implications as well as impacts on sustainability and results in environmental degradation. Thus, improving energy efficiency is crucial for long-term economic development and to meet human needs.

A noticeable interest is seen in the research and development of multi-functional coatings that additionally possess novel functions/characteristics along with the provision of protection and aesthetics to the underlying surface. These coatings play a crucial role across various industries, such as automotive, aerospace, construction, electronics, manufacturing, healthcare, and renewable energy. Since they can increase machine efficiency and have an environmental impact by lowering greenhouse gasses (like CO_2) and carcinogens (like NO_2), tribological coatings with low coefficients of friction (COF) are highly sought after by a variety of industries. In industries where water or moisture causing damage or affecting the performance of the materials, developing durable and scalable superhydrophobic coatings that can withstand mechanical wear, environmental exposure, and contamination while remaining cost-effective and sustainable is important. Catalytic coatings are essential in improving the efficiency, durability, and economic viability of sustainable hydrogen production technologies like water electrolysis. Advancements in catalytic materials, particularly non-precious metal catalysts, are critical for reducing costs and enhancing the scalability of hydrogen as a clean energy source, aligning with global sustainability goals and the transition to a low-carbon economy.

Metal-matrix composite functional coatings offer enhanced properties such as wear resistance, corrosion protection, improved hardness, tunable wettability, catalytic properties, etc., making them highly valuable across various industries. Their versatility, durability, and potential for improving performance in extreme conditions ensure their continued importance in various

sectors. As early as the 1970s, Nickel (Ni) was proposed to be a promising candidate in the area of metal matrix composite coatings due to its novel blend of properties and attributes.

The electrodeposition of composite coatings, also referred to as 'inclusion plating', 'codeposition of metals and particles' or "electro co-deposition". Electro-deposition of nickel-based composite coatings is one of the efficient methods for the modification of material surfaces, which is easy, facile, cost-effective, and doesn't require any complex equipment. For a number of applications, electro-deposited composite coatings are found to be superior to other coatings, developed by other methods. Another benefit of adopting electrodeposition technique is the ease with which grain size, coating thickness, morphology, and crystallographic orientation may be varied by changing the bath compositions and deposition parameters.

Chapter 1 gives a general introduction about recent developments in multi-functional metallic composite coatings developed by electrodeposition. Main focus of the chapter is on the properties of 2D materials (h-BN, graphene, and transition metal dichalcogenides) incorporated electroplated nickel based composite coatings. This chapter also gives a detailed experimental methodology for the development of Ni composite coatings over mild steel substrate by electrodeposition.

Chapter 2 deals with the development of Ni-h/BN composite coating over mild steel substrate. The influence of grain refinement on the microhardness, corrosion and tribological properties was also investigated. Micro hardness value of the composite coating was higher than pure Ni coating and mild steel. Under different saccharin concentrations, it has been found that the corrosion resistance of all Ni-BN coatings developed is better than that of pure nickel coated and uncoated substrates. Further, the composite coating exhibited lower COF (0.23) and excellent wear resistance. Thus the developed Ni-BN coating with improved properties indicates its potential for engineering applications.

One-step electrodeposited biomimetic Ni-graphene composite coating with pinecone-inspired hierarchical micro/nanostructures with a contact angle of 152° was developed in **Chapter 3**. It has been observed that this particular coating was mechanically durable with improved corrosion resistance. Furthermore, the coating was self-cleaning. The composite coating demonstrated consistent and good lubricating qualities with an average friction coefficient of 0.24 and a low wear rate that was more than 70% lower than that of the pure Ni coating, indicating its potential for a range of applications.

In **Chapter 4**, electrodeposited Ni and Ni-MoS_2 coatings have been successfully developed. The coatings reinforced with MoS_2 exhibit more compact structure as compared to the pure Ni coating. In terms of mechanical properties, Ni-MoS_2 coating shows a maximum hardness value of 525 HV. Compared with uncoated and pure Ni coated samples, Ni-MoS_2 composite coated sample exhibited excellent corrosion resistance and low coefficient of friction (0.08) at optimized conditions. Ni-MoS_2 coated SS mesh exhibited improved electrocatalytic activity for HER and OER can function as an efficient bi-functional catalyst for water splitting.

The development of a low friction, superhydrophobic Ni-WS_2 composite coating by one step electrodeposition is discussed in **Chapter 5**. The deposition parameters and concentration of WS_2 were fine-tuned to generate a hierarchical surface with a high water contact angle of 159°. WS_2 embedded in the Ni matrix forms a self-lubricating tribo-film resulting in a reduced friction coefficient of 0.04 in the case of composite coating. The robust surface of the as-prepared composite coatings exhibited strong corrosion resistance and self-cleaning properties in contrast to the bare substrate and pure nickel coating, offering potential for industrial applications.

Chapter 6A deals with the development of superhydrophobic - superoleophilic SS mesh with a water contact angle of 169.5^o and surface roughness of 168 nm. The combined effect of hydrophobic surface chemistry and the roughness contributes to excellent superhydrophobic-superoleophilic and self-cleaning characteristics of the developed SHSM. The oil/water separation performance of SHSM was studied and the efficiency was greater than 98 % even after multiple uses. **Chapter 6B** reveals the potential of Ni-WS_2 coated SS mesh with micro-nano hierarchical structure as a bi-functional catalyst in overall water splitting. A full-cell alkaline electrolyzer using Ni-WS_2 coated SS mesh as anode and cathode delivered a current density of 10 mA/cm^2 at an applied potential of 1.56 V.

Summary of the various studies carried out as part of the development of 2D materials incorporated multifunctional Ni composite coatings and also the future perspectives of the research work is given in **Chapter 7**.

Chapter 1

Multi-functional Metallic Composite Coatings

An Overview

Abstract

Multi-functional metallic composite coatings have emerged as a cornerstone in modern material science, offering a unique combination of properties that address diverse industrial challenges. Integrating multiple functionalities into a single coating not only simplifies the processes but also reduces the material costs. The improved properties of these multi-functional coatings make them indispensable in industries such as aerospace, automotive, healthcare, and energy sector. Thus the development of sustainable, cost-effective, durable, and versatile multifunctional composite coatings is imperative as industries strive for advancements in energy efficiency, sustainability, and scalability. Metal-matrix composite functional coatings seem to good option due to their versatility, durability, and potential for improving performance in extreme conditions. Due to the unique combination of properties, Nickel (Ni) was suggested as a suitable option in the field of metal matrix composite coatings. For nickel composite coatings, different types of materials may be utilized as second-phase particles like ceramics, carbon nanotubes, diamond, etc. In addition to that, two-dimensional (2D) layered material fillers such as graphene, boron nitride (BN), molybdenum disulphide (MoS_2), tungsten disulphide (WS_2) etc have been used as potential reinforcements to develop composite coatings with superior mechanical, tribological and other multifunctional characteristics. Electrodeposition of nickel-based composite coatings is one of the efficient techniques for surface modification, which is easy, facile, cost-effective, and doesn't require any complex equipment. This chapter describes the basic principles of electrodeposition, including metal-particle co-deposition models and other significant factors influencing the electrodeposition process. This chapter provides a thorough discussion of the development techniques, reinforcement mechanisms, distinctive mechanical characteristics, friction and lubrication performances, super-hydrophobicity, catalytic applications, potential uses, and real-world advantages of 2D material incorporated multi-functional nickel composite coatings.

1.1. Introduction

Material deterioration and excessive energy consumption are closely linked, especially in industries where the performance and longevity of materials are critical. According to the World Energy Council, it is expected that rapid industrialisation will increase the worldwide energy demand from 45% to 60% by 2030 [1]. The deterioration of materials due to corrosion, wear, friction, oxidation, fatigue, etc., can lead to increased energy use in several ways, primarily due to the loss of efficiency, increased maintenance requirements, and the need for more frequent replacement or repairs. It is estimated that annually, about $2.5 trillion loss occurs due to corrosion and wear [2]. Excessive energy consumption can have economic implications as well as impacts on sustainability and results in environmental degradation. The uncontrolled consumption of fossil fuels is a severe problem in the current scenario due to the emission of harmful greenhouse gases such as CO_2, contributing to global warming and related environmental issues [3]. Thus, improving energy efficiency is crucial for long-term economic development and to meet human needs.

In this context, with the aim of material protection and minimising energy consumption, a noticeable interest is seen in the research and development of multi-functional coatings that additionally possess novel functions/characteristics along with the provision of protection and aesthetics to the underlying surface. These coatings play a crucial role across various industries, such as automotive, aerospace, construction, electronics, manufacturing, healthcare, and renewable energy. Since they can increase machine efficiency and have an environmental impact by lowering greenhouse gasses (like CO_2) and carcinogens (like NO_2), tribological coatings with low coefficient of friction (COF) are highly sought after by a variety of industries [4]. The inorganic chromate-based coatings are mostly used for this purpose but they are toxic and carcinogenic causing lung cancer, skin irritation, and chronic ulcers. Hence there is a great need to find a sustainable, cost-effective, and versatile chromate replacement possessing multiple characteristics.

In industries where water or moisture causing damage or affecting the performance of the materials, superhydrophobic coatings can be really useful to repel water and contaminants, offering benefits in terms of self-cleaning, corrosion resistance, and reduced maintenance [5]. Developing durable and scalable coatings that can withstand mechanical wear, environmental

exposure, and contamination while remaining cost-effective and sustainable is the key to overcome these challenges and realizing the full potential of superhydrophobic surfaces.

Renewable energy is currently under focus due to the growing need for energy and depleting fossil fuel reserves. Out of all the sustainable energy sources, hydrogen is the most promising fuel candidate because of its high gravimetric energy density, comparatively more availability, and no emissions throughout consumption [6]. Catalytic coatings are essential in improving the efficiency, durability, and economic viability of sustainable hydrogen production technologies like water electrolysis. Advancements in catalytic materials, particularly non-precious metal catalysts, are critical for reducing costs and enhancing the scalability of hydrogen as a clean energy source, aligning with global sustainability goals and the transition to a low-carbon economy. Hence, there is a great need to develop sustainable, cost-effective, durable, and versatile multifunctional composite coatings as industries strive for innovations in terms of energy efficiency, sustainability, and scalability.

1.2. Electrodeposited metal composite coatings

Metal-matrix composite functional coatings offer enhanced properties such as wear resistance, corrosion protection, improved hardness, tunable wettability, catalytic properties, etc., making them highly valuable across various industries. Their versatility, durability, and potential for improving performance in extreme conditions ensure their continued importance in sectors like aerospace, automotive, energy, and manufacturing. As early as the 1970s, Nickel (Ni) was proposed to be a promising candidate in the area of metal matrix composite coatings due to its novel blend of properties and attributes [7].

Area of electrodeposition of metal matrix composite coatings is advancing at a regular pace. Electrodeposition is a “bottom-up”, “single-step” method for developing composite coatings [8].The electrodeposition of composite coatings, also referred to as ‘inclusion plating’, ‘codeposition of metals and particles’ or “electro co-deposition”. Electro-deposition of nickel-based composite coatings is one of the efficient methods for the modification of material surfaces, which is easy, facile, cost-effective, and doesn’t require any complex equipment. For a number of applications, electro-deposited composite coatings are found to be superior to other coatings, such as those resulting from flame spraying, hard chromium plating, nitriding, CVD, PVD, etc. Another

benefit of adopting electrodeposition technique is the ease with which grain size, coating thickness, morphology, and crystallographic orientation may be varied by changing the bath compositions and deposition parameters [9].

1.3. General co-deposition mechanism in composite electrodeposition

The metal matrix, the kind and size of the reinforcement particles, and the process parameters are all carefully selected in electrodeposited metal composite coatings in order to maximize the strengthening effects given off by the crystal structure [10] (**Figure 1.1.**). For example, the electrolyte composition, agitation, and current density are process parameters that are utilized to change the matrix's grain size [11]. The kinetics of electrochemical deposition, mechanisms of crystal growth and nucleation, all contribute to porosity of the electrodeposited coatings [12]. For nickel composite coatings, different types of particles like oxides, carbides, nitrides, two dimensional layered materials, diamond like carbon (DLC) can be utilised. Integration and even distribution of second phase particles might improve the material's intrinsic mechanical, tribological and electrochemical properties and open it up to a whole new area of material applications. Agitation/stirring, cathode movement and surfactant addition are the ways of suspending secondary particles. In the bath particles will attain a natural surface charge and zeta potential. Alteration of surface charge in terms of sign and size is possible by adsorption of metallic ions and also by surfactant addition.

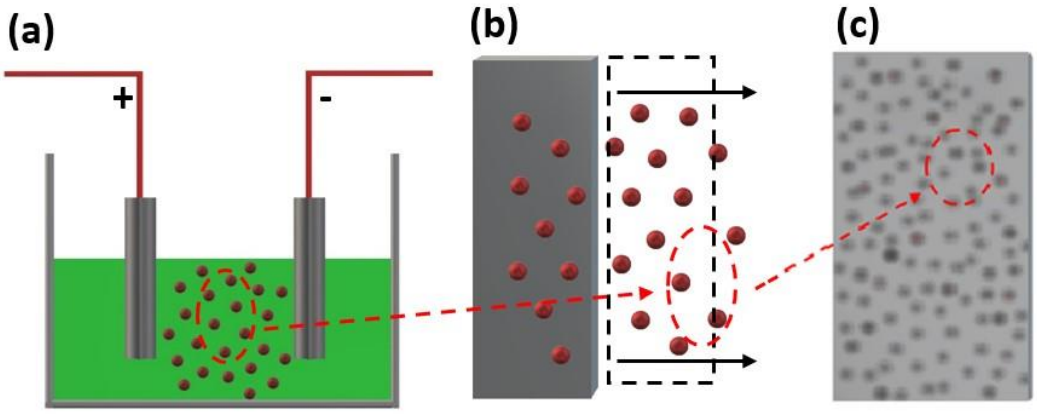

Figure 1.1. Electrodeposition of composite coating. **(a)** Particle addition to the electrolyte, **(b)** Particle entrapment by the metal and **(c)** Composite coating. Particles are encircled in red

There are many proposed models which explain particle co-deposition [13,14]. **Table 1.1.** provides the details of existing models and their main ideas.

Table 1.1. List of existing models which explain the mechanisms of particle co-deposition in composite electroplating

Guglielmi [15]	This model described co-deposition as two consecutive steps: (i) Loosely absorbed particles form a layer at the surface of the cathode by absorption. (ii) Electrophoresis where the electric field at the interface elevates potent surface adsorption and thus particles are entrapped by the growing metal. The fluid dynamic conditions were not considered in this model.
Celis et al.[16]	Devised that the movement of particles is relative to the mass transfer of ions towards cathode. Firstly ionic species forms an absorbed layer around the particles followed by the addition to the electrolytic bath, followed by transport of particles via convection-diffusion. Finally, incorporation depends upon the probability and number of transported particles.
Fransaer et al.[17]	This one use trajectory analysis to explain the suitable environment provided by the action of tangential forces on the particles enhancing rate of co-deposition.
Hwang et al.[18]	Highlighted the importance of current density in particle co-deposition. Co-deposition rates are associated with the reduction of ions adsorbed on the particles' surfaces.
Vereecken et al.[19]	The model depicted particle transport as governed by convection-diffusion taking into account hydrodynamics and assuming that particle inclusion increased with contact time at the cathode's surface.
Berçot et al.[20]	Guglielmi's model [15] was further improved by including a mathematical model that accounted for hydrodynamic conditions.

The adaptability and the credibility of all the available models still need proper proofs and verification [21,22]. One of the common mechanisms of co-deposition process have five sequential steps [23] as shown in **Figure 1.2.**

Five consecutive steps of co-deposition mechanism are:

(1) Formation of ionic clouds on the particles

(2) Convection towards the cathode

(3) Diffusion through hydrodynamic boundary layer

(4) Diffusion through concentration boundary layer

(5) Adsorption at the cathode surface where particles get deposited within metal deposit

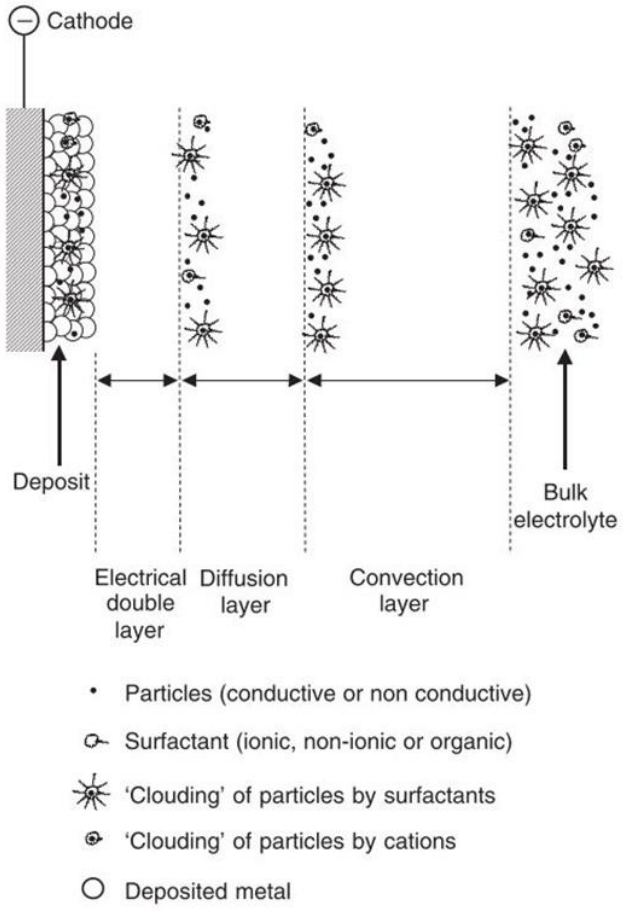

Figure 1.2. Mechanism of particle co-deposition into a metal deposit [24].

1.4. Two-dimensional layered materials as reinforcements: Scope and applications

For nickel composite coatings, different types of materials may be utilized as second-phase particles like ceramics, carbon nanotubes, diamond, etc. In addition to that, two-dimensional (2D) layered material fillers such as graphene, boron nitride (BN), molybdenum disulphide (MoS_2), tungsten disulphide (WS_2), transition metal carbides, selenides, MXenes, and other novel lamellar 2D materials, such as LDH, α-ZrP have been used as potential reinforcements to develop composite coatings with superior mechanical, tribological and other multifunctional characteristics [25].

Two-dimensional materials possess remarkable physical, chemical, electronic, and optical properties compared to existing three-dimensional (3D) materials. 2D materials are a combination of crystalline atomic chains, where the atoms are firmly linked by covalent bonds within individual atomic layers and subsequent layers are loosely connected by van der Waals forces, forming a monolayer structure with high modulus and strength. Higher specific surface area of 2D materials aids in more effective surface absorption contributing towards improved catalytic activity, and these materials can form a tribo-film between the surfaces in contact. Highly tunable layered structure of these 2D materials can also generate micro-nano roughness essential for superhydrophobicity. In addition to that, low shear resistance between the nearby atomic layers permits the easy sliding of these layered atoms [26]. Thus the soft van der Waals forces account for their outstanding tribological properties and self-lubrication performance superior to that of other nanomaterials.

2D nanomaterials can be typically classified into five categories based on their composition and atomic configuration: (1) Xenes, which are made up of single element like carbon, silicon and phosphorous. A peculiar example is graphene made of carbon atoms. (2) Transition metal carbides and nitrides (MXenes), in which M is an early transition metal (e.g. Ti, V and Mo) and X can be carbon or nitrogen. (3) Transition metal dichalcogenides (TMDs); they are composed of hexagonal metal layers in which metal atoms (M) are packed between two layers of chalcogen atoms (X) having a MX_2 stoichiometry such as MoS_2, $MoSe_2$, WSe_2 and WS_2. (4) 2D III nitrides (MN) in which M is a group III metal and N is nitrogen. An example of 2D III nitride is hexagonal boron nitride (h-BN). (5) 2D organic frameworks. They are comprised of metal-organic frameworks (2DMOFs) that contain metal ions or clusters that are bonded to organic ligands, an example is MOF-5 whereas covalent-organic frameworks (2DCOFs) forms two-dimensional structures via

interactions between organic precursors leading to strong covalent bonds, resulting in porous, stable and crystalline materials. A typical example is COF-5.

1.4.1. Graphene

Graphene (Gr) is basically a crystalline allotrope of carbon with two-dimensional properties. In graphene, sp^2-bonded carbon atoms are closely arranged in a well ordered hexagonal fashion (**Figure 1.3.**) It has a large surface area that has a close-knit contact with the metal matrix [27] and additionally has ultra-high elastic modulus, yield strength, good electrical and thermal conductivity [28]. Graphene has potential applications in the field of materials engineering specifically in resilient composite materials [29]. Possibility of using graphene as part of the composites is really useful in aerospace and automotive industries because of its superior strength, ductility and firmness as a covering especially in the area of laminated composites, altering the substrate by improving its endurance to extreme conditions that may cause wear and corrosion [30]. In addition to that, graphene incorporated metal matrix composites hold superlative thermal and mechanical properties, so that they can be utilised in the fields of surface engineering, catalysis, electronics, energy storage and so on [31]. The workability of graphene is restricted due to expensive synthesis methods, limited solubility and agglomeration tendency while utilised in the area of composite materials [32]. Pure Gr coatings are extremely vulnerable to surface defects especially when exposed to corrosive environment [33,34]. To avoid these drawbacks functionalization of graphene is considered to be an alternative choice and thus graphene oxide (GO) became popular [35],[36].

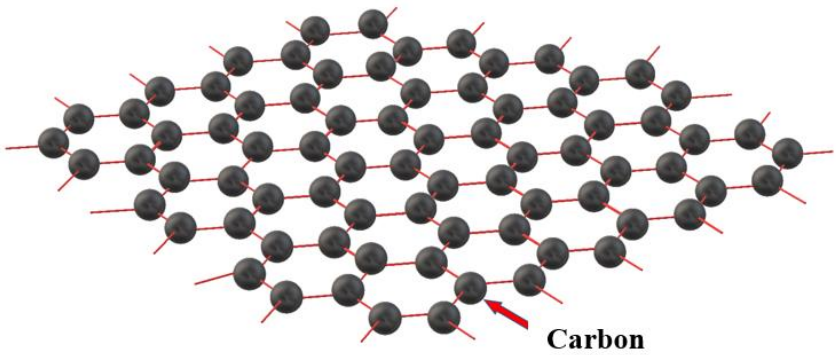

Figure 1.3. Structure of graphene

1.4.2. Boron nitride

Boron nitride (**Figure 1.4.**) is a man-made crystalline compound that is structurally similar to graphite as the alternating B and N atoms substitute for C atoms [37]. It is a refractory compound having exceptional chemical and thermal stability, high thermal conductivity, excellent electrical resistivity, non-wettability, superior lubrication properties and low dielectric constant. BN nano-particles may be directly included into polymers and metal matrices to get composite coatings which show improved corrosion resistance and high hardness [38]. An additional advantage of h-BN is that it is a very good lubricant at both low and high temperature and can be employed to generate different friction resistant composite materials [39]. Another important feature is that the viscosity of BN is maintained without water or gas entrapment in between its layers.

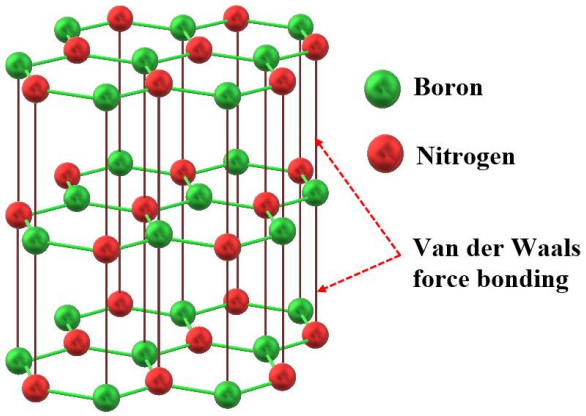

Figure 1.4. Structure of boron nitride

1.4.3. Transition metal dichalcogenides

Transition metal dichalcogenides are typically MX_2, where M is a transition metal atom (such as Mo or W) and X is a chalcogen atom (such as S, Se or Te) such as MoS_2, $MoSe_2$, WS_2, and WSe_2 (**Figure 1.5.**) They are layered materials which follow hexagonal crystal system [40,41] having strong in-plane ionic-covalent bonds and weak out-of-plane van der Waals forces. These interactions result in minimal shear and sliding of individual layers which reduces wear and friction to a greater extent [42]. The main disadvantage of these TMD based lubricants is that they are highly susceptible to humidity. These TMD based self-lubricating coatings have applications involving ultra-high vacuum, transportation and space systems comprising of satellites and launch vehicles where often liquid lubricants fail to function properly [43].

Molybdenum disulfide (MoS_2) and MoS_2-based composites have received the greatest attention among these 2D TMDs [44]. So far, MoS_2-based nanomaterials have primarily been applied in domains such as energy storage, electronic devices, and biomedical engineering [45]. MoS_2 has superior mechanical characteristics as well, including an extraordinarily high Young's modulus (0.3 TPa) and strong elasticity.

In comparison with MoS_2, WS_2 can sustain in high temperature so that it is a better solid lubricant for high temperature applications. On oxidation, WS_2 is converted to tungsten trioxide (WO_3). WO_3 also has a low friction factor and restricts the glue formation in between the surfaces that experience friction. The addition of WS_2 in Ni matrix leads to reduction in fragility of the coating and improves properties like adhesion and wear resistance of the coating [46].

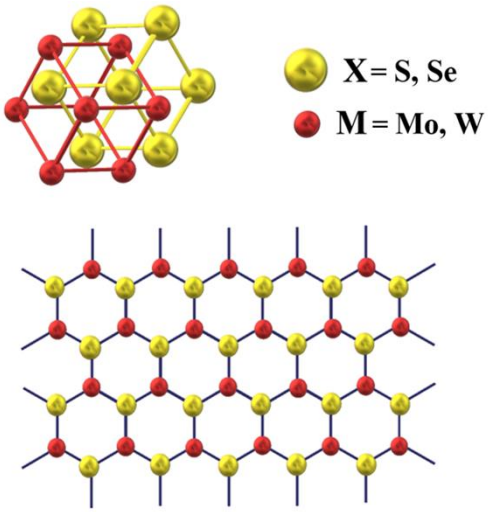

Figure 1.5. Structure of transition metal dichalcogenides

1.5. Nickel composite electrodeposition

1.5.1 Ni-Watts bath

The most common nickel plating bath is the sulphate bath known as Watts bath. Watts formulation, which was developed in 1916 by Professor Oliver P. Watts [7] is the basis of majority of the nickel plating solutions. This electrolyte is made up of nickel sulphate, nickel chloride and boric acid. Nickel sulphate is the main source of nickel ions. The limiting current density for attaining good quality deposits is determined by the nickel metal content. Anodic corrosion is provided by nickel chloride thus increasing the diffusion coefficient of nickel ions allowing a

higher limiting current density and boric acid functions as a pH buffer [47]. H_3BO_3 could also influence the nucleation and grain growth of Ni electrodeposits in the Watts electrolyte. A sufficient H_3BO_3 content improves the Ni nucleation process, resulting in a fine and bright Ni coating [48]. While the quantities may vary depending on the application, **Table 1.2.** provides a common formulation and details of operating parameters [49]. The Watts bath has four major advantages compared to the other available baths:

1. Simple and easy to use

2. Obtained in high purity grades and relatively inexpensive

3. Less aggressive to equipment (container) than nickel chloride solutions

4. Deposits plated from these solutions are less brittle and possess lower internal stress than plated from nickel chloride electrolytes.

Table 1.2. Details of Ni Watts electroplating bath

Bath composition	Nickel Sulphate ($NiSO_4.6H_2O$)	240-300 g L^{-1}
	Nickel Chloride ($NiCl_2.6H_2O$)	30-90 g L^{-1}
	Boric Acid (H_3BO_3)	30-45 g L^{-1}
Operating Parameters	Temperature	40-60 ^oC
	pH	3.5-4.5
	Current Density	2-7 A dm^{-2}
	Deposition Rate	25-85 µm h^{-1}

1.5.2. Techniques for Ni composite electrodeposition

Generally in Ni electrodeposition when an external electric field is applied, a transfer of electrons occurs across the cathode surface causing reduction of Ni ions into their metallic form [24],[50]. This process is divided into three successive steps [51].

(1). Ni ions are carried to the cathode from the bulk electrolyte by mass transport through diffusion, convection and electro-migration [52].
(2). A charge transfer occurs on the cathode and the partially reduced Ni atoms are adsorbed at the surface.
(3). Loosely bound Ni atoms will diffuse across the electrode surface to active growth sites where they are incorporated into the crystal lattice at the kink sites or an atomic step.

Passing electric current to the electrolyte is the primary function of nickel anodes in electroplating. Replacement of nickel ions that have been discharged at the cathode and distribution of current are also major functions of the Ni anode. The following reactions are most probable in the course of Ni deposition, where $Ni(OH)^{+}_{ad}$ denotes an active intermediate [53].

$$Ni^{2+} + H_2O \leftrightarrow Ni(OH)^{+}_{aq} + H^{+} \quad (\mathbf{1.1.})$$

$$Ni(OH)^{+}_{aq} \leftrightarrow Ni(OH)^{+}_{ad} \quad (\mathbf{1.2.})$$

$$Ni(OH)^{+}_{ad} + e^{-} \leftrightarrow NiOH \quad (\mathbf{1.3.})$$

$$NiOH + H^{+} + e^{-} \leftrightarrow Ni + H_2O \quad (\mathbf{1.4.})$$

Direct Current (DC) electrochemical deposition, Pulsed Current (PC) deposition and Pulsed Reverse Current (PRC) deposition are various types of electrochemical deposition. In DC method, a steady and specific current is applied throughout the coating process. One downside of this approach is the generation of residual tensile stresses, which results in the formation of cracks within the deposit. Because of its capacity to improve current distribution and mass transfer processes, the pulse technique is an effective way for controlling the microstructure and chemical composition of plated coatings. Furthermore, this process eliminates various issues such as hydrogen evolution, metallic hydride formation, uneven deposits, and local pH fluctuations. Application of an anodic current in form of a reverse pulse during nickel electrodeposition may distinctively affect quality, properties, and chemical composition of obtained coatings. Superior quality coatings may be obtained by this pulse reverse method.

1.5.3. Co-deposition mechanism in Ni-2D material incorporated composite coatings

There are studies on optimization and analysis of the underlying mechanism of co-deposition of nano materials in metallic deposition [54]. The whole co-electrodeposition process in Ni–W/BN nanocomposite coating via DC deposition can be summarized in four sequential steps as "transportation, adsorption, reduction and incorporation" (**Figure 1.6.**) according to Li et al.[55] The initial step is "transportation" in which aqueous metal ions, complexes and charged particles are moved towards the cathode by convection or an electric field. Electrophoresis has been used to transfer metallic ions and BN nanoparticles to the cathode. Agitation can increase the availability of the nickel complex at the solution/electrode interface and accelerates the mass transport which speeds up the electrodeposition process. It is followed by "adsorption". Metal ions and charged BN nanoparticles move through the diffusion layer and get adsorbed on the surface of cathode [56]. "Reduction" was the next step. Metal ions are reduced and neutralized by electron transfer in this stage and they get firmly adsorbed on the cathode. The WO_4^{2-} ion reduction may be summarised as:

$$WO_4^{2-} + 8H^+ + 6e^- \rightarrow W + 4H_2O \qquad (\mathbf{1.5.})$$

The final stage was "incorporation". The BN particles get inserted into the Ni-W alloy matrix. Thus Ni-W/BN nanocomposite coating was formed. The Ni-W/BN nanocomposite coating generation is depicted in equation (**1.6.**)

$$[(Ni)\,(HWO_4)\,(Cit)]^{2-} + 3H_2O + 8e^- + BN_s \longrightarrow Ni - W/BN + 7OH^- + Cit^{3-} \qquad (\mathbf{1.6.})$$

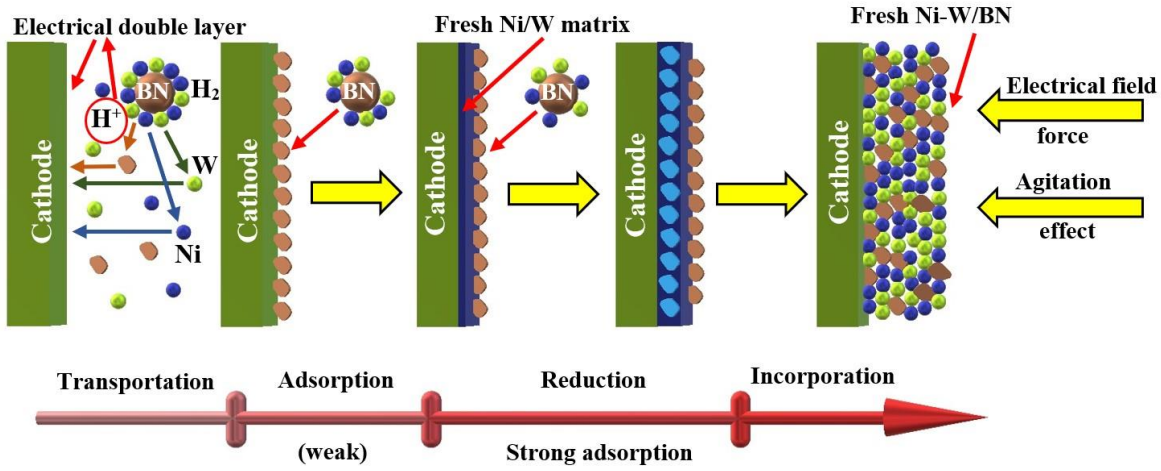

Figure 1.6. Mechanism of co-electrodeposition process in Ni–W/BN composite coating

A discussion on the mechanism of deposition and hierarchical coating growth in Ni-P-WS_2 is given by He et al.[57]. The main cathodic reaction is:

$$Ni^{2+} + 2e^- \rightarrow Ni \qquad (\mathbf{1.7.})$$

Hydrogen evolution will take place as a side reaction:

$$2H^+ + 2e^- \rightarrow H_2 \qquad (\mathbf{1.8.})$$

Reduction of hypophosphite ion at the cathode leads to phosphorus being co-deposited with nickel

$$H_2PO_2^- + e^- \rightarrow P + 2OH^- \qquad (\mathbf{1.9.})$$

Analysing Ni-P-WS_2 composite coatings, CTAB gets adsorbed by WS_2 and its quaternary ammonium groups (-NH_4^+) has a positive charge. Both convective-diffusion and electrophoretic migration help in WS_2 transportation. The incorporation of WS_2 particles into the Ni-P electrodeposit caused noticeable transformation of surface morphology from a planar smooth surface to a nodular rough surface and finally a hierarchical rough surface. Surface morphological changes are mainly due to the variation of current distribution on the surface of electrodes because of the conductive WS_2 particles [58]. Adhesion of WS_2 particles to the cathode surface is associated with a change in the electric field behaviour. The Ni-P deposits preferentially initiate growing above WS_2 particles as they have a higher current density which causes more active nickel ion reduction [59]. Thus 'broccoli-like' structures are formed (**Figure 1.7.**).

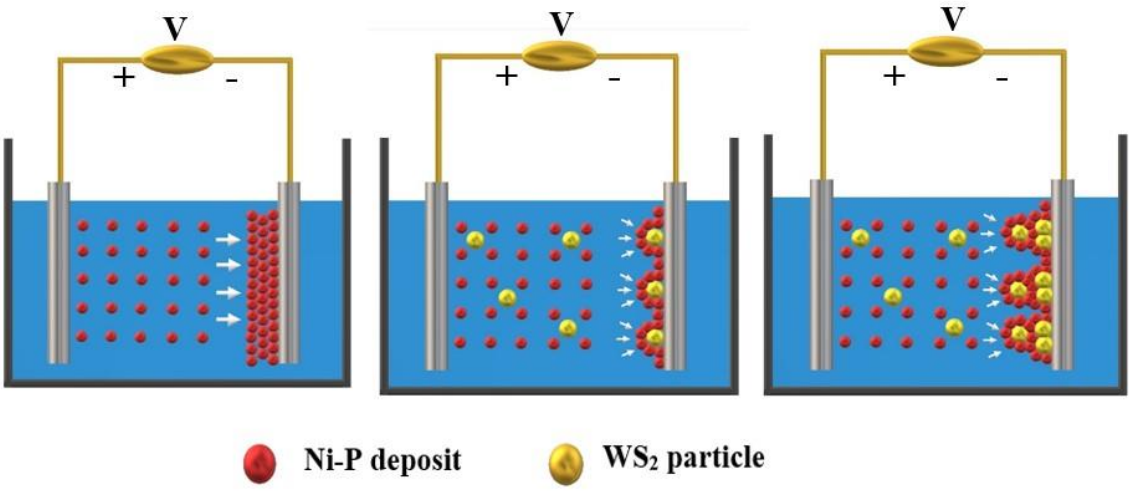

Figure 1.7. Schematic illustration of the growth process of Ni-P-WS_2 composite coating

1.6. Nickel-2D material incorporated composite coatings

1.6.1. Mechanical Properties

The enhancement in the mechanical and tribological properties of composite coatings by 2D nanomaterial reinforcement depends on numerous factors such as aspect ratio, volume fraction of nanomaterials, orientation of nanosheet and interface bonding between the filler and matrix. At a higher volume content, 2D nanomaterials are prone to self-aggregation, resulting in the deterioration of the mechanical properties. Interface bonding of 2D materials comprising hydrogen bonding, covalent bonding, ionic interactions and electrostatic interactions is another important factor influencing the improvement in composite coatings.

1.6.1.1 Micro-hardness

The electrodeposited composites being economical and having superior physical properties are promising candidates in many industries. Mechanical properties namely hardness, toughness, adhesive strength, impact and tensile strength are prominent traits of these composites. Hardness is a material's quality to withstand localised deformation. Integrated effect of Hall-Petch mechanism [60] on account of the grain size refinement and Orowan mechanism [61] due to the uniform dispersion of nano-particles is the main reason of increase in hardness. Hardness of composite coatings is primarily controlled by the hardness of metal matrix and the proportion of

reinforcement particles. The hardness and corrosion resistance of nanocrystalline-Ni coatings can be enhanced by refining the grain size [62].

The variation in micro-hardness of Ni-BN composite coating was exceptional being 3 to 4 times than that of pure nickel. Combined effect of dispersion hardening and grain refinement accounts for the greater hardness of the coating. The dispersed particles in the fine grained matrix can restrict the dislocation motions and plastic flow is ruled out [63]. The indicated resistance to deformation is actually hardness of Ni-BN composite coating. In nickel-alloy composite coatings, the hardness of nickel-rich alloy directly increases with increasing strain till a particular value followed by a decrease. Micro-hardness values of Ni–W/BN (h) (460–565 HV) coatings are comparatively more than that of Ni–W alloy coating [64]. In this instance, the lubricating action of BN can be seen. The microhardness of PC nanocomposite coating is higher than that of DC deposits. A higher over potential is the result of the superlative pulse frequency during PC deposition. Because of the dispersion strengthening effect of BN nanoparticles, which limits the dislocation movement improve the microhardness.

Mixed nitride-carbide boron particles are used as reinforcements in Ni matrix by Paydar et al. [65] resulting in hard composite coating of Ni-BN-B_4C. Hardness improvement with rise in current density up to 50 $mAcm^{-2}$ indicating the accelerated cathodic movement of adsorbed particles which is in accordance with the Guglielmi model. Higher bath temperatures results in brownian movement of the particles. This leads to more particle entrapment in the deposit and thus hardness will increase. Agitation avoids agglomeration which further improve the microhardness.

Morphology of the coating is related to microhardness in Ni-MoS_2 system. Microhardness decreased gradually in Ni-MoS_2 system from 650 to 333 HV as the MoS_2 concentration changed from 0 to 2 g L^{-1} [66]. Porous sponge-like structured coating will be obtained with increased MoS_2 concentration and has lower hardness. Shourije et al. [67] observed that with the increase in the amount of MoS_2, the coating thickness and microhardness got lowered in a consistent way.

The observed increase in hardness in Ni/IF-WS_2 composite coatings cannot be explained only by the presence of WS_2 particles, which are frequently regarded as soft materials along with other solid lubricants like MoS_2 or graphite [68]. The inclusion of WS_2 particles in the deposits results in microstructural alterations, namely refinement of crystallite size and a shift in preferred orientation, which are responsible for the observed increase in hardness in the films. Dislocation

piling up and an increase in stress concentration (Hall-Petch strengthening) occur when the size of the crystallite decreases because the movement of dislocations is more impeded by the increased number of grain boundaries. Since these planar defects impose barriers for dislocation propagation in a manner similar to that of high-angle grain boundaries, the frequency of stacking faults can also enhance hardness [69]. The increase in hardness may also be partially explained by the modifications seen in the films' crystallographic texture.

1.6.2. Corrosion properties

Enhanced corrosion resistance in comparison with pure nickel coatings has been attained by the addition of certain secondary particles in to the Ni matrix like SiC [70], CeO_2 [71,72] , TiC [73] , TiO_2 [74], Al_2O_3 [75]. Additionally layered materials like graphene, BN, WS_2 and MoS_2 are added to the nickel matrix in order to improve its corrosion resistance. Layered 2D materials can enhance the barrier protection by impeding the diffusion of oxygen, water and corrosion-promoting ions, such as Cl^- ions because of their ultra-high chemical stability [76]. In theory, the impermeable nature of the 2D sheets can not only restrict diffusion, but they can also fill pores in the coatings, extending their protection period. Grain size refinement is an important method that can be used to improve the corrosion resistance of nanocrystalline nickel [77]. A summary of recent corrosion studies in various Ni-composite systems is given in **Table 1.3.**

Table 1.3. Summary of deposition parameters and corrosion results in some Ni-composite systems

Coatings	Deposition Technique	Parameters			E_{corr} [V vs. SCE]	I_{corr} [μAcm^{-2}]	References
		pH	C.D [Adm^{-2}]	Temperature [^oC]			
Ni-graphene	DC	3 – 4	5	45 ± 5	-0.129	1.425	[78]
Ni/r-GO	DC	4 – 5	2, 5	60	-0.153	0.010	[79]
Ni-h/BN	PC	4	8	60	-0.150	0.876	[38]
Ni–W-BN	DC, PC	8	120	65	-0.309	2.5	[64]
Ni-WS_2	DC	3.5	4	40	-0.162	0.206	[80]

Graphene has become an important constituent in Ni based nanocomposite coatings which improves the corrosion resistant properties [81]. Yasin et al. [82] incorporated graphene into Watts bath and studied the influence of current density on the corrosion resistance of the developed coating. The corrosion properties of nickel–graphene composite coatings are mostly decided by the nature of dispersion of graphene sheets within the nickel matrix. A uniform dispersion of graphene in the Ni matrix is necessary to avoid the unwanted adsorption of Cl anions forming defective sites resulting in corrosion when immersed in NaCl solution. Reinforcing the nickel matrix with graphene nano sheets helps in filling the holes and cavities that may otherwise be the defects in composite coatings. Co-deposition of metal and graphene/GO by electrodeposition results in a microstructure with graphene/GO spread randomly throughout the coating. In these circumstances, the microstructure near and around the graphene/GO-metal interfaces differs from the whole in terms of grain texture, orientation, size, boundary and chemical partitioning [83]. This is actually one of the reasons behind the improved corrosion resistance of these systems. Better corrosion characteristics is interconnected to the reduced grain size and higher deposition current densities. Bai et al.[79] fabricated a Ni/r-GO anti-corrosive, self-cleaning and superhydrophobic coating on stainless steel substrate. Coating had remarkable anticorrosion properties mainly because of the presence of pinecone-like rough surface. **Figure 1.8.** depicts the anticorrosion mechanism shown by this coating. The air cushion having an approximate area of 94.03 percent created by the pinecone-like progressive micro/nanostructure provides a crucial part in avoiding chloride ions from entering the surface of coating.

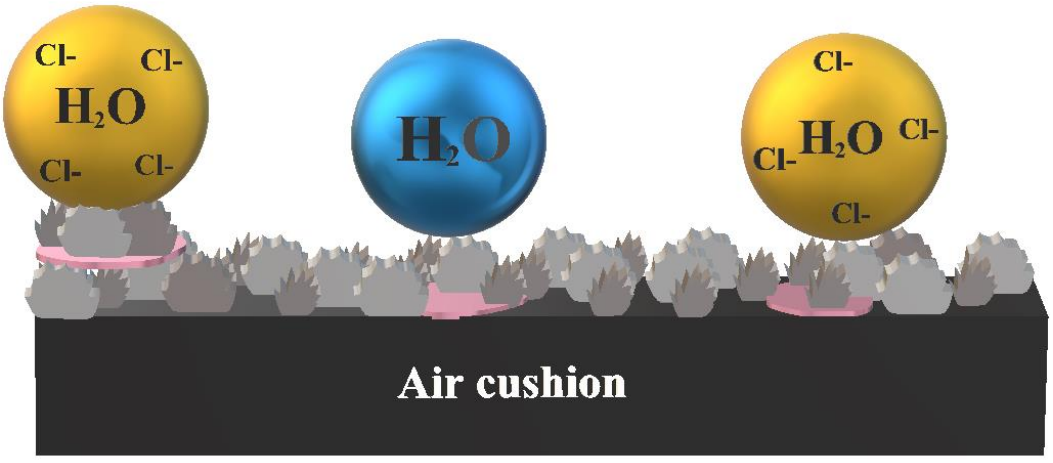

Figure 1.8. Anticorrosion mechanism of the superhydrophobic Ni/r-GO coating in NaCl solution

Li et al.[55] in their study found that as the amount of BN increases, corrosion resistance of Ni–W/BN composite coating initially increased followed by a decrease. A higher value of polarization resistance R_p was obtained when BN concentration was 5 g L^{-1} which indicated an excellent anti-corrosion property. Uniform distribution of BN particles at this particular concentration can be a reason for its corrosion resistance. MoS_2 in combination with a metal matrix displayed preferable corrosion resistant characteristics in comparison with natural MoS_2 materials [84].

Analysing the Ni-WS_2 composite coating developed by Zhao et al. [80] it was found that as the amount of WS_2 increased, current density showed a decrease and a more positive potential was generated. Anti-corrosion property of this particular coating is related to the superhydrophobic nature of the same. The trapped air within the clusters in the superhydrophobic surface can act as an effective shield to keep corrosive elements away from the surface and improve the corrosion resistance [85].

1.6.3. Tribological and wear properties

1.6.3.1. Wear

Since friction and wear account for almost a quarter of total energy losses worldwide, innovative strategies of mitigating these unfavourable impacts could be extremely valuable for the future energy-efficient economy [86]. In this regard the wear performance of different Ni and Ni-based composite coatings are extensively investigated under dry and wet sliding conditions (**Table 1.4.**).

2D materials provide interlaminar sliding and a low shear force, thus giving them superlubricity properties. Moreover, owing to their nanostructures, they can easily enter the frictional contact surface to form a lubricating film. Furthermore, they can also decrease surface roughness and repair wear. The initial high specific surface allows 2D materials to be easily adsorbed onto the surface of a substrate to form a physical film. The physical film can separate the two contact surfaces to prevent direct contact between the two sliding surfaces. In the second stage, the physical film ruptures with an increase in the frictional strength, thereby promoting the chemical reaction between the lubricant and local contact surface. This chemical reaction forms a

new tribological film and gradually replaces the physical film, and this film exists on a local contact surface. As a result, the tribological properties are improved.

Table 1.4. Summary of deposition parameters and coefficient of friction values in some Ni-composite systems

Coatings	Deposition Technique	Parameters pH	C.D [Adm^{-2}]	Temperature [^oC]	Reported Coefficient of Friction (COF) Value	References
Ni-graphene	PC	4	1	50 - 80	0.70	[87]
Ni-GO	PC	3.5 - 4.5	6 - 10	55 - 60	0.15	[88]
Ni-BN	DC	4 - 5	2 - 6	50	0.50	[39]
Ni-MoS_2	DC	2–4	4.8	50	0.40	[89]
Ni-WS_2	PC	4.8	10	50	0.11	[90]
Ni-P-WS_2	DC	2 - 3	2.5	60	0.17	[57]

Hussain et al.[33] concluded that graphene filled metal matrix coatings containing well-dispersed graphene nanosheets in the matrix improves surface durability and wear properties. The mechanism of decrease of the friction coefficient and wear rate in Ni-graphene composite coating was explained by Xiang et al.[91]. For instance, graphene is a self-lubricating material and is capable of forming a lubrication film at the sliding interface. The graphene incorporation improves the wear resistance of the coating [92]. The low surface energy of graphene also helps the Ni-graphene coating to possess minimal adhesive friction (reduce adhesion forces between particles and the substrate) and results in easy shearing being a solid lubricant [91]. Thus Ni–graphene composite coatings were shown to be ideal candidates to be used in micro devices subjected to high load and sliding speed conditions [93].

The lamellar structure of BN must be a factor which leads to low COF values. Low COF values must be caused by the lamellar structure of BN [39]. BN and B_4C particles present in the Ni matrix either block or slow down the movement of dislocations in the nickel metal matrix, reducing plastic deformation and thereby enhancing the Ni matrix's load-bearing capacity; increased hardness and wear resistance were the outcomes of this.

An irregular frictional behaviour was observed in Ni–W–MoS_2 composite coating by Cardinal et al. [66]. These coatings possess rough, non-uniform surface composed of sponge-like structures. This accounts for large deformation related to wear and the frictional curves are not smooth. In spite of this friction coefficient of Ni–W-0.5 g L^{-1} MoS_2 composite coating was found to be 50% lower than Ni-W coating. Most important conclusion derived from this study was that there seems to be a solid lubricant concentration zone by which the co-deposition of MoS_2 particles into Ni–W nanostructured alloys improves the coating's frictional qualities. It was observed that COF reduced with increasing amount of MoS_2 and on decreasing particle size [89]. MoS_2 slides readily due to weak Van der Waal's bonding between two layers, resulting in low friction. A regression equation to calculate COF by knowing the size and concentration of MoS_2 particles was another lead from this study.

Lecina et al. [68] proposed an electrodeposited Ni–WS_2 coating with a friction coefficient of 0.4 against steel. When WS_2 particles are added the crystallographic texture evolves and the intensities of the (111), (220) and (311) peaks rise at the expense of the (200) reflection. Tudela et al. [94] varied the bath agitation to upgrade the mechanical strength and vary the wear resistance of electrodeposited Ni-WS_2 coating. Das et al. [90] reported the development of pulse deposited Ni-WS_2 coating with a friction coefficient of 0.12.

In inert atmosphere and vacuum, MoS_2 has a very low COF ($\leq$0.1); in humid air, it rises to 0.3 to 0.5. Furthermore, the conversion of MoS_2 to MoO_3, which limits the mobility of the layer, can be the reason of higher coefficient of friction of MoS_2-based coatings in humid environments. It is also possible that the use of W instead of Mo contributes favourably, as WO_3 film is slightly more protective than MoO_3 and provides lower friction in air [95].

1.6.3.2. Self-lubrication

Self-lubricating composite coatings derived from the combination of a metal matrix and suitable 2D layered nanomaterial can outperform the traditional coatings in terms of tribological characteristics [96]. These solid lubricants are exposed to the surface during sliding and flow to the contact surface to form a lubricant layer [97]. This film functions as a lubricant, reducing metal-to-metal contact and improving tribological behaviour (**Figure 1.9**). As a result self-lubricating composite coating is a cutting-edge material that offers a solution to energy sustainability and efficiency in context of ecological compatibility.

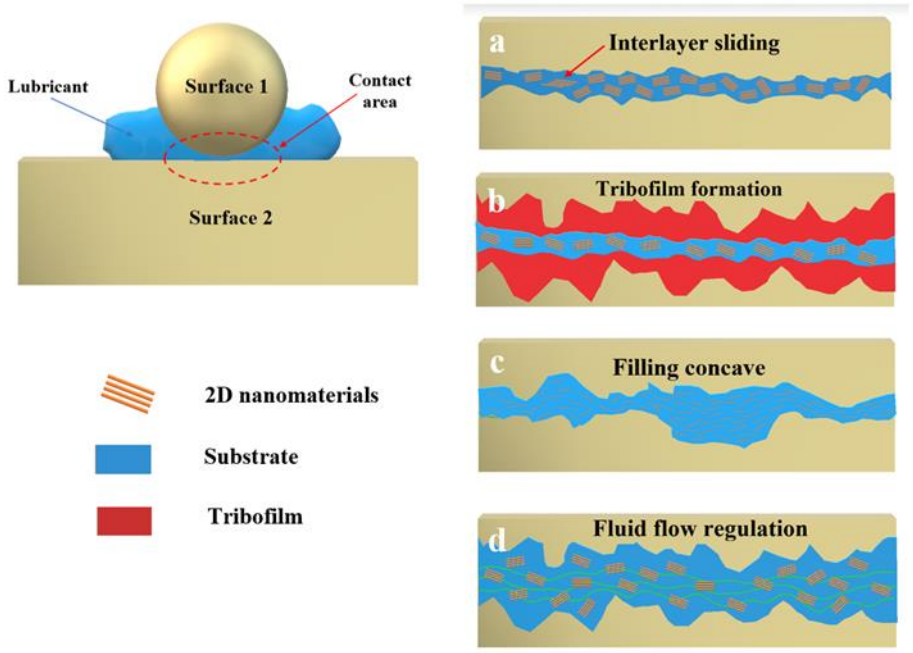

Figure 1.9. Lubrication mechanisms of 2D materials. (a) Entering the contact area of sliding surfaces, (b) Tribofilm formation, (c) Filling the pits and gaps of the contact area, (d) Affecting the fluid drag and viscosity

Graphene having remarkable mechanical strength and lubrication ability that can improve the wear resistance [93],[98]. On analysing the wear tracks of Ni–graphene composite coatings tested at varying sliding speeds it was observed that the width of wear track had undergone change in a progressive manner on increasing sliding speeds. It can be because of rise in temperature which results in the generation of nickel oxide and exfoliation of multi-layered graphene that helps in improving the lubricity of the coating [99]. Pulsed electrodeposition was employed to produce Ni-GO composite coatings on chrome steel ball and SS 440c substrates [100]. Friction and wear

characteristics had undergone refinement compared to pure Ni coating. When a load is applied, the confined GO particles emerge and create a transfer film upon the substrate providing lubricity.

The layered structure of the crystal lattice of h-BN permits sliding movement of the parallel planes. Due to the weak bonding between the planes, the shear strength is low along the direction of sliding but the compressive strength along the direction perpendicular to the shearing is high. Therefore, the addition of h-BN into the metal matrix increases the hardness of the composite as well as makes the composite more wear-resistant due to its lubricating property. Due to strong adhesion force, the lubrication film formed by h-BN adhered strongly to the substrate surface. Unlike molybdenum disulfide, lubrication by h-BN does not require a moist atmosphere. It ensures low friction in the dry atmosphere as well as in vacuum. Chemical inertness and thermal stability of h-BN gives it an advantage over graphite and MoS_2 as a solid lubricant. The coefficient of friction and rate of wear in Ni-BN composite coatings reduce as the amount of BN rises. According to the study of Zhang et al. [39], optimum addition of BN is 1.5 g L^{-1}in terms of lubricating efficiency.

MoS_2 lubrication often performs better than graphite and works well in vacuum conditions, while graphite does not. The morphologies of the mixture of MoS_2 and PTFE solid lubricant coating on stainless steel substrate offered best physical features [101]. The surface of the coating was smooth and even without any holes. This is believed to be because of self-lubricating effect of MoS_2 tribofilm [102]. High-shear mixing can be used to shear MoS_2 particles into tribo-films so that the weakly bound MoS_2 intermolecular planes align parallel to the wear track for optimal lubrication [103].

WS_2 presents a lower coefficient of friction and improvement in oxidation resistance and thermal stability, even for about 1000^oC above the well-known MoS_2. Ni/WS_2 composite coatings have markedly improved tribological performance in both lubricated and non-lubricated circumstances [104]. The Ni-WS_2 composite coating exhibited exceptional self-lubricity across a wide temperature range of 25 to 300 ^oC in a study by Cui et al. [99]. At temperatures above 400 ^oC, WS_2 gradually oxidizes into WO_3 and its lubricating capacity is lost. He et al. [57] used a versatile one-pot single-step electrodeposition to develop a superhydrophobic and self-lubricating Ni-P-WS_2 coating. A hierarchical surface with a high-water contact angle of 157 degrees was formed. The formation of a homogenous tribofilm, which resulted in a low coefficient of friction

(as low as 0.17), is ensured by a suitable amount of WS_2 in the composite coating. Because of its great abundance and low shear yield, WS_2 can reliably perform a lubricating role for an extended amount of time.

1.6.4. Superhydrophobicity

The introduction of composite particles can alter the surface roughness in a metal electrodeposit, leading to changes in wetting properties. Low surface energy particles with laminar structure such as graphene, MoS_2, and WS_2 are strong candidates for metal co-deposition to form a superhydrophobic composite coating.

Electrodeposited Ni surface has water contact angle between 79^o and 87^o [105]. Superhydrophobic Ni surfaces were developed from an aqueous solution containing additive ethylenediamine dihydrochloride capable of forming the cone-shaped Ni crystals, were first reported by Hang et al. [106]. A two step electrodeposition is carried out in which intially microcones were deposited for 10 min at 2.0 Adm^{-2} followed by the nanocone deposition at 5.0 Adm^{-2} for 1 min forming micro-nano hierarchial assembly as in **Figure 1.10.** The as-deposited surface had two-fold roughness which enabled substantial fractions of trapped air pockets and a high water contact angle of 154^o on an inherently hydrophilic material, which was explained by the Cassie–Baxter wettingstate [107].

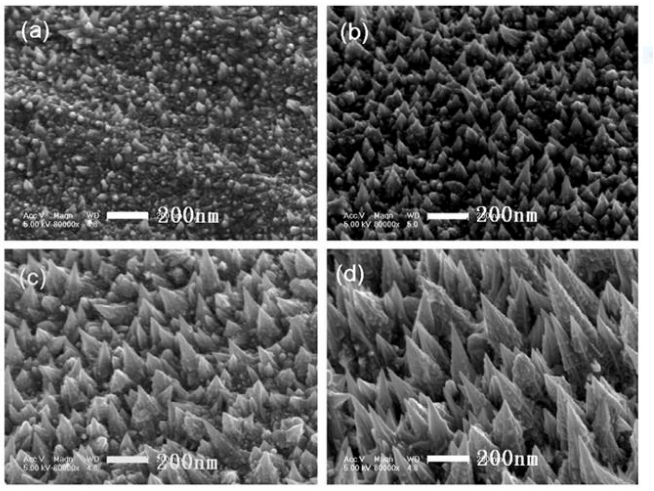

Figure 1.10. SEM image of nickel films electroplated for different current densities and times. (a) 5 Adm^{-2} 30 s (b) 5 Adm^{-2} 1 min (c) 2 Adm^{-2} 5 min (d) 2 Adm^{-2} 10 min.

Superhydrophobic Ni films with different surface structures were formed employing different plating conditions in the presence of anionic electrolytes. The ionic electrolyte was reported by Gu [108] as a deep eutectic mixture composed of choline chloride, ethylene glycol and nickel chloride. Ionic electrolytes have very low vapour pressure and good thermal stability compared to aqueous electrolytes. Storage time of coatings in air often determines the wettability and diverse nickel films with varied wettability were fabricated by Khorsand et al. [105]. The shift from superhydrophilicity to superhydrophobicity can be because of the chemical compositional change and NiO formation. A standard Watts bath was used in generation of highly ordered micro-nano structured nickel coating on copper substrate [109]. The polarisation curves and EIS measurements showed remarkable improvement in corrosion resistance subsequently by treating with (heptadecafluoro-1,1,2,2-tetradecyl) triethoxysilane. Cone size variation is possible in nickel films by regulation of electrodeposition parameters [110].

Pre-deposition of Ni along with a step-wise incrementation in current density resulted in a r-GO/Ni composite coating having micro/nanostructures similar to a pinecone with CA 162.7 ± 0.8^{o} [79]. Presence of adequate "air-pockets" formed by Ni pinecones on the r-GO sheets allowed the bouncing movement of the water droplet.

Zhao et al. [80] developed a Ni-WS_2 superhydrophobic composite coating on mild steel substrate. The water-repellent property improved in accordance with the increase in amount of WS_2. The maximum contact angle was 158.3^{o} and the sliding angle was 7.7^{o} shown by the coating with 4.88 percent WS_2. The self-cleaning effect exhibited by the coating make it suitable for industrial applications. He et al. [57] observed broccoli-like protrusions at micron scale level in Ni-P composite coatings containing 2.3 weight percent of WS_2 (WCA of 157^{o}). A combination of micron-sized broccoli-like structures, submicron-sized particles and pockets resulted in remarkable superhydrophobicity. The Ni composite coating with WC and WS_2 particles were developed on mild steel substrates followed with stearic acid modification [111]. A smooth surface without any agglomeration resulting from the combined effect WC and WS_2 particles was obtained. WCA reached 170° after surface modification.

1.6.5. Catalytic Applications

Electrochemical water splitting presents a promising method for producing high-purity hydrogen. Transition metal-based catalysts are gaining attention as an alternative to noble precious rare metal catalysts like Pt in the electrocatalytic process. These catalysts offer benefits such as low cost, widespread availability, high electrical conductivity, multiple valence states, tunable electronic structure, and favorable physical properties. Several techniques have been used to develop Ni electrocatalysts for over all water splitting. These electrocatalysts exhibit high catalytic activity, suitable hydrogen adsorption energy, strong corrosion resistance, and stability. The electrodeposition is used to directly produce Ni-based coatings on different substrates for electrocatalysis, offering a simple, eco-friendly, low-cost, energy-efficient, and highly effective approach. Among non-precious metals, nickel has been recognized as a good electrode material for the alkaline water electrolysis. This is because of its high stability and good corrosion resistance in alkaline media. Significant efforts have been devoted to enhance the performance and stability of Ni-based electroplated coatings for HER and OER. These include optimizing the electrodeposition bath composition, incorporation of composite particles, depositing multi-layer coatings, dealloying, heat treatment, and phosphorization.

1.6.5.1. Nickel-based bifunctional electrocatalysts for overall water electrolysis

It is challenging to develop a bi-functional Ni-based electrocatalyst that can effectively catalyze water splitting in acidic, neutral, and alkaline electrolytes for the industrial generation of H_2. A material that can effectively catalyze HER and OER in the same electrolyte can be generated by carefully regulating the composition, morphology, and structure of electrocatalysts [112]. Using co-precipitation, Kumar et al. produced NiFe-oxide nanocubes (NiFe-NCs) and evaluated their overall alkaline water splitting activity against NiFe oxide nanoparticles (NPs) [113]. While NiFe-NPs needed 1.90 V, NiFe-NCs provided a current density of 10 mA cm^{-2} at 1.67 V; the mesoporous structure allowed for effective mass transfer and the release of gas-evolved bubbles from the large ECSA, and the edges and corners of NCs increased the number of accessible active sites, NiFe-NCs functioned better than NiFe-NPs.

The effects of adding S to FeP and P to FeS in Ni based catalysts were assessed by Wu et al. [114]. It was found that the electrocatalytic activity is insensitive to S substitution and that the most efficient sites are produced by metal coordination with P. They found that P atoms have a

tendency to stay on the surface and serve as a sacrificial agent to partially shield Fe and S atoms from oxidation and the ensuing deactivation for HER by structural and compositional research. Lastly, they claimed that in order to successfully alter the conductivity and electrical interactions, which in turn alters the adsorption energy of intermediates, the material's surface and interior layers must be precisely controlled. Therefore, the bi-functional nickel-based electrocatalyst is the best electrocatalyst.

1.7. Industrial applications

Wear, friction and corrosion prove critical to the longevity, energy consumption and efficiency of industrial systems. These phenomena also endanger the safety of those who operate the machine. Engineers therefore go for machines that have a prolonged service life, conserve resources and have increased efficiency over their service life. In order to improve their quality, these devices or equipment composed of lighter and more economical materials such as aluminum and steel; coatings made of materials that are stronger and more chemically stable than these are employed to protect them against surface corrosion. It is estimated that metallic nano composite coatings will have a major impact on an extensive range of industries including aerospace, electronics and military [115]. Improved properties include significant improvements in fracture strength and longevity; better durability at high temperature and creep resistance; larger hardness values than those of current commercial steel and alloys; substantial increase in Young's modulus and shear modulus (compared to micro composites). These are mainly the result of the nano size reinforcements used, resulting in a suitable morphology for the products [116]. Introducing self-lubricating composites into various operating systems is a way of decreasing the use of external toxic hydrocarbon lubricants thereby reducing the environmental impact and lowering energy dissipation in industrial components for initiatives toward energy efficiency and sustainability [117].

Composite materials based on nickel and nickel alloys are ideal choices for enhancing the effectiveness of these materials [118] as in **Figure 1.11.** Furthermore, nickel electrodeposits are employed for electroforming of printing plates, phonograph record stampers, foil, tubes, screens, MEMS and a variety of other items due to their relatively good mechanical attributes [119],[120]. In the manufacturing and shaping of tools which demand excellent corrosion and wear resistance,

low friction and high thermal stability electroplated nickel composite/nanocomposite coatings are employed.

Nickel-based composite coatings are indeed very useful in the automotive industry like bumpers, exhaust trims, domestic appliances, and tools. They're commonly found in pump bodies, heat exchangers, alkaline battery cases, and food processing machinery. Since they possess high specific strength and wear resistance, graphene-based nickel composite coatings are among the most potential materials. Aside from graphene-based nano composites, composites including MoS_2 and BN have good tribological characteristics. TMDs based on selenides like WSe_2 and $MoSe_2$ are promising candidates as solid lubricants in high temperature applications. Nickel based nano composite coatings have huge relevance in aviation and aerospace sectors. Their main applications can be divided into structural components such as fuselages and wings, as well as moving components such as bearings, gears, and hatch seals [115]. Due to the in-plane mechanical isotropy of the 2D nanomaterial, two-dimensional nanomaterial-based nickel composite coatings have the capability to be used as protective and shield materials such as body armour and ambient armour.

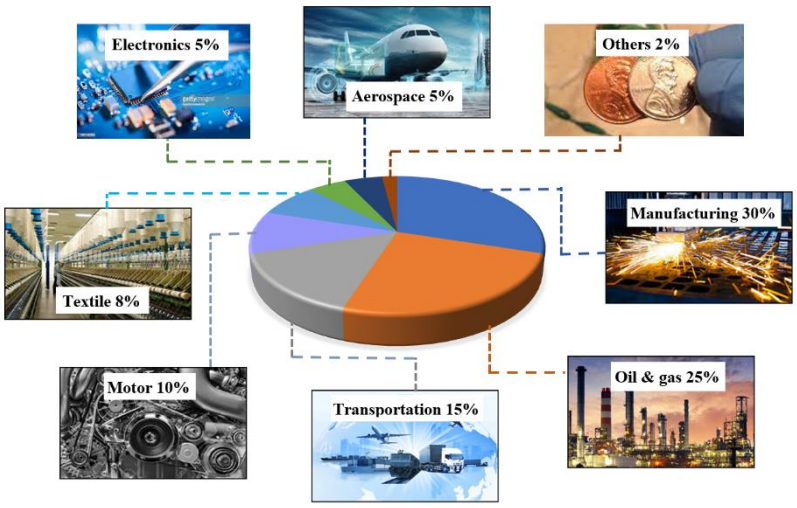

Figure 1.11. Important industrial applications of electrodeposited nickel/nickel alloy based composite coatings

1.8. Scope and objectives of the investigation

Metal-matrix composite functional coatings offer enhanced properties such as wear resistance, corrosion protection, improved hardness, tunable wettability, catalytic properties, etc, making them highly valuable across various industries. Their versatility, durability, and potential for improving performance in extreme conditions ensure their continued importance in sectors like aerospace, automotive, energy, and manufacturing. As early as the 1970s, Nickel (Ni) was proposed to be a promising candidate in the area of metal matrix composite coatings due to its novel blend of properties and attributes. Electrodeposition is a "bottom-up", "single-step" method for developing composite coatings. Electro-deposition of nickel-based composite coatings is one of the efficient methods for the modification of material surfaces, which is easy, facile, cost-effective, and doesn't require any complex equipment. For a number of applications, electro-deposited composite coatings are found to be superior to other coatings, such as those resulting from flame spraying, hard chromium plating, nitriding, CVD, PVD, etc. Another benefit of adopting electrodeposition technique is the ease with which grain size, coating thickness, morphology, and crystallographic orientation may be varied by changing the bath compositions and deposition parameters. Improved properties of typical crystalline nickel produced by electrodeposition are increased strength and hardness, low density, minimum porosity, feasibility, and excellent corrosion cum wear resistance.

For nickel composite coatings, different types of materials may be utilized as second-phase particles like ceramics, carbon nanotubes, diamond, etc. In addition to that, two-dimensional (2D) layered material fillers such as graphene, boron nitride (BN), molybdenum disulphide (MoS_2), tungsten disulphide (WS_2), transition metal carbides, selenides, MXenes, and other novel lamellar 2D materials, such as LDH, α-ZrP have been used as potential reinforcements to develop composite coatings with superior mechanical, tribological and other multifunctional characteristics [5]. Two-dimensional materials possess remarkable physical, chemical, electronic, and optical properties compared to existing three-dimensional (3D) materials. 2D materials are a combination of crystalline atomic chains, where the atoms are firmly linked by covalent bonds within individual atomic layers and subsequent layers are loosely connected by van der Waals forces, forming a monolayer structure with high modulus and strength. Higher specific surface area of 2D materials aids in more effective surface absorption contributing towards improved catalytic activity, and these materials can form a tribofilm between the surfaces in contact. Highly tunable layered

structure of these 2D materials can also generate micro-nano roughness essential for superhydrophobicity. In addition to that, low shear resistance between the nearby atomic layers permits the easy sliding of these layered atoms. Thus the soft van der Waals forces account for their outstanding tribological properties and self-lubrication performance superior to that of other nanomaterials. Out of all the 2D materials for the current investigation,

- BN which belongs to 2D III nitrides (MN) in which M is a group III metal and N is nitrogen,
- Graphene which comes under Xenes which are made up of single element like carbon, silicon and phosphorous, and
- WS_2 & MoS_2 which are transition metal dichalcogenides are selected

These four different 2D materials were selected to systematically explore and compare the influence of distinct features of each material on the properties of Ni-based composite coatings. Each 2D material was chosen based on its unique characteristics, such as catalytic activity, or lubrication behavior, to address specific functional requirements (mechanical, electrochemical, or tribological) in a progressive manner.

With this background and supportive evidence from recent studies, the primary objective of the thesis is to develop multi-functional nickel composite (graphene, BN, and TMDs) coatings by electrodeposition over mild steel (MS) substrate. The sub-objectives of the research work are:

1. Optimization of electro-deposition parameters such as, bath composition, pH, temperature, current density, stirring speed, time concentration of the reinforcement particles

2. Detailed corrosion studies of the developed composite coatings

3. Tribological study (coefficient of friction and wear rate) of the coatings

4. Wettability studies of the prepared coatings

5. Study of the catalytic behavior (HER & OER activity) of the coatings

1.9. Methodology

The experimental methodology for the development of Ni composite coated mild steel includes the pre-treatment and surface activation of the anode (Ni plate) and cathode (mild steel), preparation of Ni-Watts and Ni-composite bath, optimisation of the deposition parameters such as

current density, bath composition, concentration of reinforcement particles, temperature, time, pH, stirring speed, and electroplating of Ni composite coating over MS substrate.

1.9.1. Pre-treatment and surface activation of anode and cathode

All the MS samples (4 cm x 3 cm, purity ≥ 99.5 %) used for coating were ground using SiC papers ranging from 80 to 1000 grits, followed by degreasing in acetone and distilled water, ultrasonically cleaned, and dried in the oven. MS samples were further surface activated by dipping in 0.01M HCl for 10s and 0.1M NaOH for 20s. The anode, Ni plate (7 cm x 5 cm x 1 cm, 99.7 % purity) was polished using SiC papers of grit 80 and 100. Both the anode and cathode were further degreased in acetone and distilled water and finally dried in the oven prior to the deposition.

1.9.2. Preparation of Ni-Watts bath and Ni-composite bath

Nickel sulphate ($NiSO_4 \cdot 6H_2O$, 250 g/l), Nickel chloride ($NiCl_2 \cdot 6H_2O$, 45 g/l) and Boric acid (H_3BO_3, 40 g/l) were mixed made to a uniform solution (Watts bath). Nickel sulphate is the main origin of nickel ions. The limiting current density for attaining good quality deposits is determined by the nickel metal content. Anodic corrosion is provided by nickel chloride thus increasing the diffusion coefficient of nickel ions allowing a higher limiting current density and boric acid functions as a pH buffer. H_3BO_3 could also influence the nucleation and grain growth of Ni electrodeposits in the Watts electrolyte.

Required amount of 2D composite (BN, graphene, TMDs, ~1 µm) particles were thoroughly mixed using a magnetic stirrer and dispersed using an ultrasonicator for 1 hour. These composite particles were then added to Ni Watts bath, along with surfactants SDS/CTAB and grain refiner saccharin with proper stirring to avoid agglomeration. The Ni-composite bath was maintained at a pH of 4–4.5 by adding dilute HCl or ammonia.

1.9.3. Experimental details

Nickel plate and mild steel sample were used as anode and cathode, respectively. A DC power source (32 V, 6A) was used for all the experiments. Electrodeposition parameters, including current density (2–6 A/dm^2), temperature (40–70°C), time (5–60 min), and stirring rate (400–700 rpm), were varied. The concentration of 2D material reinforcements was also varied in the range

(1–5) wt%. Initially the experiments to optimize the electrodeposition parameters were carried out for all the Ni-composite coatings. Eventually Ni-composite coating was coated over the mild steel substrate at optimized conditions. Finally, the samples were washed and cleaned in distilled water and dried in the oven prior to further characterizations.

1.10. Characterization Techniques

A variety of techniques including scanning electron microscopy (SEM), energy dispersive X-ray spectroscopic (EDX) technique, X-ray diffraction (XRD), atomic force microscopy (AFM), contact angle measurements, micro-hardness measurement, potentiodynamic polarization, electrochemical impedance spectroscopy (EIS) and wear resistance (pin-on-disc) measurements are used to study the morphological, electrochemical, physical and mechanical properties of the developed coating.

The surface morphology and elemental analysis of the developed coatings were examined using Zeiss EVO 18 cryo-SEM (EDS attached). The phase composition of the samples was studied using X-ray diffraction (XRD) via Bruker D2 Phaser X-ray diffractometer with Cu-K_α radiation (λ = 1.5406 Å) in 0-90° range. The Vickers micro-hardness tester (Banbross) was used to measure hardness of Ni-BN coated mild steel surface under the indentation of 50 gf with 10 s dwell time. Hardness measurements at ten different locations of the specimen were done and the average value was taken.

CH Instruments electrochemical workstation (CHI608E, CH Instruments Inc.) equipped with standard three-electrode cell was used for electrochemical impedance spectroscopy and potentiodynamic polarization studies at room temperature in 3.5 wt% NaCl solution. The coated specimen with 1cm^2 exposed surface area was used as the working electrode; saturated calomel and a platinum grid were taken as the reference and counter electrodes respectively. The specimens were kept in the electrolyte for 20 min prior to the experiment for attaining their stable open circuit potential (OCP). The potentiodynamic scan was done at a rate of 1 mV/s from −250 mV to +250 mV of the OCP values. The corrosion potential (E_{corr} vs. SCE) and corrosion current density (i_{corr}) of each sample were obtained from the applied potential vs. current Tafel plot. The impedance measurements were performed using an AC signal with a perturbation of 5 mV at OCP in the frequency range of 100 kHz - 0.01 Hz. ZsimpWin software fits the generated EIS plots to

determine the electrochemical parameters. Numerous circuits were examined until the Chi-square value decreased to less than 9×10^{-4} or no further fitting improvement was observed.

Pin on disc wear testing machine (POD, 4.0 Ducom) was used to measure the wear rate and coefficient of friction under non-lubricated conditions. The measurements were done for Ni composite coated, pure Ni coated and bare mild steel samples. The pins with 6 mm diameter and 15 mm length were used against EN31 high carbon alloy steel disc. The mild steel pins were coated with pure Ni and Ni composite. Wear tests were done at a sliding velocity of 0.4 m/s under 2, 3, 4, and 5N standard loads at room temperature for 15 minutes.

References

[1] M. Tvaronavičienė, J. Baublys, J. Raudeliūnienė, D. Jatautaitė, Global energy consumption peculiarities and energy sources: Role of renewables, 2019. https://doi.org/10.1016/B978-0-12-817688-7.00001-X.

[2] K. Holmberg, A. Erdemir, Influence of tribology on global energy consumption, costs and emissions, Friction 5 (2017) 263–284. https://doi.org/10.1007/s40544-017-0183-5.

[3] G.W. Crabtree, M.S. Dresselhaus, M. V. Buchanan, The hydrogen economy, Phys. Today 57 (2004) 39–44. https://doi.org/10.1063/1.1878333.

[4] Z. Zhang, H. Dong, Recent development in low friction and wear-resistant coatings and surfaces for high-Temperature forming tools, Manuf. Rev. 1 (2014). https://doi.org/10.1051/mfreview/2015001.

[5] G. Barati Darband, M. Aliofkhazraei, S. Khorsand, S. Sokhanvar, A. Kaboli, Science and Engineering of Superhydrophobic Surfaces: Review of Corrosion Resistance, Chemical and Mechanical Stability, Arab. J. Chem. 13 (2020) 1763–1802. https://doi.org/10.1016/j.arabjc.2018.01.013.

[6] X. Li, L. Zhao, J. Yu, X. Liu, X. Zhang, H. Liu, W. Zhou, Water Splitting: From Electrode to Green Energy System, Nano-Micro Lett. 12 (2020) 1–29. https://doi.org/10.1007/s40820-020-00469-3.

[7] G.A. DiBari, Chronology of nickel electroplating, Met. Finish. 100 (2002) 34–49. https://doi.org/10.1016/S0026-0576(02)80244-6.

[8] J. Qin, X. Zhang, K. Umporntheep, V. Auejitthavorn, R. Li, P. Wangyao, Y. Boonyongmaneerat, S. Limpanart, M. Ma, R. Liu, Electrodeposition and mechanical properties of Ni-W matrix composite coatings with embedded amorphous boron particles, Int. J. Electrochem. Sci. 11 (2016) 9529–9541. https://doi.org/10.20964/2016.11.58.

[9] L.P. Bicelli, B. Bozzini, C. Mele, L. D'Urzo, A review of nanostructural aspects of metal electrodeposition, Int. J. Electrochem. Sci. 3 (2008) 356–408.

[10] A. Hovestad, L.J.J. Janssen, Electroplating of Metal Matrix Composites by Codeposition of Suspended Particles, Mod. Asp. Electrochem. (2006) 475–532. https://doi.org/10.1007/0-387-25838-8_6.

[11] O. Sadiku-Agboola, E.R. Sadiku, O.I. Ojo, O.L. Akanji, O.F. Biotidara, Influence of Operation parameters on Metal deposition in bright Nickel-plating Process, Port.

Electrochim. Acta 29 (2011) 91–100. https://doi.org/10.4152/pea.201102091.

[12] A. Juskowiak-Brenska, J. Lapinski, D. Pletcher, F.C. Walsh, Porosity of nickel electrodeposits on mild steel using electrochemical impedance spectroscopy, Trans. IMF 90 (2012) 156–160. https://doi.org/10.1179/0020296712Z.0000000007.

[13] F.C. Walsh, C. Ponce De Leon, A review of the electrodeposition of metal matrix composite coatings by inclusion of particles in a metal layer: An established and diversifying technology, Trans. Inst. Met. Finish. 92 (2014) 83–98. https://doi.org/10.1179/0020296713Z.000000000161.

[14] C.T.J. Low, R.G.A. Wills, F.C. Walsh, Electrodeposition of composite coatings containing nanoparticles in a metal deposit, Surf. Coatings Technol. 201 (2006) 371–383. https://doi.org/10.1016/j.surfcoat.2005.11.123.

[15] N. Guglielmi, Kinetics of the Deposition of Inert Particles from Electrolytic Baths, J. Electrochem. Soc. 119 (1972) 1009. https://doi.org/10.1149/1.2404383.

[16] J.P. Celis, J.R. Roos, C. Buelens, A Mathematical Model for the Electrolytic Codeposition of Particles with a Metallic Matrix, J. Electrochem. Soc. 134 (1987) 1402–1408. https://doi.org/10.1149/1.2100680.

[17] J. Fransaer, J.P. Celis, J.R. Roos, Analysis of the Electrolytic Codeposition of Non-Brownian Particles with Metals, J. Electrochem. Soc. 139 (1992) 413–425. https://doi.org/10.1149/1.2069233.

[18] B.J. Hwang, C.S. Hwang, Mechanism of Codeposition of Silicon Carbide with Electrolytic Cobalt, J. Electrochem. Soc. 140 (1993) 979–984. https://doi.org/10.1149/1.2056239.

[19] P.M. Vereecken, I. Shao, P.C. Searson, Particle Codeposition in Nanocomposite Films, J. Electrochem. Soc. 147 (2000) 2572. https://doi.org/10.1149/1.1393570.

[20] P. Berçot, E. Peña-Muñoz, J. Pagetti, Electrolytic composite Ni–PTFE coatings: an adaptation of Guglielmi's model for the phenomena of incorporation, Surf. Coatings Technol. 157 (2002) 282–289. https://doi.org/10.1016/S0257-8972(02)00180-9.

[21] N.M. Schneider, J.H. Park, J.M. Grogan, D.A. Steingart, H.H. Bau, F.M. Ross, Nanoscale evolution of interface morphology during electrodeposition, Nat. Commun. 8 (2017) 1–10. https://doi.org/10.1038/s41467-017-02364-9.

[22] F.C. Walsh, C.P. de Leon, A review of the electrodeposition of metal matrix composite

coatings by inclusion of particles in a metal layer: an established and diversifying technology, Trans. IMF 92 (2014) 83–98. https://doi.org/10.1179/0020296713Z.000000000161.

[23] H. Mahdi, K. Salloomi, H. Husam, Improvement of Microhardness and Corrosion Resistance of Stainless Steel by Nanocomposite Coating, Al-Khawarizmi Eng. J. 10 (2014) 1–10.

[24] M.S. Hussain, Synthesis of bulk nanostructured materials by high speed turbulent flow-a method of electrodepositing nanocrystalline nickel, Elsevier Inc., 2018. https://doi.org/10.1016/B978-0-12-812792-6.00003-0.

[25] Y.H. Ahmad, A.M.A. Mohamed, Electrodeposition of nanostructured Nickel-Ceramic composite coatings: A review, Int. J. Electrochem. Sci. 9 (2014) 1942–1963.

[26] Z. Ji, L. Zhang, G. Xie, W. Xu, D. Guo, J. Luo, B. Prakash, Mechanical and tribological properties of nanocomposites incorporated with two-dimensional materials, Friction 8 (2020) 813–846. https://doi.org/10.1007/s40544-020-0401-4.

[27] W. Chen, T. Yang, L.L. Dong, A. Elmasry, J. Song, N. Deng, A. Elmarakbi, X. Liu, H. Lv, Y. Fu, Advances in graphene reinforced metal matrix nanocomposites: Mechanisms, processing, modelling, properties and applications, Nanotechnol. Precis. Eng. 3 (2020) 189–210. https://doi.org/10.1016/j.npe.2020.12.003.

[28] A. Nieto, A. Bisht, D. Lahiri, C. Zhang, A. Agarwal, Graphene reinforced metal and ceramic matrix composites: a review, Int. Mater. Rev. 62 (2017) 241–302. https://doi.org/10.1080/09506608.2016.1219481.

[29] Y. Kim, J. Lee, M.S. Yeom, J.W. Shin, H. Kim, Y. Cui, J.W. Kysar, J. Hone, Y. Jung, S. Jeon, S.M. Han, Strengthening effect of single-atomic-layer graphene in metal-graphene nanolayered composites, Nat. Commun. 4 (2013). https://doi.org/10.1038/ncomms3114.

[30] S. Kumari, A. Panigrahi, S.K. Singh, S.K. Pradhan, Corrosion-Resistant Hydrophobic Nanostructured Ni-Reduced Graphene Oxide Composite Coating with Improved Mechanical Properties, J. Mater. Eng. Perform. 27 (2018) 5889–5897. https://doi.org/10.1007/s11665-018-3706-y.

[31] V.H. Pham, T. Gebre, J.H. Dickerson, Facile electrodeposition of reduced graphene oxide hydrogels for high-performance supercapacitors, Nanoscale 7 (2015) 5947–5950. https://doi.org/10.1039/c4nr07508k.

[32] T. Magne, T. de Oliveira, L. Alencar, F. Junior, S. Gemini-Piperni, S. Carneiro, L. Dutra, R. Freire, K. Golokhvast, P. Metrangolo, P. Fechine, R. Santos-Oliveira, Graphene and its derivatives: understanding the main chemical and medicinal chemistry roles for biomedical applications, J. Nanostructure Chem. (2021). https://doi.org/10.1007/s40097-021-00444-3.

[33] A.K. Hussain, U.M.B. Al Naib, Recent developments in graphene based metal matrix composite coatings for corrosion protection application: A review, J. Met. Mater. Miner. 29 (2019) 1–9. https://doi.org/10.14456/jmmm.2019.27.

[34] A. Ambrosi, M. Pumera, The structural stability of graphene anticorrosion coating materials is compromised at low potentials, Chem. - A Eur. J. 21 (2015) 7896–7901. https://doi.org/10.1002/chem.201406238.

[35] A.T. Dideikin, A.Y. Vul', Graphene oxide and derivatives: The place in graphene family, Front. Phys. 6 (2019). https://doi.org/10.3389/fphy.2018.00149.

[36] A.T. Smith, A.M. LaChance, S. Zeng, B. Liu, L. Sun, Synthesis, properties, and applications of graphene oxide/reduced graphene oxide and their nanocomposites, Nano Mater. Sci. 1 (2019) 31–47. https://doi.org/10.1016/j.nanoms.2019.02.004.

[37] D. Golberg, Y. Bando, Y. Huang, Z. Xu, X. Wei, L. Bourgeois, M.-S. Wang, H. Zeng, J. Lin, C. Zhi, Recent Advances in Boron Nitride Nanotubes and Nanosheets, Isr. J. Chem. 50 (2010) 405–416. https://doi.org/10.1002/ijch.201000049.

[38] G. Gyawali, R. Adhikari, H.S. Kim, H.-B. Cho, S.W. Lee, Effect of h-BN Nanosheets Codeposition on Electrochemical Corrosion Behavior of Electrodeposited Nickel Composite Coatings, ECS Electrochem. Lett. 2 (2012) C7–C10. https://doi.org/10.1149/2.003303eel.

[39] Y.K. Zhang, J.L. Li, D.S. Xiong, Y. Qin, Influence of boron nitride on tribological behavior of nickel-base composite coatings at high temperature, Mater. Sci. Forum 686 (2011) 711–715. https://doi.org/10.4028/www.scientific.net/MSF.686.711.

[40] V. Sorkin, H. Pan, H. Shi, S.Y. Quek, Y.W. Zhang, Nanoscale transition metal dichalcogenides: Structures, properties, and applications, Crit. Rev. Solid State Mater. Sci. 39 (2014) 319–367. https://doi.org/10.1080/10408436.2013.863176.

[41] S. Manzeli, D. Ovchinnikov, D. Pasquier, O. V. Yazyev, A. Kis, 2D transition metal dichalcogenides, Nat. Rev. Mater. 2 (2017). https://doi.org/10.1038/natrevmats.2017.33.

[42] A. Gracco, M. Dandrea, F. Deflorian, C. Zanella, A. De Stefani, G. Bruno, E. Stellini, Application of a molybdenum and tungsten disulfide coating to improve tribological properties of orthodontic archwires, Nanomaterials 9 (2019) 1–10. https://doi.org/10.3390/nano9050753.

[43] J.R. Lince, Effective Application of Solid Lubricants in Spacecraft Mechanisms, Lubricants 8 (2020). https://doi.org/10.3390/lubricants8070074.

[44] A. Joseph, M. Narayanasamy, B. Kirubasankar, S. Angaiah, Development of MoS Nanosheets Embedded Nickel Composite Coating and its Mechanical 2 Properties, ES Mater. Manuf. (2018) 2–8. https://doi.org/10.30919/esmm5f152.

[45] W. Zhang, P. Zhang, Z. Su, G. Wei, Synthesis and sensor applications of MoS2-based nanocomposites, Nanoscale 7 (2015) 18364–18378. https://doi.org/10.1039/c5nr06121k.

[46] S. Xu, X. Gao, M. Hu, J. Sun, D. Jiang, F. Zhou, W. Liu, L. Weng, Nanostructured WS2–Ni composite films for improved oxidation, resistance and tribological performance, Appl. Surf. Sci. 288 (2014) 15–25. https://doi.org/10.1016/j.apsusc.2013.09.024.

[47] U.S. Mohanty, B.C. Tripathy, P. Singh, A. Keshavarz, S. Iglauer, Roles of organic and inorganic additives on the surface quality, morphology, and polarization behavior during nickel electrodeposition from various baths: a review, J. Appl. Electrochem. 49 (2019) 847–870. https://doi.org/10.1007/s10800-019-01335-w.

[48] C. Davalos, J. Lopez, H. Ruiz, A. Méndez-Albores, R. Antaño-López, G. Trejo, Study of the Role of Boric Acid During the Electrochemical Deposition of Ni in a Sulfamate Bath, Int. J. Electrochem. Sci. 8 (2013) 9785–9800.

[49] N. Watt, Nickel plating bath, (2014) 64–67.

[50] D. Sobha Jayakrishnan, Electrodeposition: the versatile technique for nanomaterials, Woodhead Publishing Limited, 2012. https://doi.org/10.1533/9780857095800.1.86.

[51] Y.D. Gamburg, G. Zangari, Theory and Practice of Metal Electrodeposition, Springer New York, New York, NY, 2011. https://doi.org/10.1007/978-1-4419-9669-5.

[52] C. Breitkopf, K. Swider-Lyons, Modern Electrochemistry, in: Springer Handb. Electrochem. Energy, Springer Berlin Heidelberg, Berlin, Heidelberg, 2017: pp. 11–30. https://doi.org/10.1007/978-3-662-46657-5_2.

[53] S. Awasthi, S.K. Pandey, C.P. Pandey, K. Balani, Progress in Electrochemical and Electrophoretic Deposition of Nickel with Carbonaceous Allotropes: A Review, Adv.

Mater. Interfaces 7 (2020) 1–33. https://doi.org/10.1002/admi.201901096.

[54] A. Radisic, P.M. Vereecken, J.B. Hannon, P.C. Searson, F.M. Ross, Quantifying Electrochemical Nucleation and Growth of Nanoscale Clusters Using Real-Time Kinetic Data, Nano Lett. 6 (2006) 238–242. https://doi.org/10.1021/nl052175i.

[55] B. Li, D. Li, T. Mei, W. Xia, W. Zhang, Fabrication and characterization of boron nitride reinforced Ni–W nanocomposite coating by electrodeposition, J. Alloys Compd. 777 (2019) 1234–1244. https://doi.org/10.1016/j.jallcom.2018.11.081.

[56] A. Laszczyńska, J. Winiarski, B. Szczygieł, I. Szczygieł, Electrodeposition and characterization of Ni–Mo–ZrO 2 composite coatings, Appl. Surf. Sci. 369 (2016) 224–231. https://doi.org/10.1016/j.apsusc.2016.02.086.

[57] Y. He, W.T. Sun, S.C. Wang, P.A.S. Reed, F.C. Walsh, An electrodeposited Ni-P-WS2 coating with combined super-hydrophobicity and self-lubricating properties, Electrochim. Acta 245 (2017) 872–882. https://doi.org/10.1016/j.electacta.2017.05.166.

[58] X. ZHOU, Y. SHEN, H. JIN, Y. ZHENG, Microstructure and depositional mechanism of Ni–P coatings with nano-ceria particles by pulse electrodeposition, Trans. Nonferrous Met. Soc. China 22 (2012) 1981–1988. https://doi.org/10.1016/S1003-6326(11)61417-9.

[59] Y. He, S.C. Wang, F.C. Walsh, Y.-L. Chiu, P.A.S. Reed, Self-lubricating Ni-P-MoS2 composite coatings, Surf. Coatings Technol. 307 (2016) 926–934. https://doi.org/10.1016/j.surfcoat.2016.09.078.

[60] M.K. Tripathi, D.K. Singh, V.B. Singh, Electrodeposition of Ni-Fe/Bn nano-composite coatings from a non-aqueous bath and their characterization, Int. J. Electrochem. Sci. 8 (2013) 3454–3471.

[61] W. Wang, F.-Y. Hou, H. Wang, H.-T. Guo, Fabrication and characterization of Ni–ZrO 2 composite nano-coatings by pulse electrodeposition, Scr. Mater. - Scr. MATER 53 (2005) 613–618. https://doi.org/10.1016/j.scriptamat.2005.04.002.

[62] L. Feng, Y.Y. Ren, Y.H. Zhang, S. Wang, L. Li, Direct correlations among the grain size, texture, and indentation behavior of nanocrystalline nickel coatings, Metals (Basel). 9 (2019). https://doi.org/10.3390/met9020188.

[63] G.N.K. Ramesh Bapu, Electrocodeposition and characterization of nickel-titanium carbide composites, Surf. Coatings Technol. 67 (1994) 105–110. https://doi.org/https://doi.org/10.1016/S0257-8972(05)80033-7.

[64] S. Sangeetha, G.P. Kalaignan, Tribological and electrochemical corrosion behavior of Ni–W/BN (hexagonal) nano-composite coatings, Ceram. Int. 41 (2015) 10415–10424. https://doi.org/10.1016/j.ceramint.2015.04.089.

[65] S. Paydar, A. Jafari, M.E. Bahrololoom, V. Mozafari, Enhancing Ni electroplated matrix through mixed boron nitride–carbide reinforcement, Vacuum 92 (2013) 52–57. https://doi.org/10.1016/j.vacuum.2012.10.014.

[66] M.F. Cardinal, P.A. Castro, J. Baxi, H. Liang, F.J. Williams, Characterization and frictional behavior of nanostructured Ni-W-MoS2 composite coatings, Surf. Coatings Technol. 204 (2009) 85–90. https://doi.org/10.1016/j.surfcoat.2009.06.037.

[67] S.M.J.S. Shourije, M.E. Bahrololoom, Effect of current density, MoS 2 content and bath agitation on tribological properties of electrodeposited nanostructured Ni-MoS 2 composite coatings, Tribol. - Mater. Surfaces Interfaces 13 (2019) 76–87. https://doi.org/10.1080/17515831.2019.1589160.

[68] E. García-Lecina, I. García-Urrutia, J.A. Díez, J. Fornell, E. Pellicer, J. Sort, Codeposition of inorganic fullerene-like WS2 nanoparticles in an electrodeposited nickel matrix under the influence of ultrasonic agitation, Electrochim. Acta 114 (2013) 859–867. https://doi.org/10.1016/j.electacta.2013.04.088.

[69] J. Sort, J. Nogués, S. Suriñach, M.D. Baró, Microstructural aspects of the hcp-fcc allotropic phase transformation induced in cobalt by ball milling, Philos. Mag. 83 (2003) 439–455. https://doi.org/10.1080/0141861021000047159.

[70] W. Jiang, L. Shen, M. Qiu, M. Xu, Z. Tian, Microhardness, wear, and corrosion resistance of Ni–SiC composite coating with magnetic-field-assisted jet electrodeposition, Mater. Res. Express 5 (2018) 096407. https://doi.org/10.1088/2053-1591/aad72c.

[71] Y.B. Zeng, N.S. Qu, X.Y. Hu, Preparation and characterization of electrodeposited Ni-CeO2 nanocomposite coatings with high current density, Int. J. Electrochem. Sci. 9 (2014) 8145–8154.

[72] S.T. Aruna, C.N. Bindu, V. Ezhil Selvi, V.K. William Grips, K.S. Rajam, Synthesis and properties of electrodeposited Ni/ceria nanocomposite coatings, Surf. Coatings Technol. 200 (2006) 6871–6880. https://doi.org/10.1016/j.surfcoat.2005.10.035.

[73] M. Raja, G.N.K. Ramesh Bapu, J. Maharaja, R. Sekar, Electrodeposition and characterisation of Ni–TiC nanocomposite using Watts bath, Surf. Eng. 30 (2014) 697–

701. https://doi.org/10.1179/1743294414Y.0000000265.

[74] I. Birlik, N.F. Ak Azem, M. Toparli, E. Celik, T. Koc Delice, S. Yildirim, O. Bardakcioglu, T. Dikici, Preparation and Characterization of Ni–TiO2 Nanocomposite Coatings Produced by Electrodeposition Technique, Front. Mater. 3 (2016). https://doi.org/10.3389/fmats.2016.00046.

[75] B. KUCHARSKA, A. BROJANOWSKA, K. POPŁAWSKI, J.R. SOBIECKI, Corrosion Resistance of Ni/Al2O3 Nanocomposite Coatings, Mater. Sci. 22 (2016). https://doi.org/10.5755/j01.ms.22.1.7407.

[76] R. Sukanya, T.N. Barwa, Y. Luo, E. Dempsey, C.B. Breslin, Emerging Layered Materials and Their Applications in the Corrosion Protection of Metals and Alloys, Sustainability 14 (2022). https://doi.org/10.3390/su14074079.

[77] S. Kim, A comparison of the corrosion behaviour of polycrystalline and nanocrystalline cobalt, Scr. Mater. 48 (2003) 1379–1384. https://doi.org/10.1016/S1359-6462(02)00651-6.

[78] G. Yasin, M. Arif, M.N. Nizam, M. Shakeel, M.A. Khan, W.Q. Khan, T.M. Hassan, Z. Abbas, I. Farahbakhsh, Y. Zuo, Effect of surfactant concentration in electrolyte on the fabrication and properties of nickel-graphene nanocomposite coating synthesized by electrochemical co-deposition, RSC Adv. 8 (2018) 20039–20047. https://doi.org/10.1039/C7RA13651J.

[79] Z. Bai, B. Zhang, Fabrication of superhydrophobic reduced-graphene oxide/nickel coating with mechanical durability, self-cleaning and anticorrosion performance, Nano Mater. Sci. 2 (2020) 151–158. https://doi.org/10.1016/j.nanoms.2019.05.001.

[80] G. Zhao, Y. Xue, Y. Huang, Y. Ye, F.C. Walsh, J. Chen, S. Wang, One-step electrodeposition of a self-cleaning and corrosion resistant Ni/WS 2 superhydrophobic surface, RSC Adv. 6 (2016) 59104–59112. https://doi.org/10.1039/C6RA07899K.

[81] C.M.P. Kumar, T.V. Venkatesha, R. Shabadi, Preparation and corrosion behavior of Ni and Ni–graphene composite coatings, Mater. Res. Bull. 48 (2013) 1477–1483. https://doi.org/10.1016/j.materresbull.2012.12.064.

[82] G. Yasin, M. Arif, M. Shakeel, Y. Dun, Y. Zuo, W.Q. Khan, Y. Tang, A. Khan, M. Nadeem, Exploring the Nickel-Graphene Nanocomposite Coatings for Superior Corrosion Resistance: Manipulating the Effect of Deposition Current Density on its Morphology,

Mechanical Properties, and Erosion-Corrosion Performance, Adv. Eng. Mater. 20 (2018) 1701166. https://doi.org/10.1002/adem.201701166.

[83] M.Y. Rekha, C. Srivastava, High corrosion resistance of metal-graphene oxide-metal multilayer coatings, Philos. Mag. 100 (2020) 18–31. https://doi.org/10.1080/14786435.2019.1663375.

[84] S. ArunKumar, V. Jegathish, R. Soundharya, M. JesyAlka, C. Arul, S. Sathyanarayanan, S. Mayavan, Evaluating the performance of MoS2 based materials for corrosion protection of mild steel in an aggressive chloride environment, RSC Adv. 7 (2017) 17332–17335. https://doi.org/10.1039/c7ra01372h.

[85] D. Zhang, L. Wang, H. Qian, X. Li, Superhydrophobic surfaces for corrosion protection: a review of recent progresses and future directions, J. Coatings Technol. Res. 13 (2016) 11–29. https://doi.org/10.1007/s11998-015-9744-6.

[86] K. Sayfidinov, S.D. Cezan, B. Baytekin, H.T. Baytekin, Minimizing friction, wear, and energy losses by eliminating contact charging, Sci. Adv. 4 (2018).

[87] J. Chen, J. Li, D. Xiong, Y. He, Y. Ji, Y. Qin, Preparation and tribological behavior of Ni-graphene composite coating under room temperature, Appl. Surf. Sci. 361 (2016) 49–56. https://doi.org/10.1016/j.apsusc.2015.11.094.

[88] S. Singh, S. Samanta, A.K. Das, R.R. Sahoo, Tribological investigation of Ni-graphene oxide composite coating produced by pulsed electrodeposition, Surfaces and Interfaces 12 (2018) 61–70. https://doi.org/https://doi.org/10.1016/j.surfin.2018.05.001.

[89] E.S. Güler, E. Konca, I. Karakaya, Investigation of the tribological behaviour of electrocodeposited Ni-MoS2 composite coatings, Int. J. Surf. Sci. Eng. 11 (2017) 418.

[90] D. Roy, A.K. Das, R. Saini, P.K. Singh, P. Kumar, M. Hussain, A. Mandal, A.R. Dixit, Pulse current co-deposition of Ni-WS 2 nano-composite film for solid lubrication, Mater. Manuf. Process. 32 (2017) 365–372. https://doi.org/10.1080/10426914.2016.1198011.

[91] L. Xiang, Q. Shen, Y. Zhang, W. Bai, C. Nie, One-step electrodeposited Ni-graphene composite coating with excellent tribological properties, Surf. Coatings Technol. 373 (2019) 38–46. https://doi.org/10.1016/j.surfcoat.2019.05.074.

[92] A. Siddaiah, P. Kumar, A. Henderson, M. Misra, P.L. Menezes, Surface Energy and Tribology of Electrodeposited Ni and Ni–Graphene Coatings on Steel, Lubricants 7 (2019). https://doi.org/10.3390/lubricants7100087.

[93] H. Algul, M. Tokur, S. Ozcan, M. Uysal, T. Cetinkaya, H. Akbulut, A. Alp, The effect of graphene content and sliding speed on the wear mechanism of nickel-graphene nanocomposites, Appl. Surf. Sci. 359 (2015) 340–348. https://doi.org/10.1016/j.apsusc.2015.10.139.

[94] I. Tudela, Y. Zhang, M. Pal, I. Kerr, A.J. Cobley, Ultrasound-assisted electrodeposition of thin nickel-based composite coatings with lubricant particles, Surf. Coatings Technol. 276 (2015) 89–105. https://doi.org/10.1016/j.surfcoat.2015.06.030.

[95] S. Domínguez-Meister, T.C. Rojas, M. Brizuela, J.C. Sánchez-López, Solid lubricant behavior of MoS2 and WSe2-based nanocomposite coatings, Sci. Technol. Adv. Mater. 18 (2017) 122–133. https://doi.org/10.1080/14686996.2016.1275784.

[96] J.H. Lee, D.H. Cho, B.H. Park, J.S. Choi, Nanotribology of 2D materials and their macroscopic applications, J. Phys. D. Appl. Phys. 53 (2020). https://doi.org/10.1088/1361-6463/ab9670.

[97] L. Liu, M. Zhou, L. Jin, L. Li, Y. Mo, G. Su, X. Li, H. Zhu, Y. Tian, Recent advances in friction and lubrication of graphene and other 2D materials: Mechanisms and applications, Friction 7 (2019) 199–216. https://doi.org/10.1007/s40544-019-0268-4.

[98] J. Sun, S. Du, Application of graphene derivatives and their nanocomposites in tribology and lubrication: A review, RSC Adv. 9 (2019) 40642–40661. https://doi.org/10.1039/c9ra05679c.

[99] S. Cui, W.S. Li, L. He, L. Feng, G.S. An, W. Hu, C.X. Hu, Tribological behavior of a Ni-WS2 composite coating across wide temperature ranges, Rare Met. 38 (2019) 1078–1085. https://doi.org/10.1007/s12598-018-1152-5.

[100] Z. Xu, Q. Zhang, X. Shi, W. Zhai, K. Yang, Tribological Properties of TiAl Matrix Self-Lubricating Composites Containing Multilayer Graphene and Ti3SiC2 at High Temperatures, Tribol. Trans. 58 (2015) 1131–1141. https://doi.org/10.1080/10402004.2015.1046007.

[101] T. Thana, KarunaTuchinda, Study of the effect of MoS2 and PTFE based coatings on adhesive wear of stainless steel, Appl. Mech. Mater. 302 (2013) 216–222. https://doi.org/10.4028/www.scientific.net/AMM.302.216.

[102] Y. Jia, L. Chen, X. Feng, H. Zhou, J. Chen, Tribological behavior of molybdenum disulfide bonded solid lubricating coatings cured with organosiloxane-modified phosphate

binder, RSC Adv. 5 (2015) 69606–69615. https://doi.org/10.1039/c5ra08727a.

[103] N. Zhou, S. Wang, F.C. Walsh, Effective particle dispersion via high-shear mixing of the electrolyte for electroplating a nickel-molybdenum disulphide composite, Electrochim. Acta 283 (2018) 568–577. https://doi.org/10.1016/j.electacta.2018.06.187.

[104] I. Tudela, A.J. Cobley, Y. Zhang, Tribological performance of novel nickel-based composite coatings with lubricant particles, Friction 7 (2019) 169–180. https://doi.org/10.1007/s40544-018-0211-0.

[105] S. Khorsand, K. Raeissi, F. Ashrafizadeh, Corrosion resistance and long-term durability of super-hydrophobic nickel film prepared by electrodeposition process, Appl. Surf. Sci. 305 (2014) 498–505. https://doi.org/10.1016/j.apsusc.2014.03.123.

[106] T. Hang, A. Hu, H. Ling, M. Li, D. Mao, Super-hydrophobic nickel films with micro-nano hierarchical structure prepared by electrodeposition, Appl. Surf. Sci. 256 (2010) 2400–2404. https://doi.org/10.1016/j.apsusc.2009.10.074.

[107] A.B.D. Cassie, S. Baxter, Wettability of porous surfaces, Trans. Faraday Soc. 40 (1944) 546–551. https://doi.org/10.1039/TF9444000546.

[108] C. Gu, J. Tu, One-Step Fabrication of Nanostructured Ni Film with Lotus Effect from Deep Eutectic Solvent, Langmuir 27 (2011) 10132–10140. https://doi.org/10.1021/la200778a.

[109] M.J. Nine, M.A. Cole, L. Johnson, D.N.H. Tran, D. Losic, Robust Superhydrophobic Graphene-Based Composite Coatings with Self-Cleaning and Corrosion Barrier Properties, ACS Appl. Mater. \& Interfaces 7 (2015) 28482–28493. https://doi.org/10.1021/acsami.5b09611.

[110] N. Xu, D.K. Sarkar, X.G. Chen, W.P. Tong, Corrosion performance of superhydrophobic nickel stearate/nickel hydroxide thin films on aluminum alloy by a simple one-step electrodeposition process, Surf. Coatings Technol. 302 (2016) 173–184. https://doi.org/10.1016/j.surfcoat.2016.05.050.

[111] J. Zhou, G. Zhao, J. Li, J. Chen, S. Zhang, J. Wang, F.C. Walsh, S. Wang, Y. Xue, Electroplating of non-fluorinated superhydrophobic Ni/WC/WS2 composite coatings with high abrasive resistance, Appl. Surf. Sci. 487 (2019) 1329–1340. https://doi.org/10.1016/j.apsusc.2019.05.244.

[112] Z. Angeles-Olvera, A. Crespo-Yapur, O. Rodríguez, J. Cholula-Díaz, L. Martínez, M.

Videa, Nickel-Based Electrocatalysts for Water Electrolysis, Energies 15 (2022) 1609. https://doi.org/10.3390/en15051609.

[113] A. Kumar, S. Bhattacharyya, Porous NiFe-Oxide Nanocubes as Bifunctional Electrocatalysts for Efficient Water-Splitting, ACS Appl. Mater. Interfaces 9 (2017) 41906–41915. https://doi.org/10.1021/acsami.7b14096.

[114] Z. Wu, X. Li, W. Liu, Y. Zhong, Q. Gan, X. Li, H. Wang, Materials Chemistry of Iron Phosphosulfide Nanoparticles: Synthesis, Solid State Chemistry, Surface Structure, and Electrocatalysis for the Hydrogen Evolution Reaction, ACS Catal. 7 (2017) 4026–4032. https://doi.org/10.1021/acscatal.7b00466.

[115] Y. Xiao, P. Yao, K. Fan, H. Zhou, M. Deng, Z. Jin, Powder metallurgy processed metal-matrix friction materials for space applications, Friction 6 (2018) 219–229. https://doi.org/10.1007/s40544-017-0171-9.

[116] P. Nguyen-Tri, T.A. Nguyen, P. Carriere, C. Ngo Xuan, Nanocomposite Coatings: Preparation, Characterization, Properties, and Applications, Int. J. Corros. 2018 (2018) 1–19. https://doi.org/10.1155/2018/4749501.

[117] E. Omrani, A.D. Moghadam, P.L. Menezes, P.K. Rohatgi, Influences of graphite reinforcement on the tribological properties of self-lubricating aluminum matrix composites for green tribology, sustainability, and energy efficiency—a review, Int. J. Adv. Manuf. Technol. 83 (2016) 325–346. https://doi.org/10.1007/s00170-015-7528-x.

[118] R. Oriňáková, A. Turoňová, D. Kladeková, M. Gálová, R.M. Smith, Recent developments in the electrodeposition of nickel and some nickel-based alloys, J. Appl. Electrochem. 36 (2006) 957–972. https://doi.org/10.1007/s10800-006-9162-7.

[119] M.A.M. Ibrahim, R.M. Al Radadi, Role of glycine as a complexing agent in nickel electrodeposition from acidic sulphate bath, Int. J. Electrochem. Sci. 10 (2015) 4946–4971.

[120] J.K. Luo, M. Pritschow, A.J. Flewitt, S.M. Spearing, N.A. Fleck, W.I. Milne, Effects of Process Conditions on Properties of Electroplated Ni Thin Films for Microsystem Applications, J. Electrochem. Soc. 153 (2006) D155. https://doi.org/10.1149/1.2223302.

Chapter 2

Effect of grain refinement on microhardness, wear, and corrosion resistance of electroplated Ni-BN composite coatings

Abstract

Ni/h-BN composite coatings were successfully electrodeposited over mild steel substrate by dispersing 3wt% submicron h-BN powder in Ni Watts bath. The effect of saccharin addition (0–5 g/l) on the average crystallite size of the deposits was investigated by XRD. The results showed that the average crystallite size decreased, as the saccharin concentration increased from 0 to 5 g/l, while further increase in saccharin concentration had no significant effect. Compared to pure Ni coatings, Ni-BN composite coatings exhibited increased microhardness, and improved wear resistance. Potentiodynamic polarization curves and EIS impedance studies carried out in 3.5 wt% NaCl solution have shown that the Ni-BN composite coatings have increased corrosion resistance compared to both pure Ni coated mild steel and bare mild steel samples, indicating their potential for engineering applications.

2.1. Introduction

Manufacturing and engineering materials have been subjected to harsh service conditions, resulting in corrosion, wear and subsequent deterioration. Annually, corrosion and wear-related economic losses account for billions of dollars [1]. Surface modification is one of the best possible corrosion and wear prevention technique. Out of all the available surface modification techniques, metallic coatings are the most suitable, especially for steel structures. These coatings can enhance the corrosion resistance as well as the mechanical properties. In comparison with pure metallic coatings, composite coatings provide improved surface protection and better tribological characteristics as they integrate the beneficial properties of multiple materials [2]. By improving

hardness, reducing friction, and providing corrosion protection, these metallic composite coatings significantly extend the service life and reliability of components in harsh operating conditions.

Electrodeposition of composite coatings containing secondary particles in the metal matrix has drawn considerable interest in recent years due to the enhanced mechanical, tribological, and electrochemical properties of the composite coatings over pure metal electrodeposits [3]. The versatility of electrodeposition, along with its ability to tailor properties of the coating for specific applications, makes it an indispensable technology for a wide range of industries especially requiring durable and high-performance materials.

Nickel-based coatings have gained popularity due to the special characteristics of Ni, like excellent mechanical properties and non-hazardous nature so they can be used to replace carcinogenic chromium coatings [4]. To improve the properties of coatings, second-phase particles, including hard or soft nanoparticles (oxides, carbides, nitrides, solid lubricants) or polymers, are incorporated into the Ni matrix, resulting in nickel composite coatings. The particles are selected according to the nature and characteristics of the desired composite coating. Among these, hexagonal boron nitride (h-BN) is an ideal second-phase particle with excellent characteristics, including chemical inertness, high thermal and chemical stability, anti-wear, and lubricating properties [5]. Being a layered material with low coefficient of friction, it is also a perfect alternative to other solid lubricants used in engine parts as self-lubricating and high wear-resistance materials for high-performance applications.

In recent years electrodeposited Ni-BN composite coatings have gained significant attention due to their superior mechanical, tribological, and corrosion-resistant properties. Demir et al. [6] incorporated h-BN into Ni-Cr coatings deposited over AISI 1040 steel with concentrations ranging from 5 to 30 g/l using electrodepositon method. The effect of hBN additions on microstructure, nano indentation response, wear and corrosion resistance were studied. The effect of surfactant concentration on Ni-B/BN composite coatings developed by electrodeposition was studied by Tozar et al. [7]. Tripathi et al. [8] developed Ni-Fe/BN nano-composite coatings via electrodeposition from additive free nickel sulfamate-ferrous sulphate electrolytes. While Ni-BN composite coatings are well-established for their lubricating properties [8] and ability to withstand harsh environments, their performance can be further optimized through microstructural modifications, such as grain refinement.

Grain refinement which involves reduction in the average grain size of the electrodeposited material results in the improvement of physical and mechanical properties of coatings [9]. According to the Hall-Petch relationship [10], smaller grains can enhance the strength, hardness, and wear resistance of metallic coatings by restricting dislocation movement. In addition, grain refinement may lead to a more homogeneous distribution of reinforcing particles (in this case, BN), resulting in more uniform properties across the coating surface [11]. Saccharin, an organic additive plays a significant role in improving the quality of electrodeposited nickel composite coatings by refining the grain structure, enhancing the mechanical properties, and providing better wear and corrosion resistance [12]. However, the interplay between grain size, the distribution of BN particles, and overall performance of Ni-BN composite coatings remains an area of active research. While several studies have focused on the individual effects of BN incorporation and electrodeposition parameters, limited research has systematically explored the effect of grain refinement on the microhardness, wear behavior, and corrosion resistance of Ni-BN coatings.

This study aims to fill this gap by investigating the influence of grain refinement on the mechanical, tribological and electrochemical properties of electroplated Ni-BN composite coatings. The primary objectives are to evaluate how varying the grain size affects microhardness, wear resistance, and corrosion resistance, and to explore the underlying mechanisms responsible for these changes. Hard Ni-BN composite coatings tailored for industrial applications requiring enhanced durability and longevity will be developed as part of this study.

2.2. Materials & Methods

2.2.1. Materials

Nickel sulphate ($NiSO_4 \cdot 6H_2O$, 98%), Nickel chloride ($NiCl_2 \cdot 6H_2O$, 98%), Boric acid (H_3BO_3, 99.5%) and Sodium chloride (NaCl, 98%) were purchased from Merck. Sodium dodecyl sulphate (SDS, 99%) and Saccharin ($C_7H_5NO_3S$, 99.5%) were obtained from Alfa Aesar. Hexagonal boron nitride particles (h-BN, 98%, ~1 μm) were supplied by Sigma-Aldrich. All the chemicals were of analytical grade and used without further purification.

2.2.2. Coating Preparation

Ni–h/BN composite coatings were deposited on mild steel substrates from Ni Watts bath containing $NiSO_4 \cdot 6H_2O$ (250 g/l), $NiCl_2 \cdot 6H_2O$ (45 g/l), and H_3BO_3 (40 g/l). Hexagonal boron

nitride particles were dispersed in the Watts bath along with surfactant SDS (0.5 g/l) and grain refiner saccharin (3 g/l) (**Table 2.1**). The Ni-BN bath was kept at a pH of 4–4.5. Hexagonal BN particles were dispersed using an ultrasonicator for 30 min.

Nickel plate (7 cm × 5 cm × 1 cm, 99.7 % purity) and mild steel substrate (MS) (4 cm × 3 cm × 1 cm purity ≥ 99.5 %) were used as anode and cathode, respectively. All the mild steel samples used for coating were ground using SiC papers ranging from 80 to 1000 grits, followed by degreasing in acetone and distilled water, ultrasonically cleaned, and dried in the oven. MS samples were further surface activated by dipping in 0.01M HCl and 0.1M NaOH. The anode, Ni plate was polished using SiC papers of grit 80 and 100. This was followed by degreasing in acetone and distilled water and finally dried in the oven. Electrodeposition parameters including current density (2–6 A/dm^2), temperature (50–70˚C), and time (20–60 min) were varied. The concentration of h-BN particles was also varied in the range (1–5) wt% (**Table 2.1.**)

Table 2.1. Experimental conditions for Ni-BN coating over mild steel substrate

Electrodeposition parameters	Composition or parameter	Value	Optimised Conditions
Plating solution	$NiSO_4.6H_2O$	250 g/l	-
	$NiCl_2.6H_2O$	45 g/l	-
	H_3BO_3	40 g/l	-
	Saccharin	3 g/l	-
	SDS	0.5 g/l	-
Deposition Conditions	BN	1-5 wt%	3 wt%
	Current density	2-6 A/dm^2	5 A/dm^2
	Temperature	50-70°C	60°C
	Time	20-60 minutes	30 minutes
	Stirring rate	700 rpm	-

The grain refinement studies were further conducted by varying the amount of saccharin (1-5 g/l) at optimized conditions of current density 5 A/dm^2 for 30 min at a temperature of 60 ˚C with a 700 rpm stirring rate and 3 wt% concentration of h-BN particles. After the electrodeposition, the samples were cleaned in running distilled water followed by ultrasonic cleaning for 5 minutes in ethanol to remove loosely adsorbed particles and then subjected for further analysis.

2.2.3. Characterization of the coatings

The surface morphology and elemental analysis of the developed coatings were examined using Zeiss EVO 18 cryo-SEM (EDS attached). The phase composition of the samples was studied using X-ray diffraction (XRD) via a Bruker D2 Phaser X-ray diffractometer with Cu - K_α radiation (λ = 1.5406 Å) in the 0-90° range. The Vickers micro-hardness tester (Banbros) was used to measure the microhardness of the samples under the indentation of 50 gf with 10 s dwell time. Hardness measurements at five different locations of the sample were done and the average value was taken as the hardness value.

CH Instruments electrochemical workstation (CHI608E, CH Instruments Inc.) equipped with standard three-electrode cell was used for electrochemical impedance spectroscopy and potentiodynamic polarization studies at room temperature in 3.5 wt% NaCl solution. The coated specimen with 1cm^2 exposed surface area was used as the working electrode; saturated calomel and a platinum grid were taken as the reference and counter electrodes respectively. The specimens were kept in the electrolyte for 20 min prior to the experiment for attaining stable open circuit potential (OCP) values. The potentiodynamic scan was done at a rate of 1 mV/s from −250 mV to +250 mV of the OCP values. The corrosion potential (E_{corr} vs. SCE) and corrosion current density (i_{corr}) of each sample were obtained from the applied potential vs. current Tafel plot. The impedance measurements were performed using an AC signal with a perturbation of 5 mV at OCP in the frequency range of 100 kHz - 0.01 Hz. ZsimpWin software was used to fit the generated EIS plots to determine the electrochemical parameters. Numerous circuits were examined until the chi-square value decreased to less than 9×10^{-4} or no further fitting improvement was observed.

Pin on disc wear testing machine (POD 4.0, DUCOM) was used to measure the wear rate and coefficient of friction under non-lubricated conditions. The measurements were done for Ni-BN, pure Ni coated and bare mild steel samples. The pins with 6 mm diameter and 15 mm length were used as the wear samples against EN31 steel disc. The mild steel pins were coated with pure Ni and Ni-BN composite. Wear tests were done at a sliding velocity of 0.4 m/s under 2, 3, 4, and 5N standard loads at room temperature for 15 minutes.

2.3. Results & Discussion

2.3.1. Surface morphology and elemental composition

SEM micrographs of pure Ni and Ni-BN coatings deposited on mild steel are given in **Figure 2.1. (a)-(b)** and **Figure 2.2 (a)-(e)**, respectively. Both the coatings appeared to be uniform, compact with crack free surface. Both the coatings exhibited similar morphologies with a typical granular texture. However, the size of grains in the composite coating is smaller than that in the pure Ni coating. This occurs due to the grain refinement resulting from the co-deposition of BN particles within the Ni matrix. BN particles with a mean zeta potential of -19.5 mV influences the co-deposition mechanism by functioning as nucleation sites increasing the number of active sites to initiate Ni nucleation [5,8,13,14]. Simultaneously, the incorporation of BN particles at the boundaries of nickel crystallites can reduce the grain size so that the Ni-BN coating become denser than the pure Ni coating. Higher magnification of the SEM image (**Figure 2.2 (f)**) shows the presence of Ni grains composed of finer Ni crystallites (indicated by white arrows).

Elemental composition analysis (**Figure 2.3 (a)-(e)**) of the surface of Ni-BN coated MS possesses nickel (~ 90%) as the major elemental contribution. The composite coating surface had additional peaks corresponding to boron and nitrogen indicating that BN gets incorporated within the coating. **Figure 2.4 (a)-(f)** shows the cross-section of Ni-BN composite coatings. The average thickness of Ni-BN coating was found to be 40.5 µm. EDS data further indicated the presence of BN particles within the composite coating.

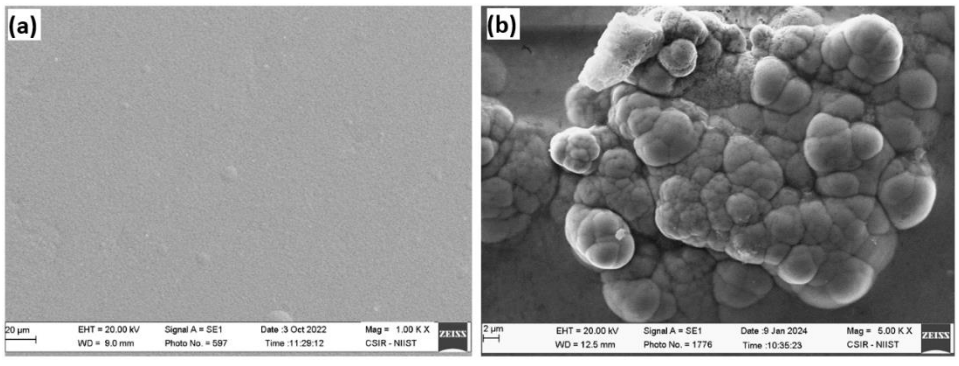

Figure 2.1 (a-b): SEM micrographs of pure Ni coated MS

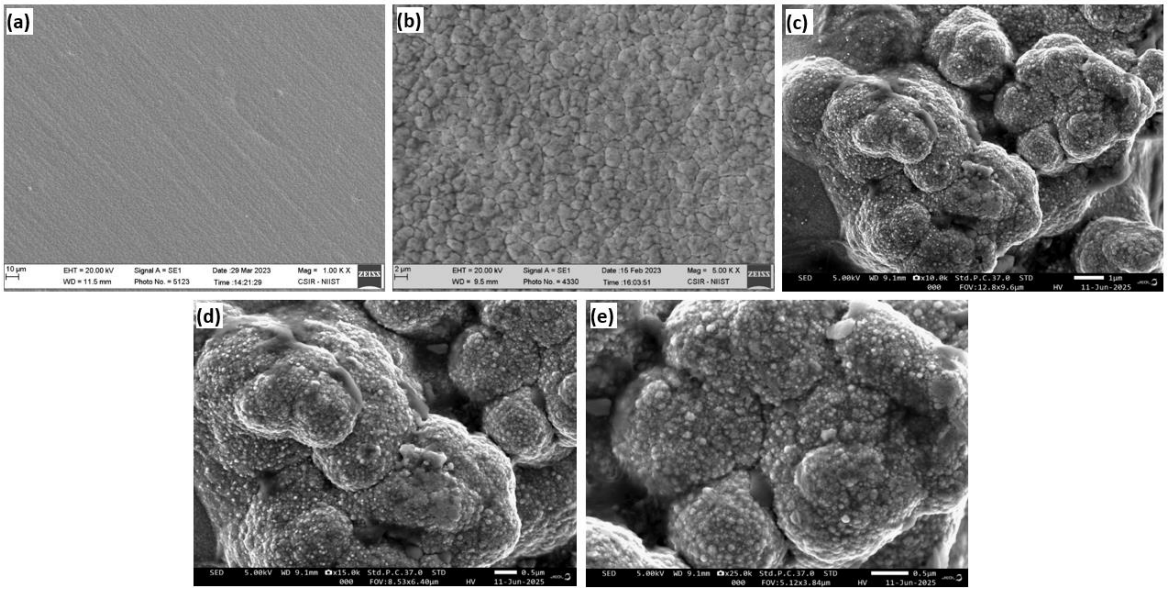

Figure 2.2 (a-e): SEM micrographs of Ni-BN coated MS

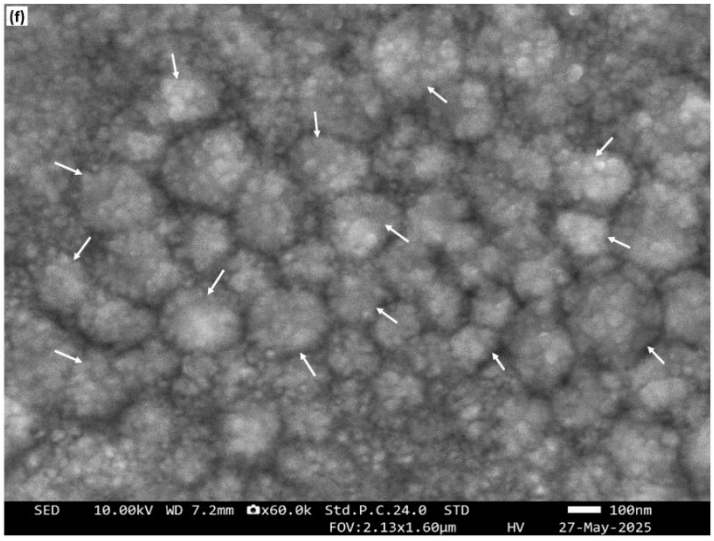

Figure 2.2 (f): Higher magnification SEM image of Ni-BN coated MS. White colored arrows indicate the Ni grains composed of finer Ni crystallites

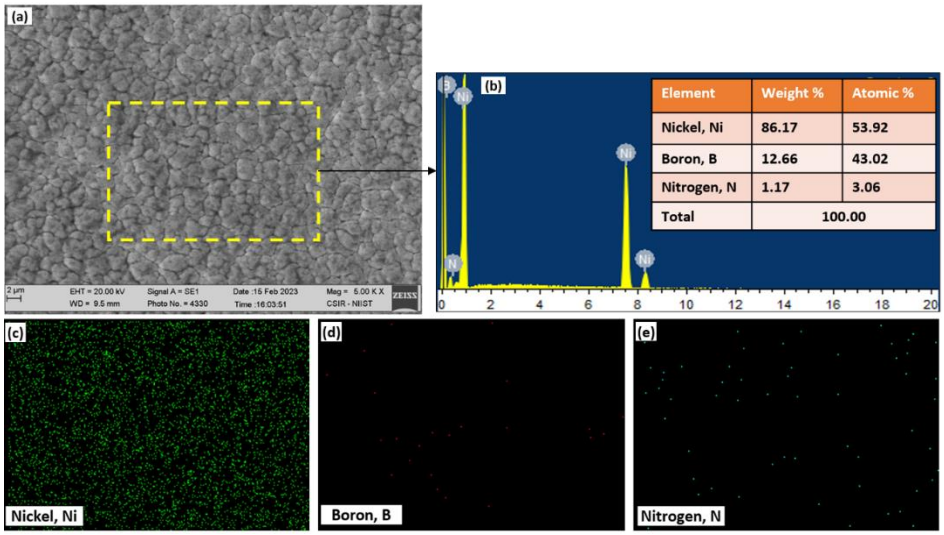

Figure 2.3 (a-e): SEM-EDS & elemental mapping of Ni-BN coated MS surface

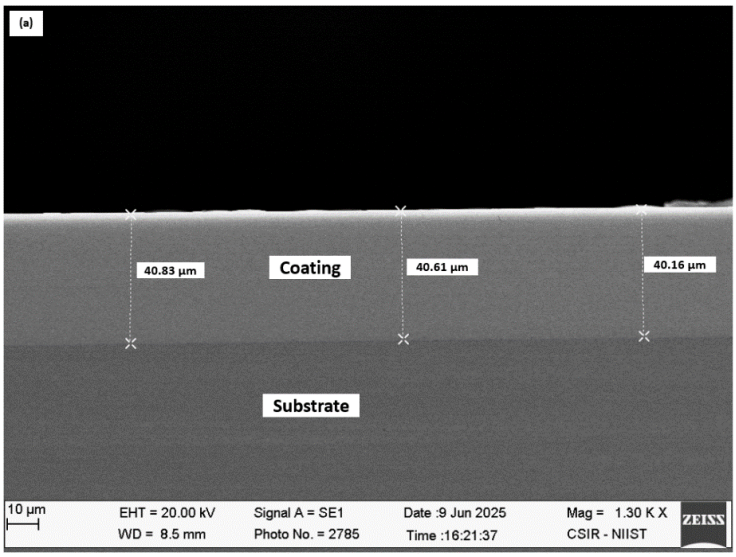

Figure 2.4 (a): Cross-sectional SEM micrographs of Ni-BN coated MS

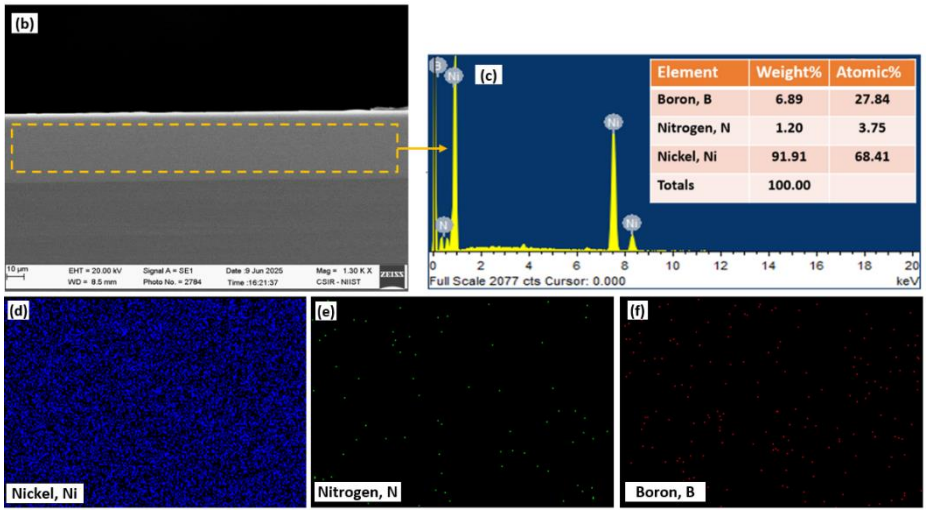

Figure 2.4 (b-f): Cross-sectional SEM-EDS & elemental mapping of Ni-BN coated MS

2.3.2. X-ray diffraction studies

X-ray diffraction patterns of pure Ni and Ni-BN coated samples with varying amount of saccharin (1-5 g/l) are shown in **Figure 2.5.** From the data, two peaks of Ni at 2θ corresponding to 44.32° and 51.77° are assigned to (111), (200) Bragg reflections of the face-centered cubic (fcc) structure of metallic nickel (JCPDS 04–0850 for Ni)[15]. Presence of BN in the coating cannot be confirmed from the XRD patterns owing to low concentration of BN. Crystallite size (grain size) of the coatings was calculated by the Scherrer equation (**Equation 2.1.**) with respect to the most intense diffraction peak of Ni (111) (**Figure 2.5**).

$$\textbf{Scherrer equation}: D = (K\,\lambda) / (\beta_{corr} \cos\theta) \qquad \textbf{(2.1.)}$$

$$\textbf{Corrected FWHM}, \beta_{corr} = \sqrt{(\beta_s)^2 - (\beta_i)^2} \qquad \textbf{(2.2.)}$$

Where, D = mean size of the crystalline domains which may be ≤ grain size, K = 0.9, Scherrer constant, β_{corr} = corrected full width at half maxima (FWHM) of the peak, θ = Bragg's diffraction angle, λ = wavelength of X-ray, 0.154 nm. Corrected FWHM (β_{corr}) was calculated by considering the instrumental broadening where β_s is FWHM of the sample and β_i is the FWHM contributed by the instrument (**Equation 2.2.**)

The grain size (crystallite size) measurements indicate that the pure Ni coating (57.4 nm) have larger grain size compared to all the Ni-BN composite coatings. The lowest crystallite size was obtained for Ni-BN composite coating with 5% saccharin (21.5 nm) (**Table 2.2**).

A significant decrease in crystallite size from 57.4 nm (pure Ni) to 23.9 nm with the addition of 1% saccharin in Ni-BN composite coating However, further addition of saccharin (from 2% to 5%) results no significant change in crystallite size, which stabilize around 22–21 nm. Saccharin basically acts as a grain-refiner during Ni-BN electrodeposition. Its role as a grain refiner in Ni-BN composite coating can be explained as follows; the lone-pair of electrons of oxygen atom of the grain refiner saccharin fill the 3d orbitals of Ni atoms, forming a stable coordination bond. As a result, there will be strong interaction between the surface atoms of Ni deposits and saccharin. Large size of coordination compound of Ni and saccharin prevents the surface migration of Ni ions and suppress it reducing the grain size of Ni deposits.

Once the surface is saturated with saccharin molecules, additional saccharin does not significantly influence the refinement of grains. Due to limited surface interaction, grain refinement reaches a plateau. This behavior is common with additives in electrodeposition; there's a threshold beyond which their effect on reducing the grain size levels off [16,17].

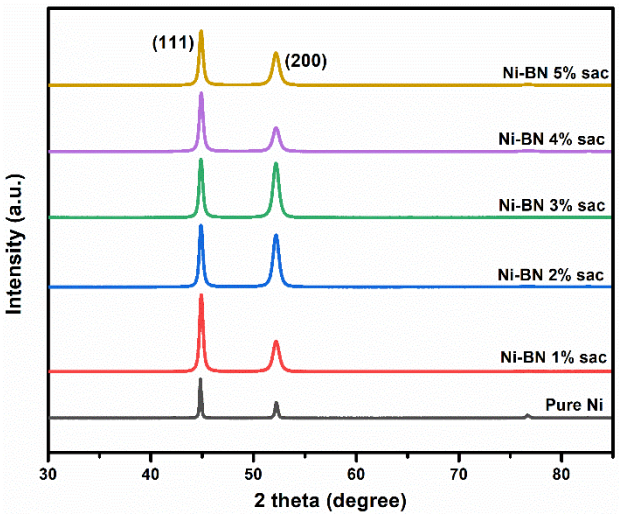

Figure 2.5. XRD pattern of pure Ni & Ni-BN coated samples with varying saccharin amount

Table 2.2. Crystallite size calculations using Scherrer equation in Ni-BN coatings

Coating	Angular position (θ) (radians)	cos θ (radians)	Full width half-maxima (FWHM) (radians)			Average crystallite size (D) (nm)
			Sample β_s	Instrument β_i	Corrected β_{corr}	
Pure Ni	0.390	0.925	2.616×10^{-3}		2.612×10^{-3}	57.4
Ni-BN 1% sac	0.390	0.925	6.280×10^{-3}		6.278×10^{-3}	23.9
Ni-BN 2% sac	0.391	0.924	6.454×10^{-3}	1.395×10^{-4}	6.453×10^{-3}	23.2
Ni-BN 3% sac	0.391	0.924	6.628×10^{-3}		6.627×10^{-3}	22.6
Ni-BN 4% sac	0.391	0.924	6.803×10^{-3}		6.801×10^{-3}	22.1
Ni-BN 5% sac	0.391	0.924	6.997×10^{-3}		6.996×10^{-3}	21.5

2.3.3. Microhardness measurements

The microhardness of Ni-BN composite coating shows exceptional high hardness values compared to mild steel and pure Ni coating (**Figure 2.6.**). Grain boundary immobilization by BN particles and the dispersion strengthening improve the hardness in the case of Ni-BN composite coating [18]. Saccharin reduces the average grain size, leading to a higher grain boundary density. Grain boundaries also act as obstacles to dislocation movement, hindering plastic deformation. The increased resistance to dislocation movement results in a harder coating. Vickers microhardness values of the samples increase in the order of mild steel (210 HV) < pure Ni (350 HV) < Ni-BN 5% saccharin (589 HV) composite coating.

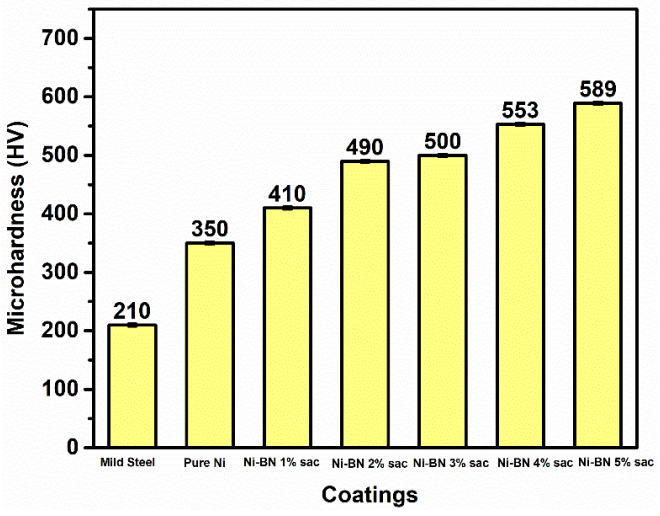

Figure 2.6. Microhardness measurements of Ni-BN grain-refined samples

2.3.4. Electrochemical characterization

Figure 2.7. (a) shows the potentiodynamic polarization curves (Tafel plots) of samples by plotting the potential scanned from cathodic region to the anodic region vs. logarithm of current density. The values of corrosion current density (i_{corr}) and corrosion potential (E_{corr}), obtained by the extrapolation of cathodic and anodic sides are given in **Table 2.3.** Variation of E_{corr} value towards more positive direction and the lower i_{corr} indicates the improved corrosion resistance of composite coatings. Presence of BN particles and the grain refinement in the coating leads to a substantial reduction in the i_{corr} value of Ni-BN to 0.471 µA cm^{-2} from 4.143 µA cm^{-2} in the case of pure Ni and 17.110 µA cm^{-2} in case of bare mild steel sample. The corresponding shift of the graph towards the left-hand side was observed. The reduction in i_{corr} values of the coated samples indicates the decreased rate of ionic diffusion on the coating surface during corrosion [19]. The Ni-BN composite coating is more cathodic with respect to other samples and possesses excellent corrosion protection (E_{corr} MS: -0.678 V, Pure Ni: -0.417 V, Ni-BN 5% saccharin: -0.251 V).

The structural modification of nickel crystallites induced with the incorporation of BN particles along with the grain refining effect of saccharin led to improved corrosion resistance [19]. The uniformly distributed h-BN particles in the deposit forms a passive layer between corrosive media and the deposited coating. By filling up the surface imperfections such as tiny holes and porosities with co-deposited particles and acting as a barrier to corrosive ion migration to the electrode surface, thus the addition of BN particles into the Ni matrix has improved the corrosion resistance behavior [20]. A passive layer is formed between the deposited coating and the corrosive media by the uniformly distributed h-BN particles in the deposit.

Saccharin acts as a grain-refiner and leveling agent in electrodeposition. It helps to create a more uniform coating**.** This will reduce the porosity and micro-cracks, which are potential paths for corrosive agents. Even if crystallite size is unchanged, a pore-free, compact surface makes it difficult for corrosive species (like Cl^- in NaCl solutions) to penetrate. Higher saccharin concentrations improve the co-deposition and uniform dispersion of BN in the Ni matrix. This creates a barrier effect, where BN particles act as obstacles to corrosive ion diffusion. Saccharin also helps to reduce internal stress, which minimizes crack formation during or after deposition. It also helps in filling up voids or gaps in the coating structure. Thus there will be fewer defects and micro-cracks which are often corrosion initiation points.

Electrochemical impedance spectroscopy measurements were performed in order to get a better understanding of the anticorrosive ability of coatings. Nyquist plots of bare mild steel, pure Ni and Ni-BN composite coatings were obtained in 3.5% NaCl medium at their respective open circuit potentials (**Figure 2.7. (b)**).The Nyquist plots of all the samples showed a single semi-circular arc in the investigated frequency region. The bare MS samples can be fitted with the circuit the equivalent electrochemical circuit (EEC) $R_s(C_{dl}R_{ct})$ (**Figure 2.7. (c)**), and all the coated samples are well fitted for the equivalent circuit of $R_s(C_cR_c(C_{dl}R_{ct}))$ (**Figure 2.7.(d)**).

R_s is the solution resistance, and R_{ct} and C_{dl} are the charge transfer resistance and double-layer capacitance, respectively. Instead of using pure capacitance due to the possibility of a dispersion effect between the metal/coating system, *C* represents a constant phase angle element (CPE). The coating offered protection by the resistance element *R*c. The parameters derived from electrochemical impedance measurements are summarized in **Table 2.3.** The results of the EIS studies showed a similar trend that was observed in potentiodynamic polarization studies. The increased radius of semicircular arc indicated better anticorrosion property of the Ni-BN composite coating than other samples. The superior value of R_{ct} obtained for Ni-BN composite coating indicating the coating's more protective nature against corrosion.

Table 2.3. Electrochemical parameters obtained and corrosion inhibition efficiency of Ni-BN coated samples

S/N	Substrate	Potentiodynamic polarisation				EIS	
		E_{corr} (V)	i_{corr} (μAcm^{-2})	η (%)	Corr.rate (mmpy)	R_{ct} (Ω cm^2)	η (%)
1.	Bare Mild Steel	-0.678	17.110	-	0.2013	3.955×10^2	-
2.	Pure Nickel	-0.417	4.143	75.78	0.0446	3.222×10^4	98.77
3.	Ni-BN 1% sac	-0.206	1.723	89.90	0.0185	4.513×10^4	99.12
4.	Ni-BN 2% sac	-0.155	1.583	90.70	0.0170	5.232×10^4	99.24
5.	Ni-BN 3% sac	-0.258	1.041	93.90	0.0112	6.627×10^4	99.40
6.	Ni-BN 4% sac	-0.184	0.687	95.90	0.0074	5.721×10^4	99.42
7.	Ni-BN 5% sac	-0.251	0.471	97.20	0.0050	9.095×10^4	99.56

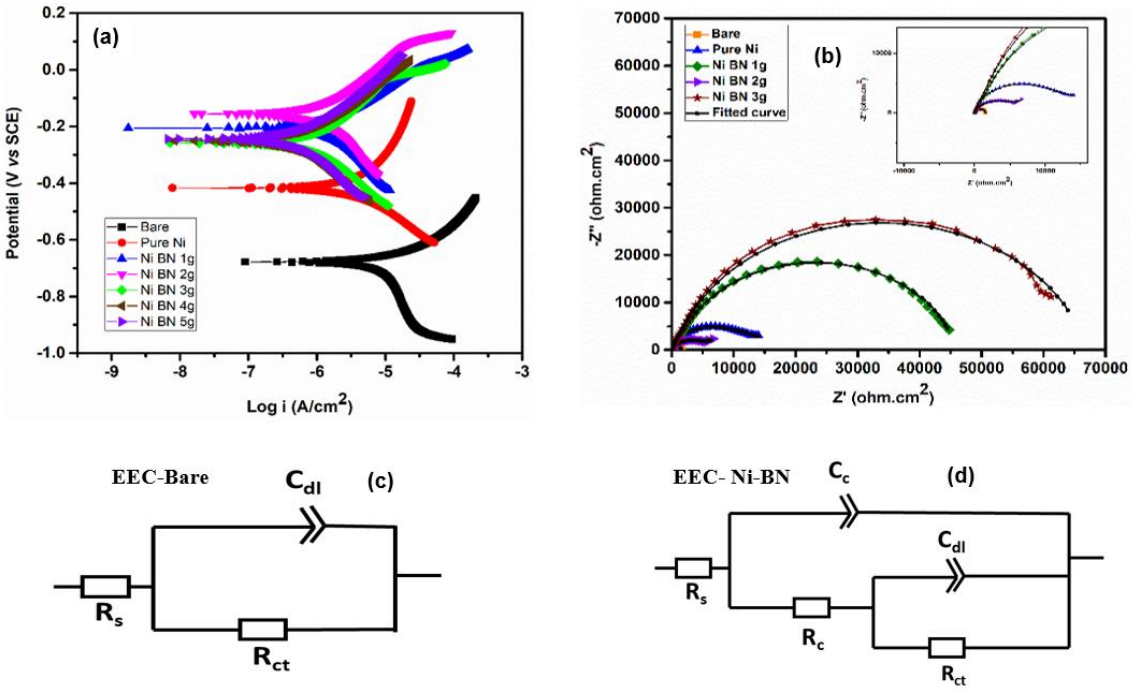

Figure 2.7. Electrochemical study for the Ni-BN composite coatings **(a)** Tafel plot, **(b)** Nyquist plot, **(c)** EEC for the bare sample, **(d)** EEC for Ni-BN coated sample

2.3.5. Tribological Characteristics

Figure 2.8. (a) shows the variation of coefficient of friction of the electrodeposited Ni-BN coating at different loads (2, 3, 4, and 5N) load for 15 min under non-lubricated conditions. Compared with the pure nickel, the friction coefficient of the Ni–BN composite coating decreased and wear resistance increased appreciably (**Figure 2.8 (b)**). The presence of BN particles and grain refinement observed in the composite coating provide lowest coefficient of friction values in comparison with pure Ni coating under different loads.

SEM studies of the worn surfaces of Ni-BN composite coatings are shown in **Figure 2.9. (a)**. BN included in the Ni matrix restricts or slows down the dislocation movements in the matrix avoiding excessive wear [21]. The layered hexagonal structure of the crystal lattice of h-BN permits sliding movement of the parallel planes. Due to the weak bonding between the planes, the shear strength is low along the sliding direction. As a result of strong adherence of BN particles to the worn surface, a solid self-lubricating tribo film is formed over the wear surfaces [22]. This film

forms an interface layer between the pin and the disc. Thus the strongly adhered lubrication film formed by h-BN prevents the surface from further wear.

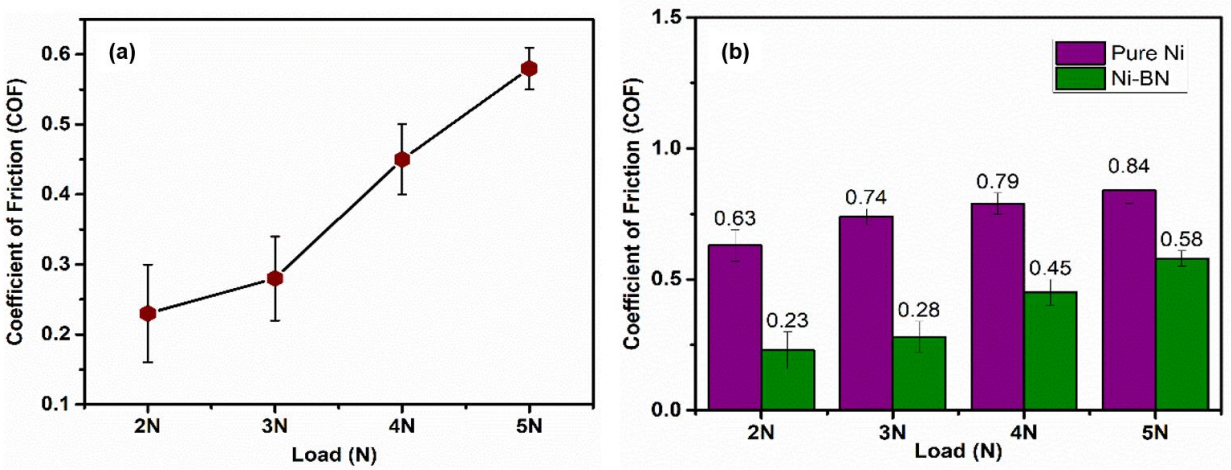

Figure 2.8. (a) Load vs COF of Ni-BN coated samples, **(b)** Comparison of COF values of pure Ni & Ni-BN coated samples under different loads

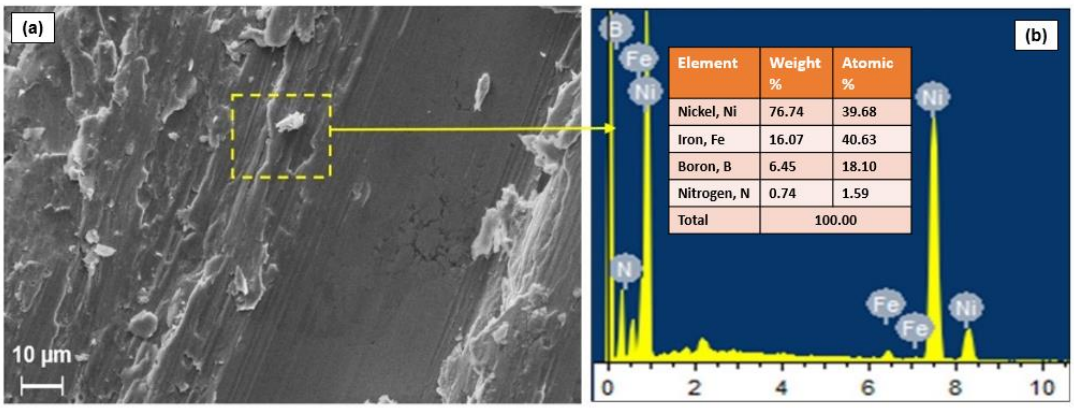

Figure 2.9. (a)-(b) SEM-EDS of the worn surface of Ni-BN coated sample

2.4. Conclusions

Ni-BN composite coating was successfully coated over mild steel via DC electrodeposition and their surface morphology, phase structure, composition, grain size, electrochemical and tribological properties were investigated. The coatings were uniform and compact without cracks. Increasing the saccharin concentration to a certain level refines the nickel grains. Additionally the incorporation of BN particles could refine grains and reduce porosity. As the saccharin concentration increases up to 5 g/l, the hardness, corrosion resistance and wear resistance of Ni-BN composite coating also increases. The Ni-BN composite coating exhibited better barrier effect due to the presence of BN particles in corrosive environment. Thus the grain refinement and uniform distribution of BN particles in the matrix has contributed to the coatings' stability indicating their potential for engineering applications.

References

[1] Z. Zhang, H. Dong, A State-of-the-art overview, Manuf. Rev. 1 (2014) 24. https://doi.org/10.1051/mfreview/2015001.

[2] I. Gurrappa, L. Binder, Electrodeposition of nanostructured coatings and their characterization—A review, Sci. Technol. Adv. Mater. 9 (2008) 043001. https://doi.org/10.1088/1468-6996/9/4/043001.

[3] C.T.J. Low, R.G.A. Wills, F.C. Walsh, Electrodeposition of composite coatings containing nanoparticles in a metal deposit, Surf. Coatings Technol. 201 (2006) 371–383. https://doi.org/10.1016/j.surfcoat.2005.11.123.

[4] S.T. Aruna, V.K. William Grips, K.S. Rajam, Ni-based electrodeposited composite coating exhibiting improved microhardness, corrosion and wear resistance properties, J. Alloys Compd. 468 (2009) 546–552. https://doi.org/10.1016/j.jallcom.2008.01.058.

[5] G. Gyawali, R. Adhikari, H.S. Kim, H.-B. Cho, S.W. Lee, Effect of h-BN Nanosheets Codeposition on Electrochemical Corrosion Behavior of Electrodeposited Nickel Composite Coatings, ECS Electrochem. Lett. 2 (2012) C7–C10. https://doi.org/10.1149/2.003303eel.

[6] M. Demir, E. Kanca, İ.H. Karahan, Characterization of electrodeposited Ni–Cr/hBN composite coatings, J. Alloys Compd. 844 (2020) 155511. https://doi.org/10.1016/j.jallcom.2020.155511.

[7] A. Tozar, İ.H. Karahan, Effect of octylphenyl ether group nonionic surfactant on the electrodepositon of the hexagonal boron nitride reinforced Ni-B matrix composite coatings, Surf. Coatings Technol. 381 (2020). https://doi.org/10.1016/j.surfcoat.2019.125131.

[8] M.K. Tripathi, D.K. Singh, V.B. Singh, Electrodeposition of Ni-Fe/Bn nano-composite coatings from a non-aqueous bath and their characterization, Int. J. Electrochem. Sci. 8 (2013) 3454–3471.

[9] M. Bhardwaj, K. Balani, R. Balasubramaniam, S. Pandey, A. Agarwal, Effect of current density and grain refining agents on pulsed electrodeposition of nanocrystalline nickel, Surf. Eng. 27 (2011) 642–648. https://doi.org/10.1179/026708410X12683118611185.

[10] F. Nasirpouri, M.R. Sanaeian, A.S. Samardak, E. V. Sukovatitsina, A. V. Ognev, L.A. Chebotkevich, M.G. Hosseini, M. Abdolmaleki, An investigation on the effect of surface

morphology and crystalline texture on corrosion behavior, structural and magnetic properties of electrodeposited nanocrystalline nickel films, Appl. Surf. Sci. 292 (2014) 795–805. https://doi.org/10.1016/j.apsusc.2013.12.053.

[11] V.N. Tseluikin, On the Structure and Properties of Composite Electrochemical Coatings. A Review, Prot. Met. Phys. Chem. Surfaces 52 (2016) 254–266. https://doi.org/10.1134/S2070205116010251.

[12] G.Q. Qadir, M.I. Awad, J.A. Juma, W.O. Karim, Z.T. Al-thagafi, B.A. Al Jahdaly, H.H. Abdallah, Influence of nicotinic acid additive on the electrodeposition of nickel from aqueous solution, Int. J. Electrochem. Sci. 19 (2024) 100745. https://doi.org/10.1016/j.ijoes.2024.100745.

[13] S. Paydar, A. Jafari, M.E. Bahrololoom, V. Mozafari, Enhancing Ni electroplated matrix through mixed boron nitride–carbide reinforcement, Vacuum 92 (2013) 52–57. https://doi.org/10.1016/j.vacuum.2012.10.014.

[14] E. Ünal, H. Karahan, Production and characterization of electrodeposited Ni-B/hBN composite coatings, Surf. Coatings Technol. 333 (2018) 125–137. https://doi.org/10.1016/j.surfcoat.2017.11.016.

[15] A. Lelevic, F.C. Walsh, Electrodeposition of Ni[sbnd]P composite coatings: A review, Surf. Coatings Technol. 378 (2019). https://doi.org/10.1016/j.surfcoat.2019.07.027.

[16] A.M. Rashidi, A. Amadeh, The effect of saccharin addition and bath temperature on the grain size of nanocrystalline nickel coatings, Surf. Coatings Technol. 204 (2009) 353–358. https://doi.org/10.1016/j.surfcoat.2009.07.036.

[17] N.P. Wasekar, P. Haridoss, S.K. Seshadri, G. Sundararajan, Influence of mode of electrodeposition, current density and saccharin on the microstructure and hardness of electrodeposited nanocrystalline nickel coatings, Surf. Coatings Technol. 291 (2016) 130–140. https://doi.org/10.1016/j.surfcoat.2016.02.024.

[18] H. Li, Y. He, T. He, D. Qing, F. Luo, Y. Fan, X. Chen, Ni-W/BN(h) electrodeposited nanocomposite coating with functionally graded microstructure, J. Alloys Compd. 704 (2017) 32–43. https://doi.org/10.1016/j.jallcom.2017.02.037.

[19] J.B. Jiang, L. Zhang, Q.D. Zhong, Q.Y. Zhou, Y. Wang, J. Luo, Preparation and characterisation of nickel-nano-B 4C composite coatings, Surf. Eng. 28 (2012) 612–619. https://doi.org/10.1179/1743294412Y.0000000038.

[20] B. Li, D. Li, T. Mei, W. Xia, W. Zhang, Fabrication and characterization of boron nitride reinforced Ni–W nanocomposite coating by electrodeposition, J. Alloys Compd. 777 (2019) 1234–1244. https://doi.org/10.1016/j.jallcom.2018.11.081.

[21] S. Paydar, A. Jafari, M.E. Bahrololoom, V. Mozafari, Influence of BN and B 4 C particulates on wear and corrosion resistance of electroplated nickel matrix composite coatings, Tribol. - Mater. Surfaces Interfaces 9 (2015) 105–110. https://doi.org/10.1179/1751584X15Y.0000000007.

[22] S. Sangeetha, G.P. Kalaignan, Tribological and electrochemical corrosion behavior of Ni–W/BN (hexagonal) nano-composite coatings, Ceram. Int. 41 (2015) 10415–10424. https://doi.org/10.1016/j.ceramint.2015.04.089.

Chapter 3

Development of multi-functional biomimetic Ni-graphene composite coating by electrodeposition

Abstract

Nickel-graphene composite coatings have been successfully coated over mild steel by electrochemical co-deposition technique. This study explores the surface morphology, phase composition, wettability, and corrosion resistance properties of the Ni-graphene composite coatings. The coatings exhibited compact and crack-free morphology, which was evident from the SEM images. Wettability studies reveal that the Ni-graphene coating has a water contact angle of 152º, indicating its superhydrophobicity. Additionally the coating possessed self-cleaning ability. The composite coatings exhibited improved corrosion and wear resistance in comparison with the pure Ni coating and bare mild steel substrates. These findings demonstrate the potential of Ni-graphene composite coatings as a multifunctional surface treatment for enhancing the durability and performance of mild steel in corrosive and wear-intensive environments.

3.1. Introduction

The need for advanced materials with multifunctional capabilities has become an important area of research in the fields of surface engineering and protective coatings [1]. With increasing demands for materials that can withstand harsh environments while maintaining high mechanical performance, the development of innovative coatings has become essential across industries such as aerospace, marine, automotive, and biomedical etc [2]. These sectors require surfaces that are not only resistant to wear and corrosion but also exhibit enhanced mechanical strength and longevity under diverse operating conditions. Recently, super-hydrophobic materials with intrinsic water contact angle (WCA) larger than 150° and a sliding angle (SA) below 10° have drawn a lot of interest due to their unique properties such as anti-icing [3], corrosion resistance [4], drag

reduction [5], and self-cleaning [6]. Fabrication of micro-nanostructured surfaces and the use of low surface energy materials results in superhydrophobic surfaces.

Nickel-based coatings have long been utilized for their remarkable properties, including excellent hardness, durability, and resistance to wear and corrosion [7]. However, further improvement of these coatings is often necessary to meet the rigorous demands of modern applications. Recent advancements in composite coatings have opened new avenues to enhance the properties of conventional nickel coatings by incorporating secondary-phase materials. Among these, graphene, a two-dimensional material composed of sp^2-hybridized carbon atoms arranged in a honeycomb lattice, has emerged as a transformative additive [8]. Its exceptional properties such as high tensile strength, excellent thermal and electrical conductivity, low friction coefficient, and superior chemical stability make it an ideal reinforcement for metal matrix composites [9].

Various graphene-based superhydrophobic surfaces have been designed [10]. In particular, nickel-graphene composite coatings have attracted attention for their ability to synergistically combine the properties of both nickel and graphene, resulting in a material with superior wear resistance, corrosion resistance, and mechanical properties. Furthermore, graphene's unique surface energy characteristics contribute to the development of superhydrophobic surfaces, which can repel water, reducing fouling and enhancing durability [11]. However, achieving a uniform dispersion of graphene within the nickel matrix, as well as optimizing the coating's microstructure and functional properties, remains a challenge.

Electrodeposition is a widely employed technique for developing nickel-based coatings due to its cost-effectiveness, scalability, and ability to produce coatings with tailored properties by varying process parameters [12]. Incorporating graphene into nickel matrix via electrodeposition offers a controllable and efficient route to develop highly durable coatings.

Co-GO coating was electrodeposited over a copper substrate was explored by Liu et al. [13] and the coating had improved wear and friction characteristics as well as corrosion resistance. Haung et al. [14] fabricated a copper-graphene coating with fewer defects, and discovered that the sample's mechanical qualities improved without affecting its electrical or thermal characteristics. According to Praveen Kumar et al. [15], graphene significantly increased the coating's hardness

and resistance to corrosion. Khorsand et al. [16] produced a superhydrophobic Ni surface with a pine-cone-like hierarchical surface with increased corrosion resistance.

In the present study to enhance the coating's functionality by tuning its wettability and further improving its tribological properties, graphene was chosen as the reinforcing material in the nickel composite coatings. In this work, thus the aim was to develop a novel Ni-graphene coating that uniquely combines superhydrophobicity, self-cleaning capabilities, mechanical durability, and superior tribological performance. By bridging fundamental research and practical applications, this work contributes to the development of robust, durable, and versatile coatings capable of meeting the demands of modern industries.

3.2. Materials & Methods

3.2.1 Materials

Nickel chloride ($NiCl_2 \cdot 6H_2O$, 98%), Boric acid (H_3BO_3, 99.5%) and Potassium chloride (KCl, 98%) were purchased from Merck. Sodium dodecyl sulphate (SDS, 99%) was obtained from Alfa Aesar. In-house graphene was used for all the experiments. All the chemicals were of analytical grade and used without further purification.

3.2.2 Coating Preparation

Ni–graphene composite coatings were deposited on mild steel substrate from electrolytic Ni bath containing $NiCl_2 \cdot 6H_2O$ (60 g/l), H_3BO_3 (9 g/l) and KCl (9 g/l). Graphene was dispersed in the Watts bath along with surfactant SDS (0.15 g/l). The Ni-graphene bath was kept at a pH of 4–4.5. Graphene was dispersed using an ultrasonicator for 1 hour.

Nickel plate (7 cm × 5 cm × 1 cm, 99.7 % purity) and mild steel substrate (SSM) (6 cm × 6 cm, purity ≥ 99.5 %) were used as anode and cathode, respectively. All the mild steel samples used for coating were ground using SiC papers ranging from 80 to 1000 grits, followed by degreasing in acetone and distilled water, ultrasonically cleaned, and dried in the oven. MS samples were further surface activated by dipping in 0.01M HCl and 0.1M NaOH. The anode, Ni plate was polished using SiC papers of grit 80 and 100. This was followed by degreasing in acetone and distilled water and finally drying in the oven. Electrodeposition parameters including current

density (2–6A/dm^2), time (5–30 min), and stirring rate (400–600 rpm) were varied. The concentration of graphene was also varied in the range (1–5) wt% (**Table 3.1.**).

Finally Ni-graphene was deposited at optimized conditions of current density of 2 A/dm^2 for 5 min at a temperature of 55°C at 600 rpm stirring rate and 1 wt% concentration of graphene. After the electrodeposition, the samples were cleaned in running distilled water followed by ultrasonic cleaning for 5 minutes in ethanol to remove loosely adsorbed particles and then subjected for further analysis.

Table 3.1. Experimental conditions for Ni-graphene coating over mild steel substrate

Electrodeposition parameters	Composition or parameter	Value	Optimised conditions
Plating solution	$NiCl_2.6H_2O$	60 g/l	-
	H_3BO_3	9 g/l	-
	KCl	9 g/l	-
	SDS	0.15 g/l	-
	Graphene	1-5 wt%	1 wt%
Deposition conditions	Current density	2-6 A/dm^2	2 A/dm^2
	Temperature	55°C	-
	Time	5-30 minutes	5 minutes
	Stirring rate	400-600 rpm	600 rpm

3.2.3. Characterization of the coatings

The surface morphology and elemental analysis of the developed coatings were examined using Zeiss EVO 18 cryo-SEM (EDS attached). The phase composition of the samples was studied using X-ray diffraction (XRD) via a Bruker D2 Phaser X-ray diffractometer with Cu - K_α radiation (λ = 1.5406 Å) in the 0-90° range. The wettability of the developed coatings was measured by Goniometer (Data Physics, Germany). The water contact angle was calculated by taking the average of five measurements taken at various points on the same sample. Mechanical stability of the developed coating was evaluated by sandpaper abrasion test. The self-cleaning action of the composite coating was analyzed using chalk powder as contaminants. Both coated and uncoated MS substrates were tilted followed by the dropping of distilled water droplets on their surface. The water rolling-off property and self-cleaning ability of both substrates were thus compared.

CH Instruments electrochemical workstation (CHI608E, CH Instruments Inc.) equipped with standard three-electrode cell was used for electrochemical impedance spectroscopy and potentiodynamic polarization studies at room temperature in 3.5 wt% NaCl solution. The coated specimen with $1cm^2$ exposed surface area was used as the working electrode; saturated calomel and a platinum grid were taken as the reference and counter electrodes respectively. The specimens were kept in the electrolyte for 20 min prior to the experiment for attaining their stable open circuit potential (OCP). The potentiodynamic scan was done at a rate of 1 mV/s from −250 mV to +250 mV of the OCP values. The corrosion potential (E_{corr} vs. SCE) and corrosion current density (i_{corr}) of each sample were obtained from the applied potential vs. current Tafel plot. The impedance measurements were performed using an AC signal with a perturbation of 5 mV at OCP in the frequency range of 100 kHz-0.01 Hz. ZsimpWin software fits the generated EIS plots to determine the electrochemical parameters. Numerous circuits were examined until the Chi-square value decreased to less than 9×10^{-4} or no further fitting improvement was observed.

Pin on disc wear testing machine (POD, 4.0, DUCOM) was used to measure the wear rate and coefficient of friction under dry condition. The measurements were done for Ni-graphene, pure Ni coated and bare mild steel samples. The pins with 6 mm diameter and 15 mm length were used against EN31 high carbon alloy steel disc. The mild steel pins were coated with pure Ni and Ni-graphene composite. Wear tests were done at a sliding velocity of 0.4 m/s under 2, 3, 4, and 5N standard loads at room temperature for 15 minutes.

3.3. Results & Discussion

3.3.1. Surface morphology and elemental composition

SEM micrographs of pure Ni and Ni-graphene composite coating deposited on mild steel are given in **Figure 3.1. (a-b)** and **Figure 3.2. (a-e)**, respectively. Both the coatings were having uniform surface without any defects such as pores and cracks. Pure Ni coating possessed large grainular surface whereas Ni graphene coating had pinecone structure. The addition of graphene with a mean zeta potential of -18.8 mV caused a change in the microstructure of the composite coating. Ni ions used graphene sheet as a template to nucleate on it. In Ni-graphene composite coating, graphene reduces the grain size by blocking the growth of Ni crystallites [18]. Due to the large specific area of graphene [19], more nucleation sites are provided for the growth of Ni.

Compared to the pure Ni coating, composite coating exhibited a rougher surface. The Ni-graphene possess pine cones having layered and hierarchical architectures (**Figure 3.2. (f),** pine cones are marked in red circles). The pine cone like structure results have higher surface area. In nickel-graphene coatings such a structure can enhance mechanical strength, anti-wear and electrochemical performance [20].

EDS analysis and elemental mapping results of Ni-graphene composite coating revealed the presence of the elements nickel and carbon which indicates the incorporation of graphene within the Ni matrix (**Figure 3.3. (a)-(d)**). No peaks originating from the steel substrate such as iron was seen, which confirms that the obtained Ni-graphene composite coating had a continuous structure. **Figure 3.4 (a)-(e)** shows the cross-section of Ni-graphene composite coating. The average thickness of Ni-graphene coating was found to be 11.37 µm. EDS data of the cross section further confirmed the presence of graphene in the composite coating.

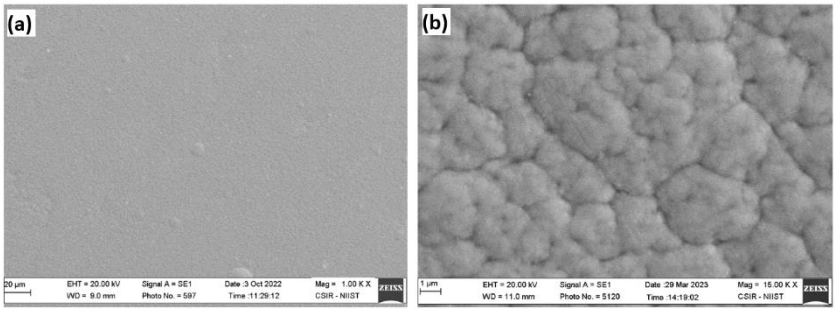

Figure 3.1 (a-b): SEM micrographs of pure Ni coated MS

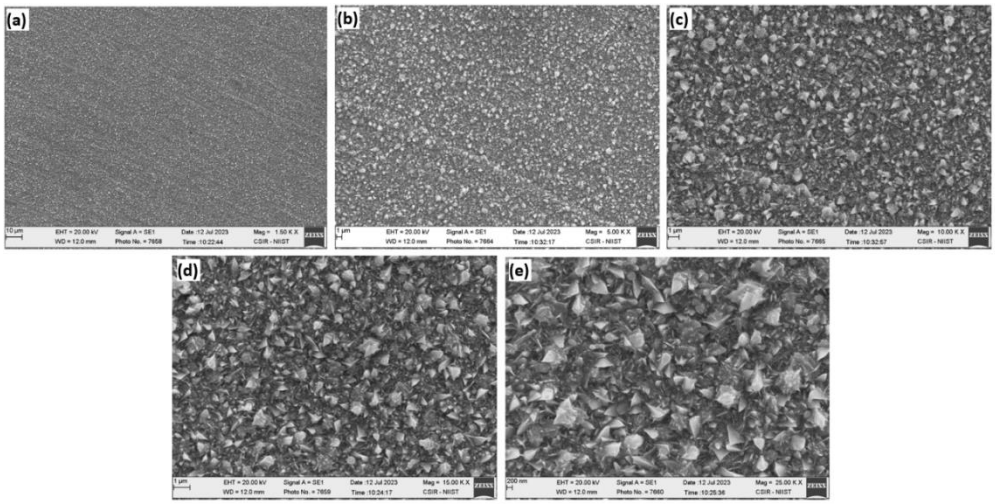

Figure 3.2 (a-e): SEM micrographs of Ni-graphene coated MS

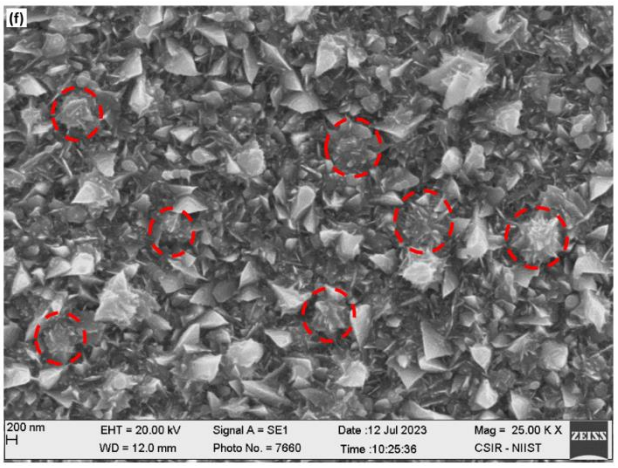

Figure 3.2 (f): Higher magnification SEM image of Ni-graphene coated MS. Pinecones are marked in red circles

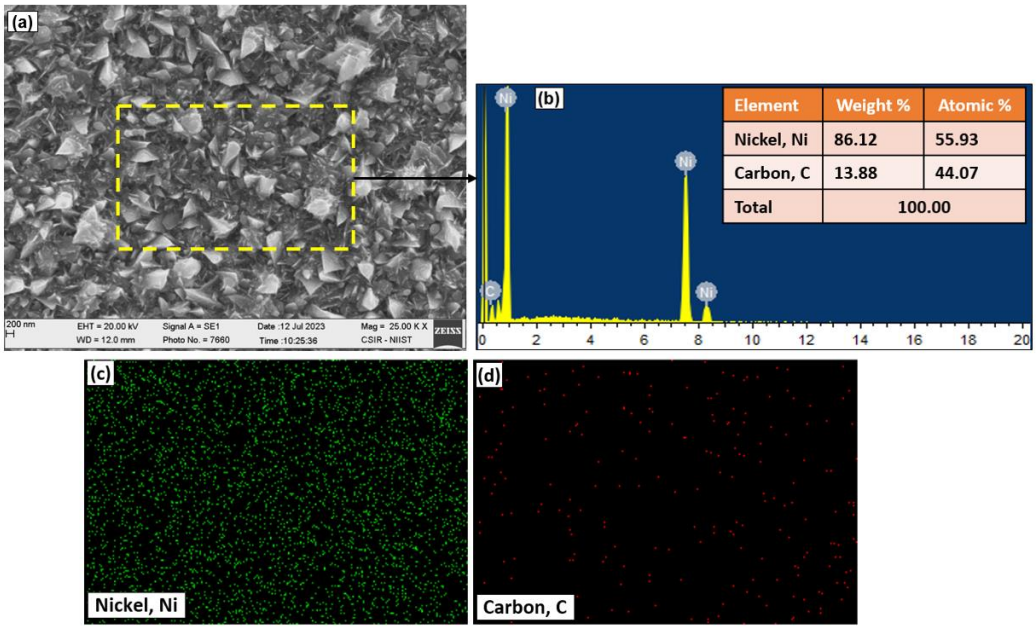

Figure 3.3 (a-d): SEM-EDS & elemental mapping of Ni-graphene coated MS surface

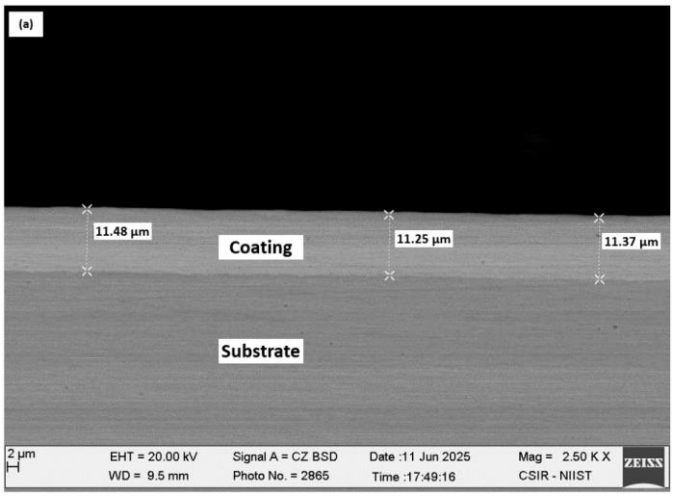

Figure 3.4 (a): Cross-sectional SEM micrograph of Ni-graphene coated MS

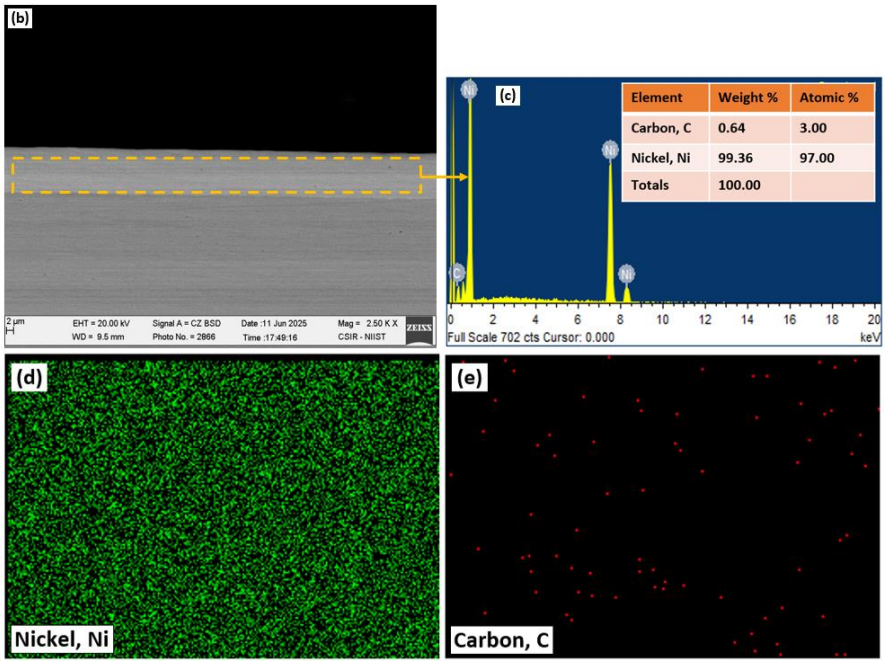

Figure 3.4 (b-e): Cross-sectional SEM-EDS & elemental mapping of Ni-graphene coated MS

3.3.2. X-ray diffraction studies

X-ray diffraction patterns of pure Ni and Ni-graphene coated samples are shown in **Figure 3.5.** respectively. From the data, three peaks of Ni at 2θ corresponding to 44.32°, 51.77° and 76.3° are assigned to (111), (200) and (220) Bragg reflections of the face-centered cubic (fcc) structure of metallic nickel [12]. The peaks corresponding to graphene ((008), (211)) are short owing to its low concentration and due to the high relative intensity of Ni peaks. The peak broadening in Ni-graphene composite coating is observed to be higher than that of pure Ni coating which is further evident from the FWHM values. This indicates a significant reduction in crystallite size in the case of composite coating (**Table 3.2**). The addition of graphene favors the crystal growth along the low-energy plane (111). This further signifies that the addition of graphene lowers the surface energy of the composite coating which also leads to positive influence on corrosion resistance as well as superhydrophobicity [21].

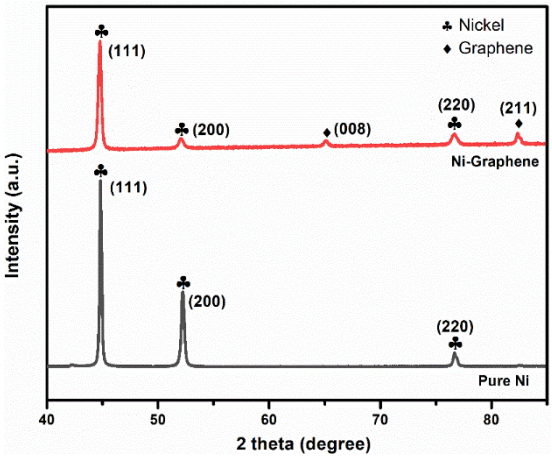

Figure 3.5: XRD pattern of pure Ni & Ni-graphene coatings

Table 3.2. Crystallite size calculations using Scherrer equation in Ni-graphene system

Coating	Angular position (θ) (radians)	cos θ (radians)	Full width half-maxima (FWHM) (radians)			Average crystallite size (D) (nm)
			Sample β_s	Instrument β_i	Corrected β_{corr}	
Pure Ni	0.390	0.925	2.616×10^{-3}	1.395×10^{-4}	2.612×10^{-3}	57.4
Ni-graphene	0.391	0.924	4.710×10^{-3}		4.709×10^{-3}	31.9

3.3.3. Wettability Studies

Chemical composition, free energy, and morphology of the surface all affect the wettability of a coating. **Figure 3.6.** shows the contact angle of the water droplet on the coated MS (pure Ni, Ni-graphene, MA-Ni-graphene) where MA is Myristic acid. As it is evident from the WCA measurements there was a gradual increase in the hydrophobicity of the surface (i.e. **123.5**° to **152**°). The pine cone micro-nanostructure along with the action of low surface energy material MA (27.4 dynes/ cm) reduces the contact area between the solid-liquid interface and water by forming a thin, strong cohesive layer on Ni-graphene coating. Whenever applied over a surface, MA can self-assemble in an organized manner through hydrogen bonding of carboxyl groups as well as hydrophobic interaction in-between methyl groups. These hydrophobic chains create a barrier that prevents water from wetting the surface. As a result, water droplets tend to bead up and roll off the surface instead of spreading out and wetting the surface.

Water droplets will exist in superhydrophobic Cassie State over the coated surface as a result of incorporation of graphene followed by modification with low surface energy material MA [22]. According to the Wenzel equation,

$$\cos \theta_w = r \cos \theta \qquad (3.1.)$$

where, θ_w is the contact angle of liquids on a rough surface, θ is the contact angle on a flat surface and r is the roughness factor [23]. This equation implies that as the roughness of the surface increases, the hydrophobic surface becomes more hydrophobic. In Ni-graphene composite coating, the micro-nano pinecone structure makes the surface rougher. It was the composite micro/nanostructure formed by Ni pinecones and graphene, which provided sufficient "air pockets" so that the water droplets bounce and roll off immediately.

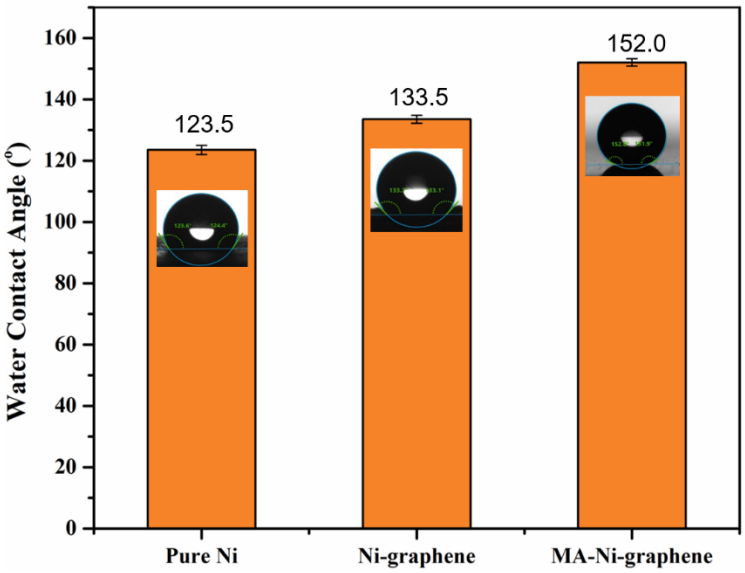

Figure 3.6. WCAs of coated sample (a) Pure Ni, (b) Ni-graphene, (c) MA-Ni-graphene

3.3.4. Mechanical stability test

Mechanical stability is a crucial measure of superhydrophobic material's practical application. A mechanical durability test was carried out to test the robustness of the developed Ni-graphene coating. The coated substrate was put on 400 grit sandpaper. Additionally, a 100 g weight was used as an outside force. In this procedure, the Ni-graphene coated substrate was moved twenty centimeters along the ruler's direction, followed by a rotation of 90°, and another twenty centimeters in the direction of the ruler. The entire procedure was referred to as a cycle.

The WCA of the sample did not change significantly after 30 cycles, and it was still greater than 140° (**Figure 3.7.**). It can be concluded that the abrasion process only damaged the outermost structure, while the internal hierarchical structure remained intact. The results indicate that the Ni-graphene coatings with rough and stable pinecone-like micro/nanostructure have better resistance to repeated mechanical abrasion, maintaining excellent superhydrophobicity after repeated cycles of sandpaper abrasion. It was observed that the incorporated graphene not only provide enough roughness but also excellent mechanical stability for the composite coating.

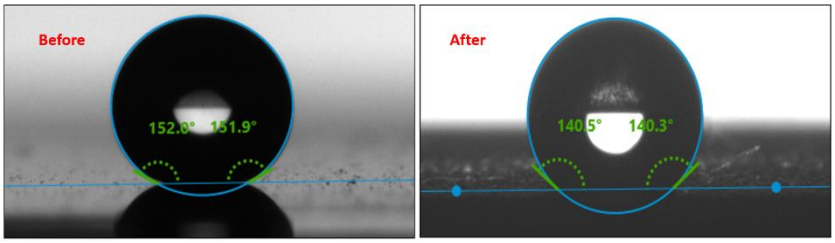

Figure 3.7. WCAs of Ni-graphene samples before and after abrasion cycles

3.3.5 Self-cleaning tests

One of the most important applications of superhydrophobic surfaces is self-cleaning. In this study, the self-cleaning action of Ni-graphene was studied using chalk powder as contaminant. Because of the superhydrophobic nature of the coating surface (**Figure 3.8.**), the droplet was still spherical, bounded with chalk powder, and got rolled out from the surface retaining its superhydrophobicity. A comparison with the uncoated MS showed that chalk powder adhered to the surface and remained sticky. The process was carried out several times till the Ni-graphene composite coating maintained its self-cleaning ability.

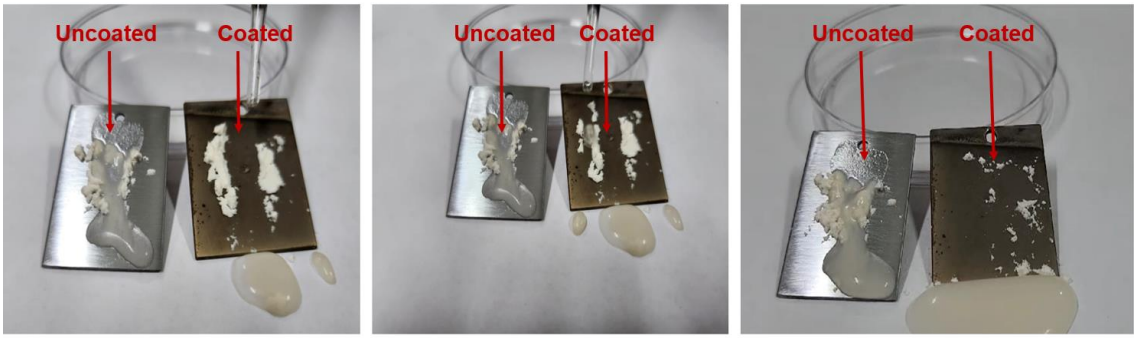

Figure 3.8. Self-cleaning action of Ni-graphene coating

3.3.6. Electrochemical characterization

Figure 3.9 (a) shows the potentiodynamic polarization curves (Tafel plots) of samples by plotting the potential scanned from cathodic region to the anodic region vs. logarithm of current density. The values of corrosion current density (i_{corr}) and corrosion potential (E_{corr}), obtained by the extrapolation of cathodic and anodic sides are given in **Table 3.3.** Variation of E_{corr} value

towards more positive direction and the lower i_{corr} indicates the improved corrosion resistance of coatings, especially in the case of composite coatings. Presence of graphene in the coating leads to a substantial reduction in the i_{corr} value of Ni-graphene to 0.516 µA cm^{-2} from 4.143 µA cm^{-2} in the case of pure Ni and 17.110 µA cm^{-2} in case of bare mild steel sample. The corresponding shift of the graph towards the left-hand side was observed. The reduction in i_{corr} values of the coated samples indicates the decreased ionic diffusion on the surface during the corrosion process. The Ni-graphene composite coating is more cathodic with respect to other samples and possesses excellent corrosion protection (E_{corr} MS: -0.678 V, Pure Ni: -0.417 V, Ni-graphene: -0.389 V).

The inclusion of graphene into the Ni matrix has improved the corrosion resistance behavior by filling surface defects such as small holes and porosities Graphene also act as a barrier to corrosive ion diffusion towards the electrode surface. The uniformly distributed graphene in the Ni matrix forms a passive layer between corrosive media and the coated surface. Thus the corrosion rate (0.0055) of Ni-graphene composite coating is exceptionally low compared to mild steel and pure Ni samples [24].

Electrochemical impedance spectroscopy measurements were performed in order to get a better understanding of the anticorrosive nature of coatings. Nyquist plots of bare mild steel, pure Ni and Ni-graphene composite coatings were obtained in 3.5% NaCl medium at the respective open circuit potentials (**Figure 3.9. (b)**). The Nyquist plots of all the samples showed a single semi-circular arc in the investigated frequency region. The bare MS samples can be fitted with the circuit the equivalent electrochemical circuit (EEC) $R_s(C_{dl}R_{ct})$ (**Figure 3.9. (c)**) and all the coated samples are well fitted for the equivalent circuit of $R_s(C_cR_c(C_{dl}R_{ct}))$ (**Figure 3.9. (d)**). R_s is the solution resistance, R_{ct} and C_{dl} are the charge transfer resistance and double-layer capacitance, respectively.

Instead of using pure capacitance due to the possibility of a dispersion effect between the metal/coating system, C represents a constant phase angle element (CPE). The coating offered protection indicated by the resistance element R_c. The results of the EIS studies also indicated a similar trend in the corrosion resistance that was observed in potentiodynamic polarization studies. The increased radius of semi-circular arc indicated better anti-corrosion property of the Ni-

graphene composite coating than other samples. The superior value of R_{ct} obtained for the composite coating suggests more protection capability against corrosion.

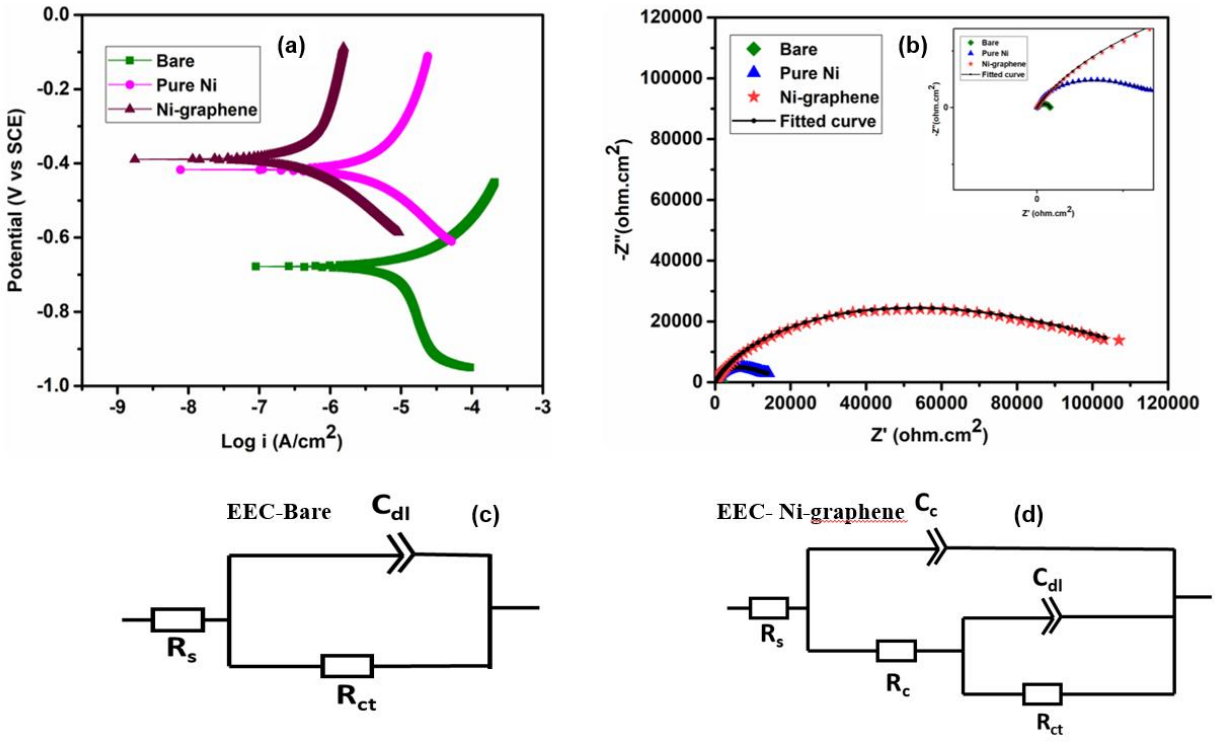

Figure 3.9. Electrochemical study for the Ni-graphene composite coatings **(a)** Tafel plot, **(b)** Nyquist plot, **(c)** EEC for the bare sample, **(d)** EEC for Ni-graphene coated sample

Table 3.3. Electrochemical parameters obtained and corrosion inhibition efficiency of Ni-graphene coated samples

S/N	Substrate	Potentiodynamic polarisation				EIS	
		E_{corr} (V)	i_{corr} (μAcm^{-2})	η (%)	Corr.rate (mmpy)	R_{ct} (Ω cm^2)	η (%)
1.	Bare Mild Steel	-0.678	17.110	-	0.2013	3.955×10^2	-
2.	Pure Nickel	-0.417	4.143	75.78	0.0446	3.222×10^4	98.77
3.	Ni-graphene	-0.389	0.516	96.98	0.0055	1.315×10^5	99.70

3.3.7. Tribological Characteristics

Figure 3.10(a) shows the variation of coefficient of friction of the electrodeposited Ni-graphene coating at different loads (2, 3, 4, and 5N) load for 15 min under non-lubricated conditions. Compared with the pure nickel, the friction coefficient of the Ni–graphene composite coating decreased and wear resistance was increased appreciably (**Figure 3.10(b)**). The presence of graphene and grain refinement observed in the developed composite coating gives the lowest coefficient of friction values in comparison with pure Ni coating under different loads. Graphene embedded in the Ni matrix blocks or delays the dislocation movements in the nickel metal matrix preventing excessive wear.

The layered hexagonal structure of the crystal lattice of graphene permits sliding movement of the parallel planes. Due to the weak bonding between the planes, the shear strength is low along the direction of sliding. With continuous friction and wear, graphene particles are pulled out from the composite coating, forming a layer of self-lubricating film between the friction pairs, which significantly improves the wear resistance of the composite coating. This film forms an interface layer between the pin and the disc. Thus the strongly adhered lubrication film formed by graphene prevents the surface from further wear.

SEM studies of the worn surfaces of Ni-graphene composite coatings are shown in **Figure 3.11**. Based on the wear results it can be concluded that the graphene incorporated within the Ni matrix block or at least delay the dislocation movements in the matrix resulting in minimal plastic deformation, resulting in enhanced load carrying capacity. This was demonstrated as improved wear resistance. The abrasive effect of the agglomerated graphene detached from the composite coating may be the cause of the pit development that results from gouging of graphene as it is dragged out of the worn surface under combined compression and shear loads. These pits resemble the etch pits on the worn surface.

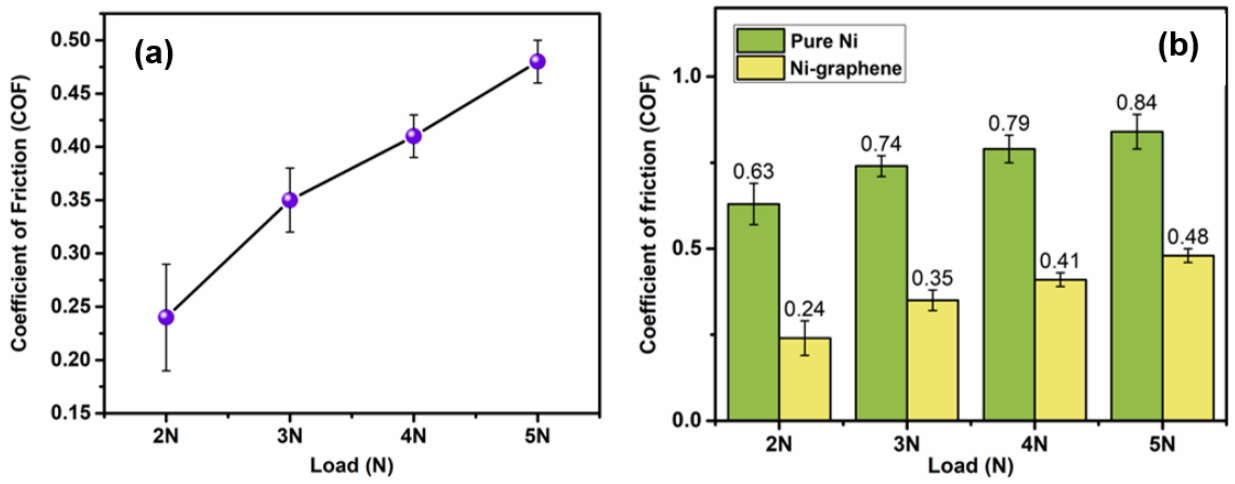

Figure 3.10. (a) Load vs COF of Ni-graphene coated samples, **(b)** Comparison of COF values of pure Ni & Ni-graphene coated samples under different loads

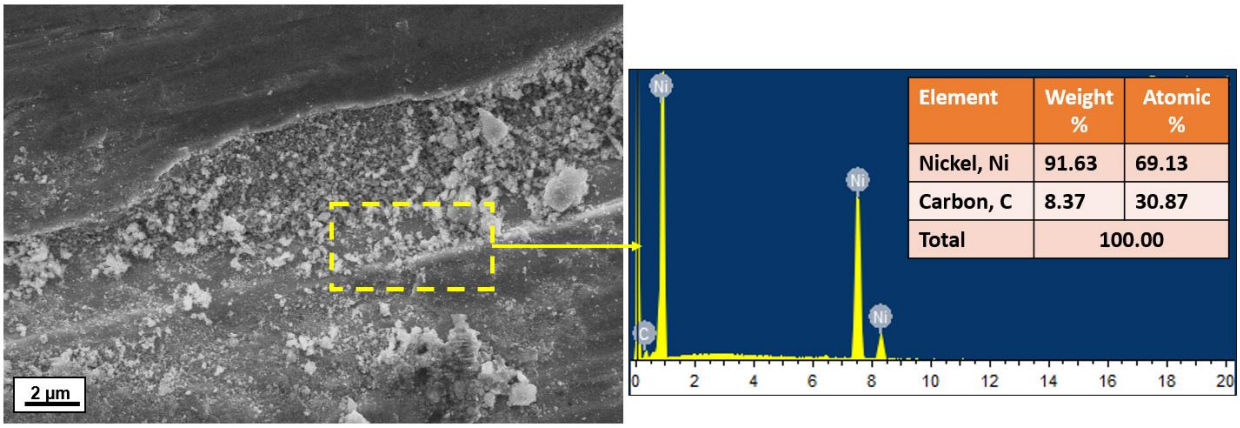

Element	Weight %	Atomic %
Nickel, Ni	91.63	69.13
Carbon, C	8.37	30.87
Total	100.00	

Figure 3.11. SEM-EDS of the worn surface of Ni-graphene coated sample

3.4. Conclusions

Nickel–graphene composite coatings have been successfully coated over mild steel by electrochemical co-deposition technique. This study explores surface morphology, phase composition, wettability, and corrosion resistance properties of the Ni –graphene composite coatings. The coatings exhibited compact and crack-free morphology, which was evident from the

SEM images. Wettability studies reveal that the Ni-graphene coating has a water contact angle (CA) of 152º, indicating its superhydrophobicity and the coating also had self-cleaning properties. The composite coatings exhibited improved corrosion resistance and wear resistance. These findings collectively demonstrate that Ni–graphene composite coatings offer a promising surface modification strategy for enhancing the functional performance of mild steel in corrosive and abrasive environments.

References

[1] G. Cieślak, M. Trzaska, Tribological properties of nanocomposite Ni/graphene coatings produced by electrochemical reduction method, Compos. Theory Pract. R. 16, nr (2016) 79–83.

[2] S. Singh, S. Samanta, A.K. Das, R.R. Sahoo, Tribological investigation of Ni-graphene oxide composite coating produced by pulsed electrodeposition, Surfaces and Interfaces 12 (2018) 61–70. https://doi.org/https://doi.org/10.1016/j.surfin.2018.05.001.

[3] N. Wang, D. Xiong, Y. Deng, Y. Shi, K. Wang, Mechanically Robust Superhydrophobic Steel Surface with Anti-Icing, UV-Durability, and Corrosion Resistance Properties, ACS Appl. Mater. \& Interfaces 7 (2015) 6260–6272. https://doi.org/10.1021/acsami.5b00558.

[4] L.B. Boinovich, S. V Gnedenkov, D.A. Alpysbaeva, V.S. Egorkin, A.M. Emelyanenko, S.L. Sinebryukhov, A.K. Zaretskaya, Corrosion resistance of composite coatings on low-carbon steel containing hydrophobic and superhydrophobic layers in combination with oxide sublayers, Corros. Sci. 55 (2012) 238–245. https://doi.org/https://doi.org/10.1016/j.corsci.2011.10.023.

[5] F. Shi, J. Niu, J. Liu, F. Liu, Z. Wang, X.Q. Feng, X. Zhang, Towards understanding why a superhydrophobic coating is needed by water striders, Adv. Mater. 19 (2007) 2257–2261. https://doi.org/10.1002/adma.200700752.

[6] S. Zheng, C. Li, Q. Fu, M. Li, W. Hu, Q. Wang, M. Du, X. Liu, Z. Chen, Fabrication of self-cleaning superhydrophobic surface on aluminum alloys with excellent corrosion resistance, Surf. Coatings Technol. 276 (2015) 341–348. https://doi.org/https://doi.org/10.1016/j.surfcoat.2015.07.002.

[7] S. VB, An Overview on the Preparation, Characterization and Properties of Electrodeposited-Metal Matrix Nanocomposites, Nanosci. Technol. Open Access 1 (2014). https://doi.org/10.15226/2374-8141/1/3/00120.

[8] V. S, S. B, B.M. Praveen, B.K. Devendra, The effect of Graphene content on the corrosion and mechanical properties of an electrodeposited Ni-Graphene coating, Appl. Surf. Sci. Adv. 11 (2022) 100310. https://doi.org/10.1016/j.apsadv.2022.100310.

[9] A. Jabbar, G. Yasin, W.Q. Khan, M.Y. Anwar, R.M. Korai, M.N. Nizam, G. Muhyodin, Electrochemical deposition of nickel graphene composite coatings effect of deposition

temperature on its surface morphology and corrosion resistance, RSC Adv. 7 (2017) 31100–31109. https://doi.org/10.1039/c6ra28755g.

[10] J. A, J. S Jayan, A. Saritha, S. A.S., G. Venu, Superhydrophobic graphene-based materials with self-cleaning and anticorrosion performance: An appraisal of neoteric advancement and future perspectives, Colloids Surfaces A Physicochem. Eng. Asp. 606 (2020) 125395. https://doi.org/https://doi.org/10.1016/j.colsurfa.2020.125395.

[11] A. Siddaiah, P. Kumar, A. Henderson, M. Misra, P.L. Menezes, Surface Energy and Tribology of Electrodeposited Ni and Ni–Graphene Coatings on Steel, Lubricants 7 (2019). https://doi.org/10.3390/lubricants7100087.

[12] L. Xiang, Q. Shen, Y. Zhang, W. Bai, C. Nie, One-step electrodeposited Ni-graphene composite coating with excellent tribological properties, Surf. Coatings Technol. 373 (2019) 38–46. https://doi.org/10.1016/j.surfcoat.2019.05.074.

[13] C. Liu, F. Su, J. Liang, Producing cobalt–graphene composite coating by pulse electrodeposition with excellent wear and corrosion resistance, Appl. Surf. Sci. 351 (2015) 889–896. https://doi.org/https://doi.org/10.1016/j.apsusc.2015.06.018.

[14] G. Huang, H. Wang, P. Cheng, H. Wang, B. Sun, S. Sun, C. Zhang, M. Chen, G. Ding, Preparation and characterization of the graphene-Cu composite film by electrodeposition process, Microelectron. Eng. 157 (2016) 7–12. https://doi.org/https://doi.org/10.1016/j.mee.2016.02.006.

[15] C.M.P. Kumar, T. V Venkatesha, R. Shabadi, Preparation and corrosion behavior of Ni and Ni–graphene composite coatings, Mater. Res. Bull. 48 (2013) 1477–1483. https://doi.org/https://doi.org/10.1016/j.materresbull.2012.12.064.

[16] S. Khorsand, K. Raeissi, F. Ashrafizadeh, Corrosion resistance and long-term durability of super-hydrophobic nickel film prepared by electrodeposition process, Appl. Surf. Sci. 305 (2014) 498–505. https://doi.org/https://doi.org/10.1016/j.apsusc.2014.03.123.

[17] G. Yasin, M.A. Khan, M. Arif, M. Shakeel, T.M. Hassan, W.Q. Khan, R.M. Korai, Z. Abbas, Y. Zuo, Synthesis of spheres-like Ni/graphene nanocomposite as an efficient anti-corrosive coating; effect of graphene content on its morphology and mechanical properties, J. Alloys Compd. 755 (2018) 79–88. https://doi.org/10.1016/j.jallcom.2018.04.321.

[18] W. Zhang, B. Li, T. Mei, M. Li, M. Hong, Z. Yuan, H. Chu, Effects of graphene oxide and

current density on structure and corrosion properties of nanocrystalline nickel coating fabricated by electrodeposition, Colloids Surfaces A Physicochem. Eng. Asp. 648 (2022) 129220. https://doi.org/https://doi.org/10.1016/j.colsurfa.2022.129220.

[19] Y. Shao, J. Wang, H. Wu, J. Liu, I.A. Aksay, Y. Lin, Graphene based electrochemical sensors and biosensors: A review, Electroanalysis 22 (2010) 1027–1036. https://doi.org/10.1002/elan.200900571.

[20] Z. Bai, B. Zhang, Fabrication of superhydrophobic reduced-graphene oxide/nickel coating with mechanical durability, self-cleaning and anticorrosion performance, Nano Mater. Sci. 2 (2020) 151–158. https://doi.org/10.1016/j.nanoms.2019.05.001.

[21] K.S. Jyotheender, C. Srivastava, Ni-graphene oxide composite coatings: Optimum graphene oxide for enhanced corrosion resistance, Compos. Part B Eng. 175 (2019) 107145. https://doi.org/10.1016/j.compositesb.2019.107145.

[22] S. Parvate, P. Dixit, S. Chattopadhyay, Superhydrophobic Surfaces: Insights from Theory and Experiment, J. Phys. Chem. B 124 (2020) 1323–1360. https://doi.org/10.1021/acs.jpcb.9b08567.

[23] H. Yang, P. Pi, Z.-Q. Cai, X. Wen, X. Wang, J. Cheng, Z. Yang, Facile preparation of super-hydrophobic and super-oleophilic silica film on stainless steel mesh via sol–gel process, Appl. Surf. Sci. 256 (2010) 4095–4102. https://doi.org/https://doi.org/10.1016/j.apsusc.2010.01.090.

[24] M.R.A. Karim, S.A. Raza, M.I. Khan, A.B. Tahir, E.U. Haq, M. Pavese, Electrodeposition of nickel–graphene nanoplatelets (GNPs) composite coatings and evaluation of their morphological, electrochemical, and thermo-mechanical properties, Appl. Phys. A Mater. Sci. Process. 128 (2022). https://doi.org/10.1007/s00339-022-05650-6.

Chapter 4
Exploring electrodeposited Ni-MoS_2 coatings for anti-corrosion, wear resistance, and catalytic performance

Abstract

This chapter deals with the development of Ni-MoS_2 coating over mild steel substrate. A uniform and compact Ni-MoS_2 coating was obtained at a current density of 5 A/dm^2 by co-deposition MoS_2 with in the nickel matrix. In comparison with pure Ni coating, Ni-MoS_2 composite coating has improved microhardness, superior corrosion resistance and lower friction coefficient. The results indicated that the layered structure and lubricity of MoS_2 particles are the main reasons for the improved tribological properties of Ni-MoS_2 coatings. The composite coatings were also studied in detail for their catalytic potential in overall water splitting by depositing Ni-MoS_2 over stainless steel mesh.

4.1. Introduction

In the pursuit of advanced surface engineering solutions, the development of multi-functional coatings has emerged as a vital area of research, driven by the need for materials that can endure harsh operational environments while offering superior performance in diverse applications [1]. Industries such as energy, transportation, chemical processing, and manufacturing require materials with enhanced properties, including corrosion resistance, anti-wear properties, and catalytic efficiency. Nickel (Ni) is a widely used as a material for coatings over metallic substrates because of its excellent corrosion resistance, thermal stability, and mechanical strength [2–4]. However, its performance can be further enhanced by incorporating functional secondary phases, such as transition metal dichalcogenides (TMDs).

MoS_2, a prominent TMD, delivers a synergistic combination of mechanical robustness, superior lubrication, wear resistance, electrochemical stability, and catalytic activity [5,6]. When incorporated into the nickel matrix, MoS_2 not only improves tribological behavior but also enhances catalytic performance, particularly in applications like overall water splitting and energy conversion processes [7].

In recent years, electrodeposition has emerged as a versatile technique for producing composite coatings with tailored properties. By combining the inherent advantages of nickel and MoS_2, electrodeposited Ni-MoS_2 coatings offer a promising solution for addressing critical challenges in diverse applications, including aerospace, automotive, and energy storage [8,9]. Electrodeposition has proven to be a versatile and cost-effective method for fabricating Ni-MoS_2 composite coatings. This technique offers significant advantages, such as precise control over the coating composition, thickness, and morphology. Furthermore, electrodeposition is scalable and compatible with complex geometries, making it suitable for industrial applications [10].

He et al. [11] developed Ni-P-MoS_2 composite coating and examined the wear resistance and mechanical characteristics. According to Cardinal et al. [1], MoS_2 self-lubrication resulted in a 50% reduction in the friction coefficient compared to Ni–W, from 0.27 to 0.14. The co-deposition of Ni-MoS_2 composite coatings using the rotating disc electrode approach has been investigated by Chang et al. [12]. They found that the weight percentage of MoS_2 in the coatings was influenced by the bath temperature and the amount of MoS_2 particles. Guler et al. [13] examined the effect of pH and surfactant concentration affected the coatings' tribological behavior. The impact of MoS_2 on the microstructure and characteristics of the Ni-based alloy coating was examined by Han et al. [14].

In order to further improve the functionality of the developed nickel composite coatings, the idea that 2D materials have good catalytic performance due to more active site was utilised in this work. The objective of this work is to explore the development, characterization, and evaluation of the multi-functional characteristics of Ni–MoS_2 composite coating demonstrating a unique combination of enhanced mechanical, tribological, and electrochemical properties. By systematically varying the deposition parameters, such as electrolyte composition, current density, and deposition time, the study aims to optimize the structural and morphological characteristics of the coatings. These parameters are correlated with the coatings' properties, including corrosion

resistance, anti-wear properties etc. The synergistic combination of Ni and MoS_2 in a composite coating can potentially leverage the best attributes of both components, leading to multifunctional coatings with diverse industrial applications. The findings could pave the way for advanced surface engineering solutions in fields such as renewable energy systems, chemical processing, and tribology.

4.2. Materials & methods

4.2.1. Materials

Nickel sulphate ($NiSO_4 \cdot 6H_2O$, 98%), Nickel chloride ($NiCl_2 \cdot 6H_2O$, 98%), Boric acid (H_3BO_3, 99.5%) and Sodium chloride (NaCl, 98%) were purchased from Merck. Sodium lauryl sulphate (SDS, 99%) and Saccharin ($C_7H_5NO_3S$, 99.5%) were obtained from Alfa Aesar. Cetyltrimethylammonium bromide (CTAB, $CH_3(CH_2)_{15}N(Br)(CH_3)_3$) and Coumarin were obtained from Himedia chemicals. Molybdenum disulphide particles (MoS_2, 98%, ~1 µm) were supplied by Sigma-Aldrich. All the chemicals were of analytical grade and used without further purification.

4.2.2. Coating preparation

Ni–MoS_2 composite coatings were deposited on mild steel substrates from Ni Watts bath containing $NiSO_4 \cdot 6H_2O$ (250 g/l), $NiCl_2 \cdot 6H_2O$ (45 g/l), and H_3BO_3 (40 g/l). Molybdenum disulphide particles were dispersed in the Watts bath along with surfactant SLS (0.5 g/l) and grain refiner saccharin (1 g/l) (Table 1). Secondary grain refiner, coumarin (4 g/l) and additional surfactant CTAB (0.5 g/l) was also added to the bath. The Ni-MoS_2 bath was kept at a pH of 4–4.5. MoS_2 particles were dispersed using an ultrasonicator for 30 min.

Nickel plate (7 cm × 5 cm × 1 cm, 99.7 % purity) and mild steel substrate (SSM) (6 cm × 6 cm, purity ≥ 99.5 %) were used as anode and cathode, respectively. All the mild steel samples used for coating were ground using SiC papers ranging from 80 to 1000 grits, followed by degreasing in acetone and distilled water, ultrasonically cleaned, and dried in the oven. MS samples were further surface activated by dipping in 0.01M HCl and 0.1M NaOH. The anode, Ni plate was polished using SiC papers of grit 80 and 100. This was followed by degreasing in acetone and distilled water and finally drying in the oven. Electrodeposition parameters including current

density (2–5A/dm^2), temperature (40–60 ˚C), time (15–30 min), and stirring rate (400–600 rpm) were varied. The concentration of MoS_2 particles was also varied in the range (1–3) wt% (**Table 4.1.**).

Finally Ni-MoS_2 was deposited at optimized conditions of current density of 5 A/dm^2 for 40 min at a temperature of 40 ˚C at a stirring rate of 400 rpm and 1 wt% concentration of MoS_2 particles. After the electrodeposition, the samples were cleaned in running distilled water followed by ultrasonic cleaning for 5 minutes in ethanol to remove loosely adsorbed particles and then subjected for further analysis.

Table 4.1. Experimental conditions for Ni-MoS_2 coating over mild steel substrate

Electrodeposition parameters	Composition or parameter	Value	Optimised Conditions
Plating solution	$NiSO_4.6H_2O$	250 g/l	-
	$NiCl_2.6H_2O$	60 g/l	-
	H_3BO_3	9 g/l	-
	Saccharin	1 g/l	-
	CTAB	0.5 g/l	-
	Coumarin	4 g/l	-
	SLS	0.5 g/l	-
Deposition Conditions	MoS_2	1-3 wt%	1 wt%
	Current density	2-5 A/dm^2	5 A/dm^2
	Temperature	40-60°C	40°C
	Time	15-30 minutes	15 minutes
	Stirring rate	400-600 rpm	400 rpm

4.2.3. Characterization of the coatings

The surface morphology and elemental analysis of the developed coatings were examined using Zeiss EVO 18 cryo-SEM (EDS attached). The phase composition of the samples was studied using X-ray diffraction (XRD) via a Bruker D2 Phaser X-ray diffractometer with Cu - K_α radiation (λ = 1.5406 Å) in the 0-90˚ range. The Vickers micro-hardness tester was used to measure hardness of Ni-MoS_2 coated mild steel surface under the indentation of 50 gf with 10 s dwell time. Hardness

measurements at five different locations of the specimen were done and the average value was taken.

CH Instruments electrochemical workstation (CHI608E, CH Instruments Inc.) equipped with standard three-electrode cell was used for electrochemical impedance spectroscopy and potentiodynamic polarization studies at room temperature in 3.5 wt% NaCl solution. The coated specimen with $1cm^2$ exposed surface area was used as the working electrode; saturated calomel and a platinum grid were taken as the reference and counter electrodes respectively. The specimens were kept in the electrolyte for 20 min prior to the experiment for attaining their stable open circuit potential (OCP). The potentiodynamic scan was done at a rate of 1 mV/s from −250 mV to +250 mV of the OCP values. The corrosion potential (E_{corr} vs. SCE) and corrosion current density (i_{corr}) of each sample were obtained from the applied potential vs. current Tafel plot. The impedance measurements were performed using an AC signal with a perturbation of 5 mV at OCP in the frequency range of 100 kHz - 0.01 Hz. ZsimpWin software fits the generated EIS plots to determine the electrochemical parameters. Numerous circuits were examined until the Chi-square value decreased to less than 9×10^{-4} or no further fitting improvement was observed.

Pin on disc wear testing machine (POD 4.0, DUCOM) was used to measure the wear rate and coefficient of friction at the dry condition. The measurements were done for Ni-MoS_2, pure Ni coated and bare mild steel samples. The pins with 6 mm diameter and 15 mm length were used against EN31 high carbon alloy steel disc. The mild steel pins were coated with pure Ni and Ni-MoS_2. Wear tests were done at a sliding velocity of 0.4 m/s under 2, 3, 4, and 5N standard loads at room temperature for 15 minutes.

To evaluate the catalytic potential, the electrochemical measurements were done using a three-electrode setup in 1 M KOH using a CHI660E electrochemical workstation. Platinum wire (working electrode), Ag/AgCl in saturated KCl (reference electrode), and Ni-MoS_2 coated SS mesh (counter electrode) are the electrodes employed. The voltammetric techniques LSV, CV, EIS and CA were used to analyse the electrochemical activity and stability of the electrode material. As a preliminary step before actual measurements, CV in a reduction potential region was carried out for several cycles to activate the materials. Once the CV curves became consistent, LSV measurements were carried out to analyse the current response. All the measurements were performed at a scan rate of 2 mV s^{-1}, and EIS measurements were taken at a frequency range (100

KHz to 100 mHz). Chronoamperometry (CA) for about 10 hours was performed to confirm the stability, and the polarisation curves before and after 1000 cycles were also recorded.

4.3. Results & Discussion

4.3.1 Surface morphology and elemental composition

SEM micrographs of pure Ni and Ni-MoS_2 composite coating deposited on mild steel are given in **Figure 4.1.(a-b)** and **Figure 4.2.(a-f)**, respectively. Both the coatings appeared to be uniform and compact. This demonstrates that the coatings had a compact and crack-free surface. The SEM micrograph of pure Ni (**Figure 4.1. (b)**) coating reveals a regular granular structure with larger grain size. The inclusion of MoS_2 having a mean zeta potential of -18.27 mV altered the microstructural characteristics of the composite coating. The dimension of grains in the Ni-MoS_2 coating is smaller than that of the pure Ni. MoS_2 particle addition inhibits the crystal growth and increases the nucleation sites for Ni ion reduction which results in reduced grain size in the composite coating [5,15]. The adsorbed MoS_2 could be the sites for the nucleation of nickel ions and could accelerate the crystal growth. The smaller Ni grains composed of finer Ni crystallites are seen in **Figure 4.2 (f)**.

The EDS analysis (**Figure 4.3. (a-e)**) was carried out for Ni-MoS_2 coating which revealed the presence of the elements nickel, molybdenum and sulfur that are present in the composite coating. No peaks originating from the steel substrate such as iron and carbon were detected. **Figure 4.4 (a)-(f)** shows the cross-section of Ni-MoS_2 composite coatings. The average thickness of Ni-MoS_2 coating was found to be 22.38 µm. EDS data further confirmed the presence of MoS_2 particles in the composite coating.

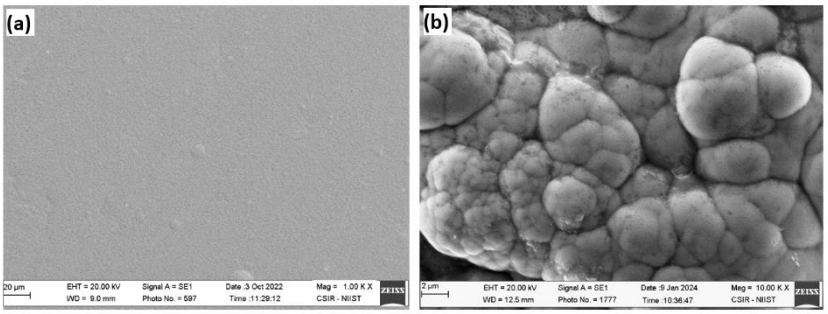

Figure 4.1 (a-b): SEM micrographs of pure Ni coated MS

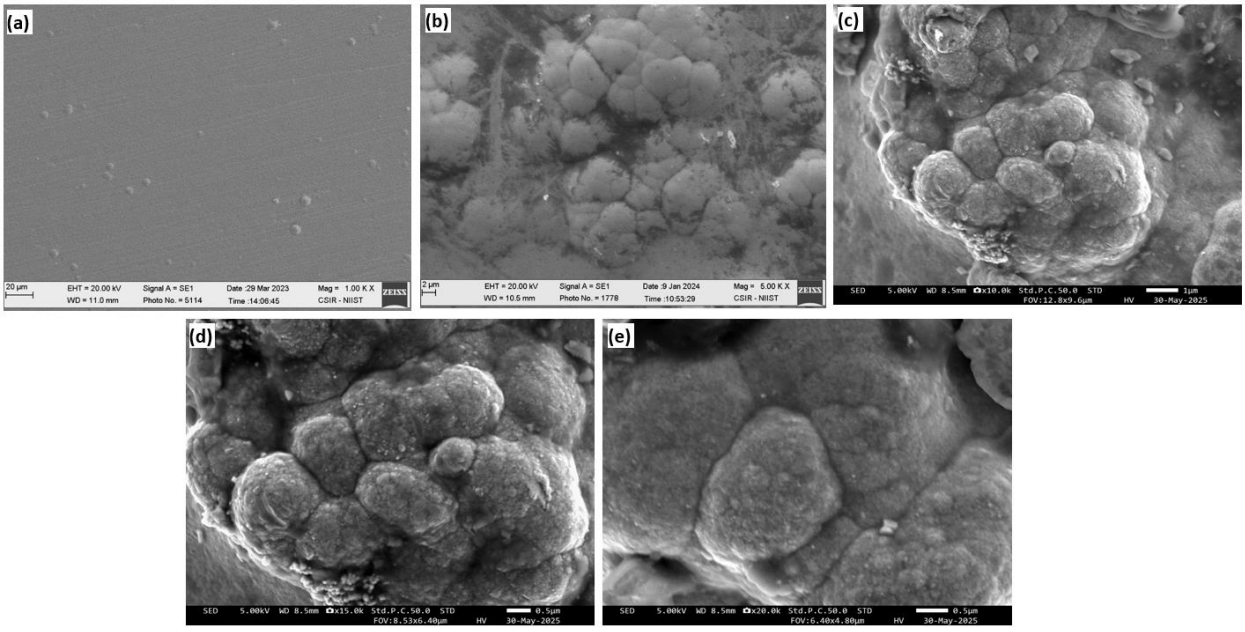

Figure 4.2 (a-e): SEM micrographs of Ni-MoS_2 coated MS

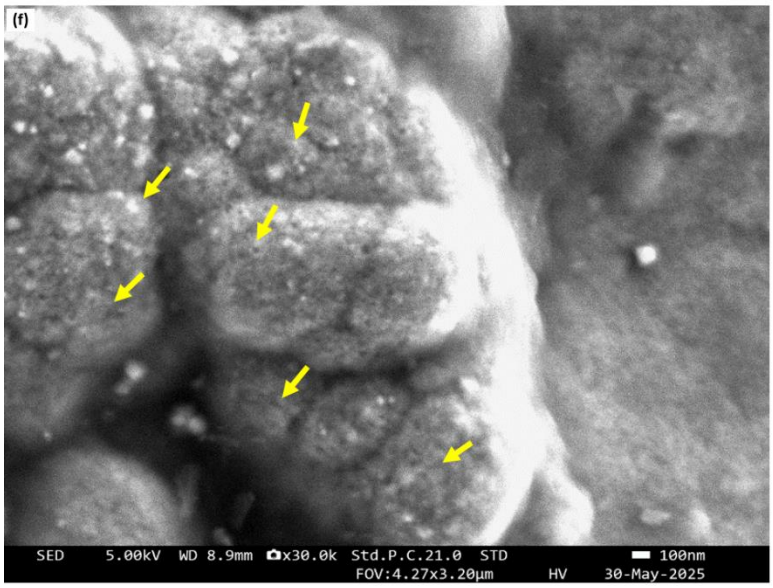

Figure 4.2 (f): Higher magnification SEM image of Ni-MoS_2 coated MS. Yellow colored arrows indicate the Ni grains composed of finer Ni crystallites

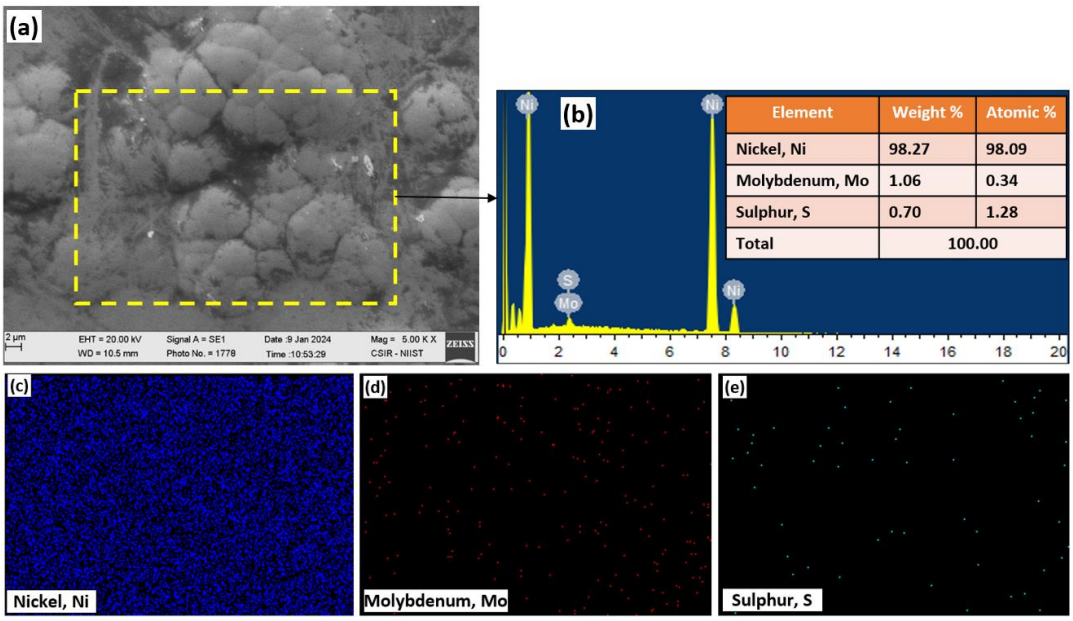

Figure 4.3 (a-e): SEM-EDS & elemental mapping of Ni-MoS_2 coated MS surface

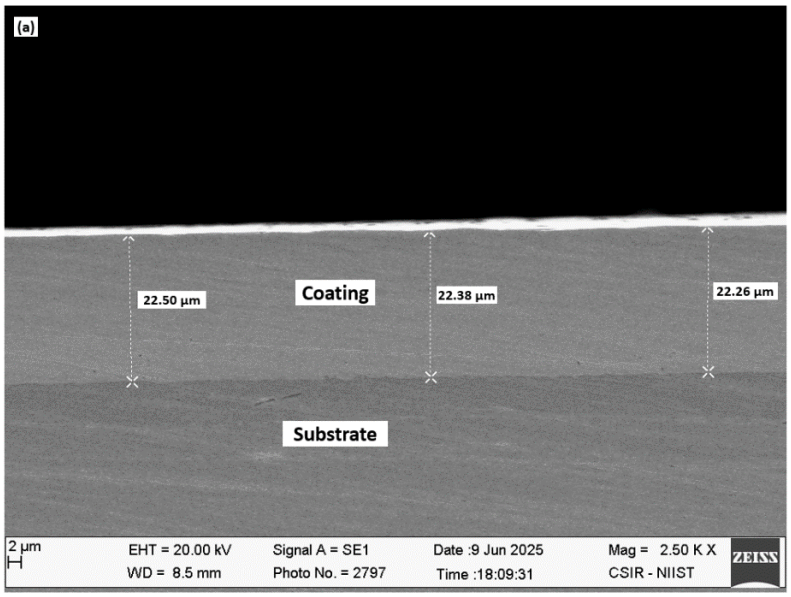

Figure 4.4 (a): Cross-sectional SEM micrograph of Ni-MoS_2 coated MS

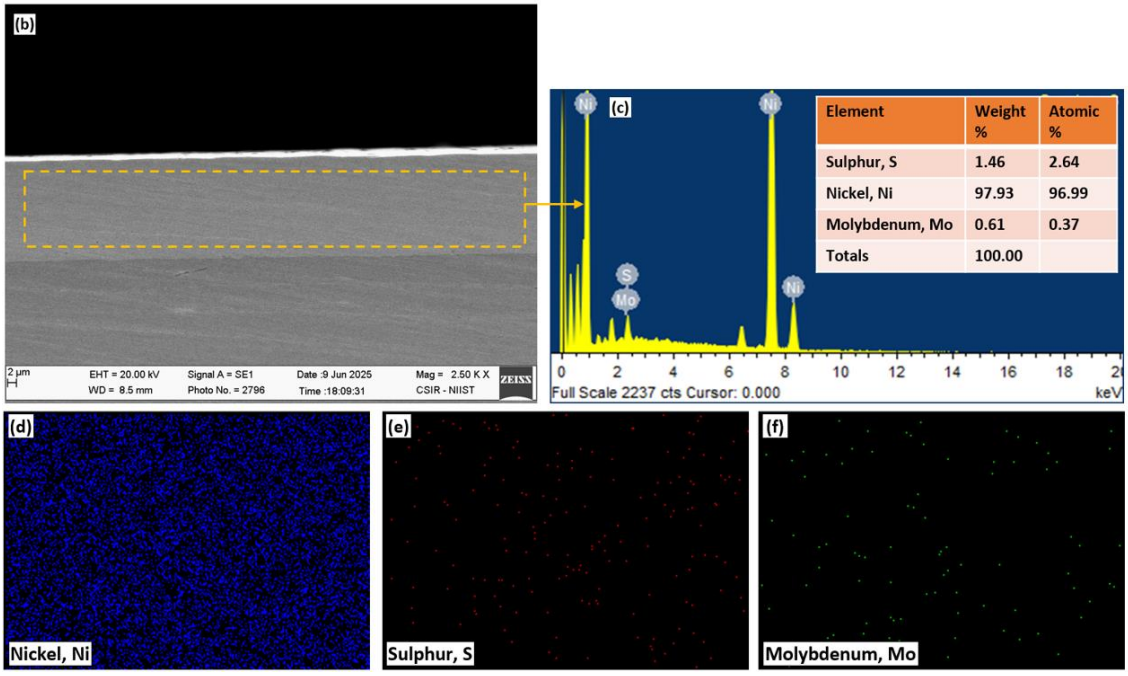

Figure 4.4 (b-f): Cross-sectional SEM-EDS & elemental mapping of Ni-MoS_2 coated MS

4.3.2. X-ray diffraction studies

X-ray diffraction patterns of pure Ni and Ni-MoS_2 coated samples are shown in **Figure 4.5.** From the data, two peaks of Ni at 2θ corresponding to 44.32° and 51.77° are assigned to (111), (200) Bragg reflections of the face-centered cubic (fcc) structure of metallic nickel. One small peak of MoS_2 is visible which can be attributed to (205) plane of hexagonal MoS_2. The peak of MoS_2 is short owing to its low concentration and due to the high relative intensity of Ni peaks. Incorporation of MoS_2 particles into the Ni matrix refines the crystallite size by providing many heterogeneous nucleation sites for the crystal growth [16]. The ideal crystal orientation for the pure Ni coating is (220), but for Ni-MoS_2 coating, the preferred crystal orientation is (111) plane. By adding MoS_2 to the Ni matrix, the preferred orientation for Ni growth is changed to a new plane and its growth is inhibited along its preferred path [17]. The grain size (crystallite size) measurements indicate that the pure Ni coating have larger grain size compared to Ni-MoS_2 composite coating (**Table 4.2**).

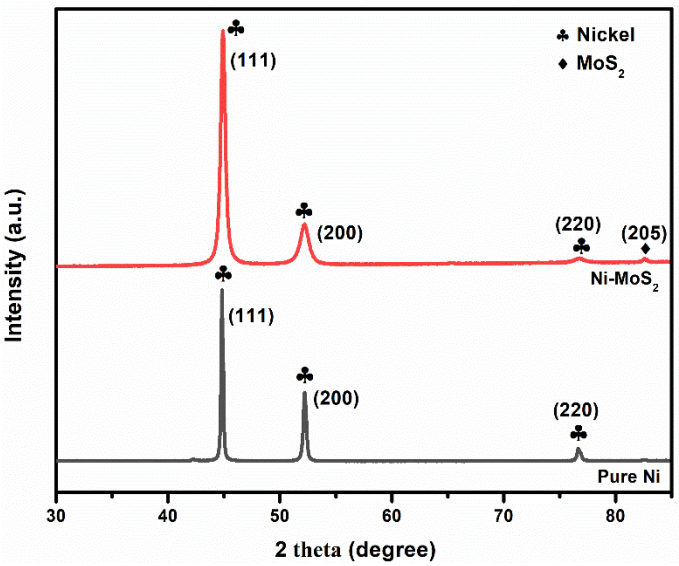

Figure 4.5: XRD pattern of pure Ni & Ni-MoS_2 coated samples

Table 4.2. Crystallite size calculations using Scherrer equation in Ni-MoS_2 system

Coating	Angular position (θ) (radians)	cos θ (radians)	Full width half-maxima (FWHM) (radians)			Average crystallite size (D) (nm)
			Sample β_s	Instrument β_i	Corrected β_{corr}	
Pure Ni	0.390	0.925	2.616×10^{-3}		2.612×10^{-3}	57.4
Ni-MoS_2	0.390	0.925	7.675×10^{-3}	1.395×10^{-4}	7.674×10^{-3}	19.5

4.3.3. Microhardness measurements

The microhardness obtained for Ni-MoS_2 composite coating (525 HV) shows higher hardness values compared to mild steel (210 HV) and pure Ni coating (350 HV) (**Figure 4.6.**). The co-deposition of MoS_2 particles within the Ni matrix resulted in the increase in microhardness of the composite coating. The MoS_2 particles are adsorbed on the Ni growth centers, preventing the nuclei growth of Ni ions. It also increases the rate of nucleation and reduction in grain size of the Ni ions. Overall, this grain refinement increases the material's strength by preventing dislocation motion and sliding of the grain boundaries. A tougher coating is produced as a result of the enhanced resistance to dislocation movement. The Hall-Petch relation explains that grain refining is primarily responsible for the increase in microhardness [18,19].

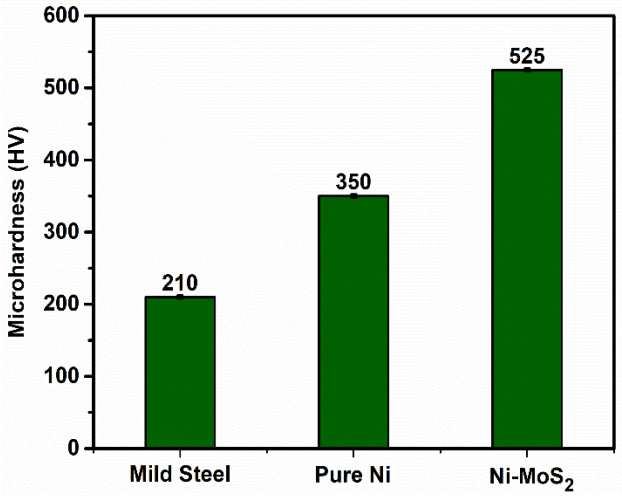

Figure 4.6. Microhardness measurements

4.3.4. Electrochemical characterization

Figure 4.7. (a) shows the potentiodynamic polarization curves (Tafel plots) of samples by plotting the potential scanned from cathodic region to the anodic region vs. logarithm of current density. The values of corrosion current density (i_{corr}) and corrosion potential (E_{corr}), obtained by the extrapolation of cathodic and anodic sides are given in **Table 4.3**. Variation of E_{corr} value towards more positive direction and the lower i_{corr} indicates the improved corrosion resistance of coatings, especially in the case of composite coatings. Presence of MoS_2 particles and the grain refinement in the coating leads to a substantial reduction in the i_{corr} value of Ni-MoS_2 to 0.923 µA cm^{-2} from 4.143 µA cm^{-2} in the case of pure Ni and 17.110 µA cm^{-2} in case of bare mild steel sample. The corresponding shift of the graph towards the left-hand side was observed. The reduction in i_{corr} values of the coated samples indicates the decreased ionic diffusion on the surface during the corrosion process. The Ni-MoS_2 composite coating is more cathodic with respect to other samples and possesses excellent corrosion protection (E_{corr} MS: -0.678 V, Pure Ni: -0.417 V, Ni-MoS_2: -0.288 V).

The inclusion of MoS_2 particles into the Ni matrix has improved the corrosion resistance behavior by filling surface defects such as small holes and porosities and acted as a barrier to corrosive ion diffusion to the electrode surface. The uniformly distributed MoS_2 particles in the deposit forms a passive layer between corrosive media and the deposited surface [20]. Thus the

corrosion rate (0.0095) of Ni-MoS_2 composite coating is exceptionally low compared to mild steel and pure Ni samples.

Electrochemical impedance spectroscopy measurements were performed in order to get a better understanding of the anticorrosive nature of coatings. Nyquist plots of bare mild steel, pure Ni and Ni-MoS_2 composite coatings were obtained in 3.5% NaCl medium at the respective open circuit potentials (**Figure 4.7. (b)**).The Nyquist plots of all the samples have showed as single semi-circular arc in the investigated frequency region. The bare MS samples can be fitted with the circuit the equivalent electrochemical circuit (EEC) $R_s(C_{dl}R_{ct})$ (**Figure 4.7 (c)**), and all the coated samples are well fitted for the equivalent circuit of $R_s(C_cR_c(C_{dl}R_{ct}))$ (**Figure 4.7 (d)**). R_s is the solution resistance, and R_{ct} and C_{dl} are the charge transfer resistance and double-layer capacitance, respectively. Instead of using pure capacitance due to the possibility of a dispersion effect between the metal/coating system, *C* represents a constant phase angle element (CPE). The coating offered protection by the resistance element *R*c. The results of the EIS studies also indicated a similar trend in the corrosion resistance that was observed in potentiodynamic polarization studies. The increased radius of semicircular arc indicated the better anticorrosion property of the Ni-MoS_2 composite coating than other samples. The superior value of R_{ct} obtained for the composite coating as offered more protection capability against corrosion.

Table 4.3. Electrochemical parameters obtained and corrosion inhibition efficiency of Ni-MoS_2 coated samples

S/N	Substrate	Potentiodynamic polarisation				EIS	
		E_{corr} (V)	i_{corr} (μAcm^{-2})	η (%)	Corr.rate (mmpy)	R_{ct} (Ω cm^2)	η (%)
1.	Bare Mild Steel	-0.678	17.110	-	0.2013	3.955×10^2	-
2.	Pure Nickel	-0.417	4.143	75.78	0.0446	3.222×10^4	98.77
3.	Ni-MoS_2	-0.288	0.923	94.60	0.0095	1.269×10^5	99.68

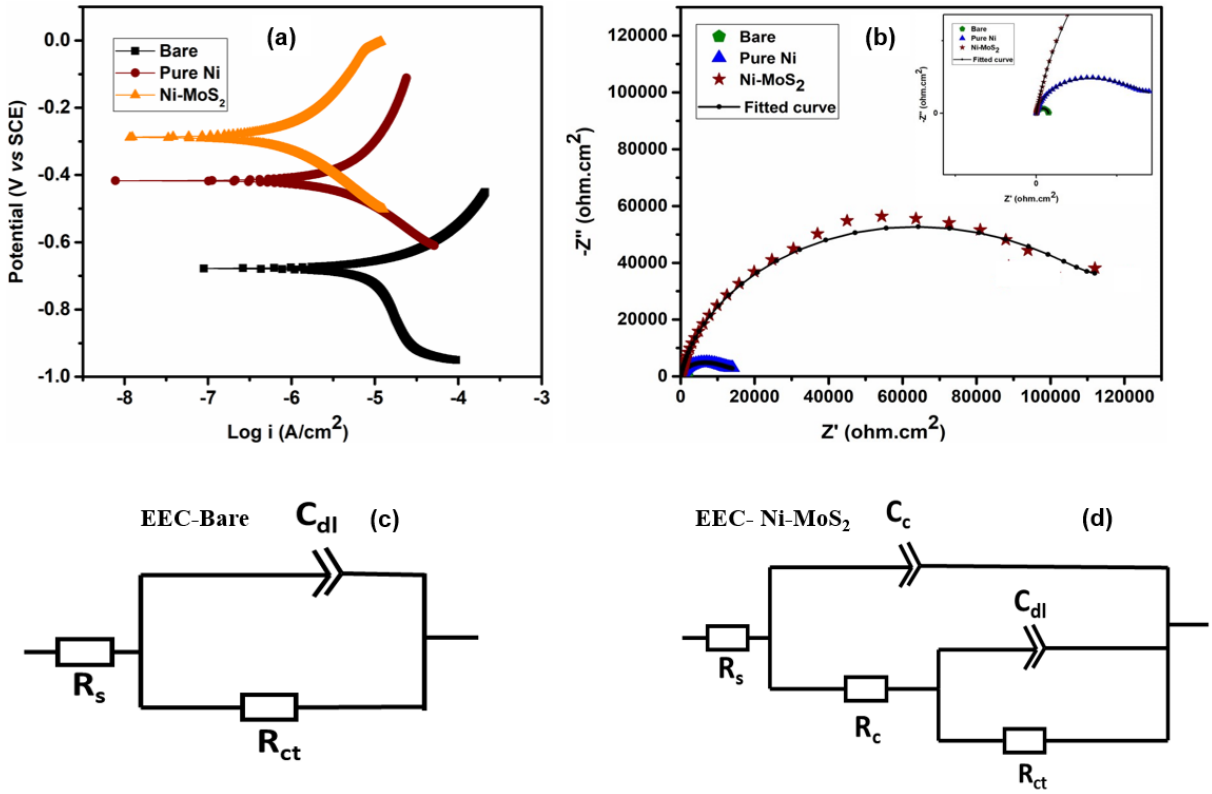

Figure 4.7. Electrochemical study for the Ni-MoS_2 composite coatings **(a)** Tafel plot, **(b)** Nyquist plot, **(c)** EEC for the bare sample, **(d)** EEC for Ni- MoS_2 coated sample

4.3.5. Tribological Characteristics

Figure 4.8. (a) shows the variation of coefficient of friction of the electrodeposited Ni-MoS_2 coating at different loads (2, 3, 4, and 5N) load for 15 min under non-lubricated conditions. Compared with the pure nickel, the friction coefficient of the Ni–MoS_2 composite coating decreased and wear resistance was increased appreciably (**Figure 4.8. (b)**). The presence of MoS_2 particles and grain refinement observed in the deposited composite coating gives the lowest coefficient of friction values in comparison with pure Ni coating under different loads. MoS_2 embedded in the Ni matrix block or delay the dislocation movements in the nickel metal matrix preventing excessive wear.

The layered hexagonal structure of the crystal lattice of MoS_2 permits sliding movement of the parallel planes. Due to the weak bonding between the planes, the shear strength is low along the direction of sliding. At the beginning of friction, MoS_2 particles are difficult to fully play the role

of lubrication between friction pairs due to insufficient MoS_2 stripping. With the continuous friction and wear, a large number of MoS_2 particles are pulled out from the composite coating, forming a layer of self-lubricating film between the friction pairs, which significantly improves the wear resistance of the composite coating. This film forms an interface layer between the pin and the disc. Thus the strongly adhered lubrication film formed by MoS_2 prevents the surface from further wear. In addition to that the grain refinement and higher microhardness also contribute to improve the wear resistance of the composite coating.

SEM studies of the worn surfaces of Ni-MoS_2 composite coatings are shown in **Figure 4.9.(a)**. Based on the wear results it can be concluded that the MoS_2 incorporated within the Ni matrix block or at least delay the dislocation movements in the matrix resulting in minimal plastic deformation, resulting in enhanced load carrying capacity. This was demonstrated as improved hardness and wear resistance. The abrasive effect of the agglomerated MoS_2 detached from the composite coating may be the cause of pit development that results from gouging of MoS_2 particles as they are dragged out of the worn surface (**Figure 4.9.(b)**) under combined compression and shear loads. These pits resemble the etch pits on the worn surface.

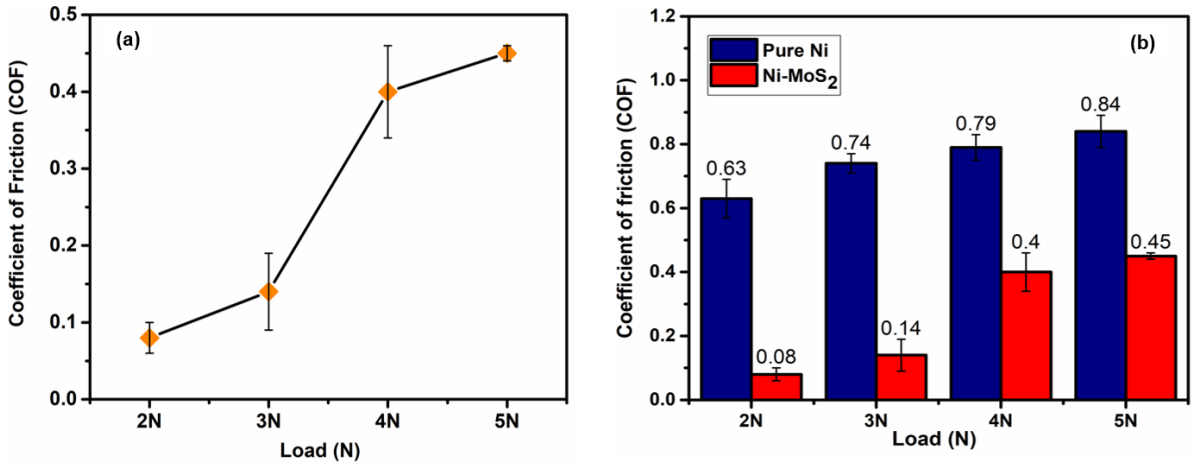

Figure 4.8. (a) Load vs COF of Ni-MoS_2 coated samples, **(b)** Comparison of COF values of pure Ni & Ni-MoS_2 coated samples under different loads

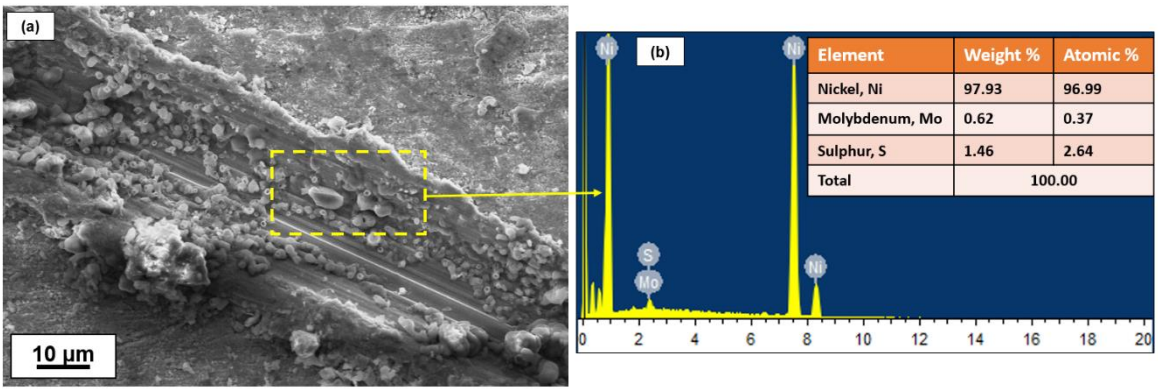

Figure 4.9. (a)-(b) SEM-EDS of the worn surface of Ni-MoS_2 coated sample

4.3.6 Electrocatalytic activity

The electrocatalytic hydrogen evolution and oxygen evolution ability of the developed catalyst materials were evaluated by linear sweep voltammetry (LSV). The lower scan rate of 2 mV/s was used to perform linear sweep analysis as it enhances the ionic and electronic movement, thereby improving the kinetics of water-splitting reactions. Hydrogen evolution was studied in the negative potential region, and **Figure 4.10. (a)** shows the HER polarization curves of the samples. The extra potential required to attain a current density of 10 mA cm^{-2}, the overpotential (η_{10}), is considered for estimating the catalytic activity of the materials [21]. Ni-MoS_2 coated SSM outperforms pure Ni coated SSM regarding η_{10}. Pure Ni coated SSM required an overpotential of 189 mV, whereas Ni-MoS_2 coated SSM needed an overpotential of 147 mV to generate a current density of 10 mA cm^{-2}. This enhancement in activity arises due to the synergistic effect of Ni and MoS_2 nanoparticles. As explained in the SEM analysis, the granular structures of Ni-MoS_2 coated SSM are beneficial for improving the electrocatalytic activity of the material. The edge sites of MoS_2 are more catalytically active than the basal planes [22]. The particular granular morphology helps more electrolyte access and exposes more edge sites of MoS_2, thereby enhancing electrocatalytic activity. Thus Ni-MoS_2 coated SSM proves to be an excellent electrode material to generate hydrogen through electrolysis of water.

Figure 4.10.(b) shows the Tafel plots of the electrode materials, which indicate the kinetics of electron transfer reactions. Tafel slope is determined from the linear portion of the voltammetric curve using the equation

$$\eta = b \log(j) \qquad (4.1.)$$

Here, out of the two electrode materials, Ni-MoS_2 coated SSM exhibited a fair tafel slope value of 145 mV dec^{-1} which indicates a faster kinetics in comparison with pure Ni coated SSM. The Tafel slope values of Ni-based systems are found to be relatively more than the theoretical value of 120 mV dec^{-1} (for Volmer pathway). However, various results with higher Tafel slope values for Ni-based alloys and composites have been reported so far [23–25]. The increase in Tafel slope may have arisen due to the presence of a surface oxide layer over the electrode surface. In this circumstance, the applied external potential will be used for initiating the HER and also to overcome the barrier caused by the oxide layer [26,27]. This indicates the faster electron adsorption-desorption mechanism by Ni-MoS_2 coated SSM.

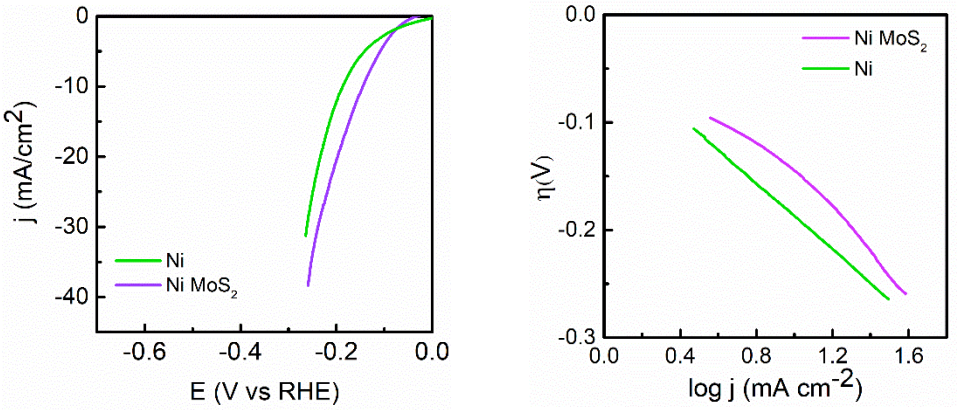

Figure 4.10. (a) HER polarisation curves, **(b)** Tafel plots of Ni-coated and Ni-MoS_2 coated SSM

Figure 4.11.(a) shows the OER polarisation curves of the catalyst materials. It is clearly evident that Ni-MoS_2 coated SSM outperforms Ni coated SSM and is suitable for OER activity. Ni coated SSM required an overpotential of 320 mV, while Ni-MoS_2 coated SSM required an overpotential of 276 mV to yield a current density of 10 mA cm^{-2}. **Figure 4.11.(b)** shows the OER Tafel plots of the electrode materials, which clearly show the enhanced oxygen evolution kinetics of Ni-MoS_2 coated SSM with a Tafel slope of 103 mV dec^{-1} whereas Ni coated SSM exhibited a Tafel slope of 118 mV dec^{-1}. OER is a four-electron transfer process in which molecular oxygen is liberated by the electro-oxidation of hydroxyl groups (OH^-) in an alkaline environment.

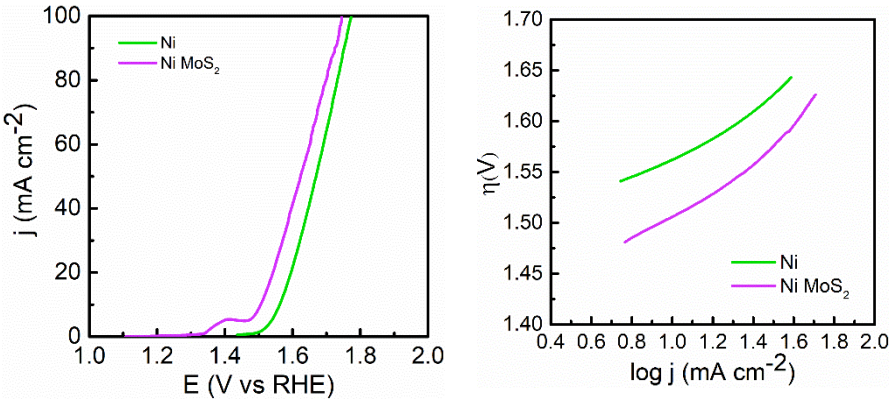

Figure 4.11. (a) OER polarisation curves, **(b)** Tafel plots of Ni-coated and Ni-MoS_2 coated SSM

The enhancement in electrocatalytic activity of Ni-MoS_2 coated SSM is due to the hierarchical growth of Ni grains and MoS_2 clusters into nodular morphology as well as due to the synergistic electrochemical properties of metallic Ni and the catalytically active TMDC–MoS_2. The material's electrocatalytic active surface area (ECSA) was calculated by recording the cyclic voltammograms in a non-Faradaic region. **Figure 4.12. (a)-(b)** show the CV curves obtained at different scan rates for Ni coated and Ni-MoS_2 coated SSM, and **Figure 4.12 (c)** shows the linear plot obtained to determine the C_{dl} value. The slope of the j vs ν curve gives the double-layer capacitance. Then, the ECSA is calculated using the equation.

$$ECSA = \frac{C_{dl}}{C_s} \qquad \textbf{(4.2.)}$$

Usually, in 0.5 M H_2SO_4, C_s is taken as 35 µF cm^{-2}; in 1M KOH it is 40 µF cm^{-2}. The Ni-MoS_2 coated SSM provided a higher ECSA value of 62.25 cm^2 while Ni coated SSM had 44 cm^2 ECSA.

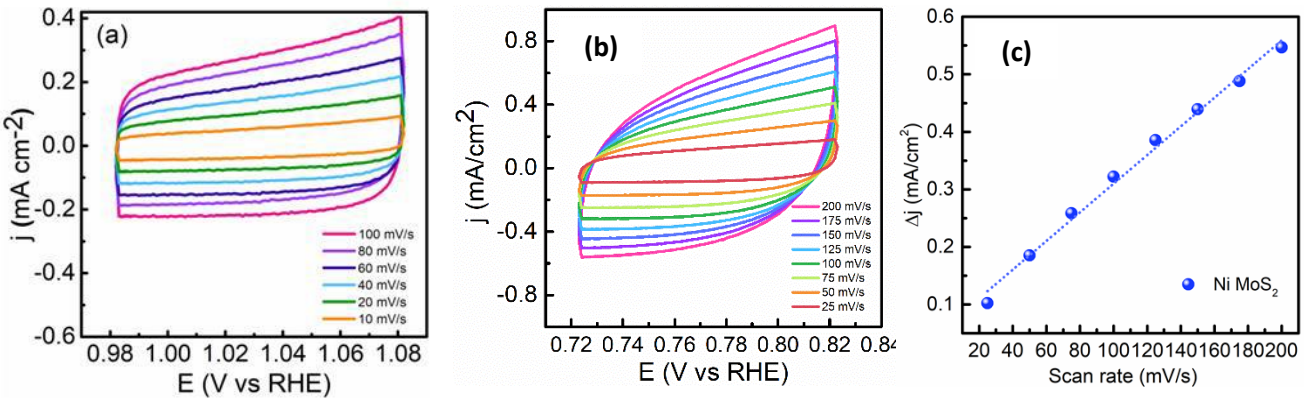

Figure 4.12. CV curves **(a)** Pure Ni, **(b)** Ni-MoS_2**, (c)** Plot of current density vs scan rate

EIS measurements were carried out to analyze the electrochemical phenomena at the electrode-electrolyte interface. **Figure 4.13.** shows the Nyquist curve of the electrode material recorded in a frequency range of 100 mHz to 100 KHz at -0.1 V.

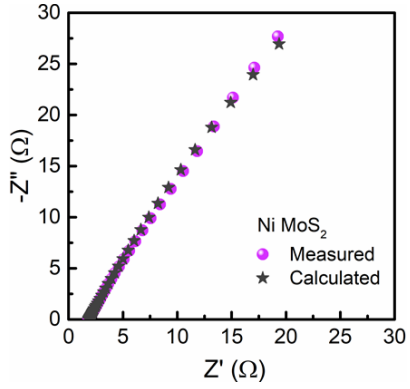

Figure 4.13. EIS Nyquist plot of Ni-MoS_2 coated SS mesh

4.4. Conclusion

Ni-MoS_2 composite coating was successfully coated over mild steel via DC electrodeposition and the surface morphology, phase structure, composition, grain size, electrochemical and tribological properties were investigated. The coatings are uniform, compact without cracks. The incorporation of MoS_2 particles could refine grains and reduce porosity since the composite particles act as nucleation sites which could inhibit the crystal growth. Compared with mild steel and pure Ni, Ni-MoS_2 composite coating exhibits higher microhardness values,

excellent corrosion resistance and low coefficient of friction at optimized conditions. The Ni-MoS_2 composite coating exhibited better barrier effect due to the presence of MoS_2 particles in corrosive environment.

The Ni-MoS_2 coated SS mesh catalyst contained a rough hierarchical surface of MoS_2 clusters and Ni cones. LSV tests showed that the overpotentials for hydrogen and oxygen evolution reactions for Ni-MoS_2 coated SS mesh were -147 mV and 276 mV respectively, much lower than pure Ni-coated mesh. The electrocatalytic activity of Ni-WS_2 coated SS mesh was higher due to the increased catalytic surface area and ready detachment of the adsorbed H_2 from the electrode surface. In light of its excellent electrocatalytic activity for HER and OER and its ease of fabrication and availability, this bi-functional composite catalyst can provide an efficient, cost-effective, and facile approach to developing large-scale industrial alkaline water electrolyzers.

References

[1] M.F. Cardinal, P.A. Castro, J. Baxi, H. Liang, F.J. Williams, Characterization and frictional behavior of nanostructured Ni-W-MoS2 composite coatings, Surf. Coatings Technol. 204 (2009) 85–90. https://doi.org/10.1016/j.surfcoat.2009.06.037.

[2] K.M. Zadeh, R.A. Shakoor, A.B. Radwan, Structural and Electrochemical Properties of Electrodeposited Ni–P nanocomposite Coatings Containing Mixed Ceramic Oxide Particles, Int. J. Electrochem. Sci. 11 (2016) 7020–7030. https://doi.org/https://doi.org/10.20964/2016.08.42.

[3] T. Guan, N. Zhang, Recent Advances in Electrodeposition of Nickel-Based Nanocomposites Enhanced with Lubricating Nanoparticles, Springer Nature Singapore, 2024. https://doi.org/10.1007/s41871-024-00245-6.

[4] C. Ma, S.C. Wang, L.P. Wang, F.C. Walsh, R.J.K. Wood, The electrodeposition and characterisation of low-friction and wear-resistant Co-Ni-P coatings, Surf. Coatings Technol. 235 (2013) 495–505. https://doi.org/https://doi.org/10.1016/j.surfcoat.2013.08.009.

[5] D. Trabelsi, M. Zouari, M. Kharrat, M. Dammak, M. Eyraud, F. Vacandio, Type and concentration effects of particulate solid lubricants on the microstructure, friction, and wear of electrodeposited Ni composite coatings, Proc. Inst. Mech. Eng. Part J J. Eng. Tribol. 233 (2019) 965–974. https://doi.org/10.1177/1350650118811057.

[6] T. Guan, Y. Lu, X. Wang, M.D. Gilchrist, F. Fang, N. Zhang, Scaling up the fabrication of wafer-scale Ni-MoS2/WS2 nanocomposite moulds using novel intermittent ultrasonic-assisted dual-bath micro-electroforming, Ultrason. Sonochem. 95 (2023) 106359. https://doi.org/10.1016/j.ultsonch.2023.106359.

[7] E. Saraloǧlu Güler, E. Konca, I. Karakaya, Effect of electrodeposition parameters on the current density of hydrogen evolution reaction in Ni and Ni-MoS2 composite coatings, Int. J. Electrochem. Sci. 8 (2013) 5496–5505.

[8] N.P. Wasekar, G. Sundararajan, Sliding wear behavior of electrodeposited Ni–W alloy and hard chrome coatings, Wear 342–343 (2015) 340–348. https://doi.org/https://doi.org/10.1016/j.wear.2015.10.003.

[9] H. Li, S. Wen, Z. Yu, J. Hu, J. Yan, X. Ren, Preparation of MoSi2-particle reinforced Ni-W alloy coatings and their anti-corrosion behavior in CO2-saturated 3.5 % NaCl solution,

Int. J. Electrochem. Sci. 19 (2024) 100708. https://doi.org/https://doi.org/10.1016/j.ijoes.2024.100708.

[10] R. Sreekumar, A.S. Nair, S. S.S, Recent trends and developments in two-dimensional materials based electrodeposited nickel nanocomposite coatings, FlatChem 36 (2022) 100434. https://doi.org/10.1016/j.flatc.2022.100434.

[11] Y. He, S.C. Wang, F.C. Walsh, Y.-L. Chiu, P.A.S. Reed, Self-lubricating Ni-P-MoS2 composite coatings, Surf. Coatings Technol. 307 (2016) 926–934. https://doi.org/https://doi.org/10.1016/j.surfcoat.2016.09.078.

[12] Y.-C. Chang, Y.-Y. Chang, C.-I. Lin, Process aspects of the electrolytic codeposition of molybdenum disulfide with nickel, Electrochim. Acta 43 (1998) 315–324. https://doi.org/https://doi.org/10.1016/S0013-4686(97)00072-8.

[13] E.S. Güler, E. Konca, I. Karakaya, Investigation of the tribological behaviour of electrocodeposited Ni-MoS2 composite coatings, Int. J. Surf. Sci. Eng. 11 (2017) 418.

[14] B. Han, M. Xue, Y. Wang, M. Yu, Influence of MoS2 on the Microstructures and Properties of Ni-Based Alloying Coating, Appl. Mech. Mater. 130–134 (2011). https://doi.org/10.4028/www.scientific.net/AMM.130-134.1276.

[15] A. Joseph, M. Narayanasamy, B. Kirubasankar, S. Angaiah, Development of MoS Nanosheets Embedded Nickel Composite Coating and its Mechanical 2 Properties, ES Mater. Manuf. (2018) 2–8. https://doi.org/10.30919/esmm5f152.

[16] S.M.J.S. Shourije, M.E. Bahrololoom, Effect of current density, MoS 2 content and bath agitation on tribological properties of electrodeposited nanostructured Ni-MoS 2 composite coatings, Tribol. - Mater. Surfaces Interfaces 13 (2019) 76–87. https://doi.org/10.1080/17515831.2019.1589160.

[17] A.G. McCormack, M.J. Pomeroy, V.J. Cunnane, Microstructural Development and Surface Characterization of Electrodeposited Nickel/Yttria Composite Coatings, J. Electrochem. Soc. 150 (2003) C356. https://doi.org/10.1149/1.1566961.

[18] T. Borkar, S. Harimkar, Microstructure and wear behaviour of pulse electrodeposited Ni–CNT composite coatings, Surf. Eng. 27 (2011) 524–530. https://doi.org/10.1179/1743294410Y.0000000001.

[19] R. Sen, S. Das, K. Das, Effect of stirring rate on the microstructure and microhardness of Ni–CeO2 nanocomposite coating and investigation of the corrosion property, Surf.

Coatings Technol. 205 (2011) 3847–3855. https://doi.org/https://doi.org/10.1016/j.surfcoat.2011.01.057.

[20] A. Joseph, M.K. Eapen, M.E. Mampilly, V. Sajith, Comparison of Corrosion Resistance Properties of Electrophoretically Deposited MoS2 and WS2 Nanosheets Coatings on Mild Steel, Metall. Mater. Trans. A Phys. Metall. Mater. Sci. 52 (2021) 3689–3693. https://doi.org/10.1007/s11661-021-06354-x.

[21] S. Niu, S. Li, Y. Du, X. Han, P. Xu, How to Reliably Report the Overpotential of an Electrocatalyst, ACS Energy Lett. 5 (2020) 1083–1087. https://doi.org/10.1021/acsenergylett.0c00321.

[22] P. V. Sarma, A. Kayal, C.H. Sharma, M. Thalakulam, J. Mitra, M.M. Shaijumon, Electrocatalysis on Edge-Rich Spiral WS2 for Hydrogen Evolution, ACS Nano 13 (2019) 10448–10455. https://doi.org/10.1021/acsnano.9b04250.

[23] D. Wang, Q. Li, C. Han, Z. Xing, X. Yang, When NiO@Ni Meets WS2 nanosheet array: A highly efficient and ultrastable electrocatalyst for overall water splitting, ACS Cent. Sci. 4 (2018) 112–119. https://doi.org/10.1021/acscentsci.7b00502.

[24] Q. Zhou, S. Liu, Y. Zhang, Z. Zhu, W. Su, M. Sheng, Fabrication of porous Cu supported Ni-P/CeO2 composite coatings for enhanced hydrogen evolution reaction in alkaline solution, Ceram. Int. 46 (2020) 20871–20877. https://doi.org/10.1016/j.ceramint.2020.05.133.

[25] F. Bao, E. Kemppainen, I. Dorbandt, R. Bors, F. Xi, R. Schlatmann, R. van de Krol, S. Calnan, Understanding the Hydrogen Evolution Reaction Kinetics of Electrodeposited Nickel-Molybdenum in Acidic, Near-Neutral, and Alkaline Conditions, ChemElectroChem 8 (2021) 195–208. https://doi.org/10.1002/celc.202001436.

[26] M. Grdeń, G. Jerkiewicz, Influence of Surface Treatment on the Kinetics of the Hydrogen Evolution Reaction on Bulk and Porous Nickel Materials, Electrocatalysis 10 (2019) 173–183. https://doi.org/10.1007/s12678-019-0506-6.

[27] Z. Liang, H.S. Ahn, A.J. Bard, A Study of the Mechanism of the Hydrogen Evolution Reaction on Nickel by Surface Interrogation Scanning Electrochemical Microscopy, J. Am. Chem. Soc. 139 (2017) 4854–4858. https://doi.org/10.1021/jacs.7b00279.

Chapter 5
Development of multi-functional (corrosion resistant, wear resistant & self-lubricating) Ni-WS_2 composite coating

Abstract

A low-friction, superhydrophobic Ni-WS_2 coating was successfully developed through a scalable single-step electrodeposition process over mild steel substrate. By optimizing WS_2 concentration and deposition parameters, a hierarchical surface with a higher WCA of 159° was produced. The incorporation of sufficient WS_2 improved the mechanical and tribological properties of the composite coating. The creation of a self-lubricating tribo-film by the incorporated WS_2 caused the friction coefficient to drop to 0.04. The composite coating demonstrated exceptional corrosion resistance in comparison to the bare mild steel substrate and pure nickel coated mild steel, indicating its potential for industrial applications.

5.1. Introduction

The demand for high-performance materials with enhanced surface properties has grown significantly in various industrial sectors, including aerospace, automotive, marine, and energy [1]. Components used in these industries often face involving wear, corrosion, and high friction. These challenges necessitate the development of advanced coatings capable of protecting surfaces and extending the service life of critical components [2]. In response, composite coatings have emerged as a promising solution, offering multi-functional capabilities by integrating diverse material properties.

Nickel-based coatings have gained considerable attention due to their excellent mechanical strength, corrosion resistance, and ease of deposition through electrochemical methods [3][4]. However, pure nickel coatings often fall short in addressing specific challenges such as wear resistance and lubrication. To overcome these limitations, incorporating solid lubricants like

tungsten disulfide (WS_2) into nickel matrices has proven to be a viable approach [5–7]. WS_2 is a well-known transition metal dichalcogenide with layered structure that facilitates low friction due to weak van der Waals forces between its layers. Furthermore, WS_2 contributes to self-lubricating properties, making it an excellent candidate for applications where reducing friction is critical [8], [9].

Ranganatha et al. [10] fabricated Ni-W-P-WS_2 composite coating by electroless plating and explored its friction and corrosion resistance. Lecina et al.[11] incorporated inorganic fullerene-like WS_2 (IF-WS_2) within Ni matrix resulting in a uniform and compact coating, with better mechanical properties and enhanced tribological performance. Polycrystalline WS_2 thin films are electrodeposited on conducting glass plates by galvanostatic route [12]. Cui et al. [13] developed a Ni-WS_2 self-lubricating composite coating with remarkable self-lubricity and lower friction coefficient at a value around 0.01–0.03.

This research focuses on the development of multi-functional Ni-WS_2 composite coatings that combine self-cleaning, corrosion resistance, wear resistance, and self-lubricating properties. The strategic incorporation of WS_2 particles into the nickel matrix aims to synergistically enhance the coating's performance. The dual-phase composition improves nickel's inherent corrosion resistance and mechanical strength while utilizing the solid lubrication and wear resistance of WS_2. This study systematically investigates the development, characterization, and performance evaluation of Ni-WS_2 composite coatings.

The outcomes of this research will provide valuable insights into the design of multi-functional composite coatings, contributing to advancements in surface engineering and material science. Additionally, the findings have the potential to address pressing challenges in industries where enhancing the durability and efficiency of critical components is paramount.

5.2. Materials & methods

5.2.1 Materials

Nickel sulphate ($NiSO_4 \cdot 6H_2O$), Nickel chloride ($NiCl_2 \cdot 6H_2O$, 98%) and Boric acid (H_3BO_3, 99.5%) were purchased from Merck. Cetyltrimethylammonium bromide (CTAB, $CH_3(CH_2)_{15}N(Br)(CH_3)_3$) and Saccharin ($C_7H_5NO_3S$) were obtained from Alfa Aesar. Tungsten disulphide particles (WS_2, ≤ 1 μm) were supplied by Sigma-Aldrich. Stearic acid

$CH_3(CH_2)_{16}COOH$ was supplied by Hi-media laboratories. All the chemicals were of analytical grade and used without further purification.

5.2.2 Coating preparation

Electrodeposition was carried out in an aqueous electrolyte of Ni Watts bath containing $NiSO_4 \cdot 6H_2O$, $NiCl_2 \cdot 6H_2O$, and H_3BO_3. WS_2 nanoparticles were dispersed in Ni bath, along with CTAB and saccharin (**Table 5.1.**). The Ni-WS_2 bath was kept at a pH of 4 - 4.5. WS_2 particles were dispersed using an ultrasonicator for 30 minutes.

Nickel plate (7 cm × 5 cm × 1 cm, 99.7 % purity) and mild steel substrate (SSM) (6 cm × 6 cm, purity ≥ 99.5 %) were used as anode and cathode, respectively. All the mild steel samples used for coating were ground using SiC papers ranging from 80 to 1000 grits, followed by degreasing in acetone and distilled water, ultrasonically cleaned, and dried in the oven. MS samples were further surface activated by dipping in 0.01M HCl and 0.1M NaOH. The anode, Ni plate was polished using SiC papers of grit 80 and 100. This was followed by degreasing in acetone and distilled water and finally drying in the oven. Electrodeposition parameters including current density (2–6A/dm^2), time (5–30 min), and stirring rate (400–600 rpm) were varied. The concentration of WS_2 was also varied in the range (1–5) wt% (**Table 5.1.**).

Finally Ni-WS_2 was deposited at optimized conditions of current density of 5 A/dm^2 for 30 mins at a temperature of 60°C with a 400 rpm stirring rate and 3wt% concentration of WS_2. After the electrodeposition, the samples were cleaned in running distilled water followed by ultrasonic cleaning for 5 minutes in ethanol to remove loosely adsorbed particles and then subjected for further analysis. The coated sample was finally modified with low surface energy material stearic acid (SA).

Table 5.1. Experimental conditions for Ni-WS_2 coating over mild steel substrate

Electrodeposition parameters	Composition or parameter	Value	Optimised conditions
Plating solution	$NiSO_4.6H_2O$	250 g/l	-
	$NiCl_2.6H_2O$	45 g/l	-
	H_3BO_3	40 g/l	-
	Saccharin	3 g/l	-
	CTAB	0.5 g/l	-
	WS_2	1-5 wt%	3 wt%
Deposition conditions	Current density	2-6 A/dm^2	5 A/dm^2
	Temperature	60°C	-
	Time	5-30 minutes	30 minutes
	Stirring rate	400-600 rpm	400 rpm

5.2.3. Characterization of the coatings

The surface morphology and elemental analysis of the developed coatings were examined using Zeiss EVO 18 cryo-SEM (EDS attached). The phase composition of the samples was studied using X-ray diffraction (XRD) via a Bruker D2 Phaser X-ray diffractometer with Cu - K_α radiation (λ = 1.5406 Å) in the 0-90° range. Coating thickness was measured using thickness measurement gauge (Elcometer). The wettability of the developed coatings was measured by Goniometer (Data Physics, Germany). The water contact angle was calculated by taking the average of five measurements taken at various points on the same sample.

CH Instruments electrochemical workstation (CHI608E, CH Instruments Inc.) equipped with standard three-electrode cell was used for electrochemical impedance spectroscopy and potentiodynamic polarization studies at room temperature in 3.5 wt% NaCl solution. The coated specimen with 1cm^2 exposed surface area was used as the working electrode; saturated calomel and a platinum grid were taken as the reference and counter electrodes respectively. The specimens were kept in the electrolyte for 20 min prior to the experiment for attaining their stable open circuit potential (OCP). The potentiodynamic scan was done at a rate of 1 mV/s from −250 mV to +250

mV of the OCP values. The corrosion potential (E_{corr} vs. SCE) and corrosion current density (i_{corr}) of each sample were obtained from the applied potential vs. current Tafel plot. The impedance measurements were performed using an AC signal with a perturbation of 5 mV at OCP in the frequency range of 100 kHz-0.01 Hz. ZsimpWin software fits the generated EIS plots to determine the electrochemical parameters. Numerous circuits were examined until the Chi-square value decreased to less than 9×10^{-4} or no further fitting improvement was observed.

Pin on disc wear testing machine (POD 4.0, DUCOM) was used to measure the wear rate and coefficient of friction at the dry condition. The measurements were done for Ni-WS_2, pure Ni coated and bare mild steel samples. The pins with 6 mm diameter and 15 mm length were used against EN31 high carbon alloy steel disc. The mild steel pins were coated with pure Ni and Ni-WS_2 composite. Wear tests were done at a sliding velocity of 0.4 m/s under 2, 3, 4, and 5N standard loads at room temperature for 15 minutes.

5.3. Results & Discussion

5.3.1 Surface morphology and elemental composition

SEM micrographs of pure Ni and Ni-WS_2 composite coating deposited on mild steel are given in **Figure 5.1. (a-b)** and **Figure 5.2. (a-e)**, respectively. Both the coatings had uniform surface without any defects such as pores and cracks. The addition of WS_2 will cause a change in the microstructure of the composite coating and makes the surface rougher. The development of a rough surface is an important factor in the preparation of special super-wetting materials [14].

During the time of deposition, Ni ions are attracted to WS_2 particles due to the electrostatic interaction between positively charged Ni ions and negatively charged WS_2 particles [15]. WS_2 particles in the plating bath exhibited negative surface charge (as indicated by a zeta potential of −14.3 mV). This negative charge facilitates electrostatic attraction with positively charged Ni^{2+} ions in the bath, leading to the formation of a localized electric double layer on the surface of WS_2. Ni^{2+} ions are thus adsorbed onto the surface of WS_2 particles, enabling the formation of a thin Ni film on WS_2. However, WS_2 particles themselves, being negatively charged, do not naturally migrate toward the negatively charged cathode under the influence of the electric field. Instead,

their transport to the cathode surface is governed primarily by convective forces, Brownian motion, and electrophoretic drag facilitated by the surrounding Ni^{2+} ionic environment.

The inclusion of cetyltrimethylammonium bromide (CTAB), a cationic surfactant, significantly alters the net surface charge of WS_2 particles. CTAB adsorbs onto the negatively charged WS_2 surfaces via electrostatic interaction, effectively neutralizing or even reversing their charge. This is further supported from the literature [16][17]. This surface modification enhances the electrophoretic mobility of WS_2 particles toward the cathode, improving their co-deposition efficiency. Overall, while the initial electrostatic attraction between Ni^{2+} and WS_2 aids in forming a composite interface, the presence of CTAB facilitates effective transport and stable incorporation of WS_2 particles into the growing nickel matrix.

The Ni-WS_2 coated MS possessed a protruding rough surface comprising pyramidal and conical structures (**Figure 5.2(e)**). This type of a structure can enhance mechanical strength, adhesion, and electrochemical performance of the Ni-WS_2 composite coating.

EDS and elemental mapping data shows the distribution of elements on the surface of Ni-WS_2 coated MS as in **Figure 5.3 (a-e)**. Ni, W and S elements are uniformly distributed on the surface of the composite coating, which indicates that WS_2 is successfully embedded in the Ni matrix. . **Figure 5.4 (a)-(f)** shows the cross-section of Ni-WS_2 composite coatings. The average thickness of Ni-WS_2 coating was found to be 39.5 µm. EDS data of the cross-section further confirmed the presence of WS_2 particles in the composite coating.

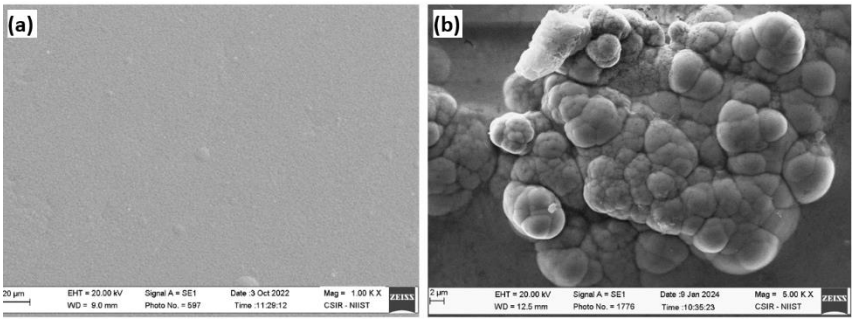

Figure 5.1 (a-b): SEM micrographs of pure Ni coated MS

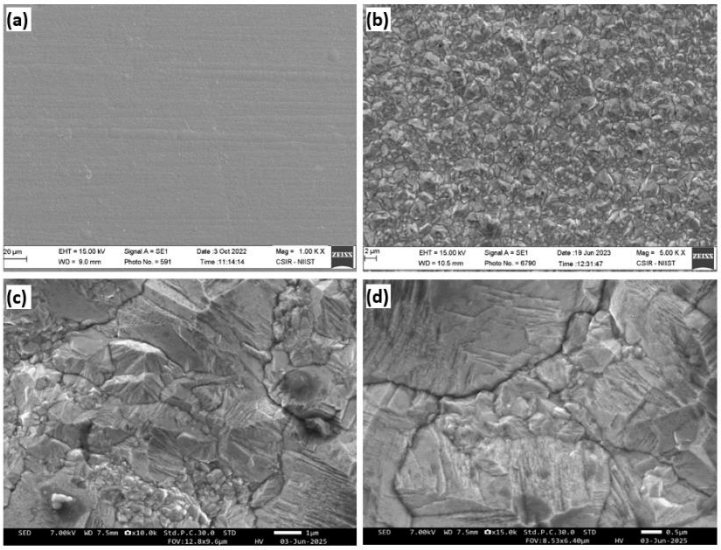

Figure 5.2 (a-d): SEM micrographs of Ni-WS_2 coated MS

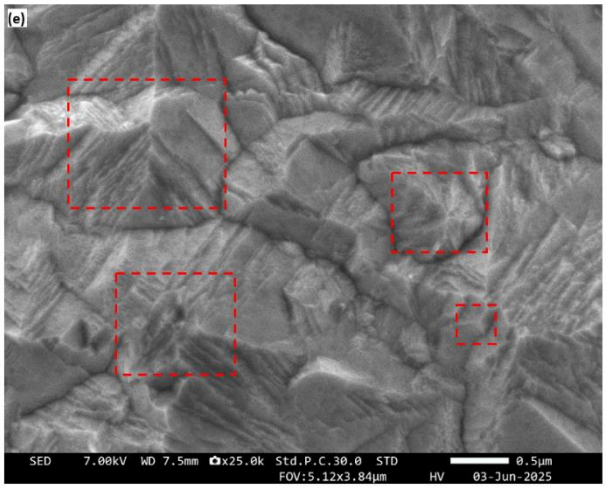

Figure 5.2 (e): Higher magnification SEM image of Ni-WS_2 coated MS. Pyramidal Ni structures are marked in red.

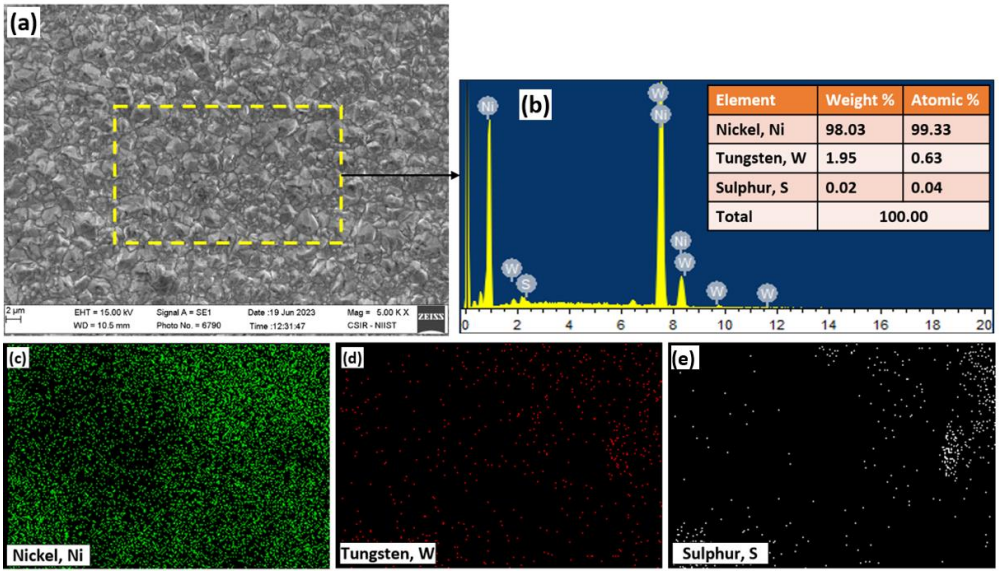

Figure 5.3 (a-e): SEM-EDS & elemental mapping of Ni-WS_2 coated MS surface

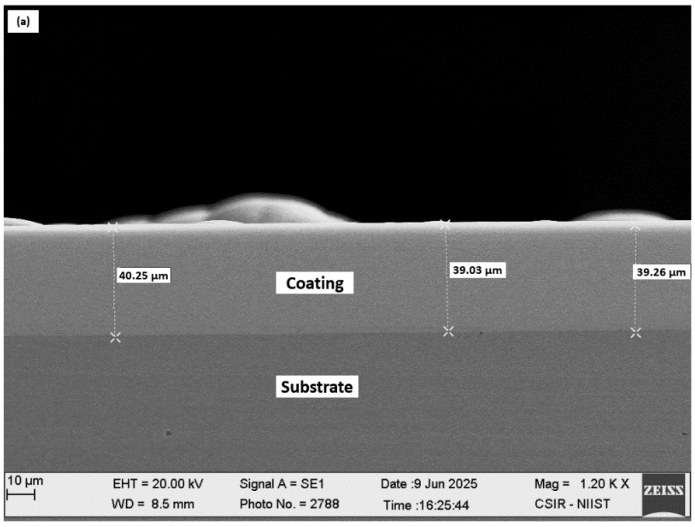

Figure 5.4 (a): Cross-sectional SEM micrograph of Ni-WS_2 coated MS

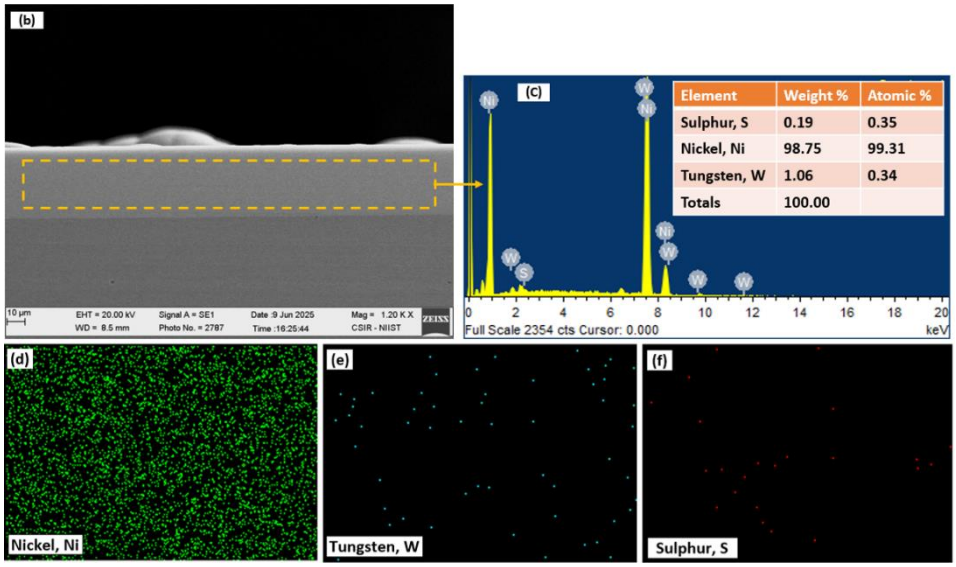

Figure 5.4 (b-f): Cross-sectional SEM-EDS & elemental mapping of Ni-WS_2 coated MS

5.3.2. X-ray diffraction studies

X-ray diffraction was employed to examine the phase composition of the coating. The XRD pattern of pure Ni-coated MS is shown in **Figure 5.5.** From the data, three peaks of Ni at 2θ corresponding to 44.32°, 51.77°, and 76.3° are assigned to (111), (200), and (220) Bragg reflections of the face-centered cubic (fcc) structure of metallic nickel [18]. The incorporation of WS_2 particles causes important microstructural changes; providing more nucleation sites. It also retards the growth of large Ni crystals, resulting in smaller grain sizes (**Table 5.2.**). Analyzing the XRD pattern of Ni-WS_2 coated sample, distinct peaks are found at 14° and 33°, correspond to (002) and (102), phases of WS_2 respectively. This confirms the hexagonal closed-packed (hcp) structure of WS_2 [19]. (**Figure 5.5.**).

Whenever Ni is deposited onto a substrate, the first few layers of atoms will tend to form (111) plane [20]. The (111) plane is one of the most densely packed planes in a crystal lattice, and it has the lowest surface energy compared to other planes. Thus the growth of the (111) plane helps to minimize the total surface energy of the crystal [21]. In this case, there is the presence of strong Ni (111) peak indicating reduced surface energy. Post electrodeposition after treatment with SA is believed that SA is chemically adsorbed on the Ni (111) surface via bi-dentate interaction, i.e. two oxygen atoms from the carboxylic acid group (-COOH) of stearic acid. This bonding interaction

prevents the water molecules from forming hydrogen bonds with the surface, enhancing the hydrophobicity [22–24].

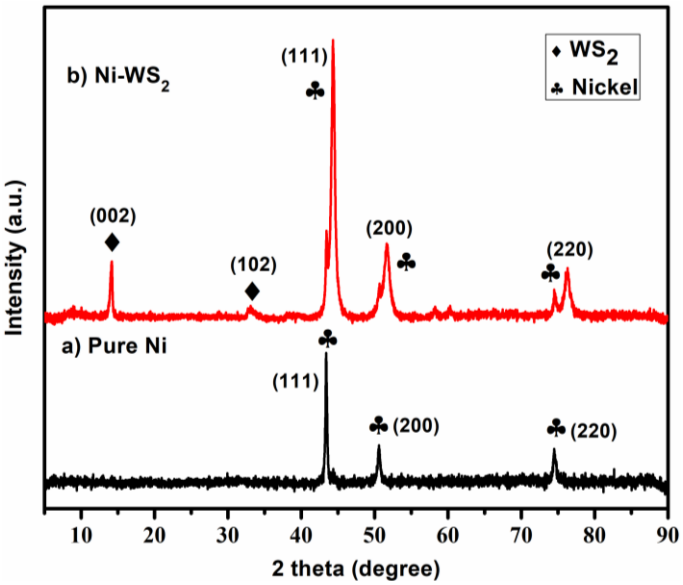

Figure 5.5. XRD pattern of pure Ni and Ni-WS_2 coating

Table 5.2. Crystallite size calculations using Scherrer equation in Ni-WS_2 system

Coating	Angular position (θ) (radians)	cos θ (radians)	Full width half-maxima (FWHM) (radians)			Average crystallite size (D) (nm)
			Sample β_s	Instrument β_i	Corrected β_{corr}	
Pure Ni	0.390	0.925	2.616×10^{-3}	1.395×10^{-4}	2.612×10^{-3}	57.4
Ni-WS_2	0.390	0.925	5.931×10^{-3}		5.930×10^{-3}	25.3

5.3.3. Wettability Studies

Chemical composition, free energy and morphology of the surface, all affect the surface wetting property of a coating. **Figure 5.6.** shows the contact angle of the water droplet on coated MS (pure Ni, Ni-WS_2, SA-Ni-WS_2). As it is evident from the WCA measurements there was a gradual increase in the hydrophobicity of the surface (i.e. **121.8°** to **159.7°**). The water droplet remained on the surface of the Ni-WS_2 coated MS in an extremely spherical fashion. The

pyramidal structure along with the action of low surface energy material SA (surface energy: 27.7 dynes/cm) reduces the contact area between the solid−liquid and water by forming a thin, strong cohesive layer on Ni-WS_2 coating.

Whenever applied over a surface, SA can self-assemble in an organized manner employing the hydrogen bonding of carboxyl groups as well as hydrophobic interaction in-between methyl groups. These hydrophobic chains create a barrier that prevents water from wetting the surface. As a result, water droplets tend to bead up and roll off the surface instead of spreading out and wetting it. The combined effect of hydrophobic surface chemistry and the roughness results in excellent superhydrophobic characteristics of the developed Ni-WS_2 coating.

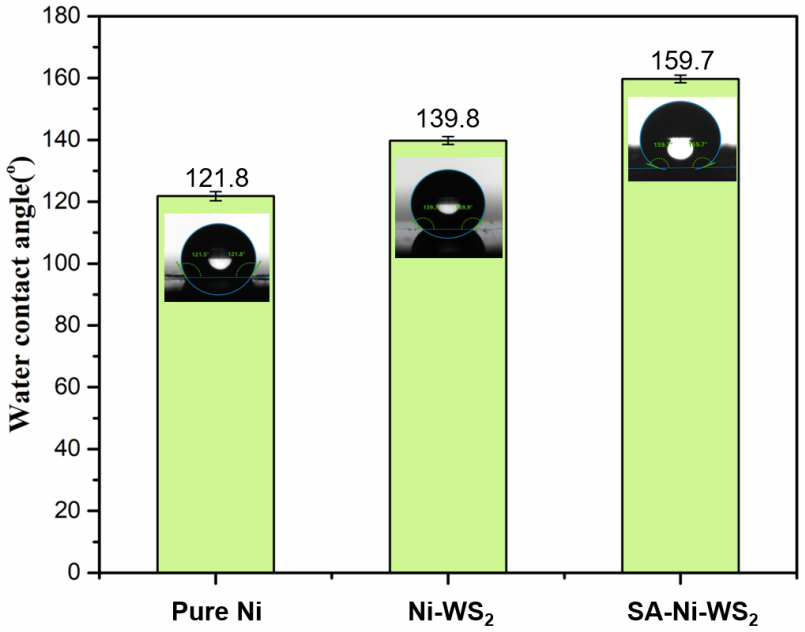

Figure 5.6. WCAs of coated sample (a) Pure Ni, (b) Ni-WS_2, (c) SA-Ni-WS_2

5.3.4. Electrochemical characterization

Figure 5.7. (a) shows the potentiodynamic polarization curves (Tafel plots) of samples by plotting the potential scanned from cathodic region to the anodic region vs. logarithm of current density. The values of corrosion current density (i_{corr}) and corrosion potential (E_{corr}), obtained by the extrapolation of cathodic and anodic sides are given in **Table 5.3.** Variation of E_{corr} value

towards more positive direction and the lower i_{corr} indicates the improved corrosion resistance of coatings, especially in the case of composite coatings. Presence of WS_2 in the coating leads to a substantial reduction in the i_{corr} value of Ni-WS_2 to 0.177 µA cm^{-2} from 4.143 µA cm^{-2} in the case of pure Ni and 17.110 µA cm^{-2} in case of bare mild steel sample. The corresponding shift of the graph towards the left-hand side was observed. The reduction in i_{corr} values of the coated samples indicates the decreased ionic diffusion on the surface during the corrosion process. The Ni-WS_2 composite coating is more cathodic with respect to other samples and possesses excellent corrosion protection (E_{corr} MS: -0.678 V, Pure Ni: -0.417 V, Ni-WS_2: -0.246 V).

WS_2 incorporation has improved the corrosion resistance of the composite coatings by filling surface defects like tiny holes and porosities with WS_2 and acted as a barrier to corrosive ion diffusion. The even distribution of WS_2 in the deposit creates a passive layer between corrosive media and the deposited surface [25]. Thus the corrosion rate (0.0019) of Ni-WS_2 composite coating is exceptionally low compared to mild steel and pure Ni samples.

Electrochemical impedance spectroscopy measurements were performed in order to get a better understanding of the anti-corrosive nature of coatings. Nyquist plots of bare mild steel, pure Ni and Ni-WS_2 composite coatings were obtained in 3.5% NaCl medium at their respective open circuit potentials (**Figure 5.7. (b)**).The Nyquist plots of all the samples have showed a single semi-circular arc in the investigated frequency region. The bare MS samples can be fitted with the circuit the equivalent electrochemical circuit (EEC) $R_s(C_{dl}R_{ct})$ (**Figure 5.7. (c)**), and all the coated samples are well fitted for the equivalent circuit of $R_s(C_cR_c(C_{dl}R_{ct}))$ (**Figure 5.7. (d)**).

R_s is the solution resistance, R_{ct} and C_{dl} are the charge transfer resistance and double-layer capacitance, respectively. Instead of using pure capacitance due to the possibility of a dispersion effect between the metal/coating system, *C* represents a constant phase angle element (CPE). The coating offered protection by the resistance element *R*c. The parameters derived from electrochemical impedance measurements are summarized in **Table 5.3.** The results of the EIS studies also indicated a similar trend in the corrosion resistance that was observed in potentiodynamic polarization studies. The increased radius of semicircular arc indicated the better anticorrosion property of the Ni-WS_2 composite coating than other samples. The superior value of R_{ct} obtained for the composite coating indicated more protection capability of the composite coating against corrosion.

Table 5.3. Electrochemical parameters obtained and corrosion inhibition efficiency of Ni-WS_2 coated samples

S/N	Substrate	Potentiodynamic polarisation				EIS	
		E_{corr} (V)	i_{corr} (μAcm^{-2})	η (%)	Corr.rate (mmpy)	R_{ct} (Ω cm^2)	η (%)
1.	Bare Mild Steel	-0.678	17.110	-	0.2013	3.955×10^2	-
2.	Pure Nickel	-0.417	4.143	75.78	0.0446	3.222×10^4	98.77
3.	Ni-WS_2	-0.246	0.177	98.96	0.0019	2.545×10^5	99.84

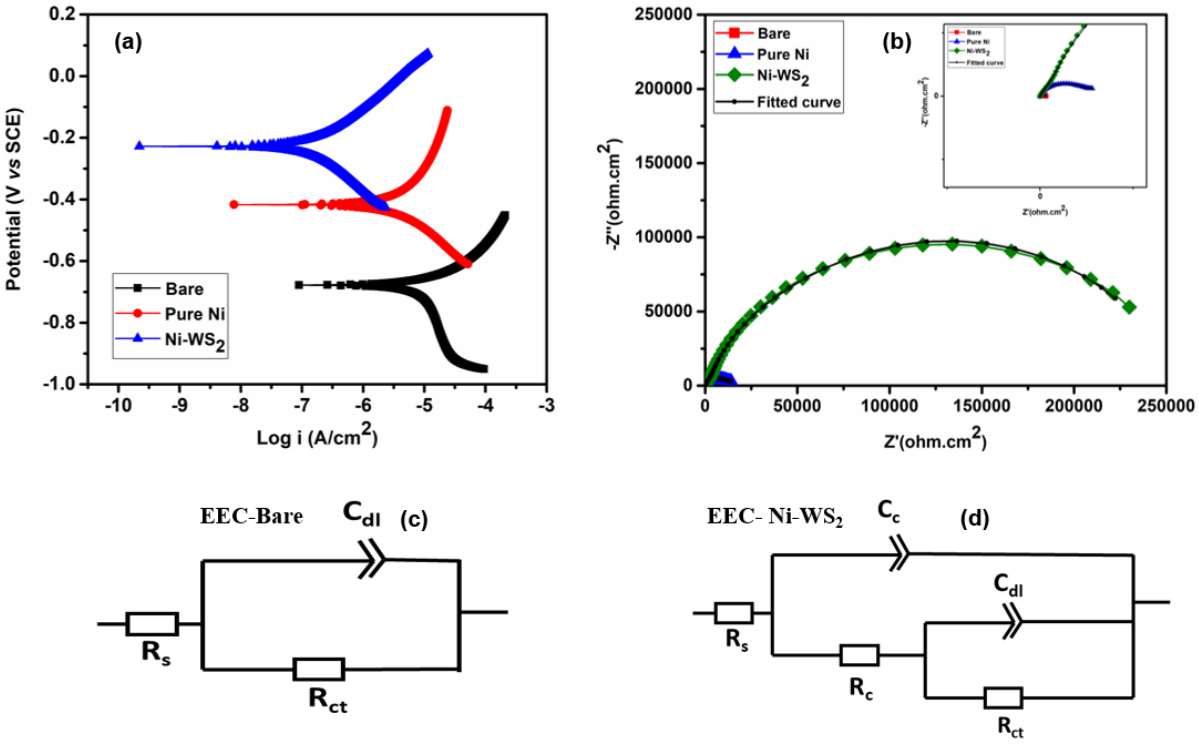

Figure 5.7. Electrochemical study for the Ni-WS_2 composite coatings **(a)** Tafel plot, **(b)** Nyquist plot, **(c)** EEC for the bare sample, **(d)** EEC for Ni- WS_2 coated sample

5.3.5. Tribological Characteristics

Figure 5.8. (a) shows the variation of coefficient of friction of the electrodeposited Ni-WS_2 coating at different loads (2, 3, 4, and 5N) load for 15 min under non-lubricated conditions. As compared to pure Ni coating, Ni–WS_2 composite coating had a lower coefficient of friction and increased wear resistance (**Figure 5.8 (b)**). The presence of WS_2 and grain refinement observed in the deposited composite coating gives the lowest coefficient of friction values in comparison with pure Ni coating under different loads. WS_2 incorporated within the Ni matrix prevents or slows down the dislocation movements in the matrix avoiding excessive wear.

The layered hexagonal structure of the crystal lattice of WS_2 permits sliding movement of the parallel planes. Due to the weak bonding between the planes, the shear strength is low along the direction of sliding. At the beginning of friction, WS_2 are difficult to fully play the role of lubrication between friction pairs due to insufficient WS_2 stripping. With the continuous friction and wear, WS_2 particles are pulled out from the composite coating, forming a layer of self-lubricating film between the friction pairs, which significantly improves the wear resistance of the composite coating [26]. This film forms an interface layer between the pin and the disc. Thus the strongly adhered lubrication film formed by WS_2 prevents the surface from further wear.

SEM-EDS studies of the worn surfaces of Ni- WS_2 composite coatings are shown in **Figure 5.9**. Based on the wear results it can be concluded that the WS_2 incorporated within the Ni matrix block or at least delay the dislocation movements in the matrix resulting in minimal plastic deformation, resulting in enhanced load carrying capacity. This was demonstrated as improved wear resistance. The abrasive effect of the agglomerated WS_2 detached from the composite coating may be the cause of the pit development that results from gouging of WS_2 particles as they are dragged out of the worn surface under combined compression and shear loads. These pits resemble the etch pits on the worn surface.

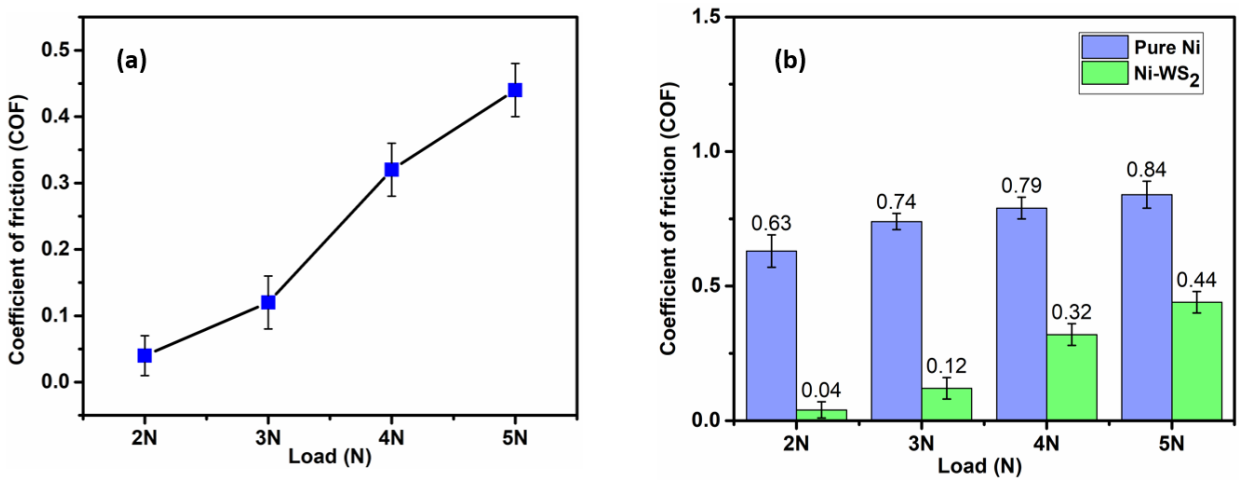

Figure 5.8. (a) Load vs COF of Ni- WS_2 coated samples, **(b)** Comparison of COF values of pure Ni & Ni- WS_2 coated samples under different loads

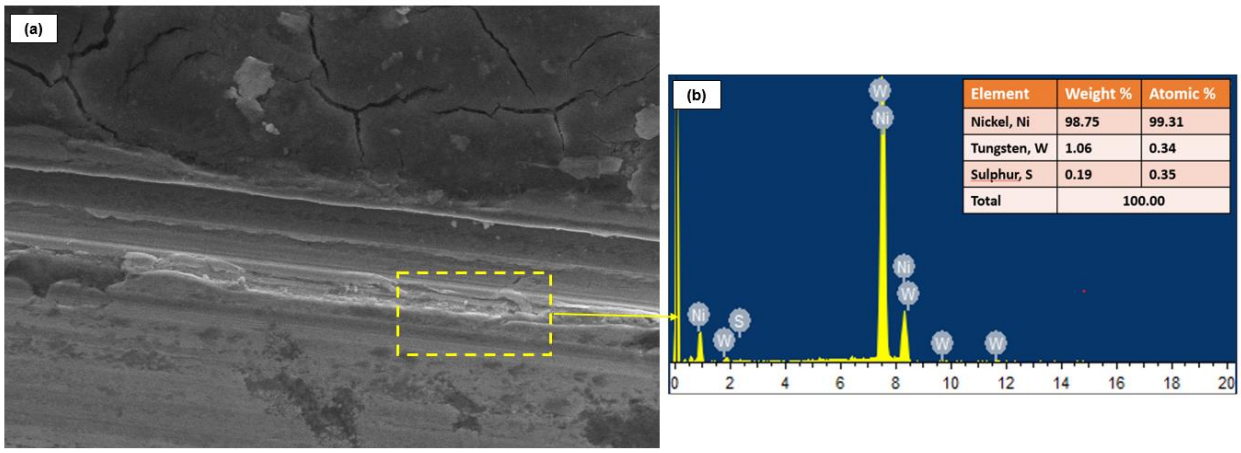

Figure 5.9. SEM-EDS of the worn surface of Ni-WS_2 coated sample

5.4. Conclusions

A low-friction, superhydrophobic Ni-WS_2 coating was successfully developed through a scalable single-step electrodeposition process. By optimizing WS_2 concentration and deposition parameters, a surface of Ni pyramids with a higher WCA of 159° was produced. The incorporation of sufficient WS_2 improved the mechanical and tribological properties of the composite coating. The creation of a self-lubricating tribo-film by the incorporated WS_2 caused the friction coefficient

to drop to 0.04. The composite coating demonstrated exceptional corrosion resistance in comparison to the bare mild steel substrate and pure nickel coated mild steel, indicating its potential for industrial applications.

References

[1] F.O.R. Corrosion, W. Resistance, SURFACE ENGINEERING Edited by, Surf. Eng. (2008) 754.

[2] S. Zhu, J. Cheng, Z. Qiao, J. Yang, High temperature solid-lubricating materials: A review, Tribol. Int. 133 (2019) 206–223. https://doi.org/https://doi.org/10.1016/j.triboint.2018.12.037.

[3] A.M. El-Sherik, U. Erb, Synthesis of bulk nanocrystalline nickel by pulsed electrodeposition, J. Mater. Sci. 30 (1995) 5743–5749. https://doi.org/10.1007/BF00356715.

[4] R. Tenne, M. Homyonfer, Y. Feldman, Nanoparticles of Layered Compounds with Hollow Cage Structures (Inorganic Fullerene-Like Structures), Chem. Mater. 10 (1998). https://doi.org/10.1021/cm9802189.

[5] A.A. Voevodin, J.P. O'Neill, J.S. Zabinski, Nanocomposite tribological coatings for aerospace applications, Surf. Coatings Technol. 116–119 (1999) 36–45. https://doi.org/https://doi.org/10.1016/S0257-8972(99)00228-5.

[6] R. Greenberg, G. Halperin, I. Etsion, R. Tenne, The effect of WS2 nanoparticles on friction reduction in various lubrication regimes, Tribol. Lett. 17 (2004) 179–186. https://doi.org/10.1023/B:TRIL.0000032443.95697.1d.

[7] L. Rapoport, N. Fleischer, R. Tenne, Fullerene-like WS2 nanoparticles: Superior lubricants for harsh conditions, Adv. Mater. 15 (2003) 651–655. https://doi.org/10.1002/adma.200301640.

[8] S. Xu, X. Gao, M. Hu, J. Sun, D. Jiang, F. Zhou, W. Liu, L. Weng, Nanostructured WS2–Ni composite films for improved oxidation, resistance and tribological performance, Appl. Surf. Sci. 288 (2014) 15–25. https://doi.org/10.1016/j.apsusc.2013.09.024.

[9] T. Ouyang, W. Lei, W. Tang, Y. Shen, C. Mo, Experimental investigation of the effect of IF-WS2 as an additive in castor oil on tribological property, Wear 486–487 (2021) 204070. https://doi.org/https://doi.org/10.1016/j.wear.2021.204070.

[10] S. Ranganatha, T. V. Venkatesha, K. Vathsala, Electroless Ni-W-P coating and its nano-WS 2 composite: Preparation and properties, Ind. Eng. Chem. Res. 51 (2012) 7932–7940. https://doi.org/10.1021/ie300104w.

[11] E. García-Lecina, I. García-Urrutia, J.A. Díez, J. Fornell, E. Pellicer, J. Sort, Codeposition of inorganic fullerene-like WS2 nanoparticles in an electrodeposited nickel matrix under the influence of ultrasonic agitation, Electrochim. Acta 114 (2013) 859–867. https://doi.org/10.1016/j.electacta.2013.04.088.

[12] J.J. Devadasan, C. Sanjeeviraja, M. Jayachandran, Electrodeposition of p-WS2 thin film and characterisation, J. Cryst. Growth 226 (2001) 67–72. https://doi.org/10.1016/S0022-0248(01)00851-X.

[13] S. Cui, W.S. Li, L. He, L. Feng, G.S. An, W. Hu, C.X. Hu, Tribological behavior of a Ni-WS2 composite coating across wide temperature ranges, Rare Met. 38 (2019) 1078–1085. https://doi.org/10.1007/s12598-018-1152-5.

[14] P. Kumari, P. Chauhan, A. Kumar, Superwetting Materials for Modification of Meshes for Oil/Water Separation, ACS Symp. Ser. 1408 (2022) 1–23. https://doi.org/10.1021/bk-2022-1408.ch001.

[15] H. Shalom, T. Bendikov, Y. Feldman, N. Lachman, A. Zak, R. Tenne, Chemical control of the surface of WS2 nanoparticles, Chem. Phys. Lett. 761 (2020) 138052. https://doi.org/10.1016/j.cplett.2020.138052.

[16] T. Guan, H. Zhang, F. Fang, N. Zhang, Synthesis of two-dimensional WS2/nickel nanocomposites via electroforming for high-performance micro/nano mould tools, Surf. Coatings Technol. 437 (2022) 128351. https://doi.org/https://doi.org/10.1016/j.surfcoat.2022.128351.

[17] T. Guan, Y. Lu, X. Wang, M.D. Gilchrist, F. Fang, N. Zhang, Scaling up the fabrication of wafer-scale Ni-MoS2/WS2 nanocomposite moulds using novel intermittent ultrasonic-assisted dual-bath micro-electroforming, Ultrason. Sonochem. 95 (2023) 106359. https://doi.org/10.1016/j.ultsonch.2023.106359.

[18] S. Mohan, S. Shriram, S. Karthikeyan, Electrodeposition of nanocrystalline nickel, Bull.

Electrochem. 18 (2002) 241–246.

[19] Y. He, W.T. Sun, S.C. Wang, P.A.S. Reed, F.C. Walsh, An electrodeposited Ni-P-WS2 coating with combined super-hydrophobicity and self-lubricating properties, Electrochim. Acta 245 (2017) 872–882. https://doi.org/10.1016/j.electacta.2017.05.166.

[20] J. Zhou, G. Zhao, J. Li, J. Chen, S. Zhang, J. Wang, F.C. Walsh, S. Wang, Y. Xue, Electroplating of non-fluorinated superhydrophobic Ni/WC/WS2 composite coatings with high abrasive resistance, Appl. Surf. Sci. 487 (2019) 1329–1340. https://doi.org/10.1016/j.apsusc.2019.05.244.

[21] J.M. Zhang, F. Ma, K.W. Xu, Calculation of the surface energy of fee metals with modified embedded-atom method, Chinese Phys. 13 (2004) 1082–1090. https://doi.org/10.1088/1009-1963/13/7/020.

[22] A. Ulman, Formation and Structure of Self-Assembled Monolayers, Chem. Rev. 96 (1996) 1533–1554. https://doi.org/10.1021/cr9502357.

[23] G. Kahl, S elf- a ssembled m onolayer (SAM), in: Dict. Genomics, Transcr. Proteomics, Wiley, 2015: pp. 1–1. https://doi.org/10.1002/9783527678679.dg11636.

[24] C.A. Thennakoon, R.B.S.D. Rajapakshe, A.U. Malikaramage, R.M. Gamini Rajapakse, Factors Affecting the Hydrophobic Property of Stearic Acid Self-Assembled on the TiO2 Substrate, ACS Omega 7 (2022) 48184–48191. https://doi.org/10.1021/acsomega.2c06217.

[25] B. Liu, S. Yan, Y. He, T. He, H. Li, Y. He, R. Song, Z. Zhang, D. Liu, J. Shangguan, Research for electrodeposited superhydrophobic Ni-W-WS2 coating and its anticorrosion and wear resistance, Colloids Surfaces A Physicochem. Eng. Asp. 655 (2022). https://doi.org/10.1016/j.colsurfa.2022.130236.

[26] D. Roy, A.K. Das, R. Saini, P.K. Singh, P. Kumar, M. Hussain, A. Mandal, A.R. Dixit, Pulse current co-deposition of Ni-WS 2 nano-composite film for solid lubrication, Mater. Manuf. Process. 32 (2017) 365–372. https://doi.org/10.1080/10426914.2016.1198011.

Chapter 6a

Fabrication of Ni-WS_2 coated stainless steel mesh for efficient oil-water separation

Abstract

A superhydrophobic - superoleophilic SS mesh with a water contact angle of 169.5° and surface roughness of 168 nm (R_a) was fabricated by electrodeposition. Ni-WS_2 coated mesh possessed a protruding rough surface comprising hierarchical WS_2 clusters. The combined effect of hydrophobic surface chemistry and roughness contributes to excellent superhydrophobic-superoleophilic and self-cleaning characteristics of the developed SHSM (superhydrophobic stainless steel mesh). The oil/water separation performance of SHSM was studied and the efficiency was greater than 98 % even after multiple uses. Further, the SHSM is highly corrosion resistant with excellent mechanical and chemical stability against strong acidic/alkaline solutions.

6a.1. Introduction

There is a growing interest in technologies for treating oily wastewater as the oil industry is one of the leading contributors to environmental pollution. The processing of oily wastewater sources is extensive, as oil industries, oil refineries, storage, transportation, and petrochemical industries produce substantial quantities of greasy wastewater. The following are the main ways in which oil pollution appears: (1) affecting the quality of potable water and groundwater reserves; (2) harming aquatic resources; (3) adversely affecting people's health; (4) environmental pollution; (5) influencing agricultural yield [1]. Floatation, gravity separation, centrifugation, filtration flocculation, and electrochemical techniques are examples of traditional oil/water separation methods [2–5]. Nevertheless, the majority of the techniques have limitations, including minimal separation efficiency and complicated operation. Compared to traditional methods, membrane filtration is facile and effective in the separation of oil-water mixtures. With the advancement of the interface theory along with the perspective of membrane wettability, filtration membranes with concurrent and opposite affinity to both oil and water are more efficient for their separation [6,7]. Furthermore, superhydrophobic and superoleophilic surfaces have resulted in remarkable research findings in the area of filtration

due to their superior self-cleaning properties [8,9]. Oil-water separation could be easily and effectively carried out by designing surfaces with special wettability [10,11].

In the past several years, numerous methods such as chemical etching [12], zeolite-coated method [13], electro-spinning [14], chemical vapor deposition (CVD) [15–17], self-assembly [18], sol-gel method [19], electrodeposition [20,21], etc are being reported for the development of superhydrophobic metallic mesh surfaces for oil-water separation. Among the metallic meshes, stainless steel meshes are more popular because of their easy availability, exceptional mechanical strength, and high efficiency.

Recently, there have been numerous studies on surface modification of stainless steel meshes for oil-water separation. For instance, Jiang et al. [22] developed a stainless steel mesh having both superhydrophobic and superoleophilic properties employing an emulsion of polytetrafluoroethylene (PTFE), polyvinyl acetate (PVAc) and polyvinyl alcohol (PVA) by spray method for oil-water separation. Using silica particles, Li et al. [23] designed highly hydrophobic and superoleophilic steel meshes for oil-water separation. Zhang et al. [24] fabricated a self-cleaning underwater superoleophobic stainless steel mesh surface using layer-by-layer assembly with sodium silicate and TiO_2 nanoparticles. However, these fabrication methods are costly, usually involving complex processes or rigorous conditions, in most cases requiring special equipment or materials, affecting their applicability [25–27].

Out of all the methods available for developing superhydrophobic surfaces, electrodeposition has specific advantages since this is an easy and quick process with high repeatability and is economical, as well as the ability to achieve a wide range of surface morphologies with high durability [28]. There are quite a few studies on the development of superhydrophobic nickel surfaces by electrodeposition [29,30].

In the present work, a novel strategy for developing superhydrophobic-superoleophilic Ni-WS_2 coated stainless steel mesh using one-step electrodeposition that will effectively resolve the long-term issue of oil-water separation in harsh conditions is presented. WS_2 particles with tunable morphology and low surface energy were incorporated into the Ni electrolyte during deposition. Deposition parameters were optimised in such a way that the developed SHSM possesses a micro-nanostructure comprising hierarchical WS_2 clusters and nodules along with Ni pine cones imparting a “cactus-like”/ “cauliflower-like” appearance. This fluorine-free method eliminates issues related to production expenses and potential environmental hazards. Flexibility of stainless steel mesh combined with stable Ni-WS_2

coating resulted in SHSM's mechanical robustness and chemical stability. Both hydrophobic surface chemistry and roughness contribute to excellent superhydrophobic-superoleophilic and self-cleaning characteristics of the developed SHSM. The thin film of air due to the micro-nano rough structure acts as a barrier that protects SHSM from corrosion. The fabricated SHSM can be reused for several cycles of oil-water separation without any degradation and thus possess unique repeatability. Since the developed SHSM is highly durable reduces the need for frequent replacements or maintenance. This can have a positive economic impact on the lifecycle of SHSM. As a result, this simple, eco-friendly, and low-cost method of fabricating SHSM would be a promising one for practical oil-water separation applications.

6a.2. Material and methods

6a.2.1. Materials

Commercial stainless steel mesh (SSM), with a pore size of less than 100 μm was supplied by Raj filters and wire mesh, India. Nickel sulphate ($NiSO_4 \cdot 6H_2O$), Nickel chloride ($NiCl_2 \cdot 6H_2O$), and Boric acid (H_3BO_3) were purchased from Merck. Cetyltrimethylammonium bromide (CTAB, $CH_3(CH_2)_{15}N(Br)(CH_3)_3$) and Saccharin ($C_7H_5NO_3S$) were obtained from Alfa Aesar. Tungsten disulphide nanoparticles (WS_2 NPs, 90 nm) were supplied by Sigma-Aldrich. Myristic acid $CH_3(CH_2)_{12}COOH$ and colouring agents like methylene blue (MB) and Sudan III (Oil Red O) were purchased from Himedia Laboratories. Solvents like toluene, n-hexane, dichloromethane (DCM), diethyl ether, and chloroform were purchased from Merck.

6a.2.2. Fabrication of Ni-WS_2 coated mesh

Electrodeposition was carried out in an aqueous electrolyte of Ni Watts bath containing $NiSO_4 \cdot 6H_2O$, $NiCl_2 \cdot 6H_2O$, and H_3BO_3. WS_2 nanoparticles were dispersed in a Ni bath, along with CTAB and saccharin (**Table 6a.1.**). The Ni-WS_2 bath was kept at a pH of 4–4.5. WS_2 nanoparticles were dispersed using an ultrasonicator for 30 min. Nickel plate (7 cm × 5 cm × 1 cm, 99.7 % purity) and stainless steel mesh (SSM) (6 cm × 6 cm, purity ≥ 99.5 %) were used as anode and cathode, respectively. SSM was cleaned by an ultrasonic cleaner with ethanol (30 min), acetone (15 min), and deionized water (15 min) followed by oven drying before deposition. Electrodeposition parameters including current density (4–6 A/dm^2), temperature (50–60 °C), time (15–30 min), and stirring rate (400–600 rpm) were varied. The concentration of WS_2 nanoparticles was also varied in the range (3–5) wt%. The electrodeposition was finally carried out at optimized conditions of the current density of 4 A/dm^2 for 15 min at a temperature

of 60°C with a 600 rpm stirring rate and 3 wt% concentration of WS_2 particles. The coated mesh was finally modified with low surface energy material Myristic acid MA.

Table 6a.1 Electrodeposition parameters for Ni-WS_2 coating

Electrodeposition parameters	Composition or parameter	Value
Plating solution	$NiSO_4.6H_2O$	250 g/l
	$NiCl_2.6H_2O$	45 g/l
	H_3BO_3	40 g/l
	CTAB	0.1 g/l
	Saccharin	1.5 g/l
	WS_2	3-5 wt%
Deposition Conditions	Current density	4-6 A/dm^2
	Temperature	50-60°C
	Time	15-30 minutes
	Stirring rate	400-600 rpm

6a.2.3. Characterization of the Ni-WS_2 coated mesh

6a.2.3.1. Morphology, phase composition & wettability studies

The surface morphology and elemental analysis of the developed coatings were examined using FE-SEM (FEI NOVA NANOSEM 450) and Zeiss EVO 18 cryo-SEM (EDS attached). Atomic Force Microscopy (AFM, Bruker Multimode-8HR system) in tapping mode was used to analyze the three-dimensional morphology to evaluate the surface roughness of the samples and the images were processed using NanoScope analysis 1.5 software package. The phase composition of the samples was studied using X-ray diffraction (XRD) via a Bruker D2 Phaser X-ray diffractometer with Cu - K_α radiation (λ = 1.5406 Å) in the 0-90° range. The wettability property (contact angle) of water droplets on coated SS mesh was explored by Goniometer (Data Physics, Germany). The water contact angle was calculated by taking the average of five measurements taken at various points on the same sample.

6a.2.3.2. Electrochemical measurements

The electrochemical measurements were done using a three-electrode setup in 1 M KOH using a CHI660E electrochemical workstation. Platinum wire (working electrode), Ag/AgCl in saturated KCl (reference electrode), and Ni-WS_2 coated SS mesh (counter electrode) are the electrodes employed. The voltammetric techniques LSV, CV, EIS and CA were used to analyse the electrochemical activity and stability of the electrode material. As a

preliminary step before actual measurements, CV in a reduction potential region was carried out for several cycles to activate the materials. Once the CV curves became consistent, LSV measurements were carried out to analyse the current response. All the measurements were performed at a scan rate of 2 mV s^{-1}, and EIS measurements were taken at a frequency range (100 KHz to 100 mHz). CA for about 10 hours was performed to confirm the stability, and the polarisation curves before and after 1000 cycles were also recorded.

6a.2.4. Durability & Performance Studies

6a.2.4.1 Stability & recyclability tests

By repeating the separation procedure for every single oil/water mixture, the recycling capacity of SHSM was evaluated for separation efficiency and corresponding water contact angle (WCA). Used SHSM was rinsed using ethanol as well as dried in a vacuum oven after the separation process and this was repeated 30 times. Mechanical stability of SHSM was evaluated by sandpaper abrasion test and chemical stability was tested by immersing it in corrosive solutions for 24 h.

6a.2.4.2 Self-cleaning test

The self-cleaning action of SHSM was analyzed using graphite particles as contaminants. Both coated and uncoated meshes were tilted followed by the dropping of distilled water droplets on their surface. The water rolling-off property and self-cleaning ability of both meshes were thus compared.

6a.2.4.3 Oil/Water Separation

Several 40 mL oil/water mixtures were made in a 1:1 volume ratio of water and oil (including toluene, n-hexane, dichloromethane, diethyl ether, chloroform, and kerosene). The oil/water mixtures were poured through SSM and gravity-based filtration was employed throughout the separation process.

The separation efficiency, η was given by $\eta = m_1/ m_0 \times 100\%$ **(6a.1.)**

where, m_0 and m_1 are the mass of oil before and after separation, respectively.

After pouring the oil-water mixture through the mesh, the permeation flux (*F*) was determined according to the equation,

$$F = V/St \qquad \textbf{(6a.2.)}$$

where, *V* is the volume of the filtrate, *S* is the area of the contacted mesh, and *t* is the time.

6a.3. Results and discussion

6a.3.1. Surface morphology and elemental composition

SEM was taken for both the original and modified stainless steel meshes. **Figure 6a.1 (a)** shows the typical image of a stainless steel mesh, suggesting that the pristine mesh has a smooth surface. Electrodeposition has an important effect on the morphology of stainless steel mesh. As can be seen in **Figure 6a.2 (a-b)**, pure nickel deposited mesh (hydrophobic) had a pine-cone structure. The pure Ni coating contained fine Ni crystals which are visible in the magnified image (**Figure 6a.2. (b)**).

With the addition of WS_2 nanoparticles, the surface became rougher. The development of a rough surface is an important factor in the preparation of special super-wetting materials [31]. During the time of electrodeposition, the deposited Ni ions are attracted to WS_2 nanoparticles because of the electrostatic interaction between positively charged Ni ions and negatively charged WS_2 nanoparticles [32]. As already reported [33], Ni ions then begin to deposit on the WS_2 particles, forming a thin film. Ni ions will continue depositing and will start to grow in size and shape.

The cauliflower-like structure is formed when the Ni ions grow in a dendritic fashion, with branches extending out from the main body of the structure. Thus the Ni-WS_2 coated mesh possessed a protruding rough surface comprising hierarchical WS_2 clusters and nodules resulting in “cactus-like”/ “cauliflower-like” structures (**Figure 6a.3(a-b)**). Thorn like projections are seen in SEM image of high-magnification of Ni-WS_2 coated SS mesh (**Figure 6a.4)**. WS_2 nanoparticles have a higher surface area, which provides more sites for the Ni ions to nucleate. Since WS_2 particles are negatively charged, they attract positively charged Ni ions. Thus the appearance of the cauliflower-like structure may be caused primarily by the preferred adsorption and growth of Ni^{2+} ions on WS_2 particles during deposition.

The "cactus/cauliflower-like" nodular structures of the coating generate more sites for MA adsorption, which leads to the formation of a hydrolysis film on these surfaces. The nodule structures are rough with high surface area so that MA molecules get more sites to bind. This increased binding leads to more MA molecules being hydrolysed, which produces a film on the mesh surface which in turn improves the hydrophobicity. In total, it may be concluded that the micron-sized spherical particles, along the nano-scale granular protuberance, resulted in a highly rough hierarchical structure that resulted in the superhydrophobic behaviour of SHSM.

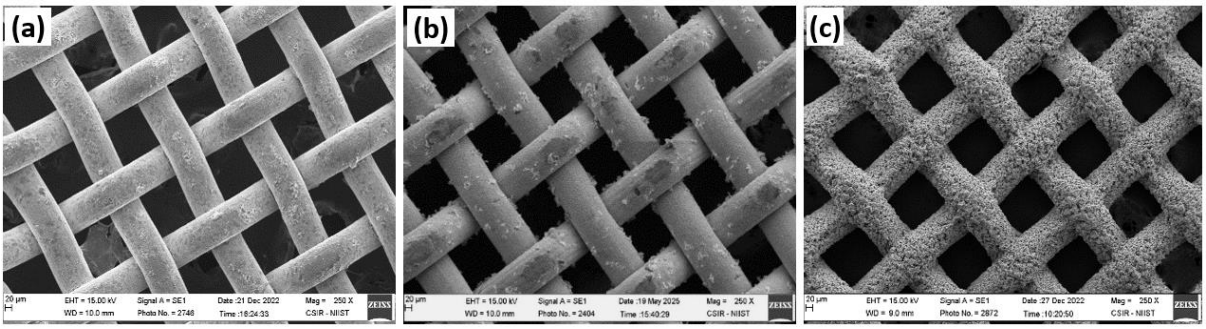

Figure 6a.1.(a) Pristine SS mesh **(b)** Pure Ni coated SS mesh **(c)** MA-Ni-WS_2 coated SS mesh

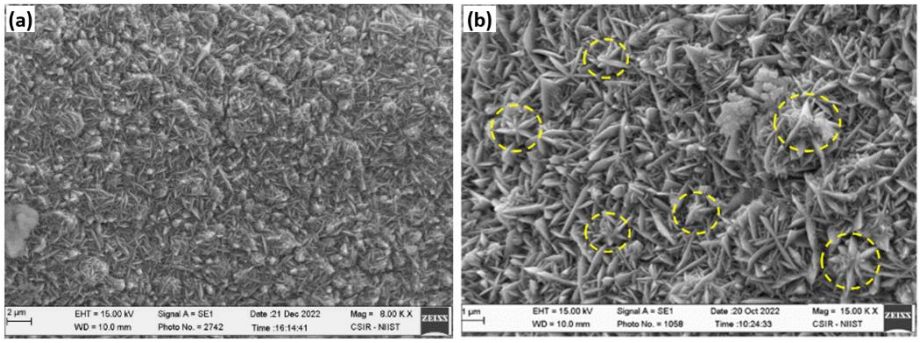

Figure 6a.2 (a-b) Pine-cone structure in pure Ni coated SS mesh

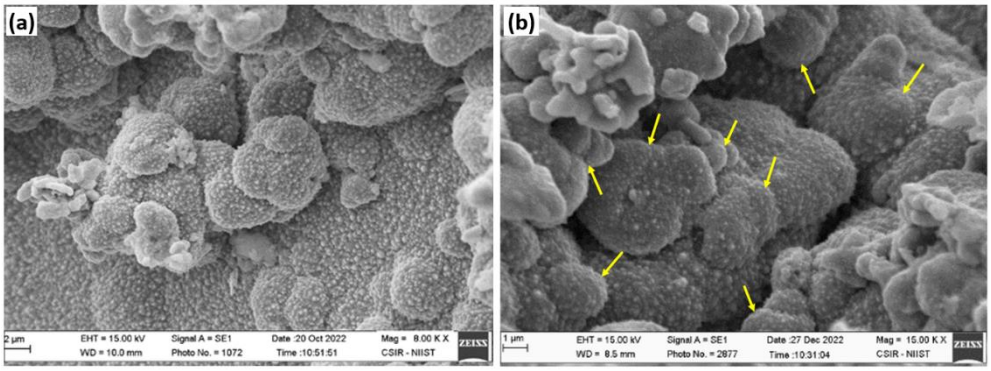

Figure 6a.3 (a,b). Cactus/cauli-flower like morphology in MA-Ni-WS_2 coated SS mesh

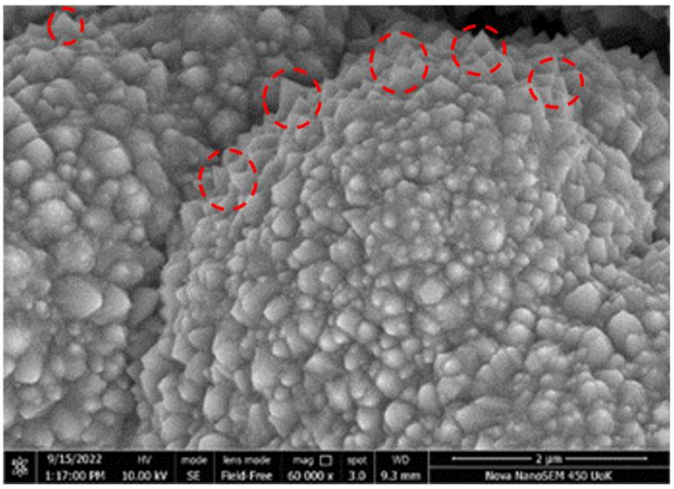

Figure 6a.4. Thorn-like projections in MA-Ni-WS_2 coated SS mesh

EDS shows the distribution of elements on the surface of Ni-WS_2 coated SS mesh as in **Figure 6a.5.** Elements like Nickel (**Ni**), tungsten (**W**), and sulphur (**S**) were found. Ni is predominantly present in the coating whereas sulphur was primarily found in the cacti-like structures.

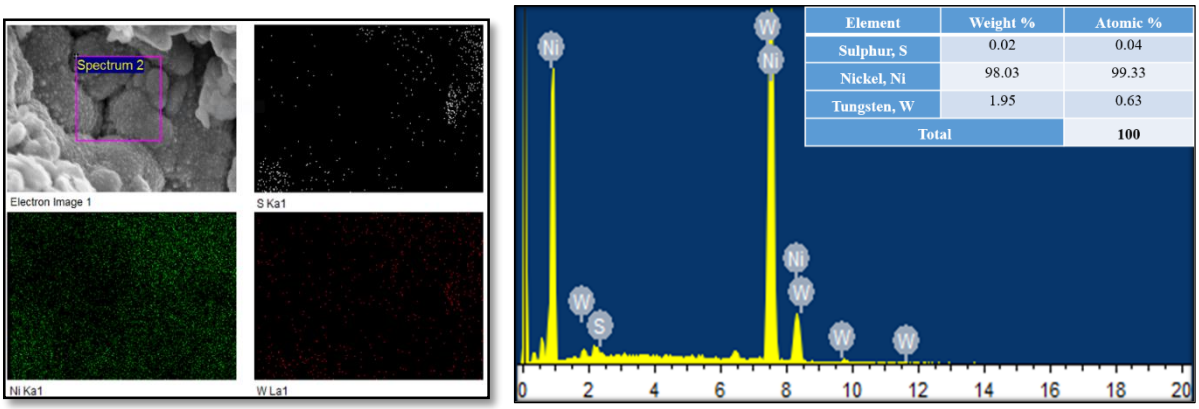

Element	Weight %	Atomic %
Sulphur, S	0.02	0.04
Nickel, Ni	98.03	99.33
Tungsten, W	1.95	0.63
Total		100

Figure 6a.5. EDS analysis of MA-Ni-WS_2 coated SS mesh

6a.3.2. AFM analysis

Figure 6a.6. (a)-(b) shows the 3D surface morphology of pure Ni coated and Ni-WS_2 coated SS meshes respectively. The average roughness (R_a), the mathematical mean deviation of the roughness profiles, is the most common way of calculating surface roughness. The surface roughness of the coated meshes significantly affects their wetting behavior. In the case of pure Ni coated mesh, R_a is 87.6 nm whereas, in the case of Ni-WS_2 coated mesh, R_a is 168 nm. This increment has been reflected in the WCA values i.e. 127.2° for pure Ni and 151.3° for Ni-WS_2 coated meshes respectively.

In the case of pure Ni-coated mesh, irregularly located clusters of varying heights are visible on the surface as seen in **Figure 6a.6.(a)**. **Figure 6a.6.(b)** of Ni-WS_2 coated mesh shows the presence of protrusions (valleys or bumps) of larger heights and sizes. The micro-nano hierarchical structure comprising of these bumps/protrusions results in the reduction of the area of contact between the solid−liquid interface and water maintaining the spherical shape of the water droplet without spreading. Thus, this micro-nano structure forms a thin film of air that acts as a barrier increasing the WCA of Ni-WS_2 coated mesh.

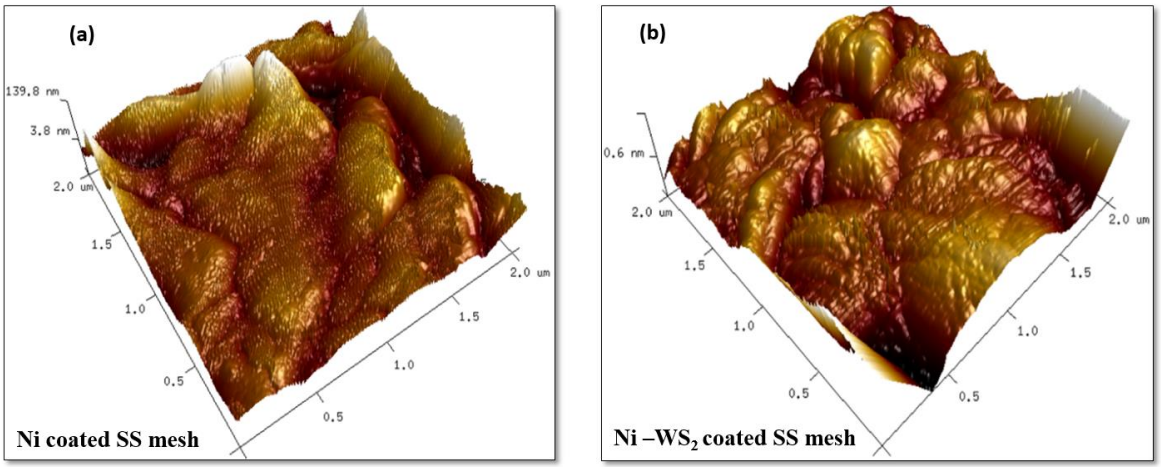

R_a = 87.6 nm; R_q = 110 nm **R_a = 168 nm; R_q = 199 nm**

Figure 6a.6. 3D surface morphologies of the developed meshes

6a.3.3. Phase Composition & Crystalline Structure Analysis

X-ray diffraction was employed to examine the crystal planes of the coating. All peaks are identified and indexed using standard Powder Diffraction Files, such as JCPDS 04-0850 for Nickel and JCPDS 84-1398 for WS_2. The XRD pattern of pure Ni-coated SS mesh is shown in **Figure 6a.7.(a)**. From the data, three peaks of Ni at 2θ corresponding to 44.32°, 51.77°, and 76.3° are assigned to (111), (200), and (220) Bragg reflections of the face-centered cubic (fcc) structure of metallic nickel [34]. The incorporation of WS_2 particles caused important microstructural changes; providing more nucleation sites. It also retards the growth of large Ni crystals, resulting in smaller grain sizes. Analyzing the XRD pattern of Ni-WS_2 coated SS mesh, distinct peaks are found at 14°, 29.1°, 33°, 40°, 49°, 58°, and 60° correspond to (002), (004), (100), (106), (110), (008) and (112) phases confirming the hexagonal closed-packed (hcp) structure of WS_2 [35] **(Figure 6a.7 (b))**.

Whenever Ni is deposited onto a substrate, the first few layers of atoms will tend to form (111) plane [36]. The (111) plane is one of the most densely packed planes in a crystal lattice, and it has the lowest surface energy compared to other planes [37]. Thus the growth of the (111) plane helps to minimize the total surface energy of the crystal. In this case, there is the presence of strong (111) Ni peaks indicating reduced surface energy [33,36,38]. Post electrodeposition after treatment with MA, it is believed that MA is chemically adsorbed on the Ni(111) surface via bi-dentate interaction, i.e. two oxygen atoms from the carboxylic acid group (-COOH) of MA with 3d orbital of Ni. This bonding interaction prevents the water molecules from forming hydrogen bonds with the surface, enhancing the hydrophobicity [39].

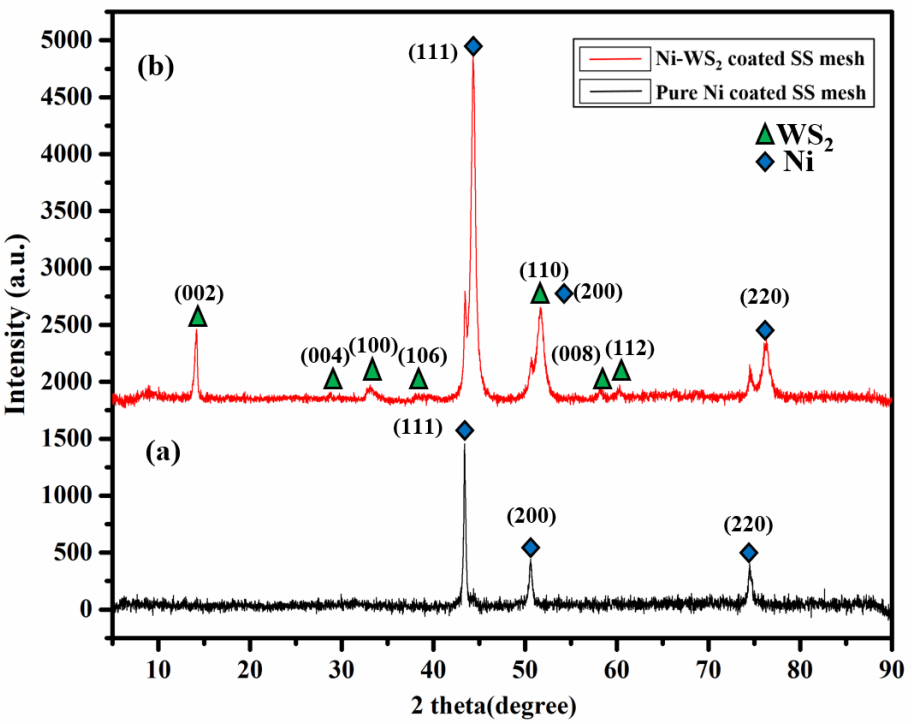

Figure 6a.7. XRD pattern of (a) Pure Ni coated SS mesh, (b) MA-Ni-WS_2 coated SS mesh

6a.3.4. Wettability Studies

Chemical composition, free energy of the surface, and surface morphology all affect the surface wetting property of a coating. **Figure 6a.8.** shows the contact angle of the water droplet on the coated SS mesh (pure Ni, Ni-WS_2, MA-Ni-WS_2). As it is evident from the WCA measurements there was a gradual increase in the hydrophobicity of the surface (i.e. **127.2°** to **169.5°**). Coated mesh exhibited wettability with the oil droplets, quickly spread while the water droplet remained on the surface of the mesh in an extremely spherical fashion. The micro-nanostructure along with the action of low surface energy material MA (27.4 dynes/cm) reduces the contact area between the solid-liquid interface and water by forming a thin, strong cohesive layer on Ni-WS_2 coating. Whenever applied over a surface, MA can self-assemble in an organized manner through hydrogen bonding of carboxyl groups as well as hydrophobic interaction in-between methyl groups. These hydrophobic chains create a barrier that prevents water from wetting the surface. As a result, water droplets tend to bead up and roll off the surface instead of spreading out and wetting the surface.

Water droplets will exist in superhydrophobic Cassie State as a result of incorporation of WS_2 nanoparticles and modification of the Ni-coated surface with low surface energy material MA [40]. According to the Wenzel equation,

$$\cos \theta_w = r \cos \theta \qquad (6a.3.)$$

where θ_w is the contact angle of liquids on a rough surface, θ is the contact angle on a flat surface and r is the roughness factor [41]. This equation implies that as the roughness of the surface increases, the hydrophobic surface becomes more hydrophobic and the oleophilic surface becomes more oleophilic. In SHSM, the micro-nano hierarchical structure makes the surface rougher. As a result, when an oil droplet is placed on Ni-WS_2 coated SS mesh, it can enter the nanostructures formed by Ni grain cells surrounded by petal-like WS_2 nanoparticles as a result of the capillary effect. The combined effect of hydrophobic surface chemistry and the roughness results in excellent superhydrophobic and superoleophilic characteristics of the developed SHSM.

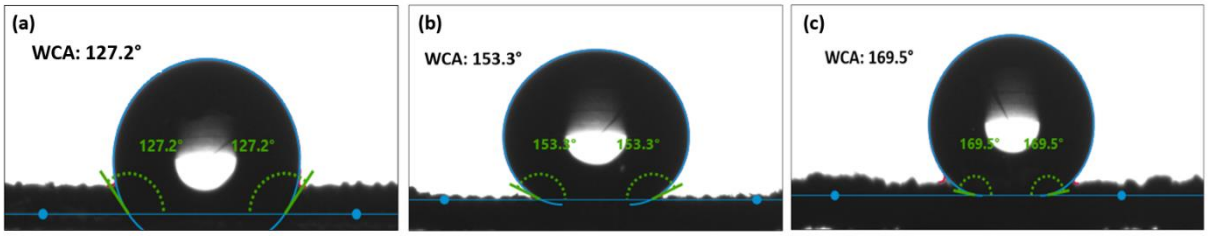

Figure 6a.8: WCAs of coated mesh (a) Pure Ni, (b) Ni-WS_2, (c) MA-Ni-WS_2

6a.3.5. Stability Tests

Mechanical stability is a crucial measure of superhydrophobic material's practical application. A mechanical durability test was carried out to test the robustness of the developed SHSM. The coated mesh was put on 400 grit sandpaper. Additionally, a 100 g weight was used as an outside force, as illustrated in **Figure 6a.9.** In this procedure, the coated mesh was moved twenty centimeters along the ruler's direction, followed by a rotation of 90°, and another twenty centimeters in the direction of the ruler. The entire procedure was referred to as a cycle. The WCA of the sample did not change significantly after 30 cycles, and it was still greater than 150° (**Figure 6a.10(a)**). From this, it may be concluded that the abrasion process only damaged the outermost structure, while the internal hierarchical structure remained intact.

The oily wastewater released by industries often turns to be acidic or alkaline. To deal with wastewater, the as-prepared mesh must be chemically stable enough to withstand harsh environmental conditions. The wettability of coated SS mesh was tested with droplets of varying pH as shown in **Figure 6a.10(b).** Ni-WS_2 coated SS mesh showed superhydrophobicity in acidic as well as alkaline range of pH. Immersion tests were conducted using corrosion solutions of HCl (pH = 1, acidic), NaCl (pH = 7, neutral), and NaOH (pH = 14, alkaline) to test the chemical stability. After placing the sample in the corrosion solution, it is believed that an air film formation took place between the corrosion solution and the sample. This particular film can hinder corrosive media from approaching the sample, preventing corrosion. Even under a highly corrosive strong acidic environment (pH = 1), the contact angle of MA-treated Ni-WS_2 SS mesh was 150°, demonstrating effective corrosion resistance of the mesh in harsh environments.

6a.3.6. Self-Cleaning Tests

One of the most important applications of superhydrophobic surfaces is self-cleaning. In this study, the self-cleaning action of SHSM was studied using black graphite particles as contaminants. Because of the superhydrophobic nature of the mesh as in **Figure 6a.11.**, the droplet was still spherical bounded with graphite particles, and rolled out from the surface retaining its superhydrophobicity. A comparison with the uncoated mesh showed that graphite particles adhered to the surface and remained sticky. The process was carried out several times still SHSM maintained its self-cleaning ability.

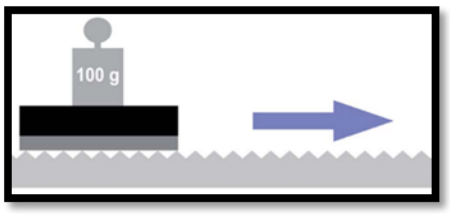

Figure 6a.9. Illustration of sandpaper abrasion test

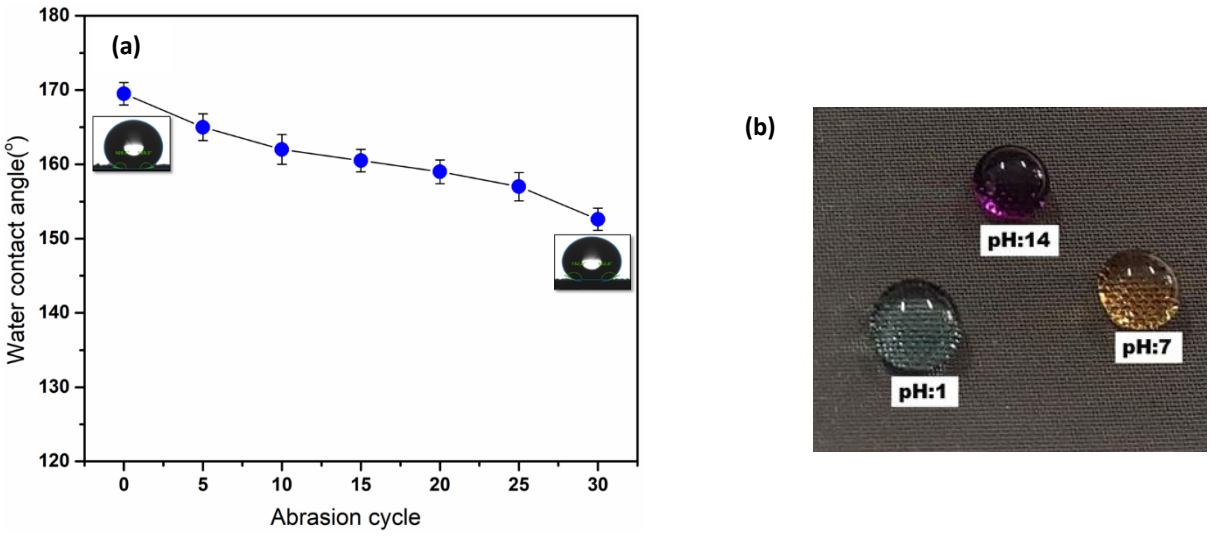

Figure 6a.10. a) Variation of WCA after different abrasion cycles **b)** Photograph of water droplets of varying pH on SHSM

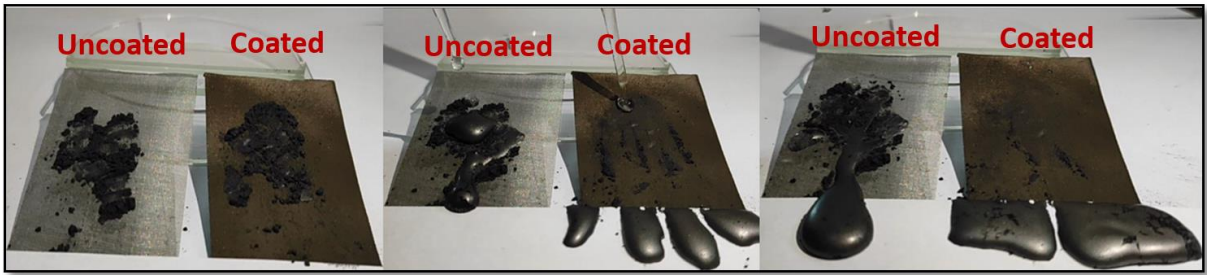

Figure 6a.11. Different stages of self-cleaning action of as-prepared SHSM (right) in contrast to uncoated mesh (left)

6a.3.7. Oil-water separation

For oil-water separation experiments, oil was colored with Sudan III (red), and water was colored with Methylene blue (blue) (**Figure 6a.12**). The contact state of water droplets on the as-prepared SHSM shifts from Cassie to Wenzel state during the separation of the oil/water mixture. The separation efficiency of the superhydrophobic mesh was evaluated by Equation 1. The initial separation efficiency for a 1:1 oil-water mixture was as high as 98.3%. After 30 separation cycles, the separation efficiency was still higher more than 98%, showing that the mesh maintained the oil−water separation ability.

In addition, the SHSM can separate different oil-water mixtures (n-hexane, diethyl ether, toluene, kerosene, dichloromethane) indicating that it can generally separate the oil−water mixture of varying surface tensions (**Figure 6a.13 (a)**). Oil flux was also calculated for various types of oils using **Equation 6a.2** (**Figure 6a.13 (b)**). Since the oil-water separation

efficiency of Ni-WS_2 coated SS mesh was greater than 98%, as a result of which the mesh can be used as a film-like material for efficient oil-water separation.

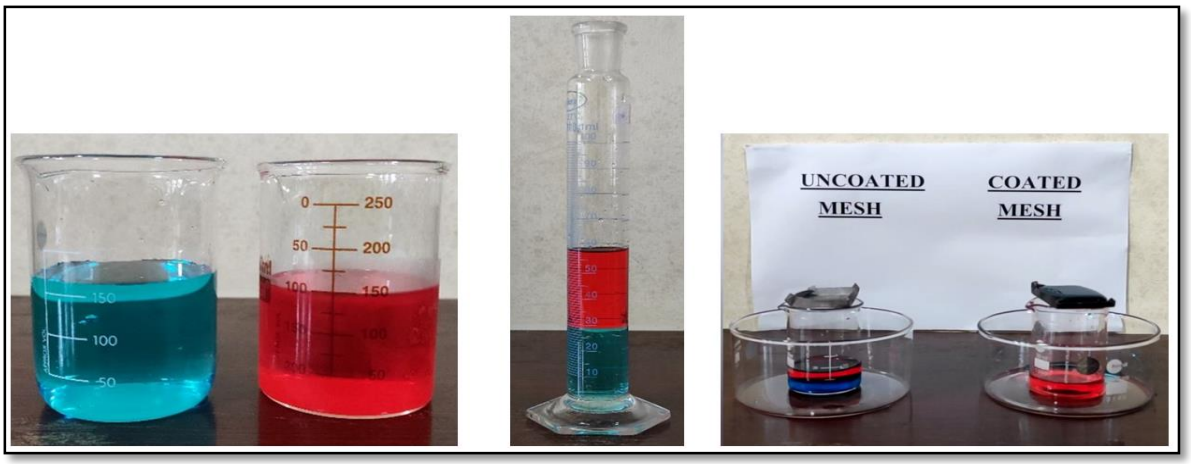

Figure 6a.12. Oil-water separation experiments; oil dyed with Sudan III (red) and water dyed with Methylene blue (blue)

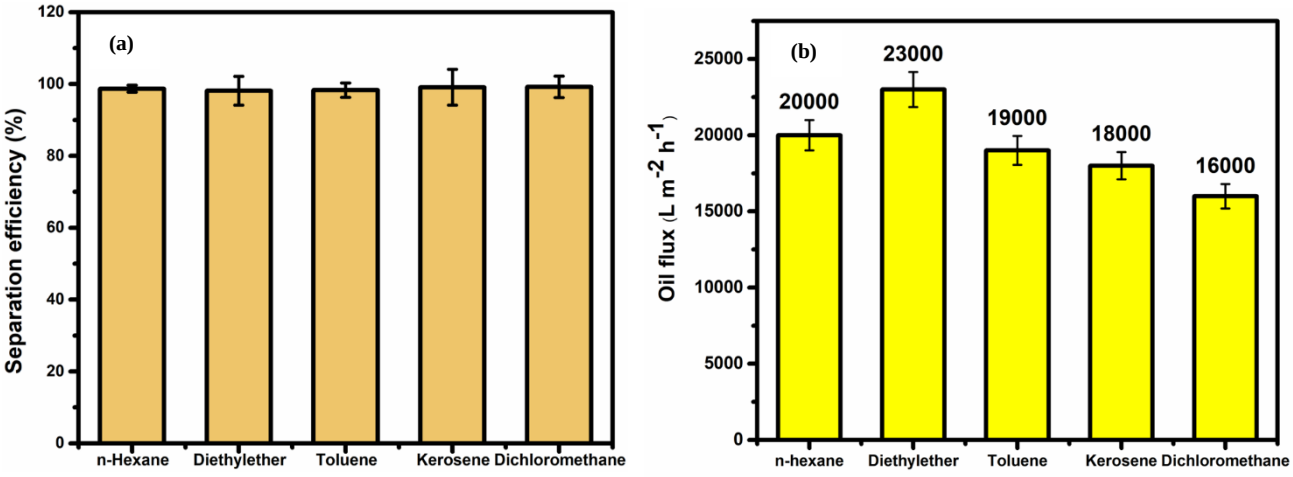

Figure 6a.13. Separation efficiencies **(a)** & flux **(b)** of SHSM for different types of oils

6a.4. Conclusions

A superhydrophobic - superoleophilic SS mesh with a water contact angle of 169.5^0 and surface roughness of 199 nm (R_q) was fabricated by electrodeposition. At the optimised concentration of WS_2 (3 wt%) and deposition parameters viz. current density of 4 A/dm^2, deposition time of 15 minutes, temperature of 60°C, and stirring speed of 600 rpm, the surface of SS mesh was effectively modified. Ni-WS_2 coated mesh possessed a protruding rough surface comprising hierarchical WS_2 clusters. The combined effect of hydrophobic surface

chemistry and the roughness contributes to excellent superhydrophobic-superoleophilic and self-cleaning characteristics of the developed SHSM. The oil/water separation performance of SHSM was studied and the efficiency was greater than 98% even after multiple uses. Further, the SHSM is highly corrosion resistant with excellent mechanical and chemical stability against strong acidic/alkaline solutions. Further, it can selectively separate different oil-water mixtures like hexane-water, diethyl ether-water, toluene-water, kerosene-water, and dichloromethane-water. Thus, the developed SS mesh has the potential in the treatment of industrial oil-water mixtures as well as environmental oil spills due to its excellent oil-water separation efficiency and durability in harsh conditions.

References

[1] L. Yu, M. Han, F. He, A review of treating oily wastewater, Arab. J. Chem. 10 (2017) S1913–S1922. https://doi.org/10.1016/j.arabjc.2013.07.020.

[2] A.B. Nordvik, J.L. Simmons, K.R. Bitting, A. Lewis, T. Strøm-Kristiansen, Oil and water separation in marine oil spill clean-up operations, Spill Sci. Technol. Bull. 3 (1996) 107–122. https://doi.org/https://doi.org/10.1016/S1353-2561(96)00021-7.

[3] K. Gaaseidnes, J. Turbeville, Separation of oil and water in oil spill recovery operations, Pure Appl. Chem. 71 (1999) 95–101. https://doi.org/10.1351/pac199971010095.

[4] B. Tansel, J. Regula, Coagulation enhanced centrifugation for treatment of petroleum hydrocarbon contaminated waters, J. Environ. Sci. Heal. Part A 35 (2000) 1557–1575. https://doi.org/10.1080/10934520009377055.

[5] B. Huang, X. Li, W. Zhang, C. Fu, Y. Wang, S. Fu, Study on demulsification-flocculation mechanism of oil-water emulsion in produced water from Alkali/Surfactant/Polymer flooding, Polymers (Basel). 11 (2019). https://doi.org/10.3390/polym11030395.

[6] D. Miller, D. Dreyer, C. Bielawski, D. Paul, B. Freeman, Surface Modification of Water Purification Membranes: a Review, Angew. Chemie 129 (2016). https://doi.org/10.1002/ange.201601509.

[7] D. Rana, T. Matsuura, Surface modifications for antifouling membranes, Chem. Rev. 110 (2010) 2448–2471. https://doi.org/10.1021/cr800208y.

[8] B. Wang, W. Liang, Z. Guo, W. Liu, Biomimetic super-lyophobic and super-lyophilic materials applied for oil/water separation: a new strategy beyond nature, Chem. Soc. Rev. 44 (2015) 336–361. https://doi.org/10.1039/C4CS00220B.

[9] G. Dunderdale, C. Urata, T. Sato, M. England, A. Hozumi, Continuous, High-Speed, and Efficient Oil/Water Separation using Meshes with Antagonistic Wetting Properties, ACS Appl. Mater. Interfaces (2015). https://doi.org/10.1021/acsami.5b06207.

[10] F. Zhang, W. Zhang, Z. Shi, D. Wang, L. Jiang, Nanowire-Haired Inorganic Membranes with Superhydrophilicity and Underwater Ultralow Adhesive

Superoleophobicity for High-Efficiency Oil/Water Separation, Adv. Mater. 25 (2013). https://doi.org/10.1002/adma.201301480.

[11] X. Yao, Y. Song, L. Jiang, Applications of bio-inspired special wettable surfaces, Adv. Mater. 23 (2011) 719–734. https://doi.org/10.1002/adma.201002689.

[12] D.K. Sarkar, N. Saleema, One-step fabrication process of superhydrophobic green coatings, Surf. Coatings Technol. 204 (2010) 2483–2486. https://doi.org/https://doi.org/10.1016/j.surfcoat.2010.01.033.

[13] Q. Wen, J. Di, L. Jiang, J. Yu, R. Xu, Zeolite-coated mesh film for efficient oil–water separation, Chem. Sci. 4 (2013) 591–595. https://doi.org/10.1039/C2SC21772D.

[14] J. Wu, N. Wang, L. Wang, H. Dong, Y. Zhao, L. Jiang, Electrospun Porous Structure Fibrous Film with High Oil Adsorption Capacity, ACS Appl. Mater. \& Interfaces 4 (2012) 3207–3212. https://doi.org/10.1021/am300544d.

[15] X. Zhou, Z. Zhang, X. Xu, X. Men, X. Zhu, Facile Fabrication of Superhydrophobic Sponge with Selective Absorption and Collection of Oil from Water, Ind. \& Eng. Chem. Res. 52 (2013) 9411–9416. https://doi.org/10.1021/ie400942t.

[16] S. Seeger, Superhyrophobic Materials: Polyester Materials with Superwetting Silicone Nanofilaments for Oil/Water Separation and Selective Oil Absorption (Adv. Funct. Mater. 24/2011), Adv. Funct. Mater. 21 (2011). https://doi.org/10.1002/adfm.201190113.

[17] C.R. Crick, J.A. Gibbins, I.P. Parkin, Superhydrophobic polymer-coated copper-mesh; membranes for highly efficient oil–water separation, J. Mater. Chem. A 1 (2013) 5943–5948. https://doi.org/10.1039/C3TA10636E.

[18] N. Liu, Y. Cao, X. Lin, Y. Chen, L. Feng, Y. Wei, A Facile Solvent-Manipulated Mesh for Reversible Oil/Water Separation, ACS Appl. Mater. \& Interfaces 6 (2014) 12821–12826. https://doi.org/10.1021/am502809h.

[19] S. Sriram, R.K. Singh, A. Kumar, Oil-water separation through an ultrahydrophobic filter paper developed by sol-gel dip-coating technique, Mater. Today Proc. 26 (2020) 2495–2501. https://doi.org/https://doi.org/10.1016/j.matpr.2020.02.531.

[20] B. Wang, Z. Guo, Superhydrophobic copper mesh films with rapid oil/water separation properties by electrochemical deposition inspired from butterfly wing, Appl. Phys.

Lett. 103 (2013). https://doi.org/10.1063/1.4817922.

[21] S. Wang, Y. Song, L. Jiang, Microscale and nanoscale hierarchical structured mesh films with superhydrophobic and superoleophilic properties induced by long-chain fatty acids, Nanotechnology 18 (2006) 15103. https://doi.org/10.1088/0957-4484/18/1/015103.

[22] L. Feng, Z. Zhang, Z. Mai, Y. Ma, B. Liu, L. Jiang, D. Zhu, A super-hydrophobic and super-oleophilic coating mesh film for the separation of oil and water, Angew. Chemie - Int. Ed. 43 (2004) 2012–2014. https://doi.org/10.1002/anie.200353381.

[23] B. Li, X. Liu, X. Zhang, W. Chai, Stainless steel mesh coated with silica for oil–water separation, Eur. Polym. J. 73 (2015) 374–379. https://doi.org/https://doi.org/10.1016/j.eurpolymj.2015.10.031.

[24] Y.K. Lai, Y.X. Tang, J.Y. Huang, F. Pan, Z. Chen, K.Q. Zhang, H. Fuchs, L.F. Chi, Bioinspired TiO2 nanostructure films with special wettability and adhesion for droplets manipulation and patterning, Sci. Rep. 3 (2013) 1–8. https://doi.org/10.1038/srep03009.

[25] M. Laad, B. Ghule, Fabrication Techniques of Superhydrophobic Coatings: A Comprehensive Review, Phys. Status Solidi Appl. Mater. Sci. 219 (2022) 1–19. https://doi.org/10.1002/pssa.202200109.

[26] H.M. Ali, M.A. Qasim, S. Malik, G. Murtaza, Techniques for the Fabrication of Super-Hydrophobic Surfaces and Their Heat Transfer Applications, Heat Transf. - Model. Methods Appl. (2018). https://doi.org/10.5772/intechopen.72820.

[27] G. Barati Darband, M. Aliofkhazraei, S. Khorsand, S. Sokhanvar, A. Kaboli, Science and Engineering of Superhydrophobic Surfaces: Review of Corrosion Resistance, Chemical and Mechanical Stability, Arab. J. Chem. 13 (2020) 1763–1802. https://doi.org/10.1016/j.arabjc.2018.01.013.

[28] T. Darmanin, E.T. De Givenchy, S. Amigoni, F. Guittard, Superhydrophobic surfaces by electrochemical processes, Adv. Mater. 25 (2013) 1378–1394. https://doi.org/10.1002/adma.201204300.

[29] S. Huang, Y. Hu, W. Pan, Relationship between the structure and hydrophobic performance of Ni–TiO2 nanocomposite coatings by electrodeposition, Surf. Coatings

Technol. 205 (2011) 3872–3876.
https://doi.org/https://doi.org/10.1016/j.surfcoat.2011.01.065.

[30] T. Xiang, S. Ding, C. Li, S. Zheng, W. Hu, J. Wang, P. Liu, Effect of current density on wettability and corrosion resistance of superhydrophobic nickel coating deposited on low carbon steel, Mater. Des. 114 (2017) 65–72.
https://doi.org/https://doi.org/10.1016/j.matdes.2016.10.047.

[31] P. Kumari, P. Chauhan, A. Kumar, Superwetting Materials for Modification of Meshes for Oil/Water Separation, ACS Symp. Ser. 1408 (2022) 1–23.
https://doi.org/10.1021/bk-2022-1408.ch001.

[32] H. Shalom, T. Bendikov, Y. Feldman, N. Lachman, A. Zak, R. Tenne, Chemical control of the surface of WS2 nanoparticles, Chem. Phys. Lett. 761 (2020) 138052.
https://doi.org/10.1016/j.cplett.2020.138052.

[33] G. Zhao, Y. Xue, Y. Huang, Y. Ye, F.C. Walsh, J. Chen, S. Wang, One-step electrodeposition of a self-cleaning and corrosion resistant Ni/WS 2 superhydrophobic surface, RSC Adv. 6 (2016) 59104–59112. https://doi.org/10.1039/C6RA07899K.

[34] S. Mohan, S. Shriram, S. Karthikeyan, Electrodeposition of nanocrystalline nickel, Bull. Electrochem. 18 (2002) 241–246.

[35] Y. He, W.T. Sun, S.C. Wang, P.A.S. Reed, F.C. Walsh, An electrodeposited Ni-P-WS2 coating with combined super-hydrophobicity and self-lubricating properties, Electrochim. Acta 245 (2017) 872–882.
https://doi.org/10.1016/j.electacta.2017.05.166.

[36] J. Zhou, G. Zhao, J. Li, J. Chen, S. Zhang, J. Wang, F.C. Walsh, S. Wang, Y. Xue, Electroplating of non-fluorinated superhydrophobic Ni/WC/WS2 composite coatings with high abrasive resistance, Appl. Surf. Sci. 487 (2019) 1329–1340.
https://doi.org/10.1016/j.apsusc.2019.05.244.

[37] J.M. Zhang, F. Ma, K.W. Xu, Calculation of the surface energy of fee metals with modified embedded-atom method, Chinese Phys. 13 (2004) 1082–1090.
https://doi.org/10.1088/1009-1963/13/7/020.

[38] E. García-Lecina, I. García-Urrutia, J.A. Díez, J. Fornell, E. Pellicer, J. Sort, Codeposition of inorganic fullerene-like WS2 nanoparticles in an electrodeposited

nickel matrix under the influence of ultrasonic agitation, Electrochim. Acta 114 (2013) 859–867. https://doi.org/10.1016/j.electacta.2013.04.088.

[39] Y. Bai, D. Kirvassilis, L. Xu, M. Mavrikakis, Atomic and molecular adsorption on Ni(111), Surf. Sci. 679 (2019) 240–253. https://doi.org/10.1016/j.susc.2018.08.004.

[40] S. Parvate, P. Dixit, S. Chattopadhyay, Superhydrophobic Surfaces: Insights from Theory and Experiment, J. Phys. Chem. B 124 (2020) 1323–1360. https://doi.org/10.1021/acs.jpcb.9b08567.

[41] H. Yang, P. Pi, Z.-Q. Cai, X. Wen, X. Wang, J. Cheng, Z. Yang, Facile preparation of super-hydrophobic and super-oleophilic silica film on stainless steel mesh via sol–gel process, Appl. Surf. Sci. 256 (2010) 4095–4102. https://doi.org/https://doi.org/10.1016/j.apsusc.2010.01.090.

Chapter 6b

Morphology tuned Ni-WS_2 coated stainless steel mesh as a bi-functional electrocatalyst for overall water splitting

Abstract

Electrocatalytic water splitting is a sustainable method for hydrogen production, but the high cost of noble metal catalysts limits its practicality. Here, we present a novel electrodeposited Ni-WS_2 coated stainless steel mesh as an efficient and cost-effective bi-functional catalyst for both the hydrogen evolution reaction (HER) and oxygen evolution reaction (OER). The innovative design of the catalyst with its hierarchical surface and the synergistic effect of Ni and WS_2, combined with a highly reactive surface and effective bubble separation, enables remarkable catalytic performance. The catalyst achieves overpotentials of 89 mV for HER and 230 mV for OER at 10 mA/cm², with robust stability for 50 hours in alkaline medium. For overall water splitting, a cell potential of 1.56 V at 10 mA/cm² was required, maintaining stability over 50 hours. This work represents a step forward in utilisation of non-precious metals like nickel for efficient, cost-effective, and sustainable hydrogen production.

6b.1. Introduction

The World Energy Council studies indicate that the global energy demand is expected to increase by 45% to 60% by the year 2030 [1]. Renewable energy is gaining prominence due to rising energy demands and depleting fossil fuels [2,3]. Out of all the sustainable energy sources, hydrogen is the most promising fuel candidate because of its high gravimetric energy density, comparatively more availability, and no emissions throughout consumption [4,5]. Conventional large-scale hydrogen production via steam reforming suffers from carbon residues and limited purity, making electrolytic water splitting a more sustainable alternative [6]. However, the process requires efficient catalysts to overcome sluggish reaction kinetics and high overpotentials.

The water-splitting reaction takes place through cathodic hydrogen evolution reaction (HER) and anodic oxygen evolution reaction (OER) [7]. At present, Pt-group metals are the most efficient HER catalysts, and Ir/Ru-based compounds serve as conventional catalysts for OER. However, the high cost, poor stability (especially in alkaline water electrolysis), and the limited availability of these metals prevent their widespread applications [8]. Bi-functional catalysts capable of performing HER and OER in a single electrolyte offer a cost-effective solution by reducing the complexity of the system and improving performance. Among all the available materials, transition metal-based materials, particularly Ni-based materials are preferred due to their low cost, high elemental abundance, strength, flexibility, corrosion resistance, thermal and electrical conductivity [9].

Ni-based compounds, including alloys, phosphides, sulphides, and oxides, have been reported for their ability to catalyse alkaline overall water splitting (OWS). Kuang et al. [10] reported the usage of $NiMoP_2$ nanowire as an electrocatalyst for both HER and OER. A unique nanostructured Ni-Fe-Co coated bi-functional 3D electrode was developed by Darband et al. [11]. A highly efficient and robust bi-functional Ni-Fe/$NiMoN_x$ electrocatalyst was developed on nickel foam by Qiu et al. [12]. Shudo et al. [13] designed a porous Ni/NiOx bi-functional oxygen electrocatalyst produced from $Ni(OH)_2$ with outstanding catalytic activity.

Morphology tuning, crystallinity alterations, surface manipulation, and synergy compositing of different materials can further improve the intrinsic electro-catalytic properties of metals like Ni. The composite materials offer larger catalytic surface area by Ni grain refinement and also by improving the intrinsic catalytic activity by generating a synergistic effect between Ni and incorporated reinforcement materials [14]. Experimental and theoretical studies have shown that the presence of two-dimensional materials changes the growth pattern and inherent activity of Ni, improving the rate of overall water splitting. Out of all the two-dimensional materials, layered transition metal dichalcogenides (TMDCs) like MoS_2 and WS_2, having exceptional electrical conductivity, highly active edge sites, tunable band structure, and a high surface area-to-volume ratio, are studied for their possible use as an electrochemical catalyst [15]. WS_2 and MoS_2 have been identified as efficient HER and OER catalysts at longer intervals due to their better chemical and environmental inertness [16].

Most of the reported electrocatalysts are amorphous and need polymer binders to be assembled before being used in water electrolysis. These binders reduce the catalytic area, and their stability at higher current densities remains a matter of concern. Creating three-dimensional nanostructures by expanding the active surface area is one of the most effective ways to increase catalytic activity. In that aspect, electrodeposition is an easy and facile method for fabricating electrocatalysts with good catalytic properties. This method can create different nanostructures by controlling and optimising the deposition parameters. Moreover, electrodeposition is a scalable process that can produce industrial electrocatalysts [17].

A combination of Ni and WS_2 known for their individual catalytic potential in alkaline water splitting remains underexplored. Here in, as per best of the author's knowledge we report for the first time the development of Ni-WS_2 coated stainless steel mesh (SSM) via electrodeposition that can function as an efficient binder-free bi-functional electrocatalyst in alkaline medium. The deposition conditions were fine-tuned so that the developed SSM has a hierarchical structure of WS_2 clusters, nodules, and Ni pine cones (micro-nano), resulting in a "cacti/cauliflower-like" appearance with highly active surface area. From the electrochemical studies, it was found that Ni-WS_2 coated SS mesh demonstrated improved electrocatalytic characteristics and is stable and durable when tested continuously over a sufficient period. As a result, this easy, environmentally friendly, and economical approach for fabricating efficient and durable bi-functional electrocatalysts would be a promising one for practical catalytic applications as a non-precious transitional metal-based alternative to Pt- and Ir/Ru-based expensive benchmark catalysts.

6b.2. Experimental

6b.2.1. Materials

Raj filters supplied stainless steel mesh (pore size < 100 µm). Nickel salts ($NiSO_4 \cdot 6H_2O$, $NiCl_2 \cdot 6H_2O$) and Boric acid (H_3BO_3) were obtained from Merck. Alfa Aesar provided Cetyltrimethylammonium bromide ($CH_3(CH_2)_{15}N(Br)(CH_3)_3$) and Saccharin ($C_7H_5NO_3S$). Tungsten disulphide nanoparticles (WS_2, 90 nm) were acquired from Sigma-Aldrich.

6b.2.2. Fabrication of Ni-WS_2 coated SS mesh

Ni-Watts bath comprising $NiSO_4 \cdot 6H_2O$, $NiCl_2 \cdot 6H_2O$, and H_3BO_3 was used for electrodeposition. WS_2 nanoparticles, CTAB, and saccharin, after ultrasonication for 30 minutes, were thoroughly mixed and added to the Ni bath. Ni-WS_2 bath was maintained at a pH of 4. The authors have reported the detailed procedure for fabricating Ni-WS_2 coated SS mesh elsewhere [18] (**Figure 6b.1.**).

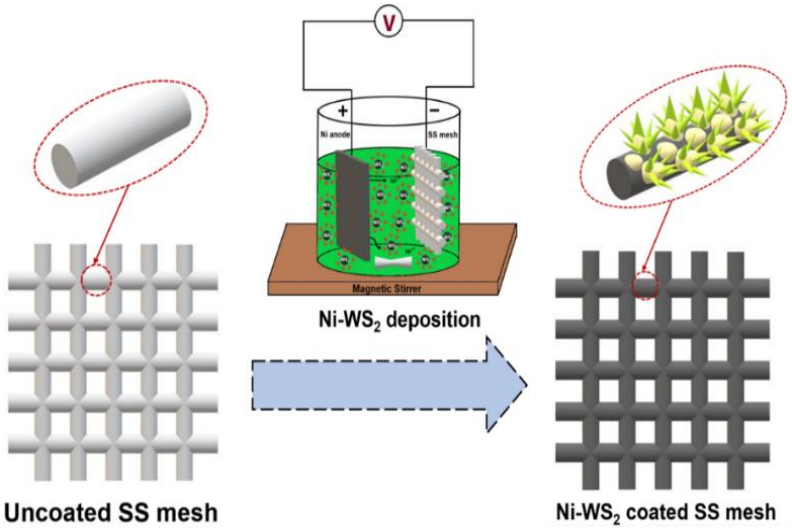

Figure 6b.1. One-step preparation process of Ni-WS_2 coated SSM

6b.2.3 Characterisation of the developed mesh

The morphologies and chemical composition of the elements present in the developed mesh were studied by FE-SEM (FEI NOVA NANOSEM 450) and Zeiss EVO 18 cryo-SEM (with EDS), respectively. The 3D morphology and roughness of samples were analysed by Atomic Force Microscopy (AFM, Bruker Multimode-8HR in tapping mode). The crystalline phase structure and composition of all the samples were studied with a Bruker D2 Phaser X-ray diffractometer with Cu - K_α radiation (λ = 1.5406 Å) in the 0-90° range.

The electrochemical measurements were done using a three-electrode setup in 1 M KOH using a CHI660E electrochemical workstation. Platinum wire (working electrode), Ag/AgCl in saturated KCl (reference electrode), and Ni-WS_2 coated SS mesh (counter electrode) are the electrodes employed. The voltammetric techniques LSV (linear sweep voltammetry), CV (cyclic voltammetry), EIS (electrochemical impedance spectroscopy) and CA (chronoamperometry) were

used to analyse the electrochemical activity and stability of the electrode material. As a preliminary step before actual measurements, CV in a reduction potential region was carried out for several cycles to activate the materials. Once the CV curves became consistent, LSV measurements were carried out to analyse the current response. All the measurements were performed at a scan rate of 2 mV s^{-1}, and EIS measurements were taken at a frequency range (100 KHz to 100 mHz). CA for about 50 hours was performed to confirm the stability, and the polarisation curves before and after 1000 cycles were also recorded.

6b.3. Results and Discussion

6b.3.1 Morphology

Figure 6b.2 (a) indicates the uniform surface of the uncoated mesh. Electrodeposition has a vital role in determining the morphology of SSM. **Figure 6b.2 (b-c)** suggests that the pure Ni-coated mesh possesses a pine-cone structure. This pine cone structure of fine Ni crystals increases the active surface area, improving the electrocatalytic activity [19]. Ni-WS_2 coated SS mesh has a rough protruding hierarchical structure of WS_2 clusters and nodules along with Ni pinecones with thorn like projections (**Figure 6b.2 (d-f)**). The progressive micro/nanostructure formation occurs due to WS_2 particle incorporation in and around the Ni matrix. Further, incorporating conductive WS_2 particles into the electrolytic bath resulted in a difference in current distribution during electrodeposition [20]. SEM image of higher magnification (**Figure 6b.3.**) indicates that the nodular structures are composed of Ni grains bound together with petal-like WS_2 particles having highly active edge sites. Since these edge sites of high active surface area are exposed maximum in the cacti/cauliflower-like structures, these peculiar structures can contribute towards the catalytic activity of the developed mesh.

Figure 6b.4.(a-e) shows the elemental distribution of Ni-WS_2 coated SS mesh. Elements such as nickel (Ni) (**Figure 6b.4 (b)**), tungsten (W) (**Figure 6b.4 (c)**), and sulphur (S) (**Figure 6b.4 (d)**) were identified. Ni is primarily seen in the base of the coating, while sulphur is mainly seen in cauliflower-like structures. The non-uniform distribution of tungsten and sulphur observed in the EDS and elemental mapping is attributed to the nature of composite electrodeposition. In Ni-WS_2 system, WS_2 particles are incorporated into the growing nickel matrix primarily through mechanical entrapment rather than electrochemical reduction. The irregular surface morphology of the SS mesh substrate and the cacti-like structure of the coating result in non-uniform current

density and local hydrodynamic conditions, which affect the transport and incorporation of WS_2 particles. Furthermore, WS_2 particles may preferentially adsorb at high-energy sites such as edges, protrusions, and defects, leading to localized enrichment of tungsten and sulphur. Similar non-uniform distribution behavior in composite coatings has also been reported in the literature [21,22].

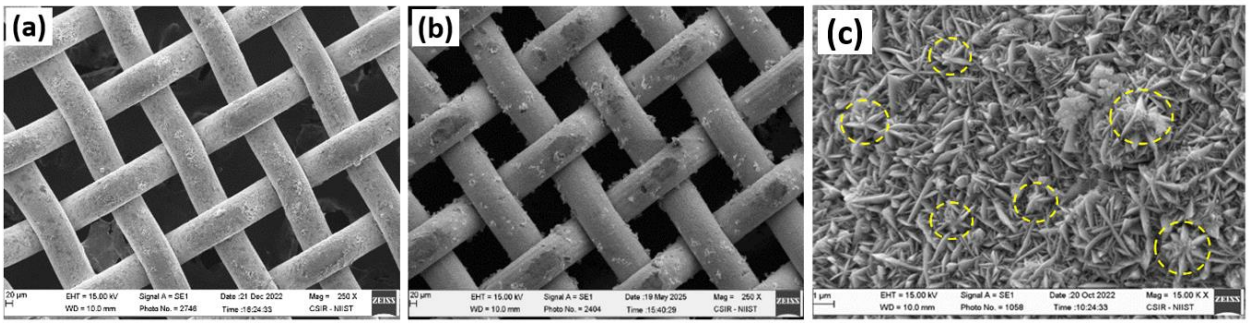

Figure 6b.2. Surface morphologies of different meshes **(a)** Uncoated stainless steel mesh, **(b)** Pure nickel coated mesh, **(c)** Pine cone like morphology in pure Ni coated mesh

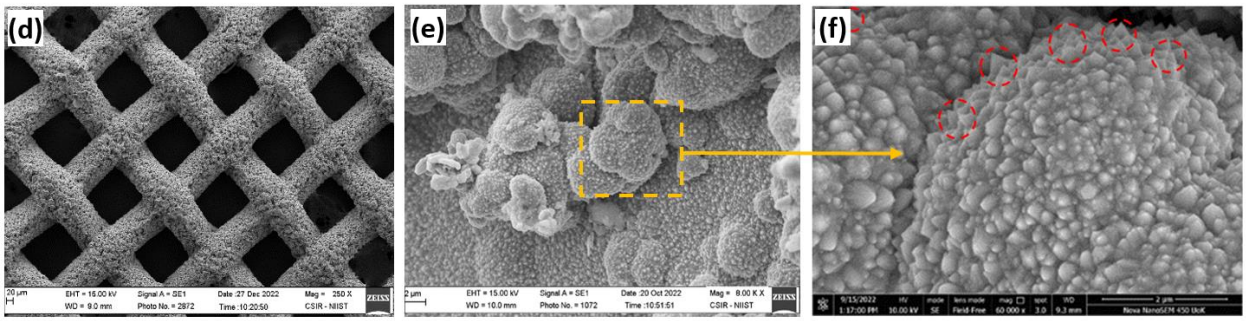

Figure 6b.2. (d) Ni-WS_2 coated stainless steel mesh, **(e)** Cacti/cauliflower like structure in Ni-WS_2 coated mesh, **(f)** High magnification SEM image showing thorn-like projections

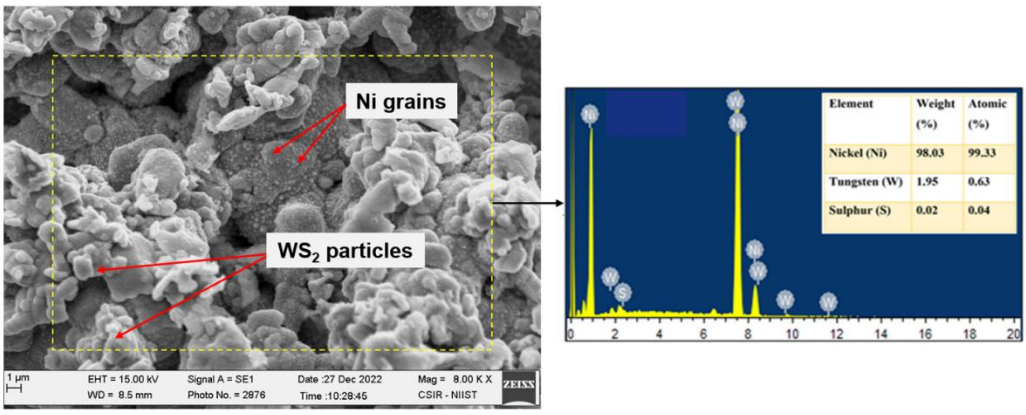

Figure 6b.3. SEM-EDS of nodular structures composed of Ni grains bound together with petal-like WS_2 particles in Ni-WS_2 coated SS mesh

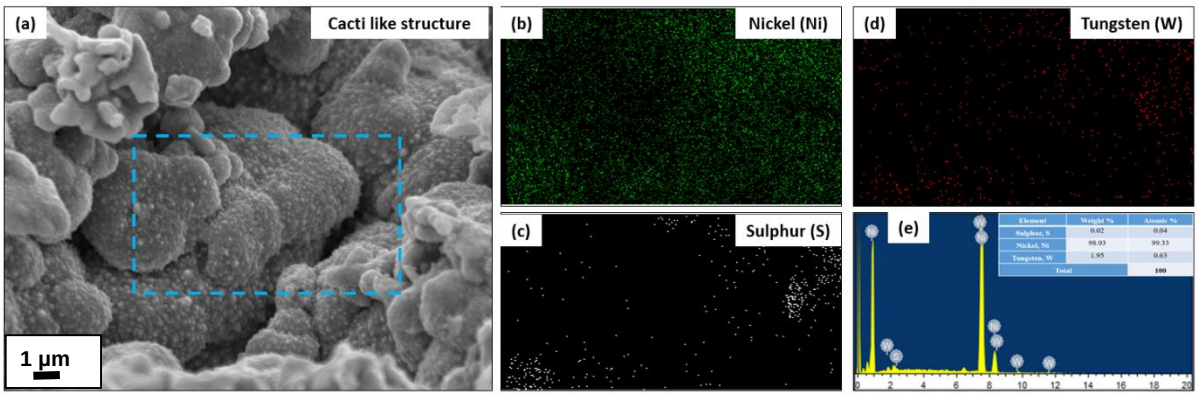

Figure 6b.4 (a-e) EDS & elemental mapping of Ni-WS_2 coated SS mesh

Pure Ni-coated mesh has an average roughness (R_a) of 87.6 nm, whereas Ni-WS_2 coated mesh has 168 nm. **Figure 6b.5 (a)** shows that the surface of pure Ni-coated mesh has unevenly placed clusters of various heights. **Figure 6b.5 (b)** of Ni-WS_2 mesh reveals protrusions (valleys or bumps) with greater heights and diameters. The topographical map reveals two distinct scales of surface roughness; at the microscale, the surface exhibits prominent undulations and protrusions with lateral dimensions ranging from approximately 1 to 2 µm, as indicated by the X and Y axes. These features correspond to the inherent structure of the coated mesh and form the first level of hierarchical roughness. Superimposed on these microscale features are nanoscale surface structures, with vertical variations in the range of few nanometers to several hundred nanometers, as depicted along the Z-axis (up to 0.6 nm). These fine-scale irregularities constitute the second level of hierarchy. The micro-nano hierarchical structure contributes to enhanced wettability, catalytic activity, and electrochemical performance of Ni WS_2 coated SS mesh.

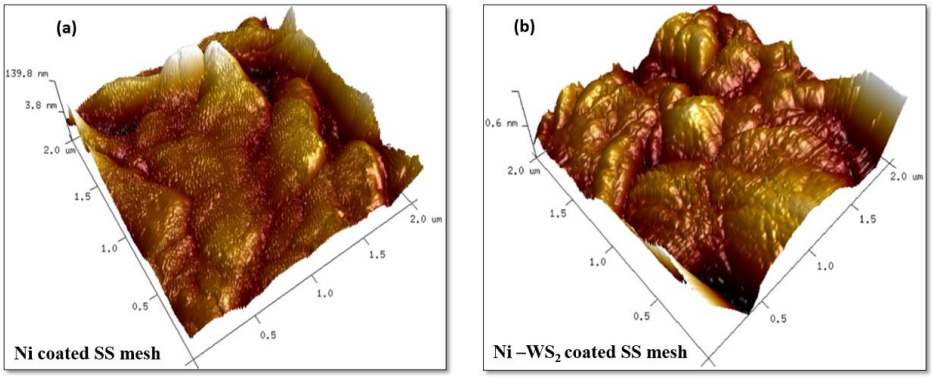

R_a = 87.6 nm; R_q = 110 nm **R_a = 168 nm; R_q = 199 nm**

Figure 6b.5. 3D surface morphologies of the developed meshes

6b.3.2 Phase Composition & Crystalline Structure Analysis

Figure **6b.6 (a)** shows the XRD graph of pure Ni-coated SS mesh. Three peaks of Ni at 44.32°(111), 51.77°(200), and 76.3°(220) indicate the fcc structure of Ni metal (JCPDS 04-0850). The typical fcc structure of Ni provides a large surface area, providing more accessible active sites for catalytic reactions and enhanced stability. Adding WS_2 particles created additional nucleation sites that caused significant microstructural changes and resulted in smaller Ni grains. Significant peaks are observed in the case of Ni-WS_2 coated SSM at 14°(002), 29.1°(004), 33°(100), 40°(103), 49°(110), 58°(008), and 60°(112) validating the hcp structure of WS_2 ((JCPDS 84-1398) (**Figure 6b.6 (b)**).The strong Ni(111) peak of Ni-WS_2 coated SSM indicates high inherent catalytic activity, appropriate hydrogen binding energy and are stable in alkaline environments.

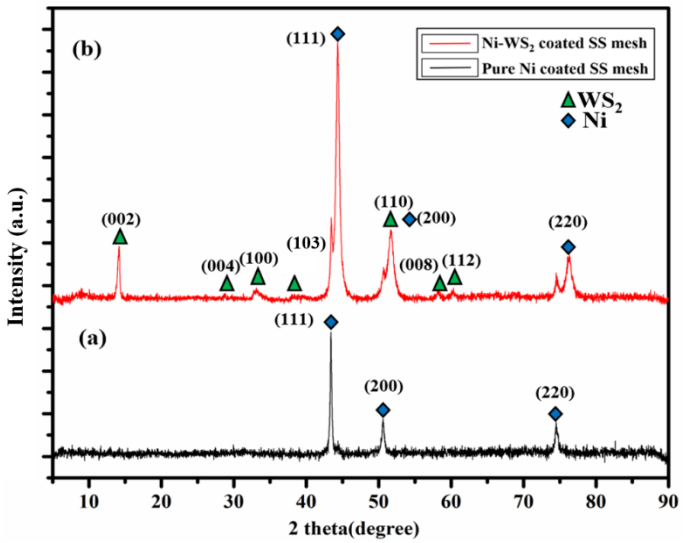

Figure 6b.6. XRD pattern of coated meshes **(a)** Pure Nickel, **(b)** Ni-WS_2

6b.3.3. Electrocatalytic activity

The electrocatalytic hydrogen evolution and oxygen evolution ability of the developed catalyst material were evaluated by LSV. The lower scan rate of 2 mV/s was used to perform the analysis as it enhances the ionic and electronic movement, thereby improving the kinetics of water-splitting reactions. Hydrogen evolution was studied in the negative potential region, and **Figure 6b.7(a)** shows the HER polarization curves of the samples. The extra potential required to attain a

current density of 10 mA cm^{-2}, the overpotential (η_{10}), is considered for estimating the catalytic activity of the materials [23]. Ni-WS_2 coated SSM outperforms pure Ni coated SSM regarding η_{10}. Pure Ni coated SSM required an overpotential of 189 mV, whereas Ni-WS_2 coated SSM needed an overpotential of 89 mV to generate a current density of 10 mA/cm^2. Although this overpotential is still higher than that of the commercial Pt/C catalyst (43 mV) [24], it is noteworthy that Ni-WS_2 coated SSM, being a non-precious and cost-effective material, demonstrates a remarkably low overpotential that approaches the performance of Pt/C.

Ni coated SSM could not deliver higher currents even when higher potentials were applied, but Ni-WS_2 coated SSM delivered higher currents on increasing the applied potential. This enhancement in the activity arises due to the synergistic effect of Ni and WS_2 nanoparticles. As explained in the SEM analysis, the "cactus-like"/ "cauliflower-like" structures of Ni-WS_2 coated SSM are beneficial for improving the electrocatalytic activity of the material. The edge sites of WS_2 are more catalytically active than the basal planes [25]. The particular micro-nano hierarchical morphology helps more electrolyte access and exposes more edge sites of WS_2, thereby enhancing electrocatalytic activity. In addition, this peculiar morphology enhances the mass and charge transfer, influencing the catalytic activity. Thus Ni-WS_2 coated SSM proves to be an excellent electrode material to generate hydrogen through electrolysis of water.

Figure 6b.7(b) shows the Tafel plots of the catalyst material, which indicate the kinetics of electron transfer reactions. Tafel slope is determined from the linear portion of the voltammetric curve using the equation

$$\eta = b \log(j) \qquad (\mathbf{6b.1})$$

Here, out of the two materials, Ni-WS_2 coated SSM exhibited a fair Tafel slope value of 102 mV dec^{-1} compared to Ni coated SSM with a slope of 151 mV dec^{-1}. This indicates the faster electron adsorption-desorption mechanism by Ni-WS_2 coated SSM. The Tafel slope values of Ni-based systems are found to be relatively more than the theoretical value of 120 mV dec^{-1} (for Volmer pathway). However, various results with higher Tafel slope values for Ni-based alloys and composites have been reported so far [26–28]. The increase in Tafel slope may have arisen due to the presence of a surface oxide layer over the electrode surface. In this circumstance, the applied external potential will be used for initiating the HER and also to overcome the barrier caused by the oxide layer [29,30].

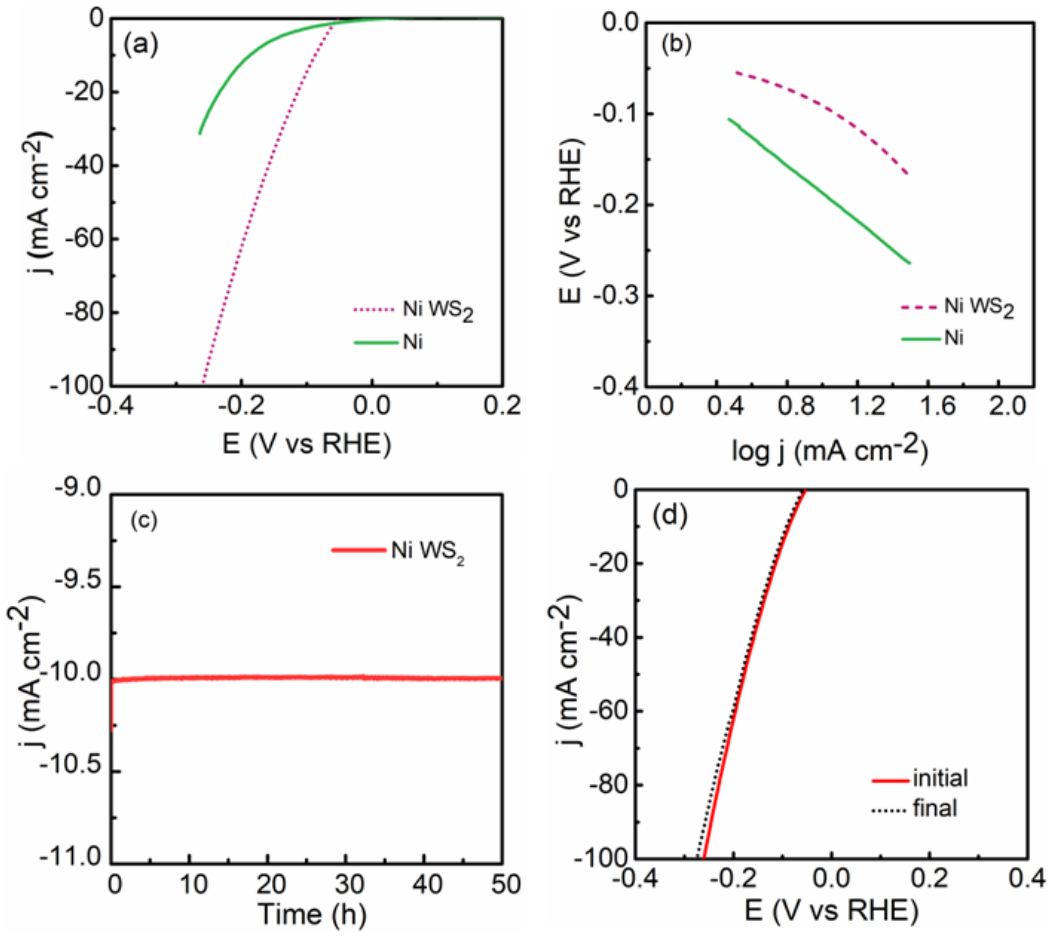

Figure 6b.7. (a) HER polarisation curves, **(b)** Tafel plots of Ni-coated and Ni-WS_2-coated SSM, **(c)** Amperometric i-t curve showing the stability of Ni-WS_2-coated SSM, and **(d)** the LSV curves before and after 1000 cycles of hydrogen evolution reaction

Along with electrocatalytic activity, electrochemical stability is an essential criterion that determines the efficiency of an electrocatalyst. The long-term stability of Ni-WS_2 coated SSM is investigated using chronoamperometry and the current response is shown in **Figure 6b.7(c)**. The CA measurements were carried out at a reduction potential of 90 mV, and Ni-WS_2 coated SS mesh generated a current density of 10 mA cm^{-2} for a higher duration of 50 hours. Even after 50 hours of continuous H_2 generation the binder-free electrode material was able to retain its activity, which is highly favourable for practical electrolyzers.

The stable performance of the material was also validated by recording the HER polarisation curves before and after 1000 cycles of continuous hydrogen generation. Figure **6b.7(d)** shows that HER polarization curves before and after 1000 cycles of CV measurement. It

can be observed from the figure that the initial curve retrace the final curve even after long cyclic measurements. The overpotentials at 10, 20 and 50 mA cm^{-2} were found to be moreover the same. This again confirms the long-term feasibility of the electrode material.

Figure 6b.8(a) shows the OER polarisation curves of the catalyst materials. It is clearly evident that Ni-WS_2 coated SSM outperforms Ni coated SSM and is suitable for OER activity. Ni coated SSM required an overpotential of 320 mV, while Ni-WS_2 coated SSM required an overpotential of 230 mV to yield a current density of 10 mA cm^{-2}, which is even better than the commercially available catalyst material, IrO_2 (310 mV) [31,32]. At the same time, to generate 20 mA cm^{-2} and 100 mA cm^{-2} current density, Ni coated SSM needed 360 mV and 540 mV of additional potential, respectively, whereas Ni-WS_2 coated SSM required extra potentials of 260 mV and 380 mV, respectively. Also, the current increased linearly for Ni-WS_2 coated SSM, which indicates faster electron transfer within the material [26].

Figure 6b.8(b) shows the OER Tafel plots of the electrode materials, which clearly show the enhanced oxygen evolution kinetics. Ni-WS_2 coated SSM had a Tafel slope of 99 mV dec^{-1} whereas Ni coated SSM exhibited a Tafel slope of 118 mV dec^{-1}. OER is a four-electron transfer process in which molecular oxygen is liberated by the electro-oxidation of hydroxyl groups (OH^-) in alkaline environment. **Figure 6b.8(c)** shows CA OER curve for Ni-WS_2 coated SSM at a potential of 250 mV. Ni-WS_2 coated SSM exhibited stable amount of oxygen generation for about fifty hours. Again, as in the case of HER activity, the electrode material exhibited stable performance even after 1000 cycles of oxygen evolution. **Figure 6b.8(d)** shows the LSV curves before and after the cyclic measurement. It is evident that the initial and the final polarisation curves varied only slightly in terms of a few milli volts. This again elucidates the long-term stable catalytic activity of the material.

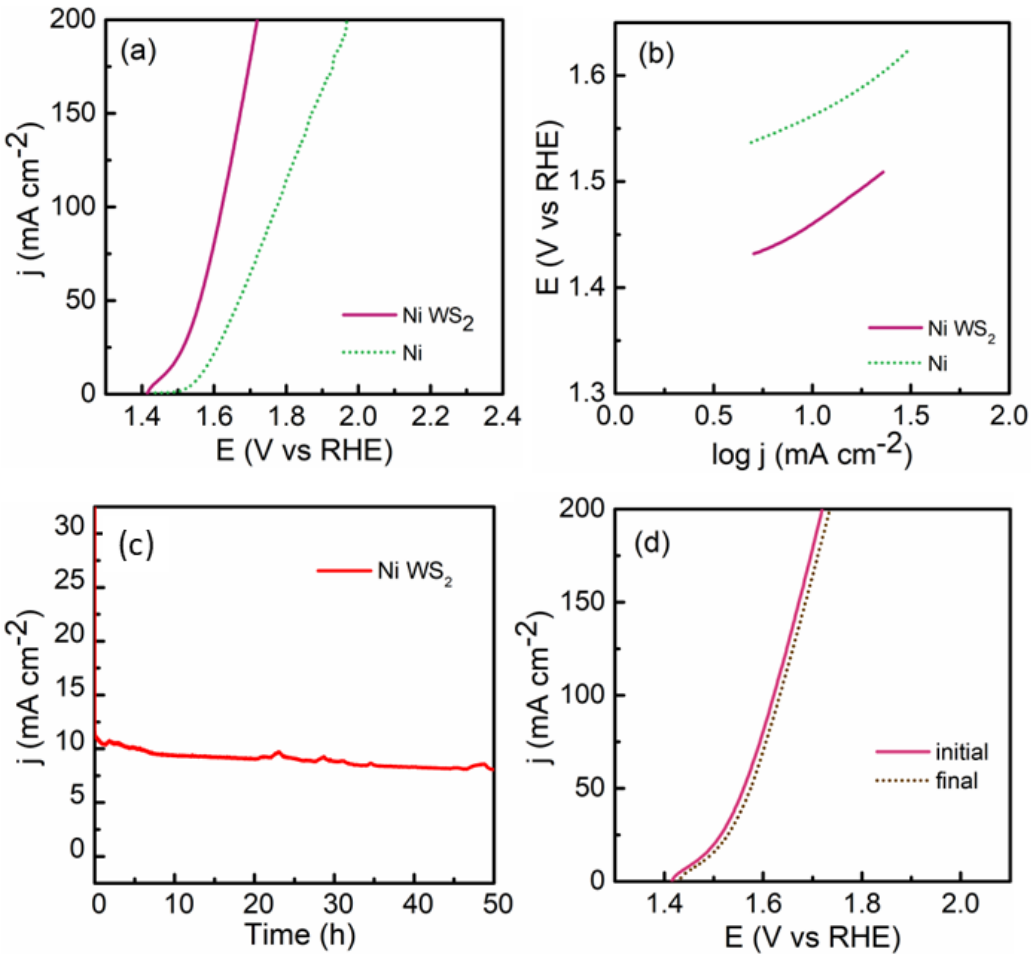

Figure 6b.8. (a) OER polarisation curves, **(b)** Tafel plots of Ni-coated and Ni-WS_2 coated SSM **(c)** Amperometric i-t curve showing the stability of Ni-WS_2 coated SSM, and **(d)** LSV curves before and after 1000 cycles of oxygen evolution reaction

The enhancement in electrocatalytic activity of Ni-WS_2 coated SSM is due to the hierarchical growth of Ni pinecones and WS_2 clusters into cacti/cauliflower-like morphology as well as due to the synergistic electrochemical properties of metallic Ni and the catalytically active TMDC–WS_2. The material's electrocatalytic active surface area (ECSA) was calculated by recording the cyclic voltammograms in a non-Faradaic region. Figure **6b.9(a)** and **(b)** show the CV curves obtained at different scan rates for Ni coated and Ni-WS_2 coated SSM respectively and **Figure 6b.10(a)** shows the linear plot obtained to determine the C_{dl} value. The slope of the j vs ν curve gives the double-layer capacitance. Then, the ECSA is calculated using the equation.

$$ECSA = \frac{C_{dl}}{C_s} \qquad (\mathbf{6b.2})$$

Usually, in 0.5 M H_2SO_4, C_s is taken as 35 µF cm^{-2}; in 1M KOH it is 40 µF cm^{-2} [33]. Ni-coated SSM exhibited a C_{dl} value of 1.78 mF cm^{-2}, significantly less than that of Ni-WS_2 coated SSM, which delivered a C_{dl} value of 35 mF cm^{-2}. Ni-WS_2 coated SSM provided a higher ECSA value of 89 cm^2 while Ni coated SSM had 44 cm^2 ECSA.

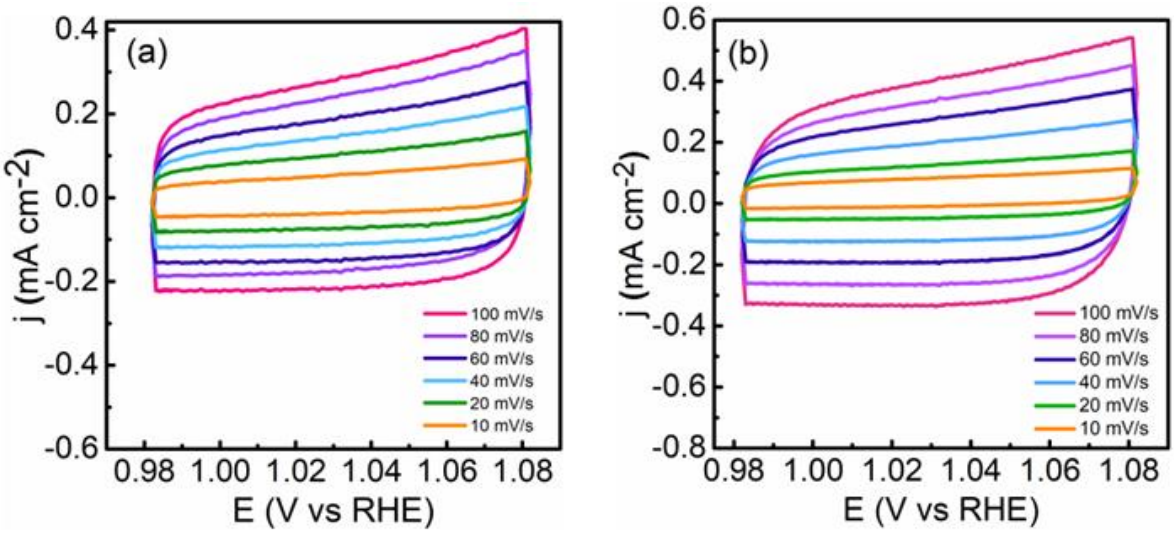

Figure 6b.9. Cyclic voltammograms of **(a)** Ni-coated and **(b)** Ni WS_2-coated SSM at different scan rates

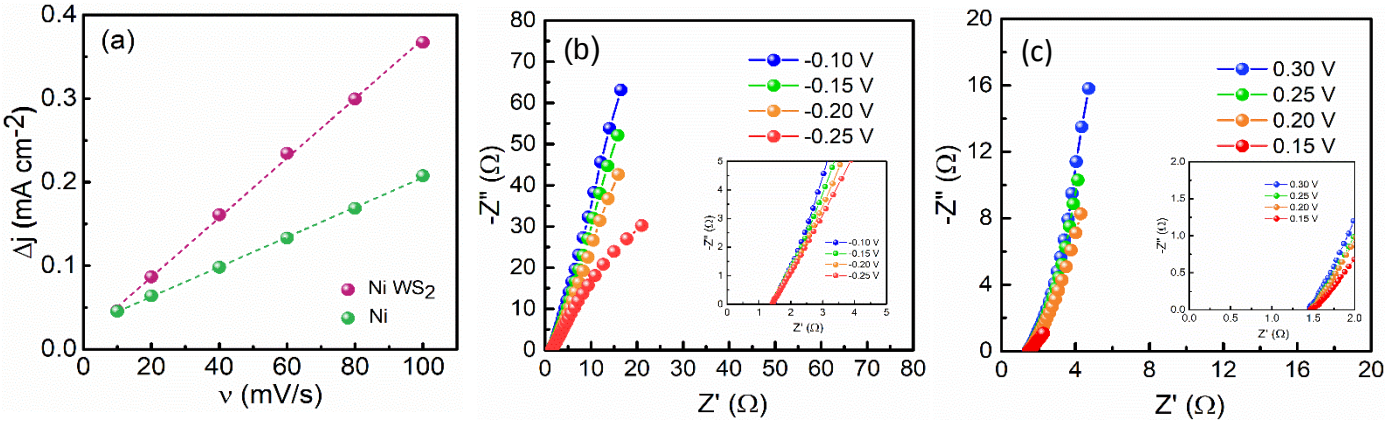

Figure 6b.10. (a) Plot of current density vs scan rate and **(b)** and **(c)** Nyquist curves of Ni WS_2 coated SSM at different potentials of HER & OER

Thus, higher ECSA (89 cm^{-2}) accounts for the higher water-splitting ability of the catalyst material Ni-WS_2 coated SSM. These observations and results indicate that the hierarchical structure of the electrodeposited Ni-WS_2 coated SSM enhanced the active surface area of the electrode, thereby resulting in increased electrolyte access. Moreover, this binder-free electrode fabrication method facilitates increased conductivity and electrolyte wettability, thereby enhancing the activity and stability of the catalyst materials.

EIS measurements were carried out to analyze the electrochemical phenomena at the electrode-electrolyte interface. The EIS measurements were carried out at different potentials slightly above and below the overpotentials of respective HER and OER. **Figure 6b.10 (b)** and **(c)** shows the Nyquist curves of Ni WS_2 recorded in a frequency range of 100 mHz to 100 KHz at different overpotentials. The Nyquist plots of Ni-WS_2 coated SS mesh for HER and OER reflect the reaction kinetics at different potentials [34–37]. Nyquist plots exhibited more capacitive behaviour than resistive behaviour, in the Non-Faradaic region (low potential region) unlike higher potentials where chemical reactions are more likely to occur. The capacitive behaviour indicates that the surface sites of the catalyst are available for charge storage, revealing how easily reactive species can adsorb onto the catalyst surface during HER and OER.

Figure 6b.11.(a) and **(b)** shows the impedance curve of Ni-WS_2 coated SSM fitted using ZSimpWIN3.21 software & inset shows the equivalent plot obtained. Analysing the equivalent circuit corresponding to the Nyquist plot of HER and OER activity. Rs accounts for the electrolytic resistance and Q_1 (CPE_1) models the double-layer capacitance, mainly due to surface roughness of the catalyst. Q_2 (CPE_2) and R_2 demonstrates the secondary surface or interfacial phenomena, such as adsorption of reaction intermediates (H*, O*, OH*) or changes in surface coverage of the catalyst. The Warburg element reflects the diffusion of protons or hydrogen species or oxygen [38,39].

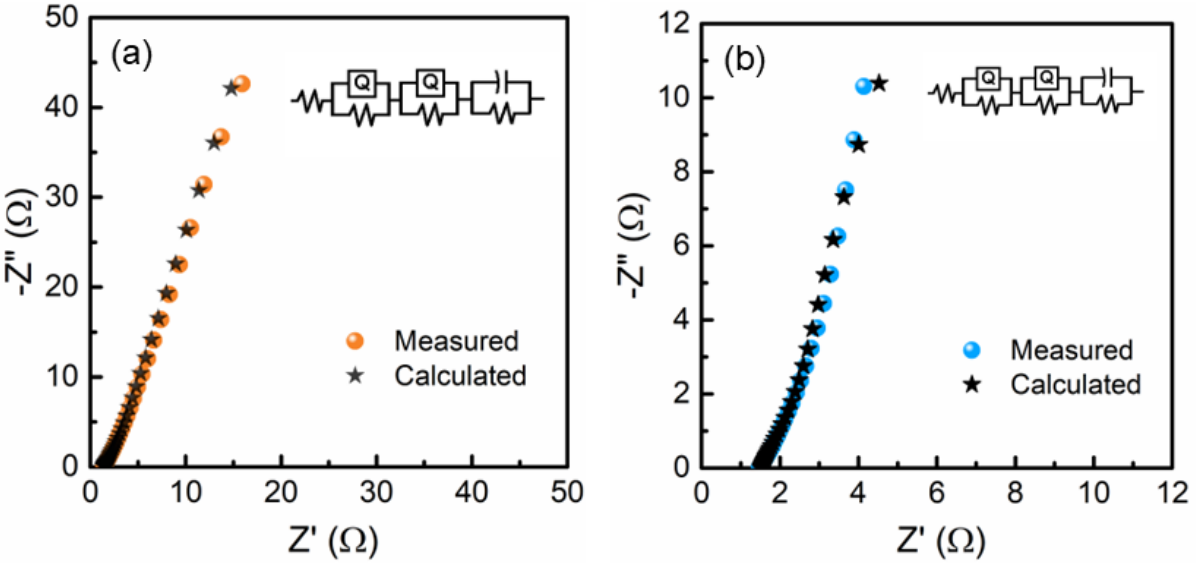

Figure 6b.11. EIS Nyquist plot fitted with equivalent EIS circuits **(a)** hydrogen evolution and **(b)** oxygen evolution

6b.3.4 Overall water splitting ability

Since Ni-WS_2 coated SSM proved to be suitable for both hydrogen and oxygen evolution, a full cell comprising the coated mesh as both anode and cathode was designed (**Figure 6b.12**). The bi-functional activity of the electrocatalyst for simultaneous hydrogen and oxygen generation was examined in the alkaline electrolyzer. **Figure 6b.13(a)** shows the polarization curve of the full cell, indicating the changes in the current generated in the electrode versus the applied voltage. To generate a current density of 10 mA/cm^2, the cell required a potential of 1.56 V. As the applied voltage increased, the current generated also increased abruptly, indicating the bi-functional activity of the electrode material.

Along with activity, the long-term stability of the material was evaluated using chronoamperometry. **Figure 6b.13(b)** shows the current versus time plot obtained for the full cell. It can be seen that the current generated remained almost constant for about 50 hours of continuous energy generation.

The electrodes were able to maintain the current density at 10 mA/cm^2 at an applied potential of 1.56 V even after continuous usage. These results indicate that Ni WS_2 coated SSM can be effectively used as a bi-functional catalyst material for overall electrochemical water

splitting in alkaline medium. By further modifying the deposition parameters and optimising the growth of Ni-WS_2 over SS mesh, the efficiency of the bi-functional catalyst can further be scaled up.

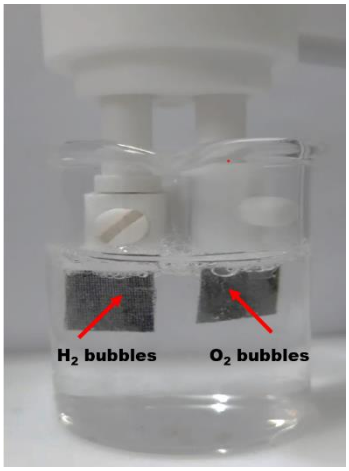

Figure 6b.12. Photograph of full cell for overall water splitting

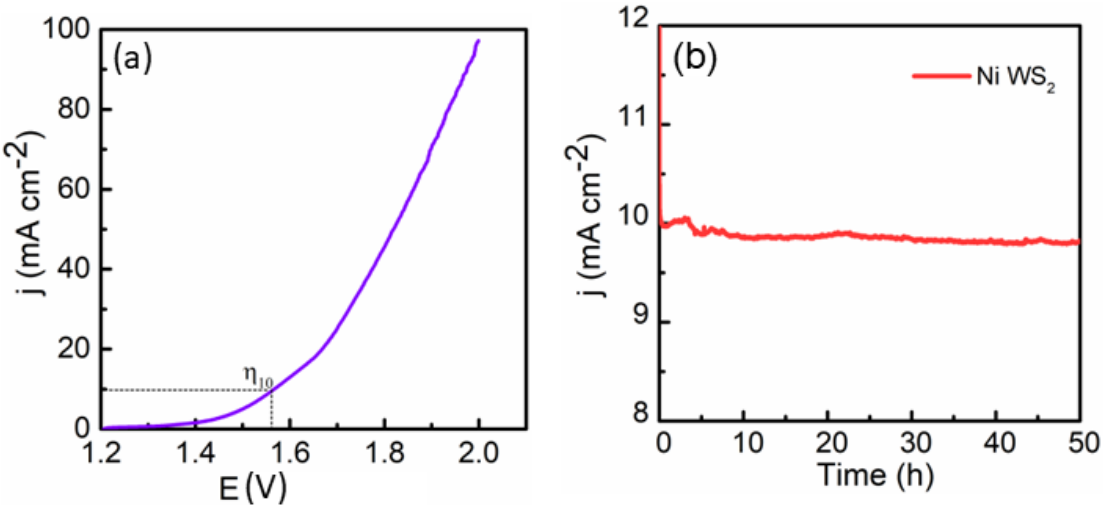

Figure 6b.13. (a) Polarization curve of the full cell using Ni WS_2 coated SSM, **(b)** Amperometric i-t curve showing the long-term stability of the full cell

The HER and OER activity of Ni-WS_2 coated SS mesh can be attributed to the active sites over both Ni and WS_2. The sulphur edges of WS_2 are active for both HER and OER. The Gibbs free energy of hydrogen or hydroxyl ion adsorption (ΔG_H/ ΔG_{OH}) of the sulfided edges make them active HER/OER sites. Various studies resonating the catalytic activity of the sulfided edges of transition metal dichalcogenides like WS_2 and MoS_2 have been reported [25]. This is further supported by our recent study of MoSSe based systems. In this study, the Gibbs free energy of

hydrogen adsorption (ΔG_H) of both sulfided and selenided edges of molybdenum was calculated. And it was found out that ΔG_H is minimum for H^+ adsorption on sulfided Mo edges [40]. Nickel provides a conductive backbone that facilitates efficient electron transfer during electrochemical reactions in water splitting. The d-band electronic structure of Ni allows optimal binding of intermediates such as hydrogen (H*) for HER or oxygen-containing species (O*, OH*) for OER [41].

Thus, the excellent bi-functional electrocatalytic activity of Ni-WS_2 coated SSM is due to: (1) Ni (111) plane and edge sites of WS_2 particles possess high inherent catalytic activity, appropriate hydrogen binding energy and are stable in alkaline environments, (2) increase in the active catalytic surface area resulting from the formation of micro-nano hierarchical structure, (3) enhancement in the intrinsic electrocatalytic activity due to the synergistic effect between Ni (low hydrogen overpotential) and WS_2 particles (high hydrogen adsorption), (4) the peculiar structure of the catalyst significantly increases ECSA as well as enables the flow of electrons and gas release, (5) the direct growth of Ni and WS_2 particles on SS mesh as a binder-free catalyst via one-step electrodeposition has several advantages, including close contact, outstanding mechanical adherence, and superior durability.

6b.4. Conclusions

A Ni-WS_2 coated SS mesh with a micro-nano hierarchical structure that can act as a bi-functional catalyst in water splitting was developed by electrodeposition. The catalyst contained a rough hierarchical surface of WS_2 clusters and Ni cones. LSV tests showed that the overpotentials for hydrogen and oxygen evolution reactions for Ni-WS_2 coated SS mesh were -89 mV and 230 mV respectively, much lower than pure Ni-coated mesh. The electrocatalytic activity of Ni-WS_2 coated SS mesh was higher due to the increased catalytic surface area and ready detachment of the adsorbed H_2 from the electrode surface. A full-cell alkaline electrolyzer using Ni-WS_2 coated SS mesh as anode and cathode delivered a current density of 10 mA/cm^{-2} at an applied potential of 1.56 V. Moreover, the electrochemical cell remained stable for 50 hours of continuous cycling. This enhanced activity arises due to the binder-free fabrication process of the electrode materials, the three-dimensional morphology of Ni-WS_2, and the catalyst material's higher electrochemical active surface area and lower charge-transfer resistance. In light of its excellent electrocatalytic activity for HER and OER and its ease of fabrication and availability, this bi-functional composite

catalyst can provide an efficient, cost-effective, and facile approach to developing large-scale industrial alkaline water electrolyzers.

References

[1] M. Tvaronavičienė, J. Baublys, J. Raudeliūnienė, D. Jatautaitė, Global energy consumption peculiarities and energy sources: Role of renewables, 2019. https://doi.org/10.1016/B978-0-12-817688-7.00001-X.

[2] M.S. Dresselhaus, I.L. Thomas, Dresselhaus, M.S. Thomas - 2001 - Alternative energy technologies, Nature 414 (2001) 332–337. www.nature.com.

[3] M.M. Najafpour, S. Salimi, M. Hołyńska, S.I. Allakhverdiev, A highly dispersible, magnetically separable and environmentally friendly nano-sized catalyst for water oxidation, Int. J. Hydrogen Energy 41 (2016) 4616–4623. https://doi.org/10.1016/j.ijhydene.2016.01.056.

[4] G.W. Crabtree, M.S. Dresselhaus, M. V. Buchanan, The hydrogen economy, Phys. Today 57 (2004) 39–44. https://doi.org/10.1063/1.1878333.

[5] S. Anwar, F. Khan, Y. Zhang, A. Djire, Recent development in electrocatalysts for hydrogen production through water electrolysis, Int. J. Hydrogen Energy 46 (2021) 32284–32317. https://doi.org/10.1016/j.ijhydene.2021.06.191.

[6] P. Häussinger, R. Lohmüller, A.M. Watson, Hydrogen, 2. Production, Ullmann's Encycl. Ind. Chem. (2011). https://doi.org/10.1002/14356007.o13_o03.

[7] V.R. Stamenkovic, D. Strmcnik, P.P. Lopes, N.M. Markovic, Energy and fuels from electrochemical interfaces, Nat. Mater. 16 (2016) 57–69. https://doi.org/10.1038/nmat4738.

[8] Y. Yan, B.Y. Xia, B. Zhao, X. Wang, A review on noble-metal-free bifunctional heterogeneous catalysts for overall electrochemical water splitting, J. Mater. Chem. A 4 (2016) 17587–17603. https://doi.org/10.1039/C6TA08075H.

[9] I. Roger, M.A. Shipman, M.D. Symes, Earth-abundant catalysts for electrochemical and photoelectrochemical water splitting, (2017). https://doi.org/10.1038/s41570-016-0003.

[10] X.-D. Wang, H.-Y. Chen, Y.-F. Xu, J.-F. Liao, B.-X. Chen, H.-S. Rao, D.-B. Kuang, C.-Y. Su, Self-supported NiMoP2 nanowires on carbon cloth as an efficient and durable electrocatalyst for overall water splitting, J. Mater. Chem. A 5 (2017) 7191–7199.

https://doi.org/10.1039/C6TA11188B.

[11] G. Barati Darband, M. Aliofkhazraei, A.S. Rouhaghdam, Facile electrodeposition of ternary Ni-Fe-Co alloy nanostructure as a binder free, cost-effective and durable electrocatalyst for high-performance overall water splitting, J. Colloid Interface Sci. 547 (2019) 407–420. https://doi.org/10.1016/j.jcis.2019.03.098.

[12] Y. Qiu, M. Sun, J. Cheng, J. Sun, D. Sun, L. Zhang, Bifunctional Ni-Fe/NiMoNx nanosheets on Ni foam for high-efficiency and durable overall water splitting, Catal. Commun. 164 (2022) 106426. https://doi.org/10.1016/j.catcom.2022.106426.

[13] Y. Shudo, M. Fukuda, M.S. Islam, K. Kuroiwa, Y. Sekine, M.R. Karim, S. Hayami, 3D porous Ni/NiO: Xas a bifunctional oxygen electrocatalyst derived from freeze-dried Ni(OH)2, Nanoscale 13 (2021) 5530–5535. https://doi.org/10.1039/d0nr08034a.

[14] L. Wang, Y. Li, M. Xia, Z. Li, Z. Chen, Z. Ma, X. Qin, G. Shao, Ni nanoparticles supported on graphene layers: An excellent 3D electrode for hydrogen evolution reaction in alkaline solution, J. Power Sources 347 (2017) 220–228. https://doi.org/10.1016/j.jpowsour.2017.02.017.

[15] L.P. Hao, A. Hanan, R. Walvekar, M. Khalid, F. Bibi, W.Y. Wong, C. Prakash, Synergistic Integration of MXene and Metal-Organic Frameworks for Enhanced Electrocatalytic Hydrogen Evolution in an Alkaline Environment, Catalysts 13 (2023) 1–13. https://doi.org/10.3390/catal13050802.

[16] A. Das, D. Roy, B. Kumar Das, M.I. Ansari, K.K. Chattopadhyay, S. Sarkar, Zinc doping induced WS2 accelerating the HER and ORR kinetics: A theoretical and experimental validation, Catal. Today 423 (2023) 113921. https://doi.org/10.1016/j.cattod.2022.10.003.

[17] G. Barati Darband, M. Aliofkhazraei, A.S. Rouhaghdam, Facile electrodeposition of ternary Ni-Fe-Co alloy nanostructure as a binder free, cost-effective and durable electrocatalyst for high-performance overall water splitting, J. Colloid Interface Sci. 547 (2019) 407–420. https://doi.org/10.1016/j.jcis.2019.03.098.

[18] R. Sreekumar, S. Eravath Thazhakkuni, S. Sukumaran Suseelamma, Fabrication of a robust superhydrophobic stainless steel mesh for efficient oil/water separation, J. Ind. Eng. Chem. 135 (2024) 425–433. https://doi.org/10.1016/j.jiec.2024.01.054.

[19] G. Barati Darband, M. Aliofkhazraei, A. Sabour Rouhaghdam, Nickel nanocones as efficient and stable catalyst for electrochemical hydrogen evolution reaction, Int. J. Hydrogen Energy 42 (2017) 14560–14565. https://doi.org/10.1016/j.ijhydene.2017.04.120.

[20] H. Shalom, T. Bendikov, Y. Feldman, N. Lachman, A. Zak, R. Tenne, Chemical control of the surface of WS2 nanoparticles, Chem. Phys. Lett. 761 (2020) 138052. https://doi.org/10.1016/j.cplett.2020.138052.

[21] C.T.J. Low, R.G.A. Wills, F.C. Walsh, Electrodeposition of composite coatings containing nanoparticles in a metal deposit, Surf. Coatings Technol. 201 (2006) 371–383. https://doi.org/10.1016/j.surfcoat.2005.11.123.

[22] M.S. Chandrasekar, M. Pushpavanam, Pulse and pulse reverse plating—Conceptual, advantages and applications, Electrochim. Acta 53 (2008) 3313–3322. https://doi.org/https://doi.org/10.1016/j.electacta.2007.11.054.

[23] S. Niu, S. Li, Y. Du, X. Han, P. Xu, How to Reliably Report the Overpotential of an Electrocatalyst, ACS Energy Lett. 5 (2020) 1083–1087. https://doi.org/10.1021/acsenergylett.0c00321.

[24] B. Jiang, S. Liu, L. Cheng, L. Zhou, H. Cui, M. Liu, M. Wen, C. Wang, W. Wang, S. Li, X. Sun, Mass synthesis of Pt/C catalysts with high Pt loading for low-overpotential hydrogen evolution, Int. J. Hydrogen Energy 58 (2024) 268–278. https://doi.org/https://doi.org/10.1016/j.ijhydene.2024.01.183.

[25] P. V. Sarma, A. Kayal, C.H. Sharma, M. Thalakulam, J. Mitra, M.M. Shaijumon, Electrocatalysis on Edge-Rich Spiral WS2 for Hydrogen Evolution, ACS Nano 13 (2019) 10448–10455. https://doi.org/10.1021/acsnano.9b04250.

[26] D. Wang, Q. Li, C. Han, Z. Xing, X. Yang, When NiO@Ni Meets WS2 nanosheet array: A highly efficient and ultrastable electrocatalyst for overall water splitting, ACS Cent. Sci. 4 (2018) 112–119. https://doi.org/10.1021/acscentsci.7b00502.

[27] Q. Zhou, S. Liu, Y. Zhang, Z. Zhu, W. Su, M. Sheng, Fabrication of porous Cu supported Ni-P/CeO2 composite coatings for enhanced hydrogen evolution reaction in alkaline solution, Ceram. Int. 46 (2020) 20871–20877.

https://doi.org/10.1016/j.ceramint.2020.05.133.

[28] F. Bao, E. Kemppainen, I. Dorbandt, R. Bors, F. Xi, R. Schlatmann, R. van de Krol, S. Calnan, Understanding the Hydrogen Evolution Reaction Kinetics of Electrodeposited Nickel-Molybdenum in Acidic, Near-Neutral, and Alkaline Conditions, ChemElectroChem 8 (2021) 195–208. https://doi.org/10.1002/celc.202001436.

[29] M. Grdeń, G. Jerkiewicz, Influence of Surface Treatment on the Kinetics of the Hydrogen Evolution Reaction on Bulk and Porous Nickel Materials, Electrocatalysis 10 (2019) 173–183. https://doi.org/10.1007/s12678-019-0506-6.

[30] Z. Liang, H.S. Ahn, A.J. Bard, A Study of the Mechanism of the Hydrogen Evolution Reaction on Nickel by Surface Interrogation Scanning Electrochemical Microscopy, J. Am. Chem. Soc. 139 (2017) 4854–4858. https://doi.org/10.1021/jacs.7b00279.

[31] Y. Huang, L.W. Jiang, B.Y. Shi, K.M. Ryan, J.J. Wang, Highly Efficient Oxygen Evolution Reaction Enabled by Phosphorus Doping of the Fe Electronic Structure in Iron–Nickel Selenide Nanosheets, Adv. Sci. 8 (2021) 1–7. https://doi.org/10.1002/advs.202101775.

[32] R. Li, H. Qi, F. Pan, W. Xie, L. Zhou, H. Liu, J. Hu, Defect Engineering in Bimetallic NiFe-BTC for Boosting Electrocatalytic Oxygen Evolution Reaction through Coordinated Ionic Liquids, ChemElectroChem 10 (2023) 1–6. https://doi.org/10.1002/celc.202300103.

[33] S.I. Perez Bakovic, P. Acharya, M. Watkins, H. Thornton, S. Hou, L.F. Greenlee, Electrochemically active surface area controls HER activity for FexNi100−x films in alkaline electrolyte, J. Catal. 394 (2021) 104–112. https://doi.org/10.1016/j.jcat.2020.12.037.

[34] M. Nazemi, G.B. Darband, A. Davoodi, Interfacial engineering of Ni–Co–Mn@Ni nanosheet–nanocone arrays as high performance non-noble metal electrocatalysts for hydrogen generation, Nanoscale 16 (2024) 10853–10863. https://doi.org/10.1039/D4NR01404A.

[35] S. Paygozar, A. Sabour Rouhaghdam, A. Seif, G.B. Darband, In-Situ Electrochemical Synthesis of Superhydrophilic NiCoMn Trimetallic-alloy nanosheets via Dynamic Hydrogen Bubble Template Method for developing High Current Density Hydrogen

Production Electrocatalyst, J. Mater. Chem. A (2024) 27558–27569. https://doi.org/10.1039/d4ta03698k.

[36] A. Fathollahi, T. Shahrabi, G.B. Darband, Modulation of active surface sites on Ni-Fe-S by the dynamic hydrogen bubble template method for energy-saving hydrogen production, J. Mater. Chem. A 12 (2024) 9038–9054. https://doi.org/10.1039/d3ta07379c.

[37] R. Andaveh, A. Sabour Rouhaghdam, A. Seif, K. Wang, M. Maleki, J. Ai, G. Barati Darband, J. Li, In Situ Assembly of a Superaerophobic CoMn/CuNiP Heterostructure as a Trifunctional Electrocatalyst for Ampere-Level Current Density Urea-Assisted Hydrogen Production, ACS Appl. Mater. Interfaces 16 (2024) 8717–8732. https://doi.org/10.1021/acsami.3c16122.

[38] A.C. Lazanas, M.I. Prodromidis, Electrochemical Impedance Spectroscopy─A Tutorial, ACS Meas. Sci. Au 3 (2023) 162–193. https://doi.org/10.1021/acsmeasuresciau.2c00070.

[39] V. V. Mohan, M. Mohan, R.B. Rakhi, High performance supercapacitors based on WS2 nanoflower electrodes with commercial-level mass-loading, Surfaces and Interfaces 42 (2023) 103496. https://doi.org/10.1016/j.surfin.2023.103496.

[40] R. Shilpa, S. Assa Aravindh, S.R. Sarath Kumar, D.D. Sarma, R.B. Rakhi, Designing Mo-based transition metal dichalcogenides for sustainable hydrogen production: Anionic substitution and DFT insight, Appl. Surf. Sci. 681 (2025) 161614. https://doi.org/https://doi.org/10.1016/j.apsusc.2024.161614.

[41] A. Shukla, S.C. Singh, C.S. Saraj, G. Verma, C. Guo, Ni-based overall water splitting electrocatalysts prepared via laser-ablation-in-liquids combined with electrophoretic deposition, Mater. Today Chem. 23 (2022) 100691. https://doi.org/https://doi.org/10.1016/j.mtchem.2021.100691.

Chapter 7

Summary & Future Perspectives

In view of the fact that material deterioration can have a significant impact on global energy demand, this doctoral investigation aims to develop multi-functional nickel composite coatings with 2D material reinforcements (BN, graphene, TMDs) that provide aesthetics, protection and mitigate the underlying causes of deterioration, such as corrosion, wear, fatigue, moisture, etc. The catalytic aspect of these coatings is also investigated since these coatings can improve the efficiency, durability, and economic viability of sustainable hydrogen production technologies like electrolytic water splitting.

Chapter 2 deals with the development of Ni-h/BN composite coating over mild steel substrate. The results indicates that the second phase h-BN particles were successfully deposited within the Ni matrix and composite coating had a compact, smooth and grain refined surface. The influence of grain refinement on the microhardness, corrosion and tribological properties was also investigated. Micro hardness value of the composite coating was higher than pure Ni coating and mild steel. Under different saccharin concentrations, it has been found that the corrosion resistance of the developed Ni-BN coating is better than that of pure nickel coating and mild steel substrate. Further the composite coating exhibited lower COF (0.23) and excellent wear resistance. Thus the developed Ni-BN coating with improved properties indicates its potential for engineering applications.

One-step electrodeposited biomimetic Ni-graphene composite coating with pinecone-inspired hierarchical micro/nanostructures with a contact angle of 152° was developed in **Chapter 3**. It was observed that this particular coating had a self-cleaning nature and it was a mechanically durable anti-corrosive coating. The composite coating also exhibited consistent and remarkable lubricating properties with an average friction coefficient of 0.24 and a low wear rate, reduced by over 70% in comparison with the pure Ni coating.

In **Chapter 4**, electrodeposited Ni and Ni-MoS_2 coatings have been successfully developed over mild steel substrate. The coatings reinforced with MoS_2 exhibited more compact structure as

compared to the pure Ni coating. In terms of mechanical and tribological properties, Ni-MoS_2 coating had a maximum hardness value of 525 HV and low coefficient of friction of 0.08. Among all the coatings, significantly lower charge-transfer resistance (R_{ct}) as well as superior inhibition efficiency (IE>90%) for MoS_2 reinforced coatings suggest better corrosion resistant behavior. In addition, LSV and CV results indicated the catalytic potential of the Ni-MoS_2 coated SS mesh for overall water splitting.

The studies in the **Chapter 5** have produced a low-friction, superhydrophobic Ni-WS_2 coating by a versatile one-pot single-step electrodeposition. By adjusting the WS_2 concentration and tuning the deposition parameters, a hierarchical surface with a high water contact angle of 159 degree was achieved. Furthermore, mechanical and friction properties of the coating were characterized, revealing that sufficient WS_2 embedded in the Ni coatings resulted in a reduced friction coefficient of 0.04 by the formation of a self-lubricating tribo-film. Compared to the substrate and pure nickel coatings, the robust surface of the as-prepared Ni-WS_2 composite coatings exhibited good self-cleaning property and corrosion resistance, providing potential for industrial applications.

Chapter 6A deals with the development of superhydrophobic - superoleophilic SS mesh with a water contact angle of 169.5^o and surface roughness of 168 nm. The combined effect of hydrophobic surface chemistry and the roughness contributes to excellent superhydrophobic-superoleophilic and self-cleaning characteristics of the developed SHSM. The oil/water separation performance of SHSM was studied and the efficiency was greater than 98 % even after multiple uses. **Chapter 6B** discuss using the Ni-WS_2 coated SS mesh with micro-nano hierarchical structure as a bi-functional catalyst in water splitting. A full-cell alkaline electrolyzer using Ni-WS_2 coated SS mesh as anode and cathode delivered a current density of 10 mA/cm^2 at an applied potential of 1.56 V.

In conclusion, this doctoral thesis demonstrates a systematic and progressive development of advanced nickel-based composite coatings by electrodeposition through the strategic incorporation of various 2D layered materials, each selected for its unique properties.

- Beginning with BN, the research initially focused on enhancing the fundamental mechanical, wear, and corrosion-resistant properties of nickel coatings.

- This foundational work was then extended by integrating graphene to impart superhydrophobicity and self-cleaning functionalities, alongside improved tribological behavior.
- Building on these advancements, the incorporation of MoS_2 introduced catalytic capabilities, expanding the functionality of the coatings into electrochemical domains.
- The research culminated in the development of a multifunctional Ni-WS_2 composite coating that successfully integrated all the desired attributes; corrosion resistance, low friction, superhydrophobicity, and catalytic activity. Notably, this work also led to a novel application of Ni-WS_2 coated stainless steel mesh for oil-water separation and as a binder-free electrocatalyst for overall water splitting.
- This sequential and thoughtful evolution of material design not only highlights the versatility of 2D materials in nickel composite coatings but also sets a strong foundation for future multi-functional surface engineering solutions.

Comparative performance of the developed multi-functional Ni composite coatings in the present work is added in **Table 7.1.**

Table 7.1. Comparative performance of the developed multi-functional Ni composite coatings in the present work

S.No	Systems studied	Microhardness (HV)	Corrosion studies		Wear studies COF at 2N	Wettability studies WCA (degree)	Catalytic studies	
			E_{corr} (V)	I_{corr} ($\mu A/cm^2$)			Overpotential (mV)	Tafel slope (mV dec^{-1})
1.	Ni-BN	589	-0.25	0.47	0.23	**NA**	**NA**	
2.	Ni-graphene	485	-0.38	0.51	0.24	152	**NA**	
3.	Ni-MoS_2	527	-0.28	0.92	0.08	**NA**	HER : 147 OER : 276	HER : 145 OER : 103
4.	Ni-WS_2	**522**	**-0.24**	**0.17**	**0.04**	**159.7**	**HER : 89** **OER : 230**	**HER : 102** **OER : 99**

Thus this thesis meticulously addresses the need to develop sustainable, cost-effective, durable and versatile multi-functional composite coatings as industries strive for innovations in terms of energy efficiency, sustainability, and scalability. This work aligns and contributes towards global sustainable development goals like clean water and sanitation, affordable and clean energy, and responsible consumption and production. Thus, the findings of this study result in exciting possibilities for innovative multi-functional composite coatings with potential implications for both academia and industry.

Future Perspectives

1. Computer-based optimization methods such as artificial neural networks and principal component optimization methods could feasibly be used to refine the electrodeposition parameters to obtain Ni composite coatings with improved properties.
2. Further investigation has to be done in incorporating suitable alloying element (Ni-Co, Ni–W, Ni-P, Ni-Mo) in these composite coatings to improve the tribological properties for high temperature applications.
3. The synergetic lubricating action and mechanism of multiple lubricants used in these Ni based self-lubricating composite coatings needs to be studied in detail.
4. Future initiatives could include the development of Ni composite coatings by pulse deposition that are functionally graded for specialised applications.
5. Further studies are needed to develop nickel composite coated mesh for oil-water emulsion separation which is an important industrial problem to be solved.

ABSTRACT

Name of the Student: **Ms. Revathy Sreekumar** Registration No.: 10CC19A39021
Faculty of Study: Chemical Sciences Year of Submission: 2025
AcSIR academic centre/CSIR Lab: CSIR-National Institute for Interdisciplinary Science and Technology (CSIR-NIIST) Name of the Supervisor: Dr. Sreejakumari S. S.

Title of the thesis: **Development of 2D materials incorporated multi-functional nickel composite coatings by electrodeposition**

Multi-functional metallic composite coatings have emerged as a cornerstone in modern material science, offering a unique combination of properties that address diverse industrial challenges. Integrating multiple functionalities into a single coating not only simplifies the processes but also reduces the material costs. The improved properties of these multi-functional coatings make them indispensable in industries such as aerospace, automotive, healthcare, and energy sector. **Chapter 1** gives a general introduction about recent developments in multi-functional metallic composite coatings developed by electrodeposition. Main focus of the chapter is on the properties of 2D materials (h-BN, graphene, and transition metal dichalcogenides) incorporated electroplated nickel based composite coatings. This chapter also gives a detailed an experimental methodology for the development of Ni composite coatings over mild steel substrate by electrodeposition.

Chapter 2 deals with the development of Ni-h/BN composite coating over mild steel substrate. The influence of grain refinement on the microhardness, corrosion and tribological properties was also investigated. Micro hardness value, wear resistance and corrosion resistance of the composite coating was higher than pure Ni coating and mild steel. Thus the developed Ni-BN coating with improved properties indicates its potential for engineering applications. One-step electrodeposited biomimetic Ni-graphene composite coating with pinecone-inspired hierarchical micro/nanostructures with a contact angle of 152° was developed in **Chapter 3**. It was observed that this particular coating had a self-cleaning nature and it was a mechanically durable anticorrosive coating. The composite coating also exhibited consistent and remarkable lubricating properties with an average friction coefficient of 0.24. In **Chapter 4**, electrodeposited Ni-MoS_2 coatings have been successfully developed. In terms of mechanical properties, Ni-MoS_2 coating showed a maximum hardness value of 525 HV. Compared with uncoated and pure Ni coated samples, Ni-MoS_2 composite coated sample exhibited excellent corrosion resistance and low coefficient of friction (0.08) at optimized conditions. Ni-MoS_2 coated SS mesh exhibited improved electrocatalytic activity for HER and OER.

Chapter 5 deals with the development of a low-friction, superhydrophobic Ni-WS_2 coating by a versatile one-pot, and single-step electrodeposition. By adjusting WS_2 concentration and tuning the deposition parameters, a hierarchical surface with a high water contact angle of 159° was achieved. Compared to the uncoated substrate and pure nickel coating, the robust surface of the as-prepared composite coatings exhibited good self-cleaning and corrosion resistance, providing potential for industrial applications. **Chapter 6A** deals with the development of superhydrophobic - superoleophilic SS mesh with a water contact angle of 169.5° and surface roughness of 168 nm. The combined effect of hydrophobic surface chemistry and the roughness contributes to excellent superhydrophobic-superoleophilic and self-cleaning characteristics of the developed SHSM. **Chapter 6B** reveals the potential of Ni-WS_2 coated SS mesh with micro-nano hierarchical structure as a bi-functional catalyst in overall water splitting. Summary of the various studies carried out and future perspectives of the research work is given in **Chapter 7**.

Details of the Publications Emanating from the Thesis Work

Published

1. **Revathy Sreekumar**, Aswathy.S.Nair, Sreejakumari S.S., "Recent trends and developments in two-dimensional materials based electrodeposited nickel nanocomposite coatings," FlatChem, 36, (2022): 100434, DOI: 10.1016/j.flatc.2022.100434

2. **Revathy Sreekumar**, Swapna Eravath Thazhakunni, Sreejakumari Sukumaran Suseelamma, "Fabrication of a robust superhydrophobic stainless steel mesh for efficient oil/water separation," Journal of Industrial and Engineering Chemistry, 135, (2024): 425-433, DOI: 10.1016/j.jiec.2024.01.054

3. **Revathy Sreekumar**, Shilpa Radhakrishna Pillai, Rakhi Raghavan Baby, Sreejakumari S.S., "Morphology tuned Ni-WS_2 coated stainless steel mesh as an efficient bi-functional electrocatalyst for water splitting," Materials Today Communications, 44, (2025): 111860, DOI: 10.1016/j.mtcomm.2025.111860

4. **Revathy Sreekumar**, M.S. Priyalekshmi, S. Parvathy, S.S. Sreejakumari, "Influence of grain refinement on microhardness, wear behaviour and corrosion resistance of electrodeposited Ni-BN composite coatings", Ceramics International, DOI: 10.1016/j.ceramint.2025.07.435

In Press

1. **Revathy Sreekumar**, S.S. Sreejakumari, "Development of a robust superhydrophobic corrosion-resistant Ni-WS_2 composite coating by electrodeposition", Journal of Electrochemical Society of India

Publications not related to thesis work

1. Ancin Maria Devis, **Revathy Sreekumar**, Subrata Das, K. Jayasankar, Sreejakumari S.S., "Fabrication of cross-linked highly stable graphene oxide membrane for dye removal" International Journal of Environmental Analytical Chemistry, 104, (2024): 7229-7245, DOI: 10.1080/03067319.2022.216471

List of conference presentations

1. **Revathy Sreekumar**, Swapna E.K., Sreejakumari S.S., "Fabrication of a superhydrophobic stainless steel mesh for efficient oil/water separation", International Symposium on Accelerated Materials Design and Additive Manufacturing: Scientific and Technological Perspectives (AMDAM) & 76th Annual Technical Meeting (ATM) **(Oral presentation)**

2. **Revathy Sreekumar**, Swapna E.K., Sreejakumari S.S., "Structural and morphological tuning of stainless steel mesh by electrodeposition for efficient oil/water separation", National Conference on Advanced Materials and Manufacturing Technologies (AMMT -2023), CSIR-NIIST Trivandrum **(Poster presentation)**

3. **Revathy Sreekumar**, Aswathy.S.Nair, Sreejakumari S.S., "Development of multi-functional Ni-graphene composite coating by electrodeposition", International Conference on Advances in Interdisciplinary Nanoscience (ICAINS – 24), Government College for Women, Thiruvananthapuram. **(Oral Presentation)**

4. **Revathy Sreekumar**, Shilpa Radhakrishna Pillai, Rakhi Raghavan Baby, Sreejakumari S.S., "Bi-functional catalytic activity of Ni-WS_2 coated stainless steel mesh for water splitting", 4th International Conference on Optoelectronic and Nanomaterials for Advanced Technology (icONMAT 2025), Cochin University of Science & Technology, Kochi **(Poster Presentation)**

Abstracts of Papers Presented

Fabrication of a Robust Superhydrophobic Stainless Steel Mesh for Efficient Oil/Water Separation

Revathy Sreekumar [a,b], Swapna E.K.[a], Sreejakumari S.S.[a,b]*

[a] *Materials Science and Technology Divison, CSIR-NIIST Trivandrum,695019, CSIR- National Institute of Interdisciplinary Science and Technology, Trivandrum, India*

[b] *Academy of Scientific and Innovative Research (AcSIR), Ghaziabad-201002, India*

Abstract

Leakage of oil or organic pollutants into the ocean arouses a global catastrophe since toxic chemicals found in oil-polluted water can harm people's health and have an adverse effect on the environment. Separation by means of materials with selective oil/water uptake is a comparatively new but sustainable area of research. The superhydrophobic materials have offered a new idea for the efficient, thorough and automated oil/water separation. Researchers have switched to interfacial superwetting porous materials to treat oily water because oil/water separation is basically an interfacial process. Metallic meshes (SS mesh and copper mesh) are commonly used as potential oil-water separation substrates because of their low cost, high plasticity, high thermal stability and good mechanical properties. Meshes with extreme, preferential wettability can effectively remove oil or water from oil/water mixtures using a simple gravity-based filtration process. In this work we have developed a robust Ni-WS_2 based superhydrophobic stainless steel mesh (SHSM) via one-step electrodeposition followed by further modification with low surface energy material. The surface morphologies, chemical composition, and wettability were characterized by means of scanning electron microscopy (SEM), X-ray diffraction (XRD) and water contact angle (WCA) measurements respectively. By tuning the mesh surface to a hierarchical structure of micron-sized protrusions and submicron-sized bumps, a high water contact angle of 150 degree with good superoleophilic properties was achieved. The SHSM was used for the separation of various oil/water mixtures (n-hexane, toluene, diethylether, dichloromethane) and the separation efficiency was up to 98.3% even after being recycled 30 times. In addition, the as-prepared mesh shows self-cleaning property with water and exhibits strong chemical stability against strong acidic/alkaline solutions.

Structural and Morphological Tuning of Stainless Steel Mesh by Electrodeposition for Efficient Oil/Water Separation

Revathy Sreekumar [a,b], Swapna E.K.[a], Sreejakumari S.S.[a,b]*

[a] *Materials Science and Technology Divison, CSIR-NIIST Trivandrum,695019, CSIR-National Institute of Interdisciplinary Science and Technology, Trivandrum, India*

[b] *Academy of Scientific and Innovative Research (AcSIR), Ghaziabad-201002, India*

Abstract

Clean water is essential for life and a critical resource for most organisms. Leakage of oil or organic pollutants into the ocean arouses a global catastrophe since toxic chemicals found in oil-polluted water can harm people's health and have an adverse effect on the environment. Separation by means of materials with selective oil/water uptake is a comparatively new but sustainable area of research. The superhydrophobic materials have offered a new idea for the efficient, thorough and automated oil/water separation. Metallic meshes (SS mesh and copper mesh) are commonly used as potential oil-water separation substrates because of their low cost, high plasticity, high thermal stability and good mechanical properties. Meshes with extreme, preferential wettability can effectively remove oil or water from oil/water mixtures using a simple gravity-based filtration process. In this work we have developed a robust Ni-WS_2 based superhydrophobic stainless steel mesh (SHSM) via one-step electrodeposition followed by further modification with low surface energy material. The surface morphologies, chemical composition, and wettability were characterized by means of scanning electron microscopy (SEM), X-ray diffraction (XRD) and water contact angle (WCA) measurements respectively. By tuning the mesh surface to a hierarchical structure of micron-sized protrusions and submicron-sized bumps, a high water contact angle of 150 degree with good superoleophilic properties was achieved. The SHSM was used for the separation of various oil/water mixtures (n-hexane, toluene, diethylether, dichloromethane) and the separation efficiency was up to 98.3% even after being recycled 30 times. In addition, the as-prepared mesh shows self-cleaning property with water and exhibits strong chemical stability against strong acidic/alkaline solutions. Thus the SHSM synthesized in this study using a facile synthetic strategy has great potential in the application of actual oil/ water separation.

Development of Multifunctional Nickel-Graphene Composite coating by Electrodeposition

Revathy Sreekumar [a,b], Aswathy.S.Nair [a,b], Dr. Sreejakumari S.S.[a,b]*

[a] Materials Science and Technology Division, CSIR- National Institute of Interdisciplinary Science and Technology, Trivandrum, India

[b] Academy of Scientific and Innovative Research (AcSIR), Ghaziabad-201002, India

Email address: revathyias26@gmail.com & sreejakumari@niist.res.in

Abstract

Long-time environmental protection of metallic materials is still required in manufacturing and engineering applications. The use of graphene-based composite as anti-corrosion and protective coatings for metallic materials is still a provocative topic worthy of debate [1]. Nickel–graphene nanocomposite coatings have been successfully coated over mild steel by electrochemical co-deposition technique. This study explores surface morphology, phase composition, wettability, and corrosion resistance properties of the Ni nanocomposite coatings. The concentration of graphene and deposition parameters like current density, time, and temperature were optimized. The coatings exhibited compact and crack-free morphology which was evident from the SEM images which was in agreement with the XRD results. Wettability studies reveal that the Ni-graphene coating has a water contact angle (CA) of 152^{o} indicating its superhydrophobicity and also possesses self-cleaning properties. Corrosion-resistant properties of the coatings were examined by potentiodynamic polarization studies and electrochemical impedance spectroscopy. Incorporating graphene sheets into a nickel metal matrix leads to enhanced surface roughness, adhesion strength, and corrosion resistance of produced composite coatings. Furthermore, the presence of graphene in composite coating exhibits reduced grain sizes and enhanced erosion–corrosion resistance properties. The simple fabrication method may provide a cost-effective way to prepare mechanically durable, anti-corrosive, self-cleaning, and superhydrophobic coatings on metal substrates.

Bi-functional Catalytic Activity of Ni-WS_2 Coated Stainless Steel Mesh for Water Splitting

Revathy Sreekumar [1,3], Shilpa.R [2], Rakhi R.B. [2,3*], Sreejakumari S.S.[1,3*]

[1] Materials Science and Technology Division, CSIR−National Institute for Interdisciplinary Science and Technology (NIIST), Thiruvananthapuram 695019, India

[2] Centre for Sustainable Energy Technologies, CSIR- National Institute for Interdisciplinary Science and Technology (NIIST), Research Centre University of Kerala, Thiruvananthapuram 695019, India

[3] Academy of Scientific and Innovative Research (AcSIR), Ghaziabad- 201002, India

*Email address: rakhiraghavanbaby@niist.res.in & sreejakumari@niist.res.in

Abstract

Electrocatalytic water splitting is a simple and environmentally friendly way of producing hydrogen. The high cost of noble metal catalysts restricts their applicability, so developing earth-abundant and inexpensive catalyst materials is vital for electrocatalytic water splitting. Nowadays, bi-functional catalysts that can perform the dual function of HER (Hydrogen evolution reaction) and OER (Oxygen evolution reaction) are in great demand. In the present work, a novel electrodeposited Ni-WS_2 coated stainless steel mesh is developed as a bi-functional catalyst for electrochemical water splitting. The synergistic effect of Ni and WS_2 particles, along with highly reactive surface area and quick separation of bubbles from the hierarchical surface, are attributed to the desirable catalytic activity of the fabricated electrode material. The developed bi-functional catalyst shows excellent performance in both HER (89 mV at 10 mA cm^{-2}) and OER (230 mV at 10 mA cm^{-2}). Chronoamperometric studies reveal that the catalyst exhibited robust stability over a period of 10 hours in alkaline medium. In overall water splitting, to generate a current density of 10 mA/cm^2, the cell only required a potential of 1.56 V and was stable over 15 hours. Thus, this work provides a new efficient electrocatalyst based on the non-precious metal Ni for overall water splitting, contributing to sustainable hydrogen energy production.

FlatChem 36 (2022) 100434

Contents lists available at ScienceDirect

FlatChem

journal homepage: www.sciencedirect.com/journal/flatchem

Recent trends and developments in two-dimensional materials based electrodeposited nickel nanocomposite coatings

Revathy Sreekumar [a,b], Aswathy S Nair [a,b], Sreejakumari S.S [a,b,*]

[a] CSIR- National Institute of Interdisciplinary Science and Technology, Trivandrum, India
[b] Academy of Scientific and Innovative Research (AcSIR), Ghaziabad 201002, India

ARTICLE INFO

Keywords:
Coatings
Hard chrome
Electrodeposition
Nickel nanocomposites
2D materials
Interface
Tribofilm
Self-lubrication
Corrosion resistance
Super-hydrophobicity

ABSTRACT

In recent years, electrodeposition has gained substantial attention due to its advantages such as being efficient, reliable, economical and simple to operate among different methods used to protect industrial components from corrosion, wear/abrasion failures. On account of their exceptional improvement in hardness, corrosion and wear properties that can be achieved from electroplated nickel nanocomposite coatings, they are being widely utilised in the manufacturing, automotive, aviation and electrical industries. Additionally, electrodeposition of nickel-based composites is an environmentally-safe alternative to traditional coatings like harmful hard chromium coatings. Scientific investigation and technological applications comprising of anti-friction, anti-wear and lubrication of 2D materials like graphene, BN, WS_2 and MoS_2 have made remarkable strides in past few years and have arisen as innovative solid lubricants having remarkable capabilities refining tribological properties. This review article provides an outline of fundamental aspects of electrodeposition such as metal-particle co-deposition models and various influential parameters affecting the electrodeposition process. Development strategies, reinforcement mechanisms, characteristic mechanical properties, friction and lubrication performances, super-hydrophobicity, characterisation techniques, possible applications and practical benefits of 2D material incorporated nickel nanocomposite coatings are comprehensively discussed in this work. Possibilities for future research in this area are also discussed. We believe that this review article serves as an important focal point for new researchers by offering an understanding of synthesis approaches and applications of two-dimensional material incorporated electrodeposited nickel nanocomposite coatings.

Introduction

Traditional chromium coatings deposited from Cr (VI) electrolyte have a wide range of engineering applications due to their excellent corrosion and wear resistant properties and are widely used in vehicle engines, hardware and tools.[1,2] Additionally chromium plated coatings possess superior hardness, low coefficient of friction and shiny lustre.[3,4] Despite many favourable characteristics and cost-effectiveness, the bath utilised for chrome deposition have hazardous Cr (VI) ions that should be abandoned according to EU directives (2000/53/WE and 2011/37/EU); and this declaration prompted investigators to go to greater extent to find alternatives to chromium.[5–7].

As early as 1970s, Nickel (Ni) was proposed to be a promising substitute for hard chromium due to its novel blend of properties and attributes.[8] Gradually it became a well-known choice within the zone of metal matrix nanocomposites (MMCs).[9,10] Area of electrodeposition of metal matrix composite coatings is advancing at a regular pace.[11] These composite coatings are used on account of their improved mechanical[12], magnetic[13], optical[14], outstanding electrochemical [15] and catalytic properties.[16,17] Electrodeposition is a "bottom-up", "single step" method for developing metal matrix nano-composites in which the source will be electroactive species which get reduced at the cathode.[18] Another benefit of adopting the electrodeposition technique is the ease with which grain size, coating thickness, morphology, and crystallographic orientation may be varied by changing the bath compositions and deposition parameters.[19] Metal matrix based nanocomposites have appreciable uses in transportation, electrical and manufacturing sectors since they have superlative mechanical properties and attributes like being light weight and higher electrical and thermal conductivity.[20–22] Improved properties of typical nano-

* Corresponding author at: Material Sciences and Technology Division, CSIR- National Institute of Interdisciplinary Science and Technology, Trivandrum 695019, India.
E-mail address: sreejakumari@niist.res.in (S. S.S).

https://doi.org/10.1016/j.flatc.2022.100434
Received 13 July 2022; Received in revised form 22 September 2022; Accepted 6 October 2022
Available online 13 October 2022

crystalline nickel produced by electrodeposition are increased strength and hardness, low density, minimum porosity, feasibility and excellent corrosion cum wear resistance.[23].

For nickel composite coatings, different types of materials may be utilised as second phase particles like ceramics [24], pure metals[25] and polymers.[26] The inclusion of nano materials into the nickel matrix imparts unique attributes that are not shown by conventional micron sized coatings.[27] Nano sized metal oxides (Al_2O_3 [28,29], ZrO_2[30], TiO_2 [31,32], Cr_2O_3[33], SiO_2[34], CeO_2[35]), carbides (SiC[36], WC [37], TiC[38], B_4C[39]), nitrides (Si_3N_4[40]), carbon-based materials (graphite,[41] diamond,[42,43] carbon nanotubes[44]) etc are included as secondary phase particles. In addition to these, layered two-dimensional (2D) nanomaterial fillers such as graphene[45], boron nitride (BN)[46], molybdenum disulphide (MoS_2)[47], transition metal carbides[48], selenides[49,50], MXenes[51,52] and other novel lamellar 2D materials, such as LDH[53], α-ZrP[54,55], mica flakes[56] have been used as potential reinforcements to develop composites with superior mechanical and tribological properties.

The present review mainly focuses on the development of electro-deposited Ni based tribological nano-composite coatings with 2D nanomaterials as reinforcements on various substrates. This review elucidates the influence of electrodeposition parameters on the physical, mechanical, microstructural and tribological characteristics of the coatings, properties like self-lubrication and super-hydrophobicity, various characterisation techniques that can be used in the detailed analysis of these coatings, applications in diverse fields and the challenges and future avenues of this ever advancing nickel based composite coating technology.

Two-dimensional layered materials as reinforcements: Scope and applications

Two-dimensional materials possess remarkable physical, chemical, electronic and optical properties compared to existing three-dimensional (3D) materials.[57] 2D materials are a combination of crystalline atomic chains, where the atoms are firmly linked by covalent bonds within individual atomic layers and subsequent layers are loosely connected by van der Waals forces, forming a monolayer structure with high modulus and strength. Higher specific surface area of 2D materials aids in more effective surface absorption and act as a barrier between the friction pair. In addition to that, low shear resistance between the nearby atomic layers permits the easy sliding of these layered atoms.[58] Thus the soft van der Waals forces account for their outstanding tribological properties and self-lubrication performance superior to that of other nanomaterials.[59].

2D nanomaterials can be typically classified into five categories based on their composition and atomic configuration: (1) Xenes, which are made up of single element like carbon, silicon and phosphorous. A peculiar example is graphene made of carbon atoms. (2) Transition metal carbides and nitrides (MXenes), in which M is an early transition metal (e.g. Ti, V and Mo) and X can be carbon or nitrogen. (3) Transition metal dichalcogenides (TMDs); they are composed of hexagonal metal layers in which metal atoms (M) are packed between two layers of chalcogen atoms (X) having a MX_2 stoichiometry such as MoS_2, $MoSe_2$, WSe_2 and WS_2. (4) 2D III nitrides (MN) in which M is a group III metal and N is nitrogen. An example of 2D III nitride is hexagonal boron nitride (h-BN). (5) 2D organic frameworks. They are comprised of metal-organic frameworks (2DMOFs) that contain metal ions or clusters that are bonded to organic ligands, an example is MOF-5 whereas covalent-organic frameworks (2DCOFs) forms two-dimensional structures via interactions between organic precursors leading to strong covalent bonds, resulting in porous, stable and crystalline materials. A typical example is COF-5. Metal composite coatings incorporating MXene or 2D MOF have not yet been explored owing to their high cost and expected defects in structure.

This paper reviews recent experimental findings related to 2D layered materials as nano-reinforcements giving more importance in analysing the performance of graphene, BN and TMDs that have been studied extensively for their tribological properties in electrodeposited nickel nano composite coatings.

Graphene

Graphene (Gr) is basically a crystalline allotrope of carbon with two-dimensional properties. In graphene, sp^2-bonded carbon atoms are closely arranged in a well ordered hexagonal fashion (Fig. 1) It has a large surface area that has a close-knit contact with the metal matrix[60] and additionally has ultra-high elastic modulus, yield strength, good electrical and thermal conductivity.[61] Graphene has potential applications in the field of materials engineering specifically in resilient composite materials.[62] Possibility of using graphene as part of the composites is really useful in aerospace and auto-motive industries because of its superior strength, ductility and firmness as a covering especially in the area of laminated composites, altering the substrate by improving its endurance to extreme conditions that may cause wear and corrosion.[63] In addition to that, graphene incorporated metal matrix composites hold superlative thermal and mechanical properties, so that they can be utilised in the fields of surface engineering, catalysis, electronics, energy storage and so on.[64] The workability of graphene is restricted due to expensive synthesis methods, limited solubility and agglomeration tendency while utilised in the area of composite materials.[65] Pure Gr coatings are extremely vulnerable to surface defects especially when exposed to corrosive environment.[66,67] To avoid these drawbacks functionalization of graphene is considered to be an alternative and thus graphene oxide (GO) became popular.[68,69] GO is the oxidized form of graphene. In GO the carbon atoms are attached to oxygen containing groups such as carbonyl, carboxyl, epoxide and hydroxyl etc. These functional groups make GO hydrophilic. It can form stable dispersions in both aqueous and non-aqueous media. Additionally GO shows better chemical activity and becomes electrically resistive because of these functional groups.[68,69] Reduced graphene oxide (r-GO) is synthesized by different methods involving suitable treatment of GO so that only minimal amount of oxygen containing functional groups are present. Obtained r-GO will have characteristics similar to that of natural graphene.[70].

Boron nitride

Boron nitride (Fig. 2) is a man-made crystalline compound that is structurally similar to graphite as the alternating B and N atoms substitute for C atoms.[71] It is a refractory compound having exceptional chemical and thermal stability, high thermal conductivity, excellent electrical resistivity, non-wettability, superior lubrication properties and low dielectric constant.[72–74] BN nano-particles may be directly included into polymers and metal matrices to get composite coatings which show improved corrosion resistance and high hardness.[75] An additional advantage of h-BN is that it is a very good lubricant at both low and high temperature and can be employed to generate different friction resistant composite materials.[76,77] Another important feature is that the viscosity of BN is maintained without water or gas entrapment in between its layers.

Transition metal dichalcogenides

Transition metal dichalcogenides are typically MX_2, where M is a transition metal atom (such as Mo or W) and X is a chalcogen atom (such as S, Se or Te) such as MoS_2, $MoSe_2$, WS_2, and WSe_2 (Fig. 3). They are layered materials which follow hexagonal crystal system[57,78] having strong in-plane ionic-covalent bonds and weak out-of-plane van der Waals forces. Ultrahigh strength composites incorporated with TMD-based nanoparticles have a wide range of applications.[79] The layered TMD based lubricants are gaining importance.[80] Van der

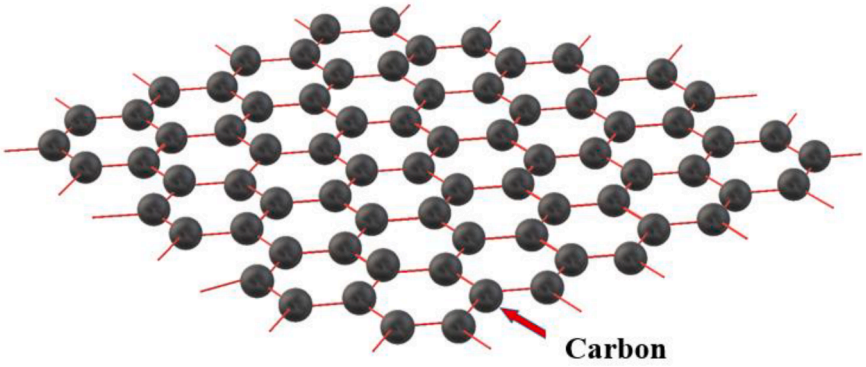

Fig. 1. Structure of graphene.

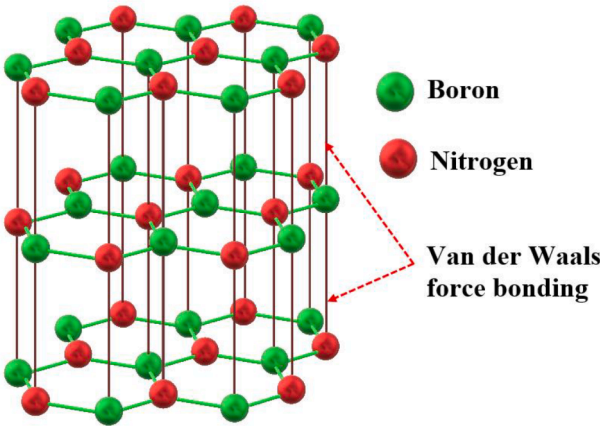

Fig. 2. Structure of boron nitride.

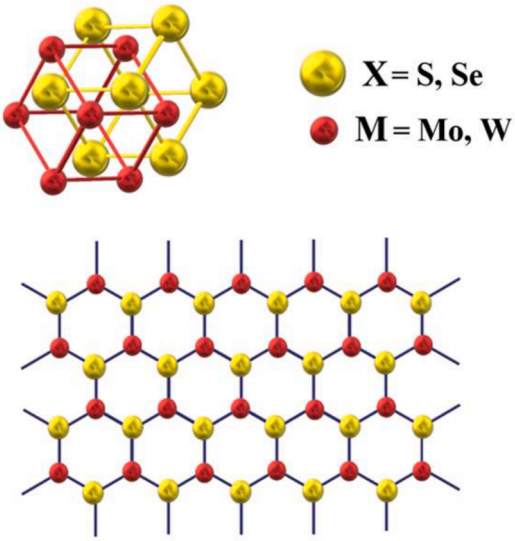

Fig. 3. Structure of transition metal dichalcogenides.

Waals interactions result in minimal shear and sliding of individual layers which reduces wear and friction to a greater extent.[81] The main disadvantage of these TMD based lubricants is that they are highly susceptible to humidity.[82] These TMD based self-lubricating coatings have applications involving ultra-high vacuum, transportation and space systems comprising of satellites and launch vehicles where often liquid lubricants fail to function properly.[83,84].

Molybdenum disulfide (MoS_2) and MoS_2-based nanocomposites have received the greatest attention among these 2D TMDs.[85] So far, MoS_2-based nanomaterials have primarily been applied in domains such as energy storage, electronic devices, and biomedical engineering.[86] MoS_2 has superior mechanical characteristics as well, including an extraordinarily high Young's modulus (0.3 TPa) and strong elasticity.[87].

In comparison with MoS_2, WS_2 can sustain in high temperature so that it is a better solid lubricant for high temperature applications. WS_2 is chemically inert and it is converted to tungsten trioxide (WO_3) as it gets oxidised. WO_3 also has a low friction factor and restricts the glue formation in between the surfaces that experience friction. The addition of WS_2 in Ni matrix leads to reduction in fragility of the coating and improves properties like adhesion and wear resistance of the coating.[88] In recent years, electrodeposition has been used extensively to develop Ni-WS_2 composite coatings having low friction coefficients and/or exceptional wear resistance. There are two types of WS_2 used for preparation of Ni/WS_2 composites: IF (inorganic fullerene-like) and 2H (layered platelets). In comparison with WS_2 platelets, the fullerene form has more superior tribological performance.

In ambient atmosphere transition metal dichalcogenides containing sulphides, typically MoS_2 and WS_2 become ineffective because of their moisture sensitive tribological behaviour unlike selenides based dichalcogenides such as tungsten diselenide (WSe_2) and $MoSe_2$ (molybdenum diselenide). $MoSe_2$ can be considered as a promising candidate to be used as a second phase reinforcement in the generation of hydrophobic surfaces due to its high thermal stability, inertness in moisture and oxygen containing atmosphere. So the incorporation of $MoSe_2$ can retain the superhydrophobicity for a considerable time period.[49] WSe_2 can be utilised as a solid lubricant in various tribological applications at different conditions like vacuum, normal atmosphere and even at high temperature around 1700 °C where the traditional liquid lubricants happens to be inefficient.[89] Therefore WSe_2 is a potential option to be a secondary particle reinforcement in Ni matrix because of its top grade tribological behaviour in ambient air as well as inert atmosphere. It is important to note that the structural and tribological parallelism of electroplated Ni-WSe_2/$MoSe_2$ composite coating on various substrates has not yet been described in detail.

General mechanism of co-deposition in composite electrodeposition

In electrodeposited nano-composites, the metal matrix, type and size of the reinforcement particles are actively chosen and the process parameters are designed to maximise the increase of the strengthening effects granted by the crystal structure[26] (Fig. 4). For instance, the process parameters: current density, agitation type and electrolyte composition are used to modify the grain size of the matrix.[90] The kinetics of electrochemical deposition, mechanisms of crystal growth

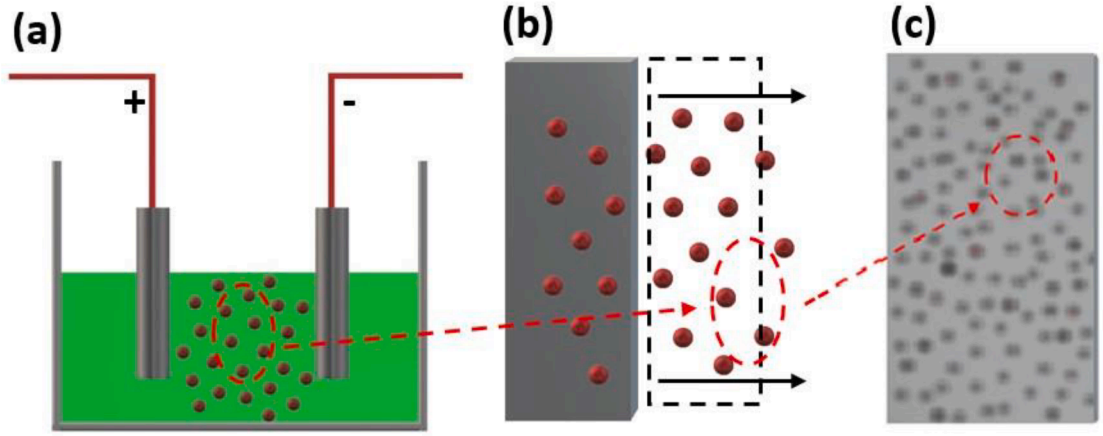

Fig. 4. Electrodeposition of composites. (a) Particle addition to the electrolyte, (b) Particle entrapment by the metal and (c) Composite coating. Particles are encircled in red.

and nucleation, all contribute to porosity of the electrodeposited coatings.[91] For nickel nanocomposite coatings, different types of particles like oxides, carbides, nitrides, two dimensional layered materials, diamond like carbon (DLC) can be utilised. Integration and even distribution of nano-meter sized second phase particles might improve the material's intrinsic mechanical, tribological and electrochemical properties and open it up to a whole new area of material applications. Agitation/stirring, cathode movement and surfactant addition are the ways of suspending secondary particles. In the bath particles will attain a natural surface charge and zeta potential. Alteration of surface charge in terms of sign and size is possible by adsorption of metallic ions and also by surfactant addition.

There are many proposed models which explain particle co-deposition.[92,93] Table 1 provides the details of existing models and their main ideas.

The adaptability and the credibility of all the available models still need proper proofs and verification.[100,101] One of the common mechanisms of co-deposition process have five sequential steps[102] as shown in Fig. 5.

Five consecutive steps of co-deposition mechanism are:

(1) Formation of ionic clouds on the particles
(2) Convection towards the cathode
(3) Diffusion through hydrodynamic boundary layer

Table 1
List of existing models which explain the mechanisms of particles co-deposition in composite electroplating.

Guglielmi [94]	This model described co-deposition as two consecutive steps:(i) Loosely absorbed particles form a layer at the surface of the cathode by absorption.(ii) Electrophoresis where the electric field at the interface elevates potent surface adsorption and thus particles are entrapped by the growing metal. The fluid dynamic conditions were not considered in this model.
Celis et al.[95]	Devised that the movement of particles is relative to the mass transfer of ions towards cathode. Firstly ionic species forms an absorbed layer around the particles followed by the addition to the electrolytic bath, followed by transport of particles via convection–diffusion. Finally, incorporation depends upon the probability and number of transported particles.
Fransaer et al. [96]	This one use trajectory analysis to explain the suitable environment provided by the action of tangential forces on the particles enhancing rate of co-deposition.
Hwang et al.[97]	Highlighted the importance of current density in particle co-deposition. Co-deposition rates are associated with the reduction of ions adsorbed on the particles' surfaces.
Vereecken et al. [98]	The model depicted particle transport as governed by convection–diffusion taking into account hydrodynamics and assuming that particle inclusion increased with contact time at the cathode's surface.
Berçot et al.[99]	Guglielmi's model [94] was further improved by including a mathematical model that accounted for hydrodynamic conditions.

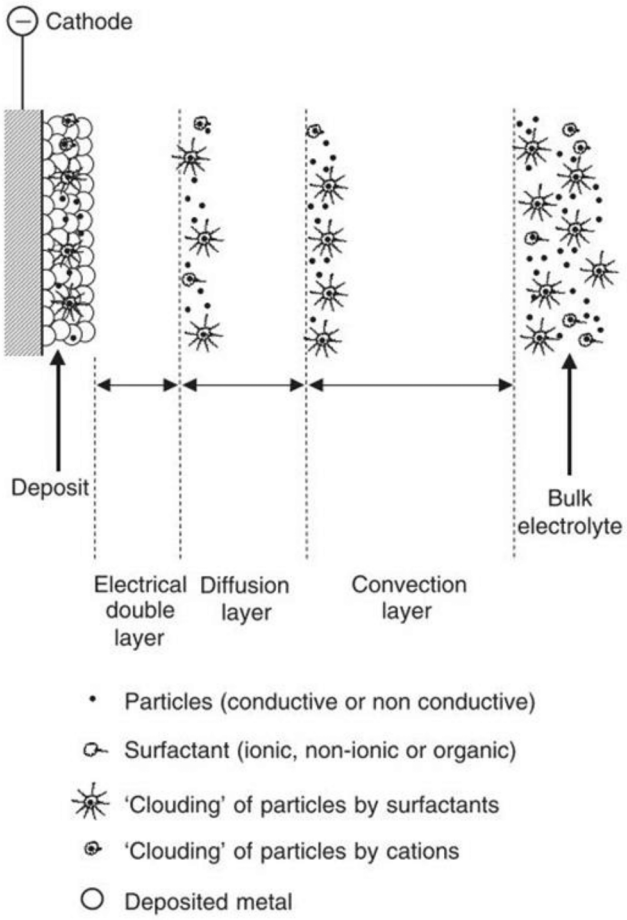

Fig. 5. Mechanisms of particle codeposition into a metal deposit. The regions include: formation of ionic clouds around the particles (bulk electrolyte, typical length in cm); convective movement toward the cathode (convection layer, typical length in mm); diffusion through a concentration boundary layer (diffusion layer, typical dimensions of hundreds of μm); electrical double layer (typical dimensions of nm) followed by adsorption and entrapment of particles. Reprinted with permission from SPS:refid::bib108[108]. © Elsevier Limited 2006.

(4) Diffusion through concentration boundary layer
(5) Adsorption at the cathode surface where particles get deposited within metal deposit

If the reinforcements are nano particles, the action of every forces will be entirely different from micron sized particles. Therefore these models need more authentication to include the concepts of nano composite coating technology.[103].

Nickel nanocomposite electrodeposition

Different types of Ni electrolytic baths

Sulphate solutions. The most common nickel plating bath is the sulphate bath known as Watts bath. Watts formulation, which was developed in 1916 by Professor Oliver P. Watts[8] is the basis of majority of the nickel plating solutions. This electrolyte is made up of nickel sulphate, nickel chloride and boric acid. Nickel sulphate is the main origin of nickel ions. The limiting current density for attaining good quality deposits is determined by the nickel metal content. Anodic corrosion is provided by nickel chloride thus increasing the diffusion coefficient of nickel ions allowing a higher limiting current density and boric acid functions as a pH buffer.[104] H_3BO_3 could also influence the nucleation and grain growth of Ni electrodeposits in the Watts electrolyte. A sufficient H_3BO_3 content improves the Ni nucleation process, resulting in a fine and bright Ni coating.[105] While the quantities may vary depending on the application, Table 2 provides a common formulation and details of operating parameters.[106].

Nickel sulfamate solutions are mostly utilized for electroforming. [107] Despite the greater cost, low stress in coatings can be obtained without the use of additives from these baths. The Watts bath has four major advantages compared to the other available baths:

1. Simple and easy to use
2. Obtained in high purity grades and relatively inexpensive
3. Less aggressive to equipment (container) than nickel chloride solutions
4. Deposits plated from these solutions are less brittle and possess lower internal stress than plated from nickel chloride electrolytes.

All Chloride Solutions. Chloride baths have an advantage over sulphate baths in deposition speed and effectively operate at high cathode current densities. Deposits from this electrolyte are smoother, finer grained, harder and stronger than those from Watts solutions and more highly stressed.

Fluoroborate Solutions. The fluoroborate solution can be operated over a wide range of nickel concentrations, temperature, current density and relatively simple to control. But the fluoroborate anion is corrosive and attack the materials that are in contact with the solution.

Hard Nickel. Developed especially for functional applications and is used where controlled hardness, improved abrasion resistance, greater tensile strength and good ductility are required without using sulphur-containing organic additives. The internal stress is slightly higher than in deposits from Watts solutions. The disadvantages of the hard-nickel bath are its tendency to form nodules on edges and low annealing temperature of the deposits.

Table 2
Details of Watts Ni electroplating solutions.

Bath composition	Nickel Sulphate (NiSO4·6H2O)	240–300 g/L
	Nickel Chloride (NiCl2·6H2O)	30–90 g/L
	Boric Acid (H3BO3)	30–45 g/L
Operating Parameters	Temperature	40–60 °C
	pH	3.5–4.5
	Current Density	2–7 A dm^{-2}
	Deposition Rate	25–85 μm h^{-1}

Techniques for Ni nanocomposite electrodeposition

Generally in Ni electrodeposition when an external electric field is applied, a transfer of electrons occurs across the cathode surface causing reduction of Ni ions into their metallic form.[108,109] This method is categorized into three successive steps[110]:

(1) Ni ions are carried to the cathode from the bulk electrolyte by mass transport through diffusion, convection and electro-migration.[111]
(2) A charge transfer occurs on the cathode and the partially reduced Ni atoms are adsorbed at the surface.
(3) Loosely bound Ni atoms will diffuse across the electrode surface to active growth sites where they are incorporated into the crystal lattice at the kink sites or an atomic step.

Passing electric current to the electrolyte is the primary function of nickel anodes in electroplating. Replacement of nickel ions that have been discharged at the cathode and distribution of current are also major functions of the Ni anode.[112] The following reactions are most probable in the course of Ni deposition, where $Ni(OH)^{+}_{ad}$ denotes an active intermediate.[113].

$$Ni^{2+} + H_2O \leftrightarrow Ni(OH)^{+}_{aq} + H^{+} \quad (1)$$

$$Ni(OH)^{+}_{aq} \leftrightarrow Ni(OH)^{+}_{ad} \quad (2)$$

$$Ni(OH)^{+}_{ad} + e^{-} \leftrightarrow NiOH \quad (3)$$

$$NiOH + H^{+} + e^{-} \leftrightarrow Ni + H_2O \quad (4)$$

Direct current electrochemical deposition (DC), pulsed electrochemical deposition (PC) and pulse reverse current electrochemical deposition (PRC) which is depicted in (Fig. 6) are various categories of electrochemical deposition. In DC method, a specific and steady current is applied throughout the coating process. One downside of this approach is the generation of residual tensile stresses, which results in the formation of cracks within the deposit. Because of its capacity to improve current distribution and mass transfer processes, the pulse technique is an effective way for controlling the microstructure and chemical composition of plated coatings. Furthermore, this process eliminates various issues such as hydrogen evolution, metallic hydride formation, uneven deposits, and local pH fluctuations. Application of an anodic current in form of a reverse pulse during nickel electrodeposition may distinctively affect quality, properties, and chemical composition of obtained coatings. Superior quality coatings may be obtained by this pulse reverse method.[114].

Mechanism of 2D material co-deposition in nickel electroplating

Due to inter-related process variables, the theoretical models for predicting particle codeposition outlined in (Table 1) are only valid in laboratory conditions. Furthermore, only the models proposed by Vereecken et al.[98] and Berçot et al.[99] were developed with submicron-size particles in consideration, while the rest of the models were built with micron-particles. As a result, the application of the proposed mechanisms in nanoparticle codeposition is limited so is the 2D material co-deposition.

There are studies on optimization and analysis of the underlying mechanism of co-deposition of nano materials in metallic deposition. [115] In case of 2D material based nanocomposite coatings, there are very few reports. The whole co-electrodeposition process in Ni–W/BN nanocomposite coating via DC deposition can be summarized in four sequential steps as “transportation, adsorption, reduction and

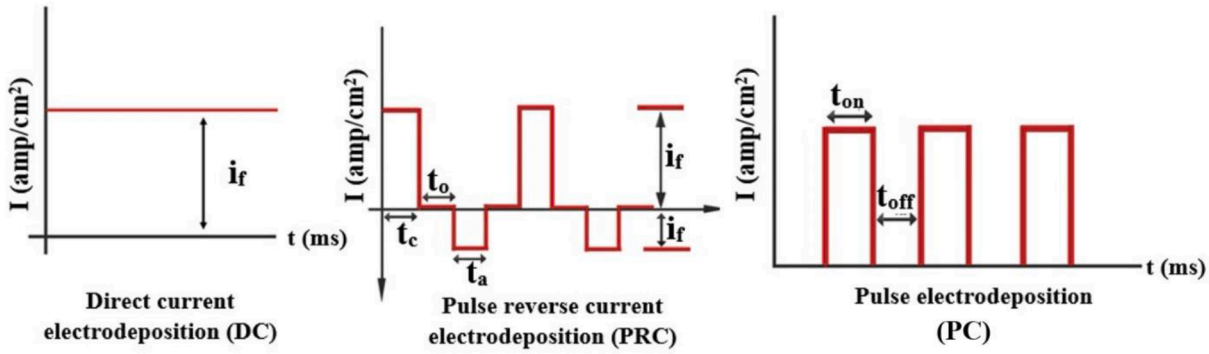

Fig. 6. Different types of electrochemical deposition.

incorporation" (Fig. 7) according to Li et al.[116] The initial step is "transportation" in which aqueous metal ions, complexes and charged particles are moved towards the cathode by convection or an electric field. Electrophoresis has been used to transfer metallic ions and BN nanoparticles to the cathode. Agitation can increase the availability of the nickel complex at the solution/electrode interface and accelerates the mass transport which speeds up the electrodeposition process. It is followed by "adsorption". Metal ions and charged BN nanoparticles move through the diffusion layer and get adsorbed on the surface of cathode.[117] "Reduction" was the next step. Metal ions are reduced and neutralized by electron transfer in this stage and they get firmly adsorbed on the cathode. The WO_4^{2-} ion reduction may be summarised as:

$$WO_4^{2-} + 8H^+ + 6e^- \rightarrow W + 4H_2O \quad (5)$$

The final stage was "incorporation". The BN particles get inserted into the Ni–W alloy matrix. Thus Ni–W/BN nanocomposite coating was formed. The Ni–W/BN nanocomposite coating generation is depicted in Eq. (6).

$$[(Ni)\,(HWO_4)\,(Cit)]^{2-} + 3H_2O + 8e^- + BN_s \rightarrow Ni - W/BN + 7OH^- + Cit^{3-} \quad (6)$$

Jiang et al.[118] suggested a set of reactions (7) to (10) responsible for the preference and significant increase in orientations of planes (111) and (220) in Ni/graphene platelet (GPL) composite coating rather than (200) plane in pure Ni coating. These reactions would occur in the electroplating bath and $Ni(OH)_2$ would be produced and get absorbed on the cathode surface, resulting in a drop in texturing coefficient at the favoured orientation (200). Ni^{2+} and $Ni[B(OH)_4]^+$ cations get attached on GPLs which prohibit the centres of Ni growth and hinders more grain growth. Therefore (111) and (220) has the highest probability of re-nucleation.

$$Ni + H_2O \rightarrow Ni(H_2O) \quad (7)$$

$$Ni(H_2O) \rightarrow Ni(OH)^+ + H^+ + 2e^- \quad (8)$$

$$Ni(OH)^+ + OH^- \rightarrow Ni(OH)_2 \quad (9)$$

$$B(OH)_3 + H_2O \leftrightarrow [B(OH)_4]^- + H^+ \quad (10)$$

An important point in understanding the progressive micro/nano structure formation in composite coatings is to analyse the optimal employment of surfactant and nanoparticles.[119] Cetyl trimethylammonium bromide (CTAB) is a cationic surfactant. After extended stirring and ultrasonic agitation, the surfaces of WC nanoparticles (NPs) and WS_2 NPs were enclosed by CTAB resulting in cationic particles. Electric field effect aids the cathodic migration of WC NPs and WS_2 NPs gets entrapped within growing nickel matrix (Fig. 8). Integrated effect of convective-diffusion and electrophoretic migration transports the CTAB capped particles and Ni^{2+} ions from the bulk solution to the electrical double layer. There will be variations in electrical resistivites of nickel matrix and the incorporated particles as a result of which the surface potential will be non-uniform. The surface structures are modified by this sequential mechanism in the presence of CTAB surfactant.

A discussion on the mechanism of deposition and hierarchical coating growth in Ni-P-WS_2 is given by He et al.[120] The main cathodic reaction is:

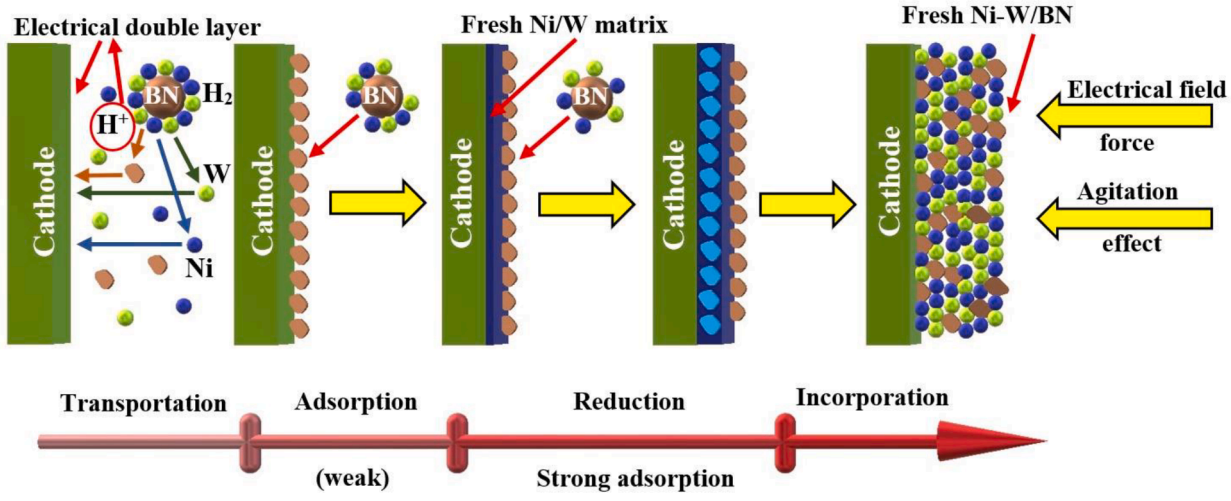

Fig. 7. Mechanism of co-electrodeposition process in Ni–W/BN composite coating. Concept adapted and redrawn from ref. [116].

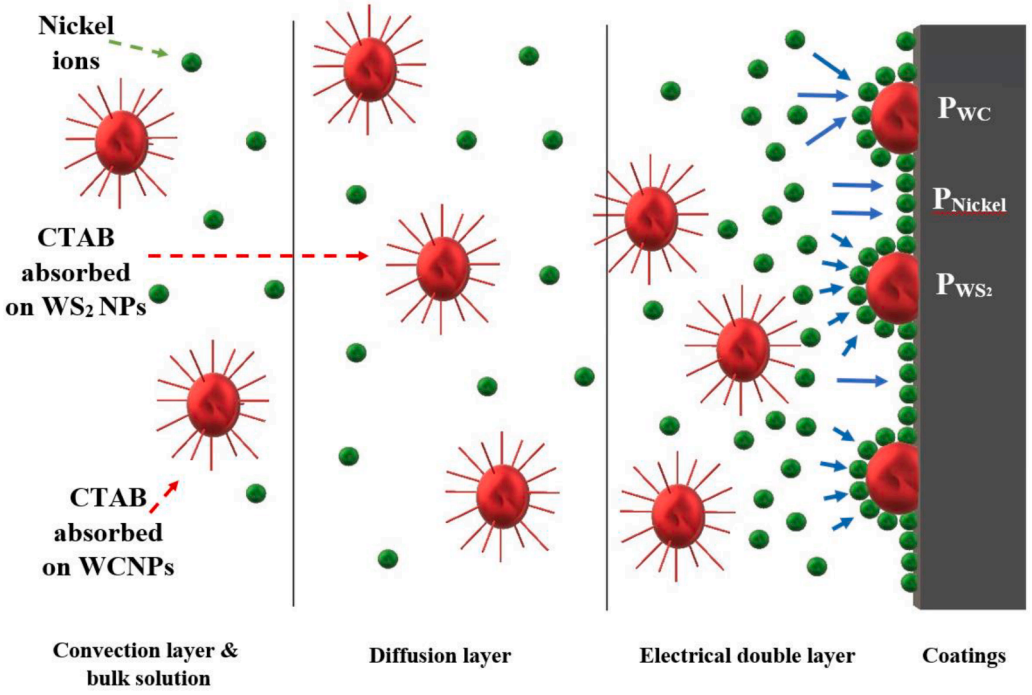

Fig. 8. Schematic illustration of co-deposition process in Ni-WC-WS_2 composite coating. Concept adapted and redrawn from ref. [119].

$$Ni^{2+} + 2e^- \rightarrow Ni \quad (11)$$

Hydrogen evolution will take place as a side reaction:

$$2H^+ + 2e^- \rightarrow H_2 \quad (12)$$

Reduction of hypophosphite ion at the cathode leads to phosphorus being co-deposited with nickel.

$$H_2PO_2^- + e^- \rightarrow P + 2OH^- \quad (13)$$

Analysing Ni-P-WS_2 composite coatings, CTAB gets adsorbed by WS_2 and its quaternary ammonium groups (-NH_4^+) has a positive charge. Both convective-diffusion and electrophoretic migration help in WS_2 transportation. The incorporation of WS_2 particles into the Ni-P electrodeposit caused noticeable transformation of surface morphology from a planar smooth surface to a nodular rough surface and finally a hierarchical rough surface. Surface morphological changes are mainly due to the variation of current distribution on the surface of electrodes because of the conductive WS_2 particles.[121] Adhesion of WS_2 particles to the cathode surface is associated with a change in the electric field behaviour. The Ni-P deposits preferentially initiate growing above WS_2 particles as they have a higher current density which causes more active nickel ion reduction.[122] Thus 'broccoli-like' structures are formed (Fig. 9).

In the present review our conclusion is also in agreement with the above mentioned studies that it is only possible to use an analogy to Guglielmi's model for composite electrodeposition to explain co-deposition mechanism in 2D materials. In the first step of the model, metal ions (Ni^{2+}) will be generated along with that there is a chance for adsorption of metal ions ((Ni^{2+}) on to the surface of 2D particles. It is followed by the migration of 2D particles with ionic cloud to the cathode surface through diffusion layer. Here, these particles will be adsorbed, losing hydrated shell by electron transfer reaction. Finally, the metal

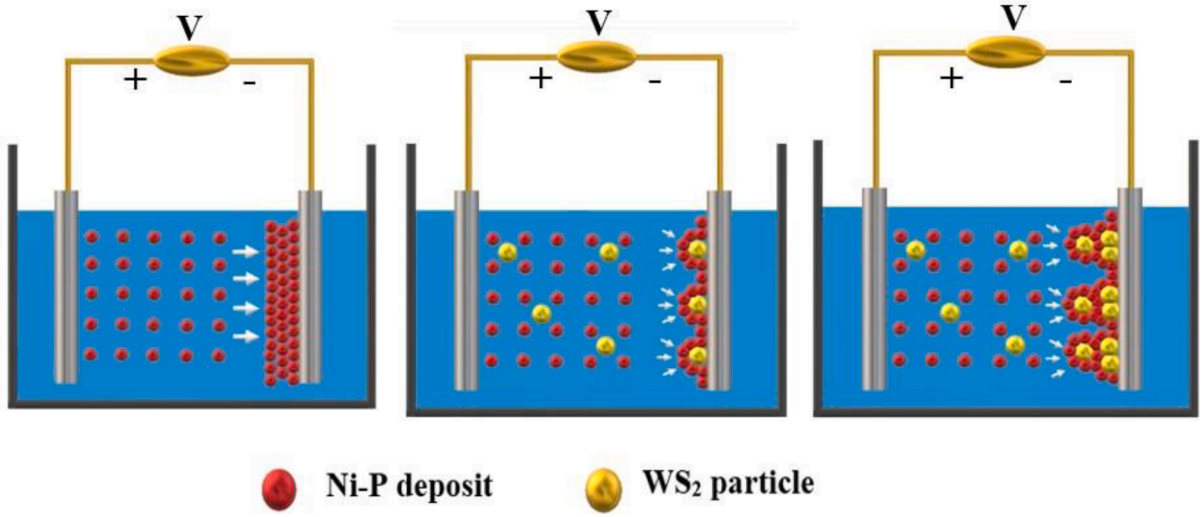

Fig. 9. Schematic illustration of the growth process of Ni-P-WS_2 composite coating. Concept adapted and redrawn from ref. [120].

(Ni) atoms were incorporated into crystal lattice surrounding 2D materials. Thus, the latter got reinforced in metal (Ni) matrix. A higher concentration of 2D particles in plating bath was found to enhance the adsorption rate, leading to a higher volume percentage of the co-deposited 2D particles.

The interaction between particles and electrolyte has a significant effect on codeposition. These interactions are often characterised by zeta-potential values and correlated to particles content, same is applicable to 2D materials. In general, dispersed materials with zeta-potential values near or < -30 mV are stable. The zeta-potential values of the h-BN, MoS_2, WS_2, $MoSe_2$ and high-temperature-sonicated graphene dispersion samples are all ~ -30 mV.

Conductivity of 2D materials has an important role in co-deposition. The presence of a porous layer in composite electrodeposition has also been observed where a conductive particle is involved. All these 2D materials have atomic-level thicknesses, but have different physical properties. For example, graphene is a conductor, h-BN an insulator and MoS_2 a semiconductor. For instance, there are reports that the addition of semi-conductive MoS_2 particles disturb the current distribution, making the electrolytic current concentrating in the vicinity of MoS_2 particles.[123] Therefore, there is a bigger electric field formed around MoS_2 to speed up its migration to the cathode, as well as the migration of Ni^{2+} ions towards MoS_2 particles.

Solvation level of 2D materials within electrolyte is another important aspect to be studied in co-deposition. There has been reports investigating the solvation states of these materials, performing molecular dynamics (MD) simulations and *ab-initio* calculations for pristine graphene, functionalized graphene (hydroxyl (−OH) and carboxyl (−COOH) groups), h-BN and MoS_2.[124] Pristine graphene has a weakly positive charge due to dangling carbon atoms, and carboxyl-functionalized graphene has a stronger positive charge due to the electron-withdrawing carboxyl groups, whereas the electron-donating hydroxyl groups render graphene flakes negatively charged. On the other hand, h-BN has an alternating charge distribution and exhibits strong polarity across the boron and nitrogen termination edges and MoS_2 shows the negative charge on the surface by S atoms and counter charges inside by Mo atoms, which exhibit moderate polarity. The numerical calculation results of interaction between the 2D materials and water show that the solvation level is highest for carboxyl-functionalized graphene, the intermediate for hydroxyl-functionalized graphene, h-BN and MoS_2, and the lowest for pristine graphene.

When multiple deposition parameters are altered, the whole electrodeposition process becomes virtually new. Future models to describe the process of codeposition would require attention to interactive variables such as the particle characteristics (type, dimensions and concentration), the operating parameters (temperature, current density, pH and hydrodynamics) and the electrolyte composition (concentrations, presence of surfactants and additives).

Characterisation techniques

The relationship between properties, preparative methods and attributes of nano-composites must be fully developed as it determines the prospective uses of these materials. Overall analysis of electrodeposition conditions and surface properties of the deposits can be evaluated by closely studying compositional, structural and morphological changes which is made possible by advanced characterisation.[125] Reinforcement state, geometry, volume content, orientation and interface bonding of reinforced nanomaterials are salient factors influencing the performance of composite coatings.[126].

A variety of techniques are used to study the morphological, electrochemical, physical and mechanical properties of the coating including scanning electron microscopy (SEM), energy dispersive X-ray spectroscopic (EDX) technique, micro-hardness measurement, X-ray diffraction (XRD), transmission electron microscopy (TEM), X-ray photoelectron spectroscopy (XPS), atomic force microscopy (AFM), electro-gravimetric analysis, wear resistance measurement, electrochemical impedance spectroscopy (EIS) and electrochemical polarization. Thermal analysis, including thermal gravimetric analysis (TGA), differential calorimetry scanning (DSC), dynamic mechanical thermal analysis (DMTA), thermal mechanical analysis (TMA) etc. are set of convenient tools for assessing the stability of nano-composite material derived coatings and various doping, curing and annealing phenomena.

The preliminary tool for the study of the microstructure of the nanocomposite coating samples is optical microscopy. Upmost care has to be taken while specimen preparation for the optimum efficiency in the imaging. It starts from the sectioning of the sample followed by mounting, grinding, polishing and finally etching. For thin macroscopic composite coating samples in transparent matrixes, optical microscopy is a viable option, but it is not preferred for microscopic nano-size coating samples. For qualitative surface morphology studies, scanning electron microscopy (SEM) can be used. Energy dispersive X-ray spectroscopic (EDX) technique is utilised for the resolving the chemical composition of a material. Essentially we can have a detailed morphology and elemental composition analysis of both surface and cross-section by SEM/EDX. Electron backscattered diffraction (EBSD) can provide a detailed and accurate representation of the sample microstructure.[127].

High resolution image viewing is possible by Transmission electron microscopy (TEM). For TEM studies, mechanical removal of the films/coatings from the substrate are usually done. The XRD characterization technique provides the crystal structure, texture and crystallite size of the metallic matrix. The particle occurrences and preferred orientation or texture can also be observed. The identification of the elemental composition can be carried out using the X-ray photo-electronic spectroscopy which follows the principles of photoelectric effect. It is a quantitative analysis which is surface sensitive. Apart from elemental composition, XPS gives an idea regarding the empirical formula, electronic as well as chemical state of the given sample. In theory, the binding energies (BE) and chemical shifts in XPS spectra can be used for nickel oxidation state analysis in the surface region. AFM does the surface morphology characterization at the nanometric scale and surface roughness values can be calculated due to high resolution imaging. Additionally the qualitative characterizations are be done by numerous technologies such as Inductively Coupled Plasma Spectroscopy (ICP), Glow Discharge Spectrometry (GDs) etc. for depth profile analysis. The tribological properties of composite coatings is an important aspect. There are many different tribometers like pin (or ball) on disc, roller on plate and block on ring that measure coefficient of friction (COF) and wear rate. The frictional force and normal load accounts for the COF. Microhardness and micro-indentation test methods are available for measuring the mechanical characteristics of plated coatings. The scratch test is a quick and simple engineering test which measures the adhesion between substrate and coating.

Electrochemical Impedance Spectroscopy (EIS) can be a useful for measuring the general barrier properties of coatings. More specifically water and ion permeability of coatings can be determined as a function of time. This information is particularly valuable in quality control, comparison of performance of different coatings and follow up of coatings in situ. The main benefit of the technique is the short time needed for a measurement: within 24 h a fingerprint of the coating is taken (duration is dependent on coating type and thickness). Since EIS does not rely on visual aspects, differences in coating performance can already be established prior to visual signs of degradation. Corrosion processes taking place underneath the coating can also be measured by means of EIS. It can be combined with an accelerated degradation test in the lab to better understand the degradation of the coating and to reduce test times.

Modelling techniques and simulation tools

A very few modelling studies in nickel composite particle systems are

currently available which include Ni-YSZ ((yttria stabilized zirconia) [128], Ni-B composites[129]etc. The design of experiment (DOE) approach is an important aspect in modelling and analysing the influence of deposition parameters and results in composite electrodeposition.[130] DOE allows minimal experimental effort.[131] Experimental observations and results are assessed on the basis of statistical techniques and by estimation of the influence of plating parameters on experimental outcomes.[132,133] Many DOE methods (Taguchi's orthogonal array[134], central composite design, response surface approach) etc. have been introduced as part of investigation on composite electrodeposition. Further, simulation tools can result in better plating results.[135,136].

The first-principles computational studies based on Density Functional Theory (DFT) were utilized to provide a new insight toward quantifying the interaction-strength between various components in the systems like Ni–graphene. The calculations based on DFT method illustrate the stacking geometry, which could be attributed to the binding/adhesion/cohesion/interaction between graphene and the Ni metal. Based on these calculations it has been reported that an approximate planar graphene sheet is constructed on Ni (111) surface. The surface of Ni (111) substrate has surface lattice constant (249 nm), whereas graphene has a surface lattice constant of (246 nm). Therefore, a layer of graphene sheet will hold two C atoms per unit cell and can be perfectly fitted on Ni (111) substrate. The nature and strength of Ni–-graphene interactions have been examined computationally by Lahiri et al.[137] and have presented a comprehensive study of graphene growth on Ni (111) substrate and the Ni–graphene interface stability using Local Density Approximation (LDA) functional of DFT approach for the geometry of Ni–graphene interface. Studies in the area of modelling of Ni systems involving 2D materials like h-BN, TMDs still needs more validation.

Mechanical properties, grain boundary segregation, chemical ordering, thermal stability, and dislocation interactions in nanocrystalline Ni-composite and Ni-alloy systems have been thoroughly investigated using computer simulation. In these studies, molecular dynamic simulation and Monte Carlo simulation have been utilized for better understating the aforementioned characteristics.[138] Nano particle co-deposition mechanism and associated enhancement in the mechanical properties of the coatings is an area that needs detailed investigation. Thus it is really important to devise a method of analysis for discovering the impact of process parameters by valid experimental design approaches to assess the quality of final deposits in the case of two dimensional material based nickel nanocomposite coatings.[139].

Plating variables and their influence

Effect of current density and distribution

In general electrodeposition, current density has a prominent influence in determining the rate of deposition.[140] It also controls the thickness of the composite coatings. Quality of the final deposit is determined by current density and distribution.[141] In case of composite deposition current density will influence the composition and morphology of secondary phase reinforced particles in the coatings. Higher the electrodeposition overvoltage in composite systems the more will be grain nucleation and subsequent grain refinement, resulting in sub-micron and perhaps even nano-crystalline coatings.[142] At higher current density the nucleation is enhanced and therefore smaller grain sizes are observed in composite electrodeposition.[111].

In the case of Ni-graphene coating as there is a rise in current density, the thickness of the coatings increases reaching an optimum value.[143] The morphology of Ni-graphene coating is influenced by varied current densities produced by pulse electrodeposition which was studied by Yu et al.[144] With an increment in the current density up to 6 Adm^{-2} the nucleation rate of Ni and the content of graphene increases. This will inhibit nucleus growth and optimization of grain structure.[145] Variation and subsequent effect of current density was utilised in modifying the hierarchical structure formation in Ni/r-GO system as in Fig. 10.[146] As cathodic polarization enhancement took place it was observed that the nickel crystal growth was arrested. [147,148].

The relationship between current density and quality of the coating was studied in Ni-BN composite coating.[149] On increasing current density from 0.5 to 2.5 Adm^{-2} the quantity of Fe decreased from 25 % to 7 % in both Ni-Fe alloy and Ni-Fe/BN composite. Degraded dull deposits with burning effect was observed at higher current densities. Paydar et al.[150] studied the relationship between hardness and current density in Ni-BN-B_4C composite coating. Low current density of 20 $mAcm^{-2}$ resulted in a low rate of nickel dissolution at the anode and subsequent transportation. When the current density was increased to 50 $mAcm^{-2}$, hardness has been enhanced due to increased cathode movement of adsorbed particles.

Effect of deposition current density on wear resistance was also analysed in Ni-BN-B_4C system.[151] Mass loss due to wear behaviour of the composite coating decreases with increasing current density until 50 $mAcm^{-2}$. Rise in the deposition current density leads to anodic depolarisation and subsequently enhanced co-deposition.[152] Therefore the quantity of absorbed BN and B_4C also increases. Sangeetha et al.[153] observed the impact of current density variations in Ni–W/BN system. At first the h-BN content in the coatings initially increased with increasing current density up to 1.2 Adm^{-2}. It is because above this limit of current density, reaction will be diffusion controlled rather than kinetic.[149].

Analysis of impact of different current densities 3, 5 and 7 Adm^{-2} on the coefficient of and content of MoS_2 in the coatings was done by Shourije et al.[154] With the increase of current density there will be an enhancement of inter-particle electrostatic attraction and more MoS_2 particles gets deposited in the metallic matrix.[76,155] Dependence of current density on the chemical composition of coatings was studied in Ni-MoS_2.[156] In this case intensity of the electric field varies directly in proportion with current density. As a consequence, the binding force between the adsorbed nickel ions and MoS_2 powder got ruptured. Particle incorporation increases with the increase of current density. With increase of current density protruding cluster formation takes place in the study of Ni/WS_2 composite coating. And it was observed that a lower current density is associated with low deposition rate and a non-rigid coating is formed at higher current density.[157].

Effect of agitation

Stirring increases the transfer/diffusion rate of metal ions from bulk solution to the electrode surface.[158] Gradually the thickness of the diffusion layer gets reduced. It decreases gas bubbles that may create pits. Therefore it is very common to use some kind of bath agitation/stirring to obtain a stable and uniform suspension.

In composite deposition, maintenance of particles within the bath and their transportation to the electrode surface is ensured by electrolyte mixing. It also determines the flow of solution by aiding in migration/adsorption process of the charged particles.[159] Normally as the agitation increases amount of particle deposition will also increase. Excessive agitation results in decrease of particle co-deposition because the particles are moved away before forming a stable layer on the cathode surface.[160] On the basis of bath agitation there are three different flow regimes: laminar, transition and turbulent.[161] In the laminar regime rotation speed doesn't have any role. For the transition regime a decrease of particle content followed by an increase is noted on increasing agitation while a continuous decrease takes place in turbulent regime. While all other conditions remain constant, the degree of agitation should vary in proportion with the current density. To eliminate coarse-grain defects caused due to the presence of impurities in the bath, agitation is followed by filtration in this process.

A non-uniform dispersion of conductive particles (MoS_2) in bath could further increase the porosity of the coating, by introducing

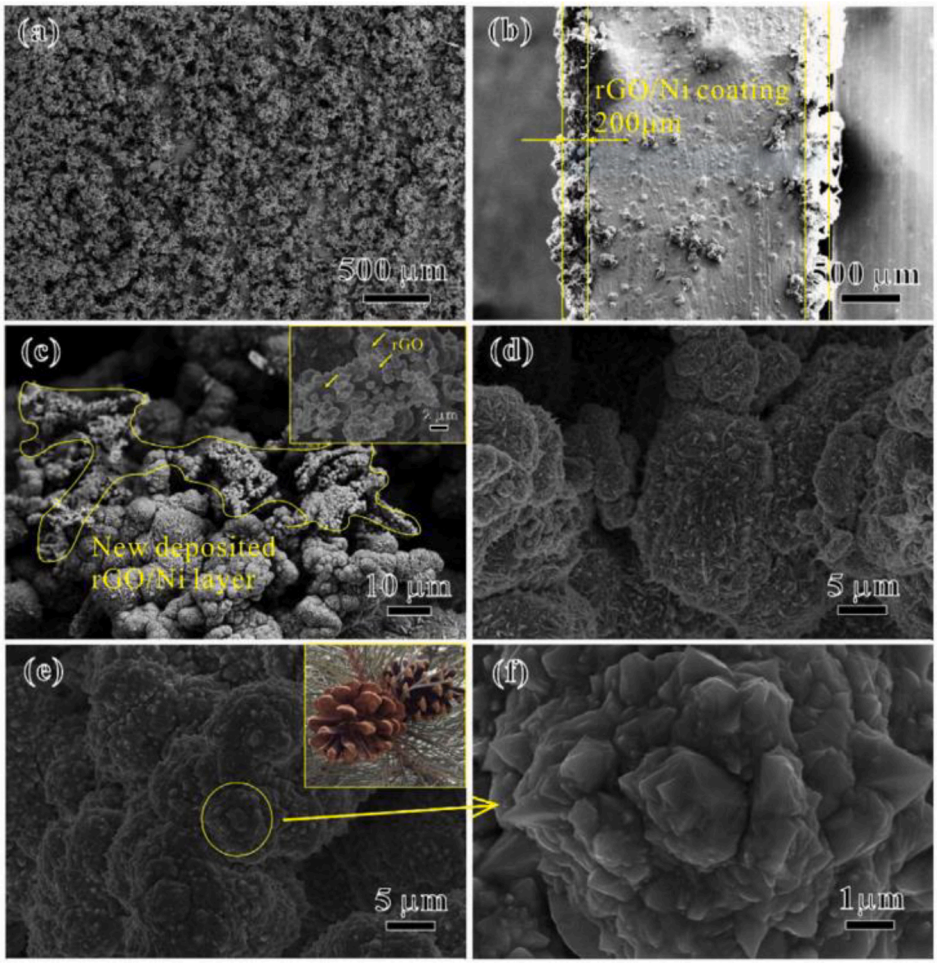

Fig. 10. SEM images of coating surfaces of (a) r-GO/Ni surface (at low-magnification) and (b) its cross-sectional view; (c) r-GO/Ni composite coating deposited at 20 mA/cm^2 current density for 5 min (d) r-GO/Ni composite coating deposited at 20 mA/cm^2 current density for 10 min (e) pinecone-like hierarchical micro/nano morphology r-GO/Ni surface and (f) close observation of r-GO/Ni surface. Reprinted with permission from [146]. © Elsevier Limited 2020.

porosities from within large particle agglomerates as well as accelerating the growth of protrusions. It is also seen that ultrasonic assisted agitation is beneficial not only in reducing porosity, but also in distributing nano particles uniformly and improving the codeposition rate, resulting in the formation of protective and highly refined coatings. [162] Thus the agitation system can probably affect the efficiency of the plating.

Mamaghani et al.[158] studied the impact of stirring rate that generated microstructure evolution of nano-crystalline nickel coatings. SEM analysis leads to the conclusion that the coating had almost a homogeneous surface containing fine crystallites and some bubbles of 100 nm diameters. High rate of agitation caused these bubbles of hydrogen to stick on to the nano-crystalline pure nickel coating. In addition to that, the crystallite size is reduced with the increase in turbulence and resulted in a cluster of nickel atoms. This cluster became a barrier for the growth of large crystals. Improvement of crystalline microstructure occurs with rising turbulence.[163] In this case there was an inverse shift in the crystal orientation degree; a sudden decrease in (111) orientation in 500 rpm sample was observed.

Different coatings were produced from baths at various magnetic stirrer rotation speeds in Ni-BN-B_4C composite coatings by Paydar et al. [150] The impact on hardness was analysed. 688 HV was the maximum hardness achieved when the speed was 700 rpm. Changes noticed in the hardness may be analysed with regard to the amount of incorporated particles which in turn depends on stirring speed. Low agitation cannot generate enough hydrodynamic force that is needed for the particles to reach cathode. For a particular bath when the particle concentration remains constant there will be laminar flow at low rate of stirring. The flow condition between 600 and 700 rpm is a transient laminar turbulent flow so that a steady state is reached and a maximum particle incorporation takes place.[164].

Shourije et al.[154] explored the role of stirring speed on the MoS_2 content in Ni- MoS_2 coatings. Increased hydrodynamics because of high agitation speed helped in easy movement of MoS_2 towards cathode. Since the flow was turbulent on changing the agitation speed from 150 to 200 rpm percentage amount of MoS_2 particles decreased from 20.1 to 6.8 %. Above 200 rpm MoS_2 particle collision happens as a result they will not hit the cathode surface properly. This phenomenon has been studied exclusively and the results are in agreement with this study. [165–168].

A change in the topography of the composite coatings is induced by the application of ultrasonic agitation. Due to ultrasonic agitation it was reported that there is an improvement in the compactness of the nickel film along with reduction in the grain size of the nickel.[169] Ultrasound agitation has a great influence in deciding the amount of particles that gets incorporated in the metal deposit. Thus there was remarkable difference in the amount of IF- WS_2 particles i.e. increased from 4.5 wt% in coatings produced with only mechanical agitation to about 7 wt% in coatings prepared by means of ultrasound agitation. Poor dispersion decreases the effective aspect ratio of 2D nanomaterials, leading to the deterioration in mechanical properties.

Effect of surfactant

The use of surfactants such as sodiumdodecyl sulphate (SDS), cetyltrimethylammonium bromide (CTAB) and saccharine (Fig. 11) can enhance the properties and durability of electrodeposited coatings. The key benefit of surfactant addition is their dispersing effect of particles. [170] As a result, the particle characteristics will be consistent on the surface. Surfactant gets absorbed to the particles and helps in the particle distribution. [92] The surface characteristics of the electrodeposited nanocrystalline nickel are influenced by the surfactants in the Watts bath. By controlling pulse parameters the grain refinement in a Ni watts bath without saccharin will be about 100 nm whereas in the presence of saccharine it can be around 30 nm. [145] The variations in properties are caused by changes in the nucleation and plating over potentials (E_n & E_p). [171].

Surfactants are classified into two types based on their charges: anionic surfactants and cationic surfactants. Secondary particle inclusion can be improved using cationic surfactants. [143] This is due to the interaction between adsorbed ions and surfactant molecules which results in the surface alterations. This adsorption aids the electrophoretic migration or cathodic movement of particles but it is pronounced if there are 2D layered nanoparticles. Because the cationic surfactant adsorbs a total positive charge on the layered material surface, its cathodic affinity improves and enhances the stability of particles in the form of suspension by preventing conglomeration. On the basis of particle type and plating solution, anionic surfactants can have a favourable or adverse effect on particle co-deposition efficiency. If there is the presence of unabsorbed free surfactants, they may deteriorate the deposit resulting in internal stress and brittleness. [172] Because the quantity of absorbed surfactant is usually quite low, their negative impacts can be negligible.

A homogeneous distribution of graphene platelets in the Ni matrix is observed when sodium dodecyl sulphate (SDS) is in electrolytic bath. [173] Lowering of surface roughness and micro-hardness reduction are important functions of SDS. The values of micro hardness are lowered when SDS is added. The decreased coating hardness of the coating and lower amount of co-deposited graphene in the Ni matrix can be because of proposed explanations: Lower interface bonding between Ni matrix and the graphene nanoparticles in the presence of SDS and the other reason is that there was an increased surface energy between the substrate and the graphene nanoparticles resulting in lesser wettability of graphene. It was observed by Yasin et al. [174] that higher concentration of SDS resulted in maximum carbon content and superior mechanical properties of Ni-graphene composite coatings. Morphology changed in to coarse because of bulge formation as in Fig. 12 on the coating surface and there is a reduction in average grain sizes on adding SDS. The suggested explanation of the influence of surfactant SDS is that initially nickel ions gets deposited on the cathode followed by graphene deposition into the freshly formed nickel matrix. Current density is more felt closer to the graphene sheets compared to other places which accounts for the bulge formation. A higher amount of SDS allows the dispersion of graphene sheets to greater extent so that more graphene sheets gets deposited. This is because surfactant adsorption on graphene sheets generates electrostatic repulsion among graphene sheets.

Employment of surfactants is more beneficial for hydrophobic particles like MoS_2. [175] Once surfactants are added there will be a change in behaviour of particles from hydrophobic to hydrophilic since surfactant gets adsorbed on the hydrophobic parts of the particles. [176] In lower MoS_2 concentrations there is noticeable role for surfactant in the case of Ni-MoS_2 composite coating. [177] For all MoS_2 concentrations as the amount of surfactant increased, coefficient of friction (COF) got decreased.

In Ni-P-WS_2 composite coating the influence of cationic surfactant CTAB was analysed. [120] It is a long chain molecule having a hydrophilic head (positively charged) and a charge less hydrophobic tail. [178] The head chain aids in dispersion of particles without accumulation. The tail is capable of the suspending particles primarily by electrostatic adsorption. The modified particles gets strongly moved towards the cathode. Thus efficient co-deposition of Ni-P and WS_2 is made possible by electrophoresis. If there is an excessive amount of CTAB several nucleation sites are created which restrict WS_2 deposition. Improvement of hardness is typically because of grain size refinement by the addition of WS_2 and CTAB. The metal (Mo vs W) influences the dispersibility at low surfactant concentrations, while the chalcogen (S vs Se) plays a more significant role as the surfactant concentration is increased, alongside the surfactant charge. [179] Effect of surfactant in Ni-BN composite coatings is yet to be done.

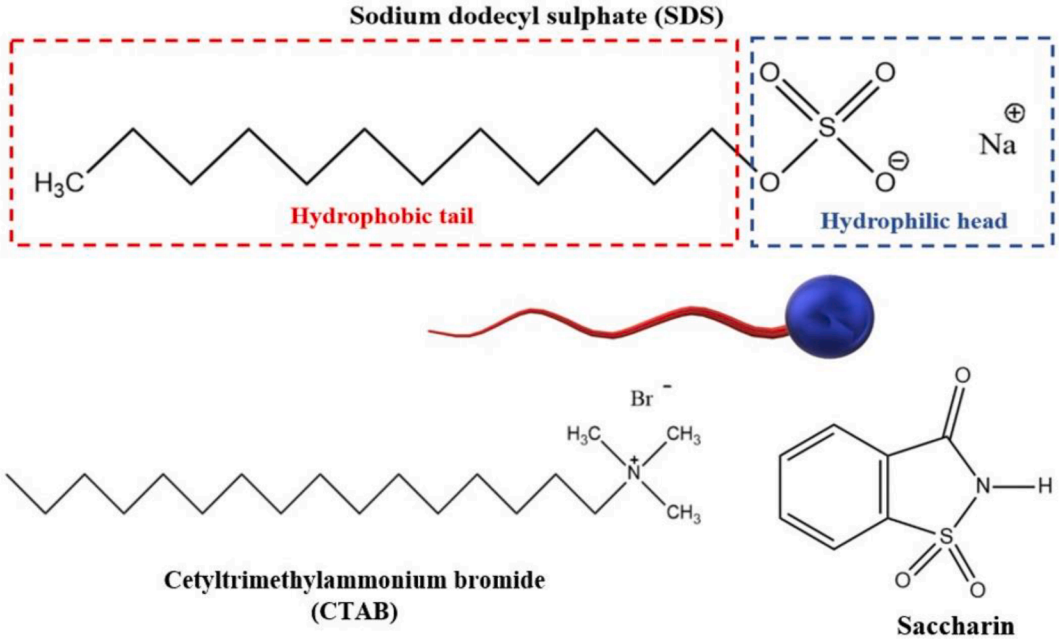

Fig. 11. Common Surfactants.

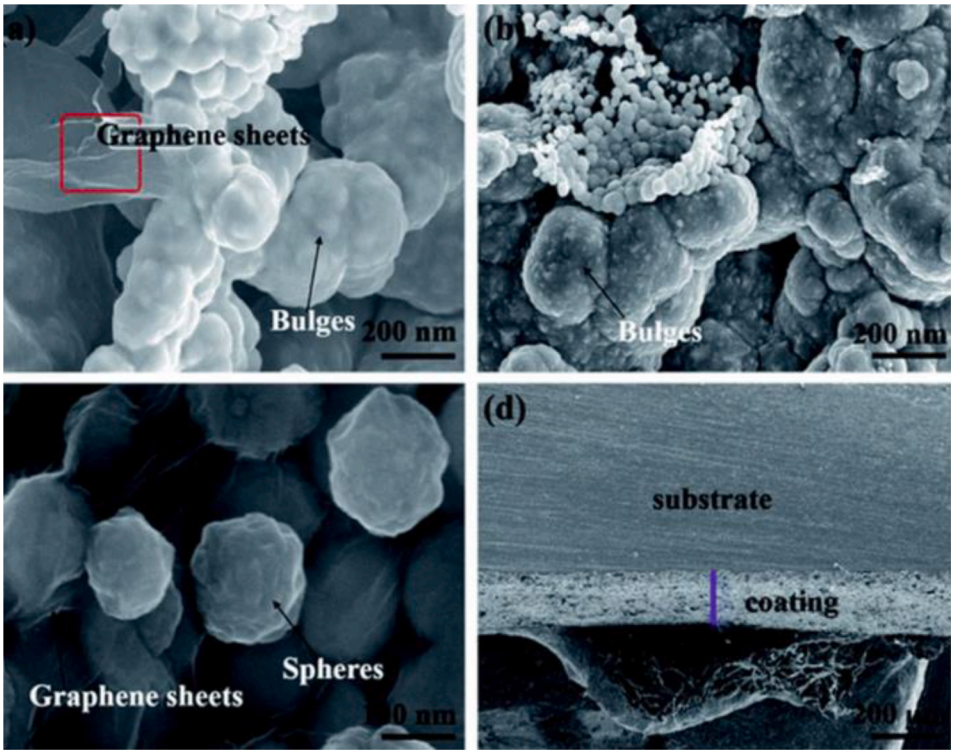

Fig. 12. SEM images: (a) marked area indicates graphene sheets, (b) bulge morphology, (c) spherical growth and (d) cross-sectional view of the nickel-graphene nanocomposite coatings. (a)-(d) Reprinted with permission from ref. [174]. © Royal Society of Chemistry 2018.

Effect of pH

pH is an important parameter that ensures quality control in electroplating. pH must be held within well-defined limits to guarantee optimum deposition rate. For instance, pH of a nickel Watts bath must be closely around 4.2–4.5 to maintain optimum current efficiency, brightness and levelling properties. The pH value depends upon the composition of the electrolytic bath. In a complex bath, pH can control equilibrium between different steps. If the anode is insoluble, oxygen evolution will occur at the anode;

$$2H_2O \rightarrow O_2 + 4H^+ + e^- \quad (14)$$

Whereas, hydrogen evolution at the cathode is followed by the production of hydroxide ion;

$$2H_2O + 2e^- \rightarrow 2OH^- + H_2 \quad (15)$$

The pH of a dispersion solution can change during sonication because of sono-chemical reactions, and this change might affect solubility. In the case of graphene, h-BN, and $MoSe_2$, the pH varies little; hence, the pH does not appear to influence their solubility. However, the MoS_2 and WS_2 solutions became acidic after sonication.

Influence of pH on the amount of secondary particle incorporation was studied in Ni-BN composite system. Increasing the pH from 3 to 5 resulted in minimal incorporation of BN (22 vol%) in the composite. [180] The decreasing trend with increasing pH may be the result of a fall in the effectiveness of nickel deposition and a subsequent rise in the viscosity of the solution.[181] For the study of the effect of pH on BN and B_4C particle deposition, the relation between pH and zeta potential of BN and B_4C particles were explored by Paydar et al.[150] The zeta potential of the BN and B_4C mixture in the electrolytic bath solution progressively rises in line with pH up to a maximum of 3.5 before approaching 0 mV (zero point of charge). The main finding was that the positive zeta potential provides an additional bonding force between inert particles and cathode, supplementing the incorporation of inherent BN and B_4C particles to the Ni matrix.

Wear rate was decreased by 84 % when there was an increment in pH from 2 to 4 in Ni-MoS_2 system.[182] It was found that the zeta potential of the particles increased with rise in pH in the case of Ni-SiC composite electroplating.[183] Based on the same analogy agglomeration of MoS_2 particles in the electrolyte is diminished by higher zeta potential hence pH thus leading to decrease in wear rate in Ni-MoS_2composite coating.

Effect of temperature

Generally in electrodeposition, increasing the bath temperature increases the solubility of metal ions and therefore the transport number which subsequently contributes to an increase in the conductivity of the solution. It also reduces viscosity of the solution rebuilding the double layer comparatively quicker. On the other hand the stress in the composite coatings/deposits is greatly affected by the current density no matter the temperature.[184] Polarization effect is an additional benefit of high temperature. So it is important to devise an optimal plating temperature to meet energy utilization and to obtain good quality coating.[185].

The temperature of deposition plays a key role in determining the surface morphologies of Ni-graphene composite coatings. As the temperature raised from 15 to 45 °C a more firm, rough and spherical morphology was observed.[186] Along with surface roughness the carbon content also showed a gradual rise up to 45 °C. Beyond that the carbon content reduced with further increase in temperature. At 60 °C some voids and cracks were found on the surface of the deposited coatings. The thickness of these coatings was in direct proportion with the deposition temperature. The SEM micrographs show surface morphologies of Ni-graphene coatings at different temperatures. (Fig. 13).

Chen et al.[187] examined the influence of plating temperature in Ni-graphene composite coating developed by using di-pulse composite

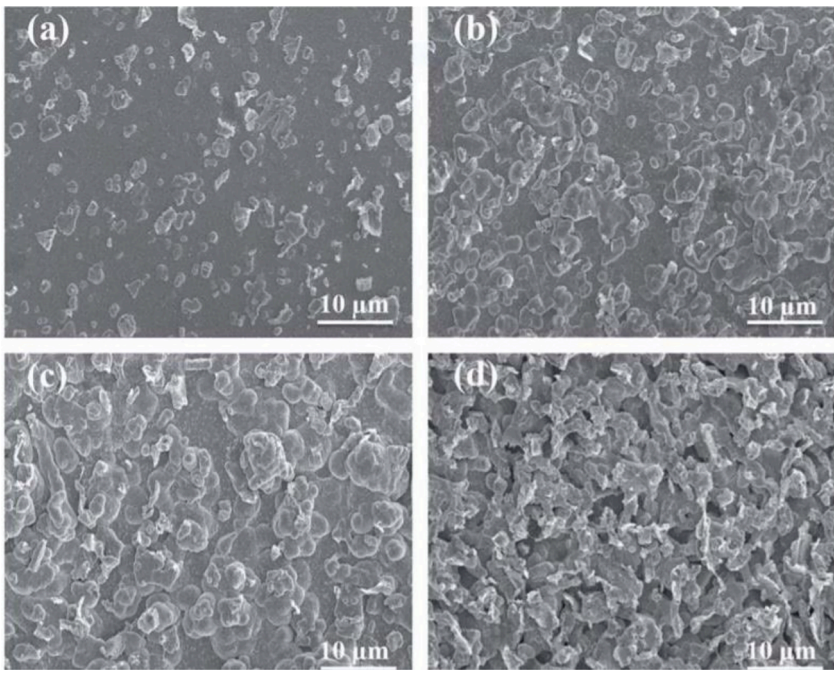

Fig. 13. SEM images: (a–d) for the surface morphologies of Ni–graphene composite coatings prepared at deposition temperatures (15, 30, 45 and 60 °C respectively). (a)-(d) Reproduced with permission from ref. [185] © Royal Society of Chemistry 2017.

electrodeposition. They concluded that the lower hardness is due to easy dislocation movement with rise in plating temperature. On varying the temperature, the friction coefficient first decreased followed by an increase. The lowest friction coefficient (about 0.68) was obtained at 60 °C.

Micro-hardness dependence on temperature of deposition in Ni-BN system was investigated by Paydar et al.[150] Higher bath temperatures result in brownian movement of the particles. This phenomenon will cause more particle collisions followed by entrapment at the cathode and thus micro-hardness increases. Temperature can also influence the zeta potential of the particles causing more positive charge to be generated on them and attracting particles to be absorbed on the surface. The influence of bath temperature on the amount of secondary particle incorporation at 40 $mAcm^{-2}$ current density was analysed in Ni–BN–B_4C composite coating.[151] With the increase in plating temperature, the content of ceramic particles in the coating was increased. Migration rate of BN and B_4C particles is accelerated with the rise in temperature.

The nature of particle controls the influence of the temperature on the quantity of deposited particles. A slight increase in the particle (MoS_2) content in coating was noted with the temperature rise from 30 to 50 °C.[132].

Effect of bath concentration and incorporated particle

In general, bath concentration has a major involvement in controlling the plating efficiency in the method of electrodeposition. The increase in concentration of the bath would increase the concentration of metal ions in the solution under normal plating conditions and the deposition rate of the plating system would then increase.[188] However the type of particles is also a significant parameter. Both conductive and non-conductive particles possess benefits over one another. Conducting particles (molybdenum disulphide, chromium carbide, zirconium diboride, graphite) usually form rough deposits and are transported towards the cathode to be the depositing points of dendritic growth.[189] Alternatively non-conductive particles forms smoother less porous deposits. Smaller particles can be agitated easily. Up to a particular point the rate and amount of particle incorporation is in proportion with the concentration of particles. In some cases the corrosion behaviour of the electrodeposited coatings depends upon the particle content and size as well as the homogeneity of the microstructure.[190].

An increase in the quantity of reinforced particles (graphene) has an effect on the reduction of crystallite size in nickel matrix and the compressive stress of the deposited coatings was a major finding by Szeptycka et al.[191] The corrosion rate lowered as the graphene content increased. Superior corrosion resistance in a 0.5 *M* NaCl solution was obtained in the case of coating containing 1 g dm^{-3} graphene in the bath. The percentage reduction of the corrosion rate in comparison with pure nickel coating was 85.84 %. A reduction of metallic surface prone to the corrosive environment can justify the premium corrosion resistance. Investigation by Jyotheender et al.[192] on electrochemical behaviour of Ni-graphene oxide composite coatings as a function of the quantity of GO had important results. An optimum concentration of GO is essential. Existence of such "optimum" has been illustrated earlier by Gupta et al. [193,194] for Sn-GO and Sn-Cu-GO composite coatings. Deposition mechanism in electrolytes with low and high concentrations of GO is depicted in (Fig. 14).

Amount of graphene in the bath is inversely proportional to the crystallite size of Ni in Ni-graphene composite coatings.[195] Incorporation of graphene is related to the fragmentation of the structure of coatings this in turn affects its material properties. Ni-graphene composite coating exhibited higher microhardness in comparison with pure nickel coatings. Improvement in the hardness of Ni-graphene coatings was explained by the fragmentation of the matrix material.[191] Chen et al.[187] correlated the quantity of graphene and the frictional properties of the Ni-graphene composite system. If the amount of graphene is above 0.3 g/L, graphene forms a lubrication film which reduces the coefficient of friction. When the amount of graphene reaches 0.4 g/L, the wear rate get reduced due to the compact structure and the high hardness of coatings. Meng et al.[196] studied the impact of varied amounts of graphene particles added within Ni–Cr–graphene coatings. Once the graphene concentration is 8 g/L in the bath there is a shift in the morphology of coatings from dendrite-like structure to compact with less porosity. Crystallite size, shape and orientation of the Ni deposits are modified by the incorporation of graphene. The crystallite size and texture of the Ni deposits also get reduced [199] The tribological

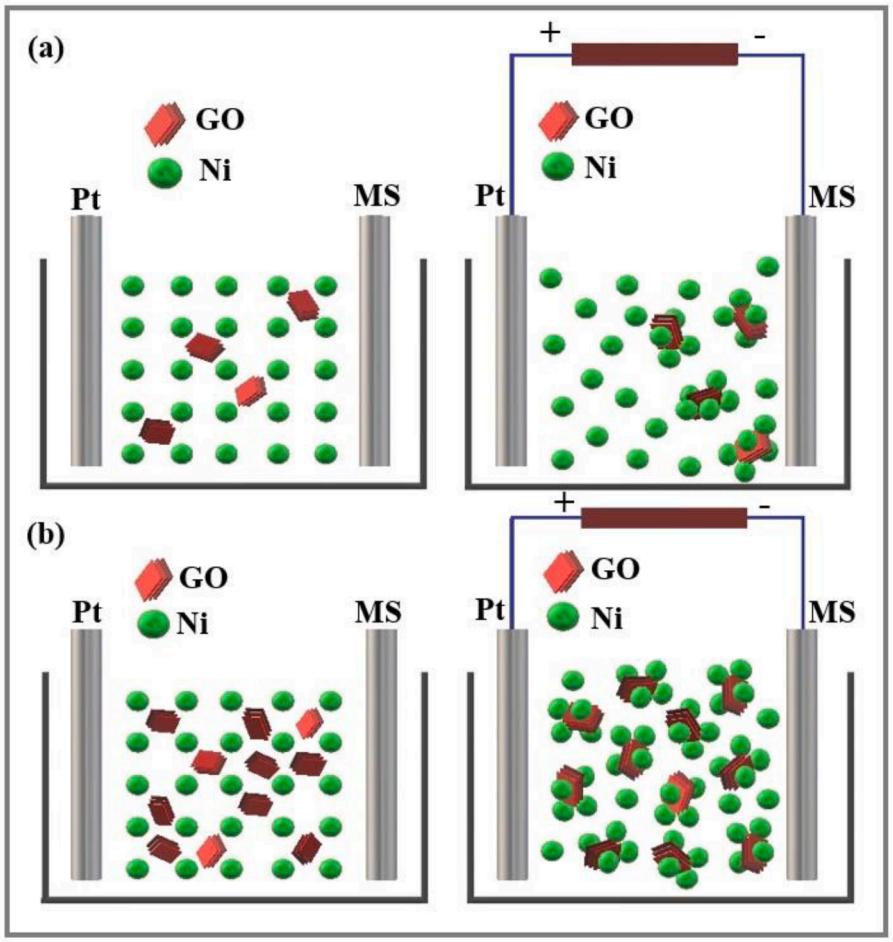

Fig. 14. Mechanism of GO deposition on cathode surface at (a) lower GO concentrations and (b) higher GO concentrations. (a)-(b) Concept adapted and redrawn from ref. [191].

properties of nickel matrix had shown drastic improvement with increasing graphene content in the electrolyte.[197].

As the amount of BN increased, the wear rate and coefficient of friction reduced in Ni-BN composite coatings.[77] It is due to the fact that the BN powder having a lamellar structure can reduce the friction between surfaces that are in constant contact. Considering the effectiveness of lubrication, the optimal addition was found to be BN concentration of 1.5 gL^{-1}. Sangeetha et al.[153] examined the effect of h-BN particle concentration on the morphology and corrosion properties of Ni-BN composite coating. Increasing h-BN particle concentration in the solution resulted in higher particle density (particles per litre) and contributed in the particle adsorption. The maximum amount of h-BN inclusion was 6 g/L. Above 6 g/L of h-BN agglomeration can occur and even the particles get settled down even being continuously stirred.

The collisions between particles and cathode controls the co-deposition of the particles. In Ni-MoS_2 system higher MoS_2 concentration reduced these collisions.[132] Zhang et al.[126] prepared Ni-Co-Al_2O_3-MoS_2 composite coatings on the surface of aluminium alloys by electrophoresis-electrodeposition with varied MoS_2 concentrations. Composite coating derived from the bath containing 1.0 g/LMoS_2 has a uniform, smooth and fine surface morphology. The conductive MoS_2 particles elevates the reactivity of nickel ions and cobalt ions creating more nucleation sites during pulse electrodeposition process.[198] With the increase of MoS_2 concentration to 1.5 and 2.0 g/L respectively, rough mushroom-like microstructure is formed due to the agglomeration of MoS_2. With the introduction of MoS_2 particles the coefficient of friction of composite coating is lower than that of pure Ni coatings indicating MoS_2 is a good lubricant. This is because of the lubricating film on the surface of the coating.

When the particle size is decreased in Ni-MoS_2 system the influence on wear rate will be more pronounced.[182] In the study of Ni-MoS_2 composite coating on copper substrate by Shourije et al.[154] it was found that on increasing the MoS_2 particle concentration, hardness of the coatings got reduced from 585 to 400HV owing to the high amount of MoS_2 in the matrix. Since MoS_2 particles are having soft nature (due to which it can form a thin film of lubrication) the hardness decreased.

The addition of second phase WSe_2 particles in various concentrations in Ni-WSe_2 composite coating has an impact on the structural and morphological development of the surface.[50] Beyond 0.5 g/L amount of WSe_2 resulted in a brittle coating. Wear study and corresponding XPS results indicated maximum oxidative wear when the amount of WSe_2 was lesser. Among all the coatings Ni-0.5 g/L WSe_2 composite coating exhibited exceptional properties with regard to hardness and wear resistance.

It was found that the coatings reinforced with $MoSe_2$ and MWCNT are having more compact structure in comparison with pure Ni coating.[49] The Ni-5 g/L$MoSe_2$-0.1 g/L MWCNT coating has super-hydrophobic nature having water contact angle (WCA) of 151.9°. It is assumed that this is because of maximum co-deposition of MWCNT generating a rough nodular structure. Values of charge-transfer resistance (R_{ctrs}) and superior inhibition efficiency (IE greater than 90 %) obtained for the 0.1 and 0.5 g/LMWCNT reinforced coatings indicates superior corrosion resistance. Overall inhibition efficiency of 94.5 % was shown by Ni-5 g/L$MoSe_2$-0.1 g/L MWCNT coating.

Effect of plating time

There are less studies on the dependence of deposition rate on plating time especially in composite coating. In general the thickness of the coating will typically increase in a way proportional with time and current density of deposition. Different nickel films with different cone sizes were generated by varying the time of deposition.[199] (Fig. 15).

Effect of the electroplating time on wettability was studied in Ni-layered graphene composite coating by Ding et al.[200] The samples have a high range of contact angle (CA) from 156 to 163° when the plating time increased from 1 to 10 min thus indicating super-hydrophobicity. The sliding angle (SA) of the coatings decreased from 40 to 4° as the time increased from 1 to 5 min. Surface changed from high to low adhesion when time reached 5 min. The sample surface maintains superhydrophobic behaviour with a CA of 157.8 ± 0.7° and a SA of 5.1 ± 0.9° after deposition for 5 min. Superhydrophobicity is maintained even after exposure in air at room temperature for 180 days. The schematic diagram of water droplet dribbled onto the surface of the sample after different deposition time is depicted in Fig. 16.

When the deposition time was 1 min, nano-structured nickel was only (Fig. 16a) formed so that the water penetration to the bottom part can occur because of single-level structure and small peak-to-base height decreasing the air pocket propensity resulting in high adhesion.[201] As the deposition time passes, the hierarchical micro-nanostructure with larger peak-to-base height was formed (Fig. 16b) and proximity of the micro-structure also increased (Fig. 16c). So the water droplets find difficult to be in contact with the bottom surface reducing the contact area between water droplets and surface. In addition, the proximity of micro-structure and nano-structure can alter the level of adhesion. In (Fig. 16b), even though the micro-structure have low density there is a possibility of impregnation of water by the nano structures. When the deposition time increased to 5 min, the water droplet can suspend on the surface as shown in (Fig. 16c). As a result SA of super-hydrophobic

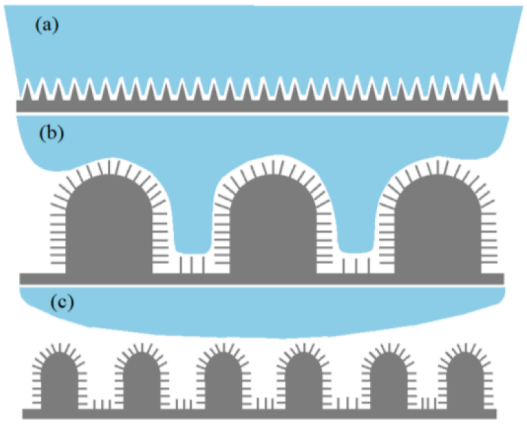

Fig.16. Schematic representation of water droplet dripped onto the sample surfaces after different deposition. (a) Nickel nano structures. (b) Nickel micro-nano structures (low density). (c) Nickel micro-nano structures (high density). Concept adapted and redrawn from ref. [199].

surface deposited in 3 min is greater than that of a surface deposited in 5 min. Moreover the CA increased to 160.4 ± 1.5° when the plating time was 5 min and when the time increased to 10 min the topography of the surface changed from model a (Fig. 16a) to model c (Fig. 16c) with deposition time. When deposition time was 10 min CA slightly decreased to 157.8 ± 1.4° while the SAs changed barely.

The variation of friction coefficient in accordance with electroplating time was studied in Ni-graphene composite coatings.[187] The friction coefficient does not show any constant trend with plating time. When the plating time was 6 h the coefficient of friction was at its lowest i.e. 0.7. It was also found that prolonging the deposition time may help in increasing the thickness of the composite coatings but minimal enhancement of wear resistance.

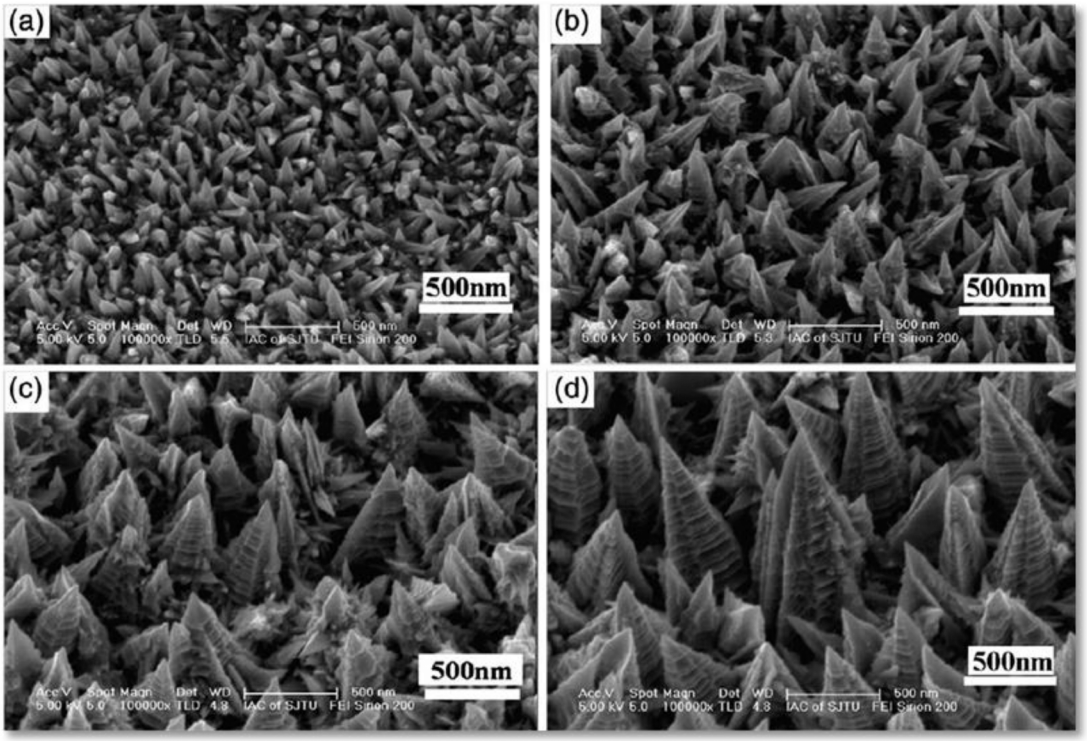

Fig. 15. SEM images of nickel surface fabricated at (a) 1 Adm^{-2} for 1 min; (b) 2 A/dm^{-2} for 2 min; (c) 2 A/dm^{-2} for 5 min; (d) 2 A/dm^{-2} for 10 min. (a)-(d) Reprinted with permission from ref. [198]. © Elsevier Limited 2013.

Mechanical properties

The enhancement in the mechanical and tribological properties of composite coatings by 2D nanomaterial reinforcement depends on numerous factors such as aspect ratio, volume fraction of nanomaterials, orientation of nanosheet and interface bonding between the filler and matrix. At a higher volume content, 2D nanomaterials are prone to self-aggregation, resulting in the deterioration of the mechanical properties. Interface bonding of 2D materials comprising hydrogen bonding, co-valent bonding, ionic interactions and electrostatic interactions is another important factor influencing the improvement in composite coatings.

Micro-hardness

The electrodeposited composites being economical and having superior physical properties are promising candidates in many industries. Mechanical properties namely hardness, toughness, adhesive strength, impact and tensile strength are prominent traits of these composites. Hardness is a material's quality to withstand localised deformation. Integrated effect of Hall-Petch mechanism[149] on account of the grain size refinement and Orowan mechanism[202] due to the uniform dispersion of nano-particles is the main reason of increase in hardness. Hardness of composite coatings is primarily controlled by the hardness of metal matrix and the proportion of reinforcement particles. The hardness and corrosion resistance of nanocrystalline-Ni coatings can be enhanced by refining the grain size.[203].

Study by Ameer et al.[143] reveals that graphene nano sheets (GNS) have potent impact in promoting the micro-hardness of metallic composite coatings. In fact involved surfactants, nonyltrimethyl ammonium bromide and dodecyl trimethyl ammonium bromide are the basis to absorb more GNS into the Ni matrix and this phenomenon led to an increase of nano hardness. It should be mentioned that GNS deposited into Ni matrix become obstacles that inhibit the Ni grain growth. It also restricts the plastic distortion of the metallic matrix. In another case of Ni-SiC-GO composite system[204] the reason behind the reduction of the hardness (7.7 GPa) of the coatings in comparison with the Ni-GO (9.4 GPa) and pure Ni coating (2.25 GPa)[205] and increase in stiffness may be due to the inclusion of the GO particles with hard SiC particles within the matrix.[63].

Pulse deposition of the composite coatings are associated with an increase in the micro-hardness values in comparison with pure nickel coatings as in the case of a study by Chronopoulou et al.[173] Microhardness values are also less compared to pure nickel coatings that are deposited by DC method which is due to irregular dispersion of graphene platelets in the Ni matrix resulting in excessive agglomeration. The Ni-exfoliated graphene composite coating developed by Xiang et al.[206] The Ni-exfoliated graphene had hardness 427 HV while pure Ni coating had only about 265 HV. The reason is Hall-Petch strengthening occurring because of the introduction of graphene in the Ni deposit. Properly dispersed graphene sheets possess distinctive structure and excellent properties that restrict the dislocation movements. Size reduction of the Ni crystallites is accompanied with increased hardness. Sometimes graphene sheets can inhibit nickel grain growth which further reduces nickel crystallite size.

The variation in micro-hardness of Ni-BN composite coating was exceptional being 3 to 4 times than that of pure nickel. Combined effect of dispersion hardening and grain refinement accounts for the greater hardness of the coating. The dispersed particles in the fine grained matrix can restrict the dislocation motions and plastic flow is ruled out.[207] The indicated resistance to deformation is actually hardness of Ni-BN composite coating. In nickel-alloy composite coatings, the hardness of nickel-rich alloy directly increases with increasing strain till a particular value followed by a decrease. Micro-hardness values of Ni–W/BN (h) (460–565 HV) coatings are comparatively more than that of Ni–W alloy coating.[153] Lubrication effect of BN is to be noted in this case. PC nanocomposite coating possess a higher microhardness compared to DC deposits. During PC deposition the superlative pulse frequency results in a higher over potential. This will supply further energy to inert particles like BN and an improvement in microhardness due to the dispersion strengthening effect of BN nanoparticles which restricts the dislocation movement.

Mixed nitride-carbide boron particles are used as reinforcements in Ni matrix by Paydar et al.[150] resulting in hard composite coating of Ni-BN-B_4C. Hardness improvement with rise in current density up to 50 $mAcm^{-2}$ indicating the accelerated cathodic movement of adsorbed particles which is in accordance with the Guglielmi model. Higher bath temperatures results in brownian movement of the particles. This leads to more particle entrapment in the deposit and thus hardness will increase. Agitation avoids agglomeration and improves the number of budding nuclei depleting the microstructure and as a result the microhardness varies.

Morphology of the coating is related to microhardness in Ni-MoS_2 system. Microhardness decreased gradually in Ni-MoS_2 system from 650 to 33 HV as the MoS_2 concentration changed from 0 to 2 g/L [167] Porous sponge-like structured coating will be obtained with increased MoS_2 concentration and has lower hardness. Shourije et al.[154] observed that that with the increase in the amount of MoS_2, the coating thickness and microhardness got lowered in a consistent way. It is because of the effect of the substrate (copper) on the coating microhardness. The correlative effects of reduction in coating thickness and soft behaviour of MoS_2 particles (these particles are softer than nano nickel) can also be thought of the reason for this. Zhang et al.[126] prepared Ni-Co-Al_2O_3 -MoS_2 composite coatings on the surface of LY12 aluminium alloys and explored the effect of MoS_2 concentration on microhardness of the coatings. On increasing the concentration of MoS_2 particles, the micro hardness of the composite coating appears to be lower because MoS_2 particles obstructs Al_2O_3 particle deposition diminishing the strengthening effect of hard particles in the composite coating.

WS_2 particles (and other solid lubricants, such as MoS_2 or graphite) are often considered as soft materials and their presence cannot explain by itself, the observed increase of hardness in the investigated Ni/IF-WS_2 composite coatings.[169] The observed increase in hardness in the films studied here is attributed to microstructural changes (primarily, crystallite size refinement and a change in preferred orientation) caused by the incorporation of WS_2 particles in the deposits. As the crystallite size decreases, the movement of dislocations is progressively hindered to a greater extent by the increased number of grain boundaries, resulting in dislocation piling up and an increase in stress concentration (Hall-Petch strengthening). The stacking fault probability can also contribute to the enhancement of hardness, since this type of planar defects impose barriers for dislocation propagation in a similar way as high-angle grain boundaries.[208] The changes observed in the crystallographic texture of the films can also partially account for the increase of hardness.

Maharana et al.[50] reported an increase in microhardness of coated substrate (485–665 HV) in comparison with uncoated substrate (209 HV). Co-deposited WSe_2 has a vital role in this improved hardness (Fig. 17) Maximum hardness was observed with 1 g/L WSe_2 was due to the combined effect of dispersion hardening and the occurrence of finer coating matrices by WSe_2 co-deposition. In addition to that RTC(111)/RTC(200) value can modify the compactness and atomic density of the resultant coating.[209].

Narayanasamy et al.[210] developed Ni-$MoSe_2$ coatings by pulse reverse plating technique that displayed excellent microhardness. It was noted that as the duty cycle was varied to higher values, the microhardness of Ni-$MoSe_2$ coating also improved because of the strengthening effect and grain refinement due to the filler.[211] Higher microhardness is reported with larger grain boundary area.[212] Adding $MoSe_2$ lowered the crystallite size, increased the grain boundaries and restricted the dislocation movement.[213] The maximum microhardness is seen at 60 % duty cycle for pure Ni and Ni-$MoSe_2$ are 415 ±

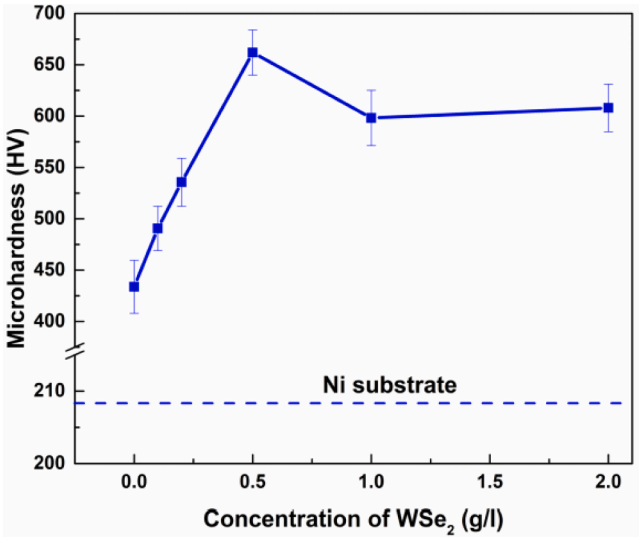

Fig. 17. Variation of microhardness of Ni-WSe_2 coatings with concentration of WSe_2. Reprinted with permission from ref. [50]. © Elsevier Limited 2018.

10 HV and 967 ± 10 HV respectively.

Corrosion properties

A substantial amount of material loss and subsequent component failure is associated with corrosion so that its prevention becomes really a matter of concern. Among all the available techniques, electrodeposited metallic nanocomposite coatings are being widely used.[214] Nickel is a popular option which is capable of acting as a host matrix which can accommodate 0D, 1D, 2D metallic, ceramic and polymeric fillers.[215,216] The nano particles that are capable of acting as a barrier can provide better corrosion resistance in comparison with pure nickel coating by causing a change at the molecular level and thus nanoparticles will attach to the surface both chemically and physically to provide complete protection against abrasion, corrosion and other damaging elements.[93,217] Enhanced corrosion resistance in comparison with pure nickel coatings has been attained by the addition of certain secondary particles in to the Ni matrix like SiC[218], CeO_2 [219,220], TiC[221], TiO_2[222], Al_2O_3[223]. Additionally layered materials like graphene, BN, WS_2 and $MoSe_2$ are added to the nickel matrix in order to improve its corrosion resistance. Layered 2D materials are interesting, as they can enhance barrier protection by impeding the diffusion of oxygen, water and corrosion-promoting ions, such as chloride anions because of their ultra-high chemical stability.[224] In theory, the impermeable nature of the 2D sheets can not only impede diffusion, but they can also be exploited to fill pores in the coatings, extending their protection period. Grain size refinement is an important method that can be used to improve the corrosion resistance of nanocrystalline nickel.[225] A summary of recent corrosion studies in various Ni-composite systems is given in Table 3.

Graphene has become an important constituent in Ni based nanocomposite coatings which improves the corrosion resistant properties. [226] Yasin et al.[227] incorporated graphene into Watts bath and studied the influence of current density on the corrosion resistance of the composite coating. The corrosion properties of nickel–graphene composite coatings are mostly decided by the nature of dispersion of graphene sheets within the nickel matrix. A uniform dispersion of graphene in the Ni matrix is necessary to avoid the unwanted adsorption of Cl anions forming defective sites resulting in corrosion when immersed in NaCl solution. Reinforcing the nickel matrix with graphene nano sheets helps in occupying the holes and cavities that may otherwise be the defects in composite coatings. Co-deposition of metal and graphene/GO using methods like electrodeposition results in a microstructure with graphene/GO spread randomly throughout the coating. In these circumstances, the microstructure near and around the graphene/GO-metal interfaces differs from the whole in terms of grain texture, orientation, size, boundary and chemical partitioning.[228] This is actually-one of the reasons behind the improved corrosion resistance of these systems. Better corrosion characteristics is interconnected to the reduced grain size and higher deposition current densities as in (Fig. 18).

Benigna et al.[191] studied the key role of graphene in providing excellent corrosion resistance compared to pure nickel coatings. It was found that the improvement in corrosion due to the uniformly added graphene particles initially decrease the corrosion rate because the

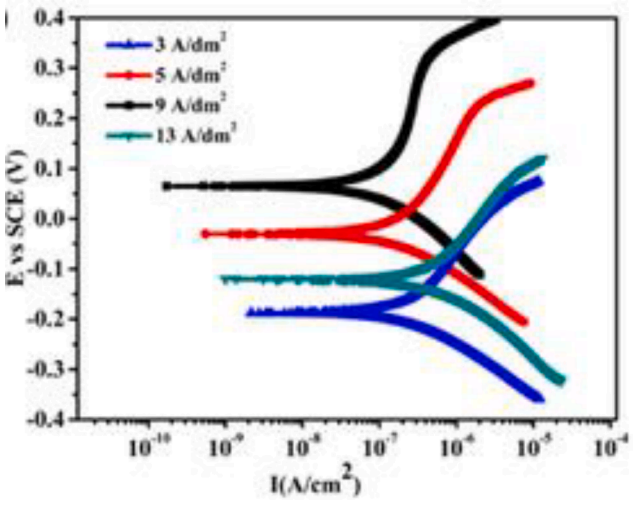

Fig. 18. Effect of deposition current density on the erosion and corrosion resistance properties of composite coatings (polarization curves). Reprinted with permission from [225]. © Wiley 2018.

Table 3
Summary of deposition parameters and corrosion results in some Ni-composite systems.

Coatings	Deposition Technique	Parameters			Corrosion Resistance	E_{corr} [V vs SCE]	I_{corr} [μAcm^{-2}]	References
		pH	C.D [Adm^{-2}]	Temperature [°C]				
Ni-graphene	DC	3 – 4	5	45 ± 5	Best with 0.4 g L^{-1} concentration of surfactant	−0.129	1.425	[174]
Ni-GO	DC	2.5	3	45 ± 2	Best with 0.6 g L^{-1} concentration of GO	−0.296	0.956	[192]
Ni/r-GO	DC	4 – 5	2, 5	60	Pinecone-like surface structure provides anticorrosion	−0.153	0.010	[146]
Ni-hBN	PC	4	8	60	Best with 20 g L^{-1} concentration of h-BN	−0.150	0.876	[75]
Ni-B_4C-BN	DC	3–4	2–5	30–60	Best at 5 A dm^{-2} & 50 °C deposition conditions	−0.222	0.653	[151]
Ni–W-BN	DC, PC	8	120	65	Best with 6 g/L concentration of BN by PC	−0.309	2.5	[153]
Ni-WS_2	DC	3.5	4	40	Trapped air pockets provide anticorrosion	−0.162	0.206	[157]
Ni-$MoSe_2$	PRC	4.5–5	4	50	Best at 60 % duty cycle	−0.511	3.91	[210]

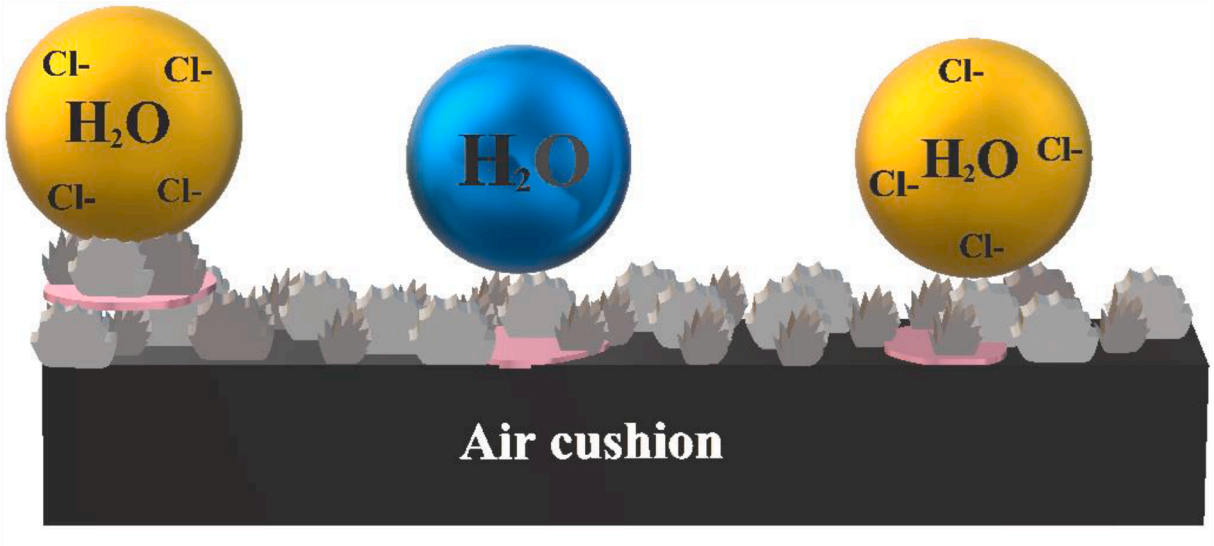

Fig. 19. Anticorrosion mechanism of the superhydrophobic Ni/r-GO coating in NaCl solution. Concept adapted and redrawn from ref. [146].

surface of metal that is exposed to corrosive environment is lowered in the presence of graphene Thus the corrosion resistance and the amount of incorporated graphene varied proportionally.

Bai et al.[146] fabricated a Ni/r-GO anti-corrosive, self-cleaning and superhydrophobic coating on stainless steel substrate. Coating had remarkable anticorrosion properties mainly because of the presence of pinecone-like rough surface. Fig. 19 depicts the anticorrosion mechanism shown by this coating. The air cushion having an approximate area of 94.03 percent created by the pinecone-like progressive micro/nano-structure provides a crucial part in avoiding chloride ions from entering the surface of coating.

Even though graphene is been used as a potential reinforcement in Ni matrix for developing coatings with anti-corrosion properties especially for load-bearing applications, the pinholes, pores and scratches in the coatings will cause increased localized corrosion due to galvanic coupling between graphene and metal. Even with relatively minimal mass loss, such local corrosion can severely degrade the material.[229] Localized corrosion tends to spread through the metal's more reactive areas, such as grain boundaries. Graphene being nobler than most common metals, metal corrosion will be accelerated at the graphene–metal interaction.[230,231].

According to new research, graphene-coated metals may corrode at even faster rates than naked metals. These significant variances in results are caused by a lack of total surface coverage, as well as the presence of irregularities such as wrinkles and cracks. These flaws are also the primary cause of poor corrosion resistance in long-term usage. For adequate corrosion resistance, the contact between the graphene sheet and the metal substrate is critical. In addition to that a high-quality graphene layer should entirely cover the metal surface, regardless of its roughness or curved shape, to produce the best barrier effect.[232] An area that has received little attention in the literature is the thorough investigation of diffusion mechanism in metallic coatings modified with graphene and graphene-derived materials. The primary process by which graphene and graphene-based metallic coatings effectively reduce corrosion is thus an area yet to be explored and a point of contradicting views.

Li et al.[116] in their study found that as the amount of BN increases, corrosion resistance of Ni–W/BN composite coating initially increased followed by a decrease. A higher value of polarization resistance R_p was obtained when BN concentration was 5 g L^{-1} which indicated an excellent anti-corrosion property. Uniform distribution of BN particles at this particular concentration can be a reason for its corrosion resistance. MoS_2 in combination with a metal matrix displayed preferable corrosion resistant characteristics in comparison with natural MoS_2 materials.[233].

Analysing the Ni-WS_2 composite coating developed by Zhao et al.[157] as the amount of WS_2 increased, current density showed a decrease and a more positive potential was generated. anti-corrosion property of this particular coating is related to the superhydrophobic nature of the same. The entrapped air within the clusters in the superhydrophobic surface can function as an efficient shield to maintain corrosive elements far from the surface and gives improved corrosion resistance in the case of plain mild steel owing to the reduced wetted area on the solid surface dipped in the aggressive solution.[234].

The $MoSe_2$ within the Ni matrix most importantly reduced the functional sites of corrosion located on the substrate.[235] The decrease in a surface area subjected to 3.5 wt% NaCl solution is due to the decline in double layer capacitance. It is clear that $MoSe_2$ minimizes superficial and structural flaws in the Ni matrix and works as a preventative barrier to restrict the dissolution of Ni.[210].

Tribological and wear properties

Wear

Since friction and wear account for almost a quarter of total energy losses worldwide, innovative strategies of mitigating these unfavourable impacts could be extremely valuable for the future energy-efficient economy.[236] In this regard the wear performance of different Ni and Ni-based composite coatings are extensively investigated under dry and wet sliding conditions (Table 4).

2D materials provide interlaminar sliding and a low shear force, thus giving them superlubricity properties. Moreover, owing to their nanostructures, they can easily enter the frictional contact surface to form a lubricating film. Furthermore, they can also decrease surface roughness and repair wear. The initial high specific surface allows 2D materials to be easily adsorbed onto the surface of a substrate to form a physical membrane. The physical membrane can separate the two contact surfaces to prevent direct contact between the two sliding surfaces. In the second stage, the physical film ruptures with an increase in the frictional strength, thereby promoting the chemical reaction between a lubricant and a local contact surface. This chemical reaction forms a new tribological film and gradually replaces the physical film, and this film exists on a local contact surface. As a result, the tribological properties are improved.

Hussain et al.[66] concluded that graphene filled metal matrix

Table 4
Summary of deposition parameters and coefficient of friction values in some Ni- composite systems.

Coatings	Deposition Technique	Parameters			Reported Coefficient of Friction (COF) Value	References
		pH	C.D [Adm^{-2}]	Temperature [^oC]		
Ni-graphene	PC	4	1	50–80	0.70	[187]
Ni- SiC-graphene	PC	3.8 – 4.5	2–8	55–60	0.15	[204]
Ni-GO	PC	3.5–4.5	6–10	55–60	0.15	[205]
Ni-BN	DC	4–5	2–6	50	0.50	[77]
Ni-MoS_2	DC	2–4	4.8	50	0.40	[177]
Ni-WS_2	PC	4.8	10	50	0.11	[237]
Ni-P-WS_2	DC	2–3	2.5	60	0.17	[120]
Ni-WSe_2	PC	4.8	10	50	0.07	[50]

coatings containing well-dispersed graphene nanosheets in the matrix improves surface durability and wear properties. The mechanism of decrease of the friction coefficient and wear rate in Ni-graphene composite coating was explained by Xiang et al.[206] For instance, graphene is a self-lubricating material and is capable of forming a lubrication film at the sliding interface. The graphene incorporation improves the wear resistance of the coating.[238] The low surface energy of graphene also helps the Ni–graphene coating to possess minimal adhesive friction (reduce adhesion forces between particles and the substrate) and results in easy shearing being a solid lubricant.[206] Thus Ni–graphene composite coatings were shown to be ideal candidates to be used in micro devices subjected to high load and sliding speed conditions.[197].

The lamellar structure of BN must be a factor which leads to low COF values.[77] Wear studies on Ni-BN-B_4C composite coating indicate that BN and B_4C particles contained in the Ni matrix either obstruct or slowdown the passage of dislocations in the nickel metal matrix, preventing plastic deformation and therefore increasing the load bearing capacity of the Ni matrix. This was manifested as increased hardness and wear resistance.

An irregular frictional behaviour was observed in Ni–W–MoS_2 composite coating by Cardinal et al.[167] These coatings possess rough, non-uniform surface composed of sponge-like structures. This accounts for large deformation related to wear and the frictional curves are not smooth. In spite of this friction coefficient of Ni–W-0.5 g/L MoS_2 composite coating was found to be 50 % lower than Ni–W coating. Most important conclusion derived from this study was that there seems to be a solid lubricant concentration zone in which co-deposition of MoS_2 particles into Ni–W nanostructured alloys improves the coating's frictional qualities. It was observed that COF reduced with increasing amount of MoS_2 and on decreasing particle size.[177] MoS_2 slides readily due to weak Van der Waal's bonding between two layers, resulting in low friction. A regression equation to calculate COF by knowing the size and concentration of MoS_2 particles was another lead from this study.

Lecina et al.[169] proposed an electrodeposited Ni–WS_2 coating with a friction coefficient of 0.4 against steel. It was discovered that the Ni film formed from Watt's solution grows favourably along the (200) orientation at first. When WS_2 particles are added the crystallographic texture evolves and the intensities of the (111), (220) and (311) peaks rise at the expense of the (200) reflection. Tudela et al.[239] varied the bath agitation to upgrade the mechanical strength and vary the wear resistance of electrodeposited Ni–WS_2 coating. Das et al.[237] reported that a pulse current electrodeposited Ni–WS_2 coating with a friction coefficient of 0.12.

Molybdenum disulphide (MoS_2) has an extremely low COF ($\leq$0.1) in vacuum and inert atmospheres, but increases to 0.3 to 0.5 in humid air. Moreover, increase in coefficient of friction of MoS_2 based coatings in humid environment can be explained as the transformation of MoS_2 to MoO_3 resulting in interruption the layer movement. It is also possible that the use of W instead of Mo contributes favourably, as WO_3 film is slightly more protective than MoO_3 and provides lower friction in air.[89].

In ambient atmosphere sulphide based transition materials, specifically MoS_2 and WS_2, become vulnerable due to their moisture sensitive tribological behaviour unlike selenides based transition metals, such as WSe_2 and $MoSe_2$. Sulphide based transition materials are comparatively less effective in humid environments as oxygen and water vapour could lead to the formation of oxides on the coating surfaces leading to an increase in coefficient of friction. In addition, sulphide based transition materials have reactive dangling bonds on the prismatic edges, which are vulnerable to oxide formation and consequently lead to the deterioration of the low friction property. Among the different candidates, the pure WSe_x stands out for its good compromise of wear resistance and friction coefficient both in ambient air and in inert environments.

Self-lubrication

Lubrication is the way of eliminating friction and wear involving two surfaces that are in immediate contact. These surfaces could be static or be in motion. The most efficient method of reducing friction and wear is to divide the two surfaces with a third body, such as a film of lubrication.[240] The duty of lubricant is to reduce friction and wear, minimize contact pressure and avoid galling and seizure. The coatings that provide lubrication are mainly used in load bearing parts.[241] The most typical examples include mechanical systems such as gears and traction devices, turbines, ball bearings and so forth.

SLMMCs (self-lubricating metal matrix composites) are a type of material that has the potential to aid engineers in meeting the needs of global efforts for green manufacturing and sustainability.[242] Several researchers have presumed that incorporating 2D layered materials in suitable metal matrix like Ni is an efficient method to combat wear and friction.[243] Additionally these materials are potential solid lubricants.[244] Graphene, BN, WS_2 and MoS_2 are the most extensively used 2D materials for this purpose. Selenide based transition metal dichalcogenides like WSe_2 are also recently been investigated in this aspect as of now. These 2-D materials have a layered structure with hexagonal closely packed atoms and the atoms within every layer are bound together by a strong covalent bond and weak Van der Waals interaction. These multilayer arrangements permit atoms in parallel planes to slide around.

Self-lubricating composite coatings derived from the combination of a metal matrix and suitable 2D layered nanomaterial can outperform the traditional coatings in terms of tribological characteristics.[245] These solid lubricants are exposed to the surface during sliding and flow to the contact surface to form a lubricant layer.[246] This film functions as a lubricant, reducing metal-to-metal contact and improving tribological behaviour (Fig. 20). As a result self-lubricating composite coating is a cutting-edge material that offers a solution to energy sustainability and efficiency in context of ecological compatibility.

Graphene having remarkable mechanical strength and lubrication ability that can improve the wear resistance.[197,247] On analysing the wear tracks of the Ni–graphene composite coatings tested at varying sliding speeds it was observed that the width of wear track had undergone change in a progressive manner on increasing sliding speeds. It can be because of rise in temperature results in the generation of nickel oxide

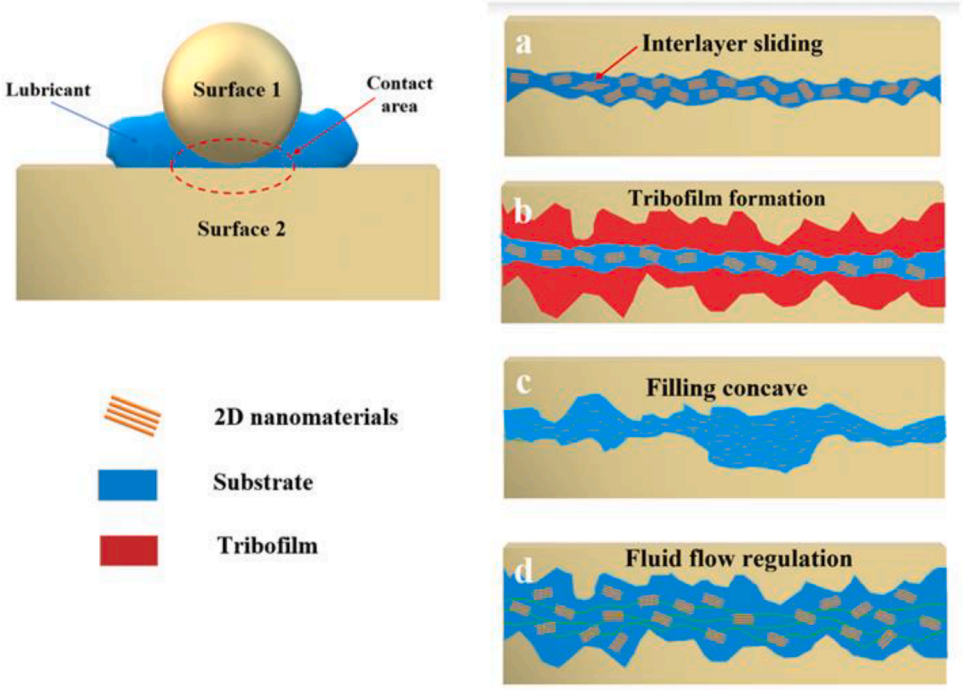

Fig. 20. Lubrication mechanisms of 2D materials. (a) Entering the contact area of sliding surfaces, (b) Tribofilm formation, (c) Filling the pits and gaps of the contact area, (d) Affecting the fluid drag and viscosity. (a)-(d) Concept adapted and redrawn from ref. [244].

and exfoliation of multi-layered graphene aids in lubrication of the coating.[248] Pulsed electrodeposition was employed to produce Ni-GO composite coatings on chrome steel ball and SS 440c substrates.[249] Friction and wear characteristics had undergone refinement compared to pure Ni coating. When a load is applied, the confined GO particles emerge and create a transfer film upon the substrate providing lubricity.

The layered structure of the crystal lattice of h-BN permits sliding movement of the parallel planes. Due to the weak bonding between the planes, the shear strength is low along the direction of sliding but the compressive strength along the direction perpendicular to the shearing is high. Therefore, the addition of h-BN into the metal matrix increases the hardness of the composite as well as makes the composite more wear-resistant due to its lubricating property. Due to strong adhesion force, the lubrication film formed by h-BN adhered strongly to the substrate surface. Unlike molybdenum disulfide, lubrication by h-BN does not require a moist atmosphere. It ensures low friction in the dry atmosphere as well as in vacuum. Chemical inertness and thermal stability of h-BN gives it an advantage over graphite and MoS_2 as a solid lubricant. The coefficient of friction and rate of wear in Ni-BN composite coatings reduce as the amount of BN rises. According to the study of Zhang et al.[77] optimum addition of BN is 1.5 g/Lin terms of lubricating efficiency.

MoS_2 lubrication performance often exceeds that of graphite and is effective in a vacuum as well whereas graphite does not. The morphologies of the mixture of MoS_2 and PTFE solid lubricant coating on stainless steel substrate offered best physical features.[250] The surfaces were smooth and even without any holes. This is believed to be because of self-lubricating effect of MoS_2 tribofilm.[251] In order to achieve maximum lubricity, MoS_2 particles need to be sheared into tribo-films with the weakly bonded MoS_2 inter-molecular planes aligning parallel with the wear track that can be achieved by high-shear mixing.[252].

WS_2 presents a lower coefficient of friction and improvement in oxidation resistance and thermal stability, even for about 100 °C above the well-known MoS_2. Ni/WS_2 composite coatings markedly increased their tribological performance in both lubricated and non-lubricated circumstances.[253] The Ni-WS_2 composite coating exhibited exceptional self-lubricity across a wide temperature range of 25 to 300 °C in a study by Cui et al.[248] At temperatures above 400 °C, WS_2 gradually oxidizes into WO_3 and its lubricating capacity is lost. He et al.[120] used a versatile one-pot mono-step electrodeposition to develop a superhydrophobic and self-lubricating Ni-P-WS_2 coating. A hierarchical surface with micron-sized protrusion arrays and submicron-sized bumps on the upper end was generated, with a high-water contact angle of 157°. A reasonable quantity of WS_2 in the composite coating will guarantee the creation of a homogenous tribofilm, which will maintain a low coefficient of friction (as low as 0.17). Low shear yield of the WS_2 and its high abundance which can consistently provide a lubrication function for a long period.

It was found that Ni-1 g/L WSe2 composite coating had a low wear rate because of higher WSe2 codeposition in the coating matrix that accelerates the solid lubricating nature of the coating.[50] WSe_2 is a more suitable second phase reinforcement than other sulfide-based reinforcements due to its moisture resistance, improved air and chemical stability.

Superhydrophobicity

Surfaces having water contact angle greater than 150° are termed as superhydrophobic surfaces. Examples for natural superhydrophobic surfaces include lotus leaves, water strider's legs and coloured-structured wings of insects. Significant attempts have been made to develop artificial superhydrophobic coatings owing to their unique features such as water repellency, self-cleaning, anti-icing and anticorrosion.[254] Replication of this self-cleaning effect is achieved by generation of rough surfaces on hydrophobic substrates or by chemical modification using low surface energy material. Based on this idea sol-gel processing, etching and lithography, chemical vapour deposition, layer-by-layer and colloidal assembly etc. have been used for developing superhydrophobic surfaces. In comparison with these techniques, electrodeposition possess certain advantages like low cost, ease of operation and appropriateness for mass production etc. The introduction of nanoparticles can alter surface roughness in a metal electrodeposit, leading to changes in wetting properties. Low surface energy nanoparticles having laminar structures such as graphene, MoS_2, WS_2, and

$MoSe_2$ are strong candidates for metal co-deposition to form a superhydrophobic composite coating.

Electrodeposited Ni surface has water contact angle between 79° and 87°.[255] Superhydrophobic Ni surfaces were developed from an aqueous solution containing additive ethylenediamine dihydrochloride capable of forming the cone-shaped Ni crystals, were first reported by Hang et al.[256] A two step electrodeposition is carried out in which intially microcones were deposited for 10 min at 2.0 Adm^{-2} followed by the nanocone deposition at 5.0 Adm^{-2} for 1 min forming micro-nano hierarchial assembly as in Fig. 21. The as-deposited surface had twofold roughness which enabled substantial fractions of trapped air pockets and a high contact angle of 154° on an inherently hydrophilic material, which was explained by the Cassie–Baxter wettingstate.[257] Fig. 22.

Superhydrophobic Ni films with different surface structures were formed employing different plating conditions in the presence of anionic electrolytes. The ionic electrolyte was reported by Gu and Tu [258] as a deep eutectic mixture composed of choline chloride, ethylene glycol and nickel chloride. Ionic electrolytes have very low vapour pressure and good thermal stability compared to aqueous electrolytes. Storage time of coatings in air often determines the wettability and diverse nickel films with varied wettability were fabricated by Khorsand et al.[255] The shift from superhydrophilicity to superhydrophobicity can be because of the chemical compositional change and NiO formation. A standard Watts bath was used in generation of highly ordered micro-nano structured nickel coating on copper substrate.[259] The polarisation curves and EIS measurements showed remarkable improvement in corrosion resistance subsequently by treating with (heptadecafluoro-1,1,2,2-tetradecyl) triethoxysilane. Cone size variation is possible in nickel films by regulation of electrodeposition parameters.[260].

Due to hydrophobicity, abrasion resistance and large specific surface area, reduced graphene oxide is an appropriate additive material for the fabrication of superhydrophobic materials.[200,259,261] Predeposition of Ni along with a step-wise incrementation in current density resulted in a r-GO/Ni composite coating having micro/nanostructures similar to a pinecone with CA 162.7 ± 0.8°.[146] Presence of adequate "air-pockets" formed by Ni pinecones on the r-GO sheets

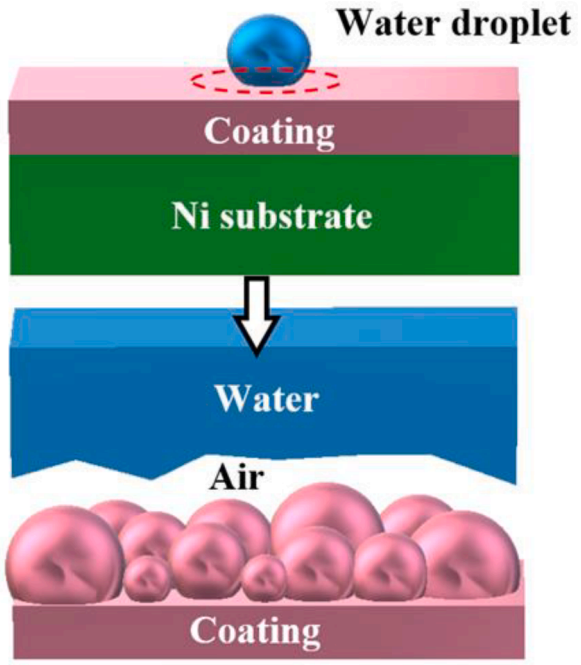

Fig. 22. Schematic illustration of the interface region between the water droplet and Ni-$MoSe_2$-0.1 g L^{-1}MWCNT coating surface. Concept adapted and redrawn from ref. [45].

allowed the bouncing movement of the water droplet.

Zhao et al.[157] developed a Ni-WS_2 superhydrophobic composite coating on mild steel substrate. The water-repellent property improved in accordance with the increase in amount of WS_2. The maximum contact angle was 158.3° and the sliding angle was 7.7° shown by the coating with 4.88 percent WS_2. The self-cleaning effect exhibited by the coating make it suitable for industrial applications. He et al.[120] observed broccoli-like protrusions at micro scale level in Ni-P composite

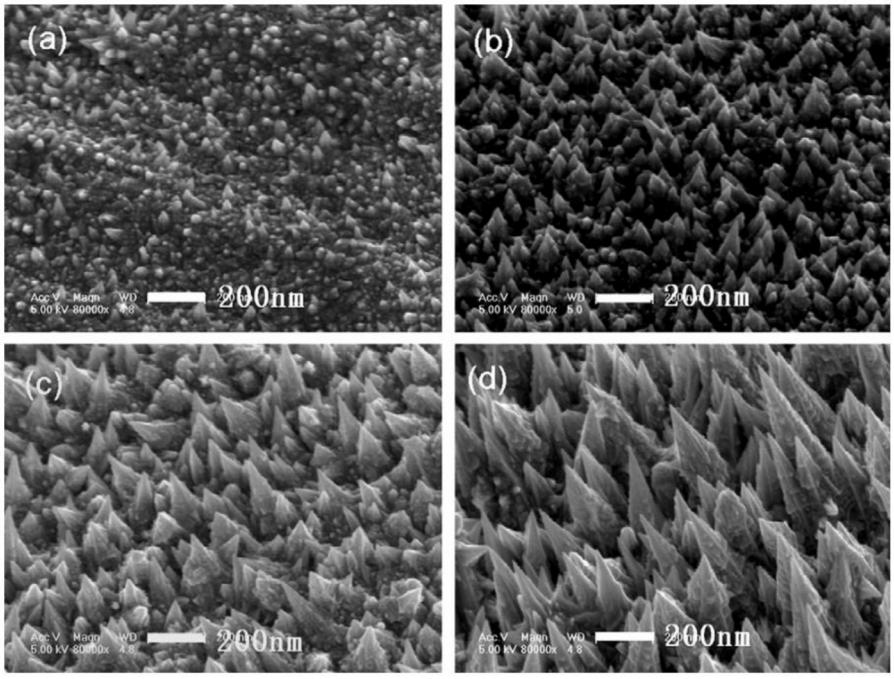

Fig. 21. SEM image of nickel films electroplated for different current densities and times. (a) 5 Adm^{-2} 30 s (b) 5 Adm^{-2} 1 min (c) 2 A/dm^{-2} 5 min (d) 2 A/dm^{-2} 10 min. (a)-(d) Reprinted with permission from ref. [254]. © Elsevier Limited 2010.

coatings containing 2.3 wt% of WS_2 (WCA of 157°). A combination of micron-sized broccoli-like structures and submicron-sized particles and pockets resulted in remarkable superhydrophobicity. The Ni composite coating with WC and WS_2 particles were developed on mild steel substrates followed with stearic acid modification.[119] A smooth surface without any agglomeration resulting from the combined effect WC and WS_2 particles was obtained. WCA reached 170° after surface modification. Abrasion test and long-term stability test justified that the coating has an abrasion bearing capacity $\geq$ 10,000 mm abrasion length and a 6-month stability pertaining with strong aerophilic behaviour.

Ni-$MoSe_2$ reinforced with multi-walled carbon nanotubes (MWCNT) composite coatings are seen to be both hydrophobic and corrosion resistant by Maharana et al.[49] Ni-$MoSe_2$ coating having composition Ni-5 g $L^{-1}$$MoSe_2$-0.1 g L^{-1}MWCNT showed notable higher roughness in comparison with the pure Ni coating. This can be credited to the appearance of random distribution of nodular structures with different sizes. There is a limited hindrance for the immediate contact in between water droplet and the surface of coating as in Fig. 23. It has a WCA of 151.9° because of maximum co-deposition of MWCNT and compact nature due to the presence of both $MoSe_2$ and MWCNT.

Applications

Wear, friction and corrosion prove critical to the longevity, energy consumption and efficiency of industrial systems. These phenomena also endanger the safety of those who operate the machine. Engineers therefore go for machines that have a prolonged service life, conserve resources and have increased efficiency over their service life. In order to improve their quality, these devices or equipment composed of lighter and more economical materials such as aluminium and steel; coatings made of materials that are stronger and more chemically stable than these are employed to protect them against surface corrosion. It is estimated that metallic nanocomposites will have a major impact on an extensive range of industries including aerospace, electronics and military.[262] Improved properties include significant improvements in fracture strength and longevity; better durability at high temperature and creep resistance; larger hardness values than those of current commercial steel and alloys; substantial increase in Young's modulus and shear modulus (compared to micro composites). These are mainly the result of the nano size reinforcements used, resulting in a suitable morphology for the products.[263] Introducing self-lubricating composites into various operating systems is a way of decreasing the use of external toxic hydrocarbon lubricants thereby reducing environmental impact and lowering energy dissipation in industrial components for initiatives toward energy efficiency and sustainability.[264].

Composite/nanocomposite materials based on nickel and nickel alloys are ideal choices for enhancing the effectiveness of these materials [265] as in Fig. 24. Furthermore, nickel electrodeposits are employed for electroforming of printing plates, phonograph record stampers, foil, tubes, screens, MEMS and a variety of other items due to their relatively good mechanical attributes.[266,267] In the manufacturing and shaping of tools [268] which demand excellent corrosion and wear resistance, low friction and high thermal stability electroplated nickel composite/nanocomposite coatings are employed.[269].

Nickel-based nanocomposite coatings are indeed very useful in the automotive industry like bumpers, exhaust trims, domestic appliances, and tools. They're commonly found in pump bodies, heat exchangers, alkaline battery cases, and food processing machinery. Since they possess high specific strength and wear resistance, graphene-based nickel nanocomposite coatings are among the most potential materials. Aside from graphene-based nano composites, composites including MoS_2 and BN have good tribological characteristics. TMDs based on selenides like WSe_2 and $MoSe_2$ are promising candidates as solid lubricants in high temperature applications. Nickel based nano composite coatings have huge relevance in aviation and aerospace sectors. Their main applications can be divided into structural components such as fuselages and wings, as well as moving components such as bearings, gears, and hatch seals.[262] Due to the in-plane mechanical isotropy of the 2D nanomaterial, two-dimensional nanomaterial-based nickel nano nanocomposite coatings have the capability to be used as protective and

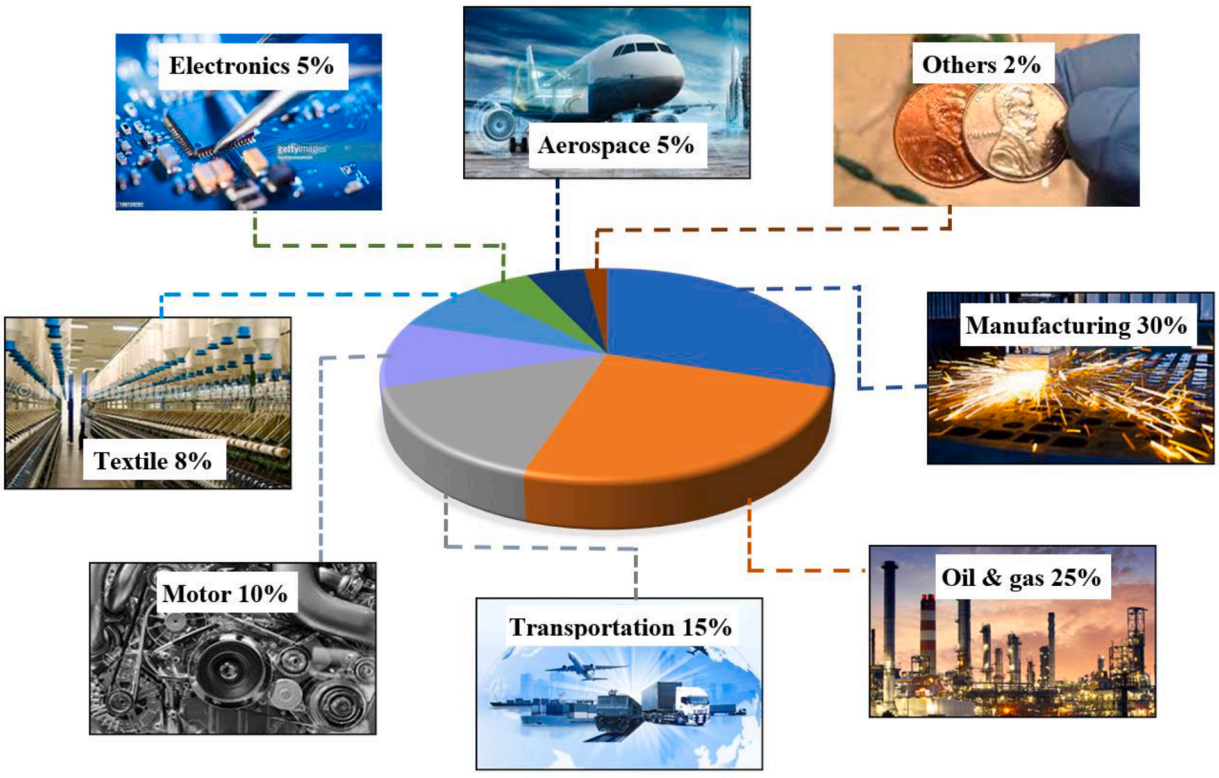

Fig. 23. Important industrial applications of electrodeposited nickel/nickel alloy based nano composite coatings.

shield materials such as body armour and ambient armour.

Conclusion & critical areas for further R & D

Electrodeposition of nickel-based composite and alloy coatings is currently-one of the most chiefly used method among many attempts made in the synthesis of surface coatings derived from non-toxic materials. 2D materials (graphene, BN, MoS_2, WS_2, $MoSe_2$ and WSe_2) based nickel nano composite coatings have shown superlative characteristics like excellent corrosion and wear resistance, premium hardness, self-lubrication and thus these coatings have exceptional capabilities to reinstate chromium-based coatings. Development of self-lubricating nanocomposite coatings is a major aspect of sustainable methods in tribology with a vision of a greener, cleaner and eco-friendly environment. To accomplish significant progress in the science and technology of Nickel nanocomposite coatings comprising uniformly dispersed secondary phase nanoparticles especially-two-dimensional layered materials, it is necessary to do additional research and development on several vital (and interconnected) areas that are underappreciated in the literature:

- It is possible to create innovative, multifunctional metal-matrix coatings by carefully combining different particles of various kinds and sizes by electrodeposition. Future initiatives could include creating and patterning innovative structures as well as gradient or layered patterns for specialised purposes. Since process equipment is simple, easy to operate, precise and being low cost, electrodeposition can be used in the manufacture of nickel based functionally graded coatings.
- The availability of bath additives for electrodeposition is likely to be limited as legislation becomes stricter and environmental concerns grow. This appears to provide a stronger emphasis on additive-free electrolytes, greater control over operational conditions, and more consideration of current control mode. Thus the development of an electrodeposited Ni composite coating from a sustainably sourced particle is of great academic and industrial interest.
- Friction and wear reductions in tribological components of electric vehicles (EVs) is an important aspect to be studied since they are viable solutions for reducing greenhouse gas emissions and maintaining a clean and healthy environment by mitigating the negative effects of using internal combustion engines (ICEs) in the transportation and energy production sectors. Self-lubricating Ni based nanocomposite coatings reinforced with 2D materials offer a solution for this and can be thought of an inevitable future material.
- There have been an increased interest in electrodeposited nickel based self-lubricating composite coatings in recent years for tribological applications with a reduced coefficient of friction at moderate to high temperatures that are capable of extending the lifetime of metal parts with complex structures under harsh conditions. Solid lubricants (graphene, BN, TMDs) can solve these problems for sliding parts with low friction under dry conditions. An interesting area that needs further investigation is the synergetic lubricating action and mechanism of multiple lubricants used in these self-lubricating composite coatings. Examples of applications requiring such materials in extreme environments include bearings and bushings for space satellites and vehicles, air-foil bearings, gas turbine seals, cylinder wall/piston ring for low-heat rejection diesel engines, various furnace components, etc.
- There are only few literature reports on aspects like Hall-Petch breakdown and grain boundary character distribution(grain boundary engineering) that account for increased micro-hardness and corrosion resistance respectively in nickel nanocomposite coatings; these need to be studied in detail. Incorporating some alloying element to alter the corrosion potential of these coatings (Ni-Co, Ni–W, Ni-P, Ni-Mo) while maintaining hardness can be considered in future directions.
- Co-deposition mechanism involving various types and concentration of nanoparticles is an area yet to be explored. There is no clear idea by which we can differentiate the co-deposition process as activation controlled or charge transfer process, mixed controlled process, and mass transport or diffusion controlled process. Elucidation of rate determining step in the process of co-deposition of nano-particles is another area that needs more clarity. When multiple nano particles are involved in the co-deposition process, mechanism becomes much more complicated. Thus we need to investigate in to the area of co-deposition more deeply.
- Obtaining a stable coating with uniform distribution of reinforced particles in electrodeposition is of critical importance. Ultrasonic assisted electrodeposition especially in the case of layered 2D material reinforcements is thus gaining importance nowadays.
- In the case of Ni deposition, pulse plating is used to reduce grain size, lower stress, and increase hardness for engineering applications. Among the various pulse plating techniques, pulse reverse deposition has already been recognised and used in certain research; however, there is a noticeable need of expansion of basic understanding in deposition mechanism and defined procedure to create an optimum film by this method.
- Given the two major factors influencing the non-wetting nature of these coatings, geometrical surface morphology and surface energy, it is easier to improve the contact angle by lowering surface energy with chemicals and/or controlling surface roughness and structure. Future advancements in this sector may include the development of novel electrolytes (such as those based on alcohol) as well as development of coatings with anti-icing properties (aircraft surfaces, engine inlets, sensors and windshields) and superhydrophobic coatings capable of oil–water separation.
- Even though the majority of the reported coating properties are based on traditional experimental methods, the use of computational methods has expanded the basic knowledge of the role of every electroplating variable on the wear and tribological properties of the fabricated coatings, as well as their effect on wear mechanism. Furthermore tools like atomistic simulation and Monte Carlo allow for systematic investigation of atomic-level interactions within the composite coating and their impact on macroscopic tribological characteristics. It is also well recognised that the mixing of various types of reinforcing secondary phases allows for a high degree of flexibility in tailoring the properties of the manufactured coatings for a particular application. However, due to the multivariable nature of such complex coatings, computer-based optimization methods such as artificial neural networks and principal component optimization methods could feasibly be used to refine the fabrication variables to those that lead to the best and most effective coating properties. To anticipate deposit particle composition and characteristics based on bath composition and operational variables, enhanced multi-physics computer modelling is required.

Declaration of Competing Interest

The authors declare that they have no known competing financial interests or personal relationships that could have appeared to influence the work reported in this paper.

Data availability

No data was used for the research described in the article.

Acknowledgements

Author Revathy Sreekumar is grateful to DST, Govt. of India for Inspire fellowship grant (IF 180987). Miss Ancin Maria Devis is highly acknowledged for proof reading and correction of this review.

References

[1] L. Anicai, Ni-W alloys coatings as ecological alternative for chromium plating - Evaluation of corrosion behaviour, Corros. Rev. 25 (2007) 607–620, https://doi.org/10.1515/CORRREV.2007.25.5-6.607.

[2] F.J. He, M. Wang, X. Lu, Properties of electrodeposited amorphous Fe-Ni-W alloy deposits, Trans. Nonferrous Met. Soc. China (English Ed. 16 (2006) 1289–1294, https://doi.org/10.1016/S1003-6326(07)60008-9.

[3] J.L. McCrea, G. Palumbo, 21 – Nanocoatings for commercial and industrial applications, in: S.H. Whang (Ed.), Nanostructured Met. Alloy., Woodhead Publishing, 2011: pp. 663–686. https://doi.org/10.1533/9780857091123.4.663.

[4] H. Khani, J.F. Brennecke, Hard chromium composite electroplating on high-strength stainless steel from a Cr(III)-ionic liquid solution, Electrochem. Commun. 107 (2019), 106537. https://doi.org/10.1016/j.elecom.2019.106537.

[5] P. Møller, L.P. Nielsen, Identifying new alternatives for hard chromium plating, Natl. Assoc. Surf. Finish. Annu. Conf. Trade Show, SUR/FIN 2014 (79) (2014) 596–620.

[6] S. Kirihara, Y. Umeda, K. Tashiro, H. Honma, O. Takai, Development of Ni-W alloy plating as a substitution of hard chromium plating, Trans. Mater. Res. Soc. Japan. 41 (2016) 35–39. https://doi.org/10.14723/tmrsj.41.35.

[7] E.W. Brooman, Corrosion performance of environmentally acceptable alternatives to cadmium and chromium coatings: Chromium - Part II, Met. Finish. 98 (2000) 39–45, https://doi.org/10.1016/S0026-0576(00)82740-3.

[8] G.A. DiBari, Chronology of nickel electroplating, Met. Finish. 100 (2002) 34–49, https://doi.org/10.1016/S0026-0576(02)80244-6.

[9] A. Lateef, R. Nazir, Metal Nanocomposites : Synthesis, Characterization and their Applications, Sci. Appl. Tailored Nanostructures. (2017) 239–256.

[10] H. Conrad, T.D. Golden, Electrodeposited Zinc-Nickel Nanocomposite Coatings, Nanocomposites - Recent Evol. (2019), https://doi.org/10.5772/intechopen.80219.

[11] S.M. Mirsaeed-ghazi, S.R. Allahkaram, A. Molaei, Tribological Behavior and Corrosion Properties of Graphite Incorporated Cu/Sic Nanocomposite Coatings Prepared by Pulse Current Electrodeposition, Inorg. Chem. - An Indian J. 13 (2018) 1–20.

[12] S. Pinate, C. Zanella, Wear behavior of Ni-based composite coatings with dual nano-sic: Graphite powder mix, Coatings. 10 (2020) 1–11, https://doi.org/10.3390/coatings10111060.

[13] R. Riedel, H.-J. Kleebe, H. Schönfelder, F. Aldinger, A covalent micro/nano-composite resistant to high-temperature oxidation, Nature. 374 (1995) 526–528, https://doi.org/10.1038/374526a0.

[14] S. Özkar, G.A. Ozin, R.A. Prokopowicz, Photooxidation of Hexacarbonylmolybdenum(0) in Sodium Zeolite Y to Yield Redox-Interconvertible Molybdenum(VI) Oxide and Molybdenum(IV) Oxide Monomers, Chem. Mater. 4 (1992) 1380–1388, https://doi.org/10.1021/cm00024a046.

[15] K. Lolupiman, P. Wangyao, J. Qin, Electrodeposition of Zn/TiO 2 composite coatings for anode materials of Zinc ion battery, 29 (2019) 120–126. https://doi.org/10.14456/jmmm.2019.55.

[16] N.S. Mbugua, M. Kang, Y. Zhang, N.J. Ndiithi, G.V. Bertrand, L. Yao, Electrochemical deposition of Ni, NiCo Alloy and NiCo-ceramic composite coatings-A critical review, Materials (Basel). 13 (2020), https://doi.org/10.3390/MA13163475.

[17] M. Cao, Z. Xue, J. Niu, J. Qin, M. Sawangphruk, X. Zhang, Facile Electrodeposition of Ni – Cu – P Dendrite Nanotube Films with Enhanced Hydrogen Evolution Reaction Activity and Durability, (2018). https://doi.org/10.1021/acsami.8b12321.

[18] J. Qin, X. Zhang, K. Umporntheep, V. Auejitthavorn, R. Li, Electrodeposition and Mechanical Properties of Ni-W Matrix Composite Coatings with Embedded Amorphous Boron Particles, 11 (2016) 9529–9541. https://doi.org/10.20964/2016.11.58.

[19] A. Aliyu, A. Gupta, C. Srivastava, Correlation Between Texture, Grain Boundary Constitution, and Corrosion Behavior of Ni-Cu Coatings, Metall. Mater. Trans. A. (2022), https://doi.org/10.1007/s11661-022-06605-5.

[20] P.S. Bains, S.S. Sidhu, H.S. Payal, Fabrication and Machining of Metal Matrix Composites: A Review, Mater. Manuf. Process. 31 (2016) 553–573, https://doi.org/10.1080/10426914.2015.1025976.

[21] L. Singh, B. Singh, K.K. Saxena, Manufacturing techniques for metal matrix composites (MMC): an overview, Adv. Mater. Process. Technol. 6 (2020) 441–457, https://doi.org/10.1080/2374068X.2020.1729603.

[22] S. Kumar, R. Singh, M.S.J. Hashmi, Metal matrix composite: a methodological review, Adv. Mater. Process. Technol. 6 (2020) 13–24, https://doi.org/10.1080/2374068X.2019.1682296.

[23] L.P. Bicelli, B. Bozzini, C. Mele, L. D'Urzo, A review of nanostructural aspects of metal electrodeposition, Int. J. Electrochem. Sci. 3 (2008) 356–408.

[24] Y.H. Ahmad, A.M.A. Mohamed, Electrodeposition of nanostructured Nickel-Ceramic composite coatings: A review, Int. J. Electrochem. Sci. 9 (2014) 1942–1963.

[25] O.S.I. Fayomi, A.A. Sode, B.U. Anyanwu, A.A. Ayoola, M.O. Nkiko, K. M. Oluwasegun, D.O. Alkhuele, D.E. Ighravwe, Experimental studies and influence of process factor on zinc-nickel based coating on mild steel, Adv. Mater. Process. Technol. (2021) 1–10, https://doi.org/10.1080/2374068X.2021.1896863.

[26] A. Hovestad, L.J.J. Janssen, Electroplating of Metal Matrix Composites by Codeposition of Suspended Particles, Mod. Asp. Electrochem. (2006) 475–532, https://doi.org/10.1007/0-387-25838-8_6.

[27] S. Fundamentals, Encyclopedia of Tribology (2013), https://doi.org/10.1007/978-0-387-92897-5.

[28] I. Corni, R.J. Chater, A.R. Boccaccini, M.P. Ryan, Electro co-deposition of Ni-Al 2O 3 composite coatings, J. Mater. Sci. 47 (2012) 5361–5373, https://doi.org/10.1007/s10853-012-6381-7.

[29] A. Góral, L. Lityńska-Dobrzyńska, M. Kot, Effect of Surface Roughness and Structure Features on Tribological Properties of Electrodeposited Nanocrystalline Ni and Ni/Al2O3 Coatings, J. Mater. Eng. Perform. 26 (2017) 2118–2128, https://doi.org/10.1007/s11665-017-2662-2.

[30] L. Benea, Electrodeposition and tribocorrosion behaviour of ZrO2–Ni composite coatings, J. Appl. Electrochem. 39 (2009) 1671–1681, https://doi.org/10.1007/s10800-009-9859-5.

[31] X.J. Sun, J.G. Li, Friction and wear properties of electrodeposited nickel-titania nanocomposite coatings, Tribol. Lett. 28 (2007) 223–228, https://doi.org/10.1007/s11249-007-9254-5.

[32] I. Birlik, N.F. Ak Azem, M. Toparli, E. Celik, T. Koc Delice, S. Yildirim, O. Bardakcioglu, T. Dikici, Preparation and characterization of Ni-TiO 2 nanocomposite coatings produced by electrodeposition technique, Front. Mater. 3 (2016) 1–7, https://doi.org/10.3389/fmats.2016.00046.

[33] S. Mbugua Nyambura, M. Kang, J. Zhu, Y. Liu, Y. Zhang, N.J. Ndiithi, Synthesis and Characterization of Ni–W/Cr2O3 Nanocomposite Coatings Using Electrochemical Deposition Technique, Coatings. 9 (2019), https://doi.org/10.3390/coatings9120815.

[34] N. Bogomazova, I. Makarava, A. Chernik, I. Zharskii, Specific features of electrodeposition of Ni-SiO2 micromounting composite coatings from complex electrolytes, Russ. J. Appl. Chem. 87 (2014) 1235–1239, https://doi.org/10.1134/S1070427214090079.

[35] C. Xiong, Y. Wang, B. Hu, L. Chen, S. Tay, A. Xu, W. Gao, Microstructure and Properties of Electrodeposited Ni-CeO2 Coatings, Int. J. Electrochem. Sci. 11 (2016) 906–914.

[36] G. Maurin, A. Lavanant, Electrodeposition of nickel/silicon carbide composite coatings on a rotating disc electrode, J. Appl. Electrochem. 25 (1995) 1113–1121, https://doi.org/10.1007/BF00242538.

[37] R.N. Gupta, A.K. Das, S.H. Nagahanumaiah, Pulse Electrocodeposited Ni–WC Composite Coating, Mater. Manuf. Process. 31 (2016) 42–47, https://doi.org/10.1080/10426914.2015.1019087.

[38] M. Raja, G.N.K.R. Bapu, J. Maharaja, R. Sekar, Electrodeposition and characterisation of Ni–TiC nanocomposite using Watts bath, Surf. Eng. 30 (2014) 697–701, https://doi.org/10.1179/1743294414Y.0000000265.

[39] J.B. Jiang, L. Zhang, Q.D. Zhong, Q.Y. Zhou, Y. Wang, J. Luo, Preparation and characterisation of nickel-nano-B 4C composite coatings, Surf. Eng. 28 (2012) 612–619, https://doi.org/10.1179/1743294412Y.0000000038.

[40] E. Budi, R. Berliana, W. Umiatin, I.S. Indrasari, Co-electrodeposition of Ni/Si3N4 composite coatings, Empower. Sci. Math. Glob. Compet. (2019).

[41] X.Z. He, X.W. Zhang, X.L. Zhou, Z.H. Fu, Study on Electrodeposition of Ni-Graphite Composite Coatings in Sulfamate Bath, in: Adv. Compos., Trans Tech Publications Ltd, 2011: pp. 1546–1550. https://doi.org/10.4028/www.scientific.net/AMR.150-151.1546.

[42] X. Zhang, J. Qin, M. Das, R. Hao, H. Zhong, A. Thueploy, S. Limpanart, Y. Boonyongmaneerat, M.Z. Ma, R. Liu, Co-electrodeposition of hard Ni-W/diamond nanocomposite coatings, Sci. Rep. 6 (2016) 22285, https://doi.org/10.1038/srep22285.

[43] X. Zhang, J. Qin, T. Perasinjaroen, W. Aeksen, M. Kumar, R. Hao, M. Ma, R. Liu, Surface & Coatings Technology Preparation and hardness of pulse electrodeposited Ni – W – diamond composite coatings, Surf. Coat. Technol. 276 (2015) 228–232, https://doi.org/10.1016/j.surfcoat.2015.06.073.

[44] L. Kodandarama, M. Krishna, H.N. Narasimha Murthy, S.C. Sharma, Development and characterization of electrocodeposited nickel-based composites coatings, J. Mater. Eng. Perform. 21 (2012) 105–113, https://doi.org/10.1007/s11665-010-9820-0.

[45] T. Van Hau, P. Van Trinh, N.P. Hoai Nam, N. Van Tu, V.D. Lam, D.D. Phuong, P. N. Minh, B.H. Thang, Electrodeposited nickel–graphene nanocomposite coating: effect of graphene nanoplatelet size on its microstructure and hardness, RSC Adv. 10 (2020) 22080–22090, https://doi.org/10.1039/D0RA03776A.

[46] S. Paydar, A. Jafari, M.E. Bahrololoom, V. Mozafari, Influence of BN and B4C particulates on wear and corrosion resistance of electroplated nickel matrix composite coatings, Tribol. - Mater. Surfaces & Interfaces. 9 (2015) 105–110, https://doi.org/10.1179/1751584X15Y.0000000007.

[47] E. Saraloğlu Güler, E. Konca, I. Karakaya, Effect of electrodeposition parameters on the current density of hydrogen evolution reaction in Ni and Ni-MoS2 composite coatings, Int. J. Electrochem. Sci. 8 (2013) 5496–5505.

[48] M. Ma, W. Sun, Y. Zhang, X. Liu, Y. Dong, J. Zi, Y. Xiao, Effect of TiC Particles Concentration on Microstructure and Properties of Ni-TiC Composite Coatings, Mater. Res. 22 (2019), https://doi.org/10.1590/1980-5373-mr-2019-0530.

[49] H.S. Maharana, P.K. Katiyar, K. Mondal, Structure dependent super-hydrophobic and corrosion resistant behavior of electrodeposited Ni-MoSe2-MWCNT coating, Appl. Surf. Sci. 478 (2019) 26–37, https://doi.org/10.1016/j.apsusc.2019.01.166.

[50] H.S. Maharana, A. Basu, K. Mondal, Structural and tribological correlation of electrodeposited solid lubricating Ni-WSe2 composite coating, Surf. Coatings Technol. 349 (2018) 328–339, https://doi.org/10.1016/j.surfcoat.2018.06.005.

[51] I. Ali, M. Faraz Ud Din, Z.G. Gu,, MXenes Thin Films: From Fabrication to Their Applications, Molecules. 27 (2022) 1–38, https://doi.org/10.3390/molecules27154925.

[52] Y. Du, X. Zhang, L. Wei, B. Yu, Y. Wang, Y. Wang, S. Ye, Electrodeposition of a Ni-P composite coating reinforced with Ti3C2Tx@TiO2/MoS2 particles, Mater. Chem. Phys. 241 (2020), 122448. https://doi.org/10.1016/j.matchemphys.2019.122448.

[53] R.E. Daugherty, M.M. Zumbach, S.F. Sanders, T.D. Golden, PT, Surf. Coat. Technol. (2018) #pagerange#. https://doi.org/10.1016/j.surfcoat.2018.05.026.
[54] H. Li, Y. He, P. Luo, Y. Fan, L. Gou, Z. Li, Y. Zhao, B. Liu, T. He, H. Zhang, Preparation of laminar α-ZrP nanosheets enhanced Ni[sbnd]W nanocomposite coating and investigation of its mechanical and anti-corrosion properties, Surf. Coatings Technol. 423 (2021), https://doi.org/10.1016/j.surfcoat.2021.127590.
[55] B. Liu, S. Yan, Y. He, T. He, Y. He, R. Song, Z. Zhang, H. Li, J. Song, Z. Li, Study on wear resistance and corrosion resistance of zirconium phenylphosphonate reinforced Ni–W composite coating, Appl. Surf. Sci. 603 (2022), 154483. https://doi.org/10.1016/j.apsusc.2022.154483.
[56] A.J. Rethinam, G.N.K.R. Bapu, R.M. Krishnan, Deposition of nickel-mica electrocomposites and characterisation, Mater. Chem. Phys. 85 (2004) 251–256, https://doi.org/10.1016/S0254-0584(03)00334-1.
[57] V. Sorkin, H. Pan, H. Shi, S.Y. Quek, Y.W. Zhang, Nanoscale transition metal dichalcogenides: Structures, properties, and applications, Crit. Rev. Solid State Mater. Sci. 39 (2014) 319–367, https://doi.org/10.1080/10408436.2013.863176.
[58] R. Zhang, R. Cheung, Mechanical Properties and Applications of Two-Dimensional Materials, in: 2016: pp. 219–246. https://doi.org/10.5772/64017.
[59] Y. He, Electrodeposition of nickel-based composite coatings for tribological applications, Univ, Southampt, 2015.
[60] W. Chen, T. Yang, L.L. Dong, A. Elmasry, J. Song, N. Deng, A. Elmarakbi, X. Liu, H. Lv, Y. Fu, Advances in graphene reinforced metal matrix nanocomposites: Mechanisms, processing, modelling, properties and applications, Nanotechnol, Precis. Eng. 3 (2020) 189–210, https://doi.org/10.1016/j.npe.2020.12.003.
[61] A. Nieto, A. Bisht, D. Lahiri, C. Zhang, A. Agarwal, Graphene reinforced metal and ceramic matrix composites: a review, Int. Mater. Rev. 62 (2017) 241–302, https://doi.org/10.1080/09506608.2016.1219481.
[62] Y. Kim, J. Lee, M.S. Yeom, J.W. Shin, H. Kim, Y. Cui, J.W. Kysar, J. Hone, Y. Jung, S. Jeon, S.M. Han, Strengthening effect of single-atomic-layer graphene in metal-graphene nanolayered composites, Nat. Commun. 4 (2013), https://doi.org/10.1038/ncomms3114.
[63] S. Kumari, A. Panigrahi, S.K. Singh, S.K. Pradhan, Corrosion-Resistant Hydrophobic Nanostructured Ni-Reduced Graphene Oxide Composite Coating with Improved Mechanical Properties, J. Mater. Eng. Perform. 27 (2018) 5889–5897, https://doi.org/10.1007/s11665-018-3706-y.
[64] V.H. Pham, T. Gebre, J.H. Dickerson, Facile electrodeposition of reduced graphene oxide hydrogels for high-performance supercapacitors, Nanoscale. 7 (2015) 5947–5950, https://doi.org/10.1039/c4nr07508k.
[65] T. Magne, T. de Oliveira, L. Alencar, F. Junior, S. Gemini-Piperni, S. Carneiro, L. Dutra, R. Freire, K. Golokhvast, P. Metrangolo, P. Fechine, R. Santos-Oliveira, Graphene and its derivatives: understanding the main chemical and medicinal chemistry roles for biomedical applications, J. Nanostructure Chem. (2021), https://doi.org/10.1007/s40097-021-00444-3.
[66] A.K. Hussain, U.M.B. Al Naib, Recent developments in graphene based metal matrix composite coatings for corrosion protection application: A review, J. Met. Mater. Miner. 29 (2019) 1–9. https://doi.org/10.14456/jmmm.2019.27.
[67] A. Ambrosi, M. Pumera, The structural stability of graphene anticorrosion coating materials is compromised at low potentials, Chem. - A Eur. J. 21 (2015) 7896–7901, https://doi.org/10.1002/chem.201406238.
[68] A.T. Dideikin, A.Y. Vul',, Graphene oxide and derivatives: The place in graphene family, Front. Phys. 6 (2019), https://doi.org/10.3389/fphy.2018.00149.
[69] A.T. Smith, A.M. LaChance, S. Zeng, B. Liu, L. Sun, Synthesis, properties, and applications of graphene oxide/reduced graphene oxide and their nanocomposites, Nano, Mater. Sci. 1 (2019) 31–47, https://doi.org/10.1016/j.nanoms.2019.02.004.
[70] A., P. Sehrawat, s. S. Islam, P. Mishra, S. Ahmad,, Reduced graphene oxide (rGO) based wideband optical sensor and the role of Temperature, Defect States and Quantum Efficiency, Sci. Rep. 8 (2018), https://doi.org/10.1038/s41598-018-21686-2.
[71] D. Golberg, Y. Bando, Y. Huang, Z. Xu, X. Wei, L. Bourgeois, M.-S. Wang, H. Zeng, J. Lin, C. Zhi, Recent Advances in Boron Nitride Nanotubes and Nanosheets, Isr. J. Chem. 50 (2010) 405–416, https://doi.org/10.1002/ijch.201000049.
[72] V. Vatanpour, S.A.N. Mehrabani, B. Keskin, N. Arabi, B. Zeytuncu, I. Koyuncu, A Comprehensive Review on the Applications of Boron Nitride Nanomaterials in Membrane Fabrication and Modification, Ind. & Eng. Chem. Res. (2021).
[73] K. Zhang, Y. Feng, F. Wang, Z. Yang, J. Wang, Two dimensional hexagonal boron nitride (2D-hBN): synthesis{,} properties and applications, J. Mater. Chem. C. 5 (2017) 11992–12022, https://doi.org/10.1039/C7TC04300G.
[74] X.F. Jiang, Q. Weng, X. Bin Wang, X. Li, J. Zhang, D. Golberg, Y. Bando, Recent Progress on Fabrications and Applications of Boron Nitride Nanomaterials: A Review, J. Mater. Sci. Technol. 31 (2015) 589–598, https://doi.org/10.1016/j.jmst.2014.12.008.
[75] G. Gyawali, R. Adhikari, H.S. Kim, H.B. Cho, S.W. Lee, Effect of h-BN nanosheets codeposition on electrochemical corrosion behavior of electrodeposited nickel composite coatings, ECS Electrochem. Lett. 2 (2013), https://doi.org/10.1149/2.003303eel.
[76] Z. Shahri, S.R. Allahkaram, Effect of particles concentration and current density on the cobalt/hexagonal boron nitride nano-composite coatings properties, Iran. J. Mater. Sci. Eng. 9 (2012) 1–7.
[77] Y.K. Zhang, J.L. Li, D.S. Xiong, Y. Qin, Influence of boron nitride on tribological behavior of nickel-base composite coatings at high temperature, Mater. Sci. Forum. 686 (2011) 711–715, https://doi.org/10.4028/www.scientific.net/MSF.686.711.
[78] S. Manzeli, D. Ovchinnikov, D. Pasquier, O.V. Yazyev, A. Kis, 2D transition metal dichalcogenides, Nat. Rev. Mater. 2 (2017), https://doi.org/10.1038/natrevmats.2017.33.
[79] J. Sun, X. Li, W. Guo, M. Zhao, X. Fan, Y. Dong, C. Xu, J. Deng, Y. Fu, Synthesis methods of two-dimensional MoS2: A brief review, Crystals. 7 (2017) 1–11, https://doi.org/10.3390/cryst7070198.
[80] T. Onodera, Y. Morlta, A. Suzuki, M. Koyama, H. Tsuboi, N. Hatakeyama, A. Endou, H. Takaba, M. Kubo, F. Dassenoy, C. Minfray, L. Joly-Pottuz, J. M. Martin, A. Miyamoto, A computational chemistry study on friction of h-MoS2. Part I. Mechanism of single sheet lubrication, J. Phys. Chem. B. 113 (2009) 16526–16536, https://doi.org/10.1021/jp9069866.
[81] A. Gracco, M. Dandrea, F. Deflorian, C. Zanella, A. De Stefani, G. Bruno, E. Stellini, Application of a molybdenum and tungsten disulfide coating to improve tribological properties of orthodontic archwires, Nanomaterials. 9 (2019) 1–10, https://doi.org/10.3390/nano9050753.
[82] L. Rapoport, Y. Bilik, Y. Feldman, M. Homyonfer, S.R. Cohen, R. Tenne, Hollow nanoparticles of WS2 as potential solid-state lubricants, Nature. 387 (1997) 791–793, https://doi.org/10.1038/42910.
[83] X. Sun, Solid Lubricants for Space Mechanisms, in: Q.J. Wang, Y.-W. Chung (Eds.), Encycl. Tribol., Springer US, Boston, MA, 2013: pp. 3165–3172. https://doi.org/10.1007/978-0-387-92897-5_1230.
[84] J.R. Lince, Effective Application of Solid Lubricants in Spacecraft Mechanisms, Lubricants. 8 (2020), https://doi.org/10.3390/lubricants8070074.
[85] A. Joseph, M. Narayanasamy, B. Kirubasankar, S. Angaiah, Development of MoS Nanosheets Embedded Nickel Composite Coating and its Mechanical 2 Properties, ES Mater. Manuf. (2018) 2–8. https://doi.org/10.30919/esmm5f152.
[86] W. Zhang, P. Zhang, Z. Su, G. Wei, Synthesis and sensor applications of MoS2-based nanocomposites, Nanoscale. 7 (2015) 18364–18378, https://doi.org/10.1039/c5nr06121k.
[87] X. Wang, W. Xing, X. Feng, L. Song, Y. Hu, MoS2/Polymer Nanocomposites: Preparation, Properties, and Applications, Polym. Rev. 57 (2017) 440–466, https://doi.org/10.1080/15583724.2017.1309662.
[88] S. Xu, X. Gao, M. Hu, J. Sun, D. Jiang, F. Zhou, W. Liu, L. Weng, Nanostructured WS2–Ni composite films for improved oxidation, resistance and tribological performance, Appl. Surf. Sci. 288 (2014) 15–25, https://doi.org/10.1016/j.apsusc.2013.09.024.
[89] S. Domínguez-Meister, T.C. Rojas, M. Brizuela, J.C. Sánchez-López, Solid lubricant behavior of MoS2 and WSe2-based nanocomposite coatings, Sci. Technol. Adv. Mater. 18 (2017) 122–133, https://doi.org/10.1080/14686996.2016.1275784.
[90] O. Sadiku-Agboola, E.R. Sadiku, O.I. Ojo, O.L. Akanji, O.F. Biotidara, Influence of Operation parameters on Metal deposition in bright Nickel-plating Process, Port. Electrochim. Acta. 29 (2011) 91–100, https://doi.org/10.4152/pea.201102091.
[91] A. Juskowiak-Brenska, J. Lapinski, D. Pletcher, F.C. Walsh, Porosity of nickel electrodeposits on mild steel using electrochemical impedance spectroscopy, Trans. IMF. 90 (2012) 156–160, https://doi.org/10.1179/0020296712Z.0000000007.
[92] F.C. Walsh, C. Ponce De Leon, A review of the electrodeposition of metal matrix composite coatings by inclusion of particles in a metal layer: An established and diversifying technology, Trans. Inst. Met. Finish. 92 (2014) 83–98, https://doi.org/10.1179/0020296713Z.000000000161.
[93] C.T.J. Low, R.G.A. Wills, F.C. Walsh, Electrodeposition of composite coatings containing nanoparticles in a metal deposit, Surf. Coatings Technol. 201 (2006) 371–383, https://doi.org/10.1016/j.surfcoat.2005.11.123.
[94] N. Guglielmi, Kinetics of the Deposition of Inert Particles from Electrolytic Baths, J. Electrochem. Soc. 119 (1972) 1009, https://doi.org/10.1149/1.2404383.
[95] J.P. Celis, J.R. Roos, C. Buelens, A Mathematical Model for the Electrolytic Codeposition of Particles with a Metallic Matrix, J. Electrochem. Soc. 134 (1987) 1402–1408, https://doi.org/10.1149/1.2100680.
[96] J. Fransaer, J.P. Celis, J.R. Roos, Analysis of the Electrolytic Codeposition of Non-Brownian Particles with Metals, J. Electrochem. Soc. 139 (1992) 413–425, https://doi.org/10.1149/1.2069233.
[97] B.J. Hwang, C.S. Hwang, Mechanism of Codeposition of Silicon Carbide with Electrolytic Cobalt, J. Electrochem. Soc. 140 (1993) 979–984, https://doi.org/10.1149/1.2056239.
[98] P.M. Vereecken, I. Shao, P.C. Searson, Particle Codeposition in Nanocomposite Films, J. Electrochem. Soc. 147 (2000) 2572, https://doi.org/10.1149/1.1393570.
[99] P. Berçot, E. Peña-Muñoz, J. Pagetti, Electrolytic composite Ni–PTFE coatings: an adaptation of Guglielmi's model for the phenomena of incorporation, Surf. Coatings Technol. 157 (2002) 282–289, https://doi.org/10.1016/S0257-8972(02)00180-9.
[100] N.M. Schneider, J.H. Park, J.M. Grogan, D.A. Steingart, H.H. Bau, F.M. Ross, Nanoscale evolution of interface morphology during electrodeposition, Nat. Commun. 8 (2017) 1–10, https://doi.org/10.1038/s41467-017-02364-9.
[101] F.C. Walsh, C.P. de Leon, A review of the electrodeposition of metal matrix composite coatings by inclusion of particles in a metal layer: an established and diversifying technology, Trans. IMF. 92 (2014) 83–98, https://doi.org/10.1179/0020296713Z.000000000161.
[102] H. Mahdi, K. Salloomi, H. Husam, Improvement of Microhardness and Corrosion Resistance of Stainless Steel by Nanocomposite Coating, Al-Khawarizmi Eng. J. 10 (2014) 1–10.
[103] D.P. Barkey, Structure and Pattern Formation in Electrodeposition (2003), https://doi.org/10.1002/3527600264.ch3.
[104] U.S. Mohanty, B.C. Tripathy, P. Singh, A. Keshavarz, S. Iglauer, Roles of organic and inorganic additives on the surface quality, morphology, and polarization

behavior during nickel electrodeposition from various baths: a review, J. Appl. Electrochem. 49 (2019) 847–870, https://doi.org/10.1007/s10800-019-01335-w.
[105] C. Davalos, J. Lopez, H. Ruiz, A. Méndez-Albores, R. Antaño-López, G. Trejo, Study of the Role of Boric Acid During the Electrochemical Deposition of Ni in a Sulfamate Bath, Int. J. Electrochem. Sci. 8 (2013) 9785–9800.
[106] N. Watt, Nickel plating bath (2014) 64–67.
[107] T. Jv, Tribological Test and Mechanical Properties of Electrodeposited Nickel Coating on the Metal Surface of Carbon Steel 4140, Ann. Chem. Sci. Res. 1 (2019) 3–6. https://doi.org/10.31031/acsr.2019.01.000513.
[108] M.S. Hussain, Synthesis of bulk nanostructured materials by high speed turbulent flow-a method of electrodepositing nanocrystalline nickel, Elsevier Inc., 2018. https://doi.org/10.1016/B978-0-12-812792-6.00003-0.
[109] D. Sobha Jayakrishnan, Electrodeposition: the versatile technique for nanomaterials, Woodhead Publishing Limited, 2012. https://doi.org/10.1533/9780857095800.1.86.
[110] Y.D. Gamburg, G. Zangari, Theory and Practice of Metal Electrodeposition, Springer, New York, New York, NY (2011), https://doi.org/10.1007/978-1-4419-9669-5.
[111] C. Breitkopf, K. Swider-Lyons, Modern Electrochemistry, in: Springer Handb. Electrochem. Energy, Springer Berlin Heidelberg, Berlin, Heidelberg, 2017: pp. 11–30. https://doi.org/10.1007/978-3-662-46657-5_2.
[112] G.A. Di Bari, Electrodeposition of Nickel, Mod. Electroplat. Fifth Ed. (2011) 79–114. https://doi.org/10.1002/9780470602638.ch3.
[113] S. Awasthi, S.K. Pandey, C.P. Pandey, K. Balani, Progress in Electrochemical and Electrophoretic Deposition of Nickel with Carbonaceous Allotropes: A Review, Adv. Mater. Interfaces. 7 (2020) 1–33, https://doi.org/10.1002/admi.201901096.
[114] J. Li, Z. An, Z. Wang, M. Toda, T. Ono, Pulse-Reverse Electrodeposition and Micromachining of Graphene-Nickel Composite: An Efficient Strategy toward High-Performance Microsystem Application, ACS Appl. Mater. Interfaces. 8 (2016) 3969–3976, https://doi.org/10.1021/acsami.5b11164.
[115] A. Radisic, P.M. Vereecken, J.B. Hannon, P.C. Searson, F.M. Ross, Quantifying Electrochemical Nucleation and Growth of Nanoscale Clusters Using Real-Time Kinetic Data, Nano Lett. 6 (2006) 238–242, https://doi.org/10.1021/nl052175i.
[116] B. Li, D. Li, T. Mei, W. Xia, W. Zhang, Fabrication and characterization of boron nitride reinforced Ni–W nanocomposite coating by electrodeposition, J. Alloys Compd. 777 (2019) 1234–1244, https://doi.org/10.1016/j.jallcom.2018.11.081.
[117] A. Laszczyńska, J. Winiarski, B. Szczygieł, I. Szczygieł, Electrodeposition and characterization of Ni–Mo–ZrO 2 composite coatings, Appl. Surf. Sci. 369 (2016) 224–231, https://doi.org/10.1016/j.apsusc.2016.02.086.
[118] K. Jiang, J. Li, J. Liu, Electrochemical codeposition of graphene platelets and nickel for improved corrosion resistant properties, RSC Adv. 4 (2014) 36245, https://doi.org/10.1039/C4RA06043A.
[119] J. Zhou, G. Zhao, J. Li, J. Chen, S. Zhang, J. Wang, F.C. Walsh, S. Wang, Y. Xue, Electroplating of non-fluorinated superhydrophobic Ni/WC/WS2 composite coatings with high abrasive resistance, Appl. Surf. Sci. 487 (2019) 1329–1340, https://doi.org/10.1016/j.apsusc.2019.05.244.
[120] Y. He, W.T. Sun, S.C. Wang, P.A.S. Reed, F.C. Walsh, An electrodeposited Ni-P-WS2 coating with combined super-hydrophobicity and self-lubricating properties, Electrochim. Acta. 245 (2017) 872–882, https://doi.org/10.1016/j.electacta.2017.05.166.
[121] X. Zhou, Y. Shen, H. Jin, Y. Zheng, Microstructure and depositional mechanism of Ni–P coatings with nano-ceria particles by pulse electrodeposition, Trans. Nonferrous Met. Soc. China. 22 (2012) 1981–1988, https://doi.org/10.1016/S1003-6326(11)61417-9.
[122] Y. He, S.C. Wang, F.C. Walsh, Y.-L. Chiu, P.A.S. Reed, Self-lubricating Ni-P-MoS2 composite coatings, Surf. Coatings Technol. 307 (2016) 926–934, https://doi.org/10.1016/j.surfcoat.2016.09.078.
[123] Q. Cheng, Z. Yao, F. Zhang, S. Zhang, M. Oleksander, Microstructure and tribological property of Ni-MoS2 composite coatings prepared by ultrasonic and mechanical stirring electrodeposition, Mater. Res. Express. 6 (2019), https://doi.org/10.1088/2053-1591/ab4e2e.
[124] J. Kim, S. Kwon, D.H. Cho, B. Kang, H. Kwon, Y. Kim, S.O. Park, G.Y. Jung, E. Shin, W.G. Kim, H. Lee, G.H. Ryu, M. Choi, T.H. Kim, J. Oh, S. Park, S.K. Kwak, S.W. Yoon, D. Byun, Z. Lee, C. Lee, Direct exfoliation and dispersion of two-dimensional materials in pure water via temperature control, Nat. Commun. 6 (2015) 1–9, https://doi.org/10.1038/ncomms9294.
[125] A. Gomes, I. Pereira, B. Fernandez, R. Pereiro, Electrodeposition of Metal Matrix Nanocomposites: Improvement of the Chemical Characterization Techniques, in: Adv. Nanocomposites - Synth. Charact. Ind. Appl., InTech, 2011. https://doi.org/10.5772/15557.
[126] Z. Ji, L. Zhang, G. Xie, W. Xu, D. Guo, J. Luo, B. Prakash, Mechanical and tribological properties of nanocomposites incorporated with two-dimensional materials, Friction. 8 (2020) 813–846, https://doi.org/10.1007/s40544-020-0401-4.
[127] I. Scharf, M. Sieber, T. Lampke, Calculation approach for current-potential behaviour during pulse electrodeposition based on double-layer characteristics, Trans. Inst. Met. Finish. 92 (2014) 325–335, https://doi.org/10.1179/0020296714Z.000000000205.
[128] S.T. Aruna, P.V.K. Srikanth, M.J. Ahamad, S. Latha, K.S. Rajam, Optimization of the properties of electrodeposited Ni-YSZ composites using Taguchi method and regression analysis, Port. Electrochim. Acta. 29 (2011) 23–37, https://doi.org/10.4152/pea.201101023.
[129] S.K. Das, P. Sahoo, Influence of Process Parameters on Microhardness of Electroless Ni-B Coatings, Adv. Mech. Eng. 4 (2012), 703168, https://doi.org/10.1155/2012/703168.
[130] J. Antony, Full Factorial Designs, Second Edi, Elsevier Ltd (2014), https://doi.org/10.1016/b978-0-08-099417-8.00006-7.
[131] M. Poroch-Seritan, S. Gutt, G. Gutt, I. Cretescu, C. Cojocaru, T. Severin, Design of experiments for statistical modeling and multi-response optimization of nickel electroplating process, Chem. Eng. Res. Des. 89 (2011) 136–147, https://doi.org/10.1016/j.cherd.2010.05.010.
[132] S.L. Kuo, The influence of process parameters on the MoS2 content of Ni-MoS2 composite coating by the robust design method, J. Chinese Inst. Eng. Trans. Chinese Inst. Eng. A/Chung-Kuo K. Ch'eng Hsuch K'an. 27 (2004) 243–251, https://doi.org/10.1080/02533839.2004.9670869.
[133] N.M. Schneider, J. Hun Park, S. Kodambaka, H.H. Bau, F.M. Ross, Estimation of Nanoscale Current Density Distributions during Electrodeposition, Microsc. Microanal. 21 (2015) 2435–2436, https://doi.org/10.1017/s1431927615012957.
[134] M. Taşyürek, C. Nazik, Improvement of mechanical properties of CNT/epoxy nano composites using the B4C by Taguchi method, Mater. Sci. Forum. 900 MSF (2017) 105–109, https://doi.org/10.4028/www.scientific.net/MSF.900.105.
[135] F. Druesne, M. Afzali, Electroplating simulation and design tool, Proc. Inst. Mech. Eng. Part B J. Eng. Manuf. 217 (2003) 705–708, https://doi.org/10.1243/095440503322011434.
[136] S.M.J.S. Shourije, M.E. Bahrololoom, Comparison of effects of simulated electric field interference and presence of a barrier in the nickel electroplating process to experimental data, Trans. Inst. Met. Finish. (2020), https://doi.org/10.1080/00202967.2020.1819021.
[137] J. Lahiri, T.S. Miller, A.J. Ross, L. Adamska, I.I. Oleynik, M. Batzill, Graphene growth and stability at nickel surfaces, New J. Phys. 13 (2011) 25001, https://doi.org/10.1088/1367-2630/13/2/025001.
[138] M.H. Allahyarzadeh, M. Aliofkhazraei, A.R. Rezvanian, V. Torabinejad, A.r., Sabour Rouhaghdam, Ni-W electrodeposited coatings: Characterization, properties and applications, Surf. Coatings Technol. 307 (2016) 978–1010. https://doi.org/10.1016/j.surfcoat.2016.09.052.
[139] N.M. Schneider, J. Hun Park, J.M. Grogan, S. Kodambaka, D.A. Steingart, F. M. Ross, H.H. Bau, Visualization of Active and Passive Control of Morphology during Electrodeposition, Microsc. Microanal. 20 (2014) 1530–1531, https://doi.org/10.1017/S1431927614009386.
[140] C.R. Raghavendra, S. Basavarajappa, I. Sogalad, Electrodeposition of Ni-nano composite coatings: a review, Inorg. Nano-Metal Chem. 48 (2018) 583–598, https://doi.org/10.1080/24701556.2019.1567537.
[141] A. Yli-Pentti, Electroplating and Electroless Plating, Elsevier (2014), https://doi.org/10.1016/B978-0-08-096532-1.00413-1.
[142] V. Lins, E. Cecconello, T. Matencio, Effect of the Current Density on Morphology, Porosity, and Tribological Properties of Electrodeposited Nickel on Copper, J. Mater. Eng. Perform. 17 (2008) 741–745, https://doi.org/10.1007/s11665-008-9205-9.
[143] M.A. Ameer, Z.A. Hamid, M. Shehata, B.M. Hassan, A.M. Fekry, The impact of cationic surfactants on the electrodeposition of nickel/graphene nano-sheet composite coatings on brass, Egypt. J. Chem. 62 (2019) 201–214. https://doi.org/10.21608/ejchem.2018.4598.1404.
[144] X. Yu, Influence of Pulse Parameters on the Morphology and Corrosion Resistance of Nickel-Graphene Composite Coating, Int. J. Electrochem. Sci. 14 (2019) 4754–4768. https://doi.org/10.20964/2019.05.48.
[145] Y. Xuetao, W. Yu, S. Dongbai, Y. Hongying, Influence of pulse parameters on the microstructure and microhardness of nickel electrodeposits, Surf. Coatings Technol. 202 (2008) 1895–1903, https://doi.org/10.1016/j.surfcoat.2007.08.023.
[146] Z. Bai, B. Zhang, Fabrication of superhydrophobic reduced-graphene oxide/nickel coating with mechanical durability, self-cleaning and anticorrosion performance, Nano, Mater. Sci. 2 (2020) 151–158, https://doi.org/10.1016/j.nanoms.2019.05.001.
[147] J. Liang, D. Li, D. Wang, K. Liu, L. Chen, Preparation of stable superhydrophobic film on stainless steel substrate by a combined approach using electrodeposition and fluorinated modification, Appl. Surf. Sci. 293 (2014) 265–270, https://doi.org/10.1016/j.apsusc.2013.12.147.
[148] S. Esmailzadeh, S. Khorsand, K. Raeissi, F. Ashrafizadeh, Microstructural evolution and corrosion resistance of super-hydrophobic electrodeposited nickel films, Surf. Coatings Technol. 283 (2015) 337–346, https://doi.org/10.1016/j.surfcoat.2015.11.005.
[149] M.K. Tripathi, D.K. Singh, V.B. Singh, Electrodeposition of Ni-Fe/Bn nano-composite coatings from a non-aqueous bath and their characterization, Int. J. Electrochem. Sci. 8 (2013) 3454–3471.
[150] S. Paydar, A. Jafari, M.E. Bahrololoom, V. Mozafari, Enhancing Ni electroplated matrix through mixed boron nitride–carbide reinforcement, Vacuum. 92 (2013) 52–57, https://doi.org/10.1016/j.vacuum.2012.10.014.
[151] S. Paydar, A. Jafari, M.E. Bahrololoom, V. Mozafari, Influence of BN and B 4 C particulates on wear and corrosion resistance of electroplated nickel matrix composite coatings, Tribol. - Mater. Surfaces, Interfaces. 9 (2015) 105–110, https://doi.org/10.1179/1751584X15Y.0000000007.
[152] A.A. Aal, K.M. Ibrahim, Z.A. Hamid, Enhancement of wear resistance of ductile cast iron by Ni-SiC composite coating, Wear. 260 (2006) 1070–1075, https://doi.org/10.1016/j.wear.2005.07.022.
[153] S. Sangeetha, G.P. Kalaignan, Tribological and electrochemical corrosion behavior of Ni–W/BN (hexagonal) nano-composite coatings, Ceram. Int. 41 (2015) 10415–10424, https://doi.org/10.1016/j.ceramint.2015.04.089.

[154] S.M.J.S. Shourije, M.E. Bahrololoom, Effect of current density, MoS 2 content and bath agitation on tribological properties of electrodeposited nanostructured Ni-MoS 2 composite coatings, Tribol. - Mater. Surfaces, Interfaces. 13 (2019) 76–87, https://doi.org/10.1080/17515831.2019.1589160.

[155] Y. Liu, L. Ren, S. Yu, Z. Han, Influence of current density on nano-Al2O3/Ni+Co bionic gradient composite coatings by electrodeposition, J. Univ. Sci. Technol. Beijing Miner. Metall. Mater. (Eng Ed) 15 (2008) 633–637, https://doi.org/10.1016/S1005-8850(08)60118-8.

[156] B. Łosiewicz, G. Dercz, M. Popczyk, Electrodeposition of the Ni+MoS_2 Composite Electrocatalysts, Solid State Phenom. 228 (2015) 125–131, https://doi.org/10.4028/www.scientific.net/SSP.228.125.

[157] G. Zhao, Y. Xue, Y. Huang, Y. Ye, F.C. Walsh, J. Chen, S. Wang, One-step electrodeposition of a self-cleaning and corrosion resistant Ni/WS 2 superhydrophobic surface, RSC Adv. 6 (2016) 59104–59112, https://doi.org/10.1039/C6RA07899K.

[158] K. Rahimi Mamaghani, The Effect of Stirring Rate on Electrodeposition of Nanocrystalline Nickel Coatings and their Corrosion Behaviors and Mechanical Characteristics, Int. J. Electrochem. Sci. 12 (2017) 5023–5035. https://doi.org/10.20964/2017.06.68.

[159] C. Ken, D. Barker, F. Walshf, J. Archer, The electrodeposition of composite coatings based on metal matrix-included particle deposits, Trans. Inst. Met. Finish. 78 (2000) 171–178, https://doi.org/10.1080/00202967.2000.11871333.

[160] R.V. Williams, P.W. Martin, Electrodeposited Composite Coatings, Trans. IMF. 42 (1964) 182–188, https://doi.org/10.1080/00202967.1964.11869925.

[161] C. Buelens, J.P. Celis, J.R. Roos, Electrochemical aspects of the codeposition of gold and copper with inert particles, J. Appl. Electrochem. 13 (1983) 541–548, https://doi.org/10.1007/BF00617528.

[162] C. Zanella, M. Lekka, S. Rossi, F.D. Orian, Study of the influence of sonication during the electrod eposition of nickel matrix nanocomposite coatings on the protective properties, Corros. Rev. 29 (2011) 253–260, https://doi.org/10.1515/CORRREV.2011.005.

[163] E. Moti, M.H. Shariat, M.E. Bahrololoom, Electrodeposition of nanocrystalline nickel by using rotating cylindrical electrodes, Mater. Chem. Phys. 111 (2008) 469–474, https://doi.org/10.1016/j.matchemphys.2008.04.051.

[164] Y. Yao, S. Yao, L. Zhang, H. Wang, Electrodeposition and mechanical and corrosion resistance properties of Ni-W/SiC nanocomposite coatings, Mater. Lett. 61 (2007) 67–70, https://doi.org/10.1016/j.matlet.2006.04.007.

[165] M. Ghorbani, M. Mazaheri, K. Khangholi, Y. Kharazi, Electrodeposition of graphite-brass composite coatings and characterization of the tribological properties, Surf. Coatings Technol. 148 (2001) 71–76, https://doi.org/10.1016/S0257-8972(01)01322-6.

[166] L. Shi, C. Sun, P. Gao, F. Zhou, W. Liu, Mechanical properties and wear and corrosion resistance of electrodeposited Ni-Co/SiC nanocomposite coating, Appl. Surf. Sci. 252 (2006) 3591–3599, https://doi.org/10.1016/j.apsusc.2005.05.035.

[167] M.F. Cardinal, P.A. Castro, J. Baxi, H. Liang, F.J. Williams, Characterization and frictional behavior of nanostructured Ni-W-MoS2 composite coatings, Surf. Coatings Technol. 204 (2009) 85–90, https://doi.org/10.1016/j.surfcoat.2009.06.037.

[168] W. chang Sun, P. Zhang, K. Zhao, M. miao Tian, Y. Wang,, Effect of graphite concentration on the friction and wear of Ni-Al2O3/graphite composite coatings by a combination of electrophoresis and electrodeposition, Wear. 342–343 (2015) 172–180, https://doi.org/10.1016/j.wear.2015.08.020.

[169] E. García-Lecina, I. García-Urrutia, J.A. Díez, J. Fornell, E. Pellicer, J. Sort, Codeposition of inorganic fullerene-like WS2 nanoparticles in an electrodeposited nickel matrix under the influence of ultrasonic agitation, Electrochim. Acta. 114 (2013) 859–867, https://doi.org/10.1016/j.electacta.2013.04.088.

[170] A. Fahami, B. Nasiri-Tabrizi, M. Rostami, R. Ebrahimi-Kahrizsangi, Influence of Surfactants on the Characteristics of Nickel Matrix Nanocomposite Coatings, ISRN Electrochem. 2013 (2013) 1–8, https://doi.org/10.1155/2013/486050.

[171] P. Das, B. Samantaray, S. Dolai, K.S. Seshu, A. Prakash, S. Gollapudi, Combined Effect of Sodium Lauryl Sulphate and Saccharin on Microstructure and Corrosion Performance of Electrodeposited Nickel Prepared from Modified Watts Bath, Metall. Mater. Trans. A Phys. Metall. Mater. Sci. 52 (2021) 1913–1926, https://doi.org/10.1007/s11661-021-06202-y.

[172] J. Qin, X. Zhang, Y. Xue, K. Das, The high concentration and uniform distribution of diamond particles in Ni-diamond composite coatings by sediment co-deposition (2015) 331–339, https://doi.org/10.1002/sia.5712.

[173] N. Chronopoulou, D. Vozios, P. Schinas, E.A. Pavlatou, ScienceDirect Electrodeposition and characterization of electroplated Ni/Graphene composite coatings, Mater. Today Proc. 5 (2018) 27653–27661, https://doi.org/10.1016/j.matpr.2018.09.086.

[174] G. Yasin, M. Arif, M.N. Nizam, M. Shakeel, M.A. Khan, W.Q. Khan, T.M. Hassan, Z. Abbas, I. Farahbakhsh, Y. Zuo, Effect of surfactant concentration in electrolyte on the fabrication and properties of nickel-graphene nanocomposite coating synthesized by electrochemical co-deposition, RSC Adv. 8 (2018) 20039–20047, https://doi.org/10.1039/C7RA13651J.

[175] L.M. Wang, Effect of surfactant BAS on MoS2 codeposition behaviour, J. Appl. Electrochem. 38 (2008) 245–249, https://doi.org/10.1007/s10800-007-9432-z.

[176] C.F. Malfatti, H.M. Veit, T.L. Menezes, J. Zoppas Ferreira, J.S. Rodriguês, J. P. Bonino, The surfactant addition effect in the elaboration of electrodepositated NiP-SiC composite coatings, Surf. Coatings Technol. 201 (2007) 6318–6324, https://doi.org/10.1016/j.surfcoat.2006.11.040.

[177] E.S. Güler, E. Konca, I. Karakaya, Investigation of the tribological behaviour of electrocodeposited Ni-MoS2 composite coatings, Int. J. Surf. Sci. Eng. 11 (2017) 418.

[178] Y. He, S.C. Wang, F.C. Walsh, W.S. Li, L. He, P.A.S. Reed, The monitoring of coating health by in situ luminescent layers, RSC Adv. 5 (2015) 42965–42970, https://doi.org/10.1039/C5RA04475H.

[179] B. Abreu, B. Almeida, P. Ferreira, R.M.F. Fernandes, D.M. Fernandes, E. F. Marques, A critical assessment of the role of ionic surfactants in the exfoliation and stabilization of 2D nanosheets: The case of the transition metal dichalcogenides MoS2, WS2 and MoSe2, J. Colloid Interface Sci. 626 (2022) 167–177. https://doi.org/10.1016/j.jcis.2022.06.097.

[180] G.N.K. Ramesh Bapu, Characteristics of Ni-BN electrocomposites, Plat. Surf. Finish. 82 (1995) 70–73.

[181] W.H. Street, Electron micrographic examination of electrodeposited dispersion-hardened nickel 3 (1973) 137–141.

[182] E. Saraloğlu Güler, İ. Karakaya, E. Konca, Effects of current density, coating thickness, temperature, pH and particle concentration on internal stress during Ni–MoS 2 electrocodeposition, Surf. Eng. 30 (2014) 109–114, https://doi.org/10.1179/1743294413Y.0000000223.

[183] S.C. Wang, W.C.J. Wei, Kinetics of electroplating process of nano-sized ceramic particle/Ni composite, Mater. Chem. Phys. 78 (2003) 574–580, https://doi.org/10.1016/S0254-0584(01)00564-8.

[184] F.A. Lowenheim, S. Senderoff, Modern Electroplating, J. Electrochem. Soc. 111 (1964) 262C, https://doi.org/10.1149/1.2425993.

[185] E.S. Güler, Effects of Electroplating Characteristics on the Coating Properties, in: Electrodepos. Compos. Mater., InTech, 2016. https://doi.org/10.5772/61745.

[186] A. Jabbar, G. Yasin, W.Q. Khan, M.Y. Anwar, R.M. Korai, M.N. Nizam, G. Muhyodin, Electrochemical deposition of nickel graphene composite coatings effect of deposition temperature on its surface morphology and corrosion resistance, RSC Adv. 7 (2017) 31100–31109, https://doi.org/10.1039/c6ra28755g.

[187] J. Chen, J. Li, D. Xiong, Y. He, Y. Ji, Y. Qin, Preparation and tribological behavior of Ni-graphene composite coating under room temperature, Appl. Surf. Sci. 361 (2016) 49–56, https://doi.org/10.1016/j.apsusc.2015.11.094.

[188] M. Kumar, R. Li, J. Qin, X. Zhang, K. Das, A. Thueploy, S. Limpanart, Y. Boonyongmaneerat, M. Ma, R. Liu, Surface & Coatings Technology Effect of electrodeposition conditions on structure and mechanical properties of Ni-W/diamond composite coatings, Surf. Coat. Technol. 309 (2017) 337–343, https://doi.org/10.1016/j.surfcoat.2016.11.074.

[189] H. Abi-Akar, C. Riley, G. Maybee, Electrocodeposition of Nickel−Diamond and Cobalt−Chromium Carbide in Low Gravity, Chem. Mater. 8 (1996) 2601–2610, https://doi.org/10.1021/cm950483j.

[190] A. Rasooli, M.S. Safavi, S. Ahmadiyeh, A. Jalali, Evaluation of TiO2 Nanoparticles Concentration and Applied Current Density Role in Determination of Microstructural, Mechanical, and Corrosion Properties of Ni–Co Alloy Coatings, Prot. Met. Phys. Chem. Surfaces. 56 (2020) 320–327, https://doi.org/10.1134/S2070205120020215.

[191] B. Szeptycka, A. Gajewska-Midzialek, T. Babul, Electrodeposition and Corrosion Resistance of Ni-Graphene Composite Coatings, J. Mater. Eng. Perform. 25 (2016) 3134–3138, https://doi.org/10.1007/s11665-016-2009-4.

[192] K.S. Jyotheender, C. Srivastava, Ni-graphene oxide composite coatings: Optimum graphene oxide for enhanced corrosion resistance, Compos. Part B Eng. 175 (2019), 107145, https://doi.org/10.1016/j.compositesb.2019.107145.

[193] A. Gupta, C. Srivastava, Enhanced corrosion resistance by SnCu-graphene oxide composite coatings, Thin Solid Films. 669 (2019) 85–95, https://doi.org/10.1016/j.tsf.2018.10.036.

[194] A. Gupta, C. Srivastava, Optimum amount of graphene oxide for enhanced corrosion resistance by tin-graphene oxide composite coatings, Thin Solid Films. 661 (2018) 98–107, https://doi.org/10.1016/j.tsf.2018.07.016.

[195] G. Cieślak, M. Trzaska, Preparation and properties of nanocrystalline Ni/graphene composite coatings deposited by electrochemical method, Polish, J Chem. Technol. 20 (2018) 29–34, https://doi.org/10.2478/pjct-2018-0005.

[196] L. Meng, Q. Hu, C. Shi, C. Huang, Roles of Graphene Additives in Optimizing the Microstructure and Properties of Ni–Cr–Graphene Coatings, Coatings. 10 (2020) 104, https://doi.org/10.3390/coatings10020104.

[197] H. Algul, M. Tokur, S. Ozcan, M. Uysal, T. Cetinkaya, H. Akbulut, A. Alp, The effect of graphene content and sliding speed on the wear mechanism of nickel-graphene nanocomposites, Appl. Surf. Sci. 359 (2015) 340–348, https://doi.org/10.1016/j.apsusc.2015.10.139.

[198] C.Y. Ma, D.Q. Zhao, F.F. Xia, H. Xia, T. Williams, H.Y. Xing, Ultrasonic-assisted electrodeposition of Ni-Al2O3 nanocomposites at various ultrasonic powers, Ceram. Int. 46 (2020) 6115–6123, https://doi.org/10.1016/j.ceramint.2019.11.075.

[199] Z. Chen, F. Tian, A. Hu, M. Li, A facile process for preparing superhydrophobic nickel films with stearic acid, Surf. Coatings Technol. 231 (2013) 88–92, https://doi.org/10.1016/j.surfcoat.2012.01.053.

[200] S. Ding, T. Xiang, C. Li, S. Zheng, J. Wang, M. Zhang, C. Dong, W. Chan, Fabrication of self-cleaning super-hydrophobic nickel/graphene hybrid film with improved corrosion resistance on mild steel, Mater. Des. 117 (2017) 280–288. https://doi.org/10.1016/j.matdes.2016.12.084.

[201] B. Bhushan, E.K. Her, Fabrication of superhydrophobic surfaces with high and low adhesion inspired from rose petal, Langmuir. 26 (2010) 8207–8217, https://doi.org/10.1021/la904585j.

[202] W. Wang, F.-Y. Hou, H. Wang, H.-T. Guo, Fabrication and characterization of Ni–ZrO 2 composite nano-coatings by pulse electrodeposition, Scr. Mater. - Scr. MATER. 53 (2005) 613–618, https://doi.org/10.1016/j.scriptamat.2005.04.002.

[203] L. Feng, Y.Y. Ren, Y.H. Zhang, S. Wang, L. Li, Direct correlations among the grain size, texture, and indentation behavior of nanocrystalline nickel coatings, Metals (Basel). 9 (2019), https://doi.org/10.3390/met9020188.

[204] S.K. Singh, S. Samanta, A.K. Das, R.R. Sahoo, Electrodeposited {SiC}-graphene oxide composite in nickel matrix for improved tribological applications, Surf. Topogr. Metrol. Prop. 7 (2019) 35004, https://doi.org/10.1088/2051-672x/ab302d.
[205] S. Singh, S. Samanta, A.K. Das, R.R. Sahoo, Tribological investigation of Ni-graphene oxide composite coating produced by pulsed electrodeposition, Surfaces and Interfaces. 12 (2018) 61–70. https://doi.org/10.1016/j.surfin.2018.05.001.
[206] L. Xiang, Q. Shen, Y. Zhang, W. Bai, C. Nie, One-step electrodeposited Ni-graphene composite coating with excellent tribological properties, Surf. Coatings Technol. 373 (2019) 38–46, https://doi.org/10.1016/j.surfcoat.2019.05.074.
[207] G.N.K. Ramesh Bapu, Electrocodeposition and characterization of nickel-titanium carbide composites, Surf. Coatings Technol. 67 (1994) 105–110. https://doi.org/10.1016/S0257-8972(05)80033-7.
[208] J. Sort, J. Nogués, S. Suriñach, M.D. Baró, Microstructural aspects of the hcp-fcc allotropic phase transformation induced in cobalt by ball milling, Philos. Mag. 83 (2003) 439–455, https://doi.org/10.1080/0141861021000047159.
[209] E. Pavlatou, M. Stroumbouli, P. Gyftou, N. Spyrellis, Hardening Effect Induced by Incorporation of SiC Particles in Ni Electrodeposits, J. Appl. Electrochem. 36 (2006) 385–394, https://doi.org/10.1007/s10800-005-9082-y.
[210] M. Narayanasamy, B. Kirubasankar, A. Joseph, C. Yan, S. Angaiah, Influence of pulse reverse current on mechanical and corrosion resistance properties of Ni-MoSe2 nanocomposite coatings, Appl. Surf. Sci. 493 (2019) 225–230, https://doi.org/10.1016/j.apsusc.2019.06.239.
[211] S. Ramalingam, K. Balakrishnan, A. Subramania, Mechanical and corrosion resistance properties of electrodeposited Cu–ZrO2 nanocomposites, Trans. IMF. 93 (2015) 262–266, https://doi.org/10.1080/00202967.2015.1114727.
[212] C.R. Raghavendra, S. Basavarajappa, I. Sogalad, S. Kumar, A review on Ni based nano composite coatings, Mater. Today Proc. 39 (2021) 6–16. https://doi.org/10.1016/j.matpr.2020.04.810.
[213] D.R. S, prof V.S. Muralidharan, S. Angaiah,, Electrodeposition and characterization of Cu-TiO 2 nanocomposite coatings, J. Solid State Electrochem. - J SOLID STATE, Electrochem. 13 (2009) 1777–1783, https://doi.org/10.1007/s10008-009-0870-x.
[214] O. Fayyaz, A. Khan, R. Shakoor, A. Hasan, M. Yusuf, M. Montemor, S. Rasul, K. Khan, M.R. Faruque, P. Okonkwo, Enhancement of mechanical and corrosion resistance properties of electrodeposited Ni–P–TiC composite coatings, Sci. Rep. 11 (2021), https://doi.org/10.1038/s41598-021-84716-6.
[215] N.K. Ngo, S. Shao, H. Conrad, S.F. Sanders, F. D'Souza, T.D. Golden, Synthesis, characterization, and the effects of organo-grafted nanoparticles in nickel coatings for enhanced corrosion protection, Mater. Today Commun. 25 (2020), 101628, https://doi.org/10.1016/j.mtcomm.2020.101628.
[216] I. Gurrappa, L. Binder, Electrodeposition of nanostructured coatings and their characterization - A review, Sci. Technol. Adv. Mater. 9 (2008), https://doi.org/10.1088/1468-6996/9/4/043001.
[217] A. Behera, P. Mallick, S.S. Mohapatra, Nanocoatings for anticorrosion, Corros. Prot. Nanoscale. (2020) 227–243, https://doi.org/10.1016/b978-0-12-819359-4.00013-1.
[218] W. Jiang, L. Shen, M. Qiu, M. Xu, Z. Tian, Microhardness, wear, and corrosion resistance of Ni–SiC composite coating with magnetic-field-assisted jet electrodeposition, Mater. Res. Express. 5 (2018), 096407, https://doi.org/10.1088/2053-1591/aad72c.
[219] Y.B. Zeng, N.S. Qu, X.Y. Hu, Preparation and characterization of electrodeposited Ni-CeO2 nanocomposite coatings with high current density, Int. J. Electrochem. Sci. 9 (2014) 8145–8154.
[220] S.T. Aruna, C.N. Bindu, V. Ezhil Selvi, V.K. William Grips, K.S. Rajam, Synthesis and properties of electrodeposited Ni/ceria nanocomposite coatings, Surf. Coatings Technol. 200 (2006) 6871–6880, https://doi.org/10.1016/j.surfcoat.2005.10.035.
[221] M. Raja, G.N.K. Ramesh Bapu, J. Maharaja, R. Sekar, Electrodeposition and characterisation of Ni–TiC nanocomposite using Watts bath, Surf. Eng. 30 (2014) 697–701, https://doi.org/10.1179/1743294414Y.0000000265.
[222] I. Birlik, N.F. Ak Azem, M. Toparli, E. Celik, T. Koc Delice, S. Yildirim, O. Bardakcioglu, T. Dikici, Preparation and Characterization of Ni–TiO2 Nanocomposite Coatings Produced by Electrodeposition Technique, Front. Mater. 3 (2016), https://doi.org/10.3389/fmats.2016.00046.
[223] B. Kucharska, A. Brojanowska, K. Popławski, J.R. Sobiecki, Corrosion Resistance of Ni/Al2O3 Nanocomposite Coatings, Mater. Sci. 22 (2016), https://doi.org/10.5755/j01.ms.22.1.7407.
[224] R. Sukanya, T.N. Barwa, Y. Luo, E. Dempsey, C.B. Breslin, Emerging Layered Materials and Their Applications in the Corrosion Protection of Metals and Alloys, Sustainability. 14 (2022), https://doi.org/10.3390/su14074079.
[225] S. Kim, A comparison of the corrosion behaviour of polycrystalline and nanocrystalline cobalt, Scr. Mater. 48 (2003) 1379–1384, https://doi.org/10.1016/S1359-6462(02)00651-6.
[226] C.M.P. Kumar, T.V. Venkatesha, R. Shabadi, Preparation and corrosion behavior of Ni and Ni–graphene composite coatings, Mater. Res. Bull. 48 (2013) 1477–1483, https://doi.org/10.1016/j.materresbull.2012.12.064.
[227] G. Yasin, M. Arif, M. Shakeel, Y. Dun, Y. Zuo, W.Q. Khan, Y. Tang, A. Khan, M. Nadeem, Exploring the Nickel-Graphene Nanocomposite Coatings for Superior Corrosion Resistance: Manipulating the Effect of Deposition Current Density on its Morphology, Mechanical Properties, and Erosion-Corrosion Performance, Adv. Eng. Mater. 20 (2018) 1701166, https://doi.org/10.1002/adem.201701166.
[228] M.Y. Rekha, C. Srivastava, High corrosion resistance of metal-graphene oxide-metal multilayer coatings, Philos. Mag. 100 (2020) 18–31, https://doi.org/10.1080/14786435.2019.1663375.
[229] C. Cui, A.T.O. Lim, J. Huang, A cautionary note on graphene anti-corrosion coatings, Nat. Nanotechnol. 12 (2017) 834–835, https://doi.org/10.1038/nnano.2017.187.
[230] M. Schriver, W. Regan, W.J. Gannett, A.M. Zaniewski, M.F. Crommie, A. Zettl, Graphene as a long-term metal oxidation barrier: Worse than nothing, ACS Nano. 7 (2013) 5763–5768, https://doi.org/10.1021/nn4014356.
[231] F. Zhou, Z. Li, G.J. Shenoy, L. Li, H. Liu, Enhanced room-temperature corrosion of copper in the presence of graphene, ACS Nano. 7 (2013) 6939–6947, https://doi.org/10.1021/nn402150t.
[232] B. Kulyk, M.A. Freitas, N.F. Santos, F. Mohseni, A.F. Carvalho, K. Yasakau, A.J. S. Fernandes, A. Bernardes, B. Figueiredo, R. Silva, J. Tedim, F.M. Costa, A critical review on the production and application of graphene and graphene-based materials in anti-corrosion coatings, Crit. Rev. Solid State Mater. Sci. (2021) 1–48, https://doi.org/10.1080/10408436.2021.1886046.
[233] S. ArunKumar, V. Jegathish, R. Soundharya, M. JesyAlka, C. Arul, S. Sathyanarayanan, S. Mayavan, Evaluating the performance of MoS2 based materials for corrosion protection of mild steel in an aggressive chloride environment, RSC Adv. 7 (2017) 17332–17335, https://doi.org/10.1039/c7ra01372h.
[234] D. Zhang, L. Wang, H. Qian, X. Li, Superhydrophobic surfaces for corrosion protection: a review of recent progresses and future directions, J. Coatings Technol. Res. 13 (2016) 11–29, https://doi.org/10.1007/s11998-015-9744-6.
[235] H. Li, Y. He, Y. Fan, W. Xu, Q. Yang, Pulse electrodeposition and corrosion behavior of Ni–W/MWCNT nanocomposite coatings, RSC Adv. 5 (2015) 68890–68899, https://doi.org/10.1039/C5RA09462C.
[236] K. Sayfidinov, S.D. Cezan, B. Baytekin, H.T. Baytekin, Minimizing friction, wear, and energy losses by eliminating contact charging, Sci. Adv. 4 (2018).
[237] D. Roy, A.K. Das, R. Saini, P.K. Singh, P. Kumar, M. Hussain, A. Mandal, A. R. Dixit, Pulse current co-deposition of Ni-WS 2 nano-composite film for solid lubrication, Mater. Manuf. Process. 32 (2017) 365–372, https://doi.org/10.1080/10426914.2016.1198011.
[238] A. Siddaiah, P. Kumar, A. Henderson, M. Misra, P.L. Menezes, Surface Energy and Tribology of Electrodeposited Ni and Ni–Graphene Coatings on Steel, Lubricants. 7 (2019), https://doi.org/10.3390/lubricants7100087.
[239] I. Tudela, Y. Zhang, M. Pal, I. Kerr, A.J. Cobley, Ultrasound-assisted electrodeposition of thin nickel-based composite coatings with lubricant particles, Surf. Coatings Technol. 276 (2015) 89–105, https://doi.org/10.1016/j.surfcoat.2015.06.030.
[240] S. Soni, M. Agarwal, Lubricants from renewable energy sources – a review, Green Chem. Lett. Rev. 7 (2014) 359–382, https://doi.org/10.1080/17518253.2014.959565.
[241] C. Group, A. Hills, Encyclopedia of Tribology (2013), https://doi.org/10.1007/978-0-387-92897-5.
[242] P.L. Menezes, P.K. Rohatgi, E. Omrani, Self-Lubricating Composites, Springer, Berlin Heidelberg, Berlin, Heidelberg (2018), https://doi.org/10.1007/978-3-662-56528-5.
[243] E.Y. Liu, Y.M. Gao, W.Z. Wang, X.L. Zhang, X. Wang, G.W. Yi, J.H. Jia, Effect of the synergetic action on tribological characteristics of Ni-based composites containing multiple-lubricants, Tribol. Lett. 47 (2012) 399–408, https://doi.org/10.1007/s11249-012-9991-y.
[244] L. Rapoport, N. Fleischer, R. Tenne, Applications of WS2 (MoS2) inorganic nanotubes and fullerene-like nanoparticles for solid lubrication and for structural nanocomposites, J. Mater. Chem. 15 (2005) 1782–1788, https://doi.org/10.1039/B417488G.
[245] J.H. Lee, D.H. Cho, B.H. Park, J.S. Choi, Nanotribology of 2D materials and their macroscopic applications, J. Phys. D. Appl. Phys. 53 (2020), https://doi.org/10.1088/1361-6463/ab9670.
[246] L. Liu, M. Zhou, L. Jin, L. Li, Y. Mo, G. Su, X. Li, H. Zhu, Y. Tian, Recent advances in friction and lubrication of graphene and other 2D materials: Mechanisms and applications, Friction. 7 (2019) 199–216, https://doi.org/10.1007/s40544-019-0268-4.
[247] J. Sun, S. Du, Application of graphene derivatives and their nanocomposites in tribology and lubrication: A review, RSC Adv. 9 (2019) 40642–40661, https://doi.org/10.1039/c9ra05679c.
[248] S. Cui, W.S. Li, L. He, L. Feng, G.S. An, W. Hu, C.X. Hu, Tribological behavior of a Ni-WS2 composite coating across wide temperature ranges, Rare Met. 38 (2019) 1078–1085, https://doi.org/10.1007/s12598-018-1152-5.
[249] Z. Xu, Q. Zhang, X. Shi, W. Zhai, K. Yang, Tribological Properties of TiAl Matrix Self-Lubricating Composites Containing Multilayer Graphene and Ti3SiC2 at High Temperatures, Tribol. Trans. 58 (2015) 1131–1141, https://doi.org/10.1080/10402004.2015.1046007.
[250] T. Thana, KarunaTuchinda, Study of the effect of MoS2 and PTFE based coatings on adhesive wear of stainless steel, Appl. Mech. Mater. 302 (2013) 216–222, https://doi.org/10.4028/www.scientific.net/AMM.302.216.
[251] Y. Jia, L. Chen, X. Feng, H. Zhou, J. Chen, Tribological behavior of molybdenum disulfide bonded solid lubricating coatings cured with organosiloxane-modified phosphate binder, RSC Adv. 5 (2015) 69606–69615, https://doi.org/10.1039/c5ra08727a.
[252] N. Zhou, S. Wang, F.C. Walsh, Effective particle dispersion via high-shear mixing of the electrolyte for electroplating a nickel-molybdenum disulphide composite, Electrochim. Acta. 283 (2018) 568–577, https://doi.org/10.1016/j.electacta.2018.06.187.
[253] I. Tudela, A.J. Cobley, Y. Zhang, Tribological performance of novel nickel-based composite coatings with lubricant particles, Friction. 7 (2019) 169–180, https://doi.org/10.1007/s40544-018-0211-0.

[254] C. Hu, X. Xie, H. Zheng, Y. Qing, K. Ren, Facile fabrication of superhydrophobic zinc coatings with corrosion resistanceviaan electrodeposition process, New J. Chem. 44 (2020) 8890–8901, https://doi.org/10.1039/d0nj00561d.
[255] S. Khorsand, K. Raeissi, F. Ashrafizadeh, Corrosion resistance and long-term durability of super-hydrophobic nickel film prepared by electrodeposition process, Appl. Surf. Sci. 305 (2014) 498–505, https://doi.org/10.1016/j.apsusc.2014.03.123.
[256] T. Hang, A. Hu, H. Ling, M. Li, D. Mao, Super-hydrophobic nickel films with micro-nano hierarchical structure prepared by electrodeposition, Appl. Surf. Sci. 256 (2010) 2400–2404, https://doi.org/10.1016/j.apsusc.2009.10.074.
[257] A.B.D. Cassie, S. Baxter, Wettability of porous surfaces, Trans. Faraday Soc. 40 (1944) 546–551, https://doi.org/10.1039/TF9444000546.
[258] C. Gu, J. Tu, One-Step Fabrication of Nanostructured Ni Film with Lotus Effect from Deep Eutectic Solvent, Langmuir. 27 (2011) 10132–10140, https://doi.org/10.1021/la200778a.
[259] M.J. Nine, M.A. Cole, L. Johnson, D.N.H. Tran, D. Losic, Robust Superhydrophobic Graphene-Based Composite Coatings with Self-Cleaning and Corrosion Barrier Properties, ACS Appl, Mater. & Interfaces. 7 (2015) 28482–28493, https://doi.org/10.1021/acsami.5b09611.
[260] N. Xu, D.K. Sarkar, X.G. Chen, W.P. Tong, Corrosion performance of superhydrophobic nickel stearate/nickel hydroxide thin films on aluminum alloy by a simple one-step electrodeposition process, Surf. Coatings Technol. 302 (2016) 173–184, https://doi.org/10.1016/j.surfcoat.2016.05.050.
[261] L. Dong, D. Yang, H. Lu, Superhydrophobic Graphene-Based Materials: Surface Construction and Functional Applications, Adv. Mater. 25 (2013) 5352–5359, https://doi.org/10.1002/adma.201302804.
[262] Y. Xiao, P. Yao, K. Fan, H. Zhou, M. Deng, Z. Jin, Powder metallurgy processed metal-matrix friction materials for space applications, Friction. 6 (2018) 219–229, https://doi.org/10.1007/s40544-017-0171-9.
[263] P. Nguyen-Tri, T.A. Nguyen, P. Carriere, C. Ngo Xuan, Nanocomposite Coatings: Preparation, Characterization, Properties, and Applications, Int. J. Corros. (2018 (2018)) 1–19, https://doi.org/10.1155/2018/4749501.
[264] E. Omrani, A.D. Moghadam, P.L. Menezes, P.K. Rohatgi, Influences of graphite reinforcement on the tribological properties of self-lubricating aluminum matrix composites for green tribology, sustainability, and energy efficiency—a review, Int. J. Adv. Manuf. Technol. 83 (2016) 325–346, https://doi.org/10.1007/s00170-015-7528-x.
[265] R. Oriňáková, A. Turoňová, D. Kladeková, M. Gálová, R.M. Smith, Recent developments in the electrodeposition of nickel and some nickel-based alloys, J. Appl. Electrochem. 36 (2006) 957–972, https://doi.org/10.1007/s10800-006-9162-7.
[266] M.A.M. Ibrahim, R.M. Al Radadi, Role of glycine as a complexing agent in nickel electrodeposition from acidic sulphate bath, Int. J. Electrochem. Sci. 10 (2015) 4946–4971.
[267] J.K. Luo, M. Pritschow, A.J. Flewitt, S.M. Spearing, N.A. Fleck, W.I. Milne, Effects of Process Conditions on Properties of Electroplated Ni Thin Films for Microsystem Applications, J. Electrochem. Soc. 153 (2006) D155, https://doi.org/10.1149/1.2223302.
[268] Z. Zhang, H. Dong, Recent development in low friction and wear-resistant coatings and surfaces for high-Temperature forming tools, Manuf. Rev. 1 (2014), https://doi.org/10.1051/mfreview/2015001.
[269] N. Malatji, P.A.I. Popoola, Tribological and Corrosion Performance of Electrodeposited Nickel Composite Coatings, Electrodepos. Compos. Mater. (2016), https://doi.org/10.5772/62170.

Journal of Industrial and Engineering Chemistry 135 (2024) 425–433

Contents lists available at ScienceDirect

Journal of Industrial and Engineering Chemistry

journal homepage: www.elsevier.com/locate/jiec

Fabrication of a robust superhydrophobic stainless steel mesh for efficient oil/water separation

Revathy Sreekumar [a,b], Swapna Eravath Thazhakkuni [a], Sreejakumari Sukumaran Suseelamma [a,b,*]

[a] *Materials Science and Technology Division, CSIR–National Institute for Interdisciplinary Science and Technology (NIIST), Thiruvananthapuram 695019, India*

[b] *Academy of Scientific and Innovative Research (AcSIR), Ghaziabad 201002, India*

ARTICLE INFO

Keywords:
Electrodeposition
Superhydrophobicity
Robust
Self-cleaning
Stainless steel mesh
Oil–water separation

ABSTRACT

Selective oil removal from water is a critical problem in the realm of environmental science and engineering. Metallic meshes are commonly used as potential oil–water separators due to their low cost and good mechanical properties. Meshes with selective wettability can effectively remove oil or water from their mixtures easily using gravity-based filtration. In this work, a mechanically robust Ni-WS_2 based superhydrophobic stainless steel mesh (SHSM) has been developed via one-step electrodeposition. The surface morphologies, surface roughness, phase composition, and wettability were studied using Scanning Electron Microscopy (SEM), Atomic Force Microscopy (AFM), X-ray diffraction (XRD), and Water Contact Angle (WCA) measurements respectively. A high water contact angle of 169.5° with excellent superhydrophobic and superoleophilic properties was achieved by tuning the surface morphology of the mesh. The oil/water separation performance of the developed SHSM was studied and the efficiency was greater than 98% even after multiple uses. Further, the SHSM is highly corrosion-resistant and exhibits self-cleaning properties with excellent mechanical and chemical stability against strong acidic/alkaline solutions. Thus, the developed multifunctional SHSM demonstrates its potential at industrial-level applications of oil–water separation under harsh environments.

Introduction

There is a growing interest in technologies for treating oily wastewater as the oil industry is one of the leading contributors to environmental pollution. The processing of oily wastewater sources is extensive, as oil industries, oil refineries, storage, transportation, and petrochemical industries produce substantial quantities of greasy wastewater during the production process. The following are the main ways in which oil pollution appears: (1) affecting the quality of potable water and groundwater reserves; (2) harming aquatic resources; (3) adversely affecting people's health; (4) environmental pollution; (5) influencing agricultural yield [1]. Floatation, gravity separation, centrifugation, filtration flocculation, and electrochemical techniques are examples of traditional oil/water separation methods [2–5]. Nevertheless, the majority of the techniques have limitations, including minimal separation efficiency and complicated operation. Compared to traditional methods, membrane filtration is facile and effective in the separation of oil–water mixtures. With the advancement of the interface theory along with the perspective of membrane wettability, filtration membranes with concurrent and opposite affinity to both oil and water are more efficient for their separation [6,7]. Furthermore, superhydrophobic and superoleophilic surfaces have resulted in remarkable research findings in the area of filtration due to their superior self-cleaning properties [8,9]. Oil-water separation could be easily and effectively carried out by designing

Abbreviations: SHSM, superhydrophobic stainless steel mesh; SEM, scanning electron microscopy; AFM, atomic force microscopy; XRD, x-ray diffraction; WCA, water contact angle; CVD, chemical vapour deposition; PTFE, polytetrafluoroethylene; PVAc, polyvinyl acetate; PVA, polyvinyl alcohol; CTAB, cetyltrimethylammonium bromide; SSM, stainless steel mesh; MB, methylene blue; MA, myristic acid; EDS, energy dispersive spectroscopy; DCM, dichloromethane; HDTMS, hexadecyltrimethoxysilane; TEOS, tetraethyl orthosilicate; PFOA, perfluorooctanoic acid.

* Corresponding author at: Materials Science and Technology Division, CSIR–National Institute for Interdisciplinary Science and Technology (NIIST), Thiruvananthapuram 695019, India.

E-mail addresses: revathyias26@gmail.com (R. Sreekumar), ekswapna1999@gmail.com (S. Eravath Thazhakkuni), sreejakumari@niist.res.in (S. Sukumaran Suseelamma).

https://doi.org/10.1016/j.jiec.2024.01.054
Received 5 October 2023; Received in revised form 5 January 2024; Accepted 24 January 2024
Available online 26 January 2024

surfaces with special wettability [10,11].

In the past several years, numerous methods such as chemical etching [12], zeolite-coated method [13], electro-spinning [14], chemical vapor deposition (CVD) [15–17], self-assembly [18], sol – gel method [19], electrodeposition [20,21], etc are being reported for the development of superhydrophobic metallic mesh surfaces for oil – water separation. Among the metallic meshes, stainless steel meshes are more popular because of their easy availability, exceptional mechanical strength, and high efficiency.

Recently, there have been numerous studies on surface modification of stainless steel meshes for oil–water separation. For instance, Jiang et al. [22] developed a stainless steel mesh having both superhydrophobic and superoleophilic properties employing an emulsion of polytetrafluoroethylene (PTFE), polyvinyl acetate (PVAc) and polyvinyl alcohol (PVA) by spray method for oil–water separation. Using silica particles, Li et al. [23] designed highly hydrophobic and superoleophilic steel meshes for oil–water separation. Zhang et al. [24] fabricated a self-cleaning underwater superoleophobic stainless steel mesh surface using layer-by-layer assembly with sodium silicate and TiO_2 nanoparticles. Liu et al. [25] designed superhydrophobic and superoleophilic stainless steel mesh surfaces by immersing in a solution of $CuCl_2$ and HCl followed by modifying the surface with stearic acid. Nature-inspired superhydrophobic micro-scale artificial hairs with eggbeater heads were fabricated by a special three-dimensional (3D) printing process by Yang et al. [26]. However, these fabrication methods are costly, usually involving complex processes or rigorous conditions, in most cases requiring special equipment or materials, affecting their applicability [27–29].

Out of all the methods available for developing superhydrophobic surfaces, electrodeposition has specific advantages since this is an easy and quick process with high repeatability and is economical, as well as the ability to achieve a wide range of surface morphologies with high durability [30]. There are quite a few studies on the development of superhydrophobic nickel surfaces by electrodeposition [31,32].

In the present work, we present a novel strategy for developing superhydrophobic-superoleophilic Ni-WS_2 coated stainless steel mesh using one-step electrodeposition that will effectively resolve the long-term issue of oil–water separation in harsh conditions.WS_2 nanoparticles with tunable morphology and low surface energy were incorporated into the Ni electrolyte during deposition. Deposition parameters were optimised in such a way that the developed SHSM possesses a micro-nanostructure comprising hierarchical WS_2 clusters and nodules along with Ni pine cones imparting a “cactus-like”/ “cauliflower-like” appearance. This fluorine-free method eliminates issues related to production expenses and potential environmental hazards. Flexibility of stainless steel mesh combined with stable Ni-WS_2 coating resulted in SHSM’s mechanical robustness and chemical stability. Both hydrophobic surface chemistry and roughness contribute to excellent superhydrophobic-superoleophilic and self-cleaning characteristics of the developed SHSM. The thin film of air due to the micro-nano rough structure acts as a barrier that protects SHSM from corrosion. The fabricated SHSM can be reused for several cycles of oil–water separation without any degradation and thus possess unique repeatability. Since the developed SHSM is highly durable reduces the need for frequent replacements or maintenance. This can have a positive economic impact on the lifecycle of SHSM. As a result, this simple, eco-friendly, and low-cost method of fabricating SHSM would be a promising one for practical oil–water separation applications.

Experimental

Materials

Commercial stainless steel mesh (SSM), with a pore size of less than 100 μm was supplied by Raj filters and wire mesh, India. Nickel sulphate ($NiSO_4{\cdot}6H_2O$), Nickel chloride ($NiCl_2{\cdot}6H_2O$), and Boric acid (H_3BO_3) were purchased from Merck. Cetyltrimethylammonium bromide (CTAB, $CH_3(CH_2)_{15}N(Br)(CH_3)_3$) and Saccharin ($C_7H_5NO_3S$) were obtained from Alfa Aesar. Tungsten disulphide nanoparticles (WS_2 NPs, 90 nm) were supplied by Sigma-Aldrich. Myristic acid $CH_3(CH_2)_{12}COOH$ and colouring agents like methylene blue (MB) and Sudan III (Oil Red O) were purchased from Himedia Laboratories. Solvents like toluene, n-hexane, dichloromethane (DCM), diethyl ether, and chloroform were purchased from Merck.

Fabrication of superhydrophobic surface

Electrodeposition was carried out in an aqueous electrolyte of Ni Watts bath containing $NiSO_4{\cdot}6H_2O$, $NiCl_2{\cdot}6H_2O$, and H_3BO_3. WS_2 nanoparticles were dispersed in a Ni bath, along with CTAB and saccharin (Table 1). The Ni- WS_2 bath was kept at a pH of 4–4.5. WS_2 nanoparticles were dispersed using an ultrasonicator for 30 min.

Nickel plate (7 cm × 5 cm × 1 cm, 99.7 % purity) and stainless steel mesh (SSM) (6 cm × 6 cm, purity ≥ 99.5 %) were used as anode and cathode, respectively. SSM was cleaned by an ultrasonic cleaner with ethanol (30 min), acetone (15 min), and deionized water (15 min) followed by oven drying before deposition. Electrodeposition parameters including current density (4–6 A/dm^2), temperature (50–60 °C), time (15–30 min), and stirring rate (400–600 rpm) were varied. The concentration of WS_2 nanoparticles was also varied in the range (3–5) wt% (Table 1). The electrodeposition was finally carried out at optimized conditions of the current density of 4 A/dm^2 for 15 min at a temperature of 60 °C with a 600 rpm stirring rate and 3 wt% concentration of WS_2 particles. The coated mesh was finally modified with low surface energy material Myristic acid MA. (Fig. 1).

Characterization of the superhydrophobic coating

The surface morphology and elemental analysis of the developed coatings were examined using FE-SEM (FEI NOVA NANOSEM 450) and Zeiss EVO 18 cryo-SEM (EDS attached). Atomic Force Microscopy (AFM, Bruker Multimode-8HR system) in tapping mode was used to analyze the three-dimensional morphology to evaluate the surface roughness of the samples and the images were processed using NanoScope analysis 1.5 software package. The phase composition of the samples was studied using X-ray diffraction (XRD) via a Bruker D2 Phaser X-ray diffractometer with Cu - K radiation (λ = 1.5406 A°) in the 0-90° range. The wettability property (contact angle) of water droplets on coated SS mesh was explored by Goniometer (Data Physics, Germany). The water contact angle was calculated by taking the average of five measurements taken at various points on the same sample. CH Instruments electrochemical workstation (CHI608E, CH Instruments Inc.) equipped with standard three-electrode cell was used for electrochemical impedance spectroscopy and potentiodynamic polarization studies.

Table 1
Electrodeposition parameters for Ni-WS_2 coatings.

Electrodeposition parameters	Composition or parameter	Value
Plating solution	$NiSO_4{\cdot}6H_2O$	250 g/dm^3
	$NiCl_2{\cdot}6H_2O$	45 g/dm^3
	H_3BO_3	40 g/dm^3
	CTAB	0.1 g/dm^3
	Saccharin	1.5 g/dm^3
	WS_2	3–5 wt%
Deposition Conditions	Current density	4–6 A/dm^2
	Temperature	50–60 °C
	Time	15–30 min
	Stirring rate	400–600 rpm

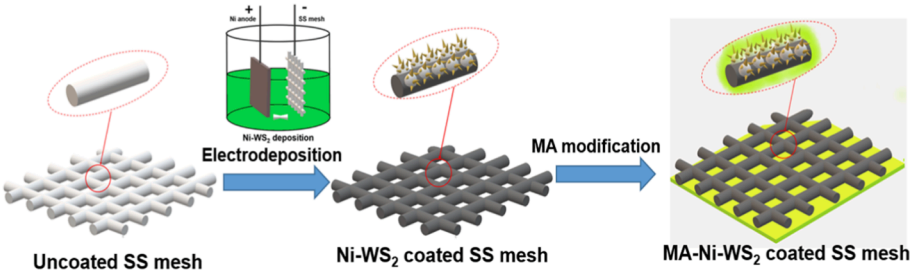

Fig. 1. The schematic illustration of preparation process of superhydrophobic stainless steel mesh.

Durability & performance studies

Stability & recyclability tests

By repeating the separation procedure for every single oil/water mixture, the recycling capacity of SHSM was evaluated for separation efficiency and corresponding water contact angle (WCA). Used SHSM was rinsed using ethanol as well as dried in a vacuum oven after the separation process and this was repeated 30 times. Mechanical stability of SHSM was evaluated by sandpaper abrasion test and chemical stability was tested by immersing it in corrosive solutions for 24 h.

Self-cleaning test

The self-cleaning action of SHSM was analyzed using graphite particles as contaminants. Both coated and uncoated meshes were tilted followed by the dropping of distilled water droplets on their surface. The water rolling-off property and self-cleaning ability of both meshes were thus compared.

Oil/Water separation

Several 40 mL oil/water mixtures were made in a 1:1 vol ratio of water and oil (including toluene, n-hexane, dichloromethane, diethyl ether, chloroform, and kerosene). The oil/water mixtures were poured through SSM and gravity-based filtration was employed throughout the separation process.

The separation efficiency, η was given by

$$\eta = \mathbf{m}_1/\mathbf{m}_0 \times 100\% \quad (1)$$

where, m_0 and m_1 are the mass of oil before and after separation, respectively.

After pouring the oil–water mixture through the mesh, the permeation flux (*F*) was determined according to the equation,

$$\mathbf{F} = \mathbf{V}/\mathbf{St} \quad (2)$$

where *V* is the volume of the filtrate, *S* is the area of contact with the mesh, and *t* is the time.

Corrosion measurements

Electrochemical impedance measurements and potentiodynamic polarisation were carried out in an electrochemical system (CH Instruments Inc., Model 680A) equipped with three electrodes: a saturated calomel electrode (SCE) as the reference electrode and a platinum mesh as the counter electrode. Pristine and modified stainless steel meshes were used as the working electrode. All electrochemical experiments were carried out at room temperature (25 ± 1 °C) in corrosive solutions (i.e., pH 4 (acidic), 7 (neutral), and 11 (alkaline)). The surface area of the sample that was in contact with the corrosive medium is about 1 cm^2. The samples were placed in the electrolyte for 25–35 min to measure their open circuit potential (OCP) until a stable value was reached. Samples were scanned from cathodic to anodic regions at the rate of 1 mV/s with reference to their corresponding OCP values. The samples' impedance was measured at the open circuit potential with a peak-to-peak amplitude of 10 mV in the frequency range of 10^5 to 10^{-1} Hz. Tafel plot was used to determine the corrosion current density (i_{corr}) and corrosion potential (E_{corr} *vs.* SCE). To validate the EIS and polarisation measurements, at least three readings were taken at each condition for all the samples.

Results and discussion

Morphology

SEM was taken for both the original and modified stainless steel meshes. Fig. 2(a) shows the typical image of a stainless steel mesh, suggesting that the pristine mesh has a smooth surface. Electrodeposition has an important effect on the morphology of stainless steel mesh. As can be seen in Fig. 3(a-b), pure nickel deposited mesh (hydrophobic) had a pine-cone structure. The pure Ni coating contained fine Ni crystals which are visible in the magnified image (Fig. 3(b)).

With the addition of WS_2 nanoparticles, the surface became rougher. The development of a rough surface is an important factor in the preparation of special super-wetting materials [33]. During the time of electrodeposition, the deposited Ni ions are attracted to WS_2 nanoparticles because of the electrostatic interaction between positively charged Ni ions and negatively charged WS_2 nanoparticles [34]. As already reported [35], Ni ions then begin to deposit on the WS_2 particles, forming a thin film. Ni ions will continue depositing and will start to grow in size and shape.

The cauliflower-like structure is formed when the Ni ions grow in a dendritic fashion, with branches extending out from the main body of the structure. Thus the Ni-WS_2 coated mesh possessed a protruding rough surface comprising hierarchical WS_2 clusters and nodules resulting in "cactus-like"/ "cauliflower-like" structures (Fig. 4). High-magnification SEM image shows that these nodular-like structures are made up of Ni grain cells wrapped around in petal-like WS_2 nanoparticles (Fig. 5). WS_2 nanoparticles have a higher surface area, which provides more sites for the Ni ions to adsorb. Since WS_2 particles are negatively charged, they attract positively charged Ni ions. Thus the appearance of the cauliflower-like structure may be caused primarily by the preferred adsorption and growth of Ni^{2+} ions on WS_2 particles during deposition.

The "cactus/cauliflower-like" nodular structures of the coating generate more sites for MA adsorption, which leads to the formation of a hydrolysis film on these surfaces. The nodule structures have a high surface area and rough surface so that MA molecules get more sites to bind. This increased binding leads to more MA molecules being hydrolysed, which produces a film on the mesh surface which in turn improves the hydrophobicity. In total, we may conclude that the micron-sized spherical particles, along the nano-scale granular protuberance, resulted in a highly rough hierarchical structure that resulted in the superhydrophobic behaviour of SHSM.

EDS shows the distribution of elements on the surface of Ni-WS_2

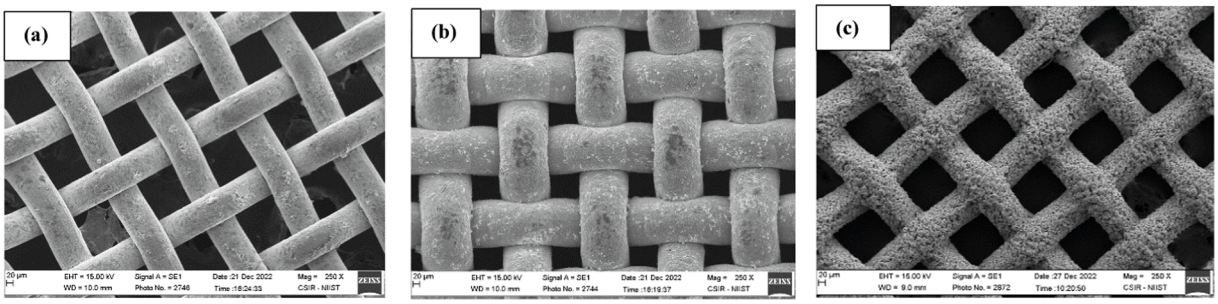

Fig. 2. (a) Pristine SS mesh (b) Pure Ni coated SS mesh (c) Ni-WS_2 coated SS mesh.

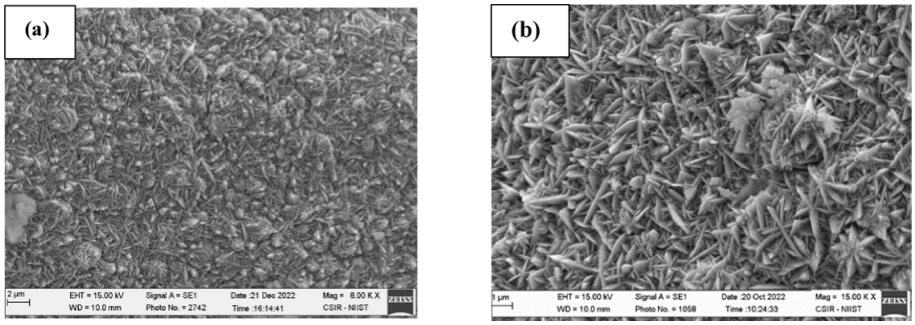

Fig. 3. (a,b). Pine-cone structure in pure Ni coated SS mesh.

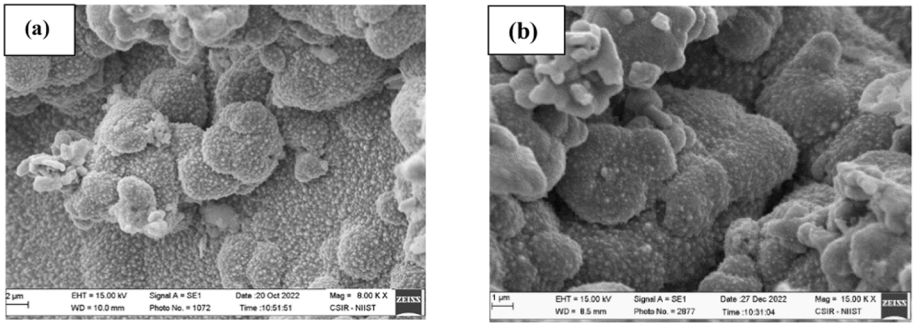

Fig. 4. (a,b): Cactus/cauli-flower like morphology in Ni-WS_2 coated SS mesh.

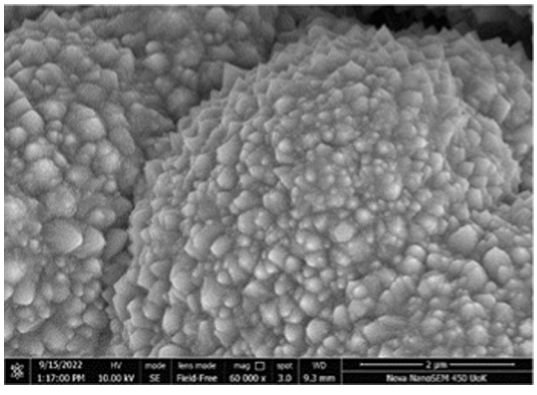

Fig. 5. Thorn-like projections in Ni-WS_2 coated SS mesh.

coated SS mesh as in Fig. 6. Elements like Nickel (**Ni**), tungsten (**W**), and sulphur (**S**) were found. Ni is predominantly present in the coating whereas sulphur was primarily found in the cacti-like structures.

Fig. S1(a), (b) shows the 3D surface morphology of pure Ni coated and Ni-WS_2 coated SS meshes respectively. The average roughness (R_a), the mathematical mean deviation of the roughness profiles, is the most common way of calculating surface roughness. The surface roughness of the coated meshes significantly affects their wetting behavior. In the case of pure Ni coated mesh, R_a is 87.6 nm whereas, in the case of Ni-WS_2 coated mesh, R_a is 168 nm. This increment has been reflected in the WCA values i.e. 127.2° for pure Ni and 151.3° for Ni-WS_2 coated meshes respectively. In the case of pure Ni-coated mesh, irregularly located clusters of varying heights are visible on the surface as seen in Fig. S1(a). Fig. S1(b) of Ni-WS_2 coated mesh shows the presence of protrusions (valleys or bumps) of larger heights and sizes. The micro-nano hierarchical structure comprising of these bumps/protrusions results in the reduction of the area of contact between the solid – liquid interface and water maintaining the spherical shape of the water droplet without spreading. Thus, this micro-nano structure forms a thin film of air that acts as a barrier increasing the WCA of Ni-WS_2 coated mesh.

Phase composition & crystalline structure analysis

X-ray diffraction was employed to examine the crystal planes of the coating. All peaks are identified and indexed using standard Powder Diffraction Files, such as JCPDS 04–0850 for Nickel and JCPDS 84–1398 for WS_2. The XRD pattern of pure Ni-coated SS mesh is shown in Fig. 7

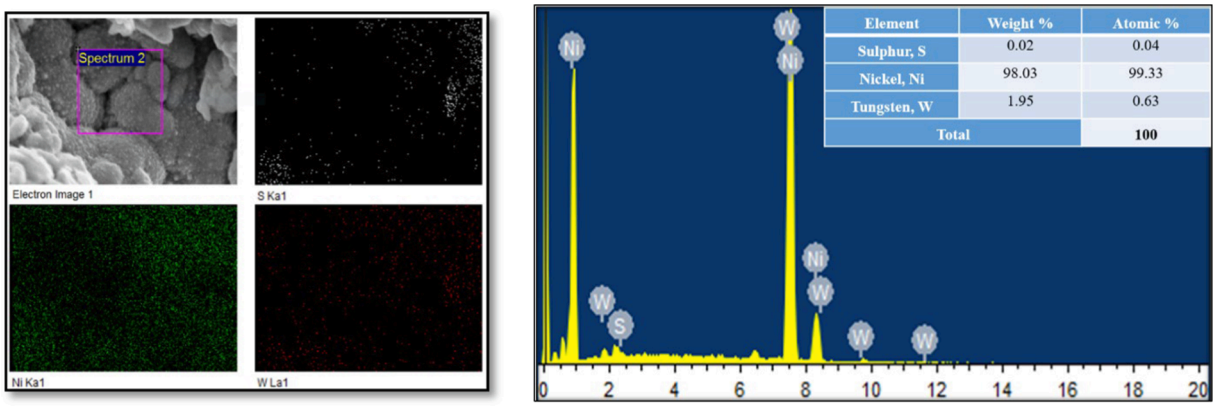

Fig. 6. EDS analysis of Ni-WS_2 coated SS mesh.

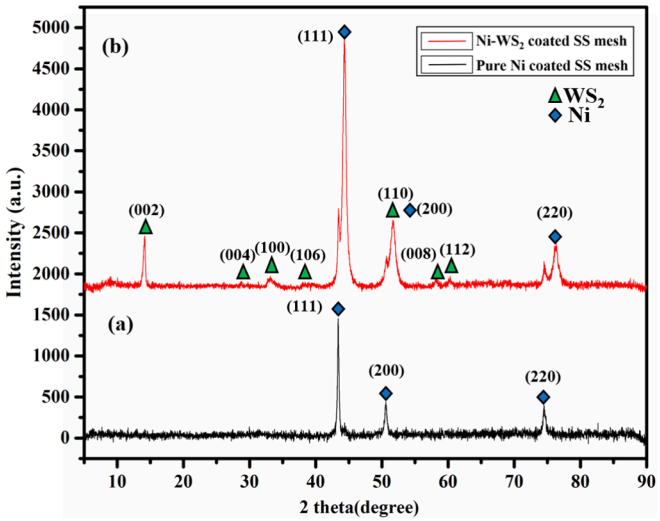

Fig. 7. XRD pattern of (a) pure Ni coated SS mesh, (b) Ni-WS_2 coated SS mesh.

(a). From the data, three peaks of Ni at 2θ corresponding to 44.32°, 51.77°, and 76.3° are assigned to (1 1 1), (2 0 0), and (2 2 0) Bragg reflections of the face-centered cubic (fcc) structure of metallic nickel [36]. The incorporation of WS_2 particles caused important microstructural changes; providing more nucleation sites. It also retards the growth of large Ni crystals, resulting in smaller grain sizes. Analyzing the XRD pattern of Ni-WS_2 coated SS mesh, distinct peaks are found at 14°, 29.1°, 33°, 40°, 49°, 58°, and 60° correspond to (0 0 2), (0 0 4), (1 0 0), (1 0 6), (1 1 0), (0 0 8) and (1 1 2) phases confirming the hexagonal closed-packed (hcp) structure of WS_2 [37] (Fig. 7(b)).

Whenever Ni is deposited onto a substrate, the first few layers of atoms will tend to form (1 1 1) plane [38]. The (1 1 1) plane is one of the most densely packed planes in a crystal lattice, and it has the lowest surface energy compared to other planes [39]. Thus the growth of the (1 1 1) plane helps to minimize the total surface energy of the crystal. In this case, there is the presence of strong (1 1 1) Ni peaks indicating reduced surface energy [35,38,40]. Post electrodeposition after treatment with MA, it is believed that MA is chemically adsorbed on the Ni (1 1 1) surface via bi-dentate interaction, i.e. two oxygen atoms from the carboxylic acid group (–COOH) of MA with 3d orbital of Ni. This bonding interaction prevents the water molecules from forming hydrogen bonds with the surface, enhancing the hydrophobicity [41].

Wettability studies

Chemical composition, free energy of the surface, and surface morphology all affect the surface wetting property of a coating. Fig. 8 shows the contact angle of the water droplet on the coated SS mesh (pure Ni, Ni-WS_2, MA-Ni-WS_2). As it is evident from the WCA measurements there was a gradual increase in the hydrophobicity of the surface (i.e. **127.2**° to **169.5**°). Coated mesh exhibited wettability with the oil droplets, quickly spread while the water droplet remained on the surface of the mesh in an extremely spherical fashion. The micro-nanostructure along with the action of low surface energy material MA (27.4 dynes/cm) reduces the contact area between the solid – liquid interface and water by forming a thin, strong cohesive layer on Ni-WS_2 coating. Whenever applied over a surface, MA can self-assemble in an organized manner through hydrogen bonding of carboxyl groups as well as hydrophobic interaction in-between methyl groups. These hydrophobic chains create a barrier that prevents water from wetting the surface. As a result, water droplets tend to bead up and roll off the surface instead of spreading out and wetting the surface.

Water droplets will exist in superhydrophobic Cassie State as a result of incorporation of WS_2 nanoparticles and modification of the Ni-coated surface with low surface energy material MA [42]. According to the Wenzel equation,

$$\cos\theta_w = r\cos\theta \tag{3}$$

where θ_w is the contact angle of liquids on a rough surface, θ is the contact angle on a flat surface and r is the roughness factor [43]. This equation implies that as the roughness of the surface increases, the hydrophobic surface becomes more hydrophobic and the oleophilic surface becomes more oleophilic. In SHSM, the micro-nano hierarchical structure makes the surface rougher. As a result, when an oil droplet is placed

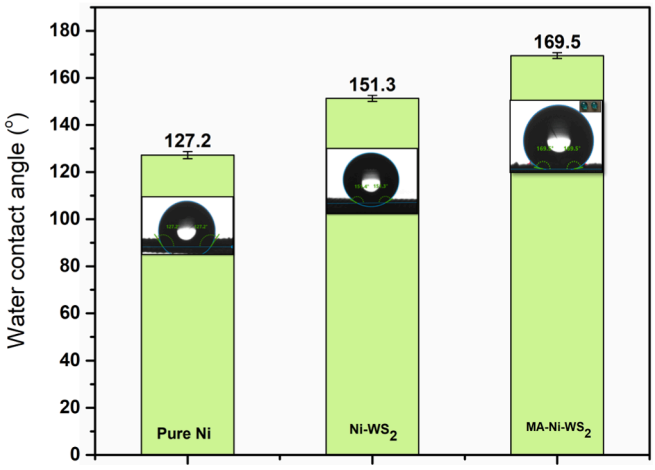

Fig. 8. WCAs of coated mesh (a) Pure Ni, (b) Ni-WS_2, (c) MA-Ni-WS_2.

on Ni-WS_2 coated SS mesh, it can enter the nanostructures formed by Ni grain cells surrounded by petal-like WS_2 nanoparticles as a result of the capillary effect. The combined effect of hydrophobic surface chemistry and the roughness results in excellent superhydrophobic and superoleophilic characteristics of the developed SHSM.

Stability tests

Mechanical stability is a crucial measure of superhydrophobic material's practical application. A mechanical durability test was carried out to test the robustness of the developed SHSM. The coated mesh was put on 400 grit sandpaper. Additionally, a 100 g weight was used as an outside force, as illustrated in Fig. 9. In this procedure, the coated mesh was moved twenty centimeters along the ruler's direction, followed by a rotation of 90°, and another twenty centimeters in the direction of the ruler. The entire procedure was referred to as a cycle. The WCA of the sample did not change significantly after 30 cycles, and it was still greater than 150° (Fig. 10). From this, we may conclude that the abrasion process only damaged the outermost structure, while the internal hierarchical structure remained intact.

The oily wastewater released by industries often turns to be acidic or alkaline. To deal with wastewater, the as-prepared mesh must be chemically stable enough to withstand harsh environmental conditions. We tested the wettability of coated SS mesh with droplets of varying pH as shown in Fig. 11. Ni-WS_2 coated SS mesh showed superhydrophobicity in acidic as well as alkaline range of pH. Immersion tests were conducted using corrosion solutions of HCl (pH = 1, acidic), NaCl (pH = 7, neutral), and NaOH (pH = 14, alkaline) to test the chemical stability. After placing the sample in the corrosion solution, it is believed that an air film formation took place between the corrosion solution and the sample. This particular film can hinder corrosive media from approaching the sample, preventing corrosion. Even under a highly corrosive strong acidic environment (pH = 1), the contact angle of MA-treated Ni-WS_2 SS mesh was 150°, demonstrating effective corrosion resistance of the mesh in harsh environments.

Self-Cleaning tests

One of the most important applications of superhydrophobic surfaces is self-cleaning. In this study, the self-cleaning action of SHSM was studied using black graphite particles as contaminants. Because of the superhydrophobic nature of the mesh as in Fig. 12, the droplet was still spherical bounded with graphite particles, and rolled out from the surface retaining its superhydrophobicity. A comparison with the uncoated mesh showed that graphite particles adhered to the surface and remained sticky (**Video 1**). The process was carried out several times still SHSM maintained its self-cleaning ability.

Oil-water separation

For oil–water separation experiments, oil was colored with Sudan III (red), and water was colored with Methylene blue (blue) (Fig. 13). The contact state of water droplets on the as-prepared SHSM shifts from Cassie to Wenzel state during the separation of the oil/water mixture. The separation efficiency of the superhydrophobic mesh was evaluated

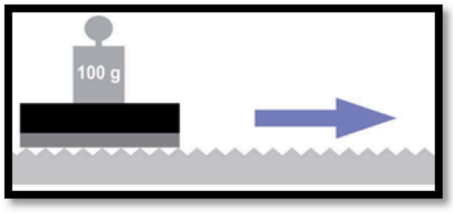

Fig. 9. Sandpaper abrasion test.

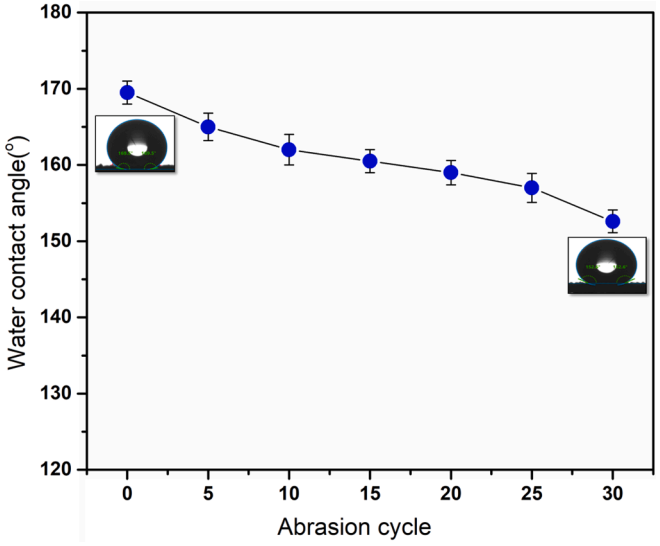

Fig. 10. Variation of WCA after different abrasion cycles.

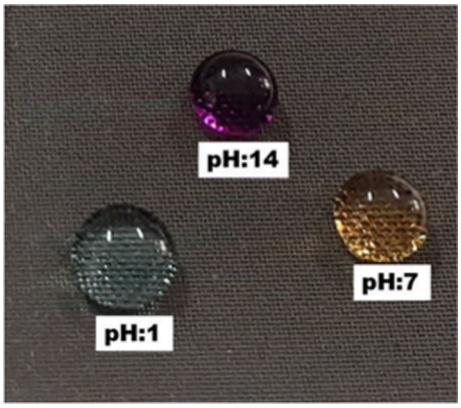

Fig. 11. Photograph of water droplets of varying pH on SHSM.

by Eq. (1). The initial separation efficiency for a 1:1 oil–water mixture was as high as 98.3 %. After 30 separation cycles, the separation efficiency was still higher more than 98 %, showing that the mesh maintained the oil − water separation ability.

In addition, the SHSM can separate different oil − water mixtures (n-hexane, diethyl ether, toluene, kerosene, dichloromethane) indicating that it can generally separate the oil − water mixture of varying surface tensions (Fig. 14(a) **Video 2**). Oil flux was also calculated for various types of oils using Eq. (2) (Fig. 14(b)). Since the oil–water separation efficiency of Ni-WS_2 coated SS mesh was greater than 98 %, as a result of which the mesh can be used as a film-like material for efficient oil − water separation compared to other superhydrophobic stainless-steel meshes already developed and reported (Table 2).

Corrosion resistance

Good anti-corrosion performance ensures stable and long-term separation efficacy of meshes at industrial-level applications in harsh environments. Corrosion experiments were carried out in acidic (pH = 1), neutral (pH = 7), and alkaline (pH = 14) mediums. The anti-corrosion property of SHSM was studied and compared with pure Ni-coated SS mesh and pristine SS mesh. The polarisation potential (E_{corr}, thermodynamic parameter) and polarisation current density (i_{corr}, kinetic parameter) of all the samples were calculated by Tafel extrapolation (Fig.S2 & Table 3). Analyzing i_{corr} values of SHSM, it is observed that i_{corr}

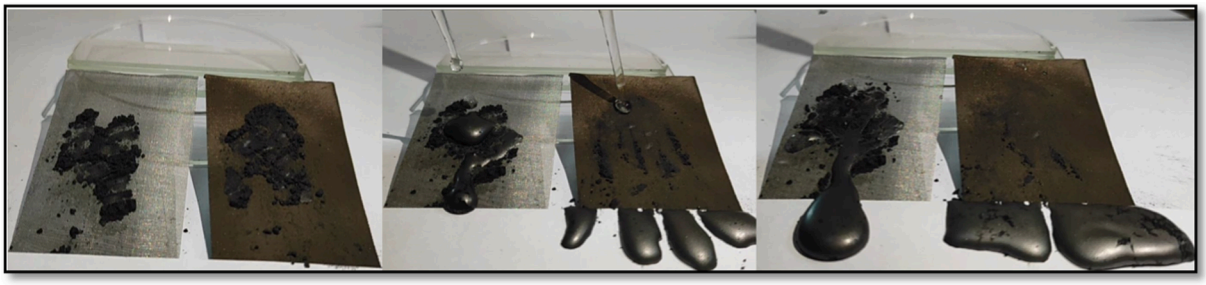

Fig. 12. Different stages of self-cleaning action of as-prepared SHSM (right) in contrast to uncoated mesh (left).

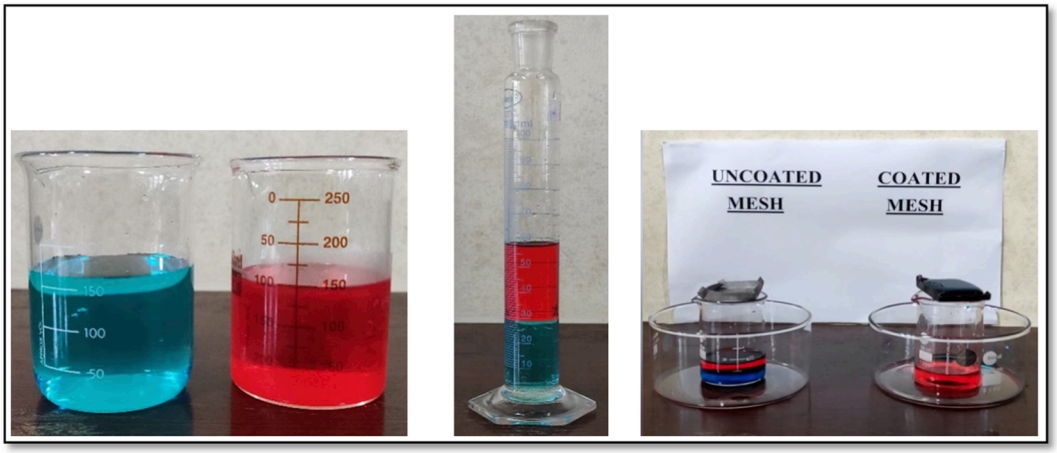

Fig. 13. Oil-water separation experiments; oil dyed with Sudan III (red) and water dyed with Methylene blue (blue). (For interpretation of the references to colour in this figure legend, the reader is referred to the web version of this article.)

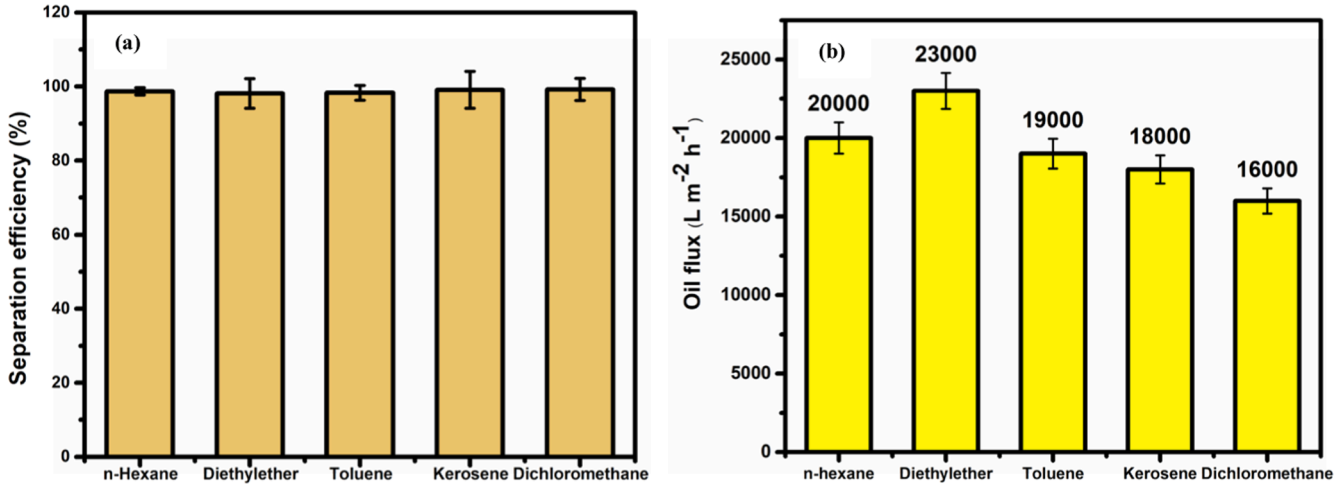

Fig. 14. Separation efficiencies (a) & flux (b) of SHSM for different types of oils.

got reduced by one order of magnitude compared with pure Ni-coated SS mesh and uncoated SS mesh indicating that incorporating WS_2 particles improved the corrosion resistance of SHSM in all the mediums.

This is further confirmed by the EIS spectra (Nyquist plots) (Fig.S3 & S4). Pure Ni-coated SS mesh and SHSM have significantly higher impedances than bare SS mesh, and it is observed that the addition of WS_2 particles further increases the impedance of pure Ni-coated mesh. Furthermore, pure Ni-coated mesh and SHSM have impedance spectra with depressed semicircles. The corrosion resistance of the coatings is determined by the diameter of the semicircle, where larger diameters suggest higher corrosion resistance [50]. Out of all the samples, SHSM has the highest impedance and the best corrosion resistance in all three mediums.

The mechanism of corrosion resistance can be interconnected to the hydrophobicity of coatings. When bare SS mesh was placed in the corrosive medium, the mesh surface appeared to be hydrophilic, and there was no barrier to delay the damage caused by the corrosive solution. A rough micro-nano hierarchical structure is present in Ni-WS_2 coated mesh that acts as a protective barrier preventing corrosive ions from reaching the mesh surface. Due to high roughness, MA-modified Ni-WS_2 coating conformed to the Cassie-Baxter state in which there will be air cushion or air pockets in between the micro nano hierarchical structures

Table 2
Comparative performance of SHSM developed in the present work with previously reported works.

Coating layer material	Fabrication Method	WCA	Oil-feed Material	Separation Efficiency (%)	Remarks	Reference
Ni/Nip	Jet electrodeposition	154°	Hexane Gasoline Kerosene Silicone oil Dichloromethane	97	–	[44]
HDTMS	Chemical etching	167°	Hexane Kerosene	98	Thermally, Mechanically and chemically stable	[45]
TEOS	Dip-coating	143°	n-Hexane Toluene Chloroform Crude oil	>99	–	[46]
PTFE	Spray coating	150°	Diesel oil	–	–	[47]
Perchloric acid-ethylene glycol PFOA	Anodic Oxidation	155°	Hexane Gasoline Kerosene Dichloromethane Cyclohexane	96	–	[48]
Nano Silica	Dip-coating	157°	Polyalphaolefin Diesel oil Vegetable oil	>95	Thermally & chemically stable	[49]
Ni-WS_2 Myristic acid	**Electrodeposition**	**169.5°**	**Hexane Diethyl ether Toluene Kerosene Dichloromethane**	**>98**	**Self-cleaning Mechanically and chemically stable**	**This work**

Table 3
Corrosion potentials (E_{corr}) and corrosion current densities (I_{corr}) from potentiodynamic polarisation test.

Sample	Acidic medium (pH:1)		Neutral medium (pH:7)		Alkaline medium (pH:14)	
	E_{corr} (V)	i_{corr} (μA/cm^2)	E_{corr} (V)	i_{corr} (μA/cm^2)	E_{corr} (V)	i_{corr} (μA/cm^2)
Uncoated SS mesh	−0.690	8.562 x 10^{-6}	−0.650	8.203 x 10^{-6}	−0.382	2.479 x 10^{-6}
Pure Ni-coated SS mesh	−0.206	1.075 x 10^{-6}	−0.168	1.148 x 10^{-6}	−0.185	1.532 x 10^{-6}
SHSM	−0.242	3.924 x 10^{-7}	−0.246	2.506 x 10^{-7}	−0.173	4.077 x 10^{-7}

preventing the attack of corrosive medium on the SHSM surface.

Conclusions

A superhydrophobic - superoleophilic SS mesh with a water contact angle of 169.5^0 and surface roughness of 168 nm (R_a) was fabricated by electrodeposition. At the optimised concentration of WS_2 (3 wt%) and deposition parameters viz. current density of 4 A/dm^2, deposition time of 15 min, temperature of 60 °C, and stirring speed of 600 rpm, the surface of SS mesh was effectively modified. Ni-WS_2 coated mesh possessed a protruding rough surface comprising hierarchical WS_2 clusters. The combined effect of hydrophobic surface chemistry and the roughness contributes to excellent superhydrophobic-superoleophilic and self-cleaning characteristics of the developed SHSM. The oil/water separation performance of SHSM was studied and the efficiency was greater than 98 % even after multiple uses. Further, the SHSM is highly corrosion resistant with excellent mechanical and chemical stability against strong acidic/alkaline solutions. Further, it can selectively separate different oil–water mixtures like hexane-water, diethyl ether-water, toluene-water, kerosene-water, and dichloromethane-water. Thus, the developed SS mesh has the potential in the treatment of industrial oil–water mixtures as well as environmental oil spills due to its excellent oil–water separation efficiency and durability in harsh conditions.

CRediT authorship contribution statement

Revathy Sreekumar: Investigation, Methodology, Formal analysis, Writing – original draft, Writing – review & editing. **Swapna Eravath Thazhakkuni:** Investigation. **Sreejakumari Sukumaran Suseelamma:** Resources, Writing – review & editing, Supervision.

Declaration of competing interest

The authors declare that they have no known competing financial interests or personal relationships that could have appeared to influence the work reported in this paper.

Acknowledgments

The first author Revathy Sreekumar is thankful to DST, Govt. of India for the Inspire fellowship grant (IF 180987). The authors are grateful to Mr. Harish Raj, Mr. Amal Raj R.B., Mr. Chandrakanth C.K., Mr. Kiran J. S., and Ms. Swathy Lekshmy V.S. for their support in the characterization of the samples. Mr. Visakh Manoj is acknowledged for his support in designing graphical abstract and schematic illustration.

Appendix A. Supplementary data

Supplementary data to this article can be found online at https://doi.org/10.1016/j.jiec.2024.01.054.

References

[1] L. Yu, M. Han, F. He, Arab. J. Chem. 10 (2017) S1913–S1922, https://doi.org/10.1016/j.arabjc.2013.07.020.
[2] A.B. Nordvik, J.L. Simmons, K.R. Bitting, A. Lewis, T. Strøm-Kristiansen, Spill Sci. Technol. Bull. 3 (3) (1996) 107–122, https://doi.org/10.1016/S1353-2561(96)00021-7.
[3] K. Gaaseidnes, J. Turbeville, Pure Appl. Chem. 71 (1) (1999) 95–101, https://doi.org/10.1351/pac199971010095.
[4] B. Tansel, J. Regula, J. Environ. Sci. Heal. Part A 35 (9) (2000) 1557–1575, https://doi.org/10.1080/10934520009377055.
[5] B. Huang, X. Li, W. Zhang, C. Fu, Y. Wang, S. Fu, Polymers (basel). 11 (2019) 3, https://doi.org/10.3390/polym11030395.
[6] D. Miller, D. Dreyer, C. Bielawski, D. Paul, B. Freeman, Angew. Chemie 129 (2016), https://doi.org/10.1002/ange.201601509.

[7] D. Rana, T. Matsuura, Chem. Rev. 110 (4) (2010) 2448–2471, https://doi.org/10.1021/cr800208y.
[8] B. Wang, W. Liang, Z. Guo, W. Liu, Chem. Soc. Rev. 44 (1) (2015) 336–361, https://doi.org/10.1039/C4CS00220B.
[9] G. Dunderdale, C. Urata, T. Sato, M. England, A. Hozumi, A.C.S. Appl, Mater. Interfaces (2015), https://doi.org/10.1021/acsami.5b06207.
[10] F. Zhang, W. Zhang, Z. Shi, D. Wang, L. Jiang, Adv. Mater. 25 (2013), https://doi.org/10.1002/adma.201301480.
[11] X. Yao, Y. Song, L. Jiang, Adv. Mater. 23 (6) (2011) 719–734, https://doi.org/10.1002/adma.201002689.
[12] D.K. Sarkar, N. Saleema, Surf. Coatings Technol. 204 (15) (2010) 2483–2486, https://doi.org/10.1016/j.surfcoat.2010.01.033.
[13] Q. Wen, J. Di, L. Jiang, J. Yu, R. Xu, Chem. Sci. 4 (2) (2013) 591–595, https://doi.org/10.1039/C2SC21772D.
[14] J. Wu, N. Wang, L. Wang, H. Dong, Y. Zhao, L. Jiang, A.C.S. Appl, Mater. & Interfaces 4(6) (2012) 3207–3212, https://doi.org/10.1021/am300544d.
[15] X. Zhou,, Z. Zhang,, X. Xu,, X. Men,, X. Zhu, Ind. \& Eng. Chem. Res. 52(27) (2013) 9411–6. 10.1021/ie400942t.
[16] S. Seeger, Adv. Funct. Mater. 21 (2011), https://doi.org/10.1002/adfm.201190113.
[17] C.R. Crick, J.A. Gibbins, I.P. Parkin, J. Mater. Chem. A 1 (19) (2013) 5943–5948, https://doi.org/10.1039/C3TA10636E.
[18] N. Liu, Y. Cao, X. Lin, Y. Chen, L. Feng, Y. Wei, A.C.S. Appl, Mater. & Interfaces 6 (15) (2014) 12821–12826, https://doi.org/10.1021/am502809h.
[19] S. Sriram, R.K. Singh, A. Kumar, Mater. Today Proc. 26 (2020) 2495–2501, https://doi.org/10.1016/j.matpr.2020.02.531.
[20] B. Wang, Z. Guo, Appl. Phys. Lett. 103 (2013) 6, https://doi.org/10.1063/1.4817922.
[21] S. Wang, Y. Song, L. Jiang, Nanotechnology 18 (1) (2006) 15103, https://doi.org/10.1088/0957-4484/18/1/015103.
[22] L. Feng, Z. Zhang, Z. Mai, Y. Ma, B. Liu, L. Jiang, D. Zhu, Angew. Chemie - Int. Ed. 43 (15) (2004) 2012–2014, https://doi.org/10.1002/anie.200353381.
[23] B. Li, X. Liu, X. Zhang, W. Chai, Eur. Polym. J. 73 (2015) 374–379, https://doi.org/10.1016/j.eurpolymj.2015.10.031.
[24] Y.K. Lai, Y.X. Tang, J.Y. Huang, F. Pan, Z. Chen, K.Q. Zhang, H. Fuchs, L.F. Chi, Sci. Rep. 3 (2013) 1–8, https://doi.org/10.1038/srep03009.
[25] Y. Liu, K. Zhang, W. Yao, J. Liu, Z. Han, L. Ren, Colloids Surfaces A Physicochem. Eng. Asp. 500 (2016) 54–63, https://doi.org/10.1016/j.colsurfa.2016.04.011.
[26] Y. Yang, X. Li, X. Zheng, Z. Chen, Q. Zhou, Y. Chen, Adv. Mater. 30 (9) (2018) 1870062, https://doi.org/10.1002/adma.201870062.
[27] M. Laad, B. Ghule, Phys. Status Solidi Appl. Mater. Sci. 219 (16) (2022) 1–19, https://doi.org/10.1002/pssa.202200109.
[28] H.M. Ali, M.A. Qasim, S. Malik, G. Murtaza, Heat Transf. - Model. Methods Appl. (2018), https://doi.org/10.5772/intechopen.72820.
[29] G. Barati Darband,, M. Aliofkhazraei,, S. Khorsand,, S. Sokhanvar,, A. Kaboli, Arab. J. Chem. 13(1) (2020) 1763–802. 10.1016/j.arabjc.2018.01.013.
[30] T. Darmanin, E.T. De Givenchy, S. Amigoni, F. Guittard, Adv. Mater. 25 (10) (2013) 1378–1394, https://doi.org/10.1002/adma.201204300.
[31] S. Huang, Y. Hu, W. Pan, Surf. Coatings Technol. 205 (13) (2011) 3872–3876, https://doi.org/10.1016/j.surfcoat.2011.01.065.
[32] T. Xiang, S. Ding, C. Li, S. Zheng, W. Hu, J. Wang, P. Liu, Mater. Des. 114 (2017) 65–72, https://doi.org/10.1016/j.matdes.2016.10.047.
[33] P. Kumari, P. Chauhan, A. Kumar, A.C.S. Symp, Ser. 1408 (2022) 1–23, https://doi.org/10.1021/bk-2022-1408.ch001.
[34] H. Shalom, T. Bendikov, Y. Feldman, N. Lachman, A. Zak, R. Tenne, Chem. Phys. Lett. 761 (2020) 138052, https://doi.org/10.1016/j.cplett.2020.138052.
[35] G. Zhao, Y. Xue, Y. Huang, Y. Ye, F.C. Walsh, J. Chen, S. Wang, RSC Adv. 6 (64) (2016) 59104–59112, https://doi.org/10.1039/C6RA07899K.
[36] S. Mohan, S. Shriram, S. Karthikeyan, Bull. Electrochem. (2002) 241–246.
[37] Y. He, W.T. Sun, S.C. Wang, P.A.S. Reed, F.C. Walsh, Electrochim. Acta 245 (2017) 872–882, https://doi.org/10.1016/j.electacta.2017.05.166.
[38] J. Zhou, G. Zhao, J. Li, J. Chen, S. Zhang, J. Wang, F.C. Walsh, S. Wang, Y. Xue, Appl. Surf. Sci. 487 (January) (2019) 1329–1340, https://doi.org/10.1016/j.apsusc.2019.05.244.
[39] J.M. Zhang, F. Ma, K.W. Xu, Chinese Phys. 13 (7) (2004) 1082–1090, https://doi.org/10.1088/1009-1963/13/7/020.
[40] E. García-Lecina, I. García-Urrutia, J.A. Díez, J. Fornell, E. Pellicer, J. Sort, Electrochim. Acta 114 (2013) 859–867, https://doi.org/10.1016/j.electacta.2013.04.088.
[41] Y. Bai, D. Kirvassilis, L. Xu, M. Mavrikakis, Surf. Sci. 679 (2019) 240–253, https://doi.org/10.1016/j.susc.2018.08.004.
[42] S. Parvate, P. Dixit, S. Chattopadhyay, J. Phys. Chem. B 124 (8) (2020) 1323–1360, https://doi.org/10.1021/acs.jpcb.9b08567.
[43] H. Yang, P. Pi, Z.-Q. Cai, X. Wen, X. Wang, J. Cheng, Z. Yang, Appl. Surf. Sci. 256 (13) (2010) 4095–4102, https://doi.org/10.1016/j.apsusc.2010.01.090.
[44] J. Xu, Y. Chen, L. Shen, J. Zhao, G. Lou, D. Huang, Y. Yang, Colloids Surfaces A Physicochem. Eng. Asp. 649 (April) (2022), https://doi.org/10.1016/j.colsurfa.2022.129434.
[45] D. Nanda, A. Sahoo, A. Kumar, B. Bhushan, J. Colloid Interface Sci. 535 (2019) 50–57, https://doi.org/10.1016/j.jcis.2018.09.088.
[46] R.A. Roslan, W.J. Lau, C.S. Ong, Y.Z. Tan, A.F. Ismail, J. Water Process Eng. 54 (May) (2023) 104063, https://doi.org/10.1016/j.jwpe.2023.104063.
[47] L. Feng, Z. Zhang, Z. Mai, Y. Ma, B. Liu, L. Jiang, D. Zhu, Angew. Chemie 116 (15) (2004) 2046–2048, https://doi.org/10.1002/ange.200353381.
[48] Y. Song, S. Yu, K. Wang, W. Li, P. Gong, H. Li, M. Zhang, D. Sun, X. Yang, Colloids Surfaces A Physicochem. Eng. Asp. (2022) 130855, https://doi.org/10.1016/j.colsurfa.2022.130855.
[49] Y. Guo, X. Zhou, X. Yi, D. Wang, Q. Xu, Appl. Nanosci. 10 (5) (2020) 1511–1520, https://doi.org/10.1007/s13204-019-01227-7.
[50] J.N. Balaraju,, V. Ezhil Selvi,, K.S. Rajam, Mater. Chem. Phys. 120(2) (2010) 546–51. 10.1016/j.matchemphys.2009.11.047.

Materials Today Communications 44 (2025) 111860

Contents lists available at ScienceDirect

Materials Today Communications

journal homepage: www.elsevier.com/locate/mtcomm

Morphology tuned Ni-WS_2 coated stainless steel mesh as an efficient bi-functional electrocatalyst for water splitting

Revathy Sreekumar [a,c,1], Shilpa Radhakrishna Pillai [b,2], Rakhi Raghavan Baby [b,c,*], Sreejakumari Sukumaran Suseelamma [a,c,**]

[a] Materials Science and Technology Division, CSIR-National Institute for Interdisciplinary Science and Technology (NIIST), Thiruvananthapuram 695019, India
[b] Centre for Sustainable Energy Technologies, CSIR-National Institute for Interdisciplinary Science and Technology (NIIST), Research Centre, University of Kerala, Thiruvananthapuram 695019, India
[c] Academy of Scientific and Innovative Research (AcSIR), Ghaziabad- 201002, India

ARTICLE INFO

Keywords:
Composite coating
Electrodeposition
Bi-functional
Water splitting
HER
OER

ABSTRACT

Electrocatalytic water splitting is a sustainable method for hydrogen production, but the high cost of noble metal catalysts limits its practicality. Here, we present a novel electrodeposited Ni-WS_2 coated stainless steel mesh as an efficient and cost-effective bi-functional catalyst for both the hydrogen evolution reaction (HER) and oxygen evolution reaction (OER). The innovative design of the catalyst with its hierarchical surface and the synergistic effect of Ni and WS_2, combined with a highly reactive surface and effective bubble separation, enables remarkable catalytic performance. The catalyst achieves overpotentials of -89 mV for HER and 230 mV for OER at 10 mA/cm^2, with robust stability for 50 h in alkaline medium. For overall water splitting at 10 mA/cm^2, a cell potential of 1.56 V was required and the cell maintained long term stability. This work represents a step forward in utilisation of non-precious metals like nickel for efficient, cost-effective, and sustainable hydrogen production.

1. Introduction

The World Energy Council expects rapid industrialisation to boost the worldwide energy demand from 45 % to 60 % by 2030 [1]. Renewable energy is gaining prominence due to rising energy demands and depleting fossil fuels [2,3]. Out of all the sustainable energy sources, hydrogen is the most promising fuel candidate because of its high gravimetric energy density, comparatively more availability, and no emissions throughout consumption [4,5]. Conventional large-scale hydrogen production via steam reforming suffers from carbon residues and limited purity, making electrolytic water splitting a more sustainable alternative [6]. However, the process requires efficient catalysts to overcome sluggish reaction kinetics and higher overpotentials.

The water-splitting reaction takes place through cathodic hydrogen evolution reaction (HER) and anodic oxygen evolution reaction (OER) [7]. At present, Pt-group metals are the most efficient HER catalysts, and Ir/Ru-based compounds serve as conventional catalysts for OER. However, the high cost, poor stability (especially in alkaline water electrolysis), and the limited availability of these metals prevent their widespread applications [8]. Bi-functional catalysts capable of

Abbreviations: SS, stainless steel; SSM, stainless steel mesh; HER, hydrogen evolution reaction; OER, oxygen evolution reaction; SEM, scanning electron microscopy; EDS, energy dispersive spectroscopy; LSV, linear sweep voltammetry; ECSA, electrocatalytic active surface area; AFM, atomic force microscopy; CV, cyclic voltammetry; FCC, face centred cubic; XRD, x-ray diffraction; CTAB, cetyltrimethylammonium bromide; TMDC, transition metal dichalcogenides; CA, chronoamperometry; EIS, electrochemical impedance spectroscopy.

* Corresponding author: Centre for Sustainable Energy Technologies, CSIR-National Institute for Interdisciplinary Science and Technology, Trivandrum 695019, India.

** Correspondence to: Materials Science and Technology Division, CSIR-National Institute for Interdisciplinary Science and Technology, Trivandrum 695019, India.

E-mail addresses: revathyias26@gmail.com (R. Sreekumar), shilparkrishnan6@gmail.com (S. Radhakrishna Pillai), rakhiraghavanbaby@niist.res.in (R. Raghavan Baby), sreejakumari@niist.res.in (S. Sukumaran Suseelamma).

[1] Materials Science and Technology Division, CSIR- National Institute for Interdisciplinary Science and Technology, Trivandrum, India- 695019

[2] Centre for Sustainable Energy Technologies, Research Centre University of Kerala, CSIR- National Institute for Interdisciplinary Science and Technology, Trivandrum, India- 695019

https://doi.org/10.1016/j.mtcomm.2025.111860
Received 10 October 2024; Received in revised form 16 January 2025; Accepted 7 February 2025
Available online 8 February 2025

performing HER and OER in a single electrolyte offer a cost-effective solution by reducing the complexity of the system and improving the overall performance. Among all the available materials, transition metal-based materials, particularly Ni-based materials are preferred due to their low cost, high elemental abundance, strength, flexibility, corrosion resistance, thermal and electrical conductivity [9].

Ni-based compounds, including alloys, phosphides, sulphides, and oxides, have been reported for their ability to catalyse alkaline overall water splitting (OWS). Kuang et al. [10] reported the usage of $NiMoP_2$ nanowire as an electrocatalyst for both HER and OER. A unique nanostructured Ni-Fe-Co coated bi-functional 3D electrode was developed by Darband et al. [11]. A highly efficient and robust bi-functional Ni-Fe/-$NiMoN_x$ electrocatalyst was developed on nickel foam by Qiu et al. [12]. Shudo et al. [13] designed a porous Ni/NiOx bi-functional oxygen electrocatalyst produced from $Ni(OH)_2$ with outstanding catalytic activity.

Morphology tuning, crystallinity alterations, surface manipulation, and synergy compositing of different materials can further improve the intrinsic electro-catalytic properties of metals like Ni. The composite materials offer larger catalytic surface area by Ni grain refinement and also by improving the intrinsic catalytic activity by generating a synergistic effect between Ni and incorporated reinforcements [14]. Experimental and theoretical studies have shown that the presence of two-dimensional materials changes the growth pattern and inherent activity of Ni, improving the rate of overall water splitting. Out of all the two-dimensional materials, layered transition metal dichalcogenides (TMDCs) like MoS_2 and WS_2, having exceptional electrical conductivity, highly active edge sites, tunable band structure, and a high surface area-to-volume ratio, are studied for their possible use as an electrochemical catalyst [15]. WS_2 and MoS_2 have been identified as efficient HER and OER catalysts at longer intervals due to their better chemical and environmental inertness [16].

Most of the reported electrocatalysts are amorphous and need polymer binders to be assembled before being used in water electrolysis. These binders reduce the catalytic area, and their stability at higher current densities remains a matter of concern. Creating three-dimensional nanostructures by expanding the active surface area is one of the most effective ways to improvecatalytic activity. In that aspect, electrodeposition is an easy and facile method for fabricating electrocatalysts with good catalytic properties. This method can create different nanostructures by controlling and optimising the deposition parameters. Moreover, electrodeposition is a scalable process that can produce industrial electrocatalysts [17].

A combination of Ni and WS_2 known for their individual catalytic potential in alkaline water splitting remains underexplored. Here in, to the best of the author's knowledge we report for the first time the development of Ni-WS_2 coated stainless steel mesh (SSM) via electrodeposition that can function as an efficient, binder-free bi-functional electrocatalyst in alkaline medium. The deposition conditions were fine-tuned so that the developed SSM has a hierarchical structure of WS_2 clusters, nodules, and Ni pine cones (micro-nano), resulting in a "cacti/cauliflower-like" appearance with highly active surface area. From the electrochemical studies, it was found that Ni-WS_2 coated SS mesh demonstrated improved electrocatalytic characteristics and is stable and durable when tested continuously over a sufficient period. As a result, this easy, environmentally friendly, and economical approach for fabricating efficient and durable bi-functional electrocatalysts would be a promising one for practical catalytic applications as a non-precious transitional metal-based alternative to Pt- and Ir/Ru-based expensive benchmark catalysts.

2. Experimental

2.1. Materials

Raj filters supplied stainless steel mesh (pore size < 100 μm). Nickel salts ($NiSO_4$•6 H_2O, $NiCl_2$•6 H_2O) and Boric acid (H_3BO_3) were obtained from Merck. Alfa Aesar provided Cetyltrimethylammonium bromide ($CH_3(CH_2)_{15}N(Br)(CH_3)_3$) and Saccharin ($C_7H_5NO_3S$). Tungsten disulphide nanoparticles (WS_2, 90 nm) were acquired from Sigma-Aldrich.

2.2. Fabrication of Ni-WS_2 coated SS mesh

Ni-Watts bath comprising $NiSO_4$•6 H_2O, $NiCl_2$•6 H_2O, and H_3BO_3 was used for electrodeposition. WS_2 nanoparticles, CTAB, and saccharin, after ultrasonication for 30 minutes, were thoroughly mixed and added to the Ni bath. Ni-WS_2 bath was maintained at a pH of 4. The authors have reported the detailed procedure for fabricating Ni-WS_2 coated SS mesh elsewhere [18] (Fig. 1).

2.3. Characterisation of the developed mesh

The morphologies and chemical composition of the elements present in the developed mesh were studied by FE-SEM (FEI NOVA NANOSEM 450) and Zeiss EVO 18 cryo-SEM (with EDS), respectively. The 3D morphology and roughness of samples were analysed by Atomic Force Microscopy (AFM, Bruker Multimode-8HR in tapping mode). The crystalline phase structure and composition of all the samples were studied with a Bruker D2 Phaser X-ray diffractometer with Cu - K_α radiation (λ = 1.5406 A°) in the 0–90° range.

The electrochemical measurements were done using a three-electrode setup in 1 M KOH using a CHI660E electrochemical workstation. Platinum wire (working electrode), Ag/AgCl in saturated KCl (reference electrode), and Ni-WS_2 coated SS mesh (counter electrode) were the electrodes employed. The voltammetric techniques LSV (linear sweep voltammetry), CV (cyclic voltammetry), EIS (electrochemical impedance spectroscopy) and CA (chronoamperometry) were used to analyse the electrochemical activity and stability of the electrode material. As a preliminary step before actual measurements, CV in a reduction potential region was carried out for several cycles to activate the materials. Once the CV curves became consistent, LSV measurements were carried out to analyse the current response. All the measurements were performed at a scan rate of 2 mVs^{-1}, and EIS measurements were taken at a frequency range (100 KHz to 100 mHz). Chronoamperometric studies for about 50 h was performed to confirm the stability, and the polarisation curves before and after 1000 cycles were also recorded.

3. Results and discussion

3.1. Morphology

Fig. 2(a) indicates the uniform surface of the uncoated mesh. Electrodeposition has a vital role in determining the morphology of SSM.

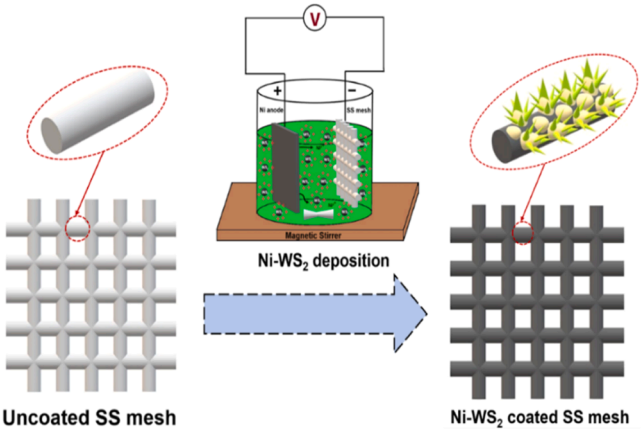

Fig. 1. One-step preparation process of Ni-WS_2 coated SSM

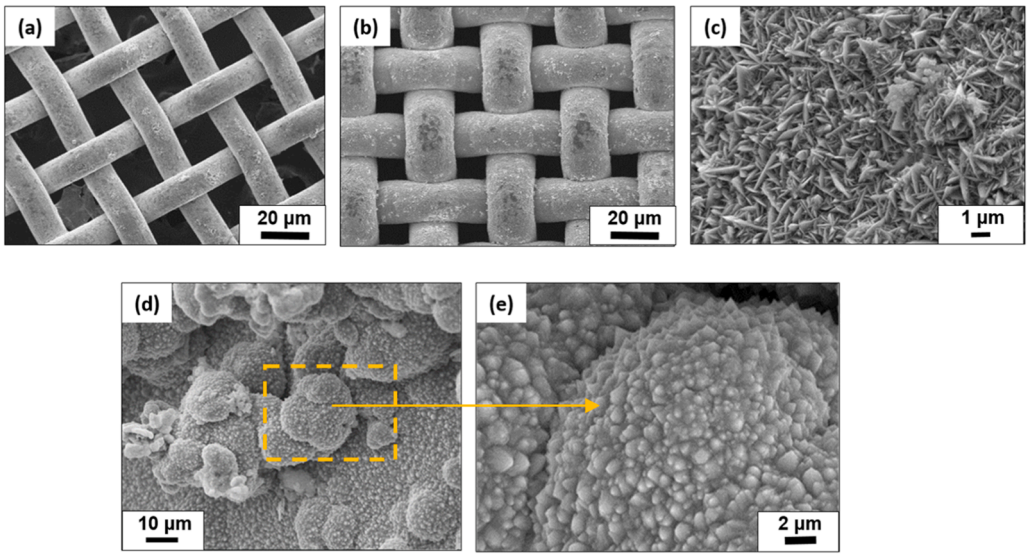

Fig. 2. Surface morphologies of different meshes (a) Uncoated stainless steel mesh, (b) Pure nickel coated mesh, (c) Pine cone like morphology in pure Ni coated mesh, (d) Cacti/cauliflower like structure in Ni-WS_2 coated mesh, (e) High magnification image of Ni-WS_2 coated mesh showing thorn-like projections

Fig. 2(b-c) suggests that the pure Ni-coated mesh possesses a pine-cone structure. This pine cone structure of fine Ni crystals increases the active surface area, improving the electrocatalytic activity [19]. Ni-WS_2 coated SS mesh has a rough protruding hierarchical structure of WS_2 clusters and nodules along with Ni pinecones (Fig. 2(d-e)). The progressive micro/nanostructure formation occurs due to WS_2 particle incorporation in and around the Ni matrix. Further, incorporating conductive WS_2 particles into the electrolytic bath resulted in a difference in current distribution during electrodeposition [20]. SEM image of higher magnification (Fig. 2(e)) indicates that the nodular structures are composed of Ni grains bound together with petal-like WS_2 particles having highly active edge sites. Since these edge sites of high active surface area are exposed maximum in the cacti/cauliflower-like structures, these peculiar structures can contribute towards the catalytic activity of the developed mesh.

Fig. 3 shows the elemental distribution of Ni-WS_2 coated SS mesh. Elements such as nickel (Ni) (Fig. 3(b)), tungsten (W) (Fig. 3(c)), and sulphur (S) (Fig. 3(d)) were identified. Ni is primarily seen in the base of the coating, while sulphur is mainly seen in cauliflower-like structures.

Pure Ni-coated mesh has an average roughness (R_a) of 87.6 nm, whereas Ni-WS_2 coated mesh has 168 nm. Fig. 4(a) shows that the surface of pure Ni-coated mesh has unevenly placed clusters of various heights. Fig. 4(b) of Ni-WS_2 mesh reveals protrusions (valleys or bumps) with greater heights and diameters. These results are in agreement with the observation of micro-nano hierarchical structure of high surface roughness factor in Ni-WS_2 coated SS mesh. These rough structures often have more exposed edges, corners or even defects usually more reactive and act as active sites for catalysis.

3.2. Phase composition and crystalline structure analysis

Fig. 5(a) shows the XRD graph of pure Ni-coated SS mesh. Three peaks of Ni at 44.32°(111), 51.77°(200), and 76.3°(220) indicate the fcc structure of Ni metal (JCPDS 04–0850). The typical fcc structure of Ni provides a large surface area, providing more accessible active sites for catalytic reactions and enhanced stability. Adding WS_2 particles created additional nucleation sites that caused significant microstructural changes and resulted in smaller Ni grains. Significant peaks are observed in the case of Ni-WS_2 SSM at 14°(002), 29.1°(004), 33°(100), 40°(103), 49°(110), 58°(008), and 60°(112) validating the hcp structure of WS_2 ((JCPDS 84–1398) (Fig. 5(b)).The strong Ni(111) peak of Ni-WS_2 coated SSM indicates high inherent catalytic activity, appropriate hydrogen binding energy and higher stability in alkaline environments.

3.3. Electrocatalytic activity

The electrocatalytic hydrogen evolution and oxygen evolution ability of the developed catalyst material were evaluated by LSV. The lower scan rate of 2 mV/s was used to perform the analysis as it enhances the ionic and electronic movement, thereby improving the kinetics of water-splitting reactions. Hydrogen evolution was studied in the negative potential region, and Fig. 6(a) shows the HER polarisation curves of the samples. The extra potential required to attain a current density of 10 mA cm^{-2}, the overpotential (η_{10}), is considered for estimating the

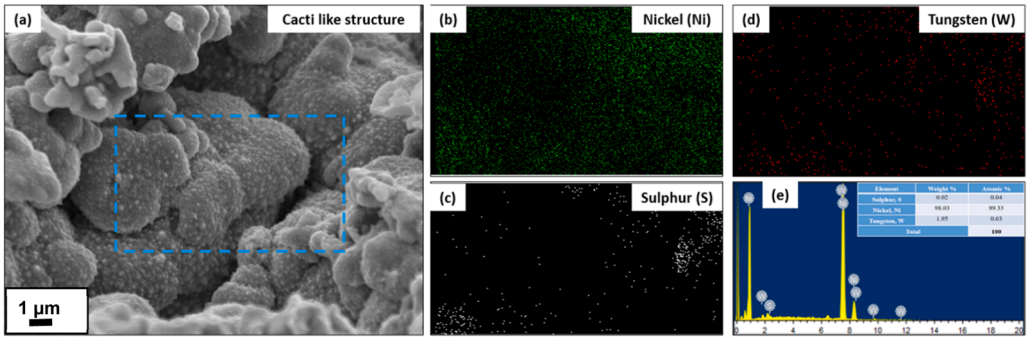

Fig. 3. EDS analysis of Ni-WS_2 coated SS mesh.

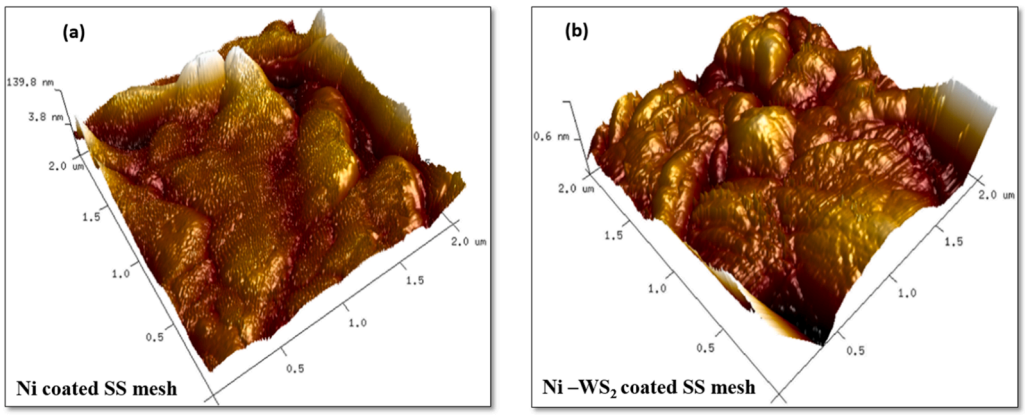

$R_a = 87.6$ nm; $R_q = 110$ nm

$R_a = 168$ nm; $R_q = 199$ nm

Fig. 4. 3D surface morphologies of the developed meshes

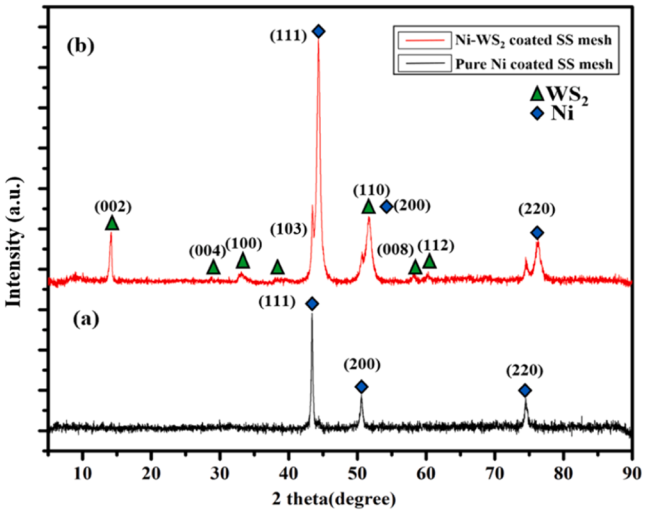

Fig. 5. XRD pattern of coated meshes (a) Pure Nickel, (b) Ni-WS_2

catalytic activity of the materials [21]. Ni-WS_2 coated SSM outperforms pure Ni coated SSM regarding η_{10}. Pure Ni coated SSM required an overpotential of 189 mV, whereas Ni-WS_2 coated SSM needed an overpotential of 89 mV to generate a current density of 10 mA/cm^2, which is comparable with that of commercially available Pt/C catalyst material having an overpotential of about 43 mV [22].

Ni coated SSM could not deliver higher currents even when higher potentials were applied, but Ni-WS_2 coated SSM delivered higher currents with increased potential. This enhancement in activity arises due to the synergistic effect of Ni and WS_2 nanoparticles. As explained in the SEM analysis, the "cactus-like"/ "cauliflower-like" structures of Ni-WS_2 coated SSM are beneficial for improving the electrocatalytic activity of the material. The edge sites of WS_2 are more catalytically active than the basal planes [23]. The particular micro-nano hierarchical morphology helps more electrolyte access and exposes more edge sites of WS_2, thereby enhancing the electrocatalytic activity. In addition, this peculiar morphology enhances the mass and charge transfer, influencing the catalytic activity. Thus Ni-WS_2 coated SSM proves to be an excellent electrode material to generate hydrogen through electrolysis of water.

Fig. 6(b) shows the Tafel plots of the catalyst material, which indicate the kinetics of electron transfer reactions. Tafel slope is determined from the linear portion of the voltammetric curve using the equation

$$\eta = b\log(j) \quad (1)$$

Here, out of the two materials, Ni-WS_2 coated SSM exhibited a fair Tafel slope value of 102 mV dec^{-1} compared to Ni coated SSM with a slope of 151 mV dec^{-1}. This indicates the faster electron adsorption-desorption mechanism of Ni-WS_2 coated SSM. The Tafel slope values of Ni-based systems are found to be relatively more than the theoretical value of 120 mV dec^{-1} (for Volmer pathway). However, various results with higher Tafel slope values for Ni-based alloys and composites have been reported so far [24–26]. The increase in Tafel slope may have arisen due to the presence of a surface oxide layer over the electrode. In this circumstance, the applied external potential will be used for initiating the HER and also to overcome the barrier caused by the oxide layer [27,28].

Along with electrocatalytic activity, electrochemical stability is an essential criterion that determines the efficiency of an electrocatalyst. The long-term stability of Ni-WS_2 coated SSM is investigated using chronoamperometry and the current response is shown in Fig. 6(c). The CA measurements were carried out at a reduction potential of 90 mV, and Ni-WS_2 coated SS mesh generated a current density of 10 mA cm^{-2} for a higher duration of 50 h. Even after 50 h of continuous hydrogen generation the binder-free electrode material was able to retain its activity, which is highly favourable for practical electrolysers. The stable performance of the material was also validated by recording the HER polarisation curves before and after 1000 cycles of continuous hydrogen generation. Fig. 6(d) shows that HER polarisation curves before and after 1000 cycles of CV measurement. It can be observed from the figure that the initial curve retrace the final curve even after long cycles of measurements. The overpotentials at 10, 20 and 50 mA cm^{-2} were found to be moreover the same. This again confirms the long-term feasibility of the electrode material.

Fig. 7(a) shows the OER polarisation curves of the catalyst materials. It is clearly evident that Ni-WS_2 coated SSM outperforms Ni coated SSM and is suitable for OER activity. Ni coated SSM required an overpotential of 320 mV, while Ni-WS_2 coated SSM required an overpotential of 230 mV to yield a current density of 10 mA cm^{-2}, which is comparable with that of commercially available IrO_2 catalyst material (310 mV) [29,30]. At the same time, to generate 20 mA cm^{-2} and 100 mA cm^{-2} current density, Ni coated SSM needed 360 mV and 540 mV of additional potential, respectively, whereas Ni-WS_2 coated SSM required extra potentials of 260 mV and 380 mV, respectively. Also, the current increased linearly for Ni-WS_2 coated SSM, which indicates faster electron transfer within the material [24].

Fig. 7(b) shows the OER Tafel plots of the electrode materials, which clearly show the enhanced oxygen evolution kinetics. The Ni-WS_2 coated SSM had a Tafel slope of 99 mV dec^{-1} whereas Ni coated SSM exhibited a Tafel slope of 118 mV dec^{-1}. OER is a four-electron transfer

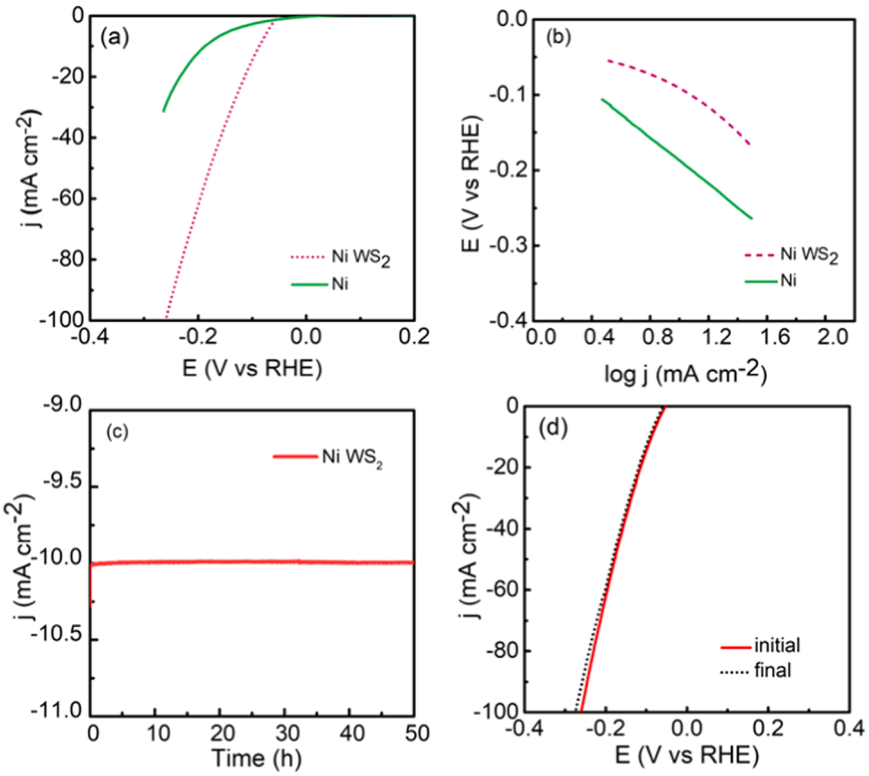

Fig. 6. (a) HER polarisation curves, (b) Tafel plots of Ni-coated and Ni-WS_2 coated SSM, (c) Amperometric i-t curve showing the stability of Ni-WS_2 coated SSM, and (d) the LSV curves before and after 1000 cycles of hydrogen evolution reaction

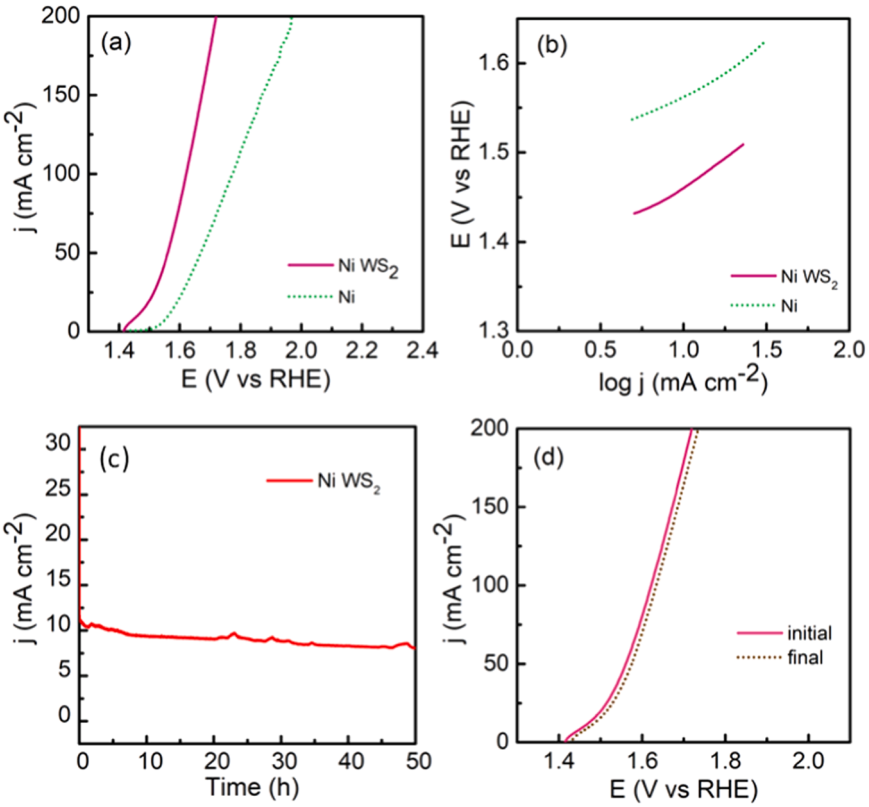

Fig. 7. (a) OER polarisation curves, (b) Tafel plots of Ni-coated and Ni-WS_2 coated SSM (c) Amperometric i-t curve showing the stability of Ni-WS_2 coated SSM, and (d) LSV curves before and after 1000 cycles of oxygen evolution reaction

process in which molecular oxygen is liberated by the electro-oxidation of hydroxyl groups (OH^-) in an alkaline environment. Fig. 7(c) shows CA OER curve for Ni-WS_2 coated SSM at a potential of 250 mV. Ni-WS_2 coated SSM exhibited stable amount of oxygen generation for about fifty h. Again, as in the case of HER activity, the electrode material exhibited stable performance even after 1000 cycles of oxygen evolution. Fig. 7(d) shows the LSV curves before and after the cyclic measurement. It is evident that the initial and the final polarisation curves vary only slightly in terms of a few milli volts. This again elucidates the long-term stable activity of the catalyst material.

The enhancement in electrocatalytic activity of Ni-WS_2 coated SSM is due to the hierarchical growth of Ni pinecones and WS_2 clusters into cacti/cauliflower-like morphology as well as due to the synergistic electrochemical properties of metallic Ni and the catalytically active TMDC–WS_2. The material's electrocatalytic active surface area (ECSA) was calculated by recording the cyclic voltammograms in a non-Faradaic region. Figure S1(a) and (b) show the CV curves obtained at different scan rates for Ni coated and Ni-WS_2 coated SSM, and Fig. 8(a) shows the linear plot obtained to determine the C_{dl} value. The slope of the j vs ν curve gives the double-layer capacitance. Then, the ECSA is calculated using the equation.

$$ECSA = \frac{C_{dl}}{C_s} \quad (2)$$

Usually, in 0.5 M H_2SO_4, C_s is taken as 35 μF cm^{-2}; in 1 M KOH it is 40 μF cm^{-2} [31]. Ni-coated SSM exhibited a C_{dl} value of 1.78 mF cm^{-2}, significantly less than that of Ni-WS_2 coated SSM, which delivered a C_{dl} value of 35 mF cm^{-2}. The Ni-WS_2 coated SSM provided a higher ECSA value of 89 cm^2 while Ni coated SSM had 44 cm^2 ECSA.

Thus, higher ECSA (89 cm^{-2}) accounts for the higher water-splitting ability of the catalyst material Ni-WS_2 coated SSM. These observations and results indicate that the hierarchical structure of the electro-deposited Ni-WS_2 coated SSM enhanced the active surface area of the electrode, thereby resulting in increased electrolyte access. Moreover, this binder-free electrode fabrication method facilitates increased conductivity and electrolyte wettability, thereby enhancing the activity and stability of the catalyst materials.

EIS measurements were carried out to analyze the electrochemical phenomena at the electrode-electrolyte interface. The EIS measurements were carried out at different potentials slightly above and below the overpotentials of respective HER and OER. Fig. 8(b) and (c) show the Nyquist curves of Ni WS_2 recorded in a frequency range of 100 mHz to 100 KHz at different overpotentials. The Nyquist plots of Ni-WS_2 coated SS mesh for HER and OER reflect the reaction kinetics at different potentials. Nyquist plots exhibited more capacitive behaviour than resistive behaviour, in the Non-Faradaic region (low potential region) unlike higher potentials where chemical reactions are more likely to occur [32-35]. The capacitive behaviour indicates that the surface sites of the catalyst are available for charge storage, revealing how easily reactive species can adsorb onto the catalyst surface during HER and OER.

Figure S2 (a) and (b) show the impedance curve of Ni-WS_2 coated SSM fitted using ZSimpWIN3.21 software & inset shows the equivalent plot obtained. Analysing the equivalent circuit corresponding to the Nyquist plot of HER and OER activity (Figure S2(a-b)), Rs accounts for the electrolytic resistance and Q_1 (CPE_1) models the double-layer capacitance, mainly due to surface roughness of the catalyst. Q_2 (CPE_2) and R_2 demonstrates the secondary surface or interfacial phenomena, such as adsorption of reaction intermediates (H*, O*, OH*) or changes in surface coverage of the catalyst. The Warburg element reflects the diffusion of protons or hydrogen species or oxygen [36,37].

3.4. Overall water splitting ability

Since Ni-WS_2 coated SSM proved to be suitable for both hydrogen and oxygen evolution, a full cell comprising the coated mesh as both anode and cathode was designed (Figure S3). The bi-functional activity of the electrocatalyst for simultaneous hydrogen and oxygen generation was examined in the alkaline environment. Fig. 9(a) shows the polarisation curve of the full cell, indicating the changes in the current generated in the electrode versus the applied voltage. To generate a current density of 10 mA/cm^2, the cell required a potential of 1.56 V. As the applied voltage increased, the current generated also increased abruptly, indicating the bi-functional activity of the electrode material. Along with electrocatalytic activity, the long-term stability of the material was evaluated using chronoamperometry. Fig. 9(b) shows the current versus time plot obtained for the full cell. It can be seen that the current generated remained almost constant for about 50 h of continuous energy generation.

The electrodes were able to maintain the current density at 10 mA/cm^2 at an applied potential of 1.56 V even after continuous usage. These results indicate that Ni WS_2 coated SSM can be effectively used as a bi-functional catalyst material for overall electrochemical water splitting in alkaline medium. A comparison of a few of the already reported Ni-based bi-functional catalysts in alkaline media was done, and it was found that the developed Ni-WS_2 coated SSM is a promising potential choice for overall water splitting (Table S1). By further modifying the deposition parameters and optimising the growth of Ni-WS_2 over SS mesh, the efficiency of the bi-functional catalyst can be scaled up.

The HER and OER activity of Ni-WS_2 coated SS mesh can be attributed to the active sites over both Ni and WS_2. The sulphur edges of WS_2 are active for both HER and OER. The Gibbs free energy of hydrogen or hydroxyl ion adsorption (ΔG_H/ ΔG_{OH}) of the sulfided edges make them active HER/OER sites. Various studies resonating the catalytic activity of the sulfided edges of transition metal dichalcogenides like WS_2 and MoS_2 have been reported [23]. This is further supported by our recent study of MoSSe based systems. In this study, the Gibbs free energy of hydrogen adsorption (ΔG_H) of both sulfided and selenided edges of molybdenum was calculated. And it was found out that ΔG_H is minimum

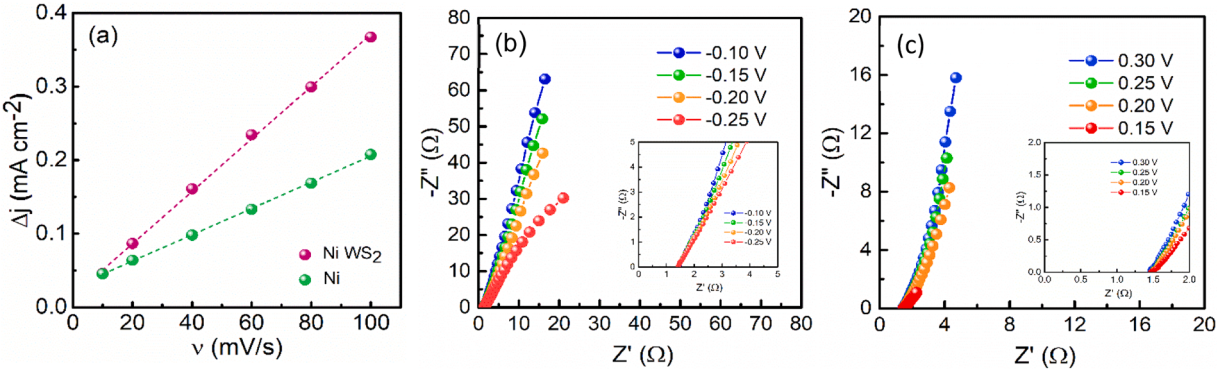

Fig. 8. (a) Plot of current density vs scan rate and (b) and (c) Nyquist curves of Ni WS_2 coated SSM at different potentials of HER & OER

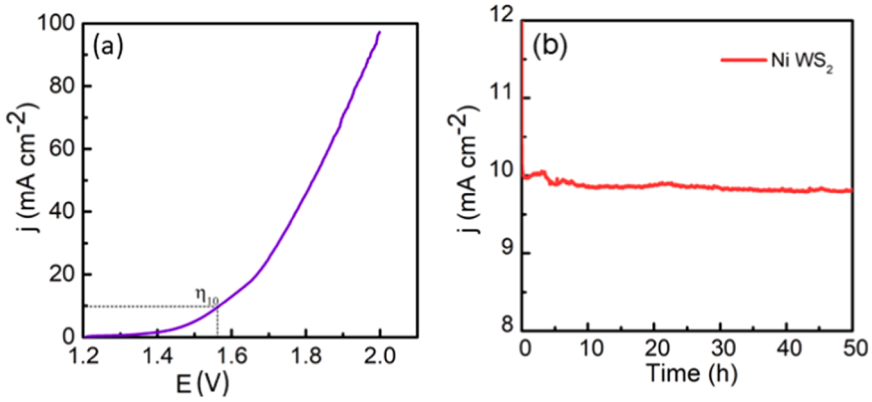

Fig. 9. (a) Polarisation curve of the full cell using Ni WS2 coated SSM, (b) Amperometric i-t curve showing the long-term stability of the full cell

for H^+ adsorption on sulfided Mo edges [38]. Nickel provides a conductive backbone that facilitates efficient electron transfer during electrochemical reactions in water splitting. The d-band electronic structure of Ni allows optimal binding of intermediates such as hydrogen (H*) for HER or oxygen-containing species (O*, OH*) for OER [39].

Thus, the excellent bi-functional electrocatalytic activity of Ni-WS_2 coated SSM is due to: (1) Ni (111) plane and edge sites of WS_2 particles possess high inherent catalytic activity, appropriate hydrogen binding energy and are stable in alkaline environments, (2) increase in the active catalytic surface area resulting from the formation of micro-nano hierarchical structure, (3) enhancement in the intrinsic electrocatalytic activity due to the synergistic effect between Ni (low hydrogen overpotential) and WS_2 particles (high hydrogen adsorption), (4) the peculiar structure of the catalyst significantly increases ECSA as well as enables the flow of electrons and gas release, (5) the direct growth of Ni and WS_2 particles on SS mesh as a binder-free catalyst via one-step electrodeposition has several advantages, including close contact, outstanding mechanical adherence, and superior durability.

4. Conclusions

A Ni-WS_2 coated SS mesh with a micro-nano hierarchical structure that can act as a bi-functional catalyst in alkaline water splitting was developed by electrodeposition. The catalyst contained a rough hierarchical surface of WS_2 clusters and Ni pinecones. LSV tests showed that the overpotentials for hydrogen and oxygen evolution reactions for Ni-WS_2 coated SS mesh were −89 mV and 230 mV respectively, much lower than pure Ni-coated mesh. The electrocatalytic activity of Ni-WS_2 coated SS mesh was higher due to the increased catalytic surface area and ready detachment of the adsorbed H_2 from the electrode surface. A full-cell alkaline electrolyser using Ni-WS_2 coated SS mesh as anode and cathode delivered a current density of 10 mA/cm^{-2} at an applied potential of 1.56 V. Moreover, the electrochemical cell remained stable for 50 h of continuous cycling. This enhanced activity arises due to the binder-free fabrication process of the electrode materials, the three-dimensional morphology of Ni-WS_2, and the catalyst material's higher electrochemical active surface area and lower charge-transfer resistance. In light of its excellent electrocatalytic activity for HER and OER and its ease of fabrication and availability, this bi-functional composite catalyst can provide an efficient, cost-effective, and facile approach to developing large-scale industrial alkaline water electrolysers.

CRediT authorship contribution statement

Revathy Sreekumar: Investigation, Methodology, Formal analysis, Writing – original draft, Writing – review & editing. **Shilpa Radhakrishna Pillai**: Investigation, Formal analysis, Writing – original draft, Writing – review & editing. **Rakhi Raghavan Baby**: Resources, Writing – review & editing, Supervision. **Sreejakumari Sukumaran Suseelamma**: Resources, Writing – review & editing, Supervision.

Declaration of Competing Interest

The authors declare that they have no known competing financial interests or personal relationships that could have appeared to influence the work reported in this paper.

Acknowledgements

The first author, Revathy Sreekumar, is grateful to DST, Government of India, for providing the Inspire fellowship grant (IF 180987). Authors Shilpa. R. and Rakhi R.B. are thankful for the financial support received from the IC MAP project (DST/TMD/IC-MAP/2K20/01) of the Technology Mission Division (Energy, Water, and all Others), Department of Science & Technology, Ministry of Science & Technology, India. The authors acknowledge Mr Harish Raj and Ms Swathy Lekshmy V.S. for their assistance in the characterisation of the samples. Mr Visakh Manoj is thanked for his help in creating the graphical abstract and schematic illustrations.

Appendix A. Supporting information

Supplementary data associated with this article can be found in the online version at doi:10.1016/j.mtcomm.2025.111860.

Data availability

No data was used for the research described in the article.

References

[1] M. Tvaronavičienė, J. Baublys, J. Raudeliūnienė, D. Jatautaitė, Global energy consumption peculiarities and energy sources: role of renewables, 2019. https://doi.org/10.1016/B978-0-12-817688-7.00001-X.
[2] M.S. Dresselhaus, I.L. Thomas, Dresselhaus, M.S. Thomas, 2001 - alternative energy technologies, Nature 414 (2001) 332–337. ⟨www.nature.com⟩.
[3] M.M. Najafpour, S. Salimi, M. Hołyńska, S.I. Allakhverdiev, A highly dispersible, magnetically separable and environmentally friendly nano-sized catalyst for water oxidation, Int. J. Hydrog. Energy 41 (2016) 4616–4623, https://doi.org/10.1016/j.ijhydene.2016.01.056.
[4] G.W. Crabtree, M.S. Dresselhaus, M.V. Buchanan, The hydrogen economy, Phys. Today 57 (2004) 39–44, https://doi.org/10.1063/1.1878333.
[5] S. Anwar, F. Khan, Y. Zhang, A. Djire, Recent development in electrocatalysts for hydrogen production through water electrolysis, Int. J. Hydrog. Energy 46 (2021) 32284–32317, https://doi.org/10.1016/j.ijhydene.2021.06.191.
[6] P. Häussinger, R. Lohmüller, A.M. Watson, Hydrogen, 2. Production, Ullmann'S. Encycl. Ind. Chem. (2011), https://doi.org/10.1002/14356007.o13_o03.
[7] V.R. Stamenkovic, D. Strmcnik, P.P. Lopes, N.M. Markovic, Energy and fuels from electrochemical interfaces, Nat. Mater. 16 (2016) 57–69, https://doi.org/10.1038/nmat4738.

[8] Y. Yan, B.Y. Xia, B. Zhao, X. Wang, A review on noble-metal-free bifunctional heterogeneous catalysts for overall electrochemical water splitting, J. Mater. Chem. A 4 (2016) 17587–17603, https://doi.org/10.1039/C6TA08075H.
[9] I. Roger, M.A. Shipman, M.D. Symes, Earth-abundant catalysts for electrochemical and photoelectrochemical water splitting, 2017. https://doi.org/10.1038/s41570-016-0003.
[10] X.-D. Wang, H.-Y. Chen, Y.-F. Xu, J.-F. Liao, B.-X. Chen, H.-S. Rao, D.-B. Kuang, C.-Y. Su, Self-supported NiMoP2 nanowires on carbon cloth as an efficient and durable electrocatalyst for overall water splitting, J. Mater. Chem. A 5 (2017) 7191–7199, https://doi.org/10.1039/C6TA11188B.
[11] G. Barati Darband, M. Aliofkhazraei, A.S. Rouhaghdam, Facile electrodeposition of ternary Ni-Fe-Co alloy nanostructure as a binder free, cost-effective and durable electrocatalyst for high-performance overall water splitting, J. Colloid Interface Sci. 547 (2019) 407–420, https://doi.org/10.1016/j.jcis.2019.03.098.
[12] Y. Qiu, M. Sun, J. Cheng, J. Sun, D. Sun, L. Zhang, Bifunctional Ni-Fe/NiMoNx nanosheets on Ni foam for high-efficiency and durable overall water splitting, Catal. Commun. 164 (2022) 106426, https://doi.org/10.1016/j.catcom.2022.106426.
[13] Y. Shudo, M. Fukuda, M.S. Islam, K. Kuroiwa, Y. Sekine, M.R. Karim, S. Hayami, 3D porous Ni/NiO: Xas a bifunctional oxygen electrocatalyst derived from freeze-dried Ni(OH)2, Nanoscale 13 (2021) 5530–5535, https://doi.org/10.1039/d0nr08034a.
[14] L. Wang, Y. Li, M. Xia, Z. Li, Z. Chen, Z. Ma, X. Qin, G. Shao, Ni nanoparticles supported on graphene layers: an excellent 3D electrode for hydrogen evolution reaction in alkaline solution, J. Power Sources 347 (2017) 220–228, https://doi.org/10.1016/j.jpowsour.2017.02.017.
[15] L.P. Hao, A. Hanan, R. Walvekar, M. Khalid, F. Bibi, W.Y. Wong, C. Prakash, Synergistic integration of mxene and metal-organic frameworks for enhanced electrocatalytic hydrogen evolution in an alkaline environment, Catalysts 13 (2023) 1–13, https://doi.org/10.3390/catal13050802.
[16] A. Das, D. Roy, B. Kumar Das, M.I. Ansari, K.K. Chattopadhyay, S. Sarkar, Zinc doping induced WS2 accelerating the HER and ORR kinetics: a theoretical and experimental validation, Catal. Today 423 (2023) 113921, https://doi.org/10.1016/j.cattod.2022.10.003.
[17] G. Barati Darband, M. Aliofkhazraei, A.S. Rouhaghdam, Facile electrodeposition of ternary Ni-Fe-Co alloy nanostructure as a binder free, cost-effective and durable electrocatalyst for high-performance overall water splitting, J. Colloid Interface Sci. 547 (2019) 407–420, https://doi.org/10.1016/j.jcis.2019.03.098.
[18] R. Sreekumar, S. Eravath Thazhakkuni, S. Sukumaran Suseelamma, Fabrication of a robust superhydrophobic stainless steel mesh for efficient oil/water separation, J. Ind. Eng. Chem. 135 (2024) 425–433, https://doi.org/10.1016/j.jiec.2024.01.054.
[19] G. Barati Darband, M. Aliofkhazraei, A. Sabour Rouhaghdam, Nickel nanocones as efficient and stable catalyst for electrochemical hydrogen evolution reaction, Int. J. Hydrog. Energy 42 (2017) 14560–14565, https://doi.org/10.1016/j.ijhydene.2017.04.120.
[20] H. Shalom, T. Bendikov, Y. Feldman, N. Lachman, A. Zak, R. Tenne, Chemical control of the surface of WS2 nanoparticles, Chem. Phys. Lett. 761 (2020) 138052, https://doi.org/10.1016/j.cplett.2020.138052.
[21] S. Niu, S. Li, Y. Du, X. Han, P. Xu, How to reliably report the overpotential of an electrocatalyst, ACS Energy Lett. 5 (2020) 1083–1087, https://doi.org/10.1021/acsenergylett.0c00321.
[22] B. Jiang, S. Liu, L. Cheng, L. Zhou, H. Cui, M. Liu, M. Wen, C. Wang, W. Wang, S. Li, X. Sun, Mass synthesis of Pt/C catalysts with high Pt loading for low-overpotential hydrogen evolution, Int. J. Hydrog. Energy 58 (2024) 268–278, https://doi.org/10.1016/j.ijhydene.2024.01.183.
[23] P.V. Sarma, A. Kayal, C.H. Sharma, M. Thalakulam, J. Mitra, M.M. Shaijumon, Electrocatalysis on edge-rich spiral WS2 for hydrogen evolution, ACS Nano 13 (2019) 10448–10455, https://doi.org/10.1021/acsnano.9b04250.
[24] D. Wang, Q. Li, C. Han, Z. Xing, X. Yang, When NiO@Ni Meets WS2 nanosheet array: A highly efficient and ultrastable electrocatalyst for overall water splitting, ACS Cent. Sci. 4 (2018) 112–119, https://doi.org/10.1021/acscentsci.7b00502.
[25] Q. Zhou, S. Liu, Y. Zhang, Z. Zhu, W. Su, M. Sheng, Fabrication of porous Cu supported Ni-P/CeO2 composite coatings for enhanced hydrogen evolution reaction in alkaline solution, Ceram. Int. 46 (2020) 20871–20877, https://doi.org/10.1016/j.ceramint.2020.05.133.
[26] F. Bao, E. Kemppainen, I. Dorbandt, R. Bors, F. Xi, R. Schlatmann, R. van de Krol, S. Calnan, Understanding the hydrogen evolution reaction kinetics of electrodeposited nickel-molybdenum in acidic, near-neutral, and alkaline conditions, ChemElectroChem 8 (2021) 195–208, https://doi.org/10.1002/celc.202001436.
[27] M. Grdeń, G. Jerkiewicz, Influence of surface treatment on the kinetics of the hydrogen evolution reaction on bulk and porous nickel materials, Electrocatalysis 10 (2019) 173–183, https://doi.org/10.1007/s12678-019-0506-6.
[28] Z. Liang, H.S. Ahn, A.J. Bard, A study of the mechanism of the hydrogen evolution reaction on nickel by surface interrogation scanning electrochemical microscopy, J. Am. Chem. Soc. 139 (2017) 4854–4858, https://doi.org/10.1021/jacs.7b00279.
[29] Y. Huang, L.W. Jiang, B.Y. Shi, K.M. Ryan, J.J. Wang, Highly efficient oxygen evolution reaction enabled by phosphorus doping of the Fe electronic structure in iron–nickel selenide nanosheets, Adv. Sci. 8 (2021) 1–7, https://doi.org/10.1002/advs.202101775.
[30] R. Li, H. Qi, F. Pan, W. Xie, L. Zhou, H. Liu, J. Hu, Defect engineering in bimetallic NiFe-BTC for boosting electrocatalytic oxygen evolution reaction through coordinated ionic liquids, ChemElectroChem 10 (2023) 1–6, https://doi.org/10.1002/celc.202300103.
[31] S.I. Perez Bakovic, P. Acharya, M. Watkins, H. Thornton, S. Hou, L.F. Greenlee, Electrochemically active surface area controls HER activity for FexNi100−x films in alkaline electrolyte, J. Catal. 394 (2021) 104–112, https://doi.org/10.1016/j.jcat.2020.12.037.
[32] M. Nazemi, G.B. Darband, A. Davoodi, Interfacial engineering of Ni–Co–Mn@Ni nanosheet–nanocone arrays as high performance non-noble metal electrocatalysts for hydrogen generation, Nanoscale 16 (2024) 10853–10863, https://doi.org/10.1039/D4NR01404A.
[33] S. Paygozar, A. Sabour Rouhaghdam, A. Seif, G.B. Darband, In-situ electrochemical synthesis of superhydrophilic NiCoMn trimetallic-alloy nanosheets via dynamic hydrogen bubble template method for developing high current density hydrogen production electrocatalyst, J. Mater. Chem. A (2024) 27558–27569, https://doi.org/10.1039/d4ta03698k.
[34] A. Fathollahi, T. Shahrabi, G.B. Darband, Modulation of active surface sites on Ni-Fe-S by the dynamic hydrogen bubble template method for energy-saving hydrogen production, J. Mater. Chem. A 12 (2024) 9038–9054, https://doi.org/10.1039/d3ta07379c.
[35] R. Andaveh, A. Sabour Rouhaghdam, A. Seif, K. Wang, M. Maleki, J. Ai, G. Barati Darband, J. Li, In situ assembly of a superaerophobic CoMn/CuNiP heterostructure as a trifunctional electrocatalyst for ampere-level current density urea-assisted hydrogen production, ACS Appl. Mater. Interfaces 16 (2024) 8717–8732, https://doi.org/10.1021/acsami.3c16122.
[36] A.C. Lazanas, M.I. Prodromidis, Electrochemical impedance spectroscopy—a tutorial, ACS Meas. Sci. Au 3 (2023) 162–193, https://doi.org/10.1021/acsmeasuresciau.2c00070.
[37] V.V. Mohan, M. Mohan, R.B. Rakhi, High performance supercapacitors based on WS2 nanoflower electrodes with commercial-level mass-loading, Surf. Interfaces 42 (2023) 103496, https://doi.org/10.1016/j.surfin.2023.103496.
[38] R. Shilpa, S. Assa Aravindh, S.R. Sarath Kumar, D.D. Sarma, R.B. Rakhi, Designing Mo-based transition metal dichalcogenides for sustainable hydrogen production: anionic substitution and DFT insight, Appl. Surf. Sci. 681 (2025) 161614, https://doi.org/10.1016/j.apsusc.2024.161614.
[39] A. Shukla, S.C. Singh, C.S. Saraj, G. Verma, C. Guo, Ni-based overall water splitting electrocatalysts prepared via laser-ablation-in-liquids combined with electrophoretic deposition, Mater. Today Chem. 23 (2022) 100691, https://doi.org/10.1016/j.mtchem.2021.100691.

Ceramics International xxx (xxxx) xxx

Contents lists available at ScienceDirect

Ceramics International

journal homepage: www.elsevier.com/locate/ceramint

Influence of grain refinement on microhardness, wear behaviour and corrosion resistance of electrodeposited Ni-BN composite coatings

Revathy Sreekumar [a,b], M.S. Priyalekshmi [a], S. Parvathy [a], S.S. Sreejakumari [a,b,*]

[a] Materials Science and Technology Division, CSIR–National Institute for Interdisciplinary Science and Technology (NIIST), Thiruvananthapuram, 695019, India
[b] Academy of Scientific and Innovative Research (AcSIR), Ghaziabad, 201002, India

ARTICLE INFO

Handling Editor: Dr P. Vincenzini

Keywords:
Composite coating
Electrodeposition
Grain refinement
Microhardness
Corrosion resistance
Tribology

ABSTRACT

The serviceability and efficiency of engineering materials can be improved by adopting a suitable surface modification technique. Ni/h-BN composite coatings were successfully coated over mild steel substrate by direct current electrodeposition at an optimised current density of 5 A/dm^2 using Ni Watts bath. The current study explores the influence of grain refinement over microhardness, wear behaviour, and corrosion properties of Ni-BN coatings. The morphology and phase structure of the coatings were assessed by scanning electron microscopy (SEM) and X-ray diffractometry (XRD) respectively. Vickers microhardness tester and pin-on-disc tribometer were employed to evaluate the tribo-mechanical behavior of the coatings. Corrosion performance of the developed coatings was analysed using potentiodynamic polarization and electrochemical impedance spectroscopy techniques in 3.5 wt% corrosive NaCl medium. XRD results revealed that the average crystallite size of Ni-BN coatings reduced when the saccharin concentration rose from 0 to 5 g/l and stabilized around 21 nm. The microhardness of the Ni coating was enhanced by approx. 68 % with the inclusion 5 % saccharin and BN particles. An increment of 5.8730 × 10^4 Ω cm^2 in the charge transfer resistance of the composite coating compared to Ni coating indicates its improved corrosion resistance. Ni–BN composite coatings offered lower coefficient of friction and wear mass loss than the pure Ni coating irrespective of saccharin incorporation. Surface modification of mild steel using electrodeposited Ni-BN composite coating significantly enhances the hardness, corrosion-resistance and wear-resistance, and thus extends service life and operational efficiency under demanding industrial conditions.

1. Introduction

Engineering materials and industrial components subjected to harsh service conditions, experience corrosion, wear and subsequent deterioration. Annually, corrosion and wear-related economic losses account for billions of dollars [1]. Consequently, tailoring surface properties of the engineering components is essential to enhance durability and achieve desired functionalities [2]. Mild steel (MS) is widely favored across sectors such as automotive, machinery, construction, and pipelines due to its cost-effectiveness, availability, excellent weldability, and versatile mechanical behavior [3]. Thus, purposeful surface modification of mild steel is a pragmatic and effective approach to improve resistance against wear and corrosion and extend the service life of the component.

Surface coating is the best possible way to prevent corrosion and wear of engineering materials. Out of all the available surface coatings, metallic coatings are the most suitable, especially for steel structures. These coatings can enhance the corrosion resistance as well as improve the mechanical properties. In comparison with pure metallic coatings, composite coatings provide improved surface protection and better tribological characteristics as they integrate the beneficial properties of both metal matrix and reinforcements [4]. By improving hardness, reducing friction, and providing corrosion protection, these metallic composite coatings significantly extend the service life and reliability of components in harsh operating conditions [5].

Electrodeposition of composite coatings containing secondary particles in the metal matrix has drawn considerable interest lately due to better mechanical, electrochemical and tribological properties of composite coatings [6]. The versatility of electrodeposition, along with its ability to tailor properties of the coating for specific applications, makes

* Corresponding author. Materials Science and Technology Division, CSIR- National Institute for Interdisciplinary Science and Technology, Trivandrum, India.
E-mail addresses: revathyias26@gmail.com (R. Sreekumar), mspriyalekshmi7356@gmail.com (M.S. Priyalekshmi), parvathyv893@gmail.com (S. Parvathy), sreejakumari@niist.res.in (S.S. Sreejakumari).

https://doi.org/10.1016/j.ceramint.2025.07.435
Received 29 April 2025; Received in revised form 30 July 2025; Accepted 31 July 2025
Available online 5 August 2025

it an indispensable technology for a wide range of industries especially requiring durable high-performance materials [7].

As an alternative to harmful hexavalent chromium coatings, nickel-based coatings have gained popularity due to the special characteristics of Ni like excellent mechanical properties and corrosion resistance [8–11]. For further improving the properties of nickel coatings, second-phase particles including hard or soft nanoparticles (oxides, carbides, nitrides, solid lubricants) or polymers, are incorporated into the Ni matrix, forming nickel composite coatings. The particles are selected according to the nature and characteristics of the desired composite coating. Among these, hexagonal boron nitride (h-BN) is an ideal second-phase particle possessing outstanding properties, like chemical inertness, wear resistance and lubrication [12].

Being a layered material with low coefficient of friction, it is a perfect alternative to other solid lubricants that can be used for high-performance applications [13]. Demir et al. [14] added h-BN into Ni-Cr coatings and it was deposited over AISI 1040 steel. It was investigated how h-BN additions affected the microstructure, corrosion resistance, wear resistance, and nano-indentation response. The effect of surfactant concentration over h-BN incorporated Ni-B coatings deposited over steel substrates was studied by Tozar et al. [15]. Tripathi et al. [16] developed Ni-Fe/BN nano-composite coatings incorporated with micron sized BN particles by varying the alloy composition from an additive free bath. While Ni-BN composite coatings are well-established for their lubricating properties [16] and ability to withstand harsh environments, their performance can be further optimised through microstructural modifications, such as grain refinement.

Grain refining leads to improvement in the mechanical and physical properties of electrodeposited coatings by reducing the material's average grain size [17]. According to the Hall-Petch relationship [18], smaller grains can enhance the strength, hardness, and wear resistance of metallic coatings by restricting dislocation movement. In addition, grain refinement may lead to a more homogeneous distribution of reinforcing particles (in this case, h-BN), resulting in a more uniform coating [19]. Saccharin (an organic additive) refines the grain structure, improves the mechanical properties, and increases corrosion resistance and anti-wear characteristics of electrodeposited nickel composite coatings [20].

However, the interplay between grain size, distribution of BN particles, and the overall performance of Ni-BN composite coatings remains an area of active research. While several studies have focused on the individual effects of BN incorporation and electrodeposition parameters, limited research has systematically explored the influence of grain refinement over microhardness, wear behaviour, and corrosion properties of Ni-BN coatings. To the best of the author's knowledge, the current study is a first attempt that seeks to fill this research gap by examining the impact of grain refinement over the mechanical and electrochemical properties of electrodeposited Ni-BN composite coatings. The primary objectives are to evaluate how the grain refinement affects microhardness, wear resistance, and corrosion resistance, and to explore the underlying mechanisms responsible for these changes. Hard Ni-BN composite coatings tailored for industrial applications requiring enhanced durability and longevity are thus developed as part of this study.

2. Experimental

2.1. Materials

Nickel sulphate hexahydrate ($NiSO_4{\cdot}6H_2O$, 98 %), Nickel chloride hexahydrate ($NiCl_2{\cdot}6H_2O$, 98 %), Boric acid (H_3BO_3, 99.5 %) and Sodium chloride (NaCl, 98 %) were purchased from Merck. Hexagonal boron nitride particles (h-BN, 98 %, ~1 μm) were supplied by Sigma-Aldrich. Sodium dodecyl sulphate (SDS, 99 %) and Saccharin ($C_7H_5NO_3S$, 99.5 %) were obtained from Alfa Aesar. All the chemicals were of analytical quality and used without additional purification.

Table 1
Experimental conditions for Ni-BN coating over mild steel substrate.

Electrodeposition parameters	Composition or parameter	Amount	Optimised Conditions
Plating solution	$NiSO_4.6H_2O$	250 g/l	–
	$NiCl_2.6H_2O$	45 g/l	–
	H_3BO_3	40 g/l	–
	Saccharin	3 g/l	–
	SDS	0.5 g/l	–
	BN	1-5 wt%	3 wt%
Deposition Conditions	Current density	2–6 A/dm^2	5 A/dm^2
	Temperature	50–70 °C	60 °C
	Time	20–60 min	30 min
	Stirring rate	700 rpm	–

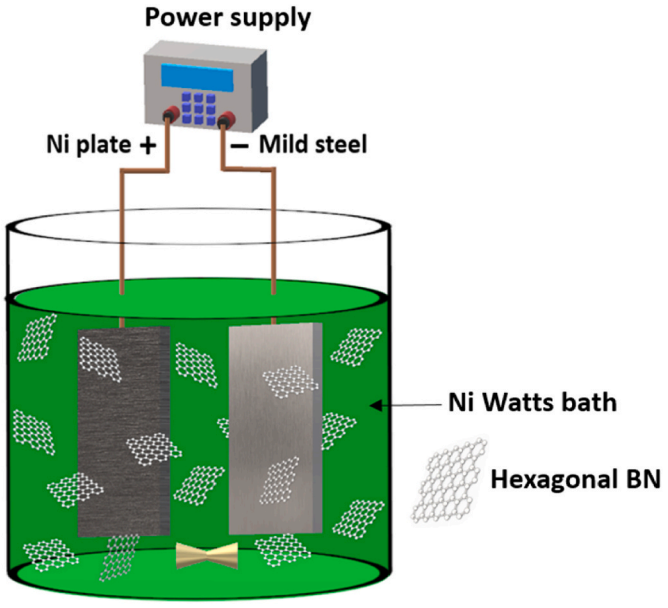

Fig. 1. Schematic illustration of experimental setup for Ni-BN electrodeposition.

2.2. Coating preparation

Ni-h/BN composite coatings were deposited on mild steel substrates from Ni Watts bath containing $NiSO_4{\cdot}6H_2O$ (250 g/l), $NiCl_2{\cdot}6H_2O$ (45 g/l), and H_3BO_3 (40 g/l). Hexagonal BN particles were dispersed in the Watts bath along with surfactant SDS (0.5 g/l) and grain refiner saccharin (3 g/l) (Table 1). The pH of Ni-BN bath was maintained between 4 and 4.5. Before electrodeposition, BN particles were dispersed using an ultrasonicator for 30 min.

Anode was Ni plate (7 cm × 5 cm × 1 cm, 99.7 % purity) and MS substrate (4 cm × 3 cm × 1 cm purity ≥99.5 %, Table S1) was used as cathode. The mild steel samples used for the coating were ground using SiC papers ranging from 80 to 1000 grits, followed by degreasing in acetone and distilled water, ultrasonically cleaned, and dried in the oven. MS samples were further surface activated by dipping in 0.01M HCl and 0.1M NaOH. The anode, Ni plate was polished using 80 and 100 SiC papers. This was followed by degreasing in acetone and distilled water and finally dried in the oven.

Electroplating was carried out at galvanostatic mode under direct current condition. The inter-electrode gap was maintained as 3 cm (Fig. 1). Electrodeposition parameters including current density (2–6 A/dm^2), stirring rate (400–700 rpm) temperature (50–70 °C), time (20–60 min) were varied. Also the amount of h-BN particles was varied between 1 and 5 wt percent (Table 1) Further grain refining studies were carried

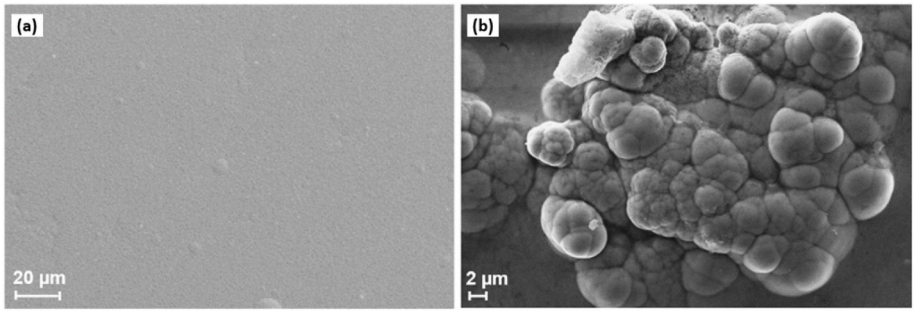

Fig. 2. (a–b): SEM micrographs of pure Ni coated MS.

out by adjusting the amount of saccharin (1–5 g/l) under ideal conditions of 5 A/dm^2 current density for 30 min at 60 °C, 700 rpm stirring rate, and 3 wt percent concentration of h-BN particles. Following electrodeposition, the samples were rinsed with running distilled water and then ultrasonically cleaned in ethanol for 5 min to get rid of any loosely adhered particles before further analysis.

2.3. Characterization of the coatings

The surface morphology and elemental composition of all the coatings were examined using scanning electron microscopy (cryo-SEM with energy dispersive spectroscopy (EDS), EVO MA 18, Carl Zeiss). X-ray diffractometry (X'Pert PRO MDD, PANalytic, Netherlands) was used for phase composition analysis. The diffractograms were obtained over a 2θ range of 10°–90°, with a step size of 0.0001°. The crystallite (grain) size of the coatings was determined using the Scherrer equation (Equation (1)) [21] with respect to the most intense diffraction peak.

Scherrer equation: $D = (K\,\lambda) / (\beta_{corr} \cos\theta)$ (1)

Corrected FWHM, $\beta_{corr} = \sqrt{(\beta_s)^2 - (\beta_i)^2}$ (2)

Where, D = mean size of the crystalline domains which may be ≤ grain size, K = 0.9, Scherrer constant, β_{corr} = corrected full width at half maxima (FWHM) of the peak, θ = Bragg's diffraction angle, λ = wavelength of X-ray, 0.154 nm. Corrected FWHM (β_{corr}) was calculated by considering the instrumental broadening where β_s is FWHM of the sample and β_i is the FWHM contributed by the instrument (Equation (2)).

The samples' microhardness was measured using the Vickers microhardness tester (VHD-1000A, Banbros Engineering) under 50 gf load and a 10-s dwell duration. The sample's hardness was determined at five distinct sites, and the average value was chosen as the hardness value.

Potentiodynamic polarization and electrochemical impedance spectroscopy were conducted at room temperature in a 3.5 wt% NaCl solution using CH Instruments (Model 600, Sinsil International) electrochemical workstation equipped with conventional three-electrode cell. The corrosion tests were carried out using a 250 mL electrochemical cell maintained at 27 ± 0.5 °C. The working electrode, coated piece with exposed area: 1 cm^2 was positioned at a distance of ~2 mm from the reference electrode (saturated calomel electrode) and ~15 mm from the counter electrode (Pt grid). To achieve a stable open circuit potential (OCP) value, the coated piece was immersed in the electrolyte for 20 min prior to the experiment. The potentiodynamic scan was performed from −250 mV to +250 mV of the OCP values with a rate of 1 mV/s. The applied potential vs. current plot (Tafel) was used to determine each sample's corrosion potential and corrosion current density. The impedance measurements were performed applying an AC signal perturbed by 5 mV at OCP in the frequency range of 100 kHz - 0.01 Hz. ZsimpWin software was used to fit the resultant EIS plots to determine the electrochemical parameters. Numerous circuits were matched until the chi-square value decreased to less than 9×10^{-4} or no further fitting improvement was observed.

Wear rate and coefficient of friction (COF) was measured using pin on disc wear testing machine (POD 4.0, DUCOM) under non-lubricated conditions (27 ± 0.5 °C). The measurements were done for Ni-BN, pure Ni coated and bare mild steel samples. The wear samples were mild steel pins (6 mm diameter & 15 mm length). EN31 steel disc having a hardness of ~750 HV was the counter surface. Wear tests were conducted for 15 min at room temperature with a sliding velocity of 0.4 m/s, sliding

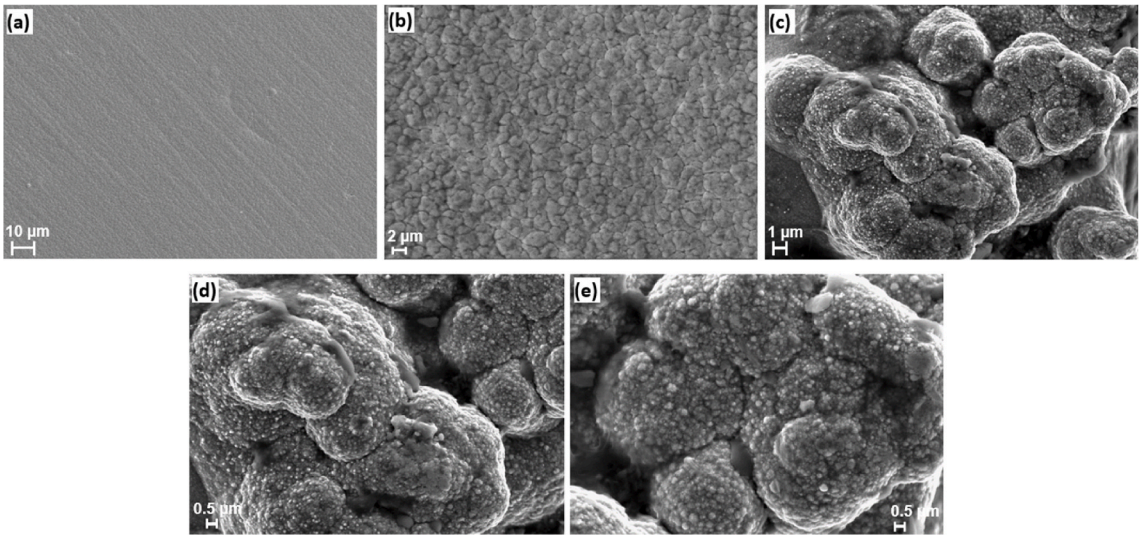

Fig. 3. (a–e): SEM micrographs of Ni-BN coated MS.

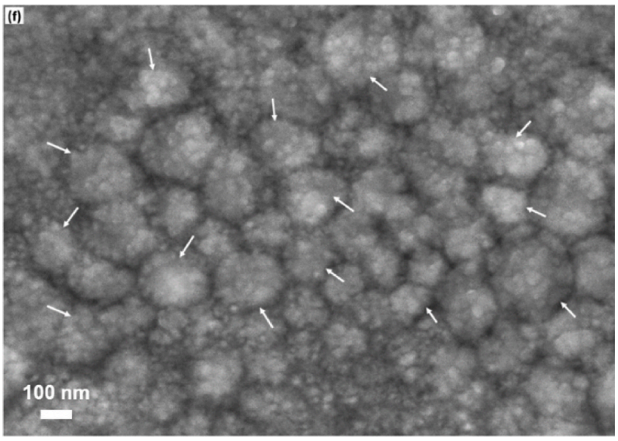

Fig. 3. (f): Higher magnification SEM image of Ni-BN coated MS. White colored arrows indicate the Ni grains composed of finer Ni crystallites.

distance of 367 m under normal loads of 2, 3, 4, and 5N.

3. Results & discussion

3.1. Morphological studies and elemental analysis

SEM micrographs of pure Ni and Ni-BN coatings (with 5 % saccharin) deposited on mild steel are given in Fig. 2(a)–(b) and Fig. 3(a)–(e), respectively. Both the coatings appeared to be uniform, compact with crack free surface. Both coatings displayed comparable surface morphologies characterized by a distinct granular texture. However, the size of grains in the composite coating is smaller than that in the pure Ni coating (Fig. S2). There is a gradual reduction in grain size as the concentration of saccharin is increased up to 5 %. This occurs due to the grain refinement resulting from the co-deposition of BN particles within the Ni matrix. BN particles with a mean zeta potential of −19.5 mV influences the co-deposition mechanism by functioning as nucleation sites increasing the number of active sites to initiate Ni nucleation [12,16,22,23]. Simultaneously, the incorporation of BN particles at the boundaries of nickel crystallites can reduce the grain size so that the Ni-BN coating become denser than the pure Ni coating. SEM image of higher magnification (Fig. 3 (f)) shows the presence of Ni grains composed of finer Ni crystallites (indicated by white arrows).

Elemental composition analysis (Fig. 4(a)–(e)) of the surface of Ni-BN coated MS possesses nickel (~90 %) as the major elemental contribution. The composite coating surface had additional peaks corresponding to boron and nitrogen indicating that BN gets incorporated within the coating. Fig. 5(a)–(f) shows the cross-section of Ni-BN composite coatings. The average thickness of Ni-BN coating was found to be 40.5 μm. EDS data further indicated the presence of BN particles within the composite coating.

3.2. X-ray diffraction studies

X-ray diffraction patterns of pure Ni and Ni-BN coated samples with varying amount of saccharin (1–5 g/l) are shown in Fig. 6. From the data, two peaks of Ni at 2θ corresponding to 44.32° and 51.77° are assigned to (111) and (200) Bragg reflections of the face-centered cubic (fcc) structure of metallic nickel (JCPDS 04–0850 for Ni) [24]. Presence of BN in the coating cannot be confirmed from the XRD patterns owing to low concentration of BN.

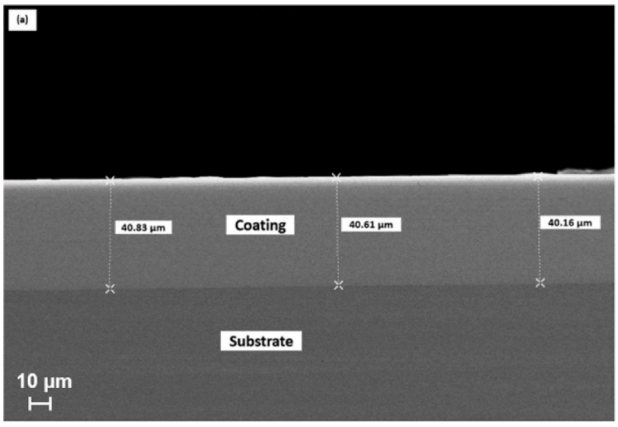

Fig. 5. (a): Cross-sectional SEM micrograph of Ni-BN coated MS.

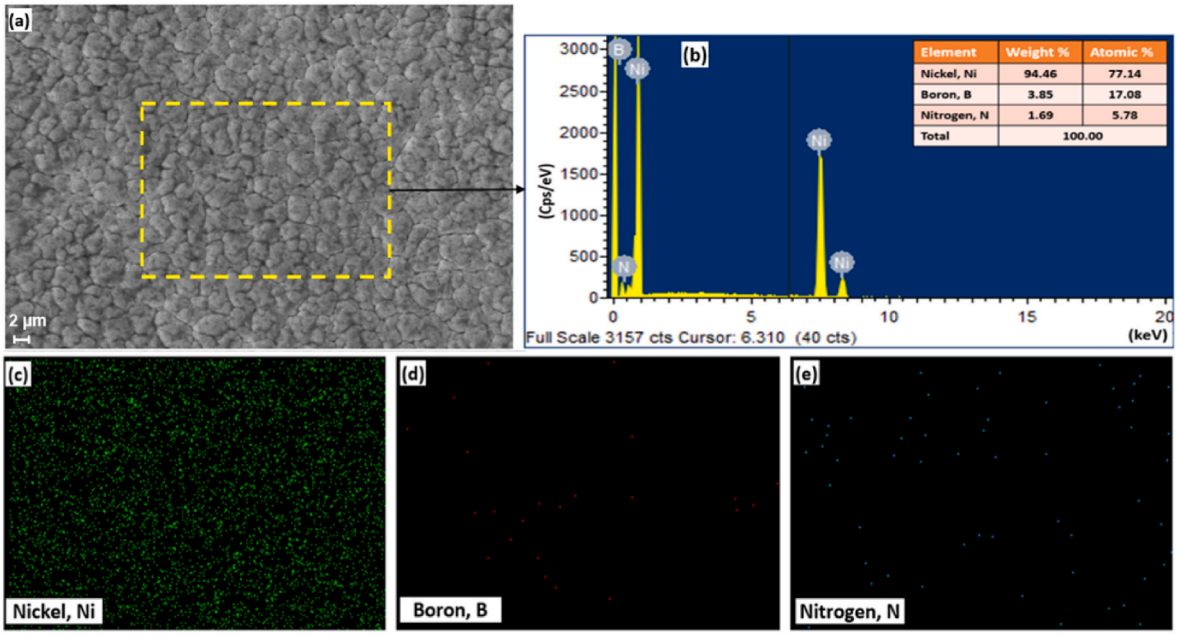

Fig. 4. (a–e): SEM-EDS & elemental mapping of Ni-BN coated MS surface.

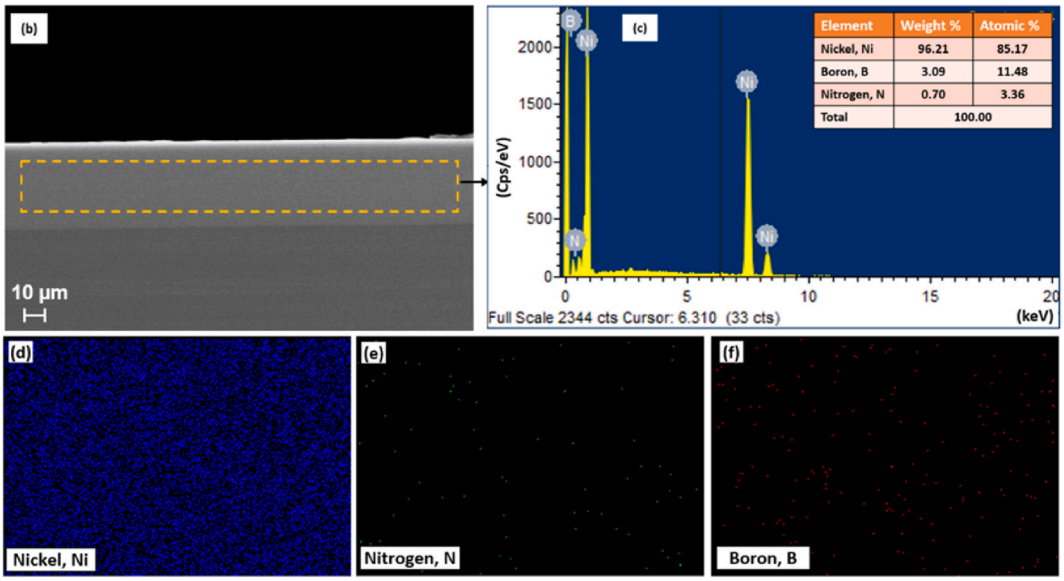

Fig. 5. (b–f): Cross-sectional SEM-EDS & elemental mapping of Ni-BN coated MS.

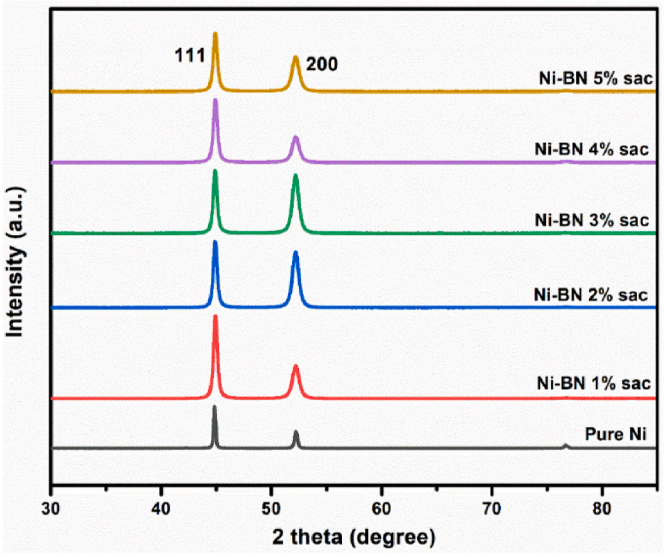

Fig. 6. XRD pattern of pure Ni & Ni-BN coated samples with varying saccharin amount.

The grain size (crystallite size) measurements indicate that the pure Ni coating (57 nm) have larger grain size compared to all the Ni-BN composite coatings. The lowest crystallite size was obtained for Ni-BN composite coating with 5 % saccharin (21 nm) (Fig. S2, Table 2).

A significant decrease in crystallite size from 57 nm (pure Ni) to 24 nm with the addition of 1 % saccharin in Ni-BN composite coating. However, further addition of saccharin (from 2 % to 5 %) results no significant change in crystallite size, which stabilize around 22-21 nm. Saccharin basically acts as a grain-refiner during Ni-BN electrodeposition. Its role as a grain refiner in Ni-BN composite coating can be explained as follows; the lone-pair of electrons of oxygen atom of the grain refiner saccharin fill the 3d orbitals of Ni atoms, forming a stable coordination bond. As a result, there will be strong interaction between the surface atoms of Ni deposits and saccharin. Large size of coordination compound of Ni and saccharin prevents the surface migration of Ni ions and suppress it reducing the grain size of Ni deposits.

Once the surface is saturated with saccharin molecules, additional saccharin does not significantly influence the refinement of grains. Due to limited surface interaction, grain refinement reaches a plateau. This behavior is common with additives in electrodeposition; there's a threshold beyond which their effect on reducing the grain size levels off [25,26].

All Ni-BN composite coatings showed a significant increase in microstrain and dislocation density values compared to pure nickel coating (Table S2). Smaller crystallite size results in higher microstrain and dislocation density due to increased presence of grain boundaries and lattice distortions [27].

3.3. Microhardness measurements

Compared to mild steel and pure Ni coating, Ni-BN composite coating exhibits exceptionally high microhardness (Fig. 7). In the case of Ni-BN composite coating, the hardness is improved by the dispersion strengthening and grain boundary immobilization by BN particles [28]. Saccharin reduces the average grain size, leading to a higher grain

Table 2
Crystallite size calculations using Scherrer equation in Ni-BN coatings.

Coating	Angular position (θ) (radians)	cos θ (radians)	Full width half-maxima (FWHM) (radians)			Average crystallite size (D) (nm)
			Sample β_s	Instrument β_i	Corrected β_{corr}	
Pure Ni	0.390	0.925	2.616×10^{-3}	1.395×10^{-4}	2.612×10^{-3}	57
Ni-BN 1 % sac	0.390	0.925	6.280×10^{-3}		6.278×10^{-3}	24
Ni-BN 2 % sac	0.391	0.924	6.454×10^{-3}		6.453×10^{-3}	23
Ni-BN 3 % sac	0.391	0.924	6.628×10^{-3}		6.627×10^{-3}	23
Ni-BN 4 % sac	0.391	0.924	6.803×10^{-3}		6.801×10^{-3}	22
Ni-BN 5 % sac	0.391	0.924	6.997×10^{-3}		6.996×10^{-3}	21

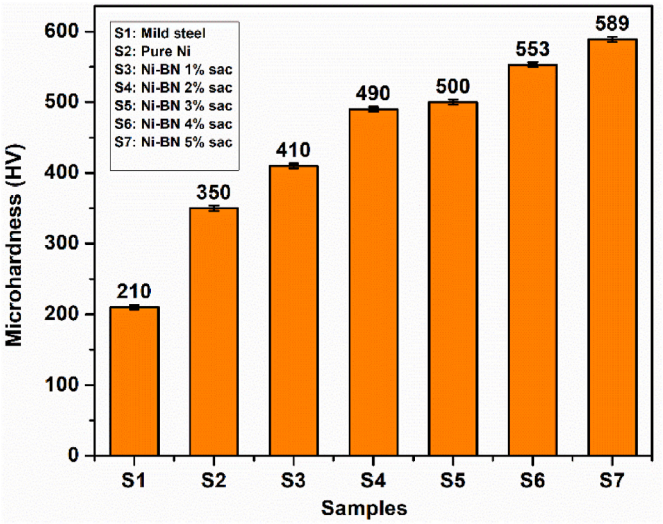

Fig. 7. Microhardness measurements of the coated samples.

boundary density further substantiated from higher microstrain and dislocation density. Grain boundaries act as obstacles to dislocation movement, hindering plastic deformation. The increased resistance to dislocation movement results in a harder coating. Vickers microhardness increase in the order of mild steel (210 HV) < pure Ni (350 HV) < Ni-BN 5 % saccharin (589 HV) composite coating.

The crystallite size is not changing significantly above 1 % saccharin, however, there is a significant increase in hardness. There are certain additional effects of saccharin other than crystallite size reduction [29]. After 1 % saccharin, even though crystallite size stabilizes, saccharin still influences other microstructural features. Saccharin molecules can modify the cathode surface properties, enhancing the adsorption of BN particles and increasing the chances that they become embedded in the growing nickel matrix. Saccharin also suppresses hydrogen evolution during electroplating, which otherwise would hinder BN incorporation by causing turbulence or gas bubble interference near the cathode surface.

Higher concentrations of saccharin can help in stabilizing the BN particles in suspension, preventing agglomeration and ensuring a more uniform distribution throughout the deposit. These BN particles once incorporated in the Ni matrix will act as barriers to dislocation motion (dispersion strengthening) enhancing the hardness. Saccharin can reduce the internal porosity of the coating. This leads to a more uniform structure improving mechanical strength of the coating [30]. Saccharin

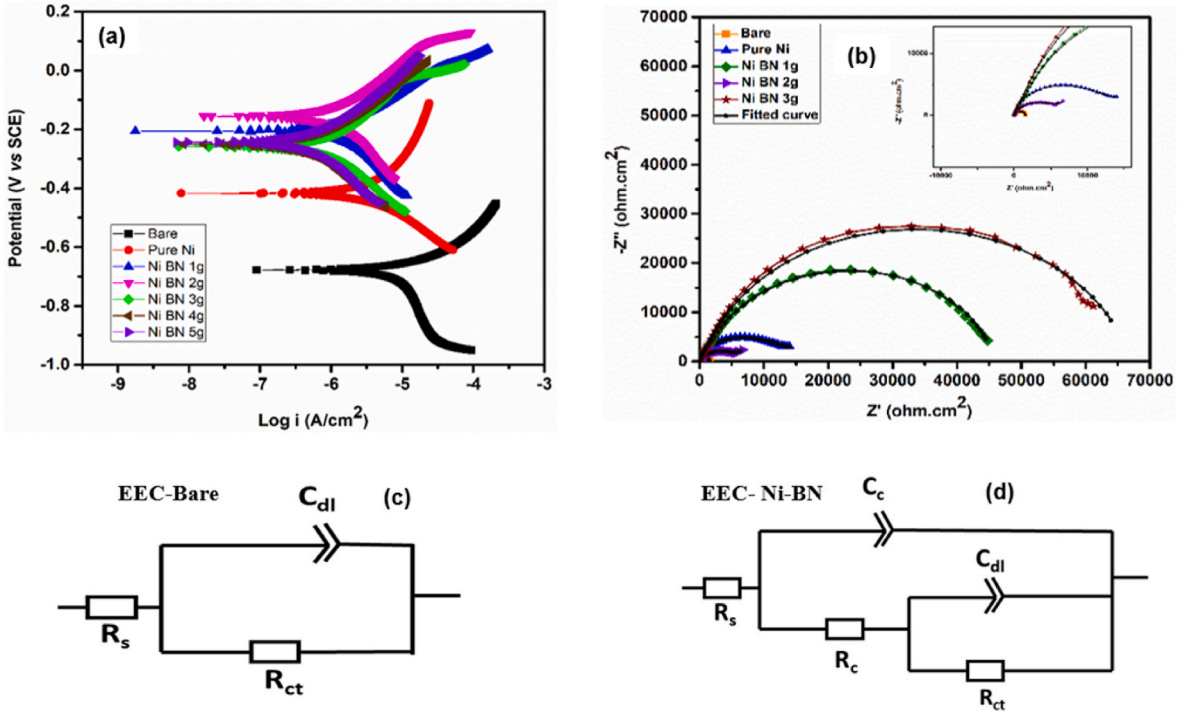

Fig. 8. Electrochemical study for the Ni-BN composite coatings **(a)** Tafel plot, **(b)** Nyquist plot, **(c)** EEC for the bare sample, **(d)** EEC for Ni-BN coated sample.

Table 3
Electrochemical parameters obtained and corrosion inhibition efficiency of Ni-BN coated samples.

S/N	Substrate	Potentiodynamic polarization				EIS	
		E_{corr} (V)	i_{corr} (μAcm^{-2})	η (%)	Corr.rate (mmpy)	R_{ct} (Ω cm^2)	η (%)
1.	Bare Mild Steel	−0.678	17.110	–	0.2013	3.955×10^2	–
2.	Pure Nickel	−0.417	4.143	75.78	0.0446	3.222×10^4	98.77
3.	Ni-BN 1 % sac	−0.206	1.723	89.90	0.0185	4.513×10^4	99.12
4.	Ni-BN 2 % sac	−0.155	1.583	90.70	0.0170	5.232×10^4	99.24
5.	Ni-BN 3 % sac	−0.258	1.041	93.90	0.0112	6.627×10^4	99.40
6.	Ni-BN 4 % sac	−0.184	0.687	95.90	0.0074	5.721×10^4	99.42
7.	Ni-BN 5 % sac	−0.251	0.471	97.20	0.0050	9.095×10^4	99.56

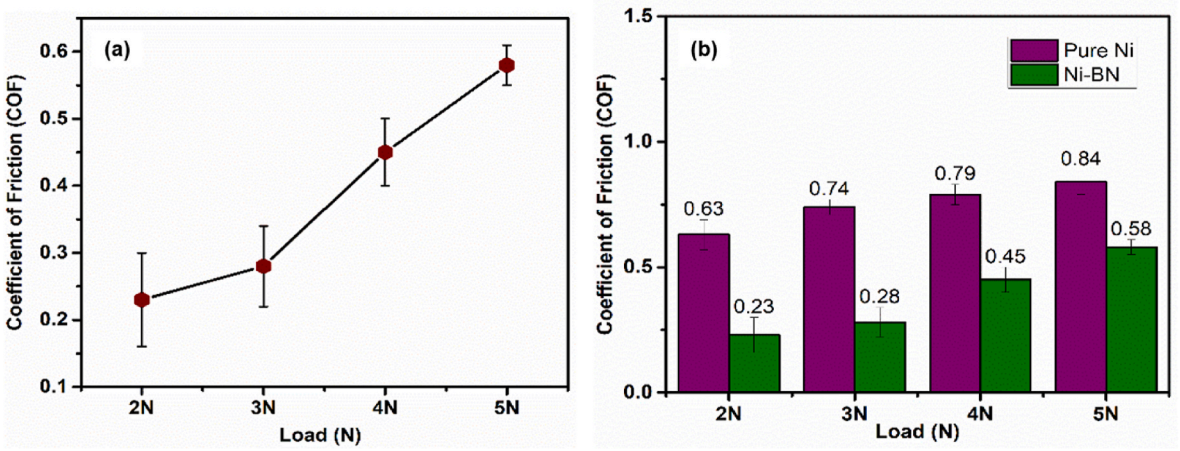

Fig. 9. **(a)** Load vs COF of Ni-BN coated samples, **(b)** Comparison of COF values of pure Ni & Ni-BN coated samples under different loads.

acts as a leveling agent, producing more compact coatings. Fewer voids or surface defects can contribute to better hardness [31].

3.4. Electrochemical characterization

Fig. 8(a) shows the Tafel plots of samples. Table 3 provides the corrosion potential (E_{corr}) and corrosion current density (i_{corr}) values that were determined by extrapolating the cathodic and anodic sides. The enhanced corrosion resistance of composite coatings is indicated by a larger positive variation in the E_{corr} value and a lower i_{corr}.

Presence of BN particles and grain refinement leads to a significant reduction in i_{corr} of Ni-BN to 0.471 μA cm^{-2} from 4.143 μA cm^{-2} in the case of pure Ni and 17.110 μA cm^{-2} in case of bare mild steel sample. The tafel graph of the composite coating correspondingly shifted towards the left side. The decrease in i_{corr} shows that there is a decrease in the rate of ion diffusion over the coating surface during corrosion [32]. Compared to other samples, the Ni-BN 5 % saccharin composite coating is more cathodic and has superior corrosion protection (E_{corr} MS: −0.678 V, Pure Ni: −0.417 V, Ni-BN 5 % saccharin: −0.251 V). The anodic and cathodic half-cell reactions are as follows:

Cathodic reactions

$$2H^+ + 2e^- = H_2 \quad (3)$$

$$O_2 + 4H^+ + 4e^- = 2H_2O \quad (4)$$

Anodic reactions.

$$Ni - 2e^- = Ni^{2+} \quad (5)$$

BN is chemically inert and generally does not undergo anodic reactions; it acts as a barrier phase in the coating. The structural modification of nickel crystallites induced with the incorporation of BN particles along with the grain refining effect of saccharin led to improved corrosion resistance [32]. A passive layer of evenly distributed h-BN particles is formed between the coating and the corrosive media. BN particles fill up the surface imperfections such as tiny voids and gaps and act as an obstacle to corrosive ion migration along the electrode surface, thus improving the anti-corrosion properties [33]. In addition to that, grain refinement in the composite coatings improves corrosion resistance by increasing the number of grain boundaries, which act as barriers to corrosive species, and by promoting more homogeneous distribution of BN particles, reducing localized corrosion. Thus the corrosion rate (0.0050) of Ni-BN composite coating is exceptionally low compared to mild steel and pure Ni samples.

The crystallite size is not changing significantly above 1 % saccharin, however, there is significant increase in corrosion resistance. Saccharin acts as a grain-refiner and levelling agent in electrodeposition. It helps to create a more uniform coating. This will reduce the porosity and micro-cracks, which are potential paths for corrosive agents. Even if crystallite size is unchanged, a pore-free, compact surface makes it harder for corrosive species (like Cl^- in NaCl solutions) to penetrate. Higher saccharin concentrations improve the co-deposition and uniform dispersion of BN in the Ni matrix. This creates a barrier effect, where BN particles act as obstacles to corrosive ion diffusion. Saccharin also helps to reduce internal stress, which minimizes crack formation during or after deposition. It also helps in filling up voids or gaps in the coating structure. Thus there will be fewer defects and micro-cracks which are often corrosion initiation points.

EIS measurements were conducted to gain a better understanding of the corrosion resistance of the coatings. Nyquist plots of bare mild steel, pure Ni and Ni-BN composite coatings were obtained in 3.5 % NaCl medium at their respective open circuit potentials (Fig. 8(b)).The Nyquist plots of all the samples showed a single semi-circular arc in the investigated frequency region. The bare MS samples can be fitted with equivalent electrochemical circuit (EEC) $R_s(C_{dl}R_{ct})$ (Fig. 8(c)), and all the coated samples are well fitted for the equivalent circuit of $R_s(C_cR_c(C_{dl}R_{ct}))$ (Fig. 8(d)).

R_s is the solution resistance, and R_{ct} and C_{dl} are the charge transfer resistance and double-layer capacitance, respectively. Instead of using pure capacitance due to the possibility of a dispersion effect between the metal/coating system, C represents a constant phase angle element (CPE). The coating offered protection by the resistance element R_c. Table 3, Table S3 & Table S4 provide a summary of the EEC components obtained from EIS measurements. The corrosion data clearly demonstrates that the inclusion of BN particles significantly enhances both R_{coat} and R_{ct} values in the Ni-BN coatings. The Ni-BN composite coating's superior anti-corrosion properties was demonstrated by the larger radius of semi-circular arc. This in turn reflects higher R_{ct} value indicating the material's ability to resist corrosive attack, hence improved protection. Simultaneously, the observed reduction in Q_{dl}, indicative of double-layer capacitance suggests the formation of a thicker electrical double layer. Overall, the combination of elevated R_{ct} and lowered Q_{dl} confirms superior corrosion resistance of the composite coating.

3.5. Tribological characteristics

Fig. 9(a) shows the variation of coefficient of friction of the electrodeposited Ni-BN coating at different loads (2, 3, 4, and 5N) load for 15 min under non-lubricated conditions. In comparison with pure Ni, the friction coefficient of Ni–BN composite coating got reduced and correspondingly the wear resistance increased (Fig. 9(b)). The incorporation of BN particles and refined grain structure of the composite coating results in lower friction coefficient in comparison with pure Ni

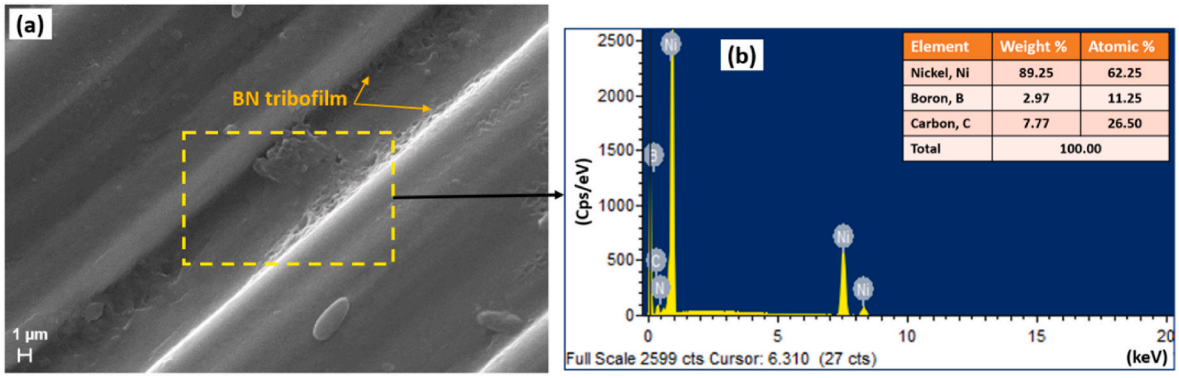

Fig. 10. (a)–(b) SEM-EDS of the worn surface of Ni-BN coated sample.

coating under different loads. Percentage of mass loss of the wear samples after wear are recorded in Table S5.

SEM-EDS of the worn surfaces of Ni-BN coatings are shown in Fig. 10 (a–b). Higher magnification sem images of the worn surface of Ni-BN coatings are included as Fig. S3. BN included in the Ni matrix restricts or slows down the dislocation movements in the matrix avoiding excessive wear [34]. In h-BN, the parallel planes can slide due to the layered hexagonal structure of the crystal lattice. The shear strength is low along the sliding direction because of the weak bonding between the planes. A solid self-lubricating tribo layer forms over the worn surfaces as a result of strong adhesion of BN particles to the surface [35]. This film forms an interface layer between the pin and the disc. Thus the strongly adhered lubrication film formed by h-BN prevents the surface from further wear.

4. Conclusions

Ni-BN composite coating was successfully coated over mild steel by DC deposition and the morphology, composition, phase structure, average grain size, microhardness, electrochemical and tribological properties were investigated. The main conclusions are outlined below;

1. All the developed coatings were uniform and compact without cracks. Increasing the saccharin concentration to a certain level (5 %) refines the nickel grains. Additionally the incorporation of BN particles refined the grains and reduced the porosity since the BN particles act as nucleation sites which could inhibit the crystal growth.
2. The presence of BN particles as well as grain refinement induced due to saccharin led to a statistically significant improvement in the microhardness (589 HV) of the coating.
3. Compared with mild steel and pure Ni, Ni-BN composite coating rendered excellent corrosion resistance (higher R_{ct} and lower Q_{dl} values) and low coefficient of friction at optimum saccharin concentration and due to BN incorporation.
4. The Ni-BN electrodeposits containing 5 % saccharin demonstrated superior tribo-mechanical and corrosion resistance properties. These findings support the effective surface modification of mild steel and promote the advancement of next-generation, high-performance, grain-refined Ni-BN composite coatings with promising applications in the automotive, construction, and pipeline industries.

CRediT authorship contribution statement

Revathy Sreekumar: Writing – review & editing, Writing – original draft, Methodology, Investigation, Data curation, Conceptualization. **M. S. Priyalekshmi:** Investigation, Data curation. **S. Parvathy:** Investigation, Data curation. **S.S. Sreejakumari:** Writing – review & editing, Validation, Supervision, Resources.

Declaration of competing interest

The authors declare that they have no known competing financial interests or personal relationships that could have appeared to influence the work reported in this paper.

Acknowledgments

The first author Revathy Sreekumar is thankful to DST, Govt. of India for the Inspire fellowship grant (IF 180987). The authors are grateful to Mr. Harish Raj and Ms.Anjali for their support in the characterization of the samples. The authors are also thankful to Mr. Visakh Manoj and Mr. Arun V.S. for their assisatnce in wear analysis of the samples.

Appendix A. Supplementary data

Supplementary data to this article can be found online at https://doi.org/10.1016/j.ceramint.2025.07.435.

References

[1] Z. Zhang, H. Dong, A state-of-the-art overview, Manuf. Rev. 1 (2014) 24, https://doi.org/10.1051/mfreview/2015001.
[2] M. Mozetič, Surface modification to improve properties of materials, Materials (Basel) 12 (2019), https://doi.org/10.3390/MA12030441.
[3] M.S. Safavi, A. Rasooli, The positive contribution of Cr2O3 reinforcing nanoparticles to enhanced corrosion and tribomechanical performance of Ni–Mo alloy layers electrodeposited from a citrate-sulfate bath, J. Mater. Res. Technol. 28 (2024) 865–878, https://doi.org/10.1016/j.jmrt.2023.12.014.
[4] I. Gurrappa, L. Binder, Electrodeposition of nanostructured coatings and their characterization—A review, Sci. Technol. Adv. Mater. 9 (2008) 043001, https://doi.org/10.1088/1468-6996/9/4/043001.
[5] E. Omrani, A. Dorri Moghadam, P.L. Menezes, P.K. Rohatgi, New emerging self-lubricating metal matrix composites for tribological applications. , 2016, https://doi.org/10.1007/978-3-319-24007-7_3.
[6] C.T.J. Low, R.G.A. Wills, F.C. Walsh, Electrodeposition of composite coatings containing nanoparticles in a metal deposit, Surf. Coating. Technol. 201 (2006) 371–383, https://doi.org/10.1016/j.surfcoat.2005.11.123.
[7] I. Fatima, O. Fayyaz, M.M. Yusuf, A. Al Ashraf, R.A. Shakoor, Enhanced electrochemical and mechanical performance of BN reinforced Ni-P based nanocomposite coatings, Diam. Relat. Mater. 130 (2022) 109454, https://doi.org/10.1016/j.diamond.2022.109454.
[8] S.T. Aruna, V.K. William Grips, K.S. Rajam, Ni-based electrodeposited composite coating exhibiting improved microhardness, corrosion and wear resistance properties, J. Alloys Compd. 468 (2009) 546–552, https://doi.org/10.1016/j.jallcom.2008.01.058.
[9] R. Sreekumar, A.S. Nair, S. S.S, Recent trends and developments in two-dimensional materials based electrodeposited nickel nanocomposite coatings, FlatChem 36 (2022) 100434, https://doi.org/10.1016/j.flatc.2022.100434.
[10] A. Rasooli, M.S. Safavi, S. Jabbarzadeh, Z. Shabzendeh Gharamaleki, Z. Jafarpour, Z. Safaralizadeh, M. Abdollahi, Enhanced tribomechanical and electrochemical performance of the Ni–P electrodeposits reinforced by duplex Cr2O3 and ZrO2 ceramic nanoparticles, J. Mater. Res. Technol. 35 (2025) 4566–4577, https://doi.org/10.1016/j.jmrt.2025.02.145.
[11] H. Zhou, N. Du, L. Zhu, J. Shang, Z. Qian, X. Shen, Characteristics investigation of Ni-diamond composite electrodeposition, Electrochim. Acta 151 (2015) 157–167, https://doi.org/10.1016/j.electacta.2014.10.122.

[12] G. Gyawali, R. Adhikari, H.S. Kim, H.-B. Cho, S.W. Lee, Effect of h-BN nanosheets codeposition on electrochemical corrosion behavior of electrodeposited nickel composite coatings, ECS Electrochem. Lett. 2 (2012) C7–C10, https://doi.org/10.1149/2.003303eel.

[13] S. Abbas, A. Abbas, Z. Liu, C. Tang, The two-dimensional boron nitride hierarchical nanostructures: controllable synthesis and superhydrophobicity, Mater. Chem. Phys. 240 (2020) 122145, https://doi.org/10.1016/j.matchemphys.2019.122145.

[14] M. Demir, E. Kanca, İ.H. Karahan, Characterization of electrodeposited Ni–Cr/hBN composite coatings, J. Alloys Compd. 844 (2020) 155511, https://doi.org/10.1016/j.jallcom.2020.155511.

[15] A. Tozar, İ.H. Karahan, Effect of octylphenyl ether group nonionic surfactant on the electrodepositon of the hexagonal boron nitride reinforced Ni-B matrix composite coatings, Surf. Coating. Technol. 381 (2020), https://doi.org/10.1016/j.surfcoat.2019.125131.

[16] M.K. Tripathi, D.K. Singh, V.B. Singh, Electrodeposition of Ni-Fe/Bn nano-composite coatings from a non-aqueous bath and their characterization, Int. J. Electrochem. Sci. 8 (2013) 3454–3471.

[17] M. Bhardwaj, K. Balani, R. Balasubramaniam, S. Pandey, A. Agarwal, Effect of current density and grain refining agents on pulsed electrodeposition of nanocrystalline nickel, Surf, Eng. 27 (2011) 642–648, https://doi.org/10.1179/026708410X12683118611185.

[18] F. Nasirpouri, M.R. Sanaeian, A.S. Samardak, E.V. Sukovatitsina, A.V. Ognev, L. A. Chebotkevich, M.G. Hosseini, M. Abdolmaleki, An investigation on the effect of surface morphology and crystalline texture on corrosion behavior, structural and magnetic properties of electrodeposited nanocrystalline nickel films, Appl. Surf. Sci. 292 (2014) 795–805, https://doi.org/10.1016/j.apsusc.2013.12.053.

[19] V.N. Tseluikin, On the structure and properties of composite electrochemical coatings. A review, Protect. Met. Phys. Chem. Surface 52 (2016) 254–266, https://doi.org/10.1134/S2070205116010251.

[20] G.Q. Qadir, M.I. Awad, J.A. Juma, W.O. Karim, Z.T. Al-thagafi, B.A. Al Jahdaly, H. H. Abdallah, Influence of nicotinic acid additive on the electrodeposition of nickel from aqueous solution, Int. J. Electrochem. Sci. 19 (2024) 100745, https://doi.org/10.1016/j.ijoes.2024.100745.

[21] S. Fatimah, R. Ragadhita, D.F. Al Husaeni, A.B.D. Nandiyanto, ASEAN journal of science and engineering how to calculate crystallite size from X-Ray diffraction (XRD) using scherrer method, ASEAN J. Sci. Eng. 2 (2022) 65–76.

[22] S. Paydar, A. Jafari, M.E. Bahrololoom, V. Mozafari, Enhancing Ni electroplated matrix through mixed boron nitride–carbide reinforcement, Vacuum 92 (2013) 52–57, https://doi.org/10.1016/j.vacuum.2012.10.014.

[23] E. Ünal, H. Karahan, Production and characterization of electrodeposited Ni-B/hBN composite coatings, Surf. Coating. Technol. 333 (2018) 125–137, https://doi.org/10.1016/j.surfcoat.2017.11.016.

[24] A. Lelevic, F.C. Walsh, Electrodeposition of ni[sbnd]p composite coatings: a review, Surf. Coating. Technol. 378 (2019), https://doi.org/10.1016/j.surfcoat.2019.07.027.

[25] A.M. Rashidi, A. Amadeh, The effect of saccharin addition and bath temperature on the grain size of nanocrystalline nickel coatings, Surf. Coating. Technol. 204 (2009) 353–358, https://doi.org/10.1016/j.surfcoat.2009.07.036.

[26] N.P. Wasekar, P. Haridoss, S.K. Seshadri, G. Sundararajan, Influence of mode of electrodeposition, current density and saccharin on the microstructure and hardness of electrodeposited nanocrystalline nickel coatings, Surf. Coating. Technol. 291 (2016) 130–140, https://doi.org/10.1016/j.surfcoat.2016.02.024.

[27] E.F.A. Zeid, I.A. Ibrahem, A.M. Ali, W.A.A. Mohamed, The effect of CdO content on the crystal structure, surface morphology, optical properties and photocatalytic efficiency of p-NiO/n-CdO nanocomposite, Results Phys. 12 (2019) 562–570, https://doi.org/10.1016/j.rinp.2018.12.009.

[28] H. Li, Y. He, T. He, D. Qing, F. Luo, Y. Fan, X. Chen, Ni-W/BN(h) electrodeposited nanocomposite coating with functionally graded microstructure, J. Alloys Compd. 704 (2017) 32–43, https://doi.org/10.1016/j.jallcom.2017.02.037.

[29] Y.W. Li, X.X. Huang, J.H. Yao, X.S. Deng, Effect of saccharin addition on the electrodeposition of nickel from a Watts-type electrolyte, Adv. Mater. Res. 189–193 (2011) 911–914. https://doi.org/10.4028/www.scientific.net/AMR.189-193.911.

[30] M. Demir, E. Kanca, I.H. Karahan, Effect of saccharin addition on formation, wear and corrosion resistance of electrodeposited Ni-Cr coatings, Mater. Sci. Pol. 41 (2023) 111–125, https://doi.org/10.2478/msp-2023-0036.

[31] V. Torabinejad, M. Aliofkhazraei, S. Assareh, M.H. Allahyarzadeh, A. S. Rouhaghdam, Electrodeposition of Ni-Fe alloys, composites, and nano coatings–A review, J. Alloys Compd. 691 (2017) 841–859, https://doi.org/10.1016/j.jallcom.2016.08.329.

[32] J.B. Jiang, L. Zhang, Q.D. Zhong, Q.Y. Zhou, Y. Wang, J. Luo, Preparation and characterisation of nickel-nano-B 4C composite coatings, Surf. Eng. 28 (2012) 612–619, https://doi.org/10.1179/1743294412Y.0000000038.

[33] B. Li, D. Li, T. Mei, W. Xia, W. Zhang, Fabrication and characterization of boron nitride reinforced Ni–W nanocomposite coating by electrodeposition, J. Alloys Compd. 777 (2019) 1234–1244, https://doi.org/10.1016/j.jallcom.2018.11.081.

[34] S. Paydar, A. Jafari, M.E. Bahrololoom, V. Mozafari, Influence of BN and B 4 C particulates on wear and corrosion resistance of electroplated nickel matrix composite coatings, Tribol. Mater. Surface Interfac. 9 (2015) 105–110, https://doi.org/10.1179/1751584X15Y.0000000007.

[35] S. Sangeetha, G.P. Kalaignan, Tribological and electrochemical corrosion behavior of Ni–W/BN (hexagonal) nano-composite coatings, Ceram. Int. 41 (2015) 10415–10424, https://doi.org/10.1016/j.ceramint.2015.04.089.